GEOMAG

Solid Ea

Upper Atmosphe

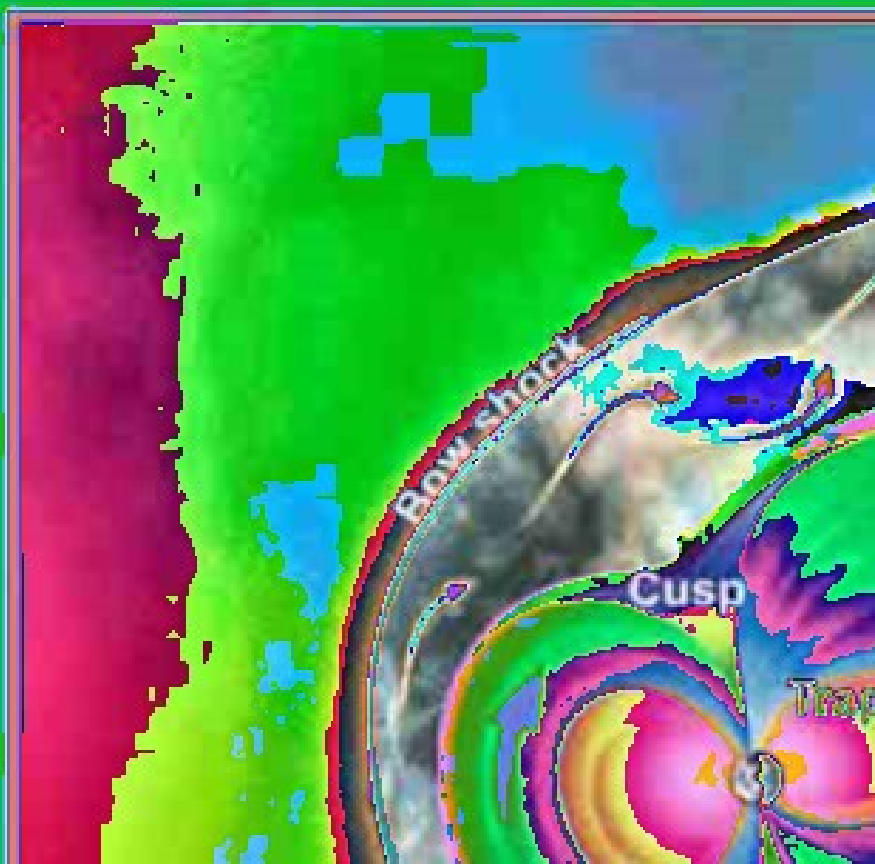

GEOMAGNETISM

Solid Earth and
Upper Atmosphere Perspectives

GEOMAGNETISM

Solid Earth and Upper Atmosphere Perspectives

By

Nathani Basavaiah

Indian Institute of Geomagnetism
Navi Mumbai, India

Springer

A C.I.P. Catalogue record for this book is available from the Library of Congress.

ISBN 978-94-007-0402-2 (HB)
ISBN 978-94-007-0403-9 (e-book)

Copublished by Springer,
P.O. Box 17, 3300 AA Dordrecht, The Netherlands
with Capital Publishing Company, New Delhi, India.

Sold and distributed in North, Central and South America by Springer,
233 Spring Street, New York 10013, USA.

In all other countries, except SAARC countries—Bangladesh, Bhutan, India, Maldives, Nepal, Pakistan and Sri Lanka—sold and distributed by Springer, Haberstrasse 7, D-69126 Heidelberg, Germany.

In SAARC countries—Bangladesh, Bhutan, India, Maldives, Nepal, Pakistan and Sri Lanka—sold and distributed by Capital Publishing Company, 7/28, Mahaveer Street, Ansari Road, Daryaganj, New Delhi, 110 002, India.

www.springer.com

Cover photos credit: *Top:* http://www.windows2universe.org/physical_science/magnetism/planetary_magnetospheres.html, *bottom left:* http://stephenschneider.stanford.edu/Publications/PDF_Papers/AllegreSHS.pdf and *bottom right:* http://geomag.usgs.gov/intro.html

Printed on acid-free paper

Printed in India.

FOREWORD

During the last century, science has taken enormous strides and tremendously impacted every segment of society. Over the years, there has been a welcome explosion of knowledge. However, this knowledge is increasingly becoming over-specialized, more complex and subtle. To be well-informed and to keep abreast with the present fast-paced scientific develop-ments, students, academics and technological fraternity need to constantly educate themselves on a wide variety of scientific phenomena. This book on geomagnetism is a step in that direction.

Geomagnetism is a relatively old stream of science but at present only a very few universities have it in their curriculum as a distinctly separate subject. Not surprisingly, research on geomagnetism is carried out today by only a few scientific organizations. Due to lack of exposure to this specialized area of study, paucity of relevant reading material is keenly felt by students and researchers alike to gain knowledge and carry out studies in the modern scientific field of geomagnetism. Most of the available literature on this subject is limited to research articles, which alone cannot provide the necessary background knowledge on the techniques and interpretative skills to the beginner. Thus, students and teachers globally find it difficult to 'identify' with the 'setting' in which the international scientists carry out their research activity and the data obtained on geomagnetic studies. The present book attempts to fill this gap.

Anyone who has used a magnetic compass utilizes at least one geomagnetic element, the declination, although the person may not be aware of it. Geomagnetism affects every individual in a myriad of ways and so the major aim of this book is to explain the 'how' and 'why' of it. The author guides the readers lucidly through the intricate maze of the world of geomagnetism as the tale of its progression is told in a fascinatingly interesting manner. The development of any scientific stream is never along one linear path. A lot of tributaries and sub-tributaries join together quite imperceptibly and seamlessly to take the form of a giant 'mainstream'. Geomagnetism too is not an exception in this regard. Right from the rudimentary declination measurements to the sophisticated ones carried out far off in space, the author takes the readers through its evolution. The processes of geomagnetism touch us all in one form

or the other, and it should be of great interest to all. Hence it is a welcome addition to the literature on geomagnetism.

The book is unique in another way. It addresses many important applications of the techniques of geomagnetism, which is quite invaluable. To explain recent occurrences of the strong earthquakes world-wide, delineation of conductive bodies substantially adds authenticity and reliability to the overall research output in this field. It also deals with the interesting geophysical features relating to hotspot traces, conductive blocks beneath the Earth, the continental collision and subduction zones, the climatic vagaries discerned through magnetic mineral changes, ancient migratory path of the various subcontinents traced through changing position of apparent magnetic poles in space and time, the crustal deformations revealed by global positioning system (GPS), and the real-time monitoring of magnetic field by magnetic observatories, all of which makes reading this book a truly enlightening experience.

Thus, the book is meant for both teachers and students who have long been starved of good quality geoscientific literature incorporating holistic examples from their own regions. The students in particular have long been faced with difficulty of finding the right up-to-date material in a consolidated manner at one place to carry out geomagnetic studies employing the scintillating examples from their own cultural and geotectonic settings. This book amply bridges that gap and, hopefully, stimulates the minds of scientists and the teachers alike to take up geomagnetic studies.

It is also our firm belief that non-specialists also will gain some seminal 'insights' into the subject from this book. The book will actually prove more useful to those research scholars actively pursuing advance research in geophysics in university departments, institutes of higher learning and other centres of excellence. It will also benefit scientists and technologists engaged in geophysical research, and development of specialized applications at the leading professional organizations in the country and abroad. The author, Nathani Basavaiah, deserves to be complimented for his commendable effort in bringing out such a textbook on geomagnetism.

Prof. Erwin Appel
University of Tübingen
72076 Tübingen, Germany

Dr. S.K. Arora
Ex-Head, Seismology Division
Bhabha Atomic Research Centre
Mumbai, India

PREFACE

The need to write this book on 'geomagnetism' stems from the fact that the book caters to the needs of specialists and students alike. The present effort is an attempt to combine the interests of both these segments by bringing forth a book that includes most of the fascinating phases in the evolution of geomagnetism and also highlights the practical applications that this stream offers to the geoscientific community at large.

The world of geomagnetism encompasses within it many strands of scientific thought that have applications in the realm of solid Earth and upper atmosphere. The progression of solid Earth geomagnetism (SEG) and upper atmosphere magnetic studies (UAS) were not coeval. The different streams that now apparently appear as part of the grand 'geomagnetic' thought were, at some point of time, isolated and segregated with their own unique qualities. The journey that these seemingly diverse branches went through and the conditions that forced them to coalesce and fuse with each other present an interesting scenario. An attempt has been made to catch a few remarkable and defining moments from the historical evolution of geomagnetism in a scintillating manner.

The contents of the book cover two broad aspects of geomagnetism: evolution and development, and research and practical applications. The first aspect is dealt within Chapters 1 to 4, which are dedicated to capturing the essence, evolution and rise of the science of geomagnetism. The second aspect of the book reflected through Chapters 5 to 8 deals mainly with research activities in the field from different parts of the world, which have a practical bearing on the academic and technological expectations. Any attempt to compile the results embedded in a large number of research papers published by all the scientists would not only be a herculean task but might even prove futile. This book tries to conceptualize the subject by taking examples from some selected, yet important, research findings relevant to the context that are seamlessly knitted together.

Geomagnetic research, like any other branch of research in a scientific discipline, has an academic as well as a practical dimension. Purely academic investigations, more often than not, provide an impetus to the practical applicability. In this sense as well, the field of geomagnetism is no different.

Extensive geomagnetic studies have been carried out generating large amount of data through a network of magnetic and other geophysical observatories spread across the world. The significance of this achievement constantly enhances the database and knowledge in this field of specialization since geomagnetic observations are not actually static but often changing from time to time.

The scientific and technological fraternity, be it researchers or teachers, is confronted today with lack of adequate study material in a consolidated single volume. This book has essentially initiated efforts to present as many geotectonic features from the subcontinents as possible. It provides in-depth coverage to research carried out using modern instrumentation and techniques such as magnetotellurics (MT), geomagnetic deep sounding (GDS), ocean bottom magnetometers (OBM), global positioning system (GPS), tectonomagnetic, palaeomagnetic and environmental magnetic studies. Studies in the area of the solid Earth geomagnetism have described many tectonic and environmental regimes across South Asia in general and the Indian subcontinent in particular. There is not a single investigation of geological or geomagnetic relevance where surveys or probes have not been launched using geomagnetic techniques.

It may appear from this book, quite erroneously though, that only SEG research is being carried out in India. This is not at all true. A few tomes have already been published, authored and edited by Indian scientists, chronicling the exploits of observatory and data analysis (ODA) and UAS studies. This textbook is a humble attempt to accord SEG its rightful place in the pantheon of geomagnetism studies.

Electromagnetic studies taken up world-wide recently have already been proved useful beyond expectations. The results obtained in the rugged terrains in northwest and northeast parts of the Himalayas have been very encouraging in particular. It is proved beyond doubt that geomagnetics can be gainfully employed to decipher and understand past climatic and environmental changes.

The selected bibliography provided at the end of the book is not only exhaustive, but truly reflective of the sequential and progressive developments in the field of modern geomagnetism. Since this field is fast emerging, the students and teachers are required to keep abreast of the latest trends and advances.

My innate desire is also to reach out to those who have an urge to acquire knowledge about the natural processes that define this Cosmos. Instead of just loading with geomagnetic concepts indiscriminately and leaving the readers to fend for themselves through a labyrinth of geomagnetic jargons, an attempt is made to guide them systematically by an extended tour of geomagnetic evolution. This, it is hoped, will help them to understand how the different concepts in geomagnetism developed over time and made the subject to gain an exalted status it now occupies in the realm of science.

While bringing out the book, special care has been taken to address the demands and requirements of the teachers and students and, at the same time,

satisfy the needs of those who are actively engaged in research and advanced studies in geophysics. Above all, the book serves as a ready reckoner for the scientists working in leading geophysical research institutes and academic institutions. I earnestly hope that the book would satisfy the geoscientific curiosity of both specialists and non-specialists alike in the subjects of geophysics, physics and geology.

I wish to gratefully acknowledge the help and assistance rendered to me by some eminent geophysicists in quintessentially consolidating the material that has eventually led to the production of this book. Amongst them are G.S. Lakhina, G.K. Rangarajan, R. Rajaram, B.P. Singh, Erwin Appel, S.K. Arora, K. Nageswara Rao and G. Karunakar. I also enjoyed substantial support from P.B. Gawali, K. Deenadayalan and staff members of three major divisions (ODA, SEG and UAS) of IIG. All figures and diagrams were redone and improved by Ramesh Borwanker.

November, 2010 **Nathani Basavaiah**

CONTENTS

ABBREVIATIONS

AF	Alternating Field
AFMAG	Audio-Frequency Magnetic Field
AMOs	Automatic Magnetic Observatories
AMPTE	Active Magnetospheric Particle Tracer Explorers
AMS	Anisotropy of Magnetic Susceptibility
AMT	Audio-Frequency Magnetotellurics
APW	Apparent Polar Wander
APWP	Apparent Polar Wander Path
ARM	Anhysteretic Remanent Magnetization
B_{EXT}	External Magnetic Field
BMZ	Balance Magnetique Zero
CA	Crack-Avalanche
Cal Yrs BP	Calibrated Years Before Present
CEJ	Counter Electrojet
ChRM	Characteristic Remanent Magnetization
CMB	Core Mantle Boundary
D	Declination
DC	Direct Current
DCC	Deep Crustal Conductor
DD	Dilatancy-Diffusion
DIM	D and I Magnetometer
DoD	Department of Defence
DRM	Detrital Remanent Magnetization
DST	Department of Science and Technology
EEJ	Equatorial Electrojet
EGO	Eastern Ghats Orogeny
EM	Electromagnetic
EMF	Earth's Magnetic Field
EPS	Equivalent Point Source
ESF	Equatorial Spread F
EUV	Extreme Ultraviolet
F	Total Field
FTIR	Fourier Transform Infrared Spectroscopy

GDS	Geomagnetic Depth Sounding
GGT	Granite Greenstone Terrain
GIC	Geomagnetically Induced Current
GMT	Greenwich Mean Time
GPS	Global Positioning System
GPTS	Geomagnetic Polarity Time Scale
GSI	Geological Survey of India
HCL	Mantle High Conductivity Layer
HGPG	Horizontal Gradient Pseudogravity
I	Inclination
ICM	Induction Coil Magnetometer
IEEY	International Equatorial Electrojet Year
IGRF	International Geomagnetic Reference Field
IGY	International Geophysical Year
IIG	Indian Institute of Geomagnetism
IMD	Indian Meteorological Department
IMF	Interplanetary Magnetic Field
IMO	Inter Magnet Observatory
IMS	International Magnetic Study
IOL	Indian Ocean Low
IRM	Isothermal Remanent Magnetization
IRSL	Infrared Stimulated Luminescence
ISEE	International Sun-Earth Explorer
IST	Indian Standard Time
ITS	Indo-Tsangpo Suture
LGM	Last Glacial Maximum
LIA	Last Ice Age
LLBL	Low-Latitude Boundary Layer
LTO	Low Temperature Oxidation
M	Magnitude (Earthquake)
Ma	Million Years
MAGSAT	Magnetic Field Satellite
MBT	Main Boundary Thrust
MCT	Main Central Thrust
MD	Multi Domain
MF	Medium Frequencies
MHD	Magnetohydrodynamics
MM	Modified Mercalli Scale
MO	Magnetic Observatory
MPS	Magnetic Polarity Scale
MPTS	Magnetic Polarity Time Scale
MRI	Magnetic Resonance Imaging
MST	Mesosphere-Stratosphere-Troposphere
MT	Magnetotelluric

N	Normal Polarity
NASA	National Aeronautics and Space Administration
NGRI	National Geophysical Research Institute
NMR	Nuclear Magnetic Resonance
NRM	Natural Remanent Magnetization
NSL	Narmada-Sone Lineament
OBE	Ocean Bottom Electrometer
OBM	Ocean Bottom Magnetometer
PCBL	Polar Cap Boundary Layer
PDRM	Post Depositional Remanent Magnetization
POGO	Polar Orbiting Geophysical Observatory
PPM	Proton Precession Magnetometer
PR	Partial Radar
PREM	Preliminary Reference Earth Model
PRR	Partial Reflection Radar
PSD	Pseudo-Single Domain
QHM	Quartz Horizontal Magnetometer
R	Reversed Polarity
R_e	Earth's Radius
RIS	Reservoir Induced Seismicity
RM	Remanent Magnetization
RS	Richter Scale
RT	Room Temperature
SAR	Synthetic Aperture Radar
SC	Sudden Commencement
SCR	Stable Continental Region
SEM	Scanning Electron Microscope
SEP	Solar Energetic Particle
SGT	Southern Granulite Terrain
SIGT	South Indian Granulite Terrain
SIOCA	South Indian Offshore Conductivity Anomaly
SIRM	Saturation Isothermal Remanent Magnetization
SOI	Survey of India
SP	Superparamagnetic
SQUID	Superconducting Quantum Interference Device
SSC	Storm Sudden Commencement
SSD	Stable Single Domain
T_b	Unblocking Temperature
T_C	Curie Temperature
TEC	Total Electron Counts
TEM	Transmission Electron Microscope
THC	Trans-Himalayan Conductor
TRM	Thermoremanent Magnetization
T_V	Verwey Transition

UFK	Ultra Fast Kelvin
ULF	Ultra-Low Frequency
VGP	Virtual Geomagnetic Pole
VHF	Very High Frequency
VLBI	Very Long Baseline Interferometry
VPPM	Vector Proton Precession Magnetometer
VRM	Viscous Remanent Magnetization
WDC	World Data Center
YD	Younger Dryas

1

THE HISTORICAL DEVELOPMENT OF (GEO)MAGNETISM

1.1 GLOBAL SCENE

Magnetism and gravity are two fundamental properties of the Earth and are innate to our planet's existence. But, the discovery of magnetism was not as dramatic as that of gravity. By deciphering the reason responsible for the fall of an apple, Newton opened the gates to understanding many of the basic principles governing the Universe. The circumstances leading to understanding of magnetism, and in essence geomagnetism, however, were slow and gradual.

A naturally occurring magnet attracts objects of iron. This knowledge was prevalent in the ancients, although it cannot be claimed with certainty that everybody was aware about this property. However, many myths and legends are associated with magnetism. According to one legend, the magnet was first discovered by a Cretan shepherd, Magnes, while he was tending to his flock. The iron nails on his sandals and iron tip of his staff got attracted to the Earth and after some digging he discovered a rock that stuck to his sandals. This was the natural magnet or lodestone, which is now known as iron ore or magnetite (Fig.1.1b). The ancient Greeks knew for certain about the lodestone and since such rocks were found near the city of Magnesia, the term magnetism must have originated. Magnesia is in Asia Minor in Turkey.

The history of magnetism started with the Greeks, but in the earliest phases it is more intimately connected with the Chinese. The Chinese were the first to crack the code of directional property of a freely suspended magnet that aligns itself in N-S direction. Here too, many myths and legends abound. One story, out of many, tells us that in 2634 BC there was a Chinese emperor who had a chariot fitted with a revolving figure of a man with one of its arms always pointing towards the north (Fig. 1.1a). This enabled the emperor to defeat his enemy by manoeuvering his way even out of a dense fog—the ancient equivalent

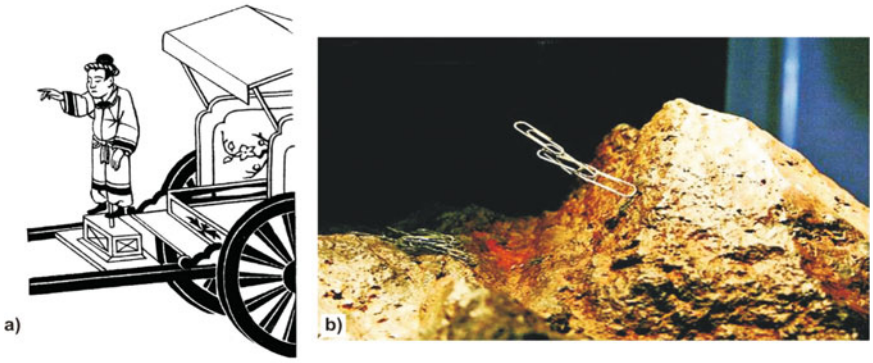

Figure 1.1. (a) The chariot of Chinese Emperor with a figure that always pointed north (Jacobs, v1, 1987). (b) A natural magnetic lodestone in the hall of Gems of the Smithsonian Museum, USA.

of the modern smokescreen. However, the firm footing on which the Chinese understanding of direction was placed can be gauged from the ancient walls of Beijing (Peking). These walls are aligned along magnetic N-S indicating the use of compass by masons, who built those walls.

The historical account, however, starts from the year 1000 BC. It was around this year that an anonymous Chinese scholar is supposed to have placed a lodestone on a boat floating into a bowl of water, and whatever its original position, it always turned south. This phenomenon was seen every time and at all places the experiment was performed. The Chinese also knew of the art of permanently magnetizing steel needles by rubbing the needle point with a lodestone.

The knowledge of magnetism and its association with the direction-specifying property was transmitted from China to Europe via the Arab world, possibly through trade links. The compass was then basically a pathfinder utility, hence became an integral part of long voyage ships. However, the phenomenon of magnetism and the reasons for the same remained shrouded in mystery. The users hadn't a clue to why compass needles pointed to a particular direction because of which the crew members were forbidden to eat garlic. They believed the pungent odour destroyed the magnetic power of a compass! The great sea voyages of Christopher Columbus, Vasco da Gama and Ferdinand Magellan were made possible by the discovery of compass, aside from other factors.

I. Problem of Latitude and Longitude

Columbus sailed across the Atlantic ocean in 1492 in search of a 'short-cut' and on a voyage of exploration to the Indies. Indies in those days included India, China, the East Indies and Japan or in general any region east of the Indus river. However, during this voyage he did not reach, where he had intended to go but landed in what is now known as the West Indies or the Caribbean

islands. Navigation in those days, the fifteenth century, was not as smooth and infallible as it is today. Global positioning system (GPS) does not allow us to 'get lost'. GPS has now made redundant the compass, maps, charts, astrolabes (ancient astronomical instruments), hourglasses and such other objects that were available as navigational tools to the ancient mariners and land travellers.

The urge to go far beyond into the horizon, away from the sight of land, necessitated the mariners of the olden days to find a way to determine their location resulting into the development of pilotage and dead reckoning. Pilotage is a method whereby known landmarks are used to determine one's position. In dead reckoning, on the other hand, a mariner recorded his course and speed every hour or every day to enable him to make a guess about his location. For this method to be of use and effective, it was necessary that the mariners never lost sight of land. Also dead reckoning could not be used at night time.

But things changed with the advent of a method designating latitude and longitude. Eratosthenes (276-194 BC) calculated the circumference of Earth and Hipparchus (160-125 BC) invented trigonometry and used it to calculate latitude and longitude with the help of north pole star, also called the polaris. The polaris is so high above the surface of the Earth that all sight lines to the star are essentially parallel. Hipparchus used this logic to determine the angle between the horizontal surface of the Earth and the polaris, which gave the precise degree of latitude. Thus, if the polaris was exactly on top of the observer, then that observer was at the north pole, i.e. at 90°N. If the angle to the polaris was zero, then the observer was at the equator at 0°. However, this method had some inherent shortcomings—the polaris cannot be sighted in a haze, bright lights of Moon can obscure it, and it is not visible from the southern hemisphere.

To circumvent these problems, the ancients decided to use the Sun, although it too had its share of lacunae. To determine the latitude, the angle to the Sun had to be taken at noon when the Sun was at zenith. But the Sun is not a fixed star (relative to Earth) and also because of the tilt of the Earth, the angle to the Sun at noon is different for each day. Thus, this method, though accurate, was a bit complicated. Improvements in deciphering latitudinal position in an easier way were made possible by the Arabs sometime between 810 and 850 AD when they developed algebra and used the system to establish the accurate position of Sun at zenith. The problem of quantification of latitude was permanently solved after 850 AD with the development of astrolabe, though later on there have been many developments in the art of knowing the positions (Fig. 1.2).

The problem of longitude was solved after a very long time. The world had to wait till 1761 because there were two very significant hurdles to cross. One was geographical and the other was the lack of an accurate timepiece. Latitude is measured with respect to equator. The latitude at equator is zero and it keeps on increasing toward either of the poles where it becomes 90°. For quantifying longitude, there wasn't any agreed reference line. The zero meridians were different for different sets of people. Ptolemy placed zero

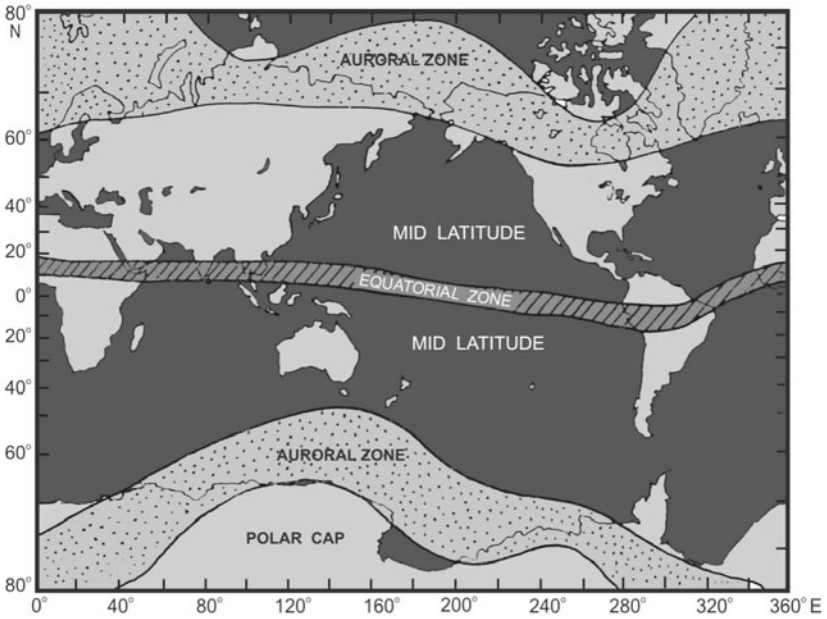

Figure 1.2. Based on the properties of changes in magnetic field, the world is divided into different latitude zones like the equatorial, mid-latitude or auroral zone (Regan et al., 1975).

meridian off the west coast of Africa, while Christian scholars placed it at Jerusalem as they considered it to be the centre of the world. In later ages, the zero meridian was calculated from Paris, Berlin, London, etc. It was only in 1884 that Greenwich, south of London was chosen as the zero (or prime) meridian for all subsequent calculations for according uniformity in maps and charts.

The ancient mariners had different methods to calculate longitude. They knew that Earth was divided into 360° of longitude and Eratosthenes had already calculated the circumference of the Earth to be 25,000 miles. Thus, if two points spaced far away observe the same event at the same time, then the difference in local time at the instant of that event can be converted into longitude. For this, they needed an accurate timepiece. John Harrison, an unschooled church clockmaker, put together the first marine chronometer in 1761.

II. Magnetic Compass—Declination and Inclination

At this juncture, it needs to ponder on why Columbus 'discovered' the West Indies and not India as was his stated purpose. His inability to reach India brings us face to face with one of Earth's (geo)magnetic elements, the 'declination (D)'.

The discovery of magnetic compass is over 1000 years old. A magnetic compass needle always aligns itself in the N-S direction and points in the direction of magnetic north. By orientation of the magnetic needle, a person can tell E or W relative to N or S. But like many matters of life that are beset with duality, direction too has its share of duality. There are two norths (or souths or easts or wests). The first is the geographic north, defined with respect to a celestial body like the Sun or pole star or planets. The other is the magnetic north. Thus, there is geographic (considered fixed) as well as magnetic north, which is variable. The angle between the two is the declination (Fig. 1.3a, b).

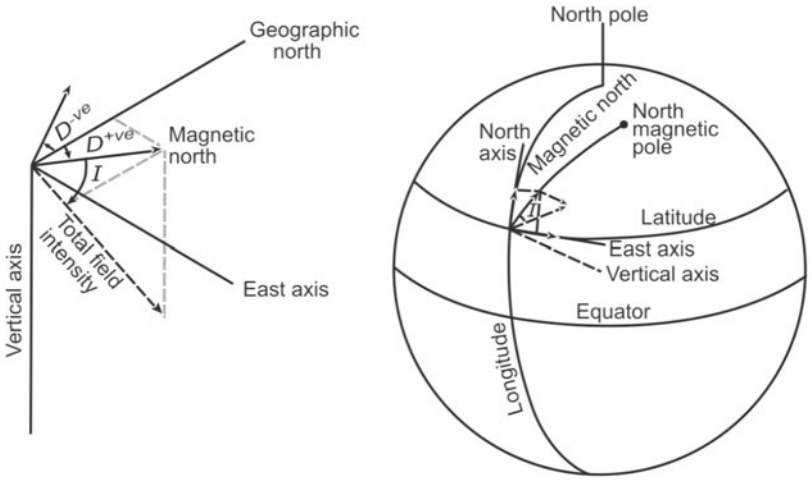

Figure 1.3. (a) The angle 'D' is declination. It is considered positive when measured 'east' of the geographic north and negative when 'west'. Angle 'I' is the inclination. (b) Viewed from the surface of the Earth, this is how D and I will 'look' (Robinson, 1982).

Declination varies from place to place. It ranges over several degrees depending upon whether the angle measured is E or W of geographic north. Declination is considered positive when the angle measured is east of the true north and negative when west. In India, D ranges from -2° to +3°. The earliest record of D comes from Columbus, who in 1492 noted its change. This magnetic property is of immense use to trading ships and to adventurous seafarers, the knowledge of which keeps them on 'track'.

The first reference of magnetic needles mounted on pivots allowing free rotation in a horizontal direction came from Alexander Neckam in 1187. The design of such a compass was also referred to in a letter written in 1269 by Petrus Peregrinus. The Europeans, like Chinese, knew that steel needles could be permanently magnetized by rubbing it with a lodestone. Their traditional way of making a compass was to take a steel needle, mount it on a pivot, balance it horizontally and then magnetize it by stroking with a lodestone. However, at the end of this entire ritual, they observed a strange thing. Right after magnetizing the needle its north pointing end slanted down, as if it had

suddenly gained weight and buckled under pressure just like a seesaw. This strange behaviour was first noted and recognized by George Hartmann in 1544.

However, for many, this was a practical nuisance and to maintain balance, the end was cut-off or a counter weight attached at the other end (the same is done even now). The phenomenon of 'slanting needle' was explained by Norman in 1580-81. He measured I with the 'dip circle' that he invented (Fig. 1.4). The second (geo)magnetic element, the dip or I is the angle between the magnetic north and the total magnetic force (Fig. 1.3a). The north seeking end of the needle will slant upward when the measurements are carried southward of the equator.

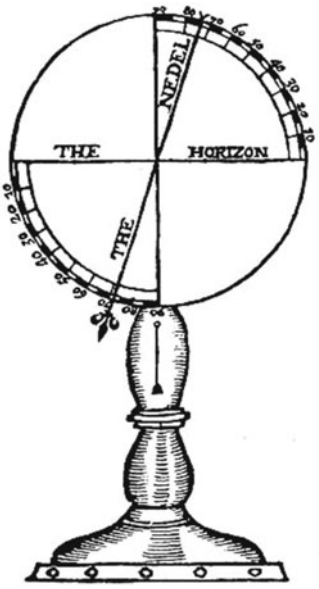

Figure 1.4. Robert Norman's dip-circle (Jacobs, v1, 1987).

For a long period of time people knew only about declination and inclination. Out of the two, D had higher utility value and it acquired an aura of indispensability in all navigational practices. Inclination, on the other hand, was considered a bit of nuisance on account of its 'dip' though it had its fleeting moments of glory by way of being used as a surrogate for magnetic latitude. However, on account of inclination measurements being more difficult and complicated, and also the idea of magnetic latitude taking a back seat, the I-measurements attracted scant attention from the mariners. Nevertheless, during the great sea voyages of exploration and conquest, unleashed by the English, Dutch, French, Spanish and Portuguese during the fourteenth and fifteenth centuries, mention of both D and I in their navigational log books can be found, though the bias is clearly in favour of declination.

III. Advent of William Gilbert

The above was the first phase that saw the seeds of geomagnetism been sown, inadvertently, by the seafarers and people like Norman. The second and the most decisive phase started with Gilbert. He was (probably) born in 1544 and became a distinguished doctor. He was the president of the Royal College of Physicians and was appointed physician to Queen Elizabeth I in 1601. By 1581, he became intensely fascinated by the phenomenon of magnetism and started collecting its information from books and all other available sources. He conducted his own experiments and much of what is now known about permanent magnetism was either enunciated or confirmed by him, though he is primarily remembered for asserting that Earth is a giant magnet which he announced to the world in his book 'De Magnete' published in the year 1600.

To arrive at this assertion, Gilbert conducted a simple experiment (he also used Norman's observations). He constructed a small replica of the Earth, a magnetized sphere, and named it terrella (Fig. 1.5), meaning 'little Earth'. He then placed a compass around the sphere and observed not just the northward pointing properties but also the dip angle.

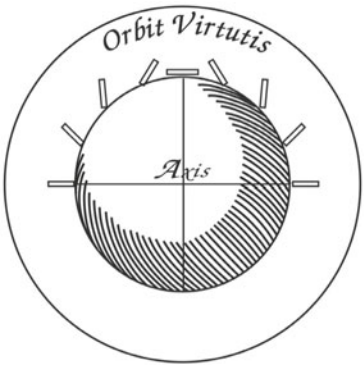

Figure 1.5. The 'Sphere of influence' of Gilbert. Note the compass needle is vertical at the poles and horizontal at the equator (Stern, 2002).

Gilbert experimentally concluded that declination would be absent if the Earth were a perfect sphere because the magnetic as well as the geomagnetic norths would then coincide. But, the Earth is not a perfect sphere. It has large irregularities on its surface. There are steep elevations (mountains) and deep depressions (oceans). Gilbert attributed magnetic attraction to the mass of Earth. Hence, he proposed that the elevated portions added to the pull while the depression decreased it. He asserted that the compass needle near the eastern and western edges of the Atlantic ocean would be deflected towards the nearby continents. This indeed was observed at the time. Gilbert had already verified the effect on his terrella on which he had cut a gash to resemble the Atlantic ocean. However, Gilbert erred on one count. He felt that the continents and oceans do not shift over the historical timescales (the theory of continental drift came much later) and so magnetic D would not change with time.

IV. Ordeal of Edmund Halley and Atlantic Declination Map

The advancement of science has necessarily been one of learning from others' mistakes. Gilbert was convinced of 'perpetual immutability' of declination. In 1634, however, Henry Gellibrand showed that the magnetic D observed near London had undergone certain changes. Later on, these changes were observed not just at London but also all over the globe without exhibiting a clear-cut pattern baffling the savants. Halley, the one who predicted the return of Halley's comet, proposed the solution that the interior of the Earth consisted of concentric spherical shells each magnetized differently and that some rotated at different rate from others.

Halley does not have just the honour of a comet named after him, but is also known for the 'Halleyan lines'. He compiled the first magnetic map of the Atlantic in 1700. In this map, the points of equal D are connected together by contour lines which came to be known as 'Halleyan lines' (Fig. 1.6a).

The longitude problem solved by Harrison and his accurate clock and Halley's plans to fix position more accurately by using the departures of magnetic north from geographic north were getting attracted by new and talented

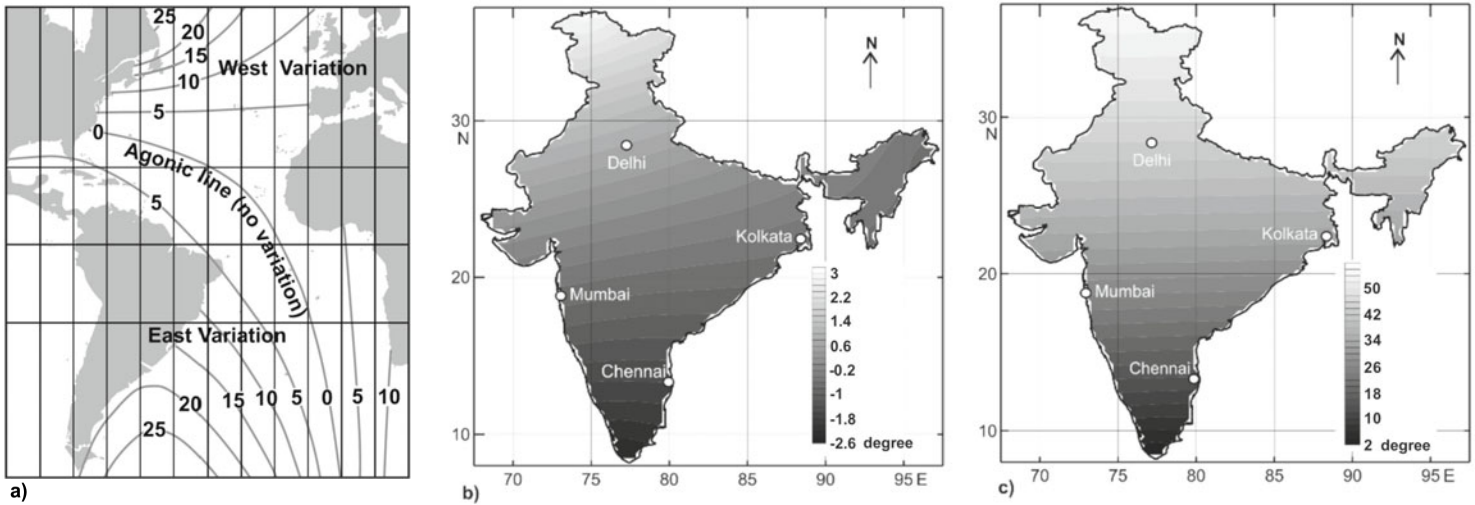

Figure 1.6. (a) Halley's map of declination, prepared in 1701, for the Atlantic (Jacobs, v1, 1987). (b) The declination map or the Halleyan lines for India. (c) India's magnetic chart of inclination angle I (IGRF11 model calculated for 2010).

minds to comprehend and decipher this geomagnetic phenomenon theoretically as well as experimentally. One such person was George Graham. In 1722, he showed that the direction of the magnetic force in London underwent a 24 hour cycle, called diurnal variation. He gauged this change by careful observation of position of the tip of a compass needle. This phenomenon was barely observable and to make it easily noticeable advanced instruments were set to be designed (details in Chapter 4 on instrumentation). Euler in 1757 used magnetic angle D to propose a theory for the EMF based on a dipole approximation. He, however, revised his theory in 1766 that enabled him with the help of polynomial expansion to calculate the D at any place on the Earth by using small number of observations.

V. Geomagnetic Field Intensity

To better understand EMF, it is not enough to have information about angles D and I alone, but the field intensity is also of immense importance. It was known that D and I changed from place to place. But doubts lingered about the true nature of intensity and whether it changed spatially. Hansteen could lay his hands on some observations of the total intensity obtained by Rossel, who participated in the 1791-1794 circumnavigation of the globe that showed the intensity increased towards the poles and away from the equator. There are also reports of scattered and sparse intensity observations even prior to Rossel's expedition. However, all these measurements were of relative magnetic intensity. It was Gauss who invented a method in 1832 for the determination of H-component intensity. The first measurements of the total field intensity (F) were obtained by timing the oscillations of a vertical dip needle disturbed

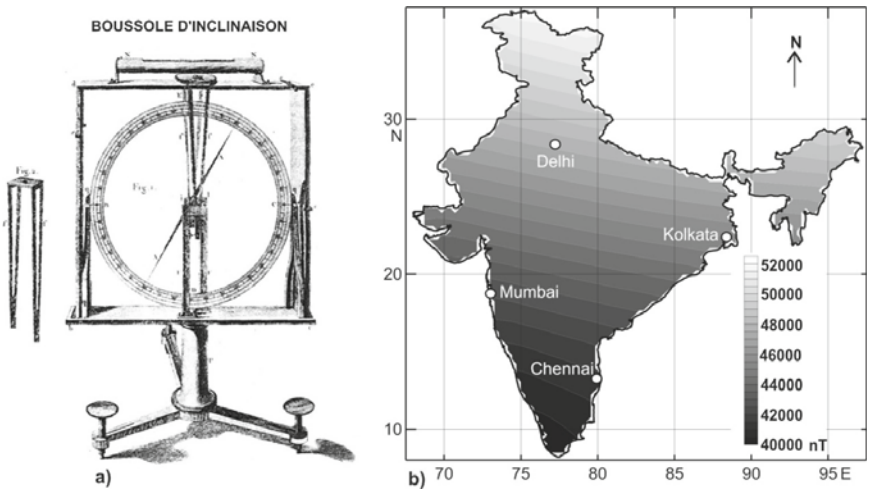

Figure 1.7. (a) Drawing of the magnetic dip needle used by Rossel (Lilley and Day, 1993). (b) India's magnetic chart of total field intensity F (IGRF11 model calculated for 2010).

from rest at different places on the globe (Fig. 1.7a). The total field intensity values based on IGRF2010 model over Indian region are shown in Fig. 1.7b.

1.2 FUNDAMENTAL SIMILARITY BETWEEN ELECTRICITY AND MAGNETISM

The next phase of development was a turning point in the history of geomagnetism that opened floodgates to the fundamental understanding of the Universe that linked magnetism to electricity and vice versa. The year 1820 is of extreme importance.

At this stage, however, we have been deliberately quiet on the events that took place between 1722 (Graham's discovery of diurnal variation) and 1820. During this period, a lot of developments did indeed occur. But, they all pertained to development of instruments (Chapter 4). To put point across, one event is picked from the timeframe between 1722 and 1820, which is inextricably associated with magnetism and electricity. Coulomb designed in 1777 an instrument known as 'torsion balance' (see Fig. 4.2). With this instrument, he showed that the magnetic repulsion between magnetic poles as also their attraction varied inversely with the square of the distance. At around 1785, he got the same relation with electric forces as well. Newton had earlier demonstrated that gravity adheres to the inverse law. The savants, capable of discerning signs of nature, almost instantly recognized the symmetry and the harmony among three of the nature's most fundamental forces – gravity, electricity and magnetism. But, there is only one point of difference with respect to gravity. Gravity always attracts, it never repels like magnetism or electricity. To know the whys and hows of these phenomena, the works of three great scientists – Oersted, Ampere and Faraday need to be combined.

I. Serendipity of Hans Christian Oersted

In hindsight, Faraday seemed to be attracted to magnetism primarily because of the observation Oersted made in 1820 of an electric current flowing in a wire deflecting a nearby compass. Oersted gave a lecture to his friends and students on electricity and magnetism in the spring of 1820. While performing the demonstration, Oersted noticed a strange thing. He saw that whenever the metallic wire was connected to the battery and a current flowed, the nearby magnetic needle moved. When the current stopped, the magnetic needle moved back to its original position. Oersted performed this experiment many times over to understand the cause of deflection.

The more he thought about it, the more was he excited and the more was he puzzled! He could see that whenever the current was passed, the magnetic needle tried to turn at right angles to the electric current. But he could not tell the reason. However, this was the first unambiguous and verifiable evidence connecting electricity and magnetism. Oersted announced these results to the world in a four-page report written in Latin on 21 July 1820.

II. Andre Marie Ampere Solves the Puzzle

The fallout of Oersted's announcement was that it reached out to a wider cross section of populace, and the experiment being simple, was repeated by many. Rive confirmed Oersted's results. A report of Oersted's magnificent discovery and the subsequent confirmation by Rive found its way to Paris. On 11 Sept 1820, the report was discussed at a meeting where Ampere was present. He went through the contents tooth and nail and ruminated over it. What followed was astounding because he solved the puzzle within a week. Ampere conducted a series of elegant experiments that proved the basic ingredient of magnetism to be the electric current and that magnetism could exist even without permanent magnets.

Ampere published his famous treatise on magnetism and electricity in 1823 and gave an explanation for this phenomenon. He declared that magnetism in a permanent magnet was due to molecular electricity.

III. Genius of Michael Faraday

In 1822, Faraday made the following entry in his notebook 'convert magnetism into electricity' in response to Oersted's experimental outcome.

He reasoned that if electricity can generate magnetism, then magnetism should also be able to produce electricity, which he demonstrated by expounding the principle of electric induction. But before looking into the experiment that converted magnetism into electricity, let us first go back again to 1820. Faraday had performed a simple experiment, first described by Peregrinus. The experiment involves sprinkling of iron filings on a piece of paper held over and above a magnet. When the paper is tapped gently the shaken filings tend to line up along arcs from the north pole to the south pole of the magnet. Faraday named these arcs as the 'magnetic lines of force' that formed a 'magnetic field'. The incisive nature of Faraday's insight can be gauged from his understanding

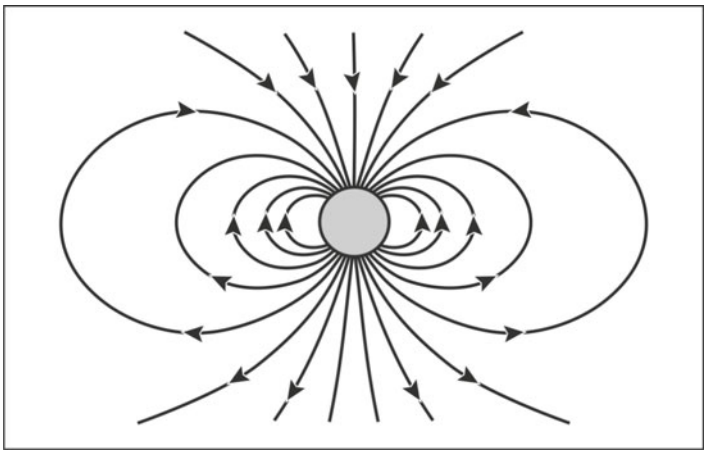

Figure 1.8. Faraday made visible the magnetic lines of force.

of the magnetic lines of force and the magnetic field. Although Gilbert had already shown on his 'terrella' that D and I displayed a certain 'direction', it was Faraday who made visible the complete picture by connecting those directions with continuous lines (Fig. 1.8).

IV. Faraday's Experiment

The knowledge of 'lines of force' is absolutely necessary to understand Faraday's experiment. On 17 Oct 1831, Faraday found a solution to converting magnetism to electricity. This is how: Faraday took a cardboard cylinder and wound around it a copper wire of 220 ft length. He also wound a twine (strong thread or cord) and placed calico cloth between the layers. He then connected the ends of the copper wire to a galvanometer. Faraday then thrust a bar magnet into the cylinder. At that instant, the galvanometer showed the presence of an electric current. He then pulled the magnet out. This time again the galvanometer moved, but in opposite direction (Fig. 1.9). Thus, Faraday showed for the first time that electric current could be produced with magnetism alone.

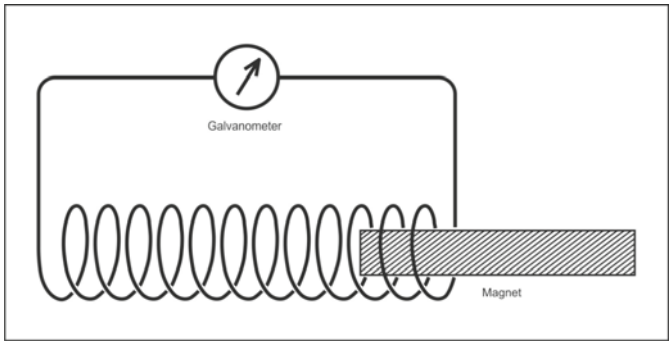

Figure 1.9. Faraday showed with this simple experiment that electricity could be produced with magnetism alone.

But this plain and simple experiment was used by Faraday to demonstrate the phenomenon to the lay and uninitiated audience. The actual experiment, where he got the 'enlightenment' and also involved a subtle thought process, was both simple and complicated. That particular experiment during which Faraday deciphered and decoded the relationship was performed thus: Faraday wound a coil of copper wire round one segment of an iron ring. He then again wound another coil of copper wire round another segment of the ring. Then he connected the first coil to a battery.

Faraday had proceeded ahead with the present experiment on an assumption and reasoning that when he sent a current through the first coil, it would create magnetic lines of force concentrated in the iron ring. This induced magnetism would then produce a current in the second coil. To detect that current, he connected the second coil to a galvanometer. But the experiment did not go according to his expectation. The flow of current in the first coil did not influence the second coil. But Faraday had made a very significant observation. He noticed

that when he turned on the current, the galvanometer needle kicked over briefly. And when he switched off the current the galvanometer needle again kicked. But this time it did in the opposite direction. Faraday guessed in an instant that it was the movement of magnetic lines of force across that wire that set up the current. It was not the magnetism *per se* that was responsible for generating electricity. When the current begins to flow in the first coil, it initiates a magnetic field. This magnetic field spreads out and in the process cuts across the second coil creating a momentary electric current. Conversely, when the current from the battery is cut off, the collapsing lines of magnetic force again cut across the wire of the second coil causing the electricity to flow, but in the opposite direction (Fig. 1.10).

With the discovery of the principle of electrical induction, Faraday was able not only to create the first 'transformer' but led directly to the creation of dynamo (generators of today) for producing electricity. It also led to Maxwell's electromagnetic theory and comes in handy to understand the generation of EMF. Faraday described his discovery of electrical induction before the royal society of London in Nov 1831.

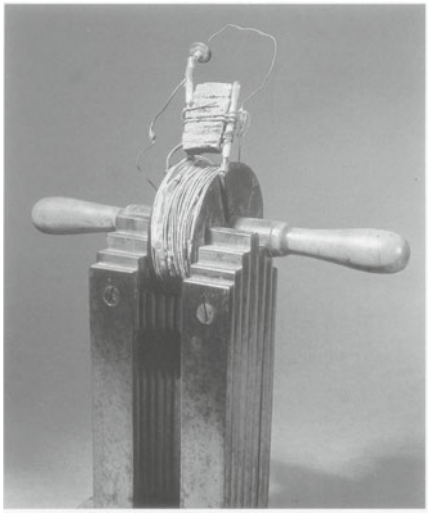

Figure 1.10. The original magnetic 'spark' apparatus. Faraday produced a spark when the handles pulled the coiled wire sharply away from the magnet (Hamilton, 1991).

V. Maxwell's Equations

Maxwell was a great admirer of Faraday and knew that Faraday had no mathematical background, although blessed with great intuition and marvellous insight. So, Maxwell, a great mathematician himself, set about in 1864 to supply mathematical analysis for Faraday's concept of lines of force.

This endeavour yielded Maxwell a set of four fundamental equations most commonly referred to as Maxwell's equations/laws (Appendix 6.1). The equations describe the nature of static and moving electrical and magnetic charges and the interrelationship that exists between them. They further suggest that electricity and magnetism are inseparable. If there is an electric field, there has to be a magnetic field at right angles to it. He found out that the magnetic and electric fields were a package of a single 'electromagnetic field' and also found that a changing electric field induced a changing magnetic field, which in turn induced a changing electric field and so on by virtue of which they flowed out together progressing outwards in all directions. Maxwell thus predicted the existence of electromagnetic radiation, possessing the properties of a waveform. This theoretical idea helped Marconi to invent radio (Chapter

3). Thus, the modern electromagnetic theory rests heavily on the work of Maxwell.

VI. Contributions of Humboldt, Gauss and Weber

Another set of scientists who have done yeomen service to the development of geomagnetism are Humboldt and Gauss. Gauss was also inspired by the work of Oersted and Ampere and was immensely impressed by their stupendous achievements. In 1828, Gauss attended a conference in Berlin and stayed as a guest with Humboldt. He was interested in magnetism and had great many collection of magnetic instruments, which he showed to Gauss and implored him to take up studying magnetism.

Gauss readily set about this task with his young assistant Weber who between them contributed a lot in understanding the EMF, through designing instruments and by formulating a mathematical method called the spherical harmonic analysis to represent the global magnetic field of the Earth. This method combines the magnetic observations at a number of diverse locations to describe the field to any desired accuracy and showed for the first time that ~90% of the total magnetic field was caused by sources inside the Earth. This led to the urge to conduct surveys on a global scale resulting in establishing permanent observatories all around the world. Gauss and Weber inspired by Humboldt's persuasion took the lead in setting up a chain of observatories by forming the 'Gottingen magnetic union' (Goettingen magnetischer verein), GMU, in 1834, which gives us a chance to introduce the Indian stream of geomagnetic thought that joined the international mainstream.

1.3 HISTORICAL PERSPECTIVE: NATIONAL SCENE AGAINST GLOBAL BACKDROP

The aim of GMU was to establish a global network of MOs. Europe had adequate number of observatories, but the rest of the world remained poorly covered. Humboldt could not ignore this shortcoming and approached the British authorities with a request to set right the situation, since the British had subjugated quite a few countries in the African and Asian continents. He also convinced the Russian Czar to facilitate setting up of observatories at Siberia, and even at Alaska.

I. First Few Magnetic Observatories in India

An MO, in the strict sense of the word, was for the very first time operated at Greenwich, England for a limited time period from June 1818 to Dec 1820, where the readings of D were regularly taken three times a day. Declination readings were also taken in Paris from 1820 to 1835. Humboldt constructed the first nonmagnetic iron-free MO in Berlin (1828). It was again Humboldt, who encouraged Gauss and Weber to form the GMU under the auspices of

which 50 magnetic stations sprang up generating copious D data facilitating drawing of worldwide magnetic charts.

For any thought to take roots and to grow into a healthy and viable intellectual stream, needs institutionalization. Institutions act as catalysts to research. The setting up of MOs helped to grow and flourish the discipline of geomagnetism into an independent branch of science.

The East India Company brought in the first set of observatories to India. They set it up at Chennai in 1792, although regular observations were recorded only from 1822 onwards till they were discontinued in 1881. Shimla also had an observatory for the limited time period from 1841 to 1845 as part of the GMU. Thiruvananthapuram, on the other hand, although an affiliate of the union, owed its presence to the king of Travancore, Rama Verma, who constructed the building in 1837. However, the actual observations started in 1841 and continued till 1870 with a brief hiatus between 1860 and 1863. The significance of the observatory at Thiruvananthapuram is: (1) an Indian had taken the initiative to establish it, and (2) it is on a unique geomagnetic (not geographic) location. The magnetic equator (a place of zero angle I) passed through this place.

The data generated at this observatory helped understand daily and seasonal magnetic variations and over different time scales effected by activities occurring on the Sun. It also revealed atmospheric currents generated in the northern and southern hemispheres impinged into each other's territories. This became possible because an array of four observatories had operated in tandem. With respect to Travancore, the first observatory was built 144 km away to the north, the second was to the south by 64 km, and the third was at Agastya Malai peak situated at a distance of 35 km towards ENE away from Travancore.

II. Colaba-Alibag Observatory

Although the earliest magnetic observations were recorded at Chennai, the history of Indian geomagnetism starts, for all practical purposes, with the establishment of the observatory at Colaba (in Mumbai).

In 1840, there was a proposal to establish MO at Aden at the entrance from the Red Sea to the Arabian Sea. However, the arrangements at Aden were found incomplete and unworthy for setting up the geomagnetic instruments. Consequently, the instruments were diverted to Colaba where an astronomical and time determination observatory was already functioning. This put Colaba and later Alibag into a profoundly honourable and respectable 'Top 4' slot. Apart from Colaba-Alibag observatories, there are just three more observatories around the world, which have been continuously and uninterruptedly (except during World War II) operational for the last 160 years. They are Greenwich-Abinger-Hartland in UK, Melbourne-Toolangi-Canberra in Australia, and Sverdlovsk in Russia.

The commencement of magnetic measurements at Colaba started in 1841, which continued till 1904. The rise in population and 'noise' generating devices

in and around Colaba made it imperative to either shift the observatory or to close it down. The first option was acted upon and an alternative site similar in all geomagnetic features to Colaba was identified at Alibag ~35 km SE of Mumbai, which became operational in April 1904. The observations at Colaba were permanently discontinued on 31 March 1906. Alibag is still functional and is acknowledged to be a prime magnetic observatory.

1.4 GEOMAGNETIC FIELD ELEMENTS AND THEIR MEASUREMENTS

I. Existence of Earth's Magnetic Field

Earth behaves as if there is a big bar magnet placed inside the Earth, whose south pole is towards the Earth's north pole and north pole is towards the Earth's south pole. This fact is supported by following experimental observations.

(i) A freely suspended magnetic needle is always in N-S direction: Two observations can be made if a freely suspended magnetic needle is placed at any point on the Earth's surface. It aligns itself with one of the ends pointing towards north pole and it does not stand horizontal but tilted upward or downward. The end pointing towards north is called north or north seeking pole and the other the south seeking pole. In case of magnets, like poles repel and the unlike poles attract. Therefore, the directive property of the magnetic needle implies that there is a giant bar magnet at the centre of the Earth and so the major magnetic influence comes from within.

(ii) A piece of iron placed inside Earth becomes a magnet: If an iron rod is placed inside the Earth in N-S direction, then it gets magnetized after some time.

(iii) Existence of neutral points: If the magnetic lines of force due to bar magnet are drawn, then neutral points are always obtained either in end-on-position or broad-on-position, where magnetic field due to bar magnet is exactly cancelled by EMF. If there is no EMF, neutral points cannot be obtained.

The Earth's main magnetic field is seen to vary in magnitude and direction on the Earth's surface. Unlike in gravity, these changes are less systematic and depend both on latitude and longitude. The variation in the Earth's main magnetic field between the two poles along a given magnetic longitude can be understood from Fig. 1.11a. The figure shows the magnetic field of a large bar magnet placed at the Earth's centre. The length of this magnet is about one-third the size of Earth's diameter (~4250 km) and is canted somewhat from the Earth's spin axis. A tangent to a field line of force cutting the ground surface indicates the direction of magnetic field. The density of the field lines represents the strength of magnetic field. Near the poles, the lines are close together giving a relatively strong field, pointing 'in' near the north geographic pole, pointing

'out' near the south geographic pole. Near the equator, the field has about half its intensity at the poles, is parallel to the surface and points north. The increase of dip and increase of strength both contribute to a pronounced increase in the vertical (Z) component of the EMF as one goes north or south from the magnetic equator, where its value is zero. In magnetic surveys of regional nature, a correction is always made for normal northward increase in the vertical component.

The EMF, therefore, can be approximated by a magnet (dipole) placed at its centre with its north pole pointing southward. Approximately, such a dipole can account for 90% of the observed field. The remaining 10% is of higher multipole in nature. The dipole axis is tilted at ~11.5° with respect to rotation axis of the Earth. The centre of the dipole is not coincident with Earth's centre; it is displaced by ~436 km towards ~15.6°N, ~150.9°E.

The direction and strength of EMF can be quantified with the help of instruments like the magnetometers. The earliest form of geomagnetic instrument was possibly a piece of lodestone, shaped into a cylinder and freely suspended at its centre. The direction it came to rest in would have depended on the location of the observation point on the globe. Later, around the eleventh century, the lodestone may have been replaced by a bar of magnetized iron or steel suspended from a fibre. The first generation of geomagnetic instruments, in use till the 1950s (when nuclear resonance instruments came into use), were improved versions of this simple system (Chapter 4).

II. Units of Measurement

Just as the gravitational force in a given direction is the derivative (rate of change) in that direction of gravity potential, so also the magnetic force in a given direction is the derivative in that direction of the magnetic potential. While the gravitational effect of a body is the sum of the effects of the mass particles constituting the body, the magnetic effect of a body is the sum of the effects of the magnetic particles or poles that give the body its magnetic state. In the magnetic case, it is further complicated because of two kinds of poles of opposite sign, resulting in a vector that may be in any direction. Therefore, unlike gravity, the magnetic case has both magnitude as well as direction (Chapter 6).

The SI units are cumbersome and inconvenient for magnetostatics as they are based on magnetic effect of current flow. The CGS and SI units of some commonly used quantities are reported in Table 1.1. The field at any point on the Earth's surface has a direction pertinent to the location and is measured in terms of the unit of nanoTesla (nT). One nT, also called gamma (γ), equals one billionth of a Tesla (T) ($1\ nT = 10^{-9}\ T$). Also the force of a magnetic field line is known as the magnetic flux, which is measured in Weber (Wb) or in older units of maxwell (maxwell is the unit of magnetic flux in the cgs (emu) system and $1\ maxwell = 10^{-8}\ Wb$). The magnetic flux density is the number of magnetic field lines passing through unit area and is measured in Tesla ($1\ T = 1\ Wb/m^2$). It is also common to use the unit gauss (G), where $10^4 G = 1\ T$. For a very small

Table 1.1 The SI and CGS symbols, units and conversion formulas for quantities most frequently used in geomagnetism

Parameter	*MKS (SI)*	*CGS (emu)*	*CGS to SI conversion factor, C*
Magnetic pole strength	Weber (Wb)	cgs pole	$4\pi \times 10^{-8}$
Magnetic field, H	A/m	Oersted (Oe)	$1000/4\pi$ Oe
Magnetic flux, Φ	Wb	maxwell (Mx)	10^{-8} Mx
Magnetic flux density, Magnetic induction, B	Tesla (T) Wb/m^2	gauss (G)	10^{-4} G
Magnetic susceptibility (volume), κ	Wb/Am	emu/cm^3	$(4\pi)^2 \times 10^{-7}$
Magnetic susceptibility (mass), χ	m^3/kg	cm^3/g	$4\pi/1000$
Magnetic moment, m	Am^2	emu	1/1000
Magnetization (volume), M	A/m	emu/cm^3	1000
Magnetization (mass), M/σ	Am^2/kg	emu/g	1
Magnetization intensity, I/J	T	emu/cm^3	$4\pi/10^4$
Permeability of free space	$4\pi \times 10^{-7}$ Hm^{-1}	1	

a. Internationally accepted unit of magnetic field intensity is the T. This is too large for practical purposes and the nanotesla (nT) is used in the literature and on maps. The nT has only recently been accepted to replace the previously used 'gamma' (γ). The EMF, depending on location on the globe, lies between 25,000 and 65,000 nT; this may also be written as 25 and 65 microteslas (μT).
b. Gaussian units and cgs emu units are the same for magnetic properties. The defining relation is $B = H + 4\pi M$.
c. Multiply a number in Gaussian units by C to convert it to SI (e.g. $1G \times 10^{-4} T/G = 10^{-4}$ T)

magnitude of the magnetic field, the unit often used is nT or γ. It follows therefore that 10^5 nT = 1 Oe or G. The EMF intensity ranges between 25,000 nT at the equator and 65,000 nT near the poles. In terms of Oe (G), it ranges from 0.25 to 0.65 Oe (G).

III. Geomagnetic Elements and Earth's Magnetic Field

The geomagnetic field at any point on the Earth's surface is represented by a vector or arrow parallel to the direction of the field, pointing in the direction of the force on a positive pole and having a length proportional to the strength of the field at that point. This vector is referred to a set of mutually perpendicular axes directed astronomically north and east and vertically downward. The vector is considered as passing diagonally from the origin to the far corner of a rectangular box (Fig. 1.11b) oriented with its edges parallel to the coordinate axes. The various magnetic elements then correspond to certain sides and angles of the parallelepiped as follows.

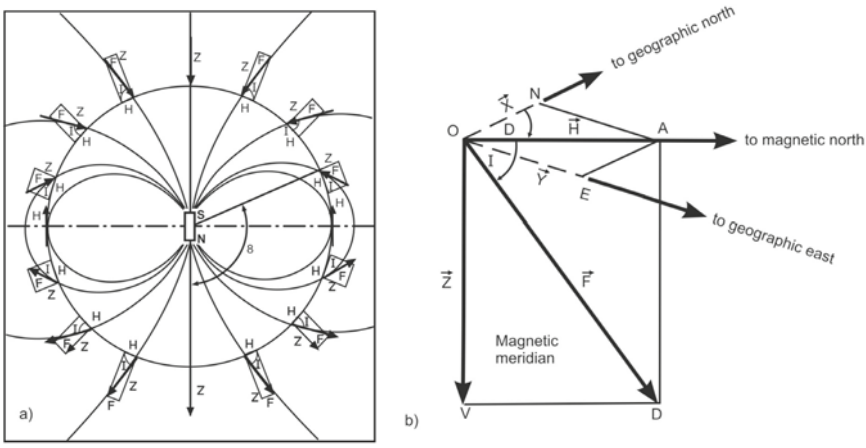

Figure 1.11. (a) A simplified model of the Earth's magnetic field. Lines of forces of eccentric dipole situated at the centre of the Earth. (b) Vector representation of the Earth's magnetic field in the northern hemisphere.

A freely-suspended magnet at a typical mid-latitude location in the northern hemisphere sets itself along the line OD (Fig. 1.11b) with its north magnetic pole dipping downwards. The plane in which it sets itself is called the magnetic meridian and this in many places makes an angle D east or west of the geographic meridian, i.e. the plane containing ON. The magnetic field, which sets the magnet at an angle inclined to the horizontal, is the total field vector F. The vector can be resolved into two vectors, OA in the horizontal plane with an intensity H, and OV in the vertical plane with value Z. The angle I made by OD with OA is called the dip or inclination. This is so named for a freely suspended magnetic needle will rest inclined at this angle from the horizontal direction. At the equator, the total field is wholly horizontal (H), i.e. I = 0° and at the two poles wholly vertical (Z), i.e. I = 90°. A suspended needle will thus rest horizontal at equator and vertical at the poles with intermediate values in between. OA in turn can be resolved in two directions, ON pointing northwards with the value X and OE pointing eastwards with magnitude Y. Each of these vectors and angles is called a geomagnetic element, and the following trigonometric relationships exist between different magnetic elements.

$X = H \cos D$ $\qquad\qquad$ $\cos D = X/H$

$Y = H \sin D$ $\qquad\qquad$ $\sin D = Y/H$

$Z = F \sin I$ $\qquad\qquad$ $\sin I = Z/F$

$H = F \cos I$ $\qquad\qquad$ $\cos I = H/F$

Angle of declination, $\tan D = Y/X$

Angle of dip, $\tan I = Z/H$

$H^2 = X^2 + Y^2$

$F^2 = H^2 + Z^2 = X^2 + Y^2 + Z^2$

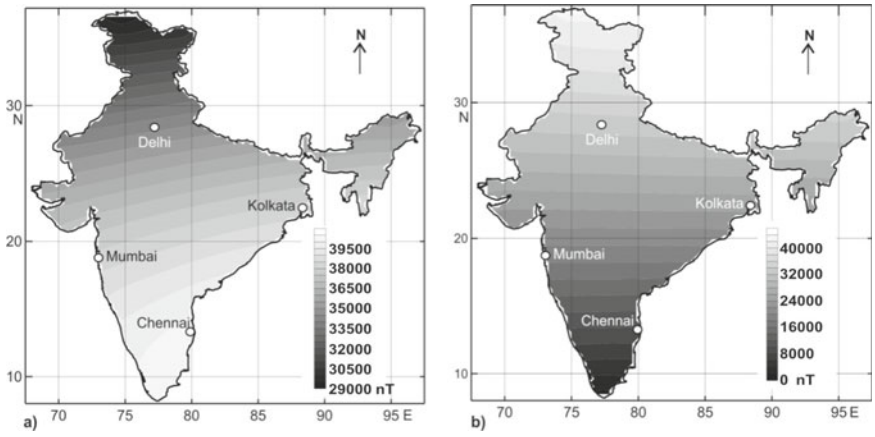

Figure 1.12. (a) India's magnetic chart of horizontal field component of magnetic field H in nT. (b) India's magnetic chart of vertical field component of magnetic field Z in nT (IGRF11 model calculated for 2010).

Thus, to completely define the geomagnetic field vector, any three independent elements out of these seven have to be measured. The vectors X, Y, Z or H, D and Z thus determine all parameters of the geomagnetic field and accurate measurement of these on a regular basis is the work of a ground-based geomagnetic observatory. Surveyers, navigators and explorers prefer to measure the quantities D, I and F for fixing direction. In magnetic prospecting, importance is accorded to Z and to a lesser extent D and H. The manner in which these components change with geographical locations encompassing the Indian region can be appreciated from Figs 1.6, 1.7 and 1.12.

IV. What is a Magnetic Observatory Setup?

The magnetic observatory is a carefully selected site, which has previously been surveyed to eliminate strong field gradients, proximity to heavy vehicular movement, industrial activity and electric traction, and where regular and continuous monitoring of the EMF is carried out. Also, the material used for constructing the observatory should be non-magnetic and immune to temperature and humidity changes in the atmosphere. Magnetic observatories are in operation worldwide with the primary objective to acquire knowledge of geomagnetic variation patterns over different latitudes and longitudes and to arrive at the cause of these variations (Chapters 3 and 5). At the observatory, two kinds of observations are carried out: (i) to measure the instantaneous values of the components of the magnetic field, and (ii) to record the continuous changes that take place on a recorder or digitally. Commonly, the first type are referred to as 'absolute measurements', and the latter as 'variations records' (Chapter 5), recording the variations with respect to a reference base value. The impression of these variations, recorded continuously for 24-hours day after day, is captured on a photographic paper called magnetogram (Fig. 1.13).

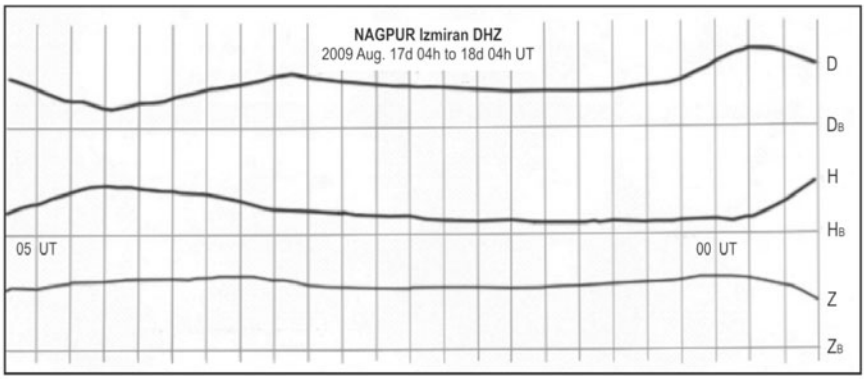

Figure 1.13. A typical quiet day magnetogram recorded at Nagpur magnetic observatory.

V. Earth's External Field

If accurate determinations of the EMF are made continuously at a fixed point, it is found that the intensity changes over short time intervals. These changes have a more or less regular daily cycle, which is approximately at the same solar time at different points but differs materially in detail from place to place and from day to day. The tidal circulation of the upper air induced by the gravitational attraction of the Sun and the Moon provides a satisfactory explanation of the daily magnetic variations. The amplitude of the daily change is greater in summer than in the winter. The range of the daily variation in vertical intensity may be as great as 100 nT.

Depending upon the nature of fluctuations recorded on a magnetogram, the days are classified as magnetically quiet or disturbed. On magnetically quiet days, geomagnetic elements undergo smooth and regular variation (Fig. 1.13). In cases of very violent magnetic activity, the disturbance field is superimposed over the average regular daily variation to be found on quiet days. The continuous magnetic records show that the average quiet day variation in the magnetic elements depends respectively on the solar (S) and lunar (L) times. The S (actual notion S_q) variation depends on the local time and is greater in magnitude during the daylight hours than those of darkness. Its amplitude varies with sunspot activity as well. The magnitude of L, on the other hand, is usually small and cannot be recognized directly on the magnetic charts. It is semi-diurnal in character and lunar tides in the atmosphere are responsible for this variation. Chapters 3 and 8 discuss aspects of magnetism that comes from outside the Earth. The S, L and magnetic storms, unlike the secular variations produce no large and long enduring changes in the EMF and hence they are called 'transient variations' or also 'diurnal variation' (Chapter 5).

In earlier days, a typical magnetogram used to be 50 cm in length having photographic traces of variations in D, H and Z (X, Y and Z at high latitudes). Nowadays all the observatories are shifting to digital recording (Chapter 5). Magnetic surveys are also carried out at many desired regions from time to

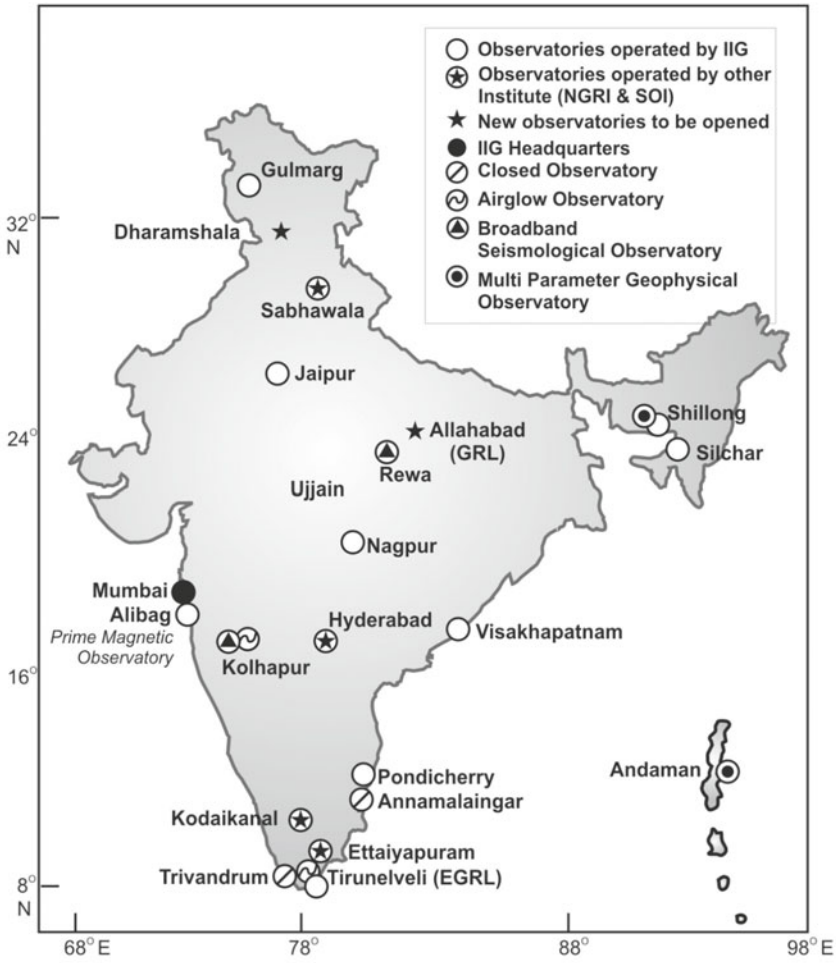

Figure 1.14. Network of geomagnetic and related observatories operated across the Indian subcontinent.

time (Chapter 6). There are 15 permanent observatories currently in operation, of which IIG maintains ten observatories (Fig. 1.14) and the remaining ones by NGRI and SOI. This Indian network of magnetic stations has latitude and longitude coverage for continuous monitoring of the ionospheric and magnetospheric phenomena. Geomagnetic data of many of these observatories are annually published in a single volume entitled 'Indian magnetic data'.

APPENDIX 1.1

Tesla

The tesla (**T**) is the compound-derived SI unit of magnetic flux density or magnetic inductivity. At the Conference General des Poids et Mesures (CGPM) in Paris in 1960, the unit was named in honour of the Serbian-American inventor and electrical engineer Nikola Tesla, who made several important contributions to the field of electromagnetism.

$1\ T = 1\ V \times s/m^2 = 1\ kg/s^2A = 1\ N/A\ m = 1\ Wb/m^2$

where V – Volt, s – second, m – metre, N – Newton, kg – kilogram and Wb – Weber.

A smaller derived unit, the Gauss = 10^{-4} T was once used.

The magnetic flux density is:

- in outer space it varies between 10^{-10} T and 10^{-8} T,
- in the Earth's magnetic field at latitude of 50°, it is 2×10^{-5} T and on the equator at a latitude of 0° is 3.1×10^{-5} T,
- in the magnetic field of a huge horseshoe magnet 0.001 T,
- in a sunspot 10 T,
- on a neutron star 10^6 T to 10^8 T,
- on a magnetar (a neutron star with a super-strong magnetic field than Earth's), it varies from 10^8 to 10^{11} T, and
- maximum theoretical field strength for a neutron star and therefore for any known phenomenon 10^{13} T.

Geophysics uses a unit of $1\ \gamma = 10^{-9}$ T (http://www.wacklepedia.com/t/te/tesla.html)

2

INTERNAL MAGNETIC FIELD

Earth is innately magnetic and owes this property to its dynamic internal physicochemical processes. The assertion that Earth is a giant magnet should be taken figuratively. The geomagnetic field is not produced by any bar magnet situated within the Earth, though the shape of the field is identical to a magnetic dipole with the south pole actually placed in the northern hemisphere. Visualising the Earth as a uniformly magnetized sphere, the lines of force near the poles are close together providing a relatively stronger field, while near the equator the field has about half the poles intensity. The farther one goes north or south from equator, the angle with the surface (magnetic dip) increases and it becomes vertical near the poles. The points on the surface of the Earth, where the continuation of the dipole axis cuts the Earth's surface, are called magnetic poles. The south magnetic pole is located in the northern part of Greenland near Thule MO (74°N and 100°W), and the north magnetic pole is at the Victoria land in Antarctica (65°S and 145°E). The magnetic axis of the Earth's geomagnetic field is situated ~436 km away from the Earth's centre, and so is referred to as the eccentric dipole field. The position of the magnetic poles varies with the passage of time known as polar wandering. Taking into consideration the Earth's magnetic field (EMF) or main field at one of the latitudes and the field intensity it produces, the magnetic moment of the Earth is estimated to be 8.1×10^{25} CGS units (~7.4×10^{22} Am^2, average over 7 ka). To know where and how EMF is produced requires delving deep into the interior of the Earth.

The cause of EMF and its impermanence are the two unsolved mysteries of geophysics. The Curie temperatures drop with increasing pressure because of which the presence of high pressure and temperature in the Earth's interior precludes magnetization. Recent studies, however, suggest that the liquid outer core of the Earth acts as a self-exciting dynamo accounting for EMF. This is because the material in the outer core is of high electrical conductivity capable of internal movement, thereby creating the main field. Also, some relation

between the rotation of the Earth and its magnetization seems probable because of approximate coincidence of magnetic axis with the axis of the Earth's rotation. Since magnetic measurements are made on the ground surface in the presence of EMF, some knowledge of the magnetic properties and conditions of the Earth are necessary to understand the contribution of the Earth to the measured magnetic effects, which decrease as the inverse cube of the distance from the observational site.

2.1 INTERIOR OF THE EARTH AND PHYSICAL PROPERTIES

The Earth is a complex body with pervasive 3D structure in its solid portions, where dominant variation in properties occurs with depth. The figure of the Earth is close to an oblate spheroid with a flattening of 0.003356. The radius to the pole is 6357 km, and the equatorial radius is 6378 km. For modelling purposes, a spheroidal Earth with a mean radius of 6371 km is considered adequate. In fact, reference models for categorizing internal structure use physical properties that depend on radius. 3D variations are normally described by deviations from a suitable reference model. In terms of planetary interiors, the Earth occupies a special position. It is the only planet, which has verifiable information on its interior, mainly from seismology, unavailable for other Cosmic entities. Also, a great deal about the Earth's interior can be inferred from surface and subsurface observations or from its gaseous envelope, e.g. elemental atmospheric compositions, chemical compositions/mineralogy of surface materials, surface geology and subsurface geophysical prospecting. The following sections discuss how ephemeral properties of temperature, pressure, density, elastic wave velocity, and electrical conductivity are used to learn about the Earth's interior.

I. Temperatures

The big bang is said to have spawned Earth (and other celestial bodies), which is yet to cool down completely. The temperature that exists at the center of the Earth is comparable with that near the Sun's surface (Fig. 2.1). The temperature of the Earth's interior is constrained through high-pressure experiments combined with geophysical and geodynamic modelling. Temperature measurements made in the deepest mine and the longest borehole drilled indicate that it rises with depth at a rate of ~30°C/km. This heat and pressure inside Earth cause rock at depths of 100–150 km to be soft, forming the asthenosphere. Here the temperature varies between 1400 and 1600°C, which is equal to the melting point of rock material. Taking into consideration of seismological evidence and the material constituents of the Earth's layers, the temperature at 6370 km is ~5000°C, ~4500°C at the outer-inner core boundary (5100 km depth) and at outer core-mantle boundary (commonly referred to as CMB at 2900 km), it is around 3527°C.

II. Pressures

The pressure like temperature increases with depth at the rate of 250 atmospheres for every km. At 50 km, it is nearly 200,000 psi (pounds/sq inch). For comparison, a typical pressure in automobile and tyre is ~35 psi. The pressure at a depth of 150 km is 5×10^4 atmospheres (1 atmosphere = 10^6 dynes/cm^2, the average pressure of atmosphere at msl); it is found to be of the order of 1.4×10^{12} dynes/cm^2 at the CMB, while it increases to 3.92×10^{12} dynes/cm^2 in the centre of the core. Thus, a large difference exists between the temperatures and pressures observed on the Earth's surface and its interior (Fig. 2.1), leading to many natural phenomena. The slow temperature dissipation and density (pressure) differences within diverse constituents of the Earth have given it a layered disposition in the form of crust, mantle and core (Fig. 2.2).

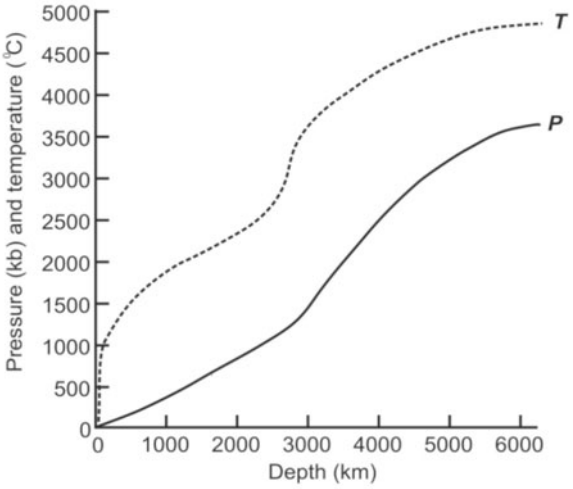

Figure 2.1. Pressure and temperature variations with depth in the Earth. Pressure increases from 1 bar (1 bar = 1 atmosphere, i.e. 10^6 dynes/cm^2) at the Earth's surface to 3.6 million bars at its centre. The temperature increases from approximately 25°C to about 4500°C and more (Hancock and Skinner, 2000).

III. Density and Gravity

Many characteristics of the Earth's interior can be delineated through density studies by understanding the ratio of mass to volume. Density also increases with depth because of increase in pressure. The extreme pressures experienced deep within the Earth (Fig. 2.1) compress rock to make it denser. Extraordinary pressures can even rearrange the minerals of the rock to create denser phases. The tendency of pressure to increase density at depth occurs in spite of the effect of enhanced temperature deep within the Earth. Most materials including rocks decrease in density with increasing temperature. Pressure overwhelms temperature as far as density is concerned.

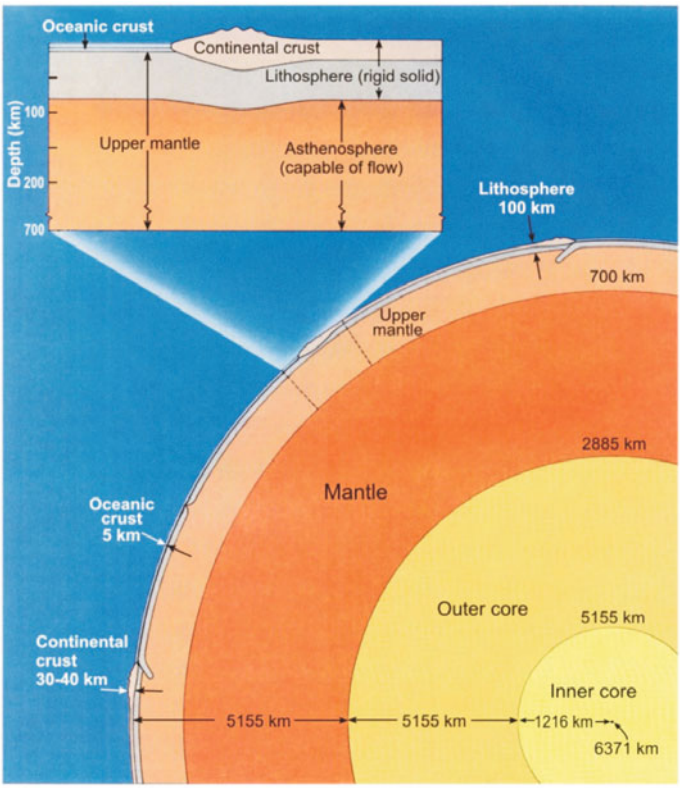

Figure 2.2. Internal structure of the Earth with the blow up of the upper mantle and crust (Tarbuck and Lutgens, 1994).

The average density (kg/m^3) close to the surface of the Earth is ~2800 kg/m^3 while at 1600 km depth it is 5000. At 2880 km, it is nearly 6000, at mantle-outer core boundary, it increases to 9400 and at the outer-inner core boundary it drops to 1150 kg/m^3. Then, there is a sudden increase to 1300 kg/m^3 in the inner core (a representative value for combined Fe and Ni at high pressure and temperature). Based on the seismically determined density of the Earth's core and the measured density of Fe at high pressure and temperature, it is certain that light elements such as S or O are in the Earth's core in addition to Fe and Ni.

The mean value of density of the Earth is estimated at 5517±0.004 kg/m^3. The profile of variation of density with depth (Fig. 2.3) for a generally accepted reference Earth model was developed by Dziewonski and Anderson. This widely used Earth model is known by its acronym, PREM (preliminary reference Earth model) and gives the low-pressure densities of cooled material with allowance for thermal expansion. Some typical measures of density (kg/m^3) of representative materials are—magnetite: 5200; hematite: 5100; pyrite: 5000; pyrrhotite: 4500–4600; galena: 7400–7600; chromite: 4800; limonite: 3600 to 4000 and siderite: 3000–3900 kg/m^3.

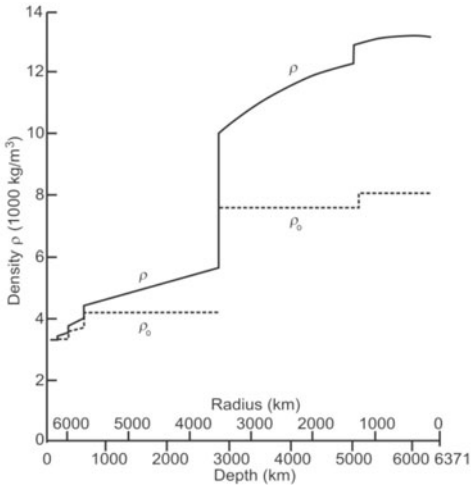

Figure 2.3. Density profile of PREM (solid line) with theoretical extrapolation to zero pressure and low temperature (broken line). Major boundaries show up as discontinuities or as abnormally rapid increases in velocity with depth (Hancock and Skinner, 2000).

Also, the gravity (g) and pressure, which are uniquely determined from the density profile of Fig. 2.3, are illustrated in Fig. 2.4. At any point in the Earth, the gravitational acceleration (g) results from the attraction of the mass

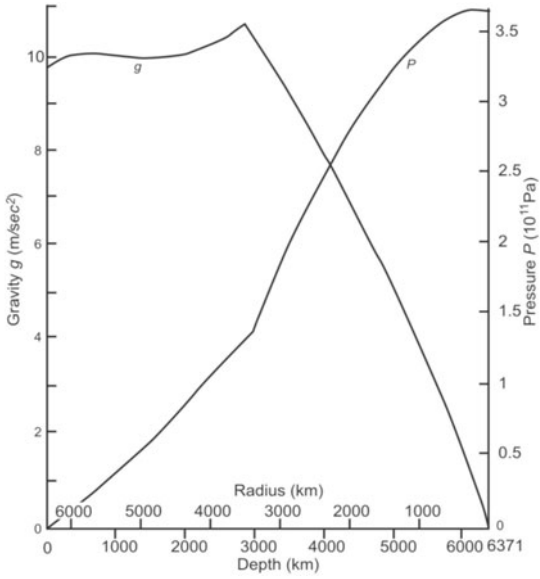

Figure 2.4. Variations in gravity (g) and pressure (P) with radius (depth) for the density profile in Fig. 2.3. Gravity (g) reaches its maximum at the mantle-core boundary (2900 km depth).

(m) contained in the sphere of radius (r) and it is expressed as $g = G \times m/r^2$ (G is the universal constant of gravitation, m is total mass of the Earth ($= 5.977 \times 10^{24}$ kg)). So, the maximum value of g is at 2900 km depth, after which, there is rapid drop to zero at the centre of Earth.

IV. Elastic Wave Velocities

The demarcation of internal units of the Earth is based essentially on probings carried out and inferred from the speed of 'P' and 'S' seismic waves, which interact differently with rocks under different pressure and temperature conditions. Generally, the wave speeds increase with depth. A 'P' or primary wave at the base of the Earth's crust (average continental crust has a thickness of ~40 km marked by Mohorovicic discontinuity) travels at a speed of 8 km/sec and at 1600 km depth, its speed is inferred to be 13 km/sec. The maximum P-wave velocity recorded in the lower mantle drops from 13.3 to 8 km/sec at the CMB. At 5120 km depth, a jump in P-wave velocity to 11.4 km/sec indicates the boundary between the outer-inner cores. The 'S' or secondary waves, on the other hand, are comparatively slower and have a velocity of 5 km/sec near the surface, increasing to 6 km/sec at 1600 km depth. As the S-waves are not transmitted through fluids, it is inferred that the outer core is fluid in behaviour, while its velocity of 3.8 km/sec approaching the centre of the Earth indicates that the inner core is a solid. Some typical measures of P-wave velocities (km/sec) of different crustal constituents are—alluvium: 0.3 to 0.6; clay and sandy clay: 2.0 to 2.6; shale: 2.0; sandstone: 2.6–4.0; limestone: 4.0–4.6; granite: 4.5–6.0; metamorphic rock: 4.0–7.0 and rock salt: 5 to 6. Thus, seismic wave speed turns out to be intimately related to material density. The more the speed of P and S, the more is the inferred compactness of the material through which these seismic waves travel.

Apart from density, the propagation of P and S waves also depends on the well-known elastic constants of the medium. For example, the velocity of P-waves is also a function of the modulus of rigidity (μ) and bulk modulus (K) of the medium, whereas S-wave velocity is influenced by the rigidity of the medium. From the familiar expression $\sqrt{(K + 4/3\ \mu)/\rho}$, for P-wave speed, one expects heavy rocks with high density values to have low speeds. Nevertheless, with increasing depth, not only ρ increases generally, but there is also a corresponding increase in the elastic constants K and μ. In fact, the increase in K and μ is much faster (sharper) as compared to that in ρ with the result that the overall control imposed by the elastic parameters outweighs that by the density alone. Hence, both P and S velocities tend to generally increase with depth even though the material density is relatively large at those depths. In case of P wave, the transmission is essentially through particle motion governed by compression and dilatation in the matter (Fig. 2.5). This behaviour is basically similar to the travel of sound waves in air.

The S wave, on the other hand, is transmitted through a transverse type of particle motion in the material (Fig. 2.6), because of which S waves cannot travel through liquids, since liquids are incapable of sustaining shear.

Figure 2.5. The dilatation and compression in the propagation of P wave having longitudinal type particle motion.

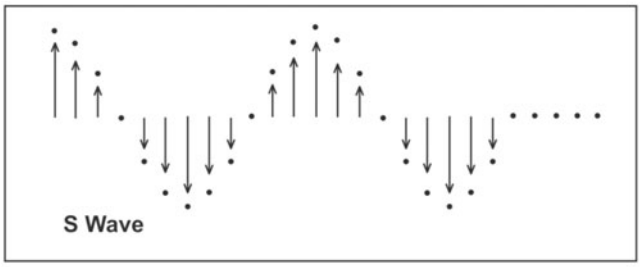

Figure 2.6. The propagation pattern of S wave through transverse type of particle motion.

V. Electrical Conductivities and Mineralogy

Observations of time-varying EMF and the associated electric currents within the Earth have led to delinate several large conductive structures in the crust and the upper mantle. Specifically, the electrical conductivity profile in Earth's interior can be obtained by EM induction methods of magnetotelluric and geomagnetic deep sounding methods. Global studies reveal that conductivity in the upper mantle is relatively low, i.e. 10^{-4} to 10^{-2} S/m. It increases with increasing depth to the top of the lower mantle. At the top of the lower mantle at 400 km, conductivity is ~1 S/m. Conductivity does not increase significantly in the lower mantle. Some studies (Fig. 2.7) have shown that the electrical conductivity of the uppermost mantle to 100 km depth is ~10^{-2}–10^{-1} S/m known as the mantle high conductivity layer (HCL). Local variations of electrical conductivity are large at shallow depths and become smaller with increasing depth. The increase in electrical conductivity in the mantle is explained in terms of the effect of temperature and phase transition of olivine and other minerals. Some typical measures of electrical conductivity (S/m) are—sea water: 4.0; molten basalt: 1.0; water saturated sedimentary rocks: 10^{-3}; igneous rocks: 10^{-4} and dry continental rocks: 10^{-6} to 10^{-3}. In general, all minerals are divided into the following three categories:

(i) High conductors are Au, Cu, Ag, PbS, graphite, etc. The general range of electrical resistivity of this particular group is 10^{-6}–10 ohm-m. All sulphides are very good conductors except sphalerite, cinnabar and stibnite (Sb_2S_3), which are typical examples of very poor conductors. The resistivity of sulphur is 10^{11} ohm-m. Certain oxides, magnetite,

pyrolusite, ilmenite and specularite (Fe_2O_3) are very good conductors. Specularite and hematite have the same chemical composition, but the former is a good conductor, and the latter a poor conductor. In all these cases, the flow of electricity is controlled by electromagnetic conductivity.

(ii) Intermediate conductors: The range of resistivity for these conductors is 10^2–10^9 ohm-m. Examples include most rocks containing anthracite having some degree of moisture (electrolytic conductivity) and all oxide minerals, except magnetite, ilmenite, pyrolusite and specularite.

(iii) Poor conductors (10^{10}–10^{15} ohm-m): Examples are all rock forming minerals in addition to phosphates, borates, carbonates, etc. Rock salt actually lies in this class of poor conductor and that is why high resistivity is obtained instead of low above a salt dome.

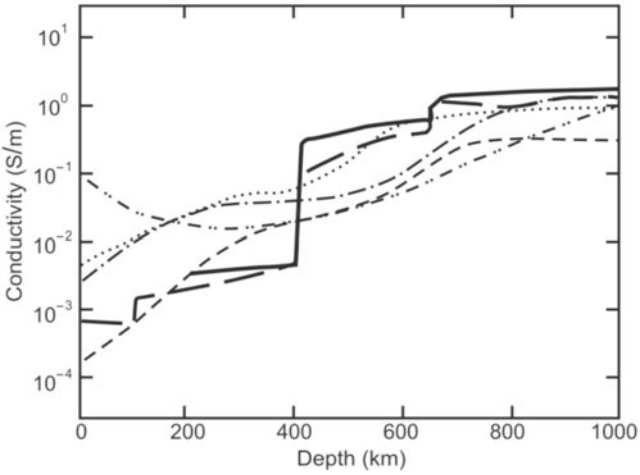

Figure 2.7. The electrical conductivity of the upper part of the mantle. Long dashed curve: north Pacific region, dotted curve: NE China, short dashed curve: Canadian shield, one-dotted dashed curve: SW USA, two-dotted dashed curve: Hawaii and thick solid curve: laboratory electrical conductivity model of Xu et al. (2000) (*courtesy:* Katsura, 2007).

2.2 EARTH STRUCTURE AND ITS MAJOR DIVISIONS

Seismology has revealed the metallic core and rocky mantle around it, but has also shown that the core consists of a solid inner part and a liquid outer shell. Beneath the thin crustal shell lies the silicate mantle, which extends to a depth of 2890 km.

I. Crust of the Earth

The crust is formed by differentiation and assimilation of primordial rock material of mantle rocks, via separation of the melt from the unmelted residuum (the present mantle rocks). Separation is achieved by the gradual upward

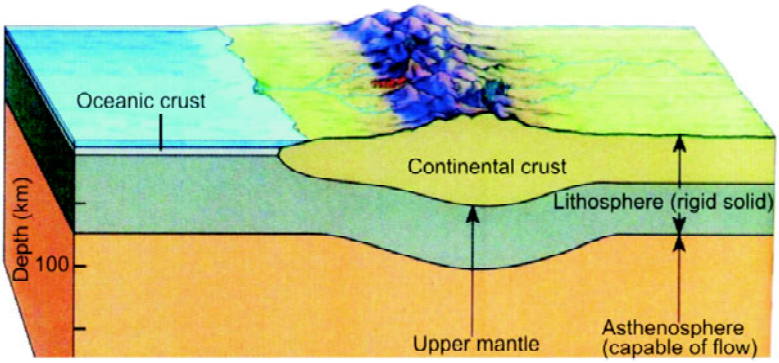

Figure 2.8. Cross-section of crust and a part of upper mantle (Tarbuck and Lutgens, 1994).

migration of the lighter magma that later solidifies to form the crust. This process can be seen even now at the mid-ocean ridges, where seafloor spreading takes place.

The crust is a thin surface layer, whose base is defined by a distinct boundary known as Mohorovičić discontinuity or Moho (Fig. 2.8). Aluminium is the most abundant metal in the Earth's crust. It is thin compared to the other two layers (mantle and core) with its thickness ranging from 8 to 16 km below the oceans and 60-80 km under mountains. The thickness of the continental crust varies more widely between 20 and 80 km with its average ranging between 30 and 40 km (Fig. 2.8). This is basically because of density differences between oceanic and continental landmass. The rock material making up the continental landmass (solidified from granitic magma) is less dense than the one observed at the oceanic landmass (solidified from basaltic magma). Thus, the thickness of the crust varies according to the principle of isostatic balance to maintain the equilibrium of mass. The concept that continents are less dense than the mantle and 'float' on it to attain gravitational equilibrium is the well known principle of isostasy. The closest analogy to this concept can be the growth of trees. Generally, the taller trees have deeper roots, and the smaller ones have shallow roots. This is the isostatic principle of Airy's compensation.

According to this principle, the masses of material columns above a certain depth of compensation are balanced; the crust is thicker beneath elevated topography compared to average crust so that extra mass of the crust is compensated by an equal mass deficit associated with the replacement of heavy mantle rock by lighter thickened crust. Similarly, the crust is thinned beneath topographic depressions, so that the mass deficit of negative topography is balanced by an equal mass excess associated with the replacement of thinned crust by heavier mantle rock. The principle of Airy compensation is well established, where it can be tested against seismic measurements of crustal thickness. The thickest crust on Earth lies below its mountainous regions (Fig. 2.8).

Conrad and Moho discontinuities: The seismic waves do not travel from the crust towards the centre of the Earth at a monotonous (constantly increasing) speed. Near the ground surface, P- and S-wave velocities are ~5.0 km/sec and 3.0 km/sec, respectively. A relative increase in P-wave velocity from 6.1 to ~6.6 km/sec occurs at contact of granitic and basaltic layers. Conrad discontinuity is the boundary between upper continental crust rich in felsic rocks such as granite (SiAl, for silica and aluminium) and lower crust madeup of magnesium-rich mafic rocks such as basalt (SiMa). During the study of seismic wave pattern of Balkan earthquake of 1909, Andrija Mohorovičić, a Croation (Yugoslav) geologist, inferred a sharp increase in seismic wave speed at a depth of ~32 km beneath the Earth's surface. This interface is named after him and called 'Moho' discontinuity, which is considered to be the base of the crust, below which lies the mantle. As this analysis is based on only a limited number of records from permanent seismic stations, knowledge of crustal structure from seismic methods has developed substantially through the use of controlled sources, i.e. explosions. Indeed most of the information on oceanic crust comes from such work. The depth of Moho varies from 20 km in rift zones to 70 km under young fold mountain ranges or the Tibetan plateau. Typical values are close to 35 km. Under the ocean basalt pile ~7 km, the Moho depth is thinner. The Moho represents either a phase change or compositional transition from gabbro to eclogite.

Continental and oceanic crust, lithosphere: The lithosphere continues from the crust into the mantle and also shows significant differences between the oceanic and continental regimes. According to plate tectonic theory, most of the lithospheric plates constituting the outer shell are composed of lighter continental and denser oceanic crust. The continental crust is located above the oceanic crust and rides on it in piggyback style. Continental and oceanic crusts differ in their layering, thickness, age, tectonic activity and igneous activity. Rocks as old as 4000 Ma are known in platform and shield areas in the continental crust, but oceanic crust is not older than 200 Ma. Evidences for folding and faulting abound in the continental crust, whereas deformation in the oceanic crust is confined just to plate margins. Oceanic environment is well known for its igneous activity (the mid-ocean ridges and island arcs), but such activity is limited across the continental crust (mountain belts like the Himalayas and Andes).

The entire oceanic lithosphere is generated by the spreading processes at mid-ocean ridges and the increase in thickness with age to at least 85 Ma is consistent with thermal cooling. Precambrian shield components of continents have a very thick, but lower density lithosphere extending to 200 km (or possibly more in some places). The lithosphere beneath Phanerozoic regions tends to be thinner, ~120 km with considerable complications in the neighbourhood of active tectonic belts.

II. Mantle of the Earth

The mantle is composed of more than 90% Fe, Si and Mg in that order. It is the region between the core and crust and is subdivided into two parts, upper and lower. The upper mantle extends from the base of the crust to a depth of ~650 km. The lower mantle continues from 650 km down to the core-mantle boundary, located at ~2900 km depth. The part of the Earth's interior that comprises the tectonic plates is referred to as the lithosphere. The rocks below the lithosphere are sufficiently hot facilitating solid-state creep. These rocks flow like a fluid comprising viscous, somewhat plastic material of a low velocity layer (asthenosphere) in the region of ~100 to 150 km within the upper mantle. The lithosphere slides over the asthenosphere with relatively little resistence. Between 400 and 650 km lies the transition zone, a region of the upper mantle, where seismic velocities tend to increase sharply. The lower mantle is known to be composed of perovskite-rich material, while the upper mantle is basically of 'olivine' type, which is rich in magnesium and iron but poor in aluminium

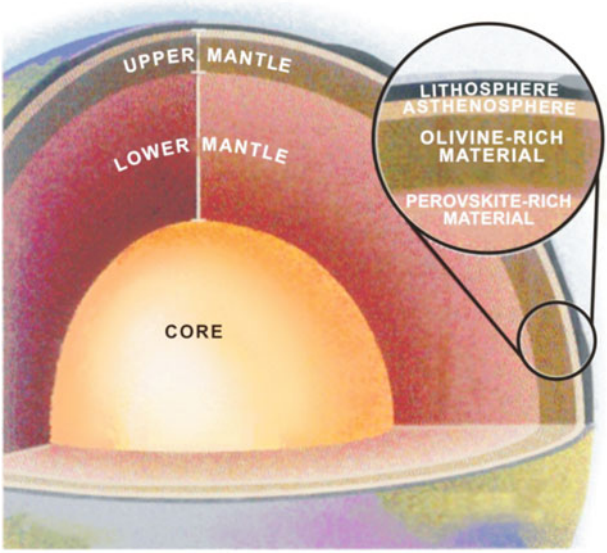

Figure 2.9. Mineralogical composition of mantle (Allegre and Schneider, 1994).

(Fig. 2.9). Assuming the mantle to be of homogeneous composition, a picture of the mineralogical distribution is given in Fig. 2.10. Geochemical and petrological studies suggest that with an increasing pressure, olivine transforms to its high-pressure polymorph, wadseleyite at 410 km depth (olivine-wadseleyite transition). Wadseleyite transforms to a further high-pressure polymorph, ringwoodite at ~520 km depth (wadseleyite-ringwoodite transition). Ringwoodite dissociates perovskite and ferropericlase at 660 km depth. These minerals form a network in each region and hence the electrical conductivity of these minerals is primarily responsible for that of the mantle itself.

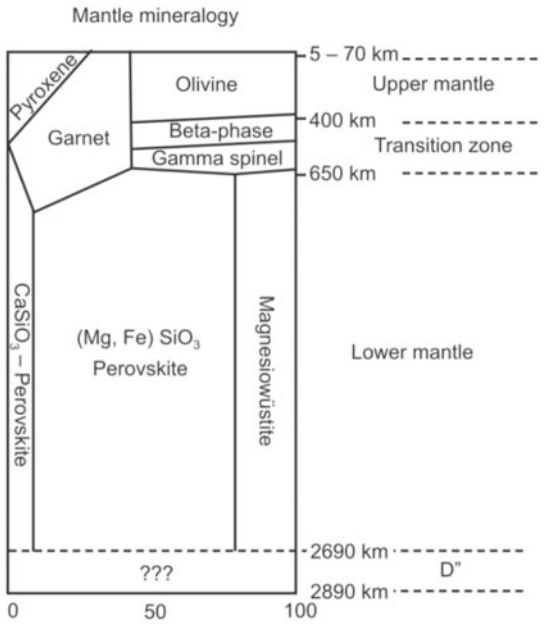

Figure 2.10. Sketch of mineralogical composition of a homogeneous mantle (Hancock and Skinner, 2000).

Additionally, some minor phases such as silicate melt that have high conductivity may also have important roles.

Gutenberg discontinuity: This boundary named in 1914 after the American geologist, Beno Gutenberg, is located at ~2900 km depth between mantle and outer core. The boundary is recognized as a discontinuity zone in seismic wave velocities, possibly caused by a distinct change in density (Figs 2.3 and 2.12). This change is interpreted to be due to a compositional change from silicate to iron-nickel. Recent evidence suggests a boundary layer represented by structural change in the perovskite mineralogy of the deep mantle. Seismic tomography studies have shown significant irregularities within the boundary zone, which are suggestive of a possible organized structure in relation to deep mantle plumes.

III. Core of the Earth

The nature, material and characteristics of the Earth's core, which is a sphere of approximately half the diameter of the whole Earth and one third of its mass, are of great geomagnetic importance. It may be recalled that the EMF is internally generated, more specifically within the liquid outer core. It was earlier conjectured that the material of the core needs to be a very common element and not a rare one since it has to occupy such a large space. The only heavy element that is very common is iron. It has the density of 7860 kg/m^3 on the

Earth's surface. But, under the enormous pressure and temperature conditions of the core, its density goes up in the range of 9000 to 12,000 kg/m^3 and is liquid in nature. Apart from iron, traces of nickel and other impurities are also conjectured to be present in the material of the core. From the propagation pattern of seismic waves, it is seen that at a depth of 2880 km, at nearly the lowermost boundary of the mantle, S waves abruptly stop, whereas P waves change their direction (Fig. 2.12). In 1906, a British geologist, Oldham, interpreted this zone to be 'liquid' in nature.

The P-wave velocity suddenly decreases at CMB, thus P-waves are refracted inward at 2900 km (Fig. 2.11). In addition, the complete absence of direct P-waves is manifested in the zone on either side of the Earth between 105° and 140° from the source of the event. This zone is called P-wave shadow (also known as core shadow) zone (Fig. 2.11), which was first recognized in 1900 by Oldham of GSI from the Indian experience.

The core is not one monotonous and continuous sphere. In 1936, Danish geologist, Inge Lehmann, proposed a discontinuity within the core at about 1280 km from the centre of the Earth that clearly distinguished between an 'inner' and 'outer' core. It is firmly established that the outer core is liquid, whereas the inner core is solid (Fig. 2.12).

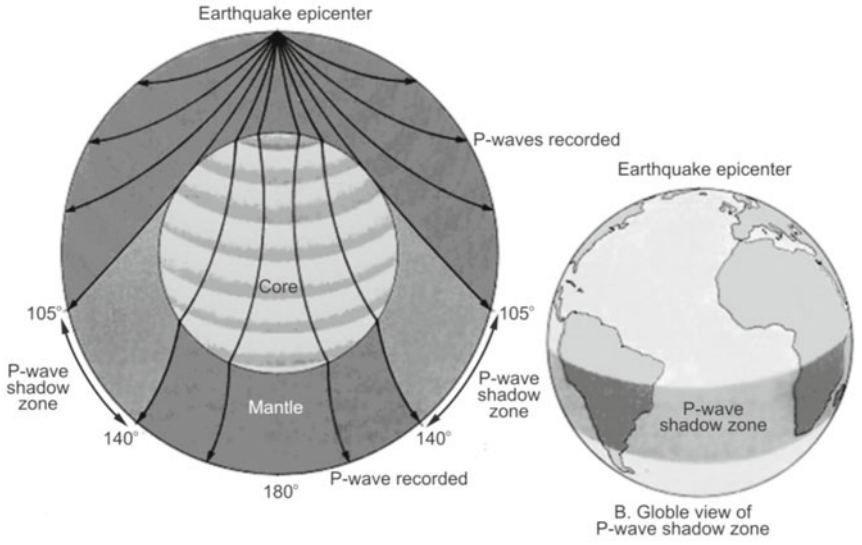

Figure 2.11. Physical properties of core and mantle inferred from the passage of seismic waves. P-waves travel through liquid and solid. S-waves travel only through solid. The abrupt change in physical properties at the mantle-core boundary causes the wave paths to bend sharply. This abrupt change in wave direction results in a shadow zone for P-waves between about 105° and 140° (Tarbuck and Lutgens, 1994).

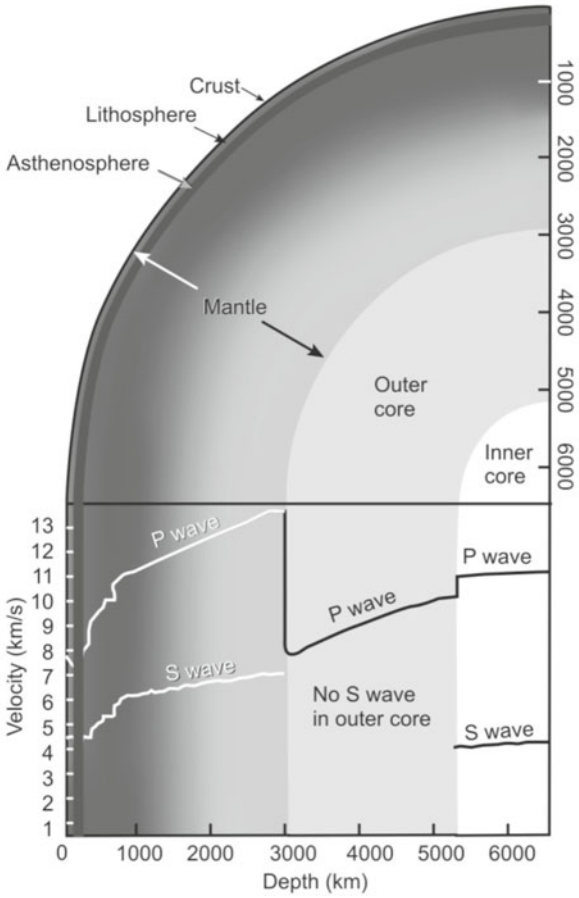

Figure 2.12. The relationship of the P- and S-waves with different layers of the Earth. The velocity of both these waves increases abruptly at the 'Moho' and then increases steadily through the mantle. At the core-mantle boundary, the Gutenberg discontinuity, S-wave velocity drops to zero and P-wave velocity is greatly retarded. Through the core, however, P-wave velocity increases steadily (Press and Siever, 2002).

2.3 MAGNETISM IN MATTER AND MAGNETIC PROPERTIES

It is now turn to direct attention from the macro to micro level by scaling down vision from the dimensions of the Earth to the tiny particles like atoms and molecules. At an atomic scale, electrons are responsible for the generation of magnetism. The fundamental law of electromagnetism states that 'a moving electrical charge creates a magnetic field'. Negatively charged electrons spin and orbit around the nucleus of an atom (Fig. 2.13), generating a magnetic field. Thus, it can be said that each electron has a magnetic moment, i.e. it behaves like a tiny magnet. Magnetic moment acts in either of the two opposing

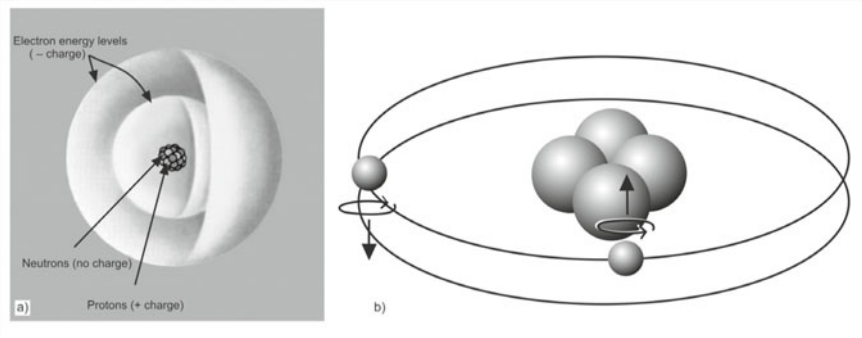

Figure 2.13. (a) Simplified model of an atom, which consists of a central nucleus, composed of protons and neutrons that are encircled by electrons (Tarbuck and Lutgens, 1994). (b) A helium atom shows two electrons spinning and orbiting around the protons and neutrons of the nucleus. The two electrons are paired, meaning that they spin and orbit in opposite directions. Since the magnetic fields produced by the motion of the electrons are in opposite directions, they add up to zero. Thus, the overall magnetic field strength of atoms with all paired electrons is zero.

directions, depending upon which properties like diamagnetism, paramagnetism and ferromagnetism arise.

I. Diamagnetic Materials

These are the ones which do not exhibit magnetism until they are placed in external magnetic fields B_{ext}. When a substance is placed in B_{ext}, a force is exerted on the electrons in orbit tending to modify the orbit in a small measure. This slows down the electrons, leading to slight changes in magnetic property. Since the effect tends to oppose the applied B_{ext}, they develop a magnetic dipole moment directed opposite to B_{ext}. If the field is nonuniform, the diamagnetic material is repelled from regions of greater magnetic field and the property is called diamagnetism.

In case of diamagnetic substances, the magnetization acquired per unit field applied, also called volume magnetic susceptibility (κ) is negative typically -10^{-5} SI. Many common natural materials including quartz, feldspar, calcite, organic matter, water, diamond, graphite, anhydrite, air, hydrogen, antimony, gold, mercury, bismuth and non-Fe containing minerals are diamagnetic.

II. Paramagnetic Materials

Materials with a weak attraction to magnets are called paramagnetic. There are many substances which do not have 'pairing' of all the electrons. Materials with one or more unpaired electrons are magnetic or slightly magnetic. This behaviour arises when magnetic dipoles align themselves parallel to the direction of applied B_{ext} to cause weak positive magnetization (Fig. 2.14). If B_{ext} is nonuniform, the paramagnetic material is attracted to regions of greater magnetic field and is called paramagnetism.

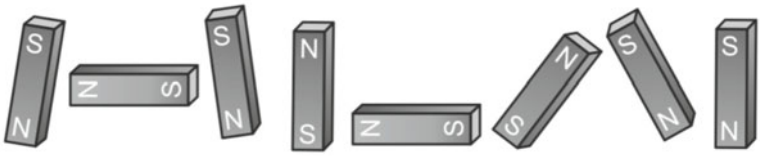

Figure 2.14. Alignment of 'paramagnetic' minerals.

The magnetic susceptibilities of paramagnetic substances are low and positive, typically in the range from 10^{-5} to 10^{-3} SI. Paramagnetic materials include lepidocrocite, ferrihydrite, ilmenite, biotite, muscovite, olivine, garnet, Fe-silicates (amphiboles, pyroxenes), aluminium, platinum, manganese and clay minerals. Carbonates of iron and manganese, pegmatites, gneisses, syenites and dolomites are also paramagnetic.

III. Ferromagnetic Materials

The basic difference between paramagnetism and ferromagnetism lies in the order of their magnetic intensity. It can be said that ferromagnetism is just an alternate name for strong paramagnetism and is characterized by large susceptibilities and spontaneous magnetization. Hence, ferromagnetic materials are used to understand the history of EMF.

Just like paramagnetic substances, atoms of ferromagnetic substances also possess a permanent magnetic dipole moment before the application of external magnetic field B_{ext}, and behave like small bar magnets. But in ferromagnetic substances, these atomic magnets due to certain mutual interaction form a large number of small effective regions known as 'domains'. Each domain has on the average 10^{17} to 10^{21} atoms or atomic magnets, whose magnetic axes are aligned in the same direction, but this direction is different from the direction of atoms of the neighbouring domains. As a result, each domain, even before the application of B_{ext}, is in the state of magnetic saturation, i.e. each domain behaves as a magnet.

In the normal state of substance, it shows no magnetism before application of B_{ext} because different domains are distributed randomly so that their resultant magnetic dipole moment in any direction is zero. This is the reason why every piece of iron is not a magnet. Figure 2.15a shows the probable directions of the magnetic dipole moments of four domains of iron. Now, if the substance is subjected to B_{ext}, magnetism or magnetic dipole moment of the substance is increased due to the following reasons—(1) due to displacement of the boundaries of domains, i.e. size of domains having magnetic dipole moment along the direction of applied B_{ext} gets increased, while those other domains gets decreased (Fig. 2.15b), (2) due to rotation of domains, i.e. domains rotate until their magnetic dipole moments are aligned up to a large extent along the direction of the B_{ext}, and (3) when B_{ext} is weak, the substance is magnetized mostly due to shifting of domains, but in strong magnetic field, the

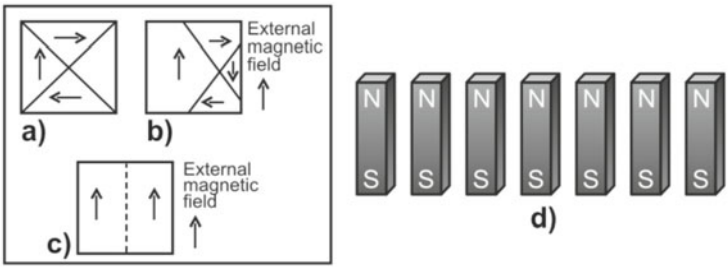

Figure 2.15. (a) The probable directions of the magnetic dipole moments of four domains. (b) The atomic dipoles within some domains suddenly swing around to line up with the direction of external field. (c) A final stage when the magnetic moments of all the domains get aligned with the direction of the external field. (d) In ferromagnetic substance like iron, all the minute magnets share a common alignment.

magnetization is due to rotation of domains. Finally, a stage is reached, when the magnetic moments of all the domains get aligned with the direction of the B_{ext} (Fig. 2.15c). When B_{ext} is removed, the substance is not demagnetized and some magnetism is left in the sample. This behaviour is called 'spontaneous magnetization' (Fig. 2.15d). If B_{ext} is nonuniform, the ferromagnetic material is attracted to regions of greater magnetic field.

Ferromagnetism is most commonly associated with Fe, but metals such as cobalt, nickel and Rare Earth elements (samarium, dysprosium and gadolinium) are also ferromagnets. These minerals normally are not found in the environment (although they are present in meteorites) nor are they always metallic and so are not of interest within the realm of geophysical exploration. Many non-metallic ferromagnets also exist, which include ferrites (mixtures of iron and other metal oxides).

Effect of heat on a ferromagnetic substance: A ferromagnetic substance retains its domain structure only up to a certain temperature called the Curie point or Curie temperature (T_C). At temperatures above the T_C, the thermal agitation causes the spontaneous alignment of the various domains to be destroyed or demagnetized so that the material beomes paramagnetic. If cooled below T_C, it again becomes ferromagnetic. For iron, T_C is 770°C, for nickel (360°C), and cobalt (1150°C). Some metals like gadolinium have their T_C close to room temperature (RT) making them ferromagnetic when cold and paramagnetic when hot. T_C is always less than the melting point as a consequence of which there are no ferromagnetic liquids.

The term Curie point is named after the French scientist Pierre Curie, who discovered that ferromagnetic substances lose their ferromagnetic properties above this critical temperature. This discovery has had great utility in providing information about the deep crust of the Earth.

Effect of heavy hammering on magnet: Magnetism can be removed by heavy hammering or by subjecting a magnetized material to an opposing magnetic

field. Hitting produces heat energy, which increases the mobility of atoms and the randomness of orientation of magnetic moments. Macroscopic net magnetism is due to predominant orientation of magnetic moments along a certain direction. Destruction of macroscopic net magnetism does not mean that individual atoms do not have a magnetic moment, but that the orientation of atomic magnetic moments is random.

IV. Ferrimagnetism and Antiferromagnetism

Ferrimagnetism and antiferromagnetism are the basic variants of ferromagnetism. Ferrimagnets have antiparallel magnetic moments of different magnitudes such that the sum of the moments pointing in one direction exceeds that in the opposite direction (Fig. 2.16). Materials of this type are the ferrites (e.g. magnetite is a natural ferrite) and are commonly used in industrial applications. Ferrimagnetic minerals include the 'cubic' and 'spinel' oxides of iron Fe_3O_4 (magnetite) and γ-Fe_2O_3 (maghemite) as well as sulphides of iron, greigite (Fe_3S_4) and pyrrhotite (~Fe_7S_8). It is often convenient to refer to natural ferrimagnets as 'magnetite', although positive identification is not always possible. Magnetites exist in various degrees of impurity including titano-magnetites (oxides of Fe and Ti), in which substitution of Ti for Fe has occurred and which are quite common in basalts.

Antiferromagnets too have antiparallel magnetic moments, but of same magnitude such that they exhibit zero bulk spontaneous magnetization (Fig. 2.16). Such a material behaves like a paramagnetic substance above the Neel temperature (T_N), at which thermal energy disrupts the magnetic ordering. Slight modification from the basic antiferromagnetism can exist, if the antiparallelism is not exact. If neighbouring spins are slightly tilted (<1°) or canted, a very small net magnetization can be produced. This is called canted or imperfect antiferromagnetism. Hematite (α-Fe_2O_3) and goethite (FeOOH) are well known examples of antiferromagnetic materials.

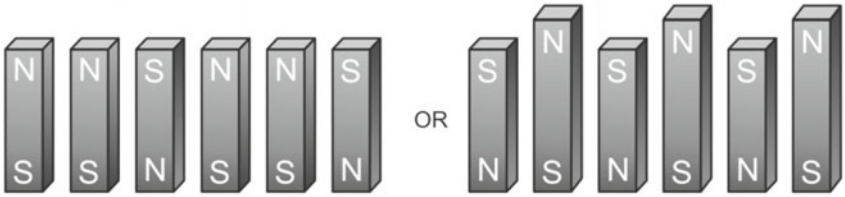

Figure 2.16. Antiferromagnetic and ferrimagnetic minerals are magnetized in favoured direction.

V. Superparamagnetism

It occurs when ferro(i)magnetic material is composed of very small crystallites (0.001 to 0.01 μm) (1 micrometre = 10^{-6} m). When particles are extremely small, they can undergo thermal vibrations, which have energies of the same order of magnitude as the interaction energy. The result is that these particles do

not have a stable magnetization, even though larger particles of the same material do. These effects were described by Neel, who asserted super-paramagnetism to be dependent upon volume and temperature of the material. The term superparamagnetic alludes to the similarity to 'paramagnetism', whereby the magnetization is field dependent with no remanence. The modifier 'super' takes note of the fact that it is the magnetization of the whole superparamagnetic particle, which is behaving in this way, not the magnetic moment of a single atom or molecule. Instead of each individual atom, the magnetic moment of the entire crystallite tends to align with the magnetic field resulting in greater magnetic susceptibility than that for simple paramagnetism. Also, superparamagnetic grains show higher frequency dependence of magnetic susceptibility.

2.4 CURIE AND NEEL TEMPERATURE

One of the most useful parameters for distinguishing the magnetic mineral(s) present in a sample is the T_C. In ferromagnetic and ferrimagnetic substances, this temperature is called the Curie temperature, while in antiferromagnetic substances, it is the Neel temperature. The T_C/T_N of some naturally occurring minerals are distinctive enough to be diagnostic, i.e. magnetite, hematite, and goethite. Other minerals have T_Cs that fall in a similar range, e.g. pyrrhotite, greigite, and titanomagnetites (Appendix 2.1). Materials having relatively high proportion of magnetite or hematite produce well defined thermomagnetic curves (Fig. 2.17a). The curves show only a small loss of magnetization at low temperatures, but as the temperature approaches the T_C, the curve steepens as the magnetization is destroyed. The Curie law ($\chi \approx 1/T$) governing the temperature dependent magnetization of paramagnetic minerals results in concave thermomagnetic curves (Fig. 2.17b).

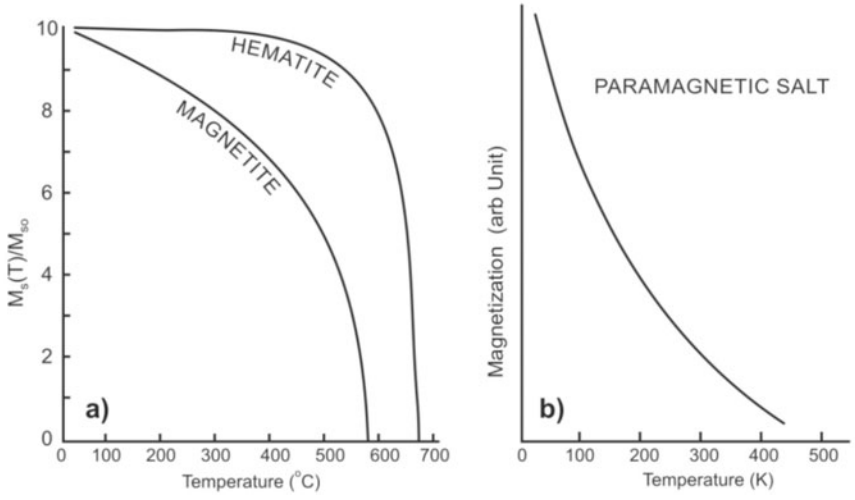

Figure 2.17. (a) Saturation magnetization curves against temperature for magnetite and hematite (Pullaiah et al., 1975). (b) The variation of paramagnetism with temperature.

Utility, depth to Curie temperature: The interior of the Earth is considerably hotter than the surface. Depth to the Curie/Neel temperature is the depth at which crustal rocks reach their Curie temperature. Supporting evidence for understanding inherent uncertainties of these Curie temperature depths comes from the magnetic properties of rocks measured in connection with palaeo, rock and environmental magnetic studies, geological mapping and mineral prospecting. Magnetomineralogical studies reveal that the dominant carriers of magnetism in rocks are Fe-Ti oxide and Fe sulphides, e.g. magnetic source mineral of Precambrian shield areas is magnetite. Indirect evidence from the study of rock magnetism on Curie temperature of rocks (or Curie/Neel temperature depth estimates from magnetic anomaly data) is important to specify the temperature of the lithosphere. The lithosphere must be relatively colder than the Curie temperature of its magnetic minerals.

2.5 ROCK FORMING MAGNETIC MINERALS AND ROCK MAGNETISM

Consider magma in a molten form at an initial temperature of 1000°C, where it slowly cools underground. While cooling, magma doesn't turn from being totally liquid to totally solid at a single temperature. Instead, different minerals crystallize over a range of temperatures (e.g. over 100° or 200°C). Thus, when the temperature falls by a small amount, a few minerals crystallize out. On further cooling, these crystals grow larger, while simultaneously forming new mineral crystals, eventually forming an interlocking network. With complete solidification, the rock displays a crystalline texture. In contrast, rapid cooling allows crystallization to occur by the nucleation of many small crystals, which ultimately form a fine-grained igneous rock. Rapid cooling is more likely at the surface, since magma comes here in contact with air or water, rather than in the hot interior of the Earth. In an extreme case, crystallization is totally inhibited and the starting liquid is quenched to form volcanic glass. Mineral crystals with Fe as a constituent tend to align with the EMF. The production of large, multi-domain (MD) magnetite grains is facilitated with slow cooling, whereas smaller, stable-single-domain (SSD) or pseudo-single-domain (PSD) grains result from rapid cooling of magma. The latter is also formed from surficial processes such as erosion, weathering, and chemical alteration.

Fe oxides are the first to be formed from molten magma having solid-solution temperatures of the order of 1400 to 1600°C. At 1000°C, Fe oxides contain Ti. The composition of Fe-Ti oxides can conveniently be displayed on TiO_2-FeO-Fe_2O_3 ternary diagram (Fig. 2.18). The lines of oxidation (increasing the Fe^{3+}/Fe^{2+} ratio) are parallel to the base of the diagram. Some oxidation also takes place during erosion, deposition or subsequent burial with consequent formation of hematite as the major magnetic constituent in most consolidated sedimentary rocks. However, in such sedimentological environments, many intermediate oxidation products may occur. Of these magnetic minerals,

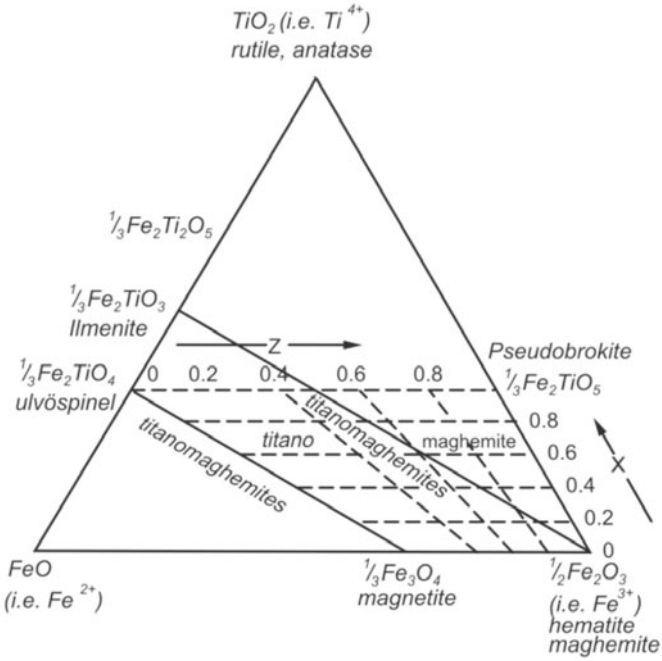

Figure 2.18. Ternary diagram representing the compositions of important Fe-Ti oxides. Positions from left to right indicate increasing ratios of ferri (Fe^{3+}) to ferrous (Fe^{2+}) iron, while positions from bottom to top indicate increasing Ti content (Ti^{4+} : total Fe). Using $\frac{1}{2}Fe_2O_3$ as the parameter for the Fe^{3+} corner normalizes the diagram to one cation, producing the convenient effect that lines of oxidation (increasing the Fe^{3+}:Fe^{2+} ratio), according to the 'addition of oxygen' mechanism, are parallel to the base of the diagram (Butler, 1992).

maghemite is important because it has a similar high intensity of magnetization as that of magnetite itself. The presence of oxygen and water also result in the formation of a number of hydroxides, of which goethite is magnetic at RT. Also, reduction of hydroxides later may lead to the production of hematite, while metamorphic processes can reverse the oxidation processes.

The use of magnetic measurements for characterizing magnetic mineralogy of rocks was initiated in the early 1960s, when it was realized that several minerals can carry natural remanent magnetization (NRM). The ferro(i)magnetic or antiferromagnetic minerals are often of a diagnostic value by themselves being the signature of various rock forming processes. In this sense, magnetite, titanomagnetite, maghemite, hematite, etc. are the chief rock forming magnetic minerals. The basic and ultrabasic rocks have minerals belonging to the titanomagnetite series, whereas acidic rocks contain minerals of ilmenohematite series. Normal cooling results in high temperature magmatic liquid, exsolving to form intergrowths between the titanomagnetite (cubic) series and the ilmenohematite (rhombohedral) series. This deuteric exsolution tends to result

in the preferential formation of two end members of each series, i.e. magnetite and ilmenite. When such igneous rocks oxidize at low temperatures (<200°–250°C), the composition of titanomagnetites moves towards that of the ilmenohematites. But these titanomagnetites are metastable, and gradually invert to ilmenohematite, especially if heated to 300°C. Oxidation of magnetites, titanomagnetites and ilmenohematites leads to the formation of hematite with varying amounts of anatase (TiO_2) and pseudobrookite (Fe_2TiO_5). Of all the Fe-Ti oxides formed by normal cooling, it is only the fairly pure forms of magnetite and hematite that have magnetic properties at RT.

I. Iron Oxides and Magnetic Properties

In the Earth's crust, Fe is the fourth most abundant element (5% by weight) after oxygen (47%), silicon (28%) and aluminium (8%). It combines with oxygen, silicon and aluminium to build up many of the commonly occurring rock-forming minerals (Fig. 2.19a-f). The composition of ferro(i)magnetic iron oxides varies from pure oxides of magnetite and maghemite to impure oxides such as titanomagnetite and titanomaghemite, in which the Fe atoms are partly substituted by atoms of Ti. There are continuous solid solutions between these two sets, which have varying Ti contents. Ti substitution reduces the Fe content and magnetic moment of the mineral; hence lowers the magnetic susceptibility. Where Ti substitution has progressed beyond a certain point, the minerals lose ferromagnetic status and become transformed into the paramagnetic titanium oxides, ilmenite and ulvospinel.

Iron oxides are the ionic crystals consisting of oxygen framework with cations in the interstices. In this group, magnetic minerals crystallize with two different ionic structures of spinel and corundum. Magnetite, ulvospinel (paramagnetic at RT), titanomagnetites, maghemite and titanomaghemites have spinel structure. On the other hand, hematite and hemoilmenites are associated with corundum structure. Other Fe oxide minerals like cassiterite (tin oxide) and zircon are magnetic due to minor impurities of ferro(i)magnetic minerals, but are quite rare, whereas manganese oxide jacobsite ($MnFe_2O_4$) is ferromagnetic at RT and carries a significant remanence.

Magnetite (Fe_3O_4): This iron ferrite is the most ubiquitous natural magnetic material and probably also the most extensively studied, since it imparts magnetic properties to rocks and produces magnetic anomalies. It occurs in most volcanic, sedimentary and metamorphic rocks and forms economically significant iron ore deposits.

(i) Origin: The challenge lies in identifying its origin from the range of possibilities including primary bed rock, tephra, secondary soil derived magnetite (difficult to distinguish from maghemite), bacterial magnetite, and industrial particulate arising from solid fuel combustion (fly ash), metal smelting or iron/steel manufacture. Rock magnetic evidence as to origin provides indications of its magnetic grain size and domain state

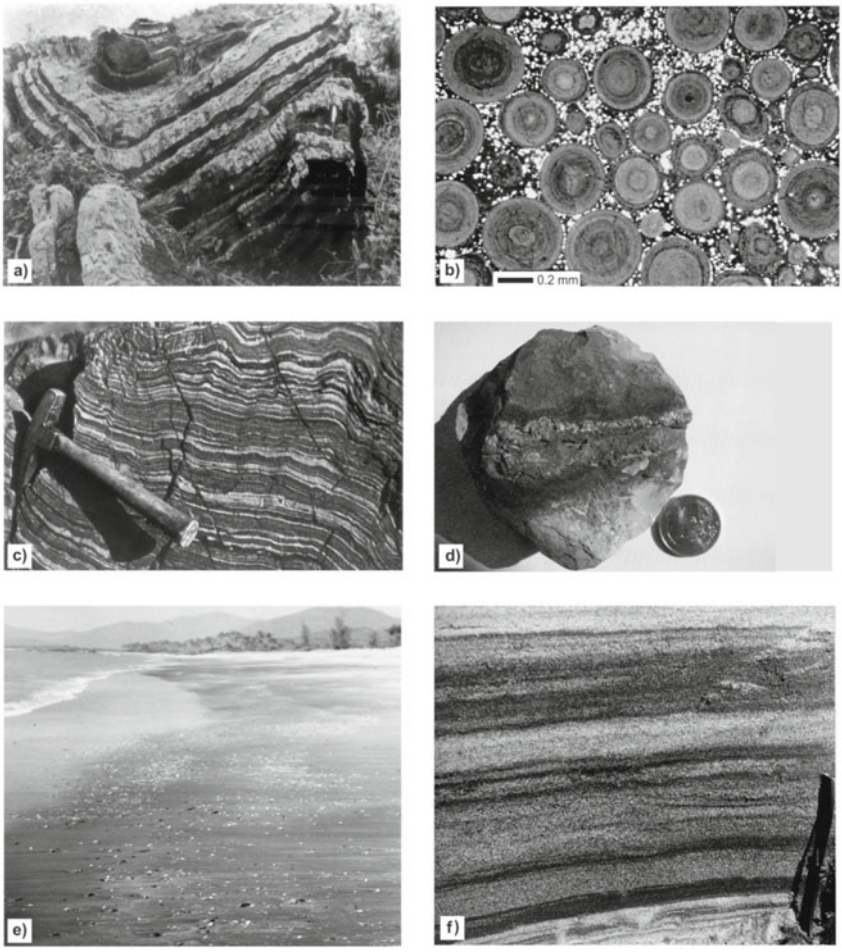

Figure 2.19. (a) Refolded iron formations, Chitradurga schist belt, SW of Tekalvatti. These are about 2.5 billion years old and are possibly formed by microbial activity (GSI memoir, 24). (b) Iron oxide ooids in a silty matrix from an iron oolite, as seen in thin section (Cornell and Schwertmann, 2003). (c) Banded iron formation found in many parts of southern India. (d) Iron oxide formation by atmospheric weathering of a pyrite vein in a limestone belt (Cornell and Schwertmann, 2003). (e) Field photograph showing black sand (mostly magnetic minerals) deposit at the mid foreshore section of a Harwada beach, Karnataka. The sand particles range in size from 0.0625 mm to 2 mm. Below the range of sand particle is the silt and clay fractions. Silt ranges in diameter from 0.0039 mm to 0.0625 mm, whereas anything less than 0.0039 mm is categorized as clay. (f) Field photograph showing alternating bands of light and heavy (magnetic) mineral layers in a vertical section of Harwada, Karnataka, beach scarp. This 'banding' is caused by the process of 'hydraulic equivalence' (Photo: Hanamgond).

(chapter 7). Magnetite is also formed biogenically by a wide variety of organisms like bacteria, algae, insects, birds, mammals and humans. Some of the magnetotactic bacteria synthesize magnetite and greigite particles from soluble Fe (Fig. 2.20).

(ii) Identification: Two of the most distinguishing and diagnostic properties are its T_C (580°C) and the Verwey transition, T_V (–150°C), which marks the change in crystallographic distribution of Fe cations (Fig. 2.21).

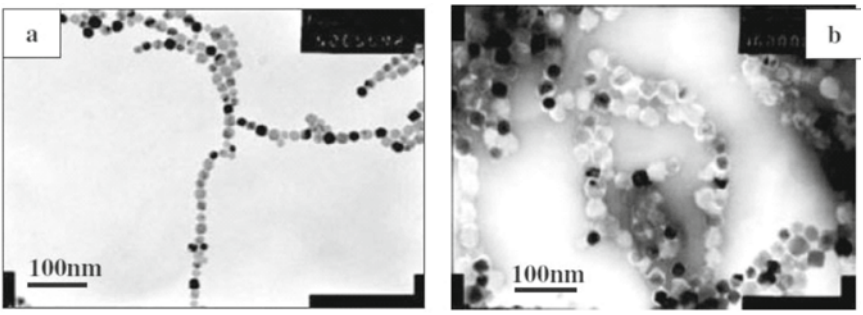

Figure 2.20. Transmission electron micrograph of bacterial magnetosome chains, formed intracelluraly by magnetotactic bacteria (Han et al., 2007).

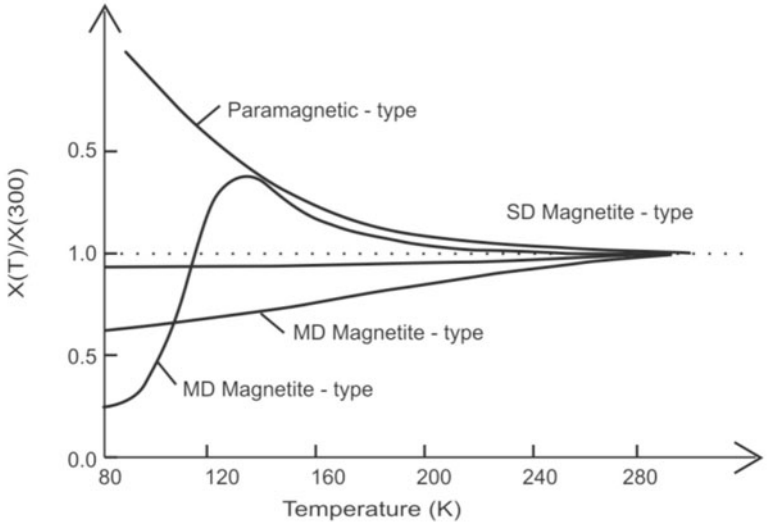

Figure 2.21. Different types of low-temperature magnetic susceptibility behaviour. Paramagnetic minerals, cation-deficient magnetite, Fe oxide grains with ilmenite lamellae, and SP hematite show a decrease in susceptibility on warming from liquid nitrogen temperatures, SSD magnetite and maghemite have an almost constant relationship with temperature, MD magnetite shows a peak associated with Verwey transition at 120 K (–150°C), and SP/SSD and Ti-rich (MD) magnetite all show an increase on warming (Radhakrishnamurty, 1993).

During this change, the previously cubic crystallographic framework gets slightly distorted to monoclinic symmetry. This is quite a subtle effect, but it alters the crystalline anisotropy resulting into many changes in magnetic as well as some of its other properties. It has a higher saturation magnetization 92 to 93 Am^2/kg (Appendix 2.1).

The coercive force of bulk samples is quite low and hence is generally not considered to be a magnetically stable material. However, when it is very fine, in terms of particle size, it has a high magnetic stability making it an important carrier of stable remanence. Also, its coercivity is dependent on grain size with maximum coercivity of 0.2 T.

It is a common component of igneous rocks (its amount increases with basicity) and of metamorphites (preferred occurrence in the katazone); skarns contain a high proportion of magnetite. It frequently occurs as a detrital mineral in sedimentary rocks. The metamorphism of magnetite generates lepidocrocite, limonite, hematite or maghemite. It is black in colour, of semi-metallic gloss and has a characteristic brown colour when viewed in reflected light. Magnetites of different forms and shapes are shown in Fig. 2.22a-e.

Maghemite (γ-Fe_2O_3): It is an oxidized (low temperature oxidation, LTO at <200°C) analog of magnetite and is common constituent of soils and deep sea sediments. In the basaltic rocks, it commonly forms at low temperatures of 200 to 300°C. In the sedimentary environment, and in soils, it forms by LTO of smaller particles of magnetite in the presence of moisture. It can also be formed in laboratory by heating various minerals such as pyrite to 400°C or lepidocrocite to 250°C. Maghemite is also known to be the source of some of the remanent magnetism found in fine-grained sediments. It is chemically unstable and on heating to ~300°C or more converts to hematite. Hematite has the same chemical composition, but has the spinel structure of magnetite. Hence, to avoid confusion, hematite is designated as α-Fe_2O_3, and maghemite as γ-Fe_2O_3.

Identification: It is ferrimagnetic and has a saturation magnetization of 83.5 Am^2/kg. It frequently forms a component, e.g. of oxivulcanites or laterite soils. The clear identification of magnetite and maghemite is difficult in many rocks because of similar magnetic properties and structure. It does not show phase transitions below RT unlike magnetite, and remanence at a given low temperature decreases monotonously on warming. Pure maghemite has a distinctive breakdown of magnetization on heating. But, after heating between 500 and 600°C, it appears to be completely destroyed as can be clearly seen from the difference between the heating and cooling curves depicted in Fig. 2.23. Maghemite, however, does not always convert to hematite on heating. The presence of certain impurities helps to stabilize the maghemite structure. Its T_C is not possible to measure directly because of its thermal instability. It is reported that its T_C lies somewhere between 545° and 675°C. It can be recognized under the microscope in reflected light at high magnification by its blue colour.

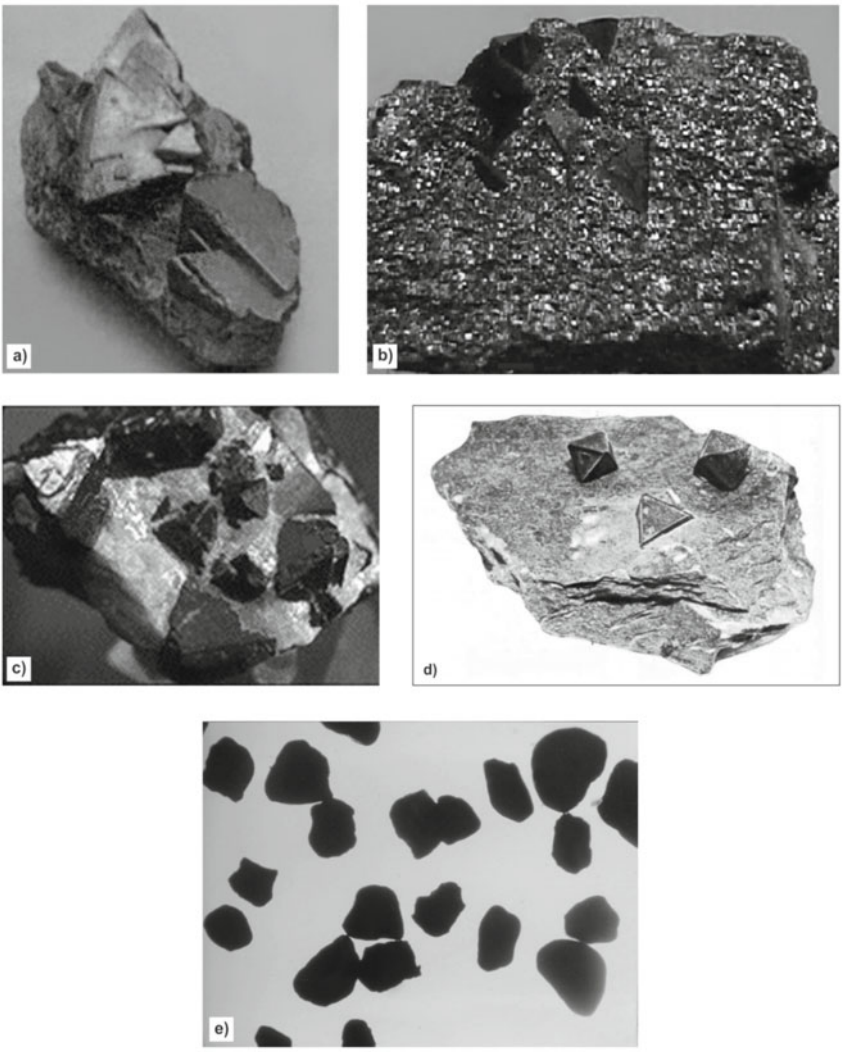

Figure 2.22. (a) Magnetite is magnetic, hence the name. Its crystal structure is octahedrons, eight sided or dodecahedrons, twelve sided. It also occurs in massive form and does not have cleavages, though it has octahedral pentin. (b) Magnetite crystals in the octahedral form. They crystallize in the cubic system and are iron-black in colour (http://mineral.galleries.com/minerals/oxides/class.htm). (c) Magnetite crystals embedded in a host rock (http://mineral.galleries.com/minerals/oxides/magnetit/magnetit.htm). (d) Magnetite in talc-chlorite schist. The octahedral shape of crystals is distinct (Milovsky, 1982). (e) Micro photograph of magnetite mineral grains taken under polarised light (Magnification×100).

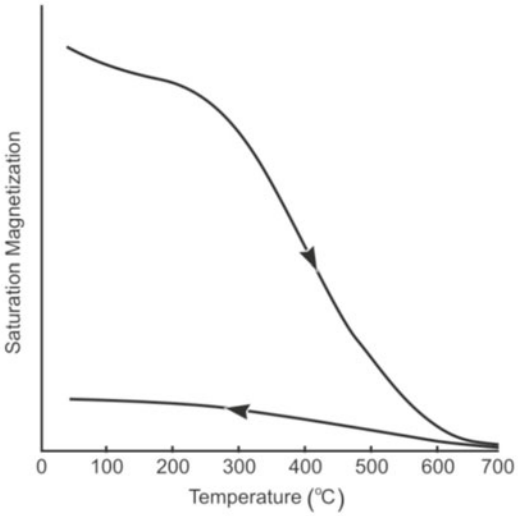

Figure 2.23. Saturation magnetisation-temperature curve for maghemite showing decrease of magnetisation on heating and cooling (Strangway, 1970).

Titanomagnetites: Titanomagnetite is the most common terrestrial natural magnetic mineral. The titanomagnetites ($Fe_{3-x}Ti_xO_4$ for $0 \geq x \geq 1$) are cubic (spinel) iron-titanium oxides at room temperature. Titanomagnetites tend to form a solid-solution series at higher temperatures (>800°C) during rapid rather than slow cooling of the magma. In practice, however, naturally occurring solid-solutions have T_C <200°C, so that any thermal remanence is likely to have low stability as the maximum associated relaxation times are only some 10^2 to 10^5 years. Figure 2.24 shows variation of T_C with compositional changes for titanomagnetites, while Fig. 2.25 illustrates their alteration mechanisms.

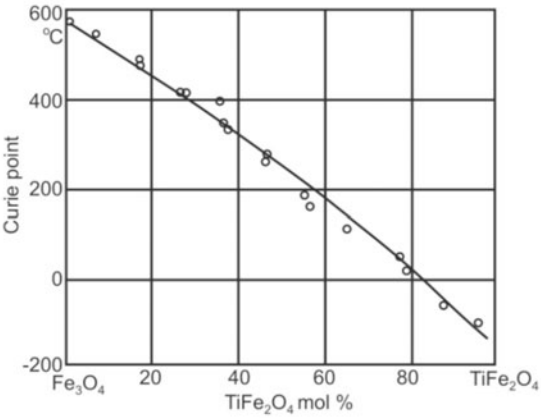

Figure 2.24. Variation of Curie points with composition for titanomagnetites (Radhakrishnamurty, 1993). Notice how the Curie temperature falls with increasing Ti content.

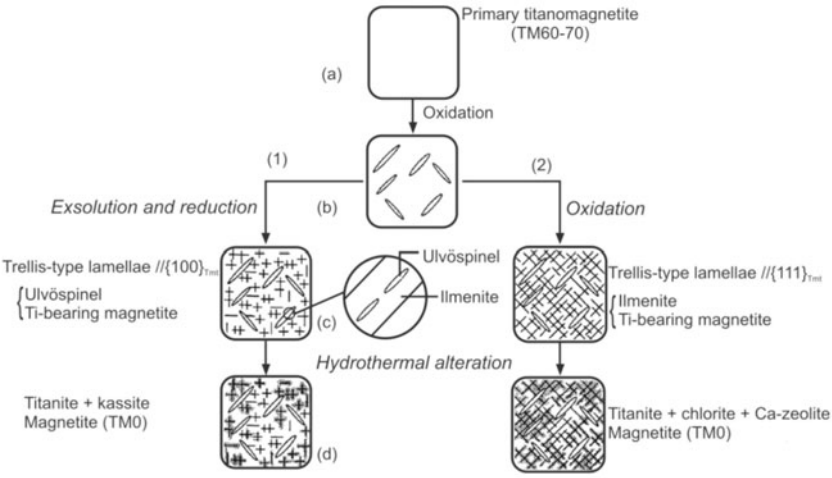

Figure 2.25. Schematic diagram showing the evolution and alteration of primary titanomagnetite from mid-ocean ridge basalt. Here the magnetite is formed by two different processes. The first stage of oxidation (paths 1 and 2) would give rise to titanomagnetite slightly depleted in Ti with a very low Curie temperature. (a) to (b) Primary titanomagnetite was first subjected to oxidation-exsolution during initial cooling. (b) to (c) The depleted titanomagnetite host in ulvöspinel then experienced (1) true exsolution of ulvöspinel (TM~87) lamellae or (2) another stage of oxidation-exsolution with formation of fine ilmenite lamellae. In path 1, ulvöspinel also formed within the ilmenite as a result of reduction reaction. (c) to (d) With the onset of hydrothermal alteration, the Ti-bearing magnetite recrystallized to end-member magnetite with loss of Ti (Shau et al., 2000).

Titanomagnetite and the proportion of Ti tend to be higher in basic rather than in acidic rocks. Oxidation at higher temperatures (>600°C) during cooling results in conversion of magnetite, whilst at lower temperatures (<400°C), oxidation produces titanomaghemite. Stable single-phase oxides exist for the composition parameter x between 0 (magnetite) and 0.96 (Fig. 2.18). The T_C falls almost linearly with increasing x (Fig. 2.24). A T_C of ~150–200°C is characteristic of stoichiometric $Fe_{2.6}Ti_{0.6}O_4$ or TM60 (x~0.6), which is the primary titanomagnetite in rapidly cooled basaltic lavas. TM60 is the dominant magnetic mineral in submarine basalts and in subaerial basalts. Unoxidized titanomagnetites typically have compositions TM60-TM70. Ti-rich titanomagnetites have only a local significance in sediments, where the eroded material from volcanic rocks is readily available. Titanomagnetites of intermediate compositions are found relatively less frequently in nature than those close to magnetite and TM60, respectively.

Ulvöspinel (Fe_2TiO_4): It occurs in volcanic rocks, whose magnetic minerals are often rich in Ti. The structure is similar to that of magnetite, except that one of the Fe ions is replaced by Ti. The result is that it no longer behaves as a ferrimagnet, but becomes antiferromagnetic because there are an equal number

of Fe ions in the two sublattices. It has a T_N estimated at 120 K (–153°C). The important feature is that it forms a solid-solution series with magnetite, so that intermediate members have properties between those of magnetite and ulvospinel. If Ti is present in magnetite, then the T_C is reduced and the saturation magnetization also decreases. In many volcanics, Fe-oxides with T_C <580°C are present and their exact Ti content can be studied by measuring the T_C.

Hematite (α-Fe_2O_3): It belongs to the trigonal system. It has a rhombohedral structure and is basically antiferromagnetic, but can carry superimposed weak ferromagnetism, often referred to as 'parasitic ferromagnetism'. Its slight departure from antiparallelism (spin canting) turns hematite into a weakly ferromagnetic mineral with a spontaneous magnetization 2.5 kA/m. Its small net saturation moment of ~0.4 Am^2/kg results primarily from a spin canting. Another mechanism that can produce a magnetic moment is presence of defects or impurity atoms in the hematite crystalline lattice. Since hematite is much less strongly magnetic than magnetite or maghemite, the two latter minerals dominate the NRM in the case when concentration of these minerals is compared.

(i) Origin: Hematite is the most stable Fe oxide in oxidizing conditions. It occurs in large amounts in sediments, e.g. in Permo-Carboniferous sandstones, in red beds and in some highly oxidized volcanic rocks. When present as fine grains (<~1 μm), it has a distinctive blood-red colour giving red beds their distinctive colour or large grains (usually >10 μm) of detrital origin referred to as specularite. It is black, dark red in colour and semi-metallic gloss (Fig. 2.26a-c) and shows a characteristic streak (Fig. 2.26d), which is its diagnostic property. It is formed as the end product of prolonged oxidation of magnetite, inversion of maghemite, dehydration of weathering products like goethite, and precipitation of ultra-fine-grained hematite cement or red pigments from Fe-rich solutions in pore spaces of clastic sediments.

(ii) Identification: It displays a low volume susceptibility of ~250×10^{-5} (SI), but a high coercive force. Hematite is more thermally stable than magnetite. The T_C of ~675°C (Fig. 2.27) coincides with the T_N at which the antiferromagnetism disappears. However, T_C 725°C is occasionally observed, which is generally attributed to defect ferromagnetism. At –15°C, it undergoes a structural transition, Morin transition, wherein the directions of preferred spin orientation changes leading to a loss of spin canting. As a consequence, its intrinsic weak ferromagnetism disappears. As in the case of the Verwey transition in magnetite, this property can be useful as a means of detecting hematite in rocks. The magnetic coercivity is strongly dependent on grain size with peak values of 3.5 to 6.5 T, for SSD sized particles (grains ~1 to 3 μm in dia). But it is virtually non-magnetic, when in particle sizes of <0.2 μm. Under supergeneous conditions, it changes to goethite, limonite and siderite and at a temperature of 1390°C into magnetite.

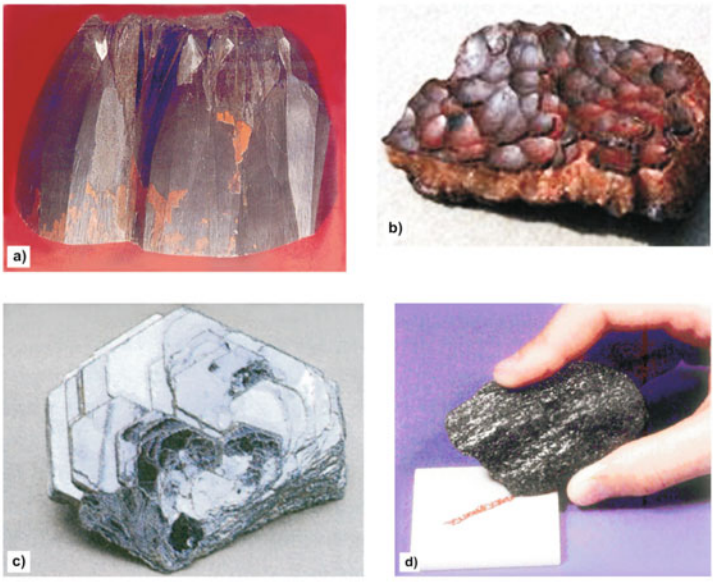

Figure 2.26. (a) Well-developed rhombohedral crystals of hematite. (b) Name hematite comes from the Greek, 'hema' meaning blood. It comes in two forms: red and gray (http://mineral.galleries.com/minerals/oxides/hematite.htm). (c) Hematite is an important ore of iron and comes in many forms like hematite rose, tiger iron, kidney ore, oolitic hematite and specularite. (d) The colour of hematite may be black, red or brown, but it always leaves a reddish streak when scratched along a ceramic plate. Streak is the colour of a mineral's powder (Press and Siever, 2002).

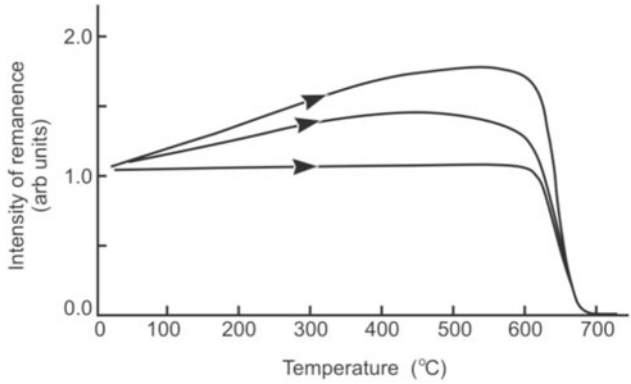

Figure 2.27. The thermomagnetic curves for hematite are somewhat variable, mainly because the fields applied are not capable of saturation magnetization of the specimen. The curves tend to be flatter for higher applied fields. Such increases can be diagnostic of the presence of hematite, although such curves also indicate the growth of new magnetic minerals. The intensity of magnetization is conventionally in arbitrary units, because the actual concentration of ferromagnetic minerals is usually not known (Tarling, 1983).

Titanohematites: Minerals intermediate in composition between hematite (Fe_2O_3) and ilmenite ($FeTiO_3$) give rise to a second solid-solution series called the titanohematites (α-$Fe_{2-y}Ti_yO_3$) (Fig. 2.18). The rhombohedral titnohematites are often referred to as hemoilmenites. Compositions close to both hematite and ilmenite are quite common in igneous rocks, while truly single-phase titanohematites of intermediate composition (y~0.5–0.7) can be preserved by rapid cooling of pyroclastic rocks and have the property of acquiring self reversed TRM. With an increase in substitution of Fe by Ti, there is linear decrease in T_C, often leading to T_C below RT (Fig. 2.24).

Ilmenite ($FeTiO_3$): Ilmenite (Fig. 2.28a-b) is the other common rhombohedral mineral that occurs in nature. It is not magnetic at RT, but becomes antiferromagnetic at –216°C. Though ilmenite is very common in igneous rocks, it cannot be used to determine the natural magnetization. In many volcanic rocks, the content of Ti is high, and the Fe-Ti minerals formed are a mixture of magnetite and ulvöspinel. As cooling proceeds, the ulvöspinel becomes mineralogically unstable and tends to oxidize to form ilmenite and magnetite.

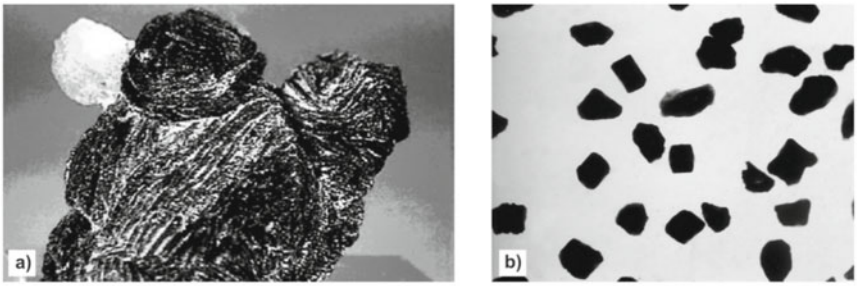

Figure 2.28. (a) Ilmenite crystallizes in the trigonal system. Crystals are thick, tabular or lamellar, commonly as embedded irregular grains. The name is derived from Ilmen mountains in the Urals (http://mineral.galleries.com/minerals/oxides/ilmenite/ilmenite.htm). (b) Micro photograph of ilmenite grains taken under polarized light. Note the presence of well developed crystals (Magnification×100).

II. Iron Sulphides and Magnetic Properties

Iron and sulphur combine in various ratios to form a number of distinct minerals. Iron sulphides can vary in composition from troilite (FeS) to pyrite (FeS_2), but troilite is very rare in terrestrial rocks, although common in meteorites and lunar rocks. Pyrite (Fig. 2.29) is common in sedimentary rocks, affected by diagenesis. Pyrite has a cubic structure and is paramagnetic at RT. Troilite has a monoclinic (pseudohexagonal) structure and is a perfect antiferromagnetic material with T_N of 320°C. Chalcopyrite ($CuFeS_2$) may be antiferromagnetic or even slightly ferrimagnetic in a high temperature cubic phase. Other Fe-S minerals (mackinawite, smythite) are often considered metastable in ambient conditions.

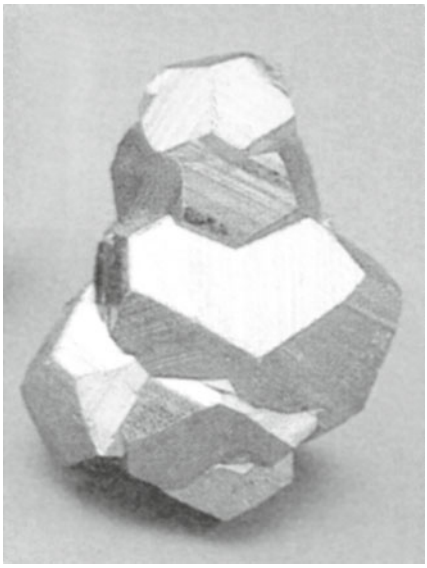

Figure 2.29. Iron pyrite, also known as 'fools gold' because of its brassy yellow colour. It tends to form in cubes. Pyrite is derived from the Greek word, pyr, meaning 'fire' (http://www.minerals.net/mineral/sulfides/pyrite/pyrite2.jpg).

In the Fe reduction conditions, fine-grained magnetite and other oxides tend to dissolve and reform as sulfides, especially pyrite. As a result, anoxic sediments are often basically nonmagnetic. But, under sulphate reducing conditions in muds and rapidly deposited sediments, greigite and pyrrhotite may be preserved. In this sense, authigenic iron sulphides, viz. greigite, are more common in saline than in freshwater environments (Fig. 2.30). However, iron sulphides may be produced in freshwater sediments in an eventuality of oxygen deficient regime. But, they exist in metamorphic and magmatic rocks as well. Of a variety of iron sulphides occurring in nature, only greigite and pyrrhotite received lot of attention in rock magnetism.

Greigite: The Fe sulfide greigite (Fe_3S_4) is the ferrimagnetic cubic mineral. Its crystal structure is comparable to magnetite in which sulfur replaces oxygen atoms. It was thought to be rare in nature, but now is known to occur widely in both freshwater and brackish/marine environments as well as in organic, gleyed soils developed as a result of water logging and lack of oxygen and even peat. It also occurs as magnetosomes originating from magnetotactic bacteria living in sulphur-rich environment.

Greigite is unstable during heating to temperature >200°C, precluding direct determination of its T_C. On initial heating, a major drop in magnetization and magnetic susceptibility is generally observed between ~250°C and 350°C, which forms often diagnostic of the presence of greigite. Typical properties of greigite are: (i) a T_C close to 330°C, (ii) no evidence of a reversible Curie

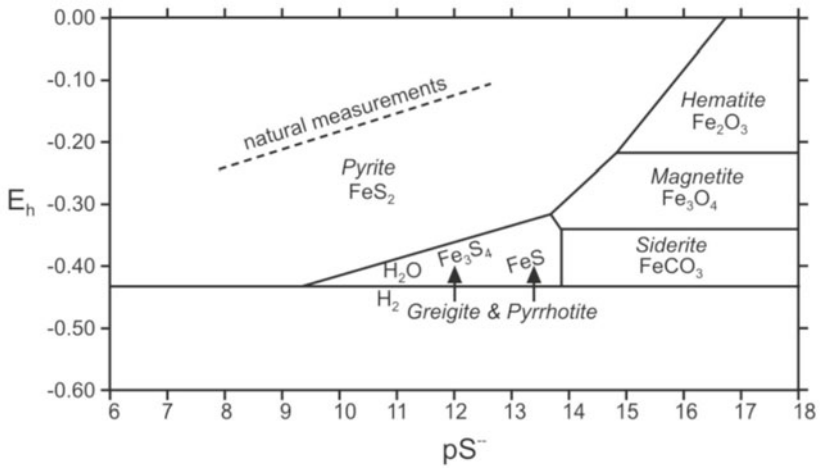

Figure 2.30. Stability fields of iron sulphides in anaerobic acqueous solutions representing average marine conditions, depicted by concentration of sulphide ions (pS^{--}) versus oxidation state. The placement of ferrimagnetic iron sulphides, greigite and pyrrhotite, in the centre of the stability diagram illustrates that their stability fields are limited with respect to pyrite, siderite and iron oxides. The formation of pyrrhotite and greigite would be favoured at intermediate pH's in the presence of lower dissolved sulphur activity (Snowball and Torii, 1999).

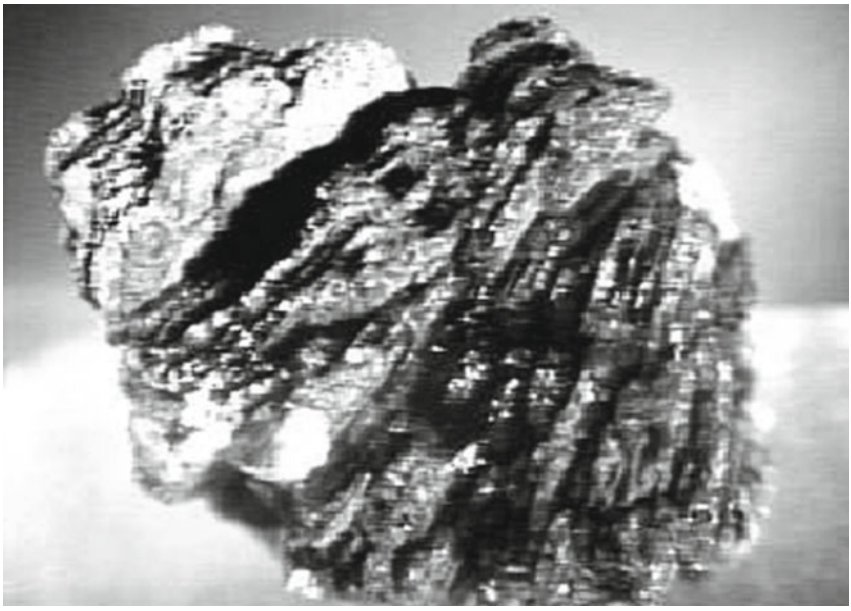

Figure 2.31. Pyrrhotite crystallizes in the hexagonal system. The name comes from the Greek 'pyrrhos', meaning fire coloured, reddish (http://mineral.galleries.com/minerals/sulfides/pyrrhoti/pyrrhoti.jpg).

temperature, (iii) maximum unblocking temperatures in the range 270–380°C and (iv) presence of distinct stable SD properties and coercivity values ranging from 13 to 67 mT.

Pyrrhotite: It crystallizes in many forms (Fig. 2.31) and is a common accessory mineral in basic deep-seated igneous rocks, amphibolites and contact-metamorphosed sediments. Its high susceptibility can produce large magnetic anomalies, helpful in mineral prospecting. Natural pyrrhotite is actually a mixture of Fe-deficient monoclinic Fe_7S_8, which is ferrimagnetic and Fe-rich antiferromagnetic hexagonal phases such as Fe_9S_{10}, $Fe_{10}S_{11}$ and $Fe_{11}S_{12}$. Monoclinic Fe_7S_8 has a few missing Fe^{2+} ions in its lattice structure, giving rise to a cation-deficient ferrimagnetic like maghemite. It has spontaneous magnetization of ~17 Am^2/kg and T_C of 320°C. It is magnetically highly anisotropic and its volume susceptibility amounts to values of the order of 10^{-1} (SI). Pyrrhotites richer in iron than Fe_7S_8 undergo crystallographic λ transition or γ transition at temperatures between ~180 and 220°C, above which they exhibit ferrimagnetism having T_C ~265°C. The Curie temperature for different compositions of hexagonal pyrrhotites varies between 210 and 270°C. The λ transition is diagnostic of hexagonal (Fe-rich) pyrrhotites. Monoclinic Fe-poor Fe_9S_{10} has no λ transition, but does have a low-temperature transition in remanence and coercivity at 30–35 K.

III. Iron Hydroxides, Oxyhydroxides and Their Magnetic Properties

Hydrous iron oxides are produced commonly by weathering of iron-bearing rocks in ambient conditions. They are ubiquitous in marine sediments. Iron oxyhydroxides are often collectively called limonite. This group contains goethite, akaganeite and lepidocrocite (respectively α, β and γ-FeOOH).

Goethite: Orthorhombic goethite (α-FeOOH) is yellowish brown to red in colour (Fig. 2.32). It is typically formed as a weathering product and is the stable Fe oxide in soils and sediments of humid climates. Most goethite is antiferromagnetic with a T_N of ~120°C. Below its T_N of 120°C, goethite is extremely magnetically hard, requiring fields in excess of 10 T to reach the magnetic saturation. When it is heated >120°C, it acquires a weak, but very stable TRM on cooling in a magnetic field. On heating, goethite dehydrates at ~300 to 400°C and forms hematite.

Akaganeite (β-FeOOH): It is not so common in nature and has a T_N between –163 and 22°C (110 and 295 K) below RT. Hence, is of very little importance in the study of natural remanence. On heating, it dehydrates to form hematite at 450°C.

Lepidocrocite (γ-FeOOH): It is brownish in colour and orthorhombic in structure. It is less common than goethite. It has a T_N of –196°C and so cannot carry remanence on its own at normal temperatures. On heating, it breaks down

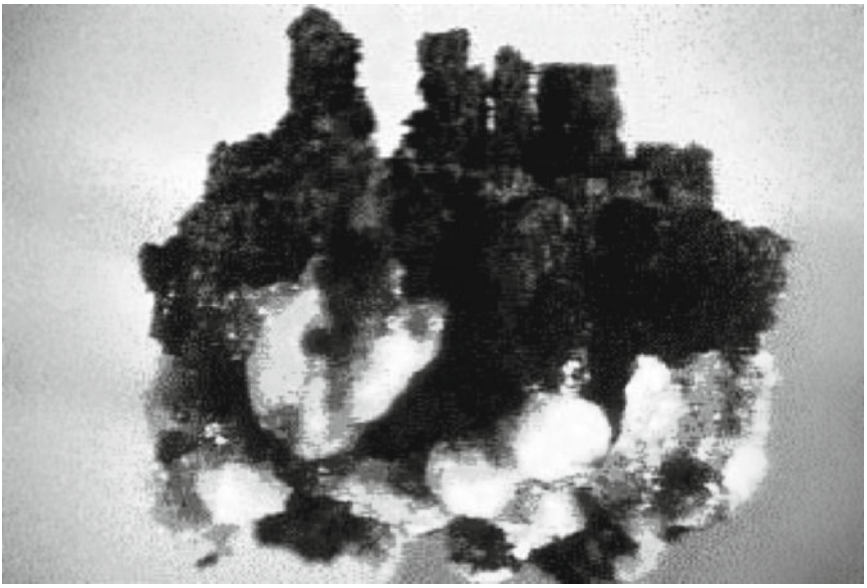

Figure 2.32. Stalactitic goethite, named after German poet and philosopher I.W. Goethe. It crystallizes in the orthorhombic system. Crystals are small, tabular, acicular, and compact in stalactitic masses (http://mineral.galleries.com/minerals/oxides/goethite/goethite.htm).

to form maghemite at 250 to 300°C. The maghemite so formed is unstable and this in turn breaks down to hematite at ~400°C. Soil scientists prefer the term ferrihydrite.

Magnetic mineralogy defines the geological and climatological setting of its formation because of which its study is important in palaeomagnetism and environmental geomagnetism. The instability of minerals also provides clues to magnetic decay products obtained at certain temperatures. Magnetic properties can further be studied through a few diagnostic parameters defined by a hysteresis loop.

2.6 HYSTERESIS LOOP

Apart from temperature, magnetization of magnetic substances also depends upon the magnetic field induced, which is best displayed by a hysteresis loop (Fig. 2.33a).

The hysteresis loop is used as a diagnostic tool to identify certain magnetic minerals in their purest form, or in combinations. When a piece of Fe is magnetized, its magnetization increases on application of the field, and the magnetization returns close to zero on removal of the field. On applying a stronger field, beyond a critical field called the coercive force, the magnetization is no longer reversible. It retains some remanent magnetization. On subjecting

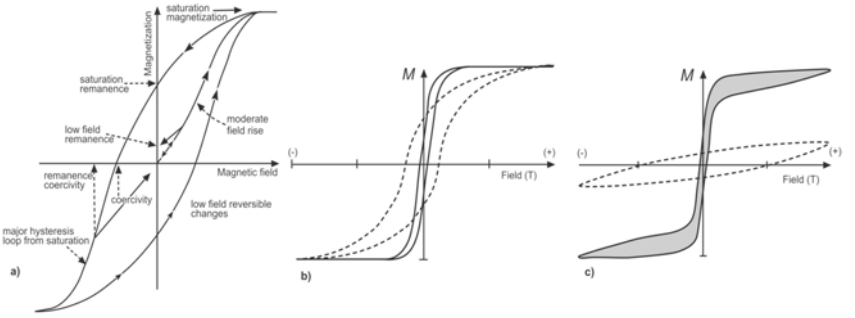

Figure 2.33. (a) A general hysteresis curve showing different parameters. (b) Hysteresis loop for SSD (dashed line) and MD (solid lines) magnetite grains. (c) Hysteresis loop for hematite (dashed line) and mixture of hard and soft minerals (solid lines).

to extreme applied field in one direction, and then in the opposite direction, and back again, a loop is formed called hysteresis loop. This loop is different for different grain sizes of the SSD or MD type (Fig. 2.33b), and for different magnetic minerals, e.g. soft magnetite and hard hematite as shown in Fig. 2.33c.

The hysteresis loop defines some of the most important magnetic parameters such as saturation magnetization, saturation remanence, coercivity and coercivity of remanence. After application of sufficiently high magnetic field, the sample acquires saturation magnetization. Removal of this field leaves the sample with its saturation remanence. But, if the original field is insufficient to achieve saturation, then the representation is just in terms of remanence. Application of a reversed field to saturation remanence eventually leads to a point, where the overall magnetization equals zero. The field necessary to achieve this is called the coercive force. However, to arrive at a point where the sample has zero remanence after the removal of magnetic field, a somewhat stronger reverse field is required. This is called the coercivity of remanence. Thus, these four key elements are used as diagnostic tools to identify the magnetic minerals, their grain size and concentration. It is important to note that paramagnetic and diamagnetic minerals do not exhibit hysteresis loops.

2.7 MAGNETIC MATERIALS, DOMAIN STATES AND GRAIN SIZES

Hysteresis properties are closely related to the arrangement of magnetic domains and spin moments. The concept of domains was invoked by Peter Weiss to explain the magnetized and demagnetized states of a ferromagnetic body, the process of magnetization in low fields, and the hysteresis phenomenon. Such material exists by splitting itself into many domains, each spontaneously

magnetized in easy directions (Fig. 2.34), ultimately rendering the domain magnetization to be overall zero. Felix Bloch, 1952 Nobel Prize winner, further suggested that zones of finite thickness separated the magnetic domains called the domain (Bloch) walls.

I. Domain Formation

Magnetic domains form to reduce the energy of the system. Consider a large uniformly magnetized single crystal (Fig. 2.34) of a ferromagnetic material with its spontaneous magnetization along an easy axis coinciding along its length rather than its width. Due to the free surface poles, a demagnetized field arises as indicated by the extraneous lines to the crystal. The demagnetization energy (magnetostatic energy), which is proportional to the square of the magnetization, can be approximately halved if the magnetization splits into two domains magnetized in opposite directions. This brings (+) and (-) charges closer together, decreasing the spatial extent of the demagnetizing field (Fig. 2.34). However, the boundary region between two oppositely (or at 45°) polarized domains, is called domain wall, and some energy is associated with its formation. The minimum energy state for the crystal is an equilibrium state of domains and domain walls.

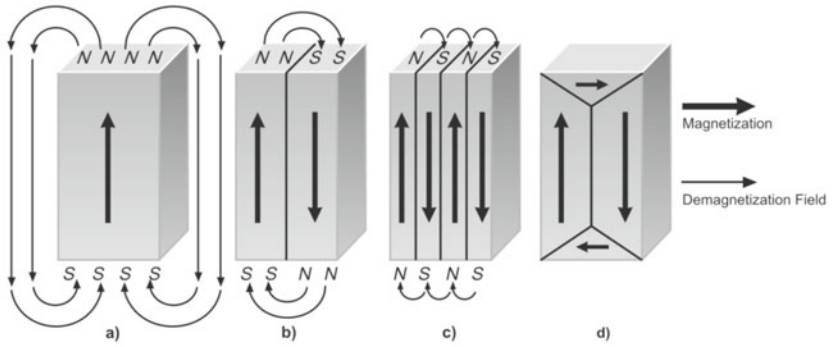

Figure 2.34. Schematic illustration of the break up of magnetization into domains: (a) single domain, (b) two domains (PSD), (c) four domains (MD), and (d) closure domains (http://www.magnets.bham.ac.uk/ magneticmaterials/domains.shtml).

This subdivision into more and more domains cannot continue indefinitely because the transition region between domains (domain wall) requires energy to be produced and maintained. Eventually, an equilibrium with number of domains is reached for a given particle size. It is very difficult to experimentally determine the dimensions of the domain and Bloch walls, but theoretical and observational factors indicate that these walls in magnetite are some 0.1 μm thick, and the domains themselves are ~0.1 to 0.05 μm thick. They may possibly be even >1.5 μm thick in hematite. However, individual domains in natural substances are likely to be very variable. This variability could be the result of the presence of impurities, and defects in the crystal lattices and other such factors.

II. Domain Status and Critical Grain Sizes

Magnetic domains are otherwise called as magnetic grains. Another control on domain status is the volume of the magnetic grain. Ferro(i)magnetic grains which can subdivide into many domains with walls between them are called MD. When the grain size is of the order of wall thickness, it cannot support a wall and will be a SD grain. The SSD size range is from <1000 Å (or wall thickness) down to a diameter equal to a few times the lattice constant of the material, and these grains are referred to as fine particles. However, thermal energy has a special effect on the fine particles, which were first investigated theoretically by Neel in 1948 in connection with magnetization process of rocks. The transition from SD to MD status is not sharply defined; it is marked by grains with intermediate domain configurations but which exhibit SD-like properties, hence are termed pseudo SD (PSD). The response to magnetization (and demagnetization) is greatly influenced by the domain status. Large MD grains respond to relatively low magnetic fields, while SD grains require high fields. SD grains have thus greater magnetic stability or are magnetically harder than MD grains.

III. Relaxation Time

Domain structure is fundamentally linked with the relaxation times and magnetic properties of a mineral. When a magnetic field is applied to an SSD particle, there is usually a component of the field that lies along one of the easy directions of the domain. The direction of magnetization within the domain tries to 'flip' into the direction of this easy axis. This flip, however, is possible only if the internal energy barriers of the domain particle are exceeded. The energy required for this flip comes from the applied magnetic field. In strong fields, the flip occurs almost immediately on application of an external field. In weak fields, the magnetic energy may be insufficient to cause a flip until thermal vibrations allow the internal barrier to be exceeded. Temperature can be taken as a statistical measure of thermal vibrations. Hence, a few electrons, at any one time, have sufficient energy to exceed the energy barrier. If the domain is then kept at the same temperature, all electrons eventually exceed the internal energy barriers, and the domain takes up an alignment along the easy direction that has a component in the direction of the applied field. The time taken by a domain to acquire magnetization with a component in the direction of the external field is the relaxation time. Each domain thus has a specific relaxation time.

The size and concentration factors of four magnetic domains are explained by magnetic properties such as frequency dependent susceptibility, coercivity, and remanence, which are illustrated below.

Stable single domain: The theoretical range of SSD size in magnetite is narrow (0.03 to 0.1 μm), whereas it is larger for hematite (0.03 to 15 μm). An SSD grain is characterized by (i) strong magnetization because all its spin moments are parallel, (ii) high coercivity, because B_{ext} must cause all the spontaneous

magnetization to rotate away from easy direction, and (iii) relatively low susceptibility. The magnetization of a SSD particle is very stable, and has relaxation time of more than 1000 Ma (Fig. 2.37). SSD grains can be very efficient carriers of remanent magnetization, and thus play an important role in palaeomagnetism.

Pseudo-single domain (PSD): When the grain size is larger (0.1 to 20 μm) than SSD with more than one domain (<2 or 3 domains), it is referred to as PSD. Grains in this range can have substantial magnetic moment. These grains can be important carriers of palaeomagnetic records in deep sea sediments.

Multidomain: Magnetic grains larger than a few μm (>20 μm) in diameter with more than two domains are the MD particles. The domains are separated from one another by ~0.1 μm thick region called the domain wall. They are magnetically soft and easy to impart a remanent magnetization. These grains exhibit anisotropy in magnetism, and used in studies determining anisotropy of magnetic susceptibility (AMS). An MD grain has: (i) smaller coercivity, since B_{ext} gradually aligns various domains in its direction, and (ii) relatively high susceptibility.

Superparamagnetic: SP grains, discovered by Neel in 1955, are extremely fine-grained magnetic particles (<0.03 μm). SP behaviour strongly depends on temperature, and is paramagnetic at RT. They exhibit ferro and ferrimagnetic properties of SSD grains at lower temperature. The magnetization of SP particles can align very quickly with an external magnetic field, giving them a high susceptibility (at low frequency) than SSD and PSD grains. For magnetite, the smallest grains <0.03 μm (for spherical shape) with short relaxation times of <150 sec are SP. At RT, the SP to SSD transition for magnetite occurs at 0.03 μm.

IV. Magnetic Grains of Magnetite

However, the actual size of magnetic grains that make up the MD, PSD, SSD and SP is very much a function of the mineral in question. In magnetite, direct microscopic observations indicate that two-domain patterns, in particular PSD, persist up to ~10^{-6} m, whereas to accommodate ~10 domains, a grain of some 10^{-4} m may be required. It must be borne in mind that the distance between atoms in solid Fe is ~3×10^{-10} m, and the wavelength of visible light is ~5×10^{-7} m. Domain behaviour can be illustrated by mapping out the various fields on a plot of grain size versus grain shape (Fig. 2.35).

V. Bulk Magnetic Properties

Magnetic properties of materials in bulk are studied to understand the domain states of magnetic grains. A pictorial summary of the basic bulk magnetic properties such as hysteresis and thermal variation of magnetization and susceptibility is given for different domain states in Fig. 2.36. The basic point to remember is that both M_S-T and χ-T curves of a sample containing SP

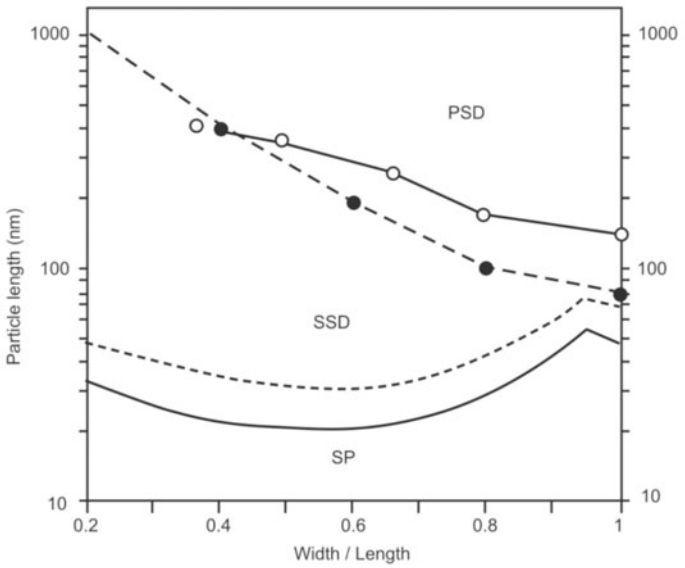

Figure 2.35. Size-shape regions for various domain states in magnetite. The lowermost curve represents a relaxation time of 100 sec. The lower dashed curve (short dashes) is similar to the curve below it but is calculated for a relaxation time of 4.5 billion years. The upper dashed curve (long dashes) was calculated from a simple energy balance model, whereas the solid line with the open circles results from a full 3D micromagnetic calculation. The SP, SSD and PSD fields are indicated (Evans and Heller, 2003).

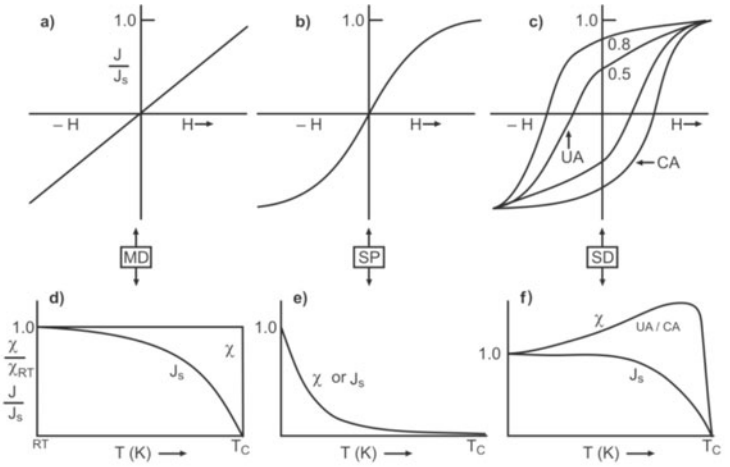

Figure 2.36. Theoretical assumed (or expected) magnetization curves with magnetic field (a, b, c), and with temperature (d, e, f) for samples containing large multidomain (MD), small superparamagnetic (SP), and optimum single domain (SD) particles distributed in a nonmagnetic matrix. Intensity of magnetization (M), saturation intensity of magnetization (M_S), uniaxial anisotropy (UA), crystalline (or cubic) anisotropy (CA), magnetic susceptibility (χ), and Curie temperature (T_C) (Radhakrishnamurty, 1993).

particles can show a concave curve rather than the convex type usually shown by ferro(i)magnetic materials (Fig. 2.36d-f).

VI. Remanence Acquisition and Temporal Scales

A magnetic mineral can acquire remanence by various means pertaining to thermal and chemical activity. An SSD particle of constant diameter, on cooling, shows an exponential increase in relaxation time as it cools from a temperature at or below its T_C. Similarly, a tiny particle, as it grows at a constant temperature, shows an exponential increase in its relaxation time. Just below the T_C, the larger SSD particles have relaxation time of the order of a few minutes (Fig. 2.37), enabling to measure their remanence. However, the smaller particles, since they have shorter relaxation times, become rapidly randomized by thermal fluctuations. On cooling to RT, the larger SSD particles have relaxation times of the order of many thousands or millions of years. The smaller particles, however, show a range of relaxation time, some of which may be of the order of a few seconds. Such fine-grained particles behave paramagnetically. It means that they have a high susceptibility in an applied magnetic field, which decays rapidly on removal of the B_{ext}. The temperature at which a relaxation time rapidly increases to geological times is called the blocking temperature (Fig. 2.37).

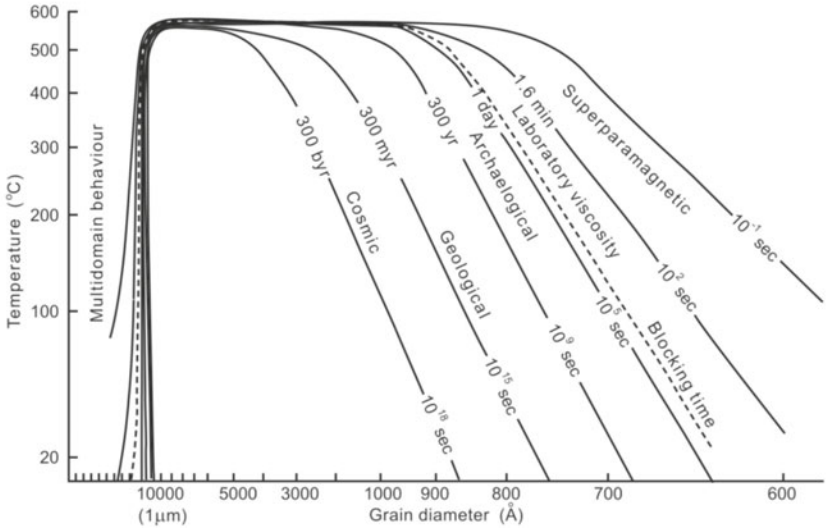

Figure 2.37. The relationship between temperature, volume and relaxation time of a titanomagnetite. The behaviour as the grain size changes from SSD to MD is very strongly controlled by the presence of imperfections in the crystal lattice and makes actual physical determinations difficult to measure. The estimated values are thus shown dashed. The onset of such MD behaviour may also take place at smaller grain sizes than indicated here (Tarling, 1983).

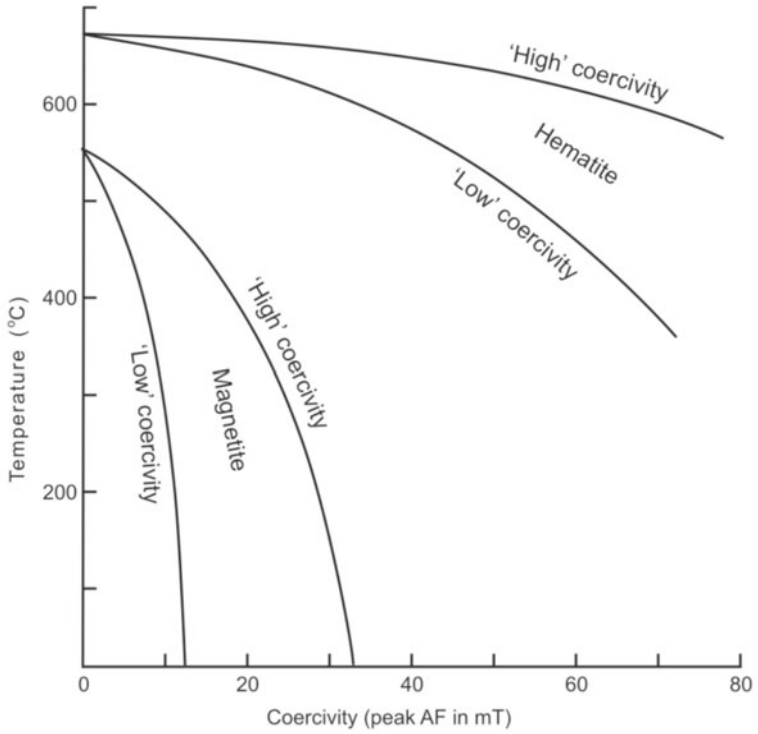

Figure 2.38. Illustrative of the relationship between blocking temperature and coercivity for magnetite and hematite. Magnetite generally has a lower coercivity and blocking temperature range than hematite. These properties are strongly influenced by grain sizes and specific composition, defects, etc. in the titanomagnetites and ilmenohematites, so that the ranges of both properties can overlap each other (Tarling, 1983).

Remanence can also be acquired during the phase of crystal growth that takes place at a constant temperature. As the crystal grows after nucleation, it behaves initially in an SP manner. On further growth of the crystal, an exponential increase is seen in its relaxation time until it reaches its blocking volume, the size at which the relaxation time is 500 seconds. Further growth sees an exponential increase in its relaxation time until it reaches dimensions, where MD behaviour commences. In hematite, the blocking volume at RT is of the order of 0.03 μm, but it is not so well defined in titanomagnetites and titanomaghemites (Fig. 2.38). They probably have a blocking volume of 0.015 to 0.04 μm. The transition from SSD to MD behaviour is even less well defined, but probably occurs well >1 μm in both the cases.

VII. Alternating Field (AF) Demagnetization

There are various types of remanent magnetizations that are strong functions of grain size. Of these, thermal remanence (TRM) and isothermal remanence

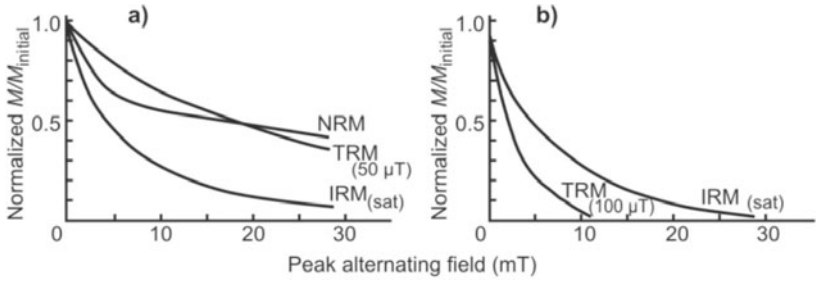

Figure 2.39. Distinguishing properties of (a) stable single domain (SSD) and (b) multidomain (MD) particles (Tarling, 1983).

(IRM) are commonly used in determining effective magnetic grain sizes. The grain size of SSD and MD particles can be determined, and identified by quite a few distinguishing factors. The first distinguishing factor is that the SSD grains that have acquired thermal remanence in a field of <1 mT show a greater stability to AF demagnetization. But, if they had saturated by a large magnetic field at RT, then they exhibit less stability to AF demagnetization (Fig. 2.39). The second distinguishing factor is that on comparison of the SSD and MD composition, it is seen that SSD particles exhibit greater stability to demagnetization after being thermally magnetized in a weak magnetic field, while MD particles show a lesser stability if the field in which they are cooled is decreased.

2.8 GENESIS OF EARTH'S MAGNETIC FIELD AND ITS DYNAMO EFFECT

EMF is produced by convective motions of the highly electrical conducting core metallic fluid, i.e. by a core dynamo. Dynamo action requires a core to be at least partly fluid. Earth metallic core is partially solidified as a result of the cooling of the core over geologic time, according to seismic exploration of the Earth. Dynamo action occurs in the molten outer core, causing it to be in a state of perpetual dynamic ferment. A dynamo is a machine that converts mechanical energy into electrical energy. The dynamo of the Earth is self-sustaining and self-perpetuating.

The factors responsible for the generation of EMF, the causes behind its changing nature, the subsurface zones that sustain the field, and the trail of anomalies that have been left behind, are issues of great scientific interest. Geomagnetists reckon high temperatures, pressures, and the rotational differences between various layers of Earth make it work eternally. The molten Fe of the outer core under intense temperature and pressure gets churned up under the rotational influence of the Earth, setting off into motion the electrical currents. The pre-condition for the emergence of these electrical currents is the presence of innate magnetic field. The electrical currents thus produced then

continuously reinforce the already existing magnetic field, and will keep on producing as long as the Earth has a searingly hot belly and its rotation around itself continues. This active geodynamo is responsible for generating almost 90–95% of the total EMF, and the magnetization of the uppermost lithosphere.

Since electricity and magnetism are commonly generated by means of dynamo, the mechanism by which EMF is created, is known as geodynamo. Permanent magnetism does occur in the crustal EMF, and contributes a small and relatively static contribution to the main internally generated magnetic field, the core field. There are also external components of the magnetic field measured at the Earth's surface. They can be distinguished from the internal core field partly because they vary on a much shorter timescale. The origin of these external fields is in the Earth's ionosphere, where charged particles in the solar wind interact with the upper atmosphere. Since solar magnetic activity changes on a timescale of a few days, short bursts of activity known as magnetic storms and substorms can be detected in magnetic observatories (Chapter 5). As the external components of the EMF are not part of geodynamo, they are not discussed further here.

I. Geodynamo: Models and Mechanisms

Many geodynamo theories have been formulated to explain magnetic field creation. Faraday proposed his 'Faraday disk' (Fig. 2.40a), while Walter Elsasser, Arthur Schuster, and Patrick Blackett tried to find mathematical solutions to the dynamo problem. Recently, Gary Glatzmaier and Paul Roberts proposed a 3D, self-consistent numerical model of the geodynamo (Fig. 2.40b). Earlier, Stanislaw Braginsky provided a mechanism, which was also endorsed by Edward Bullard. Dynamo experiments have been performed in laboratories as well. Lowes and Wilkinson performed an interesting experiment, wherein they spun two Fe cylinders, each representing an eddy, inside a container of mercury, at right angles to each other. At a certain point when the angular velocity reached an exceedingly high value, the magnetic field jumped to a higher plane. They considered this point to be the initiation of dynamo action. Along with such laboratory experiments, mathematical simulations using high-speed computers have also been used to understand the dynamo process (Fig. 2.40c).

Although the dynamo theories and experimental outcomes partially help to understand the genesis of EMF, there are still some aspects about it that cannot be satisfactorily explained. For example, it is found that the field weakens on a decadal scale by ~1%, and in some places its pattern rotates ~1° relative to the Earth's surface. Also, these models fail to account for the magnetic reversals. This backdrop suggests for a couple more mechanisms, apart from the dipole component (Fig. 2.41a), that contribute towards generating the EMF. It is conjectured that the quadrupole (Fig. 2.41b) and octupole (Fig. 2.41c) units add to the EMF. However, the nondipole input

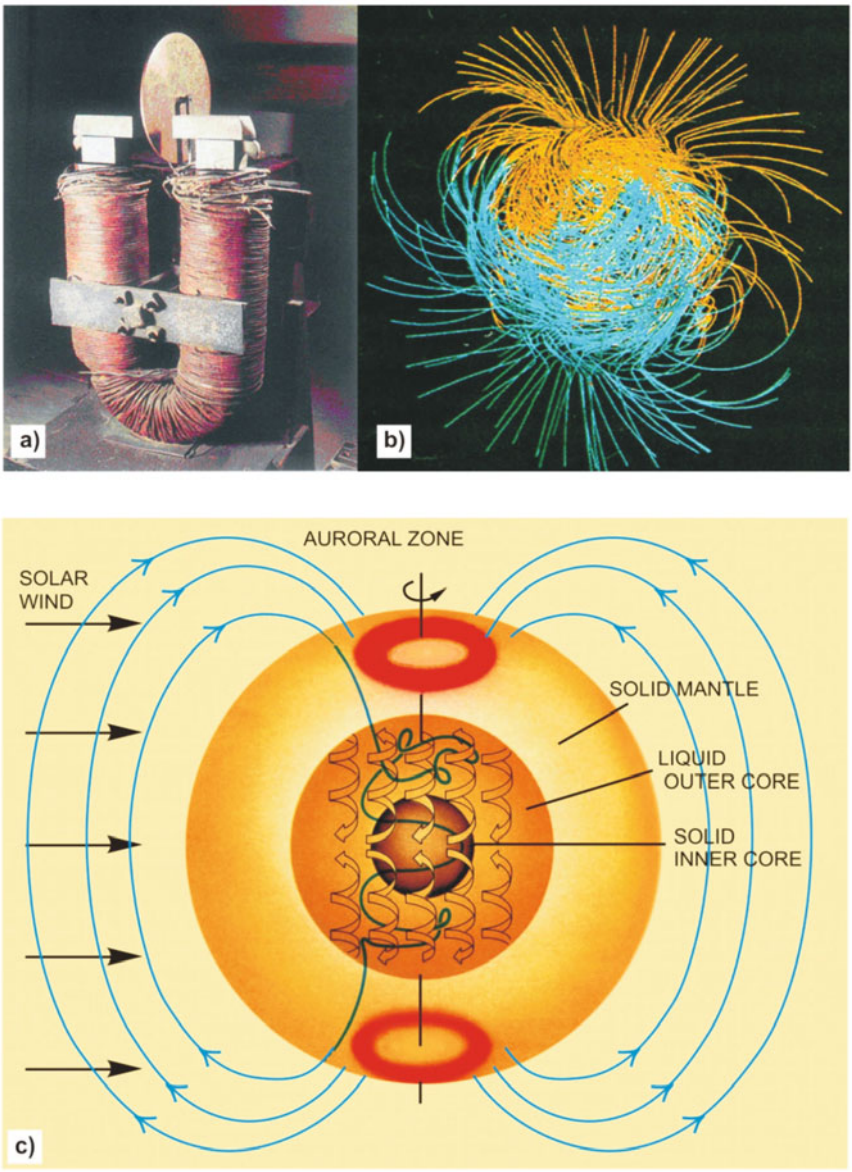

Figure 2.40. (a) Faraday's original apparatus of disk dynamo that produced electrical current by moving a magnet (Hamilton, 1991). (b) Three-dimensional magnetic field structure portrayed through lines of force plotted out to the surface of the modelled Earth (Glatzmaier and Roberts, 1995). (c) Magnetic field is generated by the action of a 'dynamo'. It is assumed that an electrically conducting metallic liquid of the core flows in screw-like rollers. The lines of force in the magnetic field thread through these rollers. A single such line (green colour line) is depicted which goes from the north to the south (http://geomag.usgs.gov/intro.html).

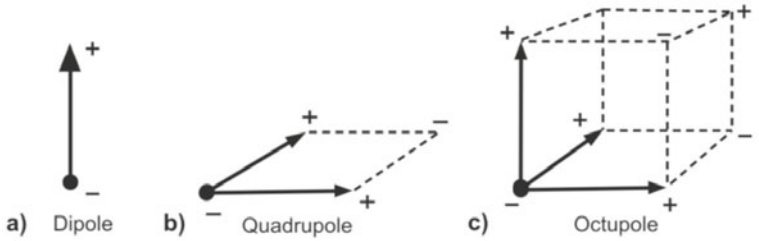

Figure 2.41. (a) The dipole component of the magnetic field. It has one 'positive' and one 'negative' pole. (b) The quadrupole has two 'positive' and two 'negative' poles. (c) The octupole has four 'positive' and four 'negative' poles.

turns out to be very sparse, and probably responsible for the secular variation of the magnetic field.

II. Magnetic Fields in Extraterrestrial Bodies

With an active dynamo, magnetic fields in planetary bodies like Earth and Mercury arise from magnetic material because of induced magnetism in the ambient field, and their earlier acquired remanent magnetism. Magnetic fields observed on the Moon and Mars in the absence of an active dynamo must be due to remanent magnetism only. These fields due to remanent magnetization or palaeomagnetic fields have been investigated with satellite-based surveys. In addition, samples brought to Earth by the Apollo missions from the Moon, and those that have come to Earth from the Moon, Mars, and asteroids in the form of meteorites provide additional palaeomagnetic data.

2.9 WEGENER AND CONTINENTAL DRIFT

The foregoing sections dealt with changing magnetic field at the equator, poles and so on leading to certain queries such as whether these changes are real or perceived or have they been changing for long or have they started to change now. To know more, the theory of continental drift, proposed by Alfred Wegener, needs to be understood. He published this radically new idea in 1915 in a German book titled *'the origin of continents and oceans'*. Wegener, possibly by serendipity (like Plachet, Francis Bacon and du Toit before him), noted that the coastlines bordering the Atlantic ocean 'fit' together rather well (Fig. 2.42a).

It was later shown by Carrey and Bullard that the edges of the continental shelf (Fig. 2.42b) fitted even better. Wegener proved the 'unity' of continents by fossil and geological evidences to declare all continents to be closer together in remote past, but are far apart now because of 'migration'. Wegener's theory was not accepted readily and met with stiff opposition, especially from the geophysicists, most notably Jeffreys. It was argued that the continents cannot drift, since they floated on a viscous material, which offered stiff resistance for any perceived movement. In fact, Wegener was considered something of a

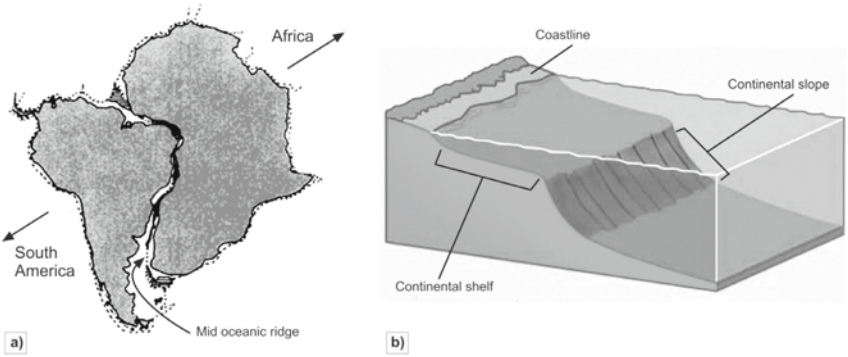

Figure 2.42. (a) The close 'fit' of eastern coastline of South America with the western coast of Africa (Tarbuck and Lutgens, 1994). (b) Schematic of different geomorphological oceanic features.

crank, who failed to secure a university position anywhere in Germany. It was in Graz, Austria, that he ended up as a Professor. Wegener died in Nov 1930, at the age of 50, on a polar expedition, where he was struck by inclement weather.

Continental drift theory, however, created a dichotomy in the geomagnetic world on whether the landmasses or magnetic poles wandered. It also put a doubt on whether the pole reversals were a fantasy or a reality. Scientists reconciled to the idea of magnetic polarity reversals through an important 'event'. Wegener's idea had not died out with him as some of his ardent supporters like du Toit kept the legacy alive, and by 1950 the scientific community had come around to accept his idea. This trick was done by the unravelling of magnetic banding (a reflection of magnetic polarity reversals)

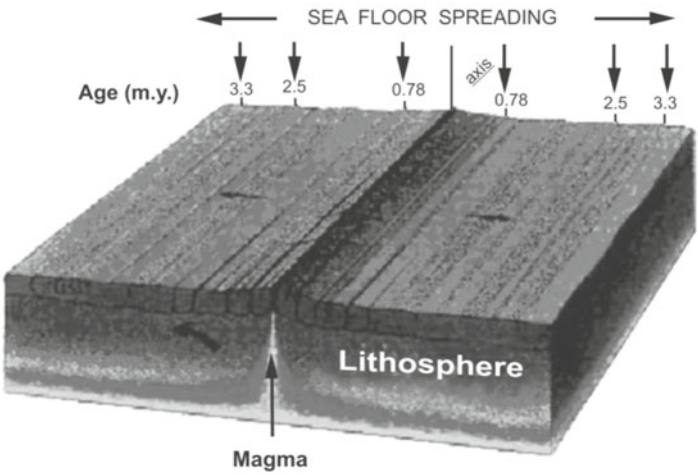

Figure 2.43. Magnetic banding, a reflection of polarity reversals, observed across the mid-Atlantic ridge. Note the increase in age towards the flanks from the centre of the ridge.

encountered across the mid-ocean ridge in the Atlantic ocean (Fig. 2.43), which opened up the field of palaeomagnetism.

2.10 PALAEOMAGNETISM: AN INDIRECT MEASUREMENT OF PAST GEOMAGNETIC FIELD

Because of EMF, magnetic particles in rocks or sediments orientate themselves relative to the ambient magnetic field. Based on magnetic properties, rocks are distinguished as highly magnetic, weakly magnetic and nonmagnetic. Generally, weakening of magnetic properties takes place with a decrease in the basicity of rocks in the order: ultrabasic, basic, acidic, terrigenous and biogenic. Geomagnetically, all these types are of immense practical importance, since the EMF influences various magnetic constituents in them. Consequently, they are magnetized by induction in the main field becoming sources of anomalous magnetic field (crustal magnetic anomalies in Chapter 6). Majority of crustal rocks possess natural remanent magnetization (NRM), which substantially differs in magnitude and direction from the induced magnetism. Studies of NRM directions of rocks help in recovering the history of EMF, essentially forming the subject matter of palaeomagnetism. NRM is a marked feature of basic igneous rocks such as basalt, gabbro and peridotite, and red coloured continental sandstones.

Volcanoes of cone or fissure type are the conduits through which the magma (molten rock) pours out on the surface of the Earth. For example, the Deccan trap basalts that cover the entire Maharashtra, and some parts of Madhya Pradesh, Gujarat, and Karnataka are the products of volcanic activity that occurred about 40–60 Ma ago. The lava that solidifies, and cools below the T_C gets magnetized in the prevailing magnetic field direction. This direction then

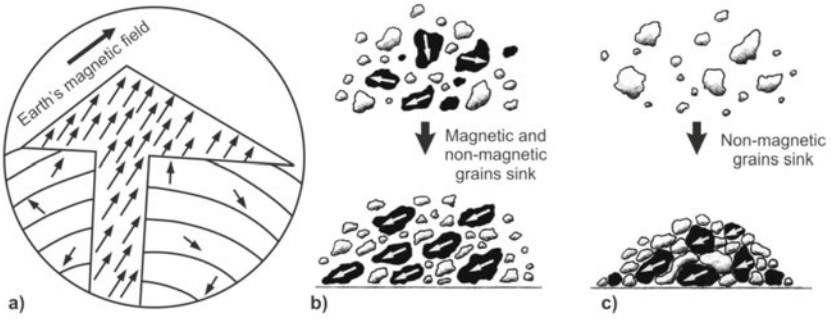

Figure 2.44. (a) In igneous rocks, the magnetic grains 'freeze' the direction of magnetization during their solidification below the Curie point as shown by a big arrow representing the ambient Earth's field direction. Remanent magnetization can be preserved in sedimentary rocks. (b) Magnetic grains that settle through water get deposited on the floor, such that their internal magnets become aligned in the direction of the prevailing magnetic field. (c) Magnetic material is being precipitated in the pore spaces between detrital grains, which get aligned in the prevalent magnetic field direction.

gets 'locked' or 'frozen' in the solidified rock, which it retains for ages (Fig. 2.44a).

In case of sedimentary rocks, individual magnetic minerals torn off from the parent rock are transported to depressions and basinal areas. When these magnetic minerals settle at the bottom of the basin, they preferentially get oriented in the prevailing EMF direction (Fig. 2.44b, c).

The same picture holds true for metamorphic rocks as well. However, some metamorphic rocks like the granulites, charnockites and gneisses of southern India have undergone quite a few episodes of metamorphism by virtue of repeated tectonic events. Consequently, the magnetic minerals portray the ambient field of the last phase of metamorphism, if at all any coherent signatures are obtained. The palaeomagnetic signatures are usually chaotic in the higher metamorphic rocks. One can, of course, obtain stable directions from low grade metamorphic rocks, like the metamorphic carbonates of the Tethyan Himalayas.

The ferrimagnetic minerals in a rock acquire a stable magnetization. By measuring the inclination of these particles, the latitude of rock formation can be deduced (Chapter 7). The magnetic directions thus obtained make sense as a whole, only if continents have moved relative to each other over the past 200 Ma, helping to reconstruct the original configuration of continents. The palaeomagnetic results supported the hypothesis of continental drift, and paved way for modern concepts such as seafloor spreading, and plate tectonics.

I. First Reports of Magnetic Reversals: An Unexpected Bonus

Magnetic signatures are chaotic and confusing in some rock types, but are still the only property of the Earth that stays put for a very long time. Delesse in 1849 carried out the first elaborate studies of magnetic properties frozen in volcanic rocks, and later by Melloni in 1853. They concluded that volcanic rocks acquire magnetization on cooling. Further, Folgerhaiter by the end of nineteenth century declared that volcanic rocks did not just acquire magnetization on cooling, but they acquire it parallel to the EMF. At this time, some magnetic reversals were also reported. A magnetic reversal is a phenomenon, whereby the north magnetic pole turns to a south magnetic pole, and vice versa. It does not mean that the Earth turns upside down, but only means that the alleged magnet, the dipole, 'reverses' its direction of polarity inside the Earth (Fig. 2.45).

However, the acceptance quotient, at least for reversals, was absolutely zero during the close of nineteenth century. Since the majority of the then scientific community found it difficult to visualize continents moving across a rigid mantle; palaeomagnetic studies in those days were carried out exclusively for geomagnetic configuration of the field, and not for confirmation of continental drift.

II. Fisher's Statistics, Approximation of Geocentric Axial Dipole

The palaeomagnetic confirmation of continental drift came much later, with Hospers, who in 1949 joined the Cambridge University to work on his doctoral

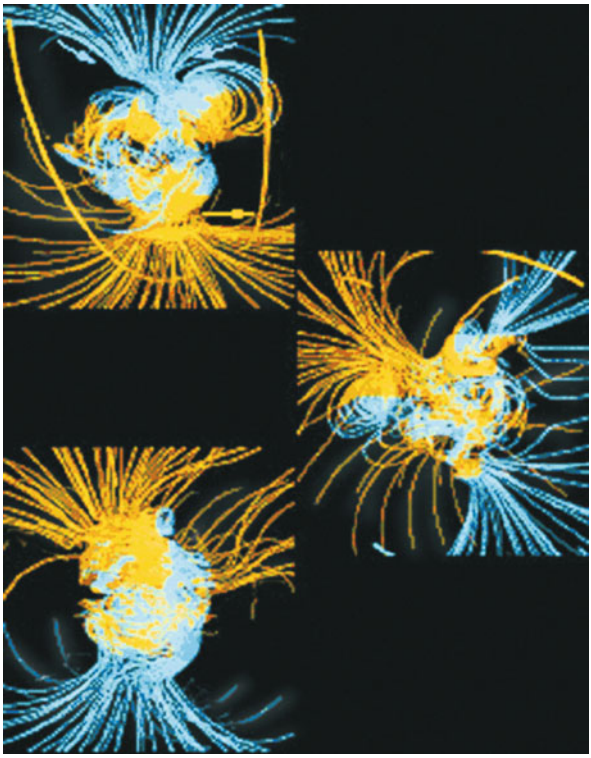

Figure 2.45. Computer simulation of a magnetic reversal. At top, blue field lines are directed towards the north pole, over a period of time reversal sets in (centre), and on complete magnetic reversal (bottom), blue field lines are directed toward south pole (http://www.windows.ucar.edu /tour/link=/glossary/ mag_field_ reversals.html).

thesis. Initially he worked on measuring the magnetic signatures of basaltic rocks of Iceland with the help of spinner magnetometer, an instrument designed by Vincenz (Chapter 4), and found two significant directions that were exactly 180° apart. These results were then shown to Runcorn, who in turn took Hospers to Fisher, the professor of genetics at Cambridge, also the progenitor of universally used statistics on spheres.

Fisher had formulated his famous 'Fisher's statistics' in 1928, but the methodology had been kept in cold storage (he published it in 1953). Fisher revived this model exclusively for Hospers data that enabled Hospers and many others after him, to consolidate their extensive data into a compact form. Hospers on applying the Fisher's statistics got an amazing result: no matter what the sign of the directions of the magnetic field were, when averaged over tens of thousands of years, it approximated closely to that of a geocentric axial dipole. This result meant that the palaeopoles which Hospers derived were of geomagnetic field that resembled the one generated by a dipole situated at the centre of the Earth (which coincided with the geographic poles).

III. Apparent Polar Wander Path and Confirmation of Continental Drift

The course of above developments intrigued many regarding what these palaeopoles represented. Did they mirror the movement of the poles or the movement of continents? What moved them? Drawing up the apparent polar wander (APW) path devised by Creer in 1954 solved this puzzle.

The magnetic directions deciphered in a rock of known age give the pole position. Rocks formed at about the same time will have the same pole position while those formed later have another pole point. Connecting these points together defines a curve that actually describes the APW. The Earth is made up of many tectonic (lithospheric) plates in a state of constant motion relative to each other. This factor puts a powerful constraint on delineating the pole position. If all the continents had the same APW path, then they had not moved at all relative to one another. This was the theory of 'fixism', which was in vogue those days. But, if each continent had its separate and distinct path, then it would be taken as an evidence of movement of continents relative to one another.

Earl Irving got interested into this problem and decided to use the situation of India to test palaeomagnetically the veracity of continental drift. Irving chose India because the movement of Indian plate has been essentially along a longitudinal path (Fig. 2.46a). Wegener had predicted that the Indian plate moved from the southern hemisphere to the northern hemisphere, which Irving most easily confirmed by calculating the palaeopoles. Thus, this method gave

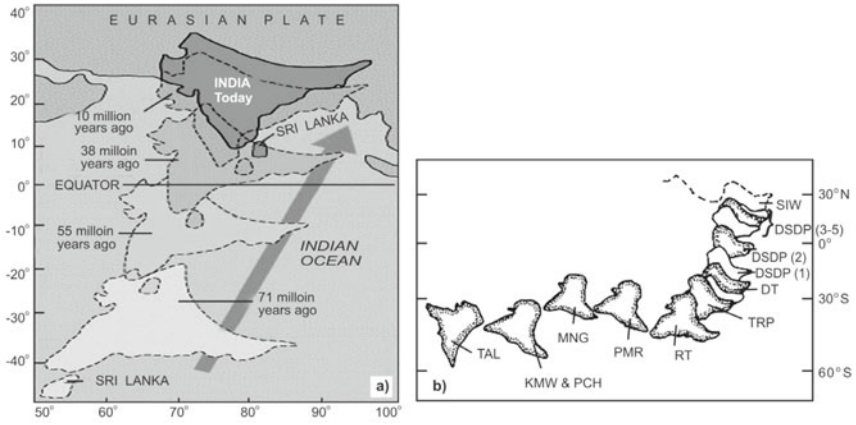

Figure 2.46. (a) The northward migration of Indian plate. (b) Northward drift of India as inferred from pole positions from different formations found at TAL (Talchir), KMW (Kamthi near Wardha), PCH (Panchet), MNG (Mangli), PMR (Panchmarhi), RT (Rajmahal trap), TRP (Tirupati), DT (Deccan trap), DSDP (Deep sea drilling project cores), SIW (Siwalik). The major northward drift of India really started after the onset of Rajmahal trap activity, about 100 Ma ago. Till that time, it was mostly latitudinal (Verma, 1989).

a physical basis of calculating large continental displacements. Further, it was observed and confirmed that the fossils and palaeomagnetic records within a single continent agreed well with each other. Consequently, by 1950, continental drift was shown to be a reality by employing the palaeomagnetic technique. The northward (N–NE) drift of India as inferred from pole positions is illustrated in Fig. 2.46b.

IV. Polarity Reversals and Mechanism of Self-Reversal

In a polarity reversal, there is an exchange of poles. Lawrence Morley of Canada developed interest in magnetic prospecting in 1939, and was well versed in aeromagnetic and remanent magnetism of rocks. During his time, Runcorn dealt with magnetic reversals on altering the directions by 180° to derive the pole positions. Balsley and Buddington, on the other hand, opposed the idea of periodically reversing EMF. Instead, they rooted for a mechanism that triggered 'self-reversals', i.e. magnetization in a direction opposite to EMF within the rock. Balsley opined that the self-reversing rocks had two main forms of ferromagnetic minerals with two differing T_Cs. When the magma having these two ferromagnetic minerals solidified, the minerals with a lower T_C trapped in the demagnetizing field of the other ferromagnetic mineral. On complete cooling, if the ferromagnetic mineral with a lower T_C has a stronger magnetic moment than the other, it leads to reverse magnetization. In June 1954, a palaeomagnetic conference was arranged in Idyllwild, Los Angeles, to which Morley was invited. This meeting was arranged ostensibly to deliberate on whether the reversely magnetized rocks portrayed the actual reversal of the EMF or was it just a manifestation of a self-reversing process. However, nothing concrete came out of the meeting as many held on to their known traditional positions.

In 1958, Morley came in contact with Larochelle, who demonstrated that the mount Yamaska volcanic plug near Montreal was negatively polarized. At about the same time, the oceanic floor was also being actively explored magnetically and many, like Mason and Raff, had found out magnetic banding to be an obvious and regular feature of the ocean floor. These disclosures aroused indefatigable curiosity in the mind of Morley, who became obsessed with finding an explanation to the regular banding pattern (Fig. 2.43). Deep down he knew that there was some fundamental property or character that related the origin as well as the geological structure of ocean basins. Remember, Morley was accustomed to chaotic magnetic signatures obtained over the continents which hardly display any clear-cut pattern. Combining his expertise gained through diverse disciplines, it did not take him long to realize that the positive and negative banding were the result of remanence. However, the generators and accumulators of this magnetic data, like Raff and Mason, had not indulged in any speculation nor was any explanation for this banding offered.

Morley was frantically searching for an explanation, and once while perusing through the literature on ocean basins, an idea hit him out of the blue.

It occurred to him that somehow, in one way or the other, this banding was related to the east Pacific ridge, because the banding was unmistakably parallel to the ridge. For more information, Morley referred to Dietz's paper on ocean floor spreading. While going through the paper, Morley was struck with the explanation. In the very own words of Morley, '*I reckoned, if the rocks at the mid-ocean ridges were rising from depth, they would become thermoremanently magnetized in the direction of the Earth's field prevailing at that time. They would then spread laterally in both the directions towards the continents, according to Dietz's theory. A million or so years later, the Earth's field would reverse, and in this way, a positive and negative banding pattern would gradually be built up. From this moment (December 1962), I never had any doubts about the concept. It locked three theories together in a mutually supporting way: the theories of continental drift, ocean floor spreading, and the periodic reversing of the Earth's field'.* Morley, in one fortuitous stroke of serendipity, cracked one of the long held mysteries of nature. However, the real credit for explaining magnetic banding has gone to Vine and Mathews, since they published their results before Morley could.

2.11 MECHANISM OF MAGNETIC BANDING

To understand the phenomenon of magnetic banding, the concept of seafloor spreading together with the continental drift needs to be brought in. Hess and Deitz proposed the hypothesis of seafloor spreading in 1960. According to them, a new seafloor formed at mid-oceanic ridges by the lava that came out, and the older seafloor went down the trenches. In simplest form, one can visualize a part of seafloor with a huge opening. This crack developed because it is right up on the surface below which the convection current is in full swing (Fig. 2.47, the top Gilbert reversal epoch).

At this opening, the convection current brings up magma from the mantle and oozes it out. On reaching the surface, this magma solidifies into a basaltic rock. While it cools, the magnetic minerals automatically align in the prevailing EMF. Since the process of convection is still operating, it breaks the solidified basaltic rock formed over the opening into two and spills out yet another dose of magma. When this hot magma cools, it 'freezes' into it the magnetic minerals that have aligned in the then existing EMF (Gauss normal epoch in Fig. 2.47). This process of the magma coming out of the opening, and breaking the pre-existing basaltic rock into two, and also pushing the broken parts away from each other continued for thousands and millions of years. When looked at this opening after those many years, an incredible symmetry is found on either side of the opening. Close to the opening, on both the sides, the age of the basaltic rock is the youngest because it formed last. At the farthest end from the opening are the oldest rocks, since they formed first, at the very beginning, giving rise to a symmetrical pattern of magnetic polarities—normal and reverse on either side of the opening.

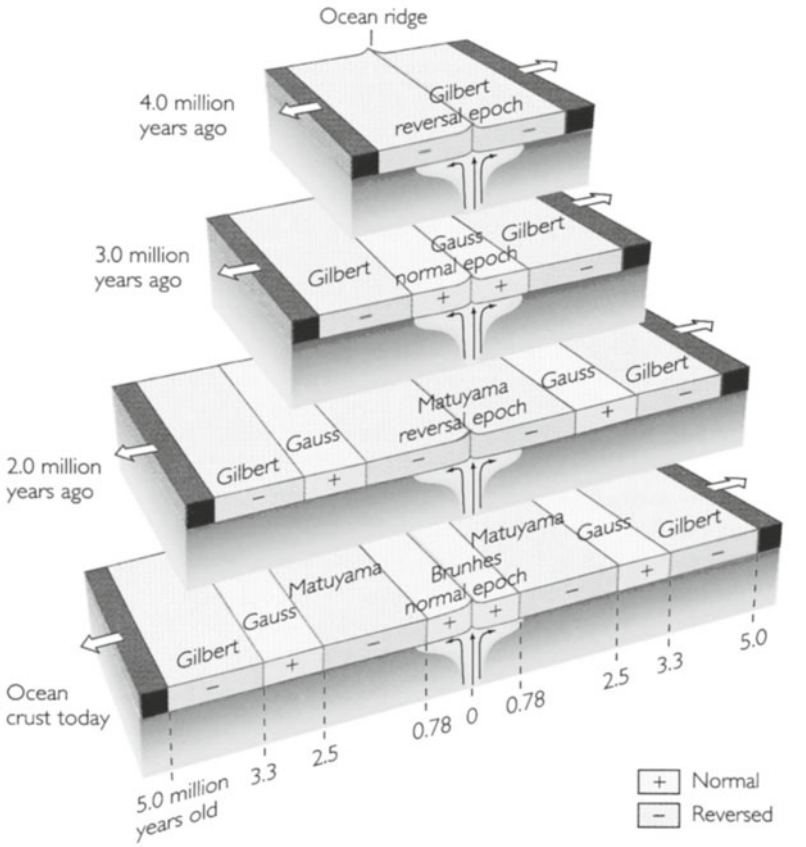

Figure 2.47. When magma comes to the surface and solidifies, magnetic minerals align in the prevailing direction of the Earth's magnetic field. The solidified material then breaks into two and moves away on either side of the crack. The ejected material containing magnetic minerals, align in the then existing magnetic field, during the course of cooling, giving rise to alternate 'normal' and 'reverse' magnetic stripes (Press and Siever, 2002).

Seafloor spreading, magnetic reversals: The interconnected concepts of magnetic reversal and sea-floor spreading share an intimate relationship to understand which, it would be wise to start again with Wegener's hypothesis of continental drift that tells present-day separated landmasses were once a single landmass, a 'supercontinent' (Fig. 2.48).

Wegener named this supercontinent Pangaea meaning 'all Earth', which broke into two—the Gondwanaland and Laurasia. India, together with Africa, South America, Antarctica and Australia was a part of Gondwanaland (Fig. 2.48). Incidentally, Gondwanaland is named after the tribe 'Gonds' found in central India. Asia and Europe formed the Laurasia (Fig. 2.48). Gondwanaland then again broke into a couple of more fragments. Wegener said that the continents broke because of the centrifugal forces arising from the rotation of

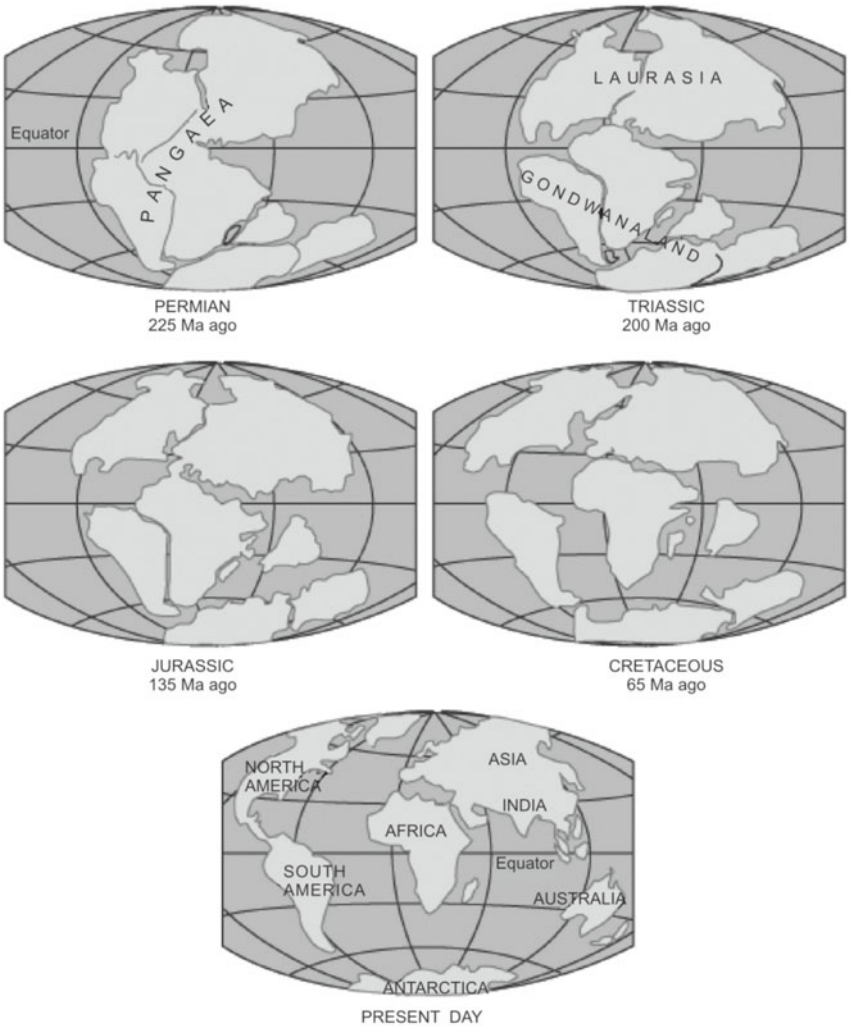

Figure 2.48. The reconstructed position of continental outlines giving a view of the postulated movements of the continental plates. The names Pangaea for the supercontinent and Laurasia and Gondwanaland for the stage after breakup date back to the time of Wegener (http://hyperphysics.phy-astr.gsu.edu/hbase/hframe.html).

the Earth as well as the lunar and solar gravitational forces that forced the movement of the continents towards the equator. This was not the case and the reason attributed by Wegener was incorrect as was proved by his opponents. The then prevailing notion was that the formation of mountains and valleys as well as the folding and faulting of the crust was because of the contraction of the Earth. The Earth to them was contracting because it was cooling. But in reality, it is neither contracting nor expanding. However, the contribution of both the opponents and proponents of Wegener's hypothesis needs to be

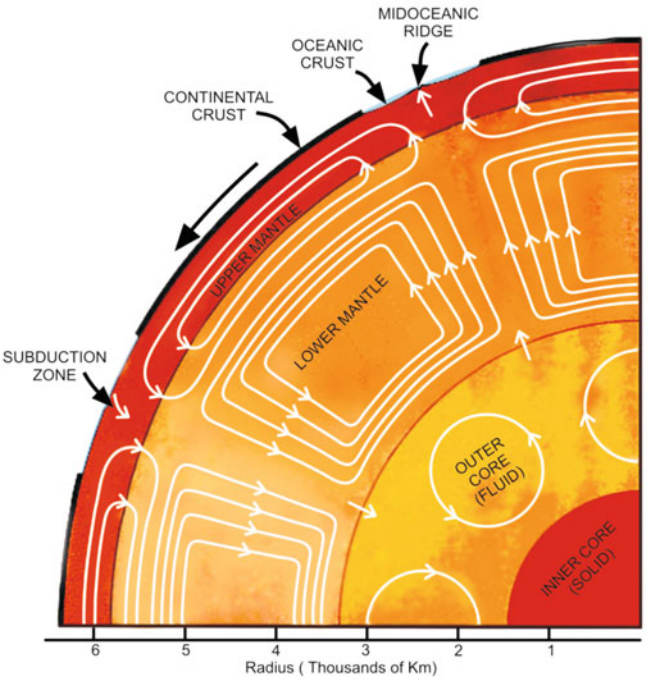

Figure 2.49. Profile of convection currents active in the mantle. When two convection currents come towards each other, they give rise to a subduction zone. When they move away from each other, a mid-ocean ridge is formed.

appreciated. None of them had access to the global tectonic and deformation processes that work within and outside the Earth.

This understanding came much later when the scientists of yore realized that the progressive increase in pressure and temperature, which occurs down the Earth, were quick to deduce the possibility that the conditions in mantle made the rocks ductile—like a soft plastic. These intense conditions, they reasoned, set in convection currents such that the warmer and hence lighter material rose up and the colder denser material consequently dropped down at the bottom (Fig. 2.49). One of the first to propose this convection model was Arthur Holmes, the English geologist, who proclaimed continental drift is caused by the convection currents operating inside the Earth.

2.12 PLATE TECTONICS AND SEISMOTECTONICS

It can be seen from Fig. 2.49 that because of convection currents, new crust is formed at the mid-ocean ridge and the older crust is destroyed at the subduction zone. Incidentally, the regions, where the crust is formed and destroyed, are the lithospheric plate margins. There are three types of plate margins. The first is the consuming/convergent/a destructive plate margin, where two plates collide

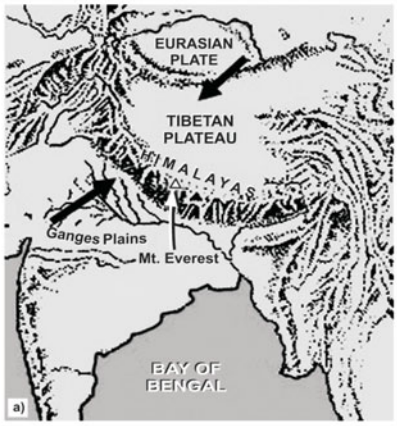

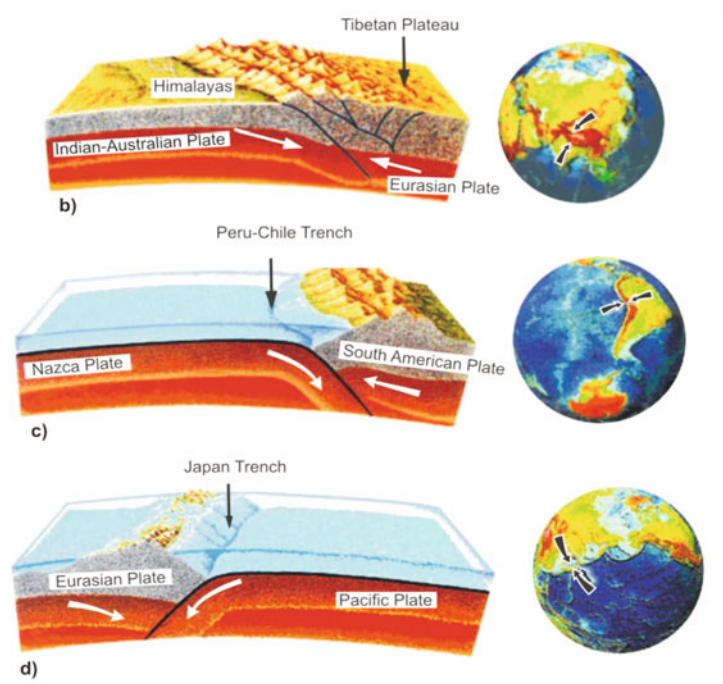

Figure 2.50. (a) Convergence between two continental blocks occurring between the Indian plate and the Eurasian plate (http://pubs.usgs.gov/publications/text/understanding.html). (b) The Eurasian plate overriding the Indian-Australian plate has created multiple thrusting and folding and double thickening of the continental crust giving rise to the Himalayan mountain chain. (c) Off the coast of South America along the Peru-Chile trench, the oceanic Nazca plate is pushing into and being subducted under the continental part of the South American plate. In turn, the overriding South American Plate is being lifted up, creating the towering Andes mountains. At this plate boundary shallow and deep focus earthquakes occur. (d) Subduction of an ocean plate beneath another ocean plate forms a volcanic island arc (Press and Siever, 2002).

(Fig.2.50 a-d) driven by convection currents in the upper mantle. The location of destructive plate margins is marked by volcanic arc on the overriding plate, which forms above the point at which partial melting commences. This type of margin is characterized by subduction, whereby one plate is thrust under the other due to collision of the plates. In this case, the crust either disappears or gets tapered. An example is when the Indian plate collided with the Asian (Eurasian) plate, the sediments in the Tethys sea lying between the plates eventually crushed into lofty mountain ranges to form the Himalayas (Fig. 2.50). Earthquakes produced in the subduction zones worldwide have hypocentral depths going to deeper levels to a few hundred kilometres.

The second type of constructive plate margin is the accreting divergent plate margin formed due to the plates moving away from each other (Fig. 2.51a, b) in more or less opposite directions. As the plates are pulled apart, the buoyant magmatic material from the mantle rises upward, thus constantly adding a new material to the existing one. Mid-ocean ridges or the mountains under the seas are formed at such margins. Mid-Atlantic ridge, Indian ocean ridge, Carlsberg ridge, etc. are some of the well known examples of this type of tectonic activity. Earthquake sources under the regions of such ridges have shallow focal depths within ~50 km.

The third kind of plate margin is of the translational type (Fig. 2.52a, b) and is commonly referred to as a conservative plate margin. This is so because

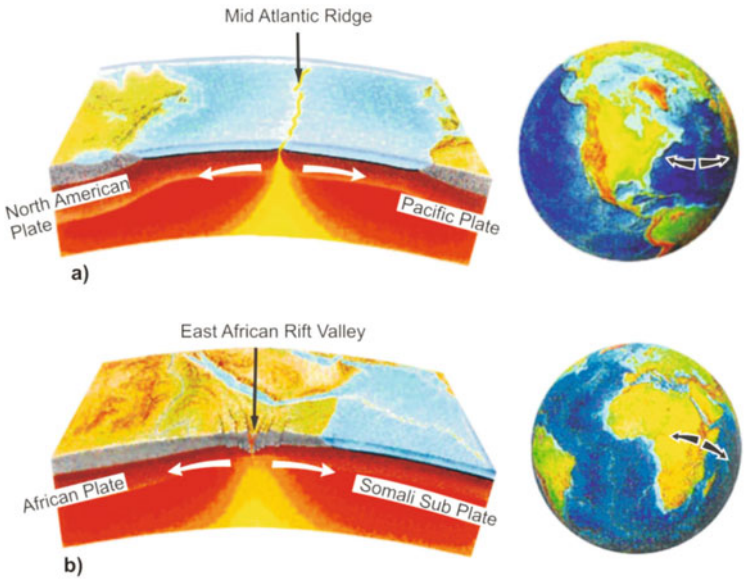

Figure 2.51. (a) Rifting and seafloor spreading along the mid-Atlantic ridge have created a mid-ocean volcanic mountain chain and a coincident earthquake belt. (b) Initiation of rifting and plate separation within a continent. Characteristic features are rift valleys, with multiple normal faults, volcanism and earthquakes (Press and Siever, 2002).

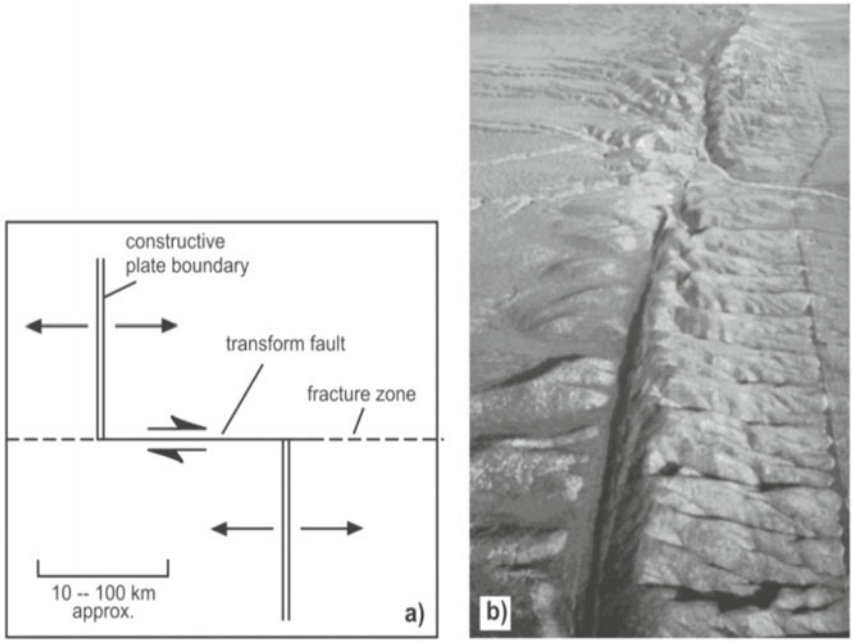

Figure 2.52. (a) A conservative plate margin, which in this case has a transform fault offsetting a constructive plate margin. (b) A section of the San Andreas translational fault (http://pubs.usgs.gov/publications/text/understanding.html).

here two plates glide or graze past each other without creating or destroying crustal material. Since no new crust is produced at this type of continental margin, it can be described as amagmatic. Conservative plate boundaries typically are formed in oceanic settings, and cause constructive plate margins to be offset by tens to hundreds of kilometres along strike-slip (transform) faults (Fig. 2.52a). The San Andreas fault in the western USA, which causes frequent earthquakes, is a prominent example of this phenomenon. It is at this kind of plate margin, and at the consuming (convergent) plate margins, that earthquakes occur more in number and magnitude. At the convergent plate margin, two huge blocks bump into each other in a head-on collision. The brute force with which they collide generates shock waves all round; somewhat similar is the case at the translational plate margin.

When two plates slide past each other, a lot of energy is generated because of friction. The enormous sliding frictional force locks up the plates temporarily in their position, thereby building up large elastic strain at the contact area. Eventually, the competence of the plate material gets exceeded by the progressively increasing stress, which results in the snapping or rupture of the faulted segments releasing the accumulated strain energy in the form of earthquake. After the stress drop (earthquake occurrence), the sliding plates resume their normal motion and prepare for the next cycle of seismotectonics.

There is also some evidence on vertical thermal plumes originating in the mantle, which may impinge vertical force on lithospheric plates giving rise to hot spot activity, rifting and fragmentation of plates.

Thus, the interior of the Earth as well as its surface houses a plethora of mysteries. The information of what lies far off in space is ample, but are quite unaware about the happenings beneath us. The knowledge of what actually goes on in the depths of the core and mantle that causes earthquakes and magnetic field changes, is still eluding us. Why does the EMF change directions from normal or reverse? As of today, nobody has a perfect clue to these processes, although it is generally agreed that magnetic reversals are the results of changing patterns of convection motions in the Earth's outer core (Fig. 2.49). Hence, the least known is that the CMB dynamics are somehow responsible for changes in EMF. This field is not just confined to the surface of the Earth, but extends far into space. How far and in what way is discussed in the next chapter.

APPENDIX 2.1

Magnetic Properties of Minerals

Metals and Alloys

Mineral	*Composition*	*Magnetic type*	*Curie temperature T_C (°C)*	σ_s *(Am^2/kg)*
Iron	Fe	Ferromagnetic	770	218
Nickel	Ni	Ferromagnetic	358	55
Cobalt	Co	Ferromagnetic	1131	161
Awaruite	Ni_3Fe	Ferromagnetic	620	120
Wairauite	CoFe	Ferromagnetic	986	235

Oxides

Mineral	*Composition*	*Magnetic type*	*Curie temperature T_C (°C)*	σ_s *(Am^2/kg)*
Magnetite	Fe_3O_4	Ferrimagnetic	575-585	90-92
Ulvospinel	Fe_2TiO_2	Anti Ferromagnetic	-153	
Hematite	∝-Fe_2O_3	Canted Antiferromagnetic	675	0.4
Ilmenite	$FeTiO_2$	Antiferromagnetic	-233	
Maghemite	ϒ-Fe_2O_3	Ferrimagnetic	~600	~80
Jacobsite	$MnFe_2O_4$	Ferrimagnetic	300	77
Trevorite	$NiFe_2O_4$	Ferrimagnetic	585	51
Magnesioferrite	$MgFe_2O_4$	Ferrimagnetic	440	21

Sulphides

Mineral	*Composition*	*Magnetic type*	*Curie temperature T_C (°C)*	σ_s *(Am^2/kg)*
Pyrrhotite	Fe_7S_8	Ferrimagnetic	320	~20
Greigite	Fe_3S_4	Ferrimagnetic	~333	~25
Troilite	FeS	Anti Ferromagnetic	305	

Oxyhydroxides

Mineral	*Composition*	*Magnetic type*	*Curie temperature T_C (°C)*	σ_s *(Am^2/kg)*
Goethite	∝-FeOOH	Antiferromagnetic, Weak ferromagnetic	~120	<1
Lepidocrocite	γ-FeOOH	Antiferromagnetic	-196	
Feroxyhyte	δ-FeOOH	Ferrimagnetic	~180	<10

σ_s = Saturation magnetization at room temperature
(http://www.irm.umn.edu/hg2m_index.html)

APPENDIX 2.2

Time Line of Reversals

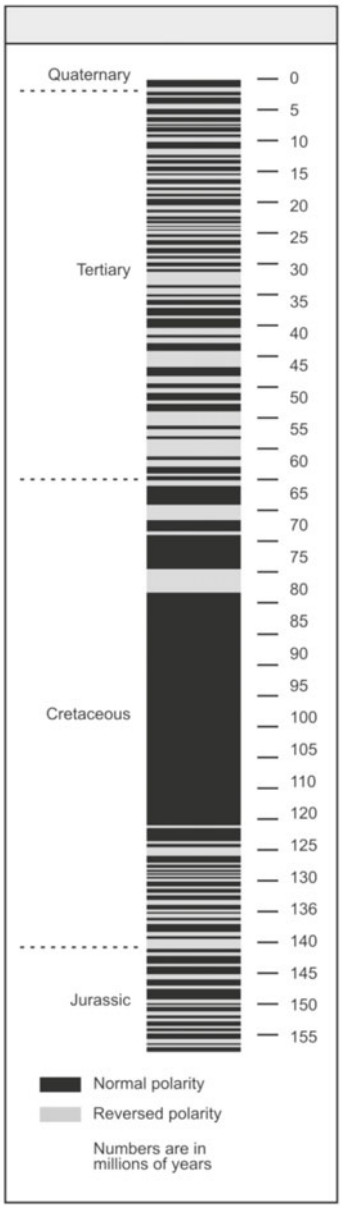

(http://www.pbs.org/wgbh/nova/magnetic/timeline.html)

APPENDIX 2.3

Migration of Pole and Its Anticipated Position in 2050

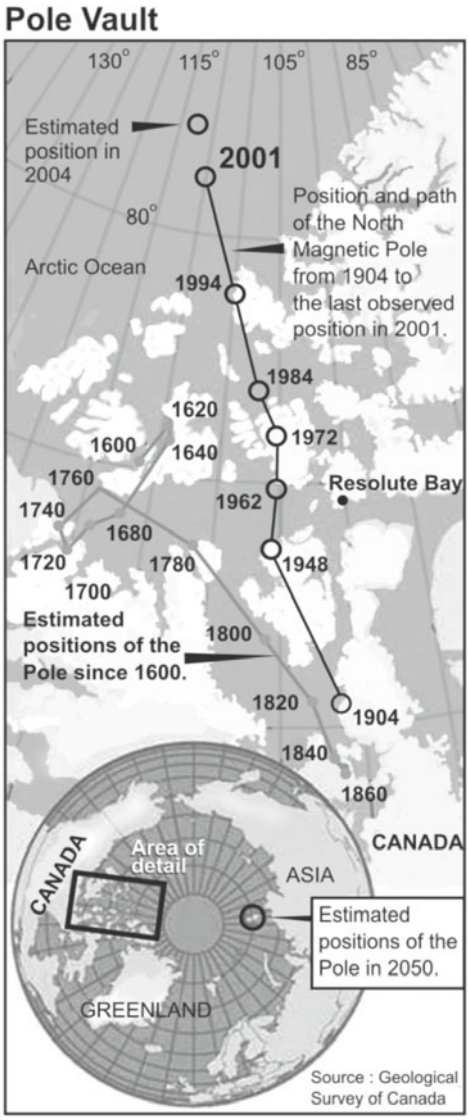

3

MAGNETIC FIELD THAT EXTENDS INTO SPACE

The advent of balloons, rockets, satellites and space probes is of great help in exploring external magnetic field and aeronomic changes. This study requires sophistication achieved by USA, Russia, and European community. The contribution by India is limited to the analyses and studies of these procured satellite and space data. The geomagnetic surface data alone provide no clue, unless the process of solar wind and solar plasma stream interactions with the geomagnetic field are better understood and modelled. The cause in the form of solar wind interaction produces various effects such as ring current, charged particle diffusion, scattering and final precipitation in the auroral zone. Simple Ohm's law and Ampere's law are at work in the production of various currents and geomagnetic field changes on the global scale. The morphological changes in the geomagnetic field play an important role in generating micropulsations and accelerating charged particles by annihilating magnetic field at the X-type neutral point in the geomagnetic tail.

Significant insight into the nature of changing geomagnetic field has been obtained only during the course of the early twentieth century, after the advent of the satellite era. While the major part of EMF emanates from within (the main field), a small but potentially significant fraction (~1 to 2 per cent) has its origin external to the Earth (the variation field), with the Sun as the main source. Even as one is separated by ~150 million kilometres from it, continuous changes in the thermal and magnetic state of the Sun are manifested in the EMF variations down to fluctuations of even very small magnitude. At the same time, observed variations of the surface magnetic field serve as a very useful diagnostic tool for deciphering the transformation processes that occur in the vast open space 'between the Sun and Earth'. Currents flowing in the ionospheric E-layer result in transient variations of magnetic field that are fairly smooth. In contrast, rapid and irregular variations are usually produced by charged particles of

solar origin. Geomagnetic field variations covering a wide range of frequencies are also very useful in understanding the physical and chemical properties of the interior of the Earth at different depths and provide clues to the locations of nonrenewable resources (chapters 2 and 6).

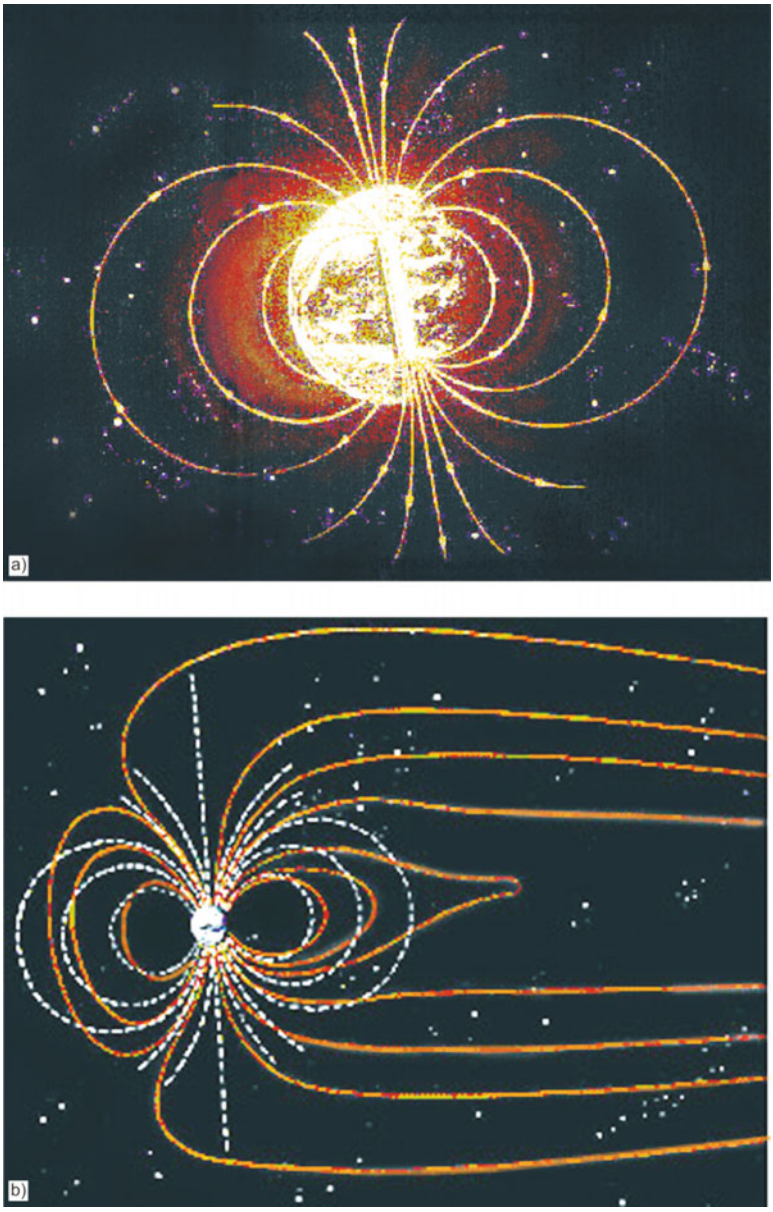

Figure 3.1. (a) Ideally the magnetic field of the Earth defines symmetry. (b) Earth's magnetic field is roughly that of a bar magnet but the solar wind tends to contract from one side (http://www-istp.gsfc.nasa.gov/Education/Imagnet.html).

The lines of force of the dipole (main field) component of EMF leave the Earth from its southern end to rejoin the globe at the northern defining symmetry (Fig. 3.1). This sphere along with the magnetic lines of force can be cut along its axial plane into two identical halves. However, in reality, this is not the case. The magnetic field lines are contracted from one side (Fig. 3.2) and the opposite side is stretched. The symmetry is lost because of the Sun. Of all the celestial bodies, Sun is the sole source of light and energy that supports and sustains life on Earth. However, if the EMF was not in its place, the Sun and other celestial bodies would (probably) have extinguished the flames of life. Sun emits visible and ultraviolet light, X-rays and charged particles, which have deleterious effects on life. Magnetic field lines that flank the Earth deflect the charged particles. This chapter focuses on the historical note of rocket-borne–balloon experiments, aeronomy, ionospheric-magnetospheric interaction, equatorial magnetic field and its solar-lunar characters, solar-interplanetary parameters and their association with low latitude geomagnetic field variations, electrojet-counter electrojet studies and low latitude scintillations/micro-pulsations/airglow.

3.1 STRUCTURE OF THE EARTH'S ATMOSPHERE: TRADITIONAL VIEW

The invention of mercury barometer (Fig. 3.2) by Torricelli and Viviani led to the discovery of finite weight of air, which was fourteen and seven tenths pound/sq inch. It also later became known that temperature changes with height.

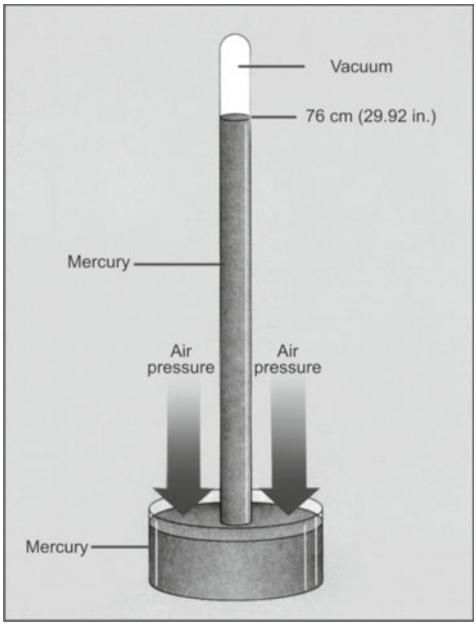

Figure 3.2. The mercury barometer (Tarbuck and Lutgens, 1994).

But there isn't any definite boundary to the atmosphere. It is transient, which fades off gradually into far-off space.

To reach physically to a height of more than few kilometres is impossible. In 1749, Wilson used a kite attached with thermometers to measure atmospheric temperatures at different altitudes. The first balloon was launched in 1782 by two French brothers Michel and Montgolfier. Three men reached an elevation of 10 km, but only one, Tissandier survived. By 1892, however, unmanned balloons with instruments went higher and came back with the data on pressure and temperature conditions which revealed temperature dropped in the first few miles in the sky. It was –55°C at 11 km, above which the temperature increased slightly.

Traditionally, the Earth's atmosphere has been studied by dividing it into various regions based on temperature profiles, conductivity or electron density (Fig. 3.3a). Each region is studied in isolation as far as the electrodynamical processes are concerned. In initial years, it was thought that atmosphere had two layers. Bort in 1908 named these two layers as troposphere and stratosphere (Fig. 3.3b).

Troposphere: In Greek, troposphere means 'the sphere of change', and is the most turbulent. It extends from the Earth's surface to ~10 km. Stratosphere means 'sphere of layers' and contains sublayers of lighter gases such as helium

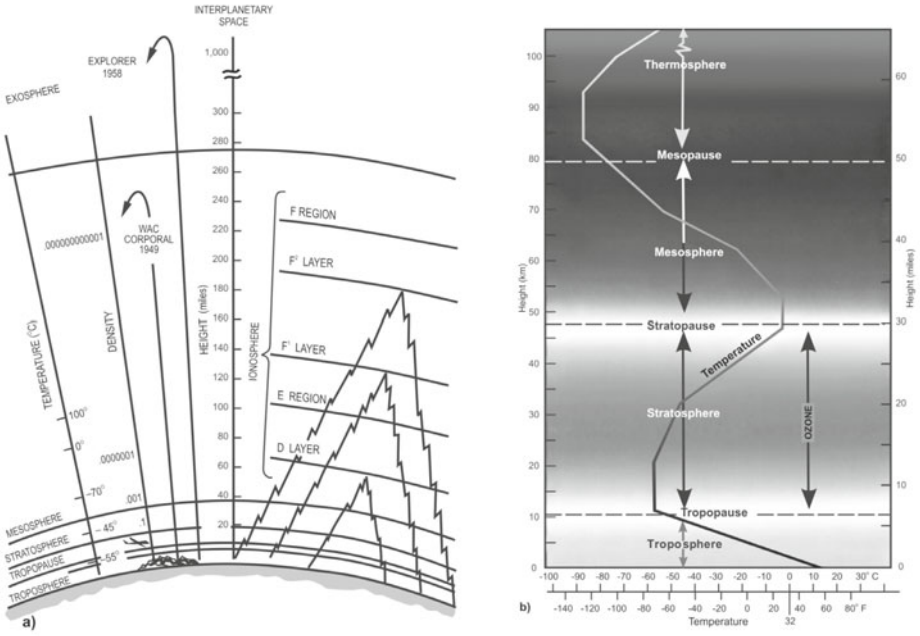

Figure 3.3. (a) Different layers of atmosphere, with their temperature and density profile (Asimov, 1979). 1 mile = 1.6 km. (b) Different layers of atmosphere with their temperature profile.

and hydrogen. Sandwiched between troposphere and stratosphere is 'tropopause' meaning 'end of change'. This was so-named because here the temperature drops from an average of 20°C on the Earth's surface to –60°C at the tropopause, whose height varies from ~16 km above msl at the equator to just ~8 km over the poles.

Stratosphere: It starts from above the tropopause (~10 km) and extends up to stratopause (~50 km), where the temperature profile attains the maximum value (Fig. 3.3b). Galactic cosmic rays are the prime source of ionization in this region. The conductivity, which is roughly of the order of 10^{-14} S/m at the Earth's surface, increases exponentially with altitude in the troposphere-stratosphere region; the main charge carriers being the small positive and negative ions.

Ten kilometres is the upper limit beyond which man cannot survive without oxygen. Hence, sealed cabins were designed, in which pressure and temperature at the Earth's surface was maintained, helping to touch the stratosphere. In 1931, Auguste and Felix reached a height of 18 km with the help of sealed cabins. Later, lighter and plastic balloons enabled man to go even higher and helped prolong his stay up there. A balloon named Explorer I went up to 21 km in 1938. By 1960, however, manned balloons had gone as high as 34 km and unmanned balloons almost to 46 km.

Rockets utility in space research: With the scaling of newer and higher altitudes, the impermanency of constant temperature established itself. The atmosphere above stratosphere was penetrated by rockets. The primitive form of rocket was used by Chinese in the thirteenth century as a means to frighten away the enemy. But, it was Tipu Sultan, who was the first to design and develop rockets in Srirangapatna (Karnataka) for their use during the Mysore wars waged against the British.

The World War II witnessed American 'Bazooka' and the Soviet 'Katusha', which were basically rocket-propelled packets of explosives. But, the use of rockets was not meant for just destructive purposes. At the fag end of the twentieth century, an idea occurred independently to Tsiolkovsky and Goddard, wherein they proposed the use of rockets to explore upper atmosphere and space. The publications of these two launched an era of space research. Telemetering was also a great help in this endeavour.

Telemetering: Telemetering measures a particular component like temperature or pressure from a 'distance'. For instance, it measures temperature in an electrical impulse, which is transmitted back to the Earth's surface, where it is 'translated' and then quantified. Molchanoff was the first to send the telemeter to atmosphere enclosed in a balloon.

Mesosphere: By the potent combination of rockets and telemetering, it was seen for the first time that above stratosphere at a height of ~48 km, the temperature rose to a maximum of –10°C. It then again dropped to a low of –90°C at 80 km height. Sydney Chapman coined the term 'mesosphere' in

1950 for this region, which witnessed the rise and fall in temperature. The major sources of ionization in the mesosphere are the solar Layman-alpha radiation, X-ray radiation and the intense auroral particle precipitation. The conductivity increases sharply in this region. The main charge carriers are electrons, positive ions (e.g. N_2^+, O_2^+, NO^+) and the negative ions (e.g. O_2^-).

Thermosphere: This is the outermost region of the Earth's atmosphere. It extends from a height of 80 km to the outer edge of the atmosphere at ~400 km above the Earth's surface. Since it receives energy directly from the Sun, the temperature in it rises from –95°C to ~400°C. Although the air is very thin, the scattering of air atoms steadily increases in temperature to ~1000°C at 480 km and above. Hence, this region is called 'thermosphere', i.e. 'the sphere of heat'. Above 480 km lies 'exosphere' which extends to as high as 1600 km and gradually merges into interplanetary space. Spitzer coined the term 'exosphere' in 1949.

Ionosphere: On account of low air pressure, the UV rays and X-rays coming from the Sun cause heavy ionization in this region. In other words, the ionosphere, which starts from the top layers of mesosphere, overlaps the thermosphere from 60 to ~500 km above the Earth's surface. The D-region of the ionosphere extends from ~60 to 90 km. The ionosphere proper (e.g. E and F regions) starts from above the mesosphere, and extends to ~500 km. The major sources of ionization in the ionosphere are EUV and X-ray radiation from the Sun and energetic particle precipitation from the magnetosphere into the auroral ionosphere. The current carriers are electrons and positive ions like NO^+, O_2^+ and O^+. Electrical conductivity becomes anisotropic in this region with parallel conductivity (with respect to geomagnetic field) exceeding the transverse conductivities by several orders of magnitude.

Svante August Arrhenius's genius: Arrhenius suggested that 'ions' were charged atoms to explain the behaviour of certain solutions that conducted electric current. He advanced this notion through his doctoral thesis in 1884. But his idea of charged atoms was revolutionary since many were unaware of charged particles residing within an atom. The electron was discovered in 1890, which made phenomenal sense of Arrhenius's doctoral thesis and was awarded the Nobel Prize in chemistry in 1903.

The discovery of ions in atmosphere came much later, made possible mainly by experimental endeavours carried by Marconi with the wireless. Marconi on 12 Dec 1901 sent signals (Morse code) from Cornwall, England to Newfoundland, Canada across the Atlantic ocean covering a distance of ~2900 km. The passage of the signal across the two cities baffled those who know that radio waves travel only in a straight line. But the distance from Cornwall and Newfoundland formed a curvature. The travel of radio waves in a curved manner became an enigma for all scientists of the day. Just a year after the Marconi's experiment, in 1902, Heaviside and Kennelly suggested a layer of charged particles situated high up in the atmosphere reflected the radio waves.

This layer was located in 1920, which has since been called the 'Kennelly-Heaviside layer'.

Discovery of Kennelly-Heaviside layer: Appleton discovered the Kennelly-Heaviside layer, which reflected back radio waves. Appleton wondered on the fading of the signal. Musing over it, he decided the fading occurred because of interference of two versions of the same signal. He reckoned that if the fading was to occur, there has to be a signal, which directly hit the receiver that was released from a transmitter and the other reached the receiver via a circuitous route by reflection from upper atmosphere. This second wave was a delayed one and so was out of phase with the first one. They thus interfere with each other partly canceling each other out causing the fading out of the signal.

Appleton located this reflecting layer by sending signals of a particular wavelength, and found to be at 104 km. Appleton also noticed the radio signals generally faded during night. He reckoned that shortly before dawn, radio waves are not reflected by the Kennelly-Heaviside layer but are reflected back from still higher layers, which begin at 224 km height. These are called the 'Appleton layers', an honour as magnificent as the Noble Prize (physics) awarded to Appleton in 1947 for these stupendous discoveries.

Ionospheric layers and space communication: Watson-Watt introduced the term 'ionosphere' in 1930 (Fig. 3.3a). The electron density in the ionosphere is especially very high in the region extending from 90 to 150 km. It is called the Kennelly-Heaviside layer (D-layer) and above which at a height of 224 km is the E-region. Another region in which electron density is very high extends from ~250 to 350 km and is called Appleton layers (F-layers) – the F_1 layer at 224 km and F_2 layer at 320 km. F_1-layer is the richest in ions, while F_2-layer is significantly stronger only during the daytime. The ionosphere reflects radio waves ranging in frequency from 2 to 30 MHz. Hence, it plays an important role in space communication. Electromagnetic waves of frequencies higher than 30 MHz penetrate through the ionosphere.

Ionosondes: Most of the data on space communication have come from ionosondes. For each concentration of electron densities, there is a plasma frequency below which all radio signals are refracted back to Earth regardless of the angle of incidence used. If the plasma frequency of the ionosphere is 5 MHz, then all radio signals transmitted vertically to the ionosphere that are <5 MHz return back to the Earth and all frequencies >5 MHz pass through the ionosphere into space. It is this characteristic of the ionosphere that is exploited to probe its properties through the ionosonde. An ionosonde is a device which combines a radio transmitter and receiver capable of transmitting pulses toward and above the ionosphere and receiving the same signal pulse as it returns back to the receiver. The pulsed ionosonde works by transmitting a series of pulses vertically upwards into the ionosphere, whereas the digisonde is highly sophisticated pulse amplitude sounder. The ionosphere is also studied through the chirp and oblique sounding methods.

3.2 STRUCTURE OF THE SUN: ASSOCIATION OF SUNSPOTS WITH TERRESTRIAL PHENOMENA

The Sun (Fig. 3.4) is the brightest star visible from Earth having surface temperatures close to 6000°C with a magnetic field strength of 0.1 to 0.2 nT. The Sun is entirely gaseous—a glowing ball of mainly incandescent hydrogen. Other elements all in gaseous state are ~10 part hydrogen to 1 part helium with a pinch of other elements like oxygen, carbon, nitrogen, magnesium and iron. The mass of the Sun is ~2×10^{30} kg. The density of the Sun at photosphere is ~140 kg/m^3, the density increases as one goes inwards to the core or the centre of the Sun, where the density is ~16000 kg/m^3 or 10 times that of ordinary metal.

Sunspot formation and magnetic fields: Magnetic fields play a great role on the Sun's photosphere. When solar material over a small area gets highly magnetized, a significant part of its thermal energy is converted into magnetic field energy and its temperature falls to ~4000 K from its initial value of ~6000 K. That is a sunspot (Fig. 3.4), an area of intense magnetic field, less bright than the surrounding area and therefore relatively dark. Sunspots greatly influence the electromagnetic state of the Earth.

The first features observed on Sun's surface are credited to Galileo, Scheiner and Fabricius. They observed the sunspots, which were first reported in 1609. The observation of the sunspots was aided by the invention of telescope designed

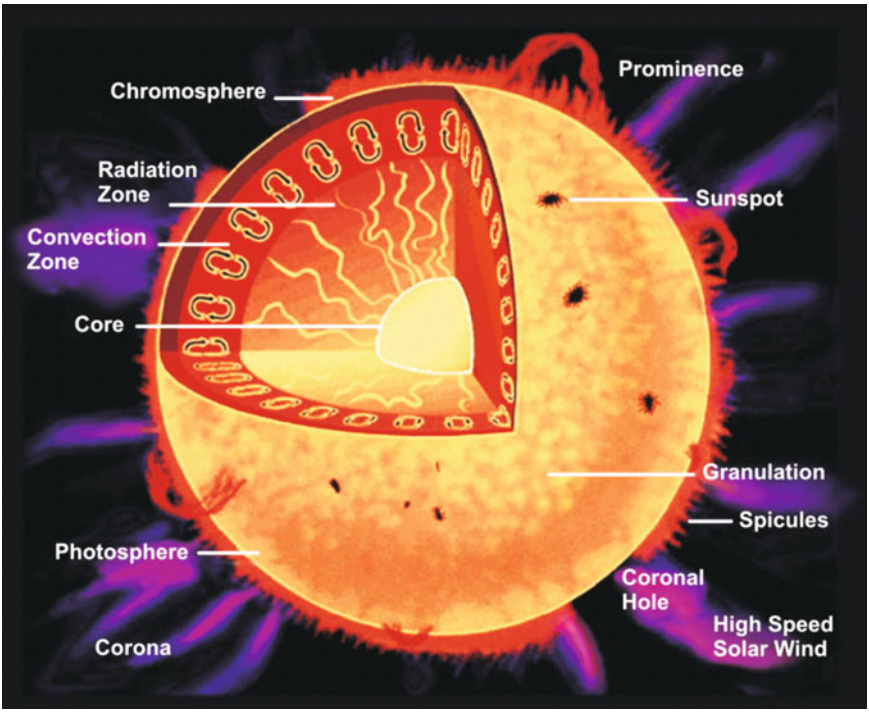

Figure 3.4. Different features associated with the Sun.

by Galileo. Scheiner later invented a safe method to project the Sun's image on a screen, so that it did not pose any threat to health. However, large sunspots are seen even with a naked eye. The initial enthusiasm for observing sunspots waned after 1645 because the sunspots disappeared completely for almost 70 years when Sun-gazers lost interest and went on to explore other phenomena.

Heinrich Schwabe perseverance: Schwabe was interested in spotting an unknown planet of the Sun. He tracked the planet that could be detected as a dark spot while passing against the bright background of the Sun. He maintained a strict vigil and kept a record of all the dark patches on the Sun. He observed the Sun for 17 years. Although he did not find the elusive planet, with the compiled observations that were at his disposal, he discerned a regular pattern in the appearance and disappearance of sunspots.

He published his findings in an article entitled 'solar observations during 1843'. Schwabe, however, found very few takers and none shared his excitement except Wolf, who was greatly impressed by his systematic observations. Some of Schwabe's excitement rubbed off on Wolf, who himself started looking out for sunspots. He collected all available sunspot data to devise the 'Zurich sunspot number' a statistical measure that gave the 11-year sunspot cycle.

The turning point came when Humboldt laid his eyes on Schwabe's article and included an updated version of the same writeup in his 'Kosmos'. This proved to be a great impetus. It acted as a catalyst and inspired many researchers to revive their interest in this neglected phenomenon. One such celebrated researcher was Carrington. His book 'observation of the spots of the Sun' published in 1863 contained observations from 1853 to 1861. Carrington on 1 Sept 1859 saw two patches of intensely bright and white light break out on the Sun. The patches grew in brightness that later faded out completely. What Carrington had seen was a solar flare, which are the great bursts of flaming hydrogen and these affect the Earth, the first inclination of which came to Carrington himself. After no more than 17 hours from the solar flare of 1 Sept 1859, Earth was bathed in a magnetic storm. '*This magnetic storm was recorded at all the Indian magnetic observatories that were in operation and the data are now used by national and international scientists to arrive at the intensity of the solar flare of 1 Sept 1859*'. The aurora produced by this storm was seen as far away as Cuba. Generally the aurora is only visible in the nearby polar region. Sabine also found an association between the sunspot cycle and occurrence of large magnetic storms. Sabine identified the source of magnetic storms with activity on the Sun.

Sunspot spectrum: Hale discovered the most prominent feature from the point of view of studies on magnetism in 1908. He deduced that the sunspots were greatly magnetic.

Newton in 1666 showed that light can be separated into a 'spectrum' of colours by passing a beam of light through a triangular-shaped prism of glass (Fig. 3.5), wherein it spreads out into a band made up of red, orange, yellow, green, blue, indigo and violet light.

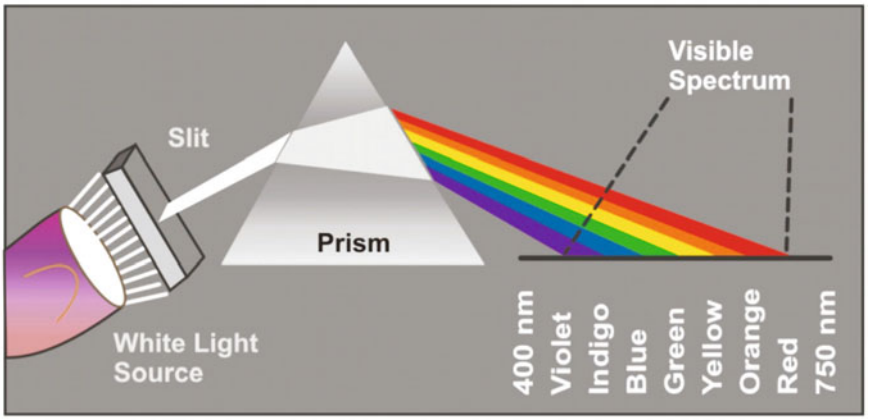

Figure 3.5. Newton showed that white light, on passing through a prism, split into 'rainbow' colours.

He also noticed that each colour faded gently into the other. By this experiment, Newton showed that sunlight (white light) is a mixture of many specific radiations. A prism separates (disperses) the colours because on passing from air into glass and from glass into air, light is bent or refracted, wherein each wavelength undergoes a different amount of refraction. The shorter the wavelength, the greater is the refraction. The short wavelengths of violet light are refracted the most, while the long wavelength of red light is refracted the least.

Utility of spectral lines: Angstrom identified hydrogen in the Sun in 1862 by the presence of spectral line characteristics of that element. Later, in 1868, Janssen while observing a total eclipse of the Sun in India sighted a spectral line that he could not identify with any known element. The line represented a new element, and so Lockyer named it helium from the Greek word for 'Sun'. Using this principle of spectral lines, a spectrograph was designed by Deslandres that produced photographic image of the Sun in a single spectral colour. However, in white light the Sun presented a dull appearance (Fig. 3.6a).

Spectroheliograph, an improvement over the spectrograph, invented by Hale, isolated light from higher layers in Sun's atmosphere and revealed many new features like the mottling of the surface, dark linear features and bright areas near sunspot (Fig. 3.6a-c).

Zeeman effect and sunspot magnetism: Hale and his collaborators found the first evidence of solar magnetic oscillation in their measurements of sunspot spectra. During these spectral studies, they discovered certain absorption lines in the spectra broadened and polarized. A strong similarity with absorption lines obtained in laboratory spectra of magnetized gases was also revealed. Zeeman, who in 1896 had discovered the 'Zeeman effect', studied such magnetized spectra. The Zeeman effect is one, where the spectral lines

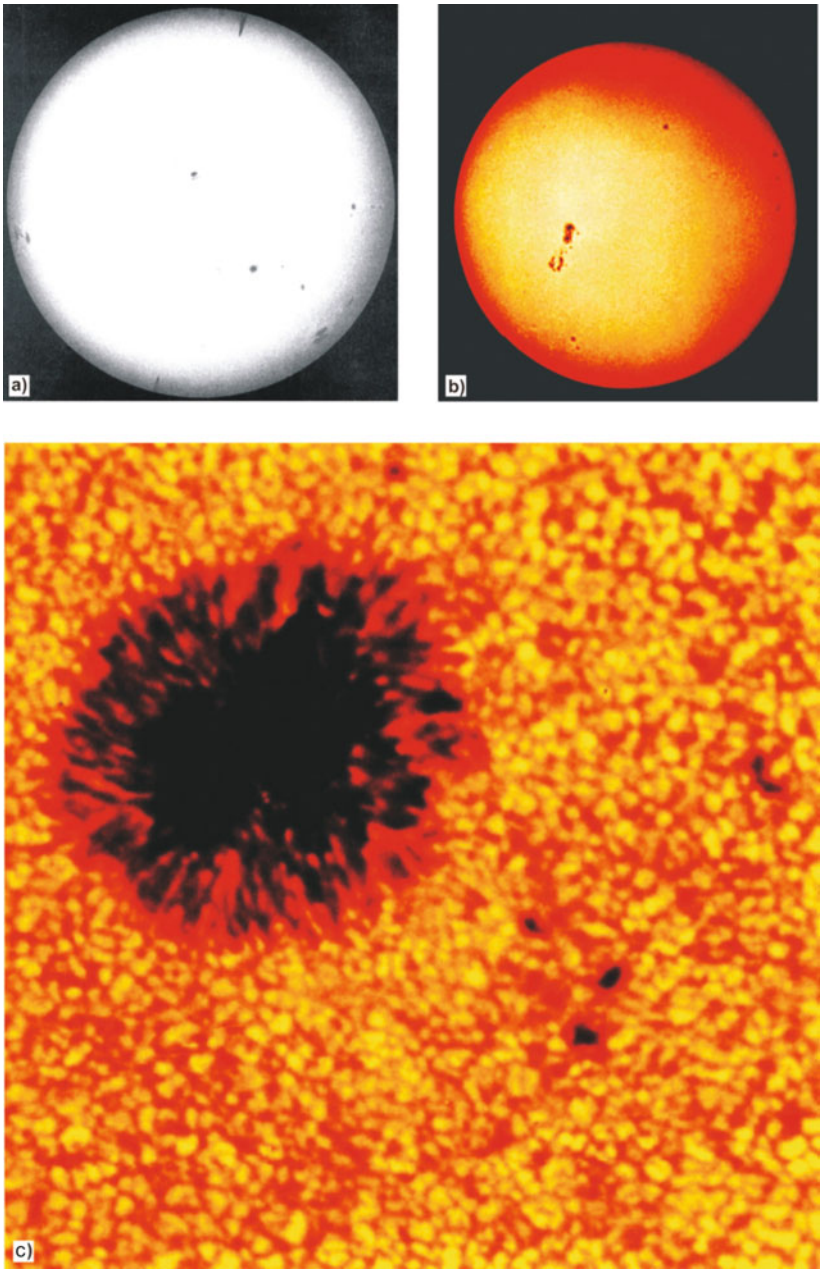

Figure 3.6. (a) A visible light photograph shows sunspots and bright areas called faculae, on the Sun's surface (http://www.eaas.co.uk/news/solar_features.html). (b) Sunspots seen over the surface of the Sun (Tarbuck and Lutgens, 1994). (c) Closer view of the 'sunspot' and the surrounding region. The fact that a magnetic field can occur in a hot, molten or gaseous body is a powerful argument in favour of the dynamo theory (Tarbuck and Lutgens, 1994).

(characteristic colours) of elements when emitted by a gas located in a magnetic field, split into two or more components of slightly different wavelengths. This separation is dependent on the intensity of the field as well. By analyzing this effect, Hale and his associates determined the strength of the magnetic field around sunspots to be between 100 and 400 nT, and also that these spots occurred in pairs that resembled giant magnetic dipoles oriented roughly parallel to solar equator. Hale's further studies enabled him to discern the so-called 11-year cycle to be actually the half of a 22-year solar magnetic cycle. During this 22-year cycle, sunspot groups reverse their polarity, wherein the switch occurred at minimum activity.

Hale's method of studying the magnetic field of sunspots and its adjoining areas were greatly refined by others like Babcock and Leighton, who used polarization of Zeeman lines and constructed a solar magnetograph. This enabled them to delineate an approximate dipole field of the Sun, which is of the order of 0.5 nT. Nevertheless, it was the confirmation of a long held view that the Sun has a magnetic field akin to that of the Earth. The Sun's magnetism is identified to extend to a substantial depth into its interior.

Variation in sunspot number and solar activity: The number of spots on the solar surface varies with time. Continuous observations for two centuries established sunspots reach a maximum number every 11.2 years on the average (Fig. 3.7a). Between, times of maxima, their number falls to a well defined minimum. During maximum of the sunspot cycle, more than 100 spots are seen on the Sun at a time. During sunspot cycle minima, very few spots are seen on the Sun. At the beginning, a few spots or group of spots appear at latitude of ±30° on the Sun. As the cycle progresses, the successive spots originate closer to the equator and by the end of the cycle they are ±5° away from the equator.

The sunspot number variation over the years 1601 to 1960 AD are computed by Waldmeier in 1961 (Fig. 3.7b). Notable highs in sunspot numbers are seen around 1725, 1780, 1840 and 1957. Since then, the highest activity seems to have occurred in 1990, in the current phase of high activity. In contrast to these notable highs in solar activity are extreme lows in activity. It was first pointed out by Spörer, Maunder and Clerke in 1890, 1894 and 1894 respectively (Table 3.1). This was confirmed by Eddy and Stuiver and Quay in 1976 and 1980

Table 3.1 Solar activity events and approximate period

Event	*Start*	*End*
Oort minimum	1040	1080
Medieval maximum	1100	1250
Wolf minimum	1280	1350
Spörer minimum	1450	1550
Maunder minimum	1645	1715
Dalton minimum	1790	1820
Modern maximum	1950	Ongoing

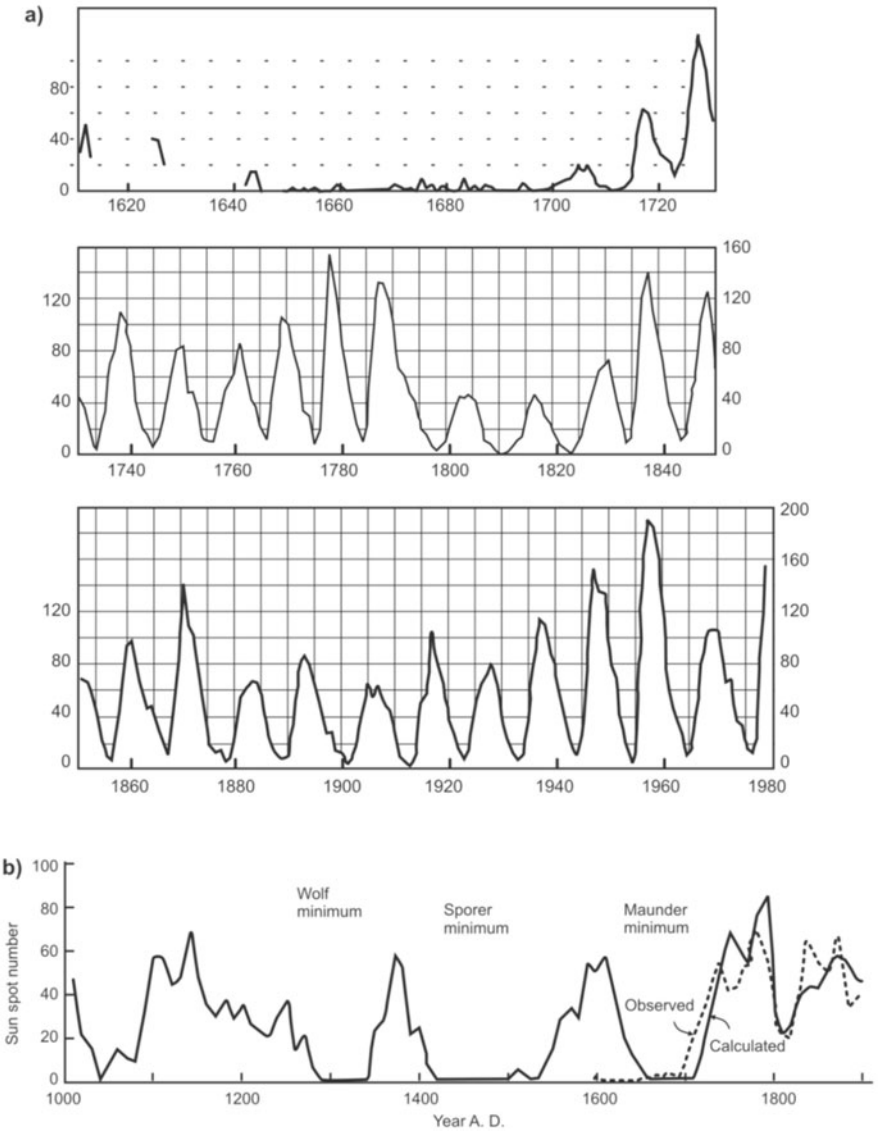

Figure 3.7. (a) Variation of the annual mean sunspot number from 1610 to 1700. The sunspots come and go on the Sun in an irregular cycle of ~11 years. (b) The Carbon-14 content in tree-rings is used to estimate the sunspot number of past centuries. The graphs for the period 1700-1900 AD show that the value calculated from ^{14}C content tally quite well with the actual values observed. This graph suggests three defined periods of very low solar activity ~1300, 1500 and 1700 AD, which are called respectively the Wolf minimum, Sporer minimum, and the Maunder minimum (Stuiver and Quay, 1980).

respectively from the examination of Carbon-14 abundances in tree rings. The work of Stuvier and Quay shows clear periods of almost zero sunspot at ~1040, 1300, 1480 and 1680 (Fig. 3.7b). Eddy in 1977 using Carbon-14 technique extended the sunspot number back to over 7000 years. It is tentatively attributed that these epochs of low solar activity coincided with ice ages on the Earth.

Sun's magnetic field: A magnetohydrodynamic dynamo operating in the Sun is most likely responsible for producing solar magnetic cycle. This dynamo is of the flux-transport type, which involves processes pertaining to generation of toroidal fields by differential rotation called the Ω-effect, regeneration of poloidal fields called the α-effect, and flux transport by meridional circulation. Thus, they have two separate components, the poloidal and toroidal field. Poloidal is a dipole field, which permeates the entire Sun and is closely aligned with the rotational axis. At the surface, it is concealed by much stronger elements of the toroidal field. The toroidal field, on the other hand, is wound from the poloidal field by differential rotation at latitudes below ~35°, where they emerge from the solar surface and are then carried polewards. An important feature of solar magnetic field is that all flux is concentrated into flux tubes and that these flux tubes are helically twisted into flux ropes. These concepts are helpful in satisfactorily explaining the equatorward migrating sunspot belt and the poleward migrating diffused fields. Lennard Fisk published a new model of the Sun's magnetic field and is quite different from other models. He suggested the magnetic field lines look like a wild tornado (Fig. 3.8), wherein in the older models they look like the path water takes while coming from a lawn sprinkler. Fisk's model takes into account the fact that the gases at the Sun's equator rotate faster than the gas at the poles and the Sun's magnetic field is constantly expanding. However, many knotty issues still remain unresolved with regard to genesis of solar magnetic field.

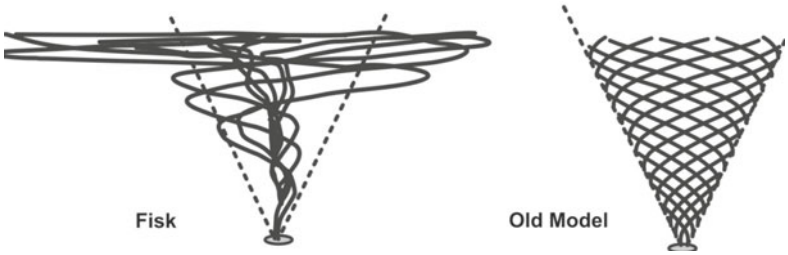

Figure 3.8. Comparison of Fisk's model to an older model (http://www.windows.ucar.edu/tour/link=/headline_universe/fisk.html).

Plasma is an ionized gas (deuterium or tritium which are isotopes of hydrogen) consisting of ions and electrons moving freely. It is found between stars and planets, where it takes the form of the solar wind. The Sun's atmosphere is overwhelmingly composed of such plasma. High temperatures reside at the

surface of the Sun and its interior and because the gas is hotter at the Sun, its atoms get converted to ion. When this ion recombines with an electron, it reverts back again to being an atom. At lower temperatures, especially at Earth's atmospheric levels, this recombining phenomenon is possible because of which there are changes in ionospheric heights. However, the chances for an ion to revert back to its atomic state are slim in solar environment.

The plasma temperature in different layers of solar atmosphere like the chromosphere, corona and solar wind (Fig. 3.4) is above millions of degrees wherein the temperatures are even more than that observed at photosphere—the layer that forms the Sun's visible surface. These hot layers of the Sun are responsible for its highly variable emissions of X-rays and of extreme ultraviolet radiation (EUV) or the wavelengths between ~100 and 1000 Angstrom units (1 Å=10^{-10} m). The chromosphere also emits a substantial fraction of the Sun's UV radiation at wavelengths between ~1600 and 3200 Å. The solar wind seems to originate from areas of corona.

Auroras: High energy particles and intense electromagnetic radiations from the Sun impinge on the Earth's upper atmosphere and produce beautiful optical displays known as aurora, which are recorded at MOs by significant changes in the geomagnetic field components. The auroras observed at northern (aurora borealis) as well as southern (aurora australis) polar regions are an absolutely magnificent display of light with brightness and incredible splendour. Figure 3.9 shows the aurora observed over Indian Antarctic station Maitri. Auroral displays are reported as far back as 1759 and credited to Canton. The aurora, however, does not occur exactly over the magnetic pole, but tends to maintain a constant distance of ~2000 to 3000 km from the respective magnetic pole.

The connection of auroral displays with the EMF was first noted by Celsius in 1741. The light that descended down from atmosphere seemed to follow the EMF. Birkeland in 1896 thought these auroras emanated by fast moving electrons that hit the higher altitudes of atmosphere. He resolved to have an experimental evidence for his reasoning. So he constructed a 'terrella', a miniature model of the Earth. He kept this terrella inside a glass vacuum chamber and directed an electron beam towards it. It travelled along the magnetic field lines right up to the poles of the terrella. By the close of nineteenth century, realization had dawned on the cognoscenti that auroral lights were associated with solar activity. Birkeland guessed that they originated in beams of electrons emitted from the Sun. In practical terms, he seemed to mean magnetic storms occurred when there was a solar flare. The flare spewed out charged particles and sent them hurtling towards the Earth. Birkeland, however, was wrong on this count. Later research proved it is not just the beams of electrons that are emitted from Sun, but there is something 'more and continuous' that is being given out, which Chapman showed are the charged particles.

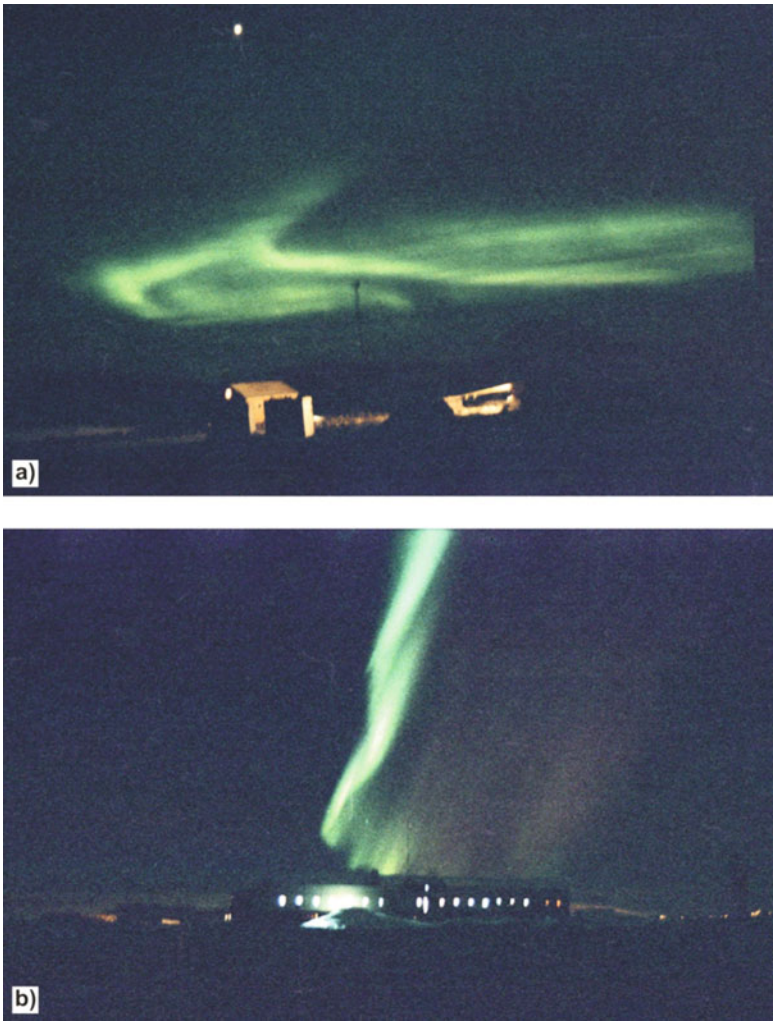

Figure 3.9. Pictures of (a) bright and (b) curtain auroras observed at Indian station Maitri at Antarctica on 19 June 2003 (photo: Hanchinal).

Detection of solar wind and realisation of magnetosphere: Chapman in 1931, while studying the Sun's corona was greatly impressed by its geographical extent. He tended to consider the charged particles that swarmed over the Earth were in fact part of the corona. He visualized either the Earth was moving around the Sun in very close proximity of its atmosphere or that the corona expanded outwards continually. If the corona expanded incessantly then it had to be perpetually renewed and rejuvenated at the surface of the Sun. Thus, there would be continuous outflow of charged particles that streamed out of the Sun in all directions. They then disturbed the EMF as they passed close to it.

The veracity of the above supposition was reinforced by work carried out in 1950s by Biermann. It was felt that the cometary tails were formed by the pressure of light from Sun. The cometary tails, however, always point away from Sun and increase in length as they approach the Sun. Biermann showed that the light pressure alone was not responsible for producing cometary tails. There was something else which had to be stronger and of the nature such that it gave a 'push' to the cometary material to turn it into a tail. These were the charged particles emitted out from the Sun. Parker went a step further and announced his proclivity for a steady outflow of particles, with additional bursts at the time of solar flares. It was Parker himself who coined the term 'solar wind' in 1958 to explain this phenomenon (Fig. 3.10).

The world did not have to wait long for the confirmation of the solar wind. The Soviet satellites Lunik I and Lunik II demonstrated their presence in 1959 and 1960, respectively. The American planetary probe Mariner II also confirmed

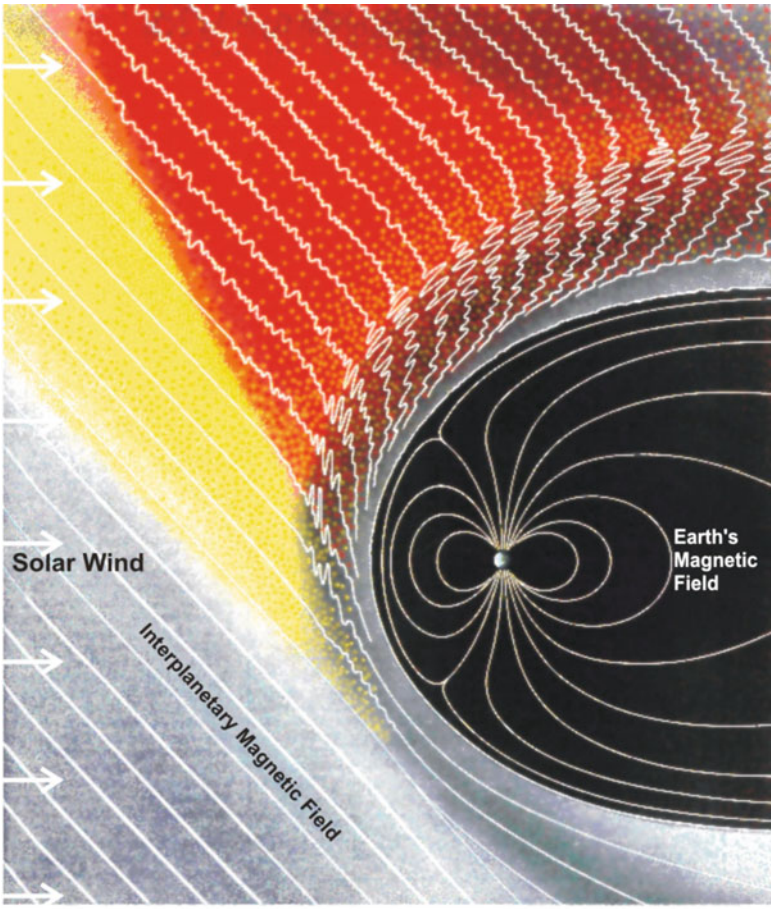

Figure 3.10. Solar wind and the interplanetary magnetic field (Sagdeev and Kennel, April 1991).

the presence of solar wind. This wind flows with a speed of as low as 260 km/sec and as fast as 750 km/sec, but typically its speed lies about 400 km/sec, whereas its density is more variable than the velocity, ranging from ~100 to 10^5 kg/m^3. Actually, it is the density fluctuations in the solar wind, which control the size of the magnetosphere. The solar wind carries magnetic field of ~5 nT that lies near the ecliptic plane in an Archimedean spiral pattern. The escape velocity of the solar wind is 625 km/sec from the surface of the Sun and because the pressure gradient falls off with radial distance more slowly than the gravitational force, the solar wind is accelerated to supersonic velocities. The solar wind is not confined to a small area, but fans out to a considerable extent in space. How far was the task given to man-made satellites to probe the levels of radiation in the topmost atmospheric layers and nearby space. They were also given the job of grading the intensity of cosmic rays beyond the atmospheric domain.

To probe the existence of charged particles, the satellites were fitted with Geiger counters, designed by Geiger in 1907, but later vastly improved and provided by Van Allen and his team. The instrument, in essence, counts the particles or the flux of radiation.

Van Allen radiation belts: The IGY was an exercise unparalleled in the history of scientific cooperation, where more than 70 nations joined the endeavour to study Earth— from within and outside. The IGY marked an 18-month period from July 1959 through Dec 1958 spanning the period of maximum sunspot activity.

The Soviets put Sputnik I that weighed 184 pounds into orbit on 4 Oct 1957. It carried with it instruments to determine and relay back to Earth, the data on pressure and temperature conditions prevalent in the atmosphere. They again sent another satellite Sputnik II into orbit on 3 Nov 1957. The US hastened its efforts and put its first satellite, Explorer I into orbit on 31 Jan 1958.

Sputnik I did not carry any Geiger counter, but Sputnik II did. It rose to a height of 1680 km. Vernov reported an increase in radiation rate between 500 and 700 km. This, as it turned out later, marked the fringes of radiation belt. However, the significance of this finding was lost on Vernov. Explorer I took to skies with a Geiger counter provided by Van Allen's team. According to Stoermer's theory, cosmic ray intensity was expected to increase with magnetic latitude. Its predicted counting rate was ~30 counts/sec. The counter detected almost the same concentrations of particles as predicted for heights below 600 km. But, at higher altitudes the count dropped. At certain heights, the count became almost zero. Explorer I had gone as high as 2520 km. The count reducing to zero would have been dismissed as an aberration with either the counter or the atmosphere, had the same pattern not been observed with Explorer III as well (Explorer II had failed to orbit). Sputnik III had also experienced the same phenomenon.

However Explorer III had carried with it a special tape recorder. Carl McIlwain, an associate of Van Allen had shown experimentally that very high particle fluxes would overwhelm the counter and consequently produce zero

counts. Van Allen and his colleagues reasoned that the count fell virtually to zero not because there was little or no radiation, but because there was too much. Hence, they fortified their old counters to handle heavy loads and launched them again into space with Explorer IV on 26 July 1958. This satellite reached the height of 2189 km and disclosed radiation intensity to be much higher than what the scientists had expected. Further, the 'Moon probes' Pioneer I and Pioneer III reached 112,000 km and 104,000 km respectively and showed two main bands of radiation. These radiation bands were named 'Van Allen radiation belts'. However, they were later renamed 'magnetosphere' by Tom Gold in line with the names given to other sections of space.

Christofilos effect: Explorer IV was launched on 26 July 1958 to know how far the magnetosphere extended, configuration of its structure, dynamical processes operative in the region and to explore the newly discovered radiation belt in greater detail. Also, under the project 'Argus', it was proposed to observe an artificial radiation belt produced by exploding nuclear bombs in the Van Allen region to release charged particles. This project was initiated to check the 'Christofilos effect' and to know whether the effect really occurs.

Christofilos studied independently the motion of charged particles in magnetic fields. He had predicted in 1957 the entrapment of charged particles along the magnetic lines of force and sent his calculations to 'experts'. However, nobody paid much heed to his erudition. It was only when they themselves arrived at the same results, they welcomed Christofilos into the California University. His idea about particle entrapment is now called 'Christofilos effect'. To check out this effect, the USA fired three rockets in Aug and Sept 1958 with nuclear bombs that were exploded into space at 480 km height.

After the explosions, the released charged particles spread out and were trapped along magnetic lines of force. The charged particles took a joy ride along the field lines and eventually ended up at polar regions to give rise to feeble auroral displays. They also had disrupted the radar for a short while.

3.3 STRUCTURE OF MAGNETOSPHERE

Gilbert proclaimed Earth to be a giant magnet and the notion of field lines forming symmetry was prevalent for a long time. This erroneous notion was abandoned once the satellite data started pouring down to Earth, especially the one sent by Explorer XIV and IMP I (interplanetary monitoring platform).

Unlike the atmosphere, the magnetosphere has a very sharp boundary (Fig. 3.11), which is called the magnetopause. The magnetosphere itself is caused by interaction of solar wind and the geomagnetic field. The solar wind is obstructed by EMF and finds it difficult to pierce through. But it is able to 'squash' it (Fig. 3.11). Thus, the observable result is the geomagnetic field on dayside compressed to a distance of 10 R_E. The opposite side of dayside, the nightside extends to ~1000 R_E and more, owing to pressure exerted by the solar wind.

Magnetosheath: The solar wind defines a direct link between Earth and Sun. The wind travels unhindered for millions of km and meets its first obstacle at the EMF, which deflects most of the tiny particles that make up its constituents. These deflected particles continue on their odyssey in a curved path called the 'bow shock' (Fig. 3.11). The particles cling along the field lines and gyrate

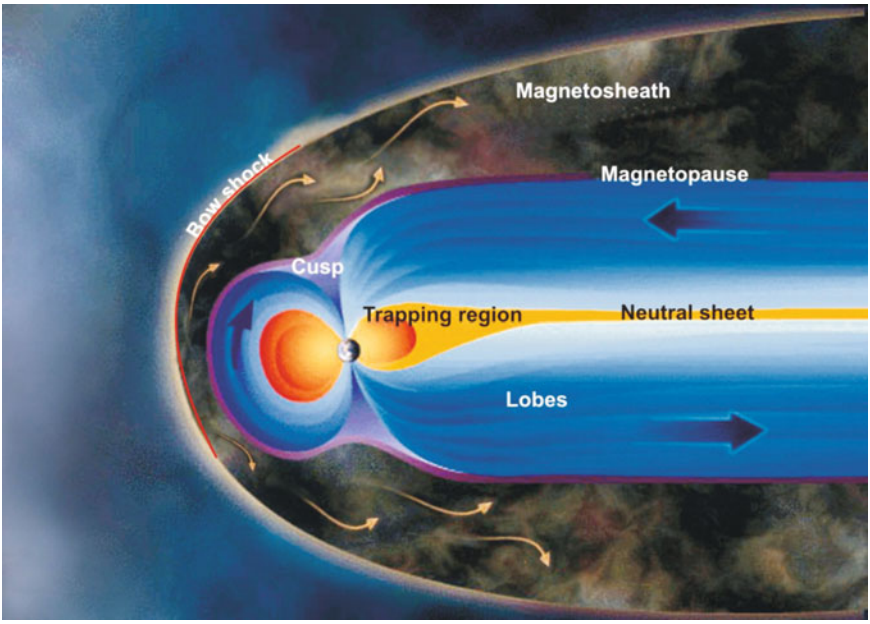

Figure 3.11. The expansive magnetosphere (http://www.windows.ucar.edu/tour/link=/earth/images/earth_magneto_gif_image.html&cdp)=/windows3.html&frp=/windows3.html).

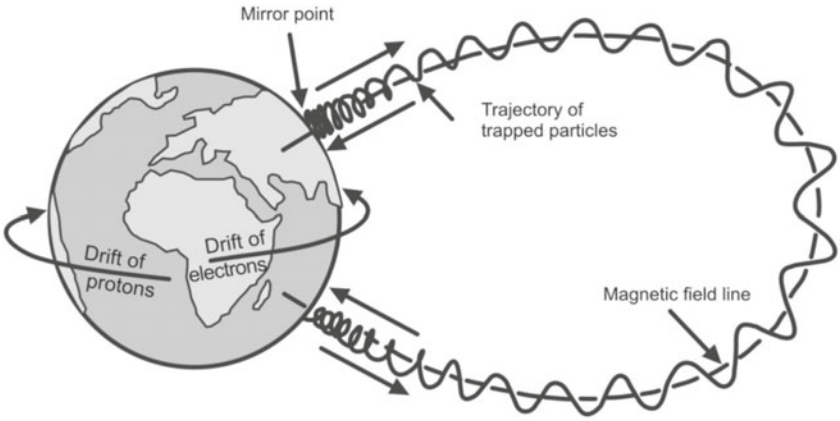

Figure 3.12. Trajectory of trapped particles through the magnetosheath (http://www.spenvis.oma.be/help/background/traprad/motion.gif).

about it and also push the magnetic field in a long tail. However, some sneaky particles leak through the magnetic barrier and are trapped inside. Some of the solar particles also rush through funnel-like openings, called cusps, at the north and south poles, releasing tremendous energy when they enter the atmosphere leading to the magnificent play of auroral lights. The particles then follow a trajectory path that goes round the Earth in a sort of cover or sheath called the 'magnetosheath' (Figs 3.11 and 3.12).

3.4 SOURCES OF ELECTRIC FIELDS

Thunderstorms are considered as the main source of electric fields in the lower atmosphere comprising troposphere-stratosphere and mesosphere. The thunderstorm activity produces vertical electric fields on a global scale. In the ionosphere, the electric fields are produced by dynamo action. Atmospheric winds and tides pull the weakly ionized ionospheric plasma across the geomagnetic field. This movement produces electromotive force and generates electric currents and fields. This is the ionospheric wind or Sq (for solar quiet) dynamo. Solar wind/magnetosphere dynamo is the major generator of electric fields in the magnetosphere.

Magnetospheric currents: The geomagnetists are sure now about the presence of number of magnetospheric and ionospheric electrical current systems. Of the magnetospheric currents, the first is the magnetopause current and the second is the ring current which is closely associated with magnetic storms. During a geomagnetic disturbance, the ring current has a global expanse, which flows in the westward direction and encircles the Earth's atmosphere over the equatorial region (Fig. 3.12). Ring current particles are identified through satellite-borne particle detectors in 1967. However, their signatures manifest on the magnetographs and magnetometers stationed at MOs across the globe in the form of magnetic storms. The third is the neutral sheet current, which divides the magnetospheric tail into two lobes of oppositely directed fields. The drifting plasma sheet particles provide energy and material for the initiation and sustenance of this current.

Geomagnetic storms: A geomagnetic storm is caused by sunspots and eruption of flares on Sun. The EMF that is continuously monitored at the MOs records the dynamical processes occurring at Sun, Earth and the intervening space between the two. For an event to be characterized as a magnetic storm, it should clearly have three phases: the initial phase (also referred to as the sudden storm commencement, SSC), the main phase and the recovery phase (Fig. 3.13).

Ionospheric currents: Some currents are also generated in the ionospheric regions. In 1839, Gauss while interpreting the fluctuations that occurred in a magnetic compass envisioned the fluctuations to be the handiwork of electric currents in atmosphere. Later, Stewart in 1882 talked of a 'great dynamo in the sky' in an article written for Encyclopedia Britannica. It was proposed that the

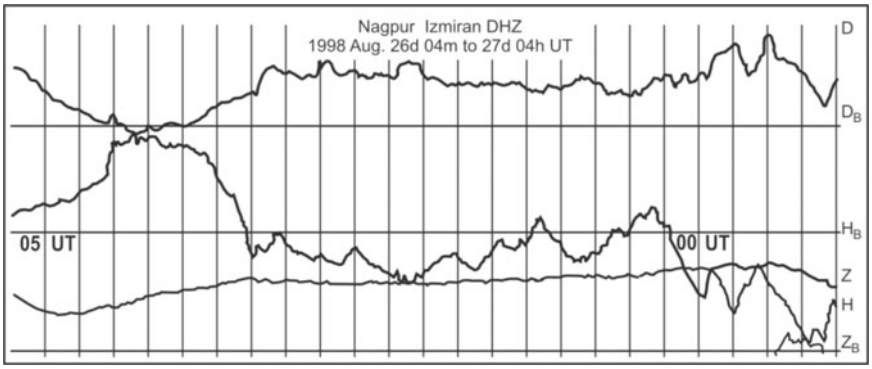

Figure 3.13. Magnetic storm recorded at Nagpur on 26-27 August 1998. Note the sudden storm commencement (SSC), the initial rise in 'H' and then the steep decline.

currents were generated in the atmosphere by the dynamo action of airflow across the geomagnetic field. Later research proved this to be correct. These ionospheric currents mainly flow in E-layers and are generated by tidal movements of ionized matter aided by solar heating (Fig. 3.14). This horizontal current sheet lies at an altitude between 100 km and 150 km in a concentric pattern over the Earth's surface. These currents are a regular feature of ionosphere irrespective of whether the solar wind is of quiet (Sq) or disturbed type.

Focus of Sq current: The Sq current system consists of two loops. The first hovers over the northern hemisphere and the second hangs in space of the southern. These currents are confined to sunlit hours. The northern hemisphere currents that define a loop, flow in an anti-clockwise direction while those in the southern flow in a clockwise manner (Fig. 3.14). The centre of each of the

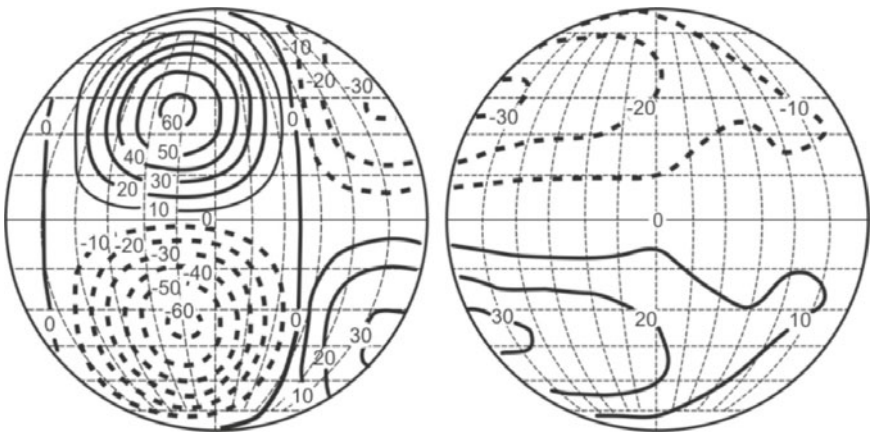

Figure 3.14. Solar daily magnetic variation on quiet days, over the day-time hemisphere (left) and the night hemisphere (right) (Jacobs, v3, 1989).

loops is called Sq focus and is situated (at 35° latitude) on either side of the equator. Sq focus and its strength change considerably from day to day or over the seasons. The current intensity between consecutive field lines is ~10^4 Å. Since these currents are tied with the Sun's energy, they are absent during the night time hours.

Equator to poles D, H and Z pattern: When variations in D, H and Z components are examined at different stations from equator to either of the poles, then a systematic variation is observed. D increases from equator to high latitudes in the northern hemisphere. In the southern hemisphere, a reverse trend is observed. This happens because in the northern hemisphere, the positive D variation reflects the eastward magnetic field generated by southward current that forms during forenoon hours. The negative D variation in the same hemisphere reflects the westward directed magnetic field formed due to northward current in afternoon hours. The H component increases systematically in the positive direction from equator to Sq focus (35° latitude) and it decreases from the Sq focus towards the pole in the northern hemisphere. The same trend can be observed in the variation of H in the southern hemisphere as well.

In terms of the current system, the variation in H in positive direction (northward) reflects the effect of the eastward flowing electric current formed during forenoon hours above MOs located between the equator and the Sq focus. Conversely, the variation in H in negative direction (southward) reveals the effect of westward flowing electric current formed during afternoon hours above MOs located between the Sq focus and poles (Fig. 3.14).

Equatorial electrojet: India occupies a unique location on the world atlas as far as geomagnetism is concerned. It is the only political entity in the world which encompasses the magnetic equator as well as the Sq focus within its boundary. The observatories situated along the magnetic equator, not just in India but everywhere else in the world, record various features in their H. It was observed that the range of daily variation in H at equator was larger by a factor of 2 to 2.5 compared to other stations several degrees beyond the equator (Fig. 3.15). This enhancement is due to a strong jet of current flowing mainly in the E-region of ionosphere during day light hours on either side of dip equator.

This phenomenon was first noticed at Hunacayo in Peru soon after the establishment of MO in 1922. The same phenomenon was also observed at Trivandrum, Annamalainagar and Tirunelveli in India, which are situated along or very close to the magnetic equator. The circulating electric currents of opposite symmetry join at the equator to form a strong flow from west to east at about 11:00 hr LT. This enhanced current flowing eastward was first identified by Egedal and the name equatorial electrojet (EEJ) was given by Chapman in 1951. Curiously, this electrojet has been discovered to reverse its direction, westward, during certain hours of the day and is known as the counter electrojet (CEJ). There is also the auroral electrojet, which is caused by field aligned currents, also known as Birkeland currents.

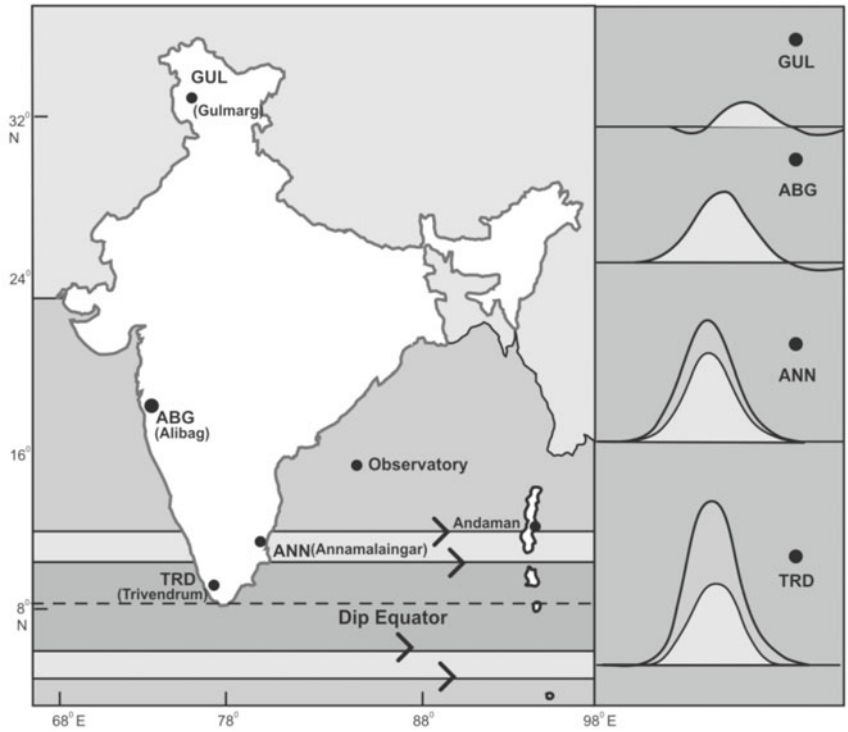

Figure 3.15. The EEJ. Note the pronounced effect seen at TRD (Trivandrum) and ANN (Annamalainagar) and lack of it at ABG (Alibag) and GUL (Gulmarg), which are located far away from the equator (Campbell et al., 1993).

3.5 RADIO WAVES: SCINTILLATION

The ionospheric irregularities are monitored with the help of radio beacons carried onboard satellites through yet another technique called scintillation. Scintillation is a rapid change in the phase or amplitude or both of a radio signal as it passes through small-scale plasma density irregularities in the ionosphere. This technique is ground based, inexpensive and highly economical. It yields information about the strength, spectrum and dynamical behaviour of metre to sub-km scale wavelength of ionospheric irregularities.

The radio waves were produced and detected by Hertz in 1887. He was generating an oscillating current from the spark of an induction coil when he detected radiation of extremely long wavelengths. These came to be called the radio waves and served a purpose by providing indirect evidences that the Earth is flooded with charged particles. It was found that a part of the radio waves generated by lightning travelled along Earth's magnetic lines of force. These waves are called 'whistlers' and was discovered by Barkhausen. The radio waves cannot follow the magnetic lines of force unless charged particles are present.

The discovery of radio waves opened a window to the far off galaxies, which later gave birth to radio astronomy. Radio astronomy has made many exciting discoveries of far off space and galaxies, the matter of which is beyond the purview of this book. However, scintillation studies, based on rapid changes encountered in phase and/or amplitude changes of a radio signal, provide useful information and clues to small-scale plasma density irregularities in the ionosphere.

The upper regions of the Earth's atmosphere (namely the mesosphere and thermosphere) and ionosphere are strongly coupled to the lower and middle atmosphere by means of chemical, dynamic and electro-dynamic processes. The observed influence of the upward propagating gravity and planetary scale waves and atmospheric tides on the thermosphere and the ionosphere is an example of dynamical coupling. The giant global electrical circuit linking the lower atmosphere to the ionosphere and the magnetosphere provides an adequate link for the electrodynamic coupling, which warrants the studies into space weather conditions.

Night airglow: The ionospheric region and beyond is composed of plasma, but below into our very own atmosphere are the gases. What might those gases be and of what composition, none had a clue before the 1930s. It was believed that hydrogen and helium may be floating over the heavier gases in the stratosphere. This was the belief of Bort. However, he was proved wrong by air samples that were brought down by Soviet balloonists in the middle of the 1930s. The upper stratosphere was found to contain oxygen and nitrogen. Troposphere, too, had these gases. But there was reason to believe that there existed some unusual gases that gave off 'airglow'. Night airglow is the feeble illumination of night sky even in the absence of moonlight.

What caused the feeble light that thinly illuminates the sky remained a mystery for quite a while. Then in 1928 came a breakthrough. Slipher, while analyzing the spectral lines obtained for the airglow of the nebulae in 1864 by Huggins, considered it to be an unfamiliar element 'nebulium'. In 1927, several experiments were carried out in the laboratory where the same kind of spectral lines as that considered to be of nebulium were generated. Ira Bowen showed it to be coming from the 'atomic oxygen'. Atomic oxygen is a single atom and not a combined two-atom molecule that is normally encountered. During the same period, research was going on over the spectral lines emanating from aurora. These spectral lines turned out to be the handiwork of 'atomic nitrogen'. The two, atomic oxygen and nitrogen, are produced by energetic radiation of the Sun, which breaks down the molecules into single atoms. This suggestion came in 1931 from Chapman and is one mechanism out of many others by which nature absorbs or weakens the harmful radiation before reaching the Earth.

Chapman further elaborated that the airglow was caused by the recombination at night of atoms that are split apart by solar energy during the

day. During the recombination process, atoms give up some of the energy they absorbed in splitting. Thus, the airglow is some kind of a delayed and very feeble return of sunlight in a new and specialized form.

Direct evidences of airglow were found by rocket experiments carried out in the 1950s. Spectroscopes carried by rockets recorded the green lines of atomic oxygen most strongly at a height of 96 km. The red light of atomic nitrogen was prominent at a height of 250 km. Slipher also found spectral lines in the airglow emitted by sodium. But the idea of sodium existing high up in the atmosphere was so embarrassing that it was rejected immediately. The reason, sodium is not a gas. It is a reactive metal and is always combined with other elements. In 1938, French scientists were emphatic in their suggestion of existence of sodium, based on the characteristics of spectral lines. The rocket experiments again gave concrete evidence. Their spectroscopes recorded the yellow light of sodium. Lithium was also found, in 1958, to be contributing to the airglow.

Creation of artificial airglow: Murray Zelikoff and his team created artificial airglow in 1956. They carried nitric oxide gas on a rocket and released it in the atmosphere at an altitude of 96 km. This gas accelerated the process of recombination of oxygen atoms. The observers on land easily sighted this glow. A similar experiment was also carried out with sodium vapour. It too created a clearly visible yellow glow.

Like night-time, there is also a daytime airglow, but because of the presence of strong solar background brightness, its contribution cannot be easily deciphered. There have been only a few ground and satellite-based measurements of visible airglow emissions during the daytime. The daytime airglow emissions are obtained by comparing blue-sky spectrum with solar spectrum, since the former is different from the latter in terms of atmospheric emissions, atmospheric scattering, and depth of the telluric absorption lines.

Space weather: The importance of research dealing with solar-terrestrial physics carried out through geomagnetic studies has helped understand the more distant universe, the intricate web of plasma phenomena, magnetic fields and particle acceleration. But there also exists a practical angle to this research. In a world increasingly dependent on electricity and electronics, the ‘space weather’ outside the atmosphere can have serious effects, in particular on human communications (Chapter 8).

Plasmas in the Earth's Magnetosphere

	Density N	*Electron velocity Ve*	*Proton velocity Vp*	*Electron temperature Te*	*Proton temperature Tp*	*Magnetic field*	*Comments*
Solar wind	1-10 cm^{-3}	200-600 km/sec	200-600 km/sec	6×10^4 to 3×10^5 °K	2×10^4 to 2×10^5 °K	2-15 nT	• High speed streams associated with coronal hole • Low speed streams near sector boundaries
Magnetosheath	2-50 cm^{-3}	200-500 km/sec	200-500 km/sec	10^5 to 10^6 °K	5×10^5 to 5×10^6 °K	2-15 nT	• Turbulent solar wind plasma and magnetic fields
High latitude boundary layer	0.5-50 cm^{-3}	No reported measurements	100-300 km/sec	10^5 to 10^6 °K	5×10^5 to 8×10^6 °K	10-30 nT	• Entry layer into the magnetosphere of magnetosheath plasma
Plasma sheet boundary layer	0.1-1.0 cm^{-3}	500-5000 km/sec	100-1500 km/sec	2×10^6 to 10^7 °K	10^7 to 5×10^7 °K	20-50 nT at 20 Re	• Region which maps to auroral zone producing discrete auroral arcs
Plasma sheet	0.1-1.0 cm^{-3}	10-50 km/sec	10-1000 km/sec	2×10^6 to 2×10^7 °K	Always hotter by a factor of 3 to 5 such that Tp/Te>1	9 nT in deep tail	• Thickness of 4 to 6 Re • Forms into the ring current at 5-6 Re from Earth
Lobe	10^{-3} to 10^{-2} cm^{-3}	No reported measurements	No reported measurements	$<10^6$ °K	$<10^7$ °K	Increases with southward IMF	• Lowest densities found in the magnetospheric cavity

(http://ssdoo.gsfc.nasa.gov/education/lectures/magnetosphere/Table_1.jpg)

APPENDIX 3.2

Classification of Geomagnetic Variation with Typical Periods, Amplitudes and Penetration Depths

Type of variation	*Symbol*	*Typical period*	*Typical amplitude*	*Typical penetration depth*
Solar cycle variations		11 yrs	10-20 nT	>2000 km
Annual variation		12 months	5 nT	1500–2000 km
Semi-annual variation		6 months	5 nT	
Short-time variation	Dst	Hours to weeks	50–500 nT	300–1000 km
Regular daily variation		24 hrs and harmonics		
at mid-latitudes	Sq		20-50 nT	300–600 km
at low latitudes	EEJ		50–100 nT	
Substorms	DP	10 minutes to 2 hrs	100 nT (1000 nT at p.l.)	100–300 km
Pulsations (=Ultra low frequency waves)	ULF	0.2–600 sec		20–100 km
regular	pc	150–600 sec (pc5)	10 nT (100 nT at p.l.)	
continuous		45–150 sec (pc4)	2 nT	
pulsations		5–45 sec (pc2,3)	0.5 nT	
		0.2–5 sec (pc1)	0.1 nT	
Irregular transient pulsations	Pi	1-150 sec	1 nT	
Extreme low frequency waves	ELF sferics	1/5–1/1000 sec	<0.1 nT	Tens of metres – kilometres
Schumann resonance oscillations		1/8 sec	<0.1 nT	
Very low frequency waves, whistlers	VLF	10-5–10-3 sec		Few metres – tens of kilometres

Note: If amplitude depends significantly on latitude, values are also given for polar latitudes (p.l., dipole latitude>65°)
(courtesy: Olsen, 2007 and Schmucker, 1985).

4

TECHNIQUE OF MAGNETIC MEASUREMENTS

Any form of data whether acquired at an observatory or through experiments concerning studies of space and solid Earth described in this book, need instruments. These instruments, essentially magnetometers, are distinguished not only by the component of the field they measure, but also by the principle of their working. The principles employed in magnetometers range from the elementary laws of forces acting on a magnetic needle, to the technique of optical pumping. There are different types of magnetometers, which include theodolite magnetometers, torsion magnetometers, variometers, Lloyd's and Schmidt's balances and Earth inductors. The recent additions are the nuclear magnetic resonance magnetometers, saturable-core magnetometers (fluxgate magnetometers), induction magnetometers and more. The magnetometers introduced in the late twentieth century include proton precession magnetometers (PPM), optical pumped sensors, super quantum interference devices (Squids) and others. The most important change in instrumentation in the last half-century, however, is the automation of observation and the direct connection of sensors to data storage and computational facilities. This chapter outlines the importance and use of three categories of instruments in magnetic measurements: magnetic observatories, ground and marine magnetic surveys and laboratory magnetometers. Some 'current' instruments are also included in these three categories of magnetic measurements.

I. Instruments in Early Navigation and Science

The directional property of a lodestone was well known by the year 1000 and the Chinese mounted it on a boat for N-S direction. The year 1187 marked the first recorded feature of magnetic needles mounted on a pivot, which were free to rotate in a horizontal plane, much like modern day compass needles. Such

design was also mentioned by Peregrinus in 1269. The slant of the magnetized pivoted needle was noted by Hartmann in 1544. Norman explained this to be inclination in 1580–81 (Fig. 4.1).

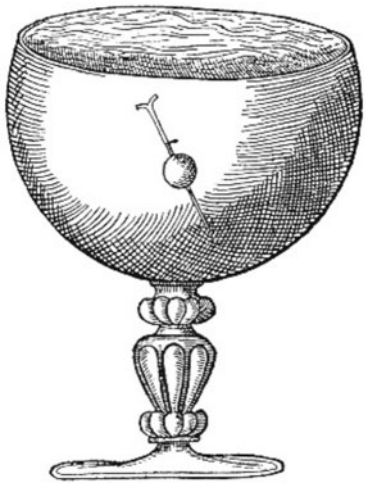

Figure 4.1. Norman's experiment for determining inclination.

These aforementioned luminaries represent an ethos of mixing of the practical goals of navigators and more esoteric goals of improving instruments and studying the phenomena revealed by them. Nunes and Castro developed an improved 'variation compass' and mentioned magnetic D in the 1530s. Norman focussed on the dipping needle, conceived the dip circle (first described in print in 1581) and concluded that the seat of magnetism is within the Earth. Borough concentrated on improving instruments for measuring declination and Gilbert assembled the most complete resume of magnetic experiments. No fundamental changes in instrument design occurred until 1800. Nevertheless, two fundamental discoveries were made using improved instruments: Gellibrand (in 1634) discovered that declination varies over time and Graham (in 1722) showed that declination varies daily according to a set pattern. During the eighteenth century, artisans modified the variation compass with lighter needles, a box to enclose the needle and the addition of reading microscopes and vernier scales. Another eighteenth century innovation was the tall azimuth visor, which allowed mariners to sight celestial objects high above the horizon.

II. Torsion Balance

The Paris Academy of Sciences, in 1773, offered a prize money for the best manner of 'constructing magnetic needles, of suspending them, of making sure that they are in the true magnetic meridian and finally of accounting for their regular diurnal variations'. Coulomb pocketed the prize in 1777 by designing the torsion balance (Fig. 4.2). In fact, his instrument was so good that for a few centuries, it served as a model for designing magnetic instruments.

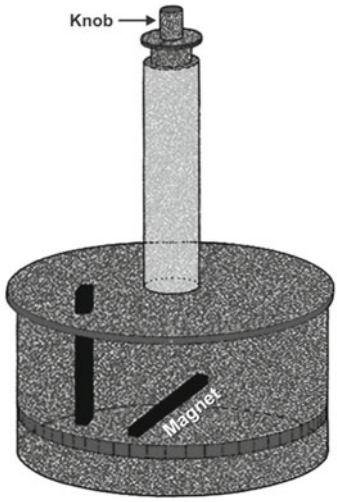

Figure 4.2. Coulomb's torsion balance.

In his torsion balance, Coulomb suspended a magnetic needle from a long

and thin wire that could be twisted around such that even a small torque produced a notable twist. To measure the twist, he attached a small mirror just above the needle and observed the shifts of spot of light reflected from it. This instrument was so sensitive that Coulomb had to place it inside a glass enclosure to shield it from air currents. Sometimes, he also found the static electric charges to be interfering with its working. Coulomb, equipped with his torsion balance, showed that the magnetic repulsion (and attraction) between magnetic poles varied inversely with the square of their distance.

The art of instrumentation took a big leap forward after the meeting of Gauss with Humboldt in 1828. Gauss pursued (geo)magnetic studies along with his young assistant Weber, who together set up a magnetic laboratory of their own, wherein they constructed their own magnetic telegraph and devised a new suspension for observatory magnets. In 1832, they also devised a method of using an auxiliary magnet to measure not only the direction of the Earth's magnetic force, but also its intensity. This ingenious method revolutionized the concept of instrumentation in the magnetic world and made possible the establishement of global MO network (Chapter 5).

III. Magnetometers

Magnetometers were developed by Schmidt around 1915, which became quite popular in mining and petroleum industries. They are also known as magnetic balances and magnetic variometers because they measure the variations in the Z and H components rather than their absolute values. But in these variometers, the magnetic system is brought to the null position by applying a twist to the torsion fibre supporting the magnetic system (Fig. 4.2). The additional twist thus applied is the measure of the change in the magnetic field. Such an instrument was also developed by Haalck in 1956, which was easier and quicker to operate and capable of large station coverage. Even then, they have not ever been able to replace the Schmidt's balances.

The magnetometers that do not utilise a moving magnet are the fluxgate, PPM, electron beam and optical pumping magnetometers. Fluxgate magnetometers measure either the Z or H or the F, and are essentially variometers. The others are absolute instruments and measure only the total field. Magnetometers are classified as scalar, when they give only the value of the field without its direction and vector when they are organized to record the field value with a definite direction. These instruments are definitely superior to the mechanical magnetometers because they are not only extremely sensitive but can also be used in space.

4.1 MAGNETOMETERY FOR GEOMAGNETIC OBSERVATORIES

Measurement of EMF variations is usually made in MOs. In abolsute measurements, the total vector of the magnetic field is obtained by measuring

atleast three magnetic elements such as F, D and H. Instruments like magnetic theodolite, quartz horizontal magnetometer (QHM), balance magnetique zero (BMZ) and magnetic variaometers have automatic recording.

I. Classic Semi-absolute Instruments

The ultimate instruments along traditional lines were devised by La Cour of Denmark in 1933. His QHM and BMZ were 'semi-absolute' instruments. The QHM's high standard of accuracy with one nT kept it into use even into the 1980s. The QHM provides quick and accurate observations of H and D (Fig. 4.3). BMZ is a portable balance, which measures Z by the zero method. The QHM and BMZ, though they form the class of absolute instruments, are treated as a 'secondary standard' because they need to be calibrated periodically to check that their instrumental constants specified by the manufacturers have not changed.

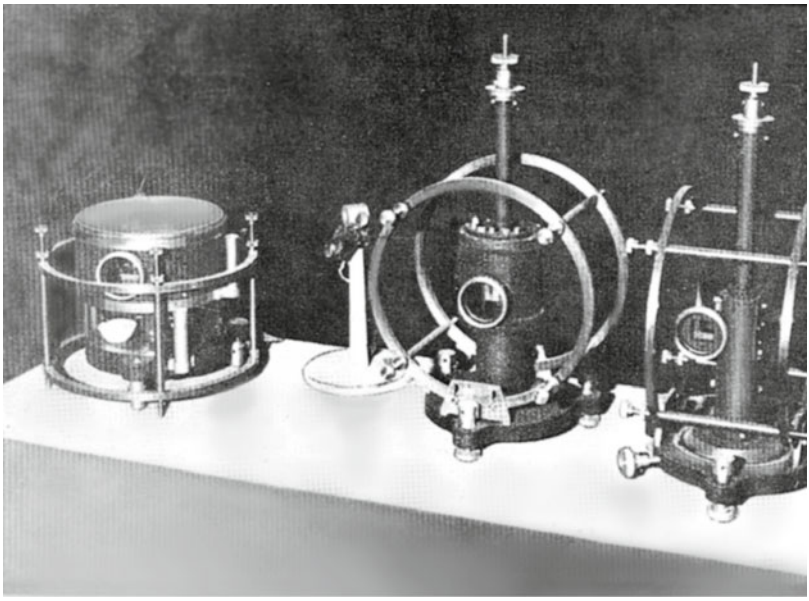

Figure 4.3. La Cour variometers D, H and Z.

II. Classic Variometers

It is almost impossible to continuously carry out absolute measurements and, therefore, it becomes essential to automatically record the variations. The changes in the amplitude and phase of each magnetic element are continuously recorded using instruments called variometers. They can then be combined with a few absolute observations during the day to provide absolute data for any instant of time. Figure 4.4 shows the functioning of a variometer.

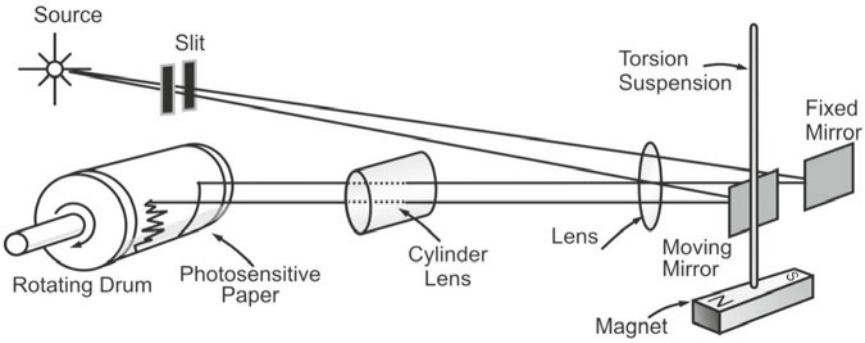

Figure 4.4. Schematic representation of a variometer (Campbell, 1997).

Essentially, the variometer consists of a magnet with a mirror attached and is oriented suitably (along N-S for recording D, along E-W for H and pivoted to oscillate in a vertical plane for Z). A beam of light from a straight filament lamp gets reflected from the mirror and passes through a long focal length lens, at the focus of which is placed a rotating drum with photographic paper. A short focal length cylindrical lens in front of the recorder enables to focus the filament image to a point on the photopaper. With the change in time, the variation in the form of angular deviation of the magnet gets registered on the photographic paper. A mirror fixed in the variometer not connected to the moving magnet will leave a straight line trace serving as a reference level. Time marks on the magnetogram are generated at definite time intervals of 1-hour each. The photographic paper fixed on the drum gets exposed by two spots of light, one of which leads to a straight line called the baseline and the second is the variable trace. When the photopaper is removed from the drum, developed and dried, a day's magnetogram distinctly depicts the subtle changes in the three components (e.g. Fig. 1.13).

The photographic paper recorder appeared in nineteenth century. The invention of the fluxgate in the early 1900s permitted the development of the triaxial electronic variometer and the DI-flux, which are in use today in most of the MOs (Fig. 4.10). Observatory fluxgate variometers include three fluxgate sensors arranged orthogonally on a stable support made of marble or quartz. This trihedron is then oriented by the variometer frame according to the three components set one wishes to observe (Fig. 4.10).

III. Vector Proton Precession Magnetometer (VPPM)

The PPM can serve as a variometer by measuring the vector components of the magnetic field by cancelling out one of the components by means of a Helmholtz coil, and is called a VPPM (Fig. 4.5).

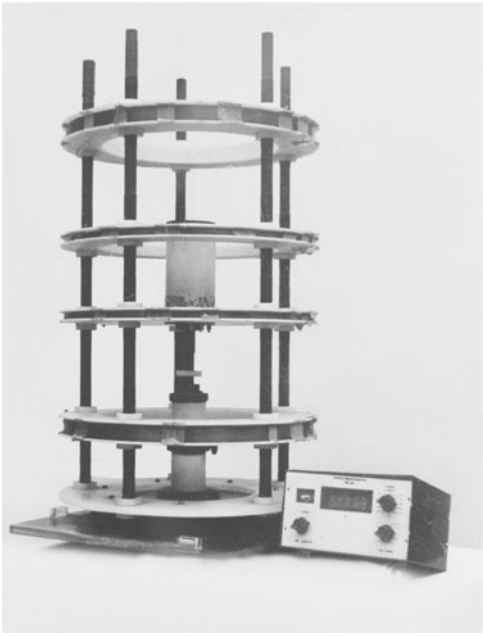

Figure 4.5. Vector coil and PPM used for absolute measurements at an observatory.

IV. Helmholtz Coil System

The torsion type variometers were first replaced by the nuclear resonance magnetometer to which the PPM belongs. Several standard designs of coil systems are available in literature to produce uniform magnetic field at the centre directed along the axis of the coil system to selectively cancel or add to one component of the ambient field. Well known among these are the Helmholtz coil system, where the two circular coils are separated by a distance equal to the radius or its variant of square coils separated by a distance 0.5445 times the

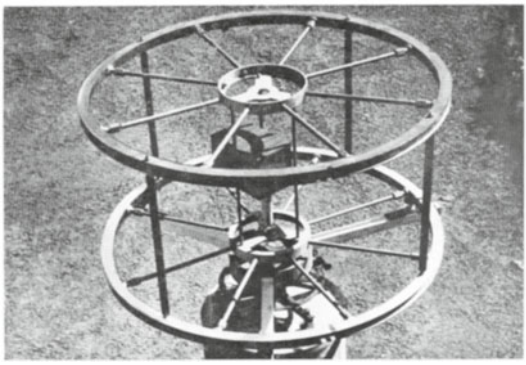

Figure 4.6. 'Helmholtz' biasing coil system for determination of absolute H using proton magnetometer.

length of one side (Fig. 4.6). The field at the centre of these two coils are given by $A = 89.92$ NI/R for circular coil, $A = 88.68$ NI/d for square coil, where N is number of coil turns in each coil, I is the current in mA, R is the radius (spacing) of the coil in cm and d spacing of the coil in cm [$d = 0.5445 \times$ side length]. In Nelson's method, one intensity component (H or Z) is measured using a PPM at the coil centre by compensating for the other component.

V. Proton Precesssion Magnetometer

The measurement of magnetic field intensity by the method of free precession of protons in a hydrogen-rich sample (e.g. water, alcohol, kerosene) can be considered as one of the most important developments in the Earth field magnetometry. Because of the simplicity of operation, its reliance only on a fundamental constant—'the proton gyromagnetic ratio' and the higher level of accuracy, PPM has almost totally replaced the classical equipment in observatory practice. The PPM could be successfully used in geomagnetic surveys by land, sea and air and on board rockets and satellites.

Protons within a hydrogen-rich sample, which possess magnetic moment due to their spin, align themselves parallel or anti-parallel to the ambient magnetic field. Due to the angular momentum, they do not move in line with the ambient field but tend to precess about the field direction with random phase like a spinning top subject to the torque imposed by gravity and the reaction of the support on the point (Fig. 4.7).

The sensor consists of a container of proton-rich fluid and is surrounded by a coil, serving the dual purpose of applying periodically a polarizing field to the liquid and picking up the signal from the precessing protons after cutting off the polarizing field. When an external magnetic field is applied, the protons, which are normally in random orientation, tend to align or group themselves either in a parallel or antiparallel direction with reference to direction of the external field. The group of nuclei, which takes up the anti-parallel position, has a higher level of energy than that of the other group. If a strong magnetic field is applied in a direction approximately perpendicular to the EMF, all protons align themselves parallel to the applied field. When the current is suddenly switched off, the protons begin to relax into their previous orientation under the EMF by 'precessing' around that field at a certain frequency. The precession of the protons under the influence of the EMF produces an emf in the coil. The signal induced in the coil is the Larmor precession frequency ω of the proton given by: $F = (2\pi/\gamma_p)\ \omega = 23.4874\omega$, where F is expressed in units of nT and γ_p is the gyromagnetic ratio (magnetic moment/angular momentum) of the proton, given by $q/(2mc)$. An electronic console amplifies the precession signal and performs a frequency measurement of it with the required accuracy. This measurement is then scaled using γ_p, which is directly proportional to the intensity of the EMF in Tesla.

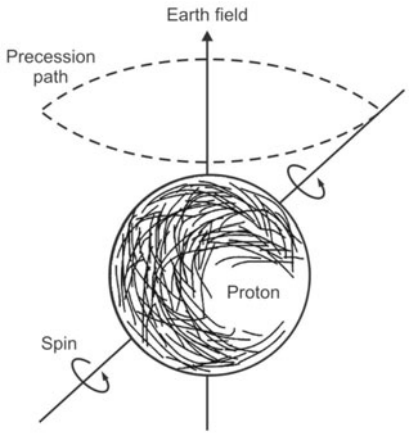

Figure 4.7. The precession (reorientation) path of proton (Rangarajan, 1992).

Modern PPMs are quite compact and have high resolution and sampling rate (typically 0.01 nT and 3 Hz, respectively). However, there are two disadvantages amongst many advantages of PPM: Firstly, measurement of fields <15,000 nT is difficult because of a low signal-to-noise ratio. Secondly, the readings of the PPM are discrete, not continuous. This is because the field produced in the coil for polarising the protons has to be on for typically 2 to 3 sec, and no readings can be taken within this time. The simplest way to make the readings continuous is to use two PPMs functioning at alternate intervals. Other methods use physical principles to achieve continuity. As the measurement is made in a sequential form, the PPM cannot give continuous output of the scalar magnetic field. One method by Overhauser uses coupling between the spin energy of protons and electrons. The other method is optical pumping, which is used in another popular type of instrument namely the metastable helium, rubidium and cesium magnetometers. All these magnetometers make use of optically pumping technique. They are highly sensitive and also enable the measurement of the vertical gradient of the EMF employing two magnetometers kept separated vertically apart from each other.

The optically pumped magnetometer depends on the Zeeman splitting of the atomic energy levels into sublevels in the presence of a magnetic field. The separation between the energy sublevels depends on: (1) the intensity of the magnetic field and (2) the alignment of the magnetic moment of the atoms relative to this field. The transition frequency generated is proportional to the energy separation levels and it is this which is monitored.

VI. Fluxgate Magnetometer

This magnetometer was the first airborne geophysical instrument successfully used to detect submarines during the World War II. It is used for measuring the component of the magnetic field vector along its sensor's axis. The fluxgate

principle uses the nonlinear field and induction relationship of easily saturable ferromagnetic core. The sensor or the main element of a fluxgate magnetometer, usually a rod or a ring, is subjected to both DC field to be measured and the auxiliary AC field produced by a coil and an electronic oscillator. This offset sinusoidal excitation creates a distorted AC signal in a pickup coil surrounding the core. The detection of its even harmonics provides a DC signal proportional to the field to be measured.

Fluxgate sensors consist of a pair of identical strips of mumetal. Mumetal is a heat-treated alloy of iron and nickel, having a narrow hysteresis loop and high initial permeability of about 10,000 cgs units. It can be saturated in a relatively weak field of ~3 Oe, equivalent to EMF intensity. Two identical primary coils (E1 and E2), kept in N-S direction and connected to a common source of AC current, are wound one on each core so that the magnetization produced in one of the cores is exactly opposite to the one in the other. Thus, in the absence of any external field, no voltages are produced across the terminals of a secondary winding surrounding the primary (Fig. 4.8a). The situation is, however, different in the presence of the EMF, because Earth's field aids the magnetizing field of one of the cores and opposes the field of the other. This

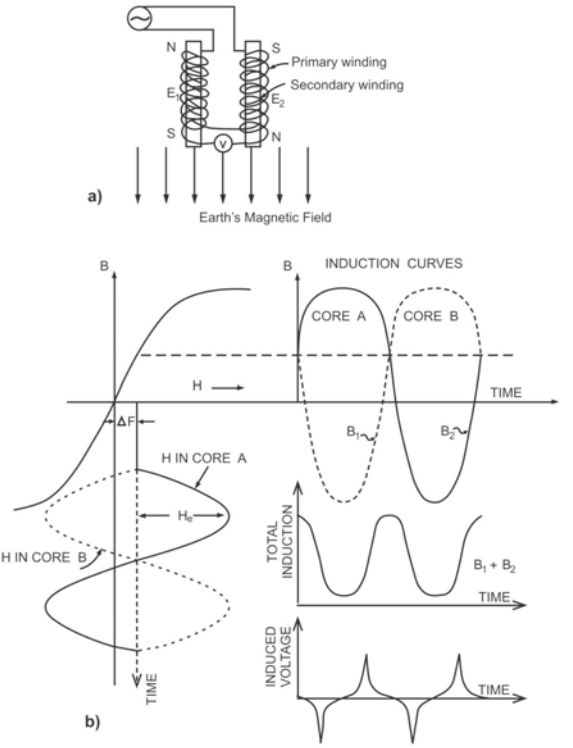

Figure 4.8. (a) Sketch illustrating the principle of fluxgate magnetometer. (b) Principle of working of peak voltage fluxgate magnetometer (Rao and Murthy, 1978).

causes a dissimilarity of the induction curves B1 and B2 (Fig. 4.8b) of the individual cores and the total flux B1+B2 of the system fluctuates with a frequency 2*f*. According to the rate of change of the total flux, a secondary voltage is developed in the secondary coil, which is in the form of steep pulses, reccurring 2*f* times/sec and having a height proportional to the EMF. By suitable phase sensitive detector circuits, the signal and hence the magnetic field can be detected.

VII. Indian Scenario

In India, the stream of instrumentation dedicated to designing, fabricating and maintaining geomagnetic equipment was started in 1972. Developmental work in India includes the fabrication of timers, electronic crystal clocks, constant current sources, calibrating coils, DC/AC inverters, battery chargers and remote control panels. PPM (VPPM) is fabricated and redesigned to operate on minimum power (Fig. 4.9). Since 1980s, microprocessor-based instruments are developed; amongst these are a cassette datalogger, a numeric printer for automatic printing of data and PC-based data logger, which is developed as part of AMOS (automatic magnetic observatory system).

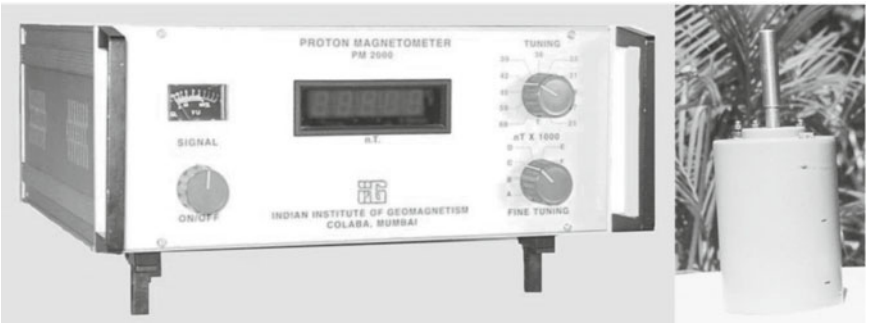

Figure 4.9. Proton precession magnetometer fabricated by IIG.

With the advent of computers and easy programmability of micro-controllers, the Indian scientists are able to incorporate DSP technique for signal processing. The use of this technique has improved the sensitivity ten-fold, i.e. from the existing 1 to 0.1 nT, culminating into fabrication of a computer-based VPPM prototype. The system has an interface and the software to give a 0.1 nT output and a digitally programmable current source controlled by the computer. The PPM designed and fabricated by IIG is used in a number of campaigns and observatories, which are updated regularly. A portable micro-controller-based PPM with 0.1 nT sensitivity is also developed for its use in survey work.

Indian observatories, an upgrade: Since 1990s, classical magnetometers are being gradually replaced by the fluxgate triaxial tilt compensated variometer (model FGE) plus scalar magnetometers of indigenous PPM type in a bid to reorganize and modernize MOs in India. The observatories are upgraded with contemporary instruments such as Danish fluxgate magnetometers (DFM) with appropriate data loggers (Fig. 4.10), and D and I magnetometer (DIM) with indigenously fabricated VPPM as the principal means of calibrating the observatory variometers. The modernized digital acquisition systems are installed to provide high resolution digital geomagnetic data with more stable baselines.

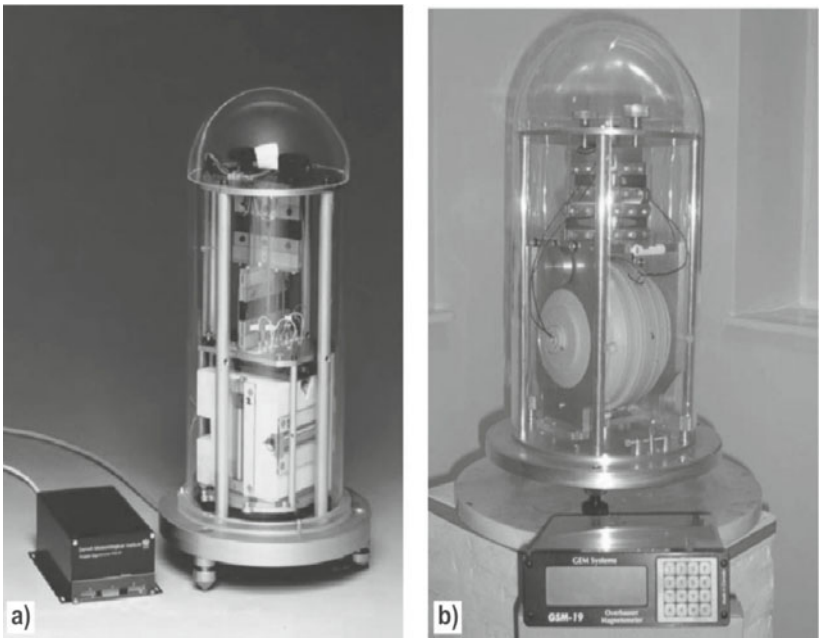

Figure 4.10. Danish triaxial fluxgate magnetometers: (a) delta inclination (dI) and (b) delta declination (dD) systems.

4.2 MAGNETIC SURVEY INSTRUMENTS: FLUXGATE AND INDUCTION MAGNETOMETERS

In ground magnetic surveys, the relative value of vertical or horizontal components or the total magnetic field with respect to some base stations, is regarded as the first step in magnetic prospecting. Different magnetometers are available for conducting magnetic and EM surveys, which may be classified under the following types. Different types of magnetic instruments and their operational principles are shown chronologically in Table 4.1.

Table 4.1 Different types of magnetic instruments

Magnetometer	*Principle of operation*	*Quantity measured*	*Sensitivity*	*Status*	*Remarks*
Dip needle	Balancing magnetic force against gravity	Z	100	Currently not used	For land use
Needle magnetometer (Schmidt balance)	Balancing magnetic force against gravity	Z and H	10	-do-	-do-
Fluxgate magnetometer	Saturable core	H, Z and F	0.1	Currently used	For land and airborne use
Torsion magnetometer	Balancing magnetic force against twist	Z and H	1	-do-	For land use
Proton precession magnetometer	Free precession of protons	F	0.05	-do-	For land, marine and airborne use
Alkali vapour magnetometer	Zeeman effect	F	0.01	-do-	For land and airborne use
Super conductor quantum interference device	Josephson effect	Z and H	0.001	-do-	-do-

I. Geomagnetic Depth Sounding (GDS) Measurement

In addition to the permanent MOs, there are also some temporary observatories involving close-spaced ground magnetometer arrays. These short-term magnetometer arrays are planned for mapping of subsurface conductivity structures or for exploratory purposes. In such cases, the delicate and sensitive instruments of the MOs are of very little practical use.

The instruments required for such purposes should be portable, free from interaction of sensors and have good thermal compensation and also easily installable. Exploring the anomalies in lateral extent with the use of an array of three component (H, D and Z) magnetometers is termed as GDS or magnetometer array studies (Chapter 6). The array study involves a number of magnetic variometers recording simultaneously across a single dimension (linear) or two dimensions area. The instruments record all the three components of EMF temporal variations. In actual practice, generally minimum 5-10 instruments are used. The station spacing and number of stations largely depend on the objective of the study. The recording period in GDS over an area is for a limited period of, say, a couple of months. The selected magnetometers need to respond to short period variation events, i.e. for a period of the length of a day to a couple of minutes (SSC). Together with the PPM, the rugged and portable fluxgate type of magnetometers (Fig. 4.11 a-c) are the most widely used magnetometers in surveys and arrays.

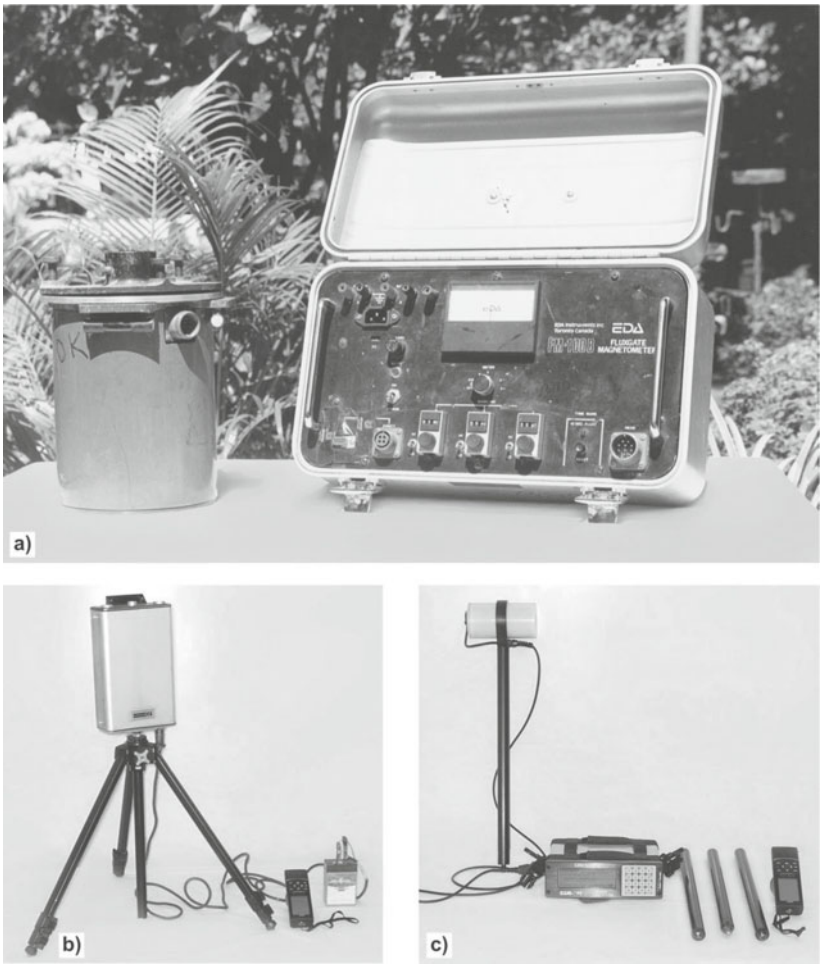

Figure 4.11. (a) Rugged and portable variants of magnetometer used in land surveys. (b) Scientrex fluxgate magnetometer used in ground magnetic surveys. It measures the vertical field Z. Also seen are the battery and GPS unit. (c) Geometrix proton precession magnetometer used in ground magnetic surveys. It measures the total field F. At the extreme right is the hand-held GPS unit.

II. Magnetotelluric (MT) Surveys

Unlike controlled source methods, the MT method uses the natural variations of the EMF. The conventional MT stations consist of sensors for the horizontal components of the electric field (E) and of the magnetic field (B), selective amplifiers and a data logger or a real-time processing system. The so-called apparent resistivity curve is obtained as a function of frequency from the field data. The MT method is used as a powerful tool for reconnaissance surveys of sedimentary basins for target exploration in hydrothermal areas. This is achieved through the integration of MT data with that obtained from GDS.

In this method, time-varying horizontal components of B and E fields at the Earth's surface are measured. The most common types of instruments used in exploring the Earth through this technique are the fluxgates for longer periods (≥100 sec) and induction coils for relatively shorter periods (Fig. 4.12). This technique involves recording of E, which is generated by inserting two electrodes in the ground separated by a distance from 25 to 1000 m. The difference in potential is then recorded with a high-impedance voltmeter.

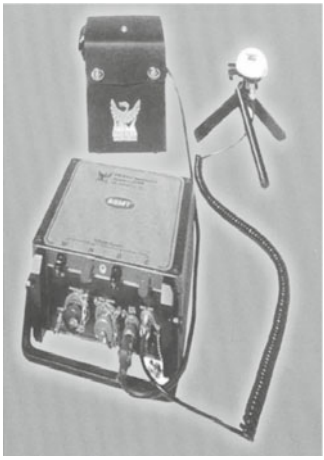

Figure 4.12. Advanced magnetotelluric system that uses 24-bit analog-to-digital converter.

III. Ocean Bottom Magnetometer (OBM) Surveys

The aforementioned are all land-based instruments. Efforts are on to generate geomagnetic data along the ocean floor in which the magnetometers are towed behind the ship to record the signatures given out by the ocean floor. The knowledge of sea floor spreading as well as the magnetic reversals became apparent because of this 'towing'. But, there is another set of equipment, the magnetometer, which can be sent to the ocean floor, allowed to stay underwater for a month or so and then commanded back to the surface. In the intervening period, the magnetometer sits down on the ocean floor and records the changes that occur in the geomagnetic field at the surface of the ocean floor. Such a magnetometer is termed the ocean bottom magnetometer (OBM) (Fig. 4.13).

The OBM is a similar kind of magnetometer used on land. It encompasses a fluxgate type of magnetometer and records three elements of EMF, viz. X, Y and Z. The sensor is suspended whereby it records Z rather accurately. As for the other two components, they are in two random directions in horizontal plane because the OBM settles down in any random direction. It records the three components at an interval of one minute for an entire month and stores it

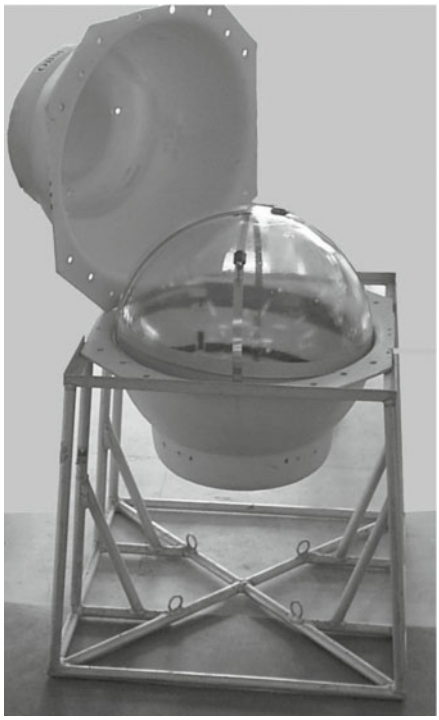

Figure 4.13. Ocean bottom magnetometer.

in a memory card. The OBM is powered by a Ni-Cd battery and the entire system is then enclosed in a pressure tight glass sphere which can withstand hydrostatic pressures at depths up to 6000 m.

The OBMs are taken to the area in oceans singled out for detailed study and are lowered down at pre-selected sites, whose exact position is noted with the help of a GPS unit aboard a ship. No rope or lifeline is attached to it, although a strong lead-weight is tied to the OBM so that it sinks down under its own weight. This unit can be sent down without a contraption to pull it back up because a sonar device is fixed to it to help track the instrument as it goes down. After the OBM settles on the sea floor, recording starts automatically at a pre-fixed time. To bring up the OBM, signals are sent through a sonar unit to initiate electrolytic reactions into the salty sea-water which corrodes and dissolves the wire to which the lead-weight is attached. On detachment of the lead-weight, the OBM rises up due to buoyancy and ascends to the sea surface. When it reaches the surface, it beams out high frequency radio signals to help scientists aboard the ship to track them down. The flasher attached to the OBM also comes in handy if the unit surfaces up during dark hours or night.

Ocean bottom electromagnetometer (OBE): Recently a new form of OBM has been developed which is called OBE (Fig. 4.14), and whose principle remains the same as that of OBM. However, in the case of OBE, it is not

required to be brought back to the surface to retrieve the data. The OBE is lowered to the bottom of the ocean, where it sits comfortably and starts recording the magnetic field variation. Then, after some time, the ship is taken over the site, where the OBE has been lowered and sonar signals are sent. At the receipt of the signal, the OBE starts transmitting the data, which is collected by a receiver aboard the ship. In this way, it is not required to pop the device up from the seafloor. A new version of OBE equipment has been developed that can be kept at the sea bottom on a permanent basis. It is powered by a long-life battery, whereby it works for an extended period of time. The electric field and magnetic field data are collected and stored in memory. The ship is taken to the site at regular intervals (say once in three months) to retrieve the data. The data are transferred from the equipment to the ship through sonar signals.

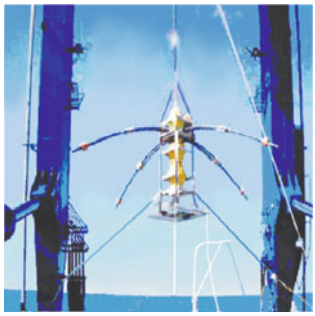

Figure 4.14. Ocean bottom electromagnetometer before deployment into the sea.

IV. Induction Coil Magnetometer

The induction coil (or search-coil) magnetometer's (ICM) operation principle is based on the Maxwell equation, which can be written in integral form as: $e = -d\varphi/dt$, where e is the emf, φ is the magnetic flux and t is the time. In its simplest form, an ICM contains a coil with many turns of copper wire connected to the input of a voltage amplifier. It utilizes the fact that, when the magnetic flux across a circuit changes, an induced emf is generated in the circuit, whose magnitude is proportional to the rate of change of the flux density and the effective 'area turns' (NA). The coils are presumed to have a large number of turns (N) with a small loop area (A). An ICM can be used only for the measurement of a time-varying magnetic flux. Its component collinear with the coil's axis intercepts the coil loops and generates an emf at the coil's terminals, which is further amplified to an easily measurable level.

To increase the ICM sensitivity, a high permeability ferromagnetic material is used as a core inside the multiturn winding. Due to their relative simplicity, ICMs are widely used for many applications, mainly in geophysics. In MOs, they are used for the study of EMF pulsations, where the fluxgate magnetometer is not a suitable instrument to record the variation of short-range pulsations. Their operational frequency band covers a range from about 10^{-4} to 10^{7} Hz, and the dynamic range of measurement covers from fractions of femotesla to tens of tesla. In spite of an apparent simplicity, the creation of a high-class ICM needs complicated calculations to establish an optimal matching of the sensor coil with the amplifier. Modern ICMs are quite compact; the electronics are configured to have flat passbands over the frequency range of interest and

the output can be easily logged on a standard data logging system for further analysis.

4.3 LABORATORY MAGNETIC INSTRUMENTS

The classic astatic/spinner/Squid magnetometers and AF/thermal demagnetizers are used to measure remanent magnetization (RM) directions and intensities of oriented rock samples. Rock magnetic instruments are used for the discrimination of magnetic minerals and their magnetic properties. For palaeomagnetism, the main consideration is to measure the stable RM vector in a rock, whereas for environmental magnetism, the requirement is to identify sample's magnetic mineralogy and grain size distribution. In either case, the magnetometers employed operate either by the use of magnetization of the sample to induce a current in a sensing coil, or the magnetization can create a force, which is measured by a variety of methods.

I. Sampling

Standard palaeomagnetic samples are 2.5-cm dia cores, ~2.2 cm in length, and most palaeomagnetic magnetometers are designed for this sample size. For measurement purpose, rock specimen is considered to be a homogeneously magnetized sphere. Hence, they are cut in cylindrical and cubical forms using laboratory rock-cutting instruments (Fig. 4.15). The major exception of this is whole core sections commonly collected from lake and deep-sea sediments used in environmental studies. These cores are typically 10 cm in dia and can be several metres in length.

It is also necessary to take precautions for possible contamination during drilling and slicing of samples, which at times leave metallic particles. Use of phosphor-bronze cutting surfaces as well as nonmagnetic grinding powder such as bauxilite (Al_2O_3) eliminates some of these contaminations.

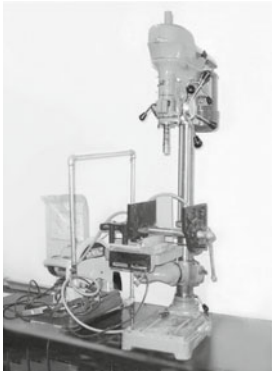

Figure 4.15. Rock coring (right) and rock cutting (left) equipments.

II. Astatic Magnetometer

These magnetometers were the most common type of instrument in palaeomagnetic laboratories in the 1950s and 1960s. They are force-type magnetometers, where the sample's magnetization is used to exert a force on a pair of identical suspended magnets. Two bar magnets of the same magnetic moment but antiparallel in polarity are set one above the other with their axis horizontal and are suspended vertically by a torsion wire (Fig. 4.16). The RM component is isolated by measuring the antiparallel deflections along three

orthogonal axes, and combining them to give the resultant vector. Their typical sensitivities are $<10^{-8}$ Am^2.

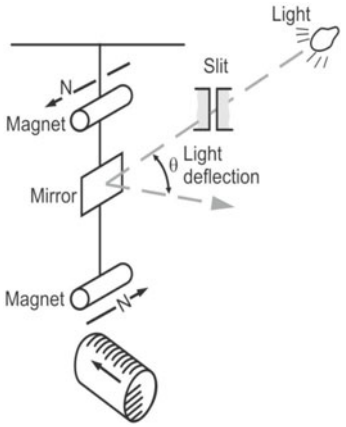

Figure 4.16. Astatic magnetometer (Campbell, 1997).

III. Spinner Magnetometer

This instrument is used for laboratory measurements of the direction and magnitude of remanent magnetization of the rock specimen. Remanent magnetization Jr is a vector: the measurement must therefore provide magnitude and direction, defined with angles D and I. The three components of Jr are obtained in the specimen reference system (x, y, z), and then transformed to the geographic system using the field orientation of the sample. Magnetometers do not measure Jr directly, but the magnetic field B the specimen generates in the surrounding space. Assuming that the field is that of a dipole, the magnetic moment M is derived and from it, assumed to be homogeneous within the specimen, Jr is computed. To satisfy the first hypothesis, the shape of the specimens must approximate the sphere as closely as possible: standard shapes are the cube and the cylinder with height/diameter ratio $h/\theta = 0.9$. The lack of homogeneity of M, and hence that of Jr in the rock, is often limited and the related errors can be reduced by repeating the measurements in different specimen/sensor relative positions. Sensor and specimen are appropriately shielded against external magnetic fields, to prevent the presence of induced magnetization Ji (EMF) and minimize noise (artificial fields).

Typical spinner magnetometer applications are: (1) Palaeomagnetism: palaeomagnetic dating of rocks, solving some tectonic problems in particular terrains and dating the development of mineralization of ore deposits; (2) Archaeomagnetism: changes of EMF in human history. These investigations are mostly applicable to dating archaeological materials; (3) Mineralogy: impurities of ferro (i) magnetic grains in para or diamagnetic materials can be investigated; (4) Magnetic fabric studies: measurements of the anisotropy of IRM can help in the separation of ferromagnetic and paramagnetic fraction of

a rock, and (5) Magnetometry: in the interpretation of ground or airborne magnetic measurements, it is useful to know whether the rock's magnetization is due to its induced or remanent component. Investigation of RM can help to solve this problem.

Measuring principle: The principle is very simple and is based on Faraday's EM induction law. Rock specimen fixed in a specimen holder, rotates at a constant angular speed in the surrounding two orthogonal coils, which are shielded with a multilayer permalloy shield. A rotating magnetized specimen produces an alternating emf in coils. The signal frequency is equal to revolution rate, and its amplitude is proportional to the component of the magnetic moment perpendicular to the axis of revolution. The spinning system generates a reference signal whose phase allows to split the signal to two orthogonal components proportional to the two components of the magnetic moment. Repeating measurements in different mutually orthogonal positions of x, y and z marked on the sample, the three components are obtained.

The simplest sensor is an induction coil placed around the sample chamber. The signal output increases with sample size (limited by the induction coil size) and with rotation frequency. The highest sensitivities for such instruments approach 10^{-10} Am^2. Fluxgate sensors may be used instead of induction coils, or increased sensitivity can be obtained using Squid detector. The Agico's spinner magnetometers of the JR series, which have a high sensitivity of the order of 10^{-6} A/m (for cubic specimens with sides 2 cm) and Molspin's minispin fluxgate magnetometer (sensitivity 10^{-3} A/m), are shown in Figs 4.17 and 4.18. With these popular commercial instruments, the practical lower limit of NRM

Figure 4.17. Laboratory induced remanent magnetization called anhysteretic remanent magnetization (ARM) and isothermal remanent magnetization (IRM) is imparted and measured by highly sensitive JR-6 spinner magnetometer. Rock and sedimentary samples of defined shape and size rotate at a constant angular speed in the pick-up unit inside a pair of coils. An AC voltage is induced in the coils whose amplitude and phase depend on the magnitude and direction of the magnetic remanence vector of the specimen. By Fourier analysis the computer calculates two rectangular components of the projection of remanence vector into the plane perpendicular to the axis of rotation.

Table 4.2 Measurement specifications of Molspin Minispin and AGICO JR6 spinner magnetometers

Specifications	*Molspin Minispin*	*AGICO JR6*
Speed of rotation (rev/sec)	5 (Long) or 4 (Short)	87.7 (High) or 16.7 (Low)
Measuring range (A/m)	0.1 to 2500	0 to 12500
Noise/Sensitivity (μA/m)	35	2.4

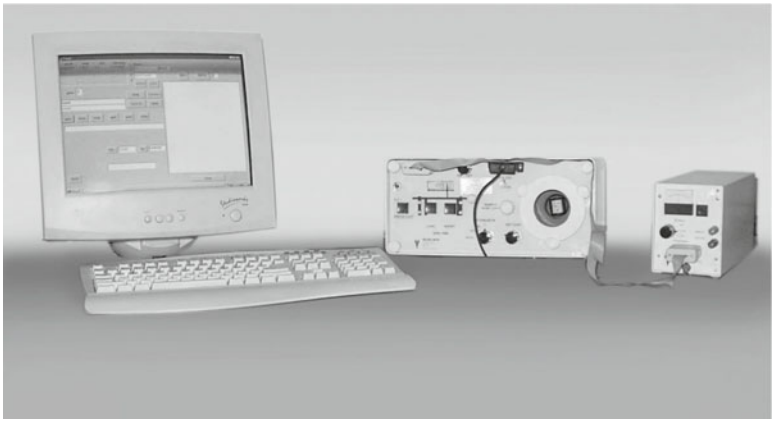

Figure 4.18. Laboratory induced remanent magnetization of ARMs and IRMs measured by Minispin spinner magnetometer of Molspin. It is a portable and low speed spinner magnetometer. Rock and sedimentary samples are spun at 6 Hz about a vertical axis inside an annulus-shaped fluxgate surrounded by a triple layer cylindrical mumetal shield. The output signal is integrated over either 6 sec or 24 sec and is then displayed as two orthogonal horizontal components of magnetization of the specimen on a 6-digit liquid crystal panel. To obtain complete vector results, it is necessary to perform a sequence of measurements with the specimen in different orientations.

for routine measurements is 5×10^{-6} Am^2/kg, with a measurement time of ~5 minute/sample and an accuracy of direction of 2–4°.

IV. Cryogenic Squid Magnetometer

This type of magnetometer is mainly associated with super-conductivity. Its sensor is called Squid. The magnetometer is contained within an insulated vacuum space cooled by helium. A metal ring of superconductor material is maintained below the critical temperature. When a magnetized specimen is moved close to it, the magnetic flux φ linked to the ring changes, and the change $\Delta\phi$ induces in the ring an electrical current whose intensity depends on the component of the field B of the specimen parallel to the axis of the ring. The sensors are installed inside a Dewar vessel, shaped in such a way so as to enable the specimen kept at ambient temperature to be moved close to it. Having

three mutually orthogonal Squids, the three components of B can be measured all in one go.

Modern instruments provide reliable measurements of magnetic moments $M=10^{-10}$ Am^2, and useful for specimens with weak magnetization ($Jr = 10^{-5}$ A/m), as for example carbonate rocks. Basic effusive rocks can exhibit values up to Jr=10 A/m; higher values are observed in particular cases (mineralizations, lightning strikes).

V. Alternating Field and Thermal Demagnetizers

The NRM can consist of more than one component, each with a different geological and chronological meaning. The measured vector (J_{NRM}) is the resultant of the various components; so the problem of identifying them needs to be confronted. This is mathematically impossible because a vector can be resolved into components in infinite different ways. Resolution can instead be possible through physics, based on a simple principle. If a rock has multiple magnetization components, each of them involves a different population of ferromagnetic grains: if they have different magnetic properties, for example different T_b or H_c, the components can be cancelled out one at a time, and this allows to isolate them (Fig. 4.19).

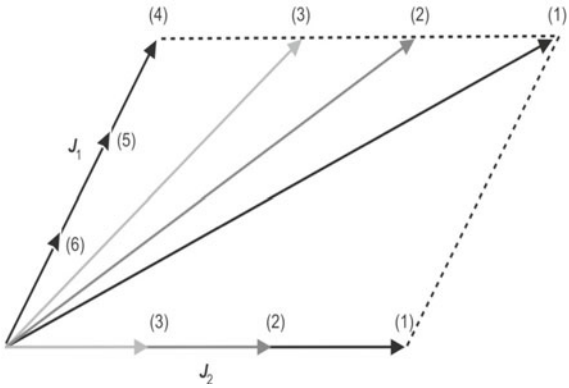

Figure 4.19. Stepwise demagnetization of a NRM consisting of two components with different blocking temperature or coercivity spectra. As the less stable component J2 is erased, the direction of the measured remanence varies (steps 1 to 4); when J2 is completely erased, only the more stable component J1 survives; direction does not change any more, intensity progressively decreases (steps 4 to 6).

To cancel a magnetization, thermal or magnetic energy must be provided. Thermal demagnetization is performed with an oven shielded from all external magnetic fields and built in such a way that the magnetic fields caused by the heating current cancel each other out (Fig. 4.20). The magnetic domains with $Tb \leq T_1$ lose their magnetization, which they reacquire when the specimen cool

down to ambient temperature, always within the magnetic shield. Since there is no field, there is no preferential direction. So each domain is magnetized in its easy direction and the resultant of the domains with $T_b = T_1$ is zero. The process is repeated step by step until $J(T_n) = 0$, i.e. when the maximum value of T_b has been attained.

Figure 4.20. MMTD 80 sample thermal demagnetizer isolates the primary component which carries the remanence acquired at the time of formation of the rock. A sample is heated and cooled in zero field for a series of increasing temperatures. After each step the remaining remanence is measured at room temperature. Only those grains with blocking temperatures below the demagnetization temperature will be demagnetized.

Demagnetization in AF is wholly similar to thermal, and is based on the magnetic hysteresis principle. Instead of the oven, a solenoid shielded from external magnetic fields is used (Fig. 4.21). It carries an alternating current,

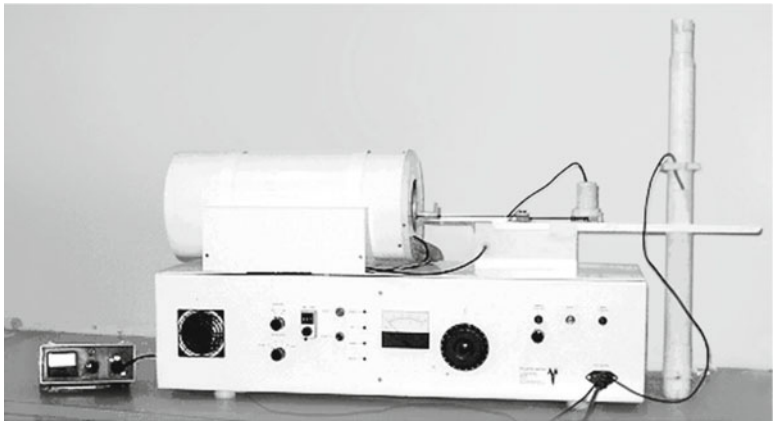

Figure 4.21. Molspin alternating field demagnetizer with ARM attachment removes the secondary components having low coercivities. A sample is subjected to alternating field that is smoothly reduced to zero from some peak value. The AF demagnetization curve is measured by exposing the sample to a series of increasing AF peak values (5, 10, 15, 20, …100 mT). After each demagnetizing step the remaining remanence is measured. Remanences in grains with low coercivities are eased out first while grains with higher coercivities remain unaltered.

which generates an AF that is parallel to the axis of the solenoid and has a peak value of H_1. Domains with $H_c \leq H_1$ follow the oscillations of the field; when it is made to decrease (Fig. 4.22), each domain is remagnetized as the field passes its H_c value. The two opposite senses of the AF are two preferential directions, and when H=0, domain magnetization is statistically distributed half in one sense, half in the opposite, thereby yielding a zero resultant. A second step is done with H_2 and so on as in thermal procedure.

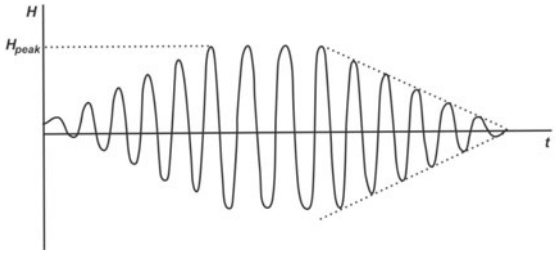

Figure 4.22. Alternating field (AF) demagnetization. The intensity of the field increases up to and for a few seconds remains at maximum value, H_{peak}; then linearly decays to zero.

VI. Rock- and Environmental-magnetic Instrument Kit

Many instruments founded on various principles serve to determine the fundamental magnetic properties of complex natural samples. Many of the instruments of palaeomagnetism are also used for environmental magnetic measurements. The basic environmental magnetism laboratory comprises a susceptibility kappabridge/meter (and suitable sensors), a magnetometer, a pulse magnetizer, and AF demagnetizer with an apparatus for imparting anhysteretic remanent magnetization to samples.

For environmental work using mineral magnetic measurements, the remanent magnetizations are induced into the samples within the laboratory by the use of artificial, as opposed to natural, magnetic fields. The remanence induced can be measured in a single orientation by the spinner magnetometer. Artificial magnetic fields suitable for inducing remanence in geological samples for mineral magnetic work can be generated by the use of electromagnets. The pulse magnetizer (Fig. 4.23) generates fields between 0 and 9 T. The remanence induced in a sample in this way is known as IRM, and the remanence acquired at a particular field size is referred to as IRM_{20mT}, IRM_{40mT}, etc. The pulse magnetizer operates using a capacitor system in which electrical charge is built up to the necessary level and required magnetic field is then generated as a short duration pulse. Measurement of full hysteresis loops is done using equipment such as Molspin vibrating sample magnetometer (Fig. 4.26). Low and high temperature dependence (–196° to 700°C) of magnetic susceptibility provide useful additional information on the Curie temperature using AGICO's KLY4S Kappabridge/Bartington thermal susceptibility system (Figs 4.24 and 4.25).

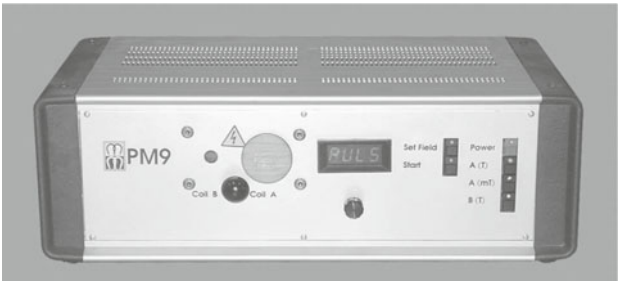

Figure 4.23. The pulse magnetizer. The IRM of a sample is the magnetization retained by that sample when a known field is imparted to the sample. Imparting IRM to a rock or sedimentary sample in a laboratory is achieved by subjecting it to increasing fields, in stages from 1 mT to 9 T by using the pulse magnetizer. The saturation IRM or SIRM is the maximum remanence that a sample can acquire, indicating the type of magnetic mineral present.

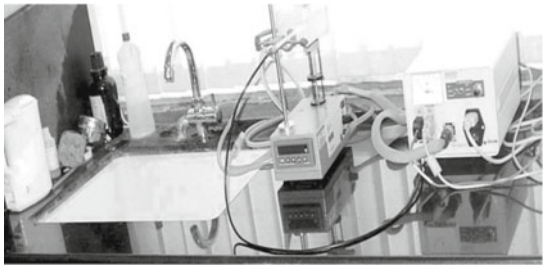

Figure 4.24. Bartington temperature variation of magnetic susceptibility meter, operating over the temperature range -200° C to +900° C, is used to investigate magnetic mineralogy, grain size and for the determination of Curie transition temperatures.

Figure 4.25. Anisotropy of magnetic susceptibility kappabridge (KLY-4S) and temperature variation apparatus (CS-3). The kappabridge is used to measure magnetic susceptibility of rock and sedimentary samples, as also its anisotropy. Its operation is based on measurements of inductivity changes in coil due to a rock/sedimentary specimen. This instrument is attached with high and low temperature apparatus CS-3/ CS-L to monitor temperature variations of magnetic susceptibility.

(i) Vibrating sample magnetometer (VSM): This magnetometer is used for discrimination of magnetic minerals. The VSM is generally used for high-field measurements, such as hysteresis properties. The sample is mounted at one end of a vertical cantilever, the other end of which is attached to the bottom of a resonator unit. The sample is mechanically vibrated at a fixed frequency (Fig. 4.26). The sensing coils have an emf induced within them due to the changing flux produced by the vibrating sample. For a sample magnetization M, the induced voltage V in the sensing coils is given by $V = \mu_0 GM\omega A \sin \omega t$, where ω is the angular frequency of the vibration, A is the vibration amplitude and G is a factor relating to the geometry of the sensing coils. A uniform magnetic field in the region of the sample is provided by an electromagnet or superconducting solenoid if fields >3 T are required. A heater or cryostat can be suitably fitted for variable temperature measurement.

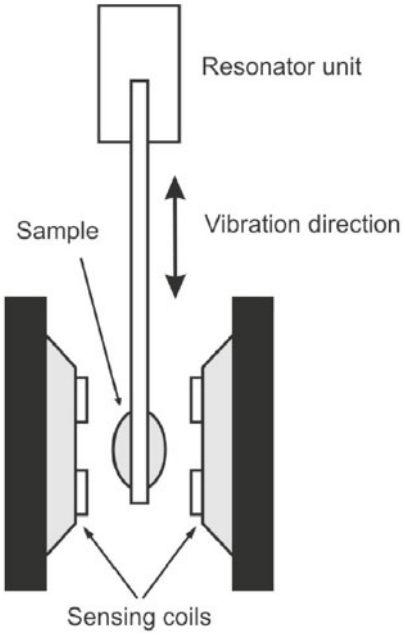

Figure 4.26. A schematic of a vibrating sample magnetometer. The sample is vibrated mechanically, and the induced signal in the sensing coils will be proportional to its magnetization (*courtesy:* Williams).

(ii) Susceptibility meter/Kappabridge: Magnetic susceptibility is a measure of the concentration of ferrimagnetic minerals by rapid and non-destructive means. It can be measured both in the laboratory and directly in the field. There are three field versions (MS2D, MS2F and KT Kappameter) and two laboratory (MS2B and Kappabridges of KLY and MFK1 series), commonly used to measure magnetic susceptibility (Figs 4.25 and 4.27).

The MS2 magnetic susceptibility system consists of a MS2 meter with interchangeable field probes, MS2D and MS2F, and the laboratory probe MS2B (Figs 4.27 and 4.28a). The field sensors are used in conjunction with a MS2 probe handle. It is submersible to a depth of the handle length. The MS2 meter allows data acquisition with a 4-digit display (range: 10^{-1}–10^{-6} SI). The other sensor is a portable KT-6 Kappameter of almost pocket size (66 mm dia) with a data range of 10^{-4}–10^{-9} SI (Fig. 4.28b). Generally, the laboratory MS2B and KLY-2 Kappabridge probes give true susceptibility values. As these sensors do not work at the same frequency and induction field (Table 4.3), measurement differences are to be expected for materials with a possible frequency and AC dependence of susceptibility (Figs 4.25 and 4.27).

Table 4.3 Measurement specifications of Bartington MS2B and AGICO Kappabridges

Specifications	*Bartington*	*AGICO*	
	MS2B	*KLY-4S*	*MFK1-FA*
Frequency (Hz)	470 & 4700	875	976, 3904 & 15616
Alternating field (A/m)	80	3 to 450	2 to 700
Sensitivity (SI)	2×10^{-6}	3×10^{-8}	2×10^{-8}
Measuring range (SI)	0-0.1	0-0.2	0-0.9

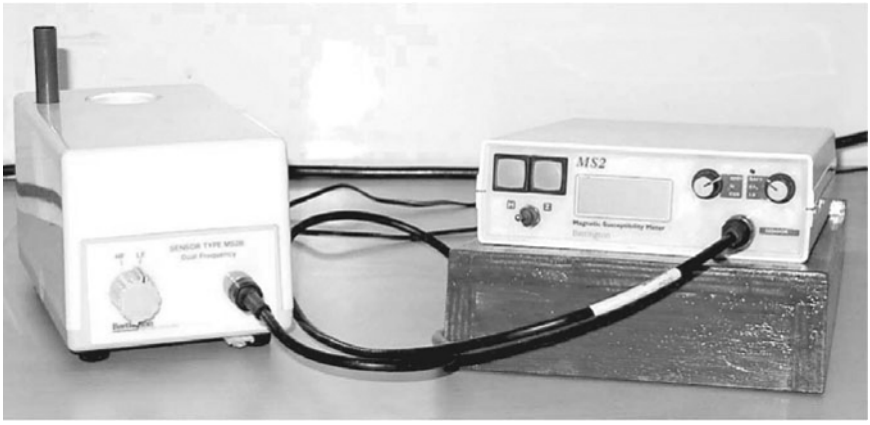

Figure 4.27. MS2 Bartington susceptibility meter attached with a dual frequency MS2B sensor can rapidly measure low field or initial susceptibility. The sensor subjects the sample to a non-saturating field that has the advantage of measuring initial susceptibility without destroying magnetic remanence of the sample.

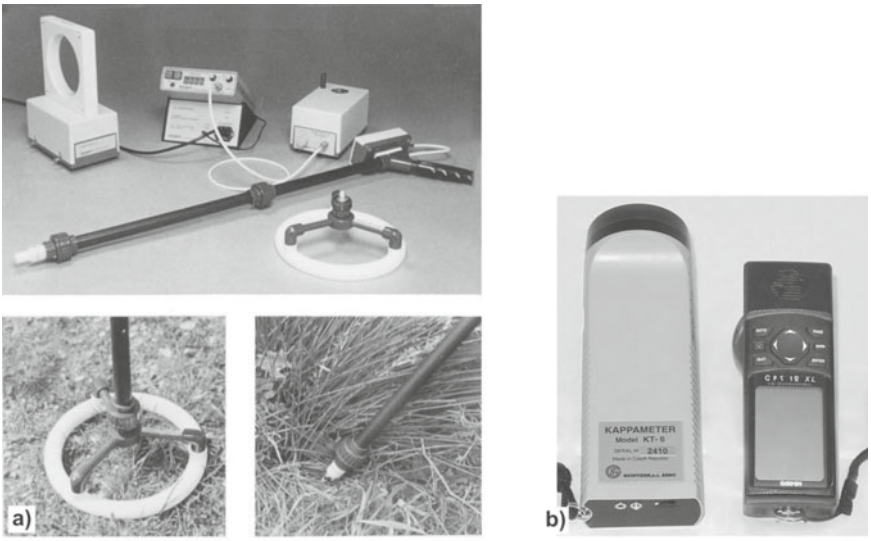

Figure 4.28. (a) A set of Bartington susceptibility meters and sensors. (b) The Kappameter used for in situ susceptibility measurements and hand held GPS unit for getting the exact location.

5

MAGNETIC OBSERVATORIES AND DATA ANALYSIS

The geophysical discipline of geomagnetism carries out scientific study of the Earth's external and internal field comprising secular change, and magnetic reversals. This is a multidisciplinary science and magnetic observatories (MOs) provide data to those institutes, whose interests range from geology, subsurface structural mapping, geophysics (including seismology and earthquake prediction), meteorology, solar-terrestrial physics, and astronomy. Most of the surface magnetic phenomena exhibit strong dependence on both latitude and longitude. A worldwide network of magnetic stations is, therefore, absolutely essential for continuous monitoring of the ionospheric and magnetospheric phenomenon. Much depends on the accuracy and stability of the input magnetic data from magnetic observatories.

Global distribution of ground-based MOs (Fig. 5.1) support these pursuits by providing accurate records of the magnetic field direction and intensity at fixed locations over long periods of time. First few MOs began operation in the early nineteenth century in response to the influence of Humboldt and Gauss. Establishment of MOs recognizes geomagnetic field to be a continuum (though transient and fleeting), which connects Earth to itself and to space. The earliest known regular measurements of declination were carried out at Greenwich from 1816 to calibrate ship's compasses. The practical use of MO includes help in space, ground navigation systems and monitoring earthquake activity. The data generated at the observatory is passed through a series of quality control measures that involves data processing.

To support scientific research in geomagnetism, Colaba-Alibag Observatory (CAO) was separated from the Indian Meteorological Department (IMD) in 1971. It was also done because major gains were being made in the arena of space exploration, which had a direct bearing on studies related to space magnetism. The CAO and the then existing equatorial observatories were

reconstituted as Indian Institute of Geomagnetism (IIG). It is an autonomous organization, working directly under the Department of Science and Technology (DST). Till 2003, it was located at Colaba, but now the head-quarter has been moved over to a new campus in Navi Mumbai. The growth and development of geomagnetism in India is interminably associated with IIG, which continues to make single largest contribution to studies in geomagnetism.

I. Overview and Observatory Characteristics

Monitoring the strength and direction of EMF accurately and continuously over many years with a time resolution of at least a minute is carried out at MOs. Their data reveal field changes on a wide range of timescales from seconds to centuries, which are important for understanding processes both inside and outside the Earth.

A network of ~180 observatories is currently operating around the world (Fig. 5.1), although their distribution is mainly determined by the location of habitable land and availability of local expertise. This has resulted in its scarce presence in some regions. Consequently, vast tracts of ocean and southern hemisphere have poor coverage (Fig. 5.1). International scientific campaigns such as international polar years 1882–1883 and 1932–1933, and the international geophysical year (IGY) 1957–1958 saw the establishment of many observatories around the world.

Figure 5.1. Location of currently operating magnetic observatories around the world.

The variometer and absolute are the two main categories of instruments at an observatory. They make continuous measurements of elements of the geomagnetic field vector in arbitrary units on photographic paper variographs and electrical voltage for fluxgates (Chapter 4). The resulting data from analog

and digital variometers are, however, not absolute. But the PPM (measuring total field intensity) and fluxgate theodolites (measuring D and I) can make measurements of the magnetic field in terms of absolute physical basic units or universal physical constants (Chapter 4). This data is subjected to application of baseline so that it closely fits the absolute data after which it is ready for use in data analysis. Many instrumental effects of long-term drifts in the variometer data, scaling factors, offsets, sensor alignments, temperature responses and timing events, have been removed with modern digital variometers. Once a continuous time series of data reduced to the observatory reference location is obtained, final observatory products are produced and disseminated. These include 1-min means, hourly means, daily means, annual means, k-indices and some more.

InterMagnet (international magnetic observatory network) was created in late 1980s to establish a worldwide network of cooperating digital magnetic observatories. These observatories agreed to adopt global standards in the measurement, recording and near real time dissemination. There are now ~100 observatories operating to InterMagnet standards. Besides this, the combination of observatory data with magnetic survey satellites such as Magsat, Oersted, CHAMP and SAC-C provides a rich research resource into understanding diverse topics ranging from core processes to effects of space weather on technological systems during magnetic storms and many others. The ongoing programmes to replace analog systems with digital systems will undoubtedly increase the utility of observatory data.

II. Magnetic Observatories in India

Magnetic observatories in India are in operation for well over 180 years. Geomagnetism started in India with observations at Chennai (Madras) (1822–1881), Shimla (1841–1845), and Thiruvananthapuram (Trivandrum) observatory (1841–1871). The first geomagnetic observations were carried out in 1823 at Colaba, Mumbai (Bombay), but the magnetic observatory (MO) was formally established in 1841, after which readings were regularly taken. Values of magnetic elements from 1845 onwards exist as printed volumes. Because of the magnetic perturbations due to the introduction of a DC electric tram system in Mumbai in 1900, the Colaba observatory was moved to Alibag in 1904, a low-latitude station outside the equatorial electrojet domain. A standard Alibag magnetic observatory (ABO) was established in April 1904, and the observations are still continuing. The measurements were overlapped with Colaba records for a period of two years (1904-1906) after which recordings at Colaba were stopped. Thus, at present, CAO data form a long series of >180 years.

In 1993, a digital MO under InterMagnet (IMO) was commissioned at Alibag and since then 1-min data are being regularly transferred to the geomagnetic information nodes (GINs), which are the collection and

dissemination points for near real-time data within the InterMagnet. These nodes are connected to the IMOs by satellite, computer and telephone networks.

A magnetic observatory functioned at Kodaikanal between 1902 and 1923, and again from 1949 to date. The Sabhawala observatory carried out observations during 1902–1943, and from 1964 to date. The IGY years of 1957–1959 saw the establishment of two new MOs at Thiruvananthapuram and Annamalainagar to study the equatorial electrojet (EEJ). The decade of 1960 saw the operation of MOs at places like Kodaikanal, Sabhawala (near Dehradun) and Hyderabad. Geoelectric observatories were setup at Choutuppal near Hyderabad and at Etaiyapuram near Kodaikanal.

A collaborative programme was established by IIG with the Institute of Ionosphere and Terrestrial Magnetism (IZMIRAN) from the erstwhile Soviet Union to set up 'project geomagnetic meridian', whose emphasis was on 145° meridian. Under this project, geomagnetic observatories were set up at Ujjain and Jaipur in 1975. These places were selected to have a control station outside the influence but having practically similar kind of variations to decipher the complexities and intricacies of EEJ. Shillong MO (1975) was commissioned to bridge a large gap in the distribution of MOs and also to study the ionospheric current systems. The Gulmarg MO, which is close to the latitude of focus of quiet time ionospheric current system, became operational in 1977. This gave rise to a unique chain of observatories right from the dip equator, Trivandrum to the north pole, if the chain of observatories operated by the erstwhile Soviet Union is also considered as a continuous chain along a single longitudinal belt (~79°E).

Trivandrum MO was shifted to Tirunelveli in 1996 and Annamalainagar to Pondicherry in 1993. New observatories became operational at Nagpur, Visakhapatnam, Silchar, Rajkot and Port Blair. They were commissioned in 1991, 1994, 1998, 2007, and 2007, respectively. Data from Alibag and Ujjain (closed in 2004) MOs highlighted certain EEJ features. However, Alibag being a coastal station, its magnetic recordings are influenced by the induced currents from the Arabian Sea. Also, in the literature of palaeomagnetism, the ancient poles were all reduced to the latitude and longitude of a central place in the country, because of which Nagpur was chosen for the installation of a permanent observatory. The choice of Visakhapatnam was dictated by the presence of Alibag observatory. A need was felt to have another station, on the same geographic latitude as that of Alibag, on the eastern coast of India, to unravel the hitherto unknown oceanic effects between the two coasts. The station at Visakhapatnam is also expected to serve as a base station for marine magnetic measurements carried out off Bay of Bengal.

The MOs at Alibag, Jaipur, Rajkot, Nagpur, Visakhapatnam and Allahabad ensure proper regional coverage. Rajkot is the first modern observatory monitoring geomagnetic variations at 1 Hz sampling rate. The locations of Shillong and Silchar MOs are ideally suited to monitor tectonic and geomagnetic changes occurring across the Dauki fault. They are located respectively to the

north and south of the Dauki fault. Port Blair was chosen to ascertain the geomagnetic changes caused by the tectonics of the arc region, leading to increased seismic activity in Andaman and adjoining areas.

Table 5.1 gives geographic coordinates and geomagnetic (IGRF models 1990 and 2010) coordinates of the 17 Indian magnetic observatories. Locations of the Indian permanent observatories are such that they cover a wide range of latitudes extending from the dip equator up to the focus of the Sq current system. Thus, the magnetic data recorded continuously at these observatories provide a unique opportunity to study the associated phenomena of ionospheric Sq current system as well as the EEJ and counter EEJ. The establishment of the equatorial geophysical research laboratory (EGRL) at Tirunelveli near the latitude of the dip equator is expected in providing the basic infrastructure required for the study of EEJ and other upper atmosphere features.

III. Indian Observatories: Automation

The modernized digital acquisition systems at the Indian MOs are installed to provide high resolution digital geomagnetic data with more stable baselines (Chapter 4). The digital MOs are in the process of being linked to a centralized station, so that the data are readily accessible to scientists, who can do quality check and pass appropriate instructions for corrective measures, if the data are found incompatible. Acquisition and transmission of 1-sec digital data of the three magnetic components recorded from the InterMagnet system at Alibag and computation and publishing of EEJ index are being done in an exceptionally expeditious way. The calibration of Indian navy, airforce, SOI, NGRI and GSI compasses is also extensively modernized.

IV. Observatory Data: Services

Descriptions of the observatories, their results, instruments and methods are found in the magnetic year-book. In today's world, dissemination of magnetic data by internet for instant access and analyses has become important, and this is done through InterMagnet (WDC) as well as through IIG's website (iigs.iigm.res.in/world.htm). One-sec data are useful for research into external magnetic fields. Data at this time resolution are also required for modelling geomagnetically induced currents, which are of interest to the electricity distribution industry, especially those at high latitudes. A further modern-day application, important to hydrocarbon production around India, is the use of accurate magnetic reference data to correct well-logging survey measurements. Observatory data are also used in the analysis of records gained by ground and aeromagnetic surveys (see Chapter 9).

5.1 MEASUREMENT AND DATA

The modern MOs have a fluxgate magnetometer, which gives vectorial data, conventionally expressed in terms of either the Cartesian components X, Y,

Table 5.1 The geographic and geomagnetic latitudes of the 21 geomagnetic observatories operated by India

Station	*Geographic co-ordinates (In degrees)*		*Geomagnetic co-ordinates (In degrees)*			
			1990 model		*2010 model*	
	Latitude	*Longitude*	*Latitude*	*Longitude*	*Latitude*	*Longitude*
Trivandrum (TRD)	8.48 N	76.95 E	- 0.77 S	148.45 E	- 0.11 S	149.54 E
Tirunelveli (TIR)	8.70 N	77.80 E	- 0.64 S	149.30 E	0.03 N	150.40 E
Eitaiyapuram (ETT)	9.17 N	78.00 E	- 0.19 S	149.55 E	0.48 N	150.64 E
Kodaikanal (KOD)	10.23 N	77.47 E	0.92 N	149.13 E	1.59 N	150.21 E
Annamalainagar(ANN)	11.37 N	79.68 E	1.85 N	151.40 E	2.54 N	152.47 E
Port Blair	11.68 N	92.72 E	1.23 N	164.17 E	2.03 N	165.25 E
Pondicherry (PON)	11.92 N	79.92 E	2.37 N	151.69 E	3.07 N	152.75 E
Hyderabad (HYB)	17.42 N	78.55 E	7.97 N	150.88 E	8.66 N	151.88 E
Visakhapatnam (VSK)	17.68 N	83.32 E	7.83 N	155.47 E	8.56 N	156.49 E
Alibag (ABG)	18.62 N	72.87 E	9.73 N	145.57 E	10.36 N	146.54 E
Nagpur (NGP)	21.15 N	79.08 E	11.64 N	151.75 E	12.33 N	152.71 E
Rajkot (RJK)	22.30 N	70.93 E	13.60 N	144.16 E	14.21 N	145.08 E
Ujjain (UJJ)	23.18 N	75.78 E	13.97 N	148.84 E	14.63 N	149.77 E
Silchar (SIL)	24.93 N	92.82 E	14.46 N	164.98 E	15.27 N	165.96 E
Allahabad (ALH)	25.28 N	81.54 E	15.54 N	154.46 E	16.26 N	155.39 E
Shillong (SHI)	25.92 N	91.88 E	15.49 N	164.16 E	16.30 N	165.12 E
Jaipur (JAI)	26.92 N	75.80 E	17.68 N	149.27 E	18.35 N	150.16 E
Sabhawala (SAB)	30.37 N	77.80 E	20.93 N	151.51 E	21.62 N	152.37 E
Hanle (HAN)	32.76 N	78.95 E	23.20 N	152.83 E	23.91 N	153.67 E
Gulmarg (GUL)	34.08 N	74.40 E	24.93 N	148.85 E	25.60 N	149.65 E
Maitri (MAl)	- 70.75 S	11.75 E	-66.84 S	56.29 E	-67.49 S	58.91 E

The Antarctic observatory at Maitri operates all the year round. The geomagnetic coordinates are based on the IGRF models 1990 and 2010.

and Z or the horizontal-polar components ($H = [X_2 + Y_2]^{1/2}$, D = arctan[Y/X], and Z). A PPM measures the total absolute field intensity, $F = (X^2 + Y^2 + Z^2)^{1/2}$. A series of measurements using the theodolite at the observatory provides D and I = arctan(Z/H). This absolute magnetic direction data are then used to calibrate the fluxgate data, so as to compensate for long-term drift in the fluxgate magnetometer. Production of definitive observatory data involves processing. The resulting data have an absolute accuracy of better than 5 nT. Low and mid latitude Indian MOs record magnetic variations in D, H and Z. However, at Maitri in Antarctica, X, Y and Z are measured. This is because the field aligned currents cause very rapid fluctuations in D at higher north and south latitudes of >75°.

I. Solar Terrestrial Effects from Observatory

An invisible force, the magnetic field, envelopes the Earth, which originates deep within the Earth and extends many thousands of km into geospace. The geospace comprises the atmosphere, ionosphere and magnetosphere. On the basis of the solar-terrestrial interaction process, the Earth is broadly divided into four regions (Fig. 5.2a) with distinct and clearly demarcated characteristics. The network of global MOs to which the Indian chain of 17 stations belong, provide an invaluable source of data to understand these intricacies. The advent of space age since 1957 catapulted man to physically and instrumentally observe the interplanetary space, helping confirm the earlier hypotheses of solar sources of magnetic storms and auroras. As the Earth rotates under overhead current system in the upper atmosphere, a smoothly varying magnetic field is produced whose magnitude and shape depend upon the station location, time of day and the season of the year. They thus offer clues to the vagaries of the upper atmosphere, particularly its electrical state. Close to the equator, this current is enhanced abnormally called EEJ. The observations that catch up this anomalous current lie close to the tip of the peninsula.

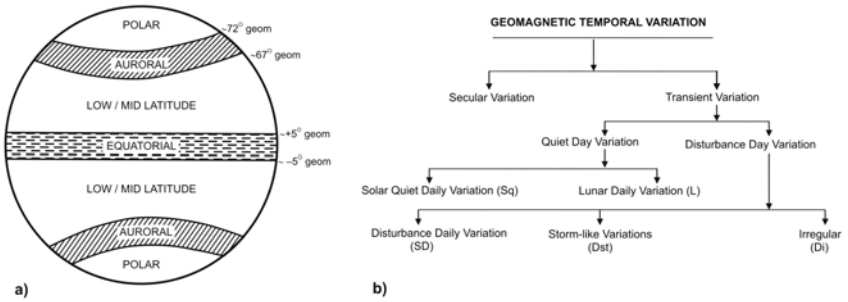

Figure 5.2. (a) Broad latitudinal categorization of the Earth, on the basis of geophysical phenomena occurring as a consequence of the solar-terrestrial energy coupling (Rajaram and Pisharoty, 1998). (b) Schematic of geomagnetic variations on different timescales.

Magnetic charts are an inexpensive tool to monitor signatures of temporal and spatial characteristics of the large-scale over-head currents and the geomagnetic field (Fig. 5.2b). The morphological and geographical location of India in the global scenario is ideal for monitoring the equatorial and low latitude dynamics and its associated effect in the global Sq current system, equatorial ionization anomaly and low latitude ionospheric irregularities. Interestingly, Indian observatory network from dip equator to Sq focus complements the magnetometer chain along a single longitudinal belt (~79°E) through Russia to the North Pole. The magnetic measurements from the Indian longitudinal chain form a unique database in investigating the ionosphere-magnetosphere coupling processes, as the entire network can cover the locations spanning from equator to the North Pole in the Indo-Russian longitude.

II. Observatory Data Based Investigation

Observatory data on its own or coupled with satellite observations are used to launch investigations into an array of diverse topics from the realm of solid Earth to atmosphere to interplanetary space. This is done by applying a range of mathematical and statistical techniques to qualify and quantify the field variations. Numerous numerical models are built to decipher the quiet and disturbed time dynamics of the ionosphere and magnetosphere. The processes of energetic reconnection and vigorous coupling of atmosphere-ionosphere-magnetosphere are a hot topic for investigation (Chapters 3 and 8). Since the equatorial and polar electric current systems are genetically different, the data from low latitude observatories are used to standardize the EEJ indices. Geomagnetic storm processes impact low latitudes in quite different way compared to high latitudes and hence these changes are examined in association with the interplanetary features. The disturbance fields indicative of space weather conditions, are characterized by various geomagnetic activity indices. The correlations between selective features on the Sun and the surface magnetic field changes enable to predict the possibility of the occurrence of violent geomagnetic disturbances. Repeat measurements of the magnetic field aid in preparing regional magnetic field model and monitoring secular acceleration towards tectonic change interpretation. The surveys in the vicinity of equatorial locations are carried out periodically to update or monitor information on the location and movement of the dip equator. The variations in geomagnetic field recorded on the ground or in the magnetosphere cavity, when interpreted skillfully can yield clues to physical processes at work in (1) the entire magnetospheric cavity, (2) in interplanetary space, (3) on the Sun, and (4) within the Earth.

III. Temporal Variation of Geomagnetism Spectrum

The painstaking measurements carried out by astronomers, clockmakers, and the like revealed some novel features. To them, there were slow changes in the strength and direction of the magnetic field spanning several years, regular

smooth daily variations and occasional violent outbursts of short duration, which they linked to the Sun. These discoveries stimulated the curiosity to unravel the causative agents and look for the inter-relationships between all the cosmic entities to use this knowledge for predictive purposes. Hence, the intricacies and vagaries of the geomagnetic field are studied since the variations encompass several types of information. This knowledge is gained out from a few important frequency bands, the details of which follow in the next paragraph.

Variations are normally studied by analyzing how changes in the geomagnetic field are distributed as a function of frequency. This is done by estimating the spectrum of geomagnetic variations. The power spectral density S(f) is a measure of the power in geomagnetic field variations at frequency f. When integrated over all frequencies, it measures the total variance in the geomagnetic field. Figure 5.3a shows a schematic of the various processes that contribute to the geomagnetic field, and these can be roughly divided according to the frequency range in which they operate.

The bulk of EMF is generated at the liquid outer core, where fluid flow produces secular variation in the magnetic field, which propagates upward through mantle and crust. Short-term changes in the core field are attenuated by their passage through the mantle so that at periods less than a few months most of the changes are of external origin. The electrically conductive ionosphere supports Sq currents with a diurnal variation as a result of dayside solar heating. Lightning generates high-frequency Schuman resonances in the Earth/ionosphere cavity. Outside the Earth, the magnetosphere, the manifestation of core dynamo, is deformed and modulated by the solar wind, compressed on the dayside and elongated on the night-side. At a distance of $\sim 3R_E$, the magnetospheric ring current acts to oppose the main field, and is modulated by solar activity. A recent composite spectrum by Constable and Constable (Fig. 5.3b) uses spectral estimates from palaeointensity variations at long periods. Between 10^{-10} and 1 Hz, the spectrum is from Filloux and for above 1 Hz, the results of Nichols and his coworkers are included.

5.2 GEOMAGNETISM AND SECULAR VARIATION

The observed temporal variations of the EMF are due to two distinct (external and internal) source regions with respect to the Earth's surface. The short-period variations of the EMF have an external origin, while long-period variations have an internal one. However, the boundary between these two domains, if it exists, is not known accurately. Fluctuations of the external field range from millisec to a few decades, whereas the longer periods are related to variations of the solar magnetic field (22 and 11 years). The magnetic field is not a pure dipole. It has substantial quadrupole and higher order polarity components adding to its complexity, which is unravelled only by examining various components of its behaviour. The SV of the geomagnetic field is one such aspect.

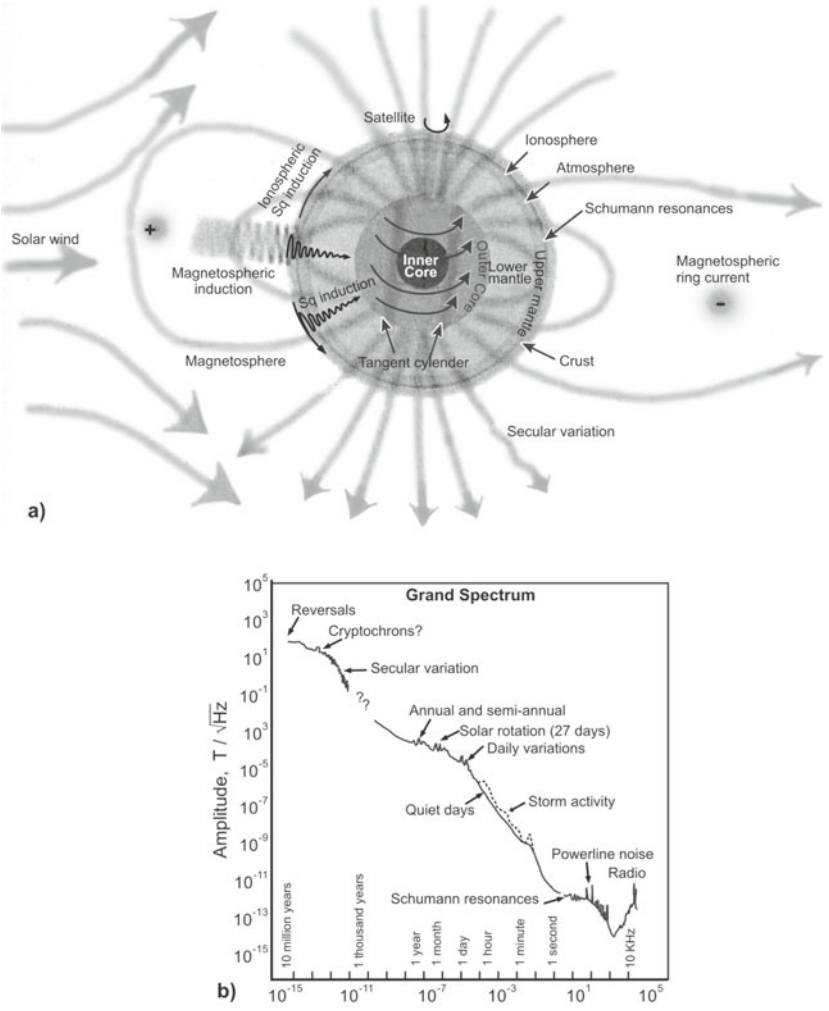

Figure 5.3. (a) Schematic illustration of the physical processes, contribute to the geomagnetic field (courtesy: Constable and Constable, 2004). (b) Composite amplitude spectrum of geomagnetic variations as a function of frequency. Annotations indicate the predominant physical processes at various scales (Constable, 2007). Note this is an amplitude rather than power spectrum, i.e. the square root of power spectral density.

I. Long-period Variations of Internal Geomagnetic Field

Changes of the internal field range from a few million years (reversals of the internal dipole) through a few hundreds of years for changes in intensity of the dipole to a few years for phenomena like the magnetic jerk (Chapters 2 and 7). The more recent historical past is covered under archaeomagnetism. Slow changes in the geomagnetic field in the time frame of hundreds of years form the secular variation. Earth's magnetic moment has so far varied with a

periodicity of ~7000 year, with values ranging from 6.5 to 11.5×10^6 (Fig. 5.4). This interlude is attributed to be stable natural period of the Earth's internal dynamo. There exists another SV of 300 to 100 years, ascribed to originate in convective motions within the geodynamo. Other periodicities observed are of 600 and 60 years. These are attributed to inhomogeneous processes at the core-mantle boundary.

Archaeomagnetic data indicate that the total field intensity has over the past 2000 years dropped from a value of 4.2 to ~3.2 nT, but that over the preceding 3000 years, it had increased by practically the same value. For the last 150 years, the geomagnetic field intensity has been dropping at a yearly rate of 15 nT, with the jump accelerating to 22 nT/year in the 1960s and to 29 nT/year in the 1980s (Fig. 5.4). If this fall is linearly extrapolated, the dipole field may disappear in 1000 years! Palaeomagnetic studies, however, show situations in the past, where the dipole attained zero, and then recovered rapidly with either the same or reversed polarity. Hence, it is difficult to predict just how this field intensity changes in future.

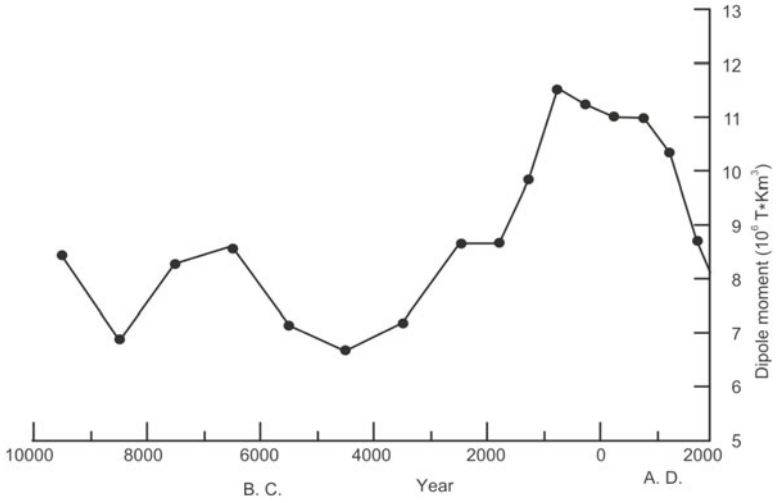

Figure 5.4. Archaeomagnetic data show the change in the magnetic dipole moment of the Earth since 10,000 BC to date. Note a sharp rise in dipole moment since 2000 BC before a sharp drop at ~800 AD till the present (Cain, 1987).

Other notable SV features are: (1) the non-dipole part of the field, which is currently drifting westward (WD) with an average angular velocity of ~0.3°/year, and is growing or decaying at ~10 nT/year. Halley was the first to observe the WD in the Atlantic ocean, where lines of zero D moved steadily westward during the past few centuries (Fig. 1.6a), and (2) the magnetic moment of the dipole which over the past century is decaying at an average rate of ~0.4%/year.

Secular trends at the Indian observatories: The plots of the annual mean values of D, H and Z for quiet days during 1958-1990 at six stations are shown in Fig. 5.5a-c together with their best-fitting curves: a parabola for D, a quadratic for H and a cubic for Z. Secular trends show a region of demarcation between equatorial and low latitude stations. The secular jerk around 1960-70 is not seen in D but is noted in H and Z components. A comparison between the observed annual means and IGRF models indicates very low SV anomaly in the Indian region.

At Alibag, H component attained a maximum by 1965, and is decreasing presently at the rate of 20 nT/year. The diurnal variation in the Z component close to the dip equator will be small, but analysis shows a significant internal contribution due to channelling of induced currents in the Palk Strait between India and Sri Lanka. Another notable feature of the region is the location of one of the foci of H, and H maximum close to the Andaman islands. The parallelism in the secular trend of Alibag, Hyderabad and Sabhawala indicate that the feature has a regional coverage, whose southern latitudinal extent is just above the edge of the EEJ belt. The secular trend for D is a smooth parabola with the broad maximum near the same epoch as for H. Z component, on the other hand, shows a near-sinusoidal secular trend with ~80 years periodicity, the so-called Gleissberg cycle. In the Indian sector, the dip equator shifted northward from 1928 to 1967 at 2 to 3°/year, after which it started drifting southward.

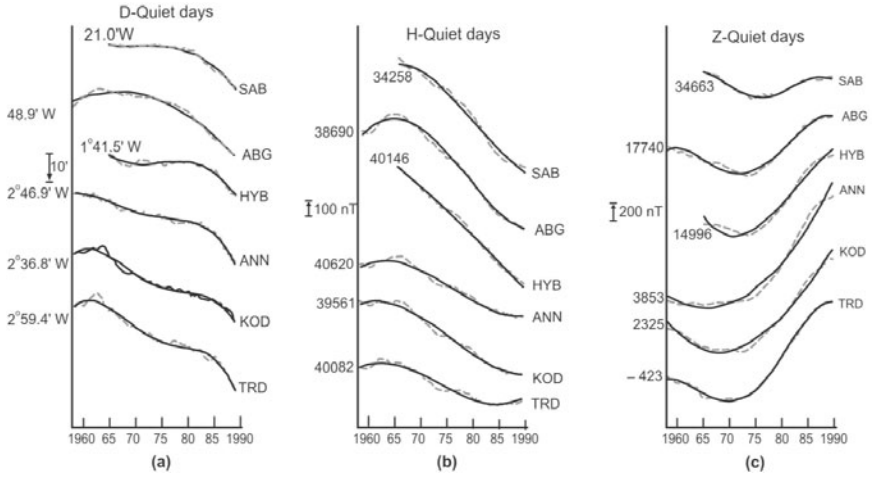

Figure 5.5. Observed annual mean values for quiet days at six Indian stations from 1958-1990, together with their best-fitting curves of (a) D, westerly-increasing D is plotted downwards, (b) H-component and (c) Z-component (Bhardwaj and Rangarajan, 1997).

II. Short-period Variations of External Geomagnetic Field

The external field variations originate in space around the Earth, generally have shorter time-periods of a few years (22 years solar magnetic reversal cycle and 11-year solar sunspot cycle), through a few days (magnetic storms) to a few sec (ULF pulsations). A periodicity of one year may be linked to variable distances during the Earth's orbital motion around the Sun, and a semi-annual periodicity is understood to be associated with the differing tilt of the Earth's axis of rotation with respect to the plane of the ecliptic.

At the faster end of the spectra is: (1) 27-day variation connected with solar active regions rotating with the Sun's period of rotation, (2) 24-hour variation and its sub-harmonics connected with Sunrise and Sunset (referred to as Sq variation), (3) variations of lunar origin with period 50.5-min longer than the Sq, (4) 2 to 4-day variation associated with the main phase and decay of geomagnetic storms, (5) 1 to 3-hour variation connected with the growth and decay of sub-storms, (6) periodicities of a few min to an hour which are set due to (i) X-rays from solar flares, (ii) decreased currents in the ionosphere caused by rapid recombination of ionization during a solar eclipse, and finally (7) pulsations with periods ranging from 0.3 sec to 30 min, which originate in the distant magnetosphere. Atmospheric lightning too leaves an oscillatory signature with periods of <0.1 sec.

5.3 CAUSES OF GEOMAGNETIC FIELD VARIATION: EXTERNAL ORIGIN

The maximum contribution to the geomagnetic field (97–99%) comes from the main internal field. The remaining 1% originates directly in currents flowing in the Earth's space environment of ionosphere, magnetotail and magnetopause (Chapter 8). This tiny component of the geomagnetic field exhibits marked variations of both regular and irregular kind, and it can be as small as 100 nT in a background total field of ~40,000 nT (Figure 5.6 showing variations at Alibag). The variation field is mainly caused by: (1) thermal tidal forces in the atmosphere caused by solar heating, (2) interaction of the Earth's gaseous and plasma environment with charged particles and wave radiation intermittently emitted by the Sun, and (3) gravitational tidal pulls exerted on the Earth's gaseous environment, predominantly by Moon or to a lesser extent by the Sun.

I. Quiet Time Variation and the Ionosphere

Variations in the geomagnetic field are strongly affected by solar phenomena. Annual variation of the geomagnetic field caused by magnetic effects associated with solar activity is examined by expanding the annual mean values of the D, H and Z components at selected observatories into spherical harmonic series. At most places on the Earth, the measured geomagnetic field starts rising in value at ~06 hr LT, reaches a peak at 11-12 LT, and regains low levels at 17-18

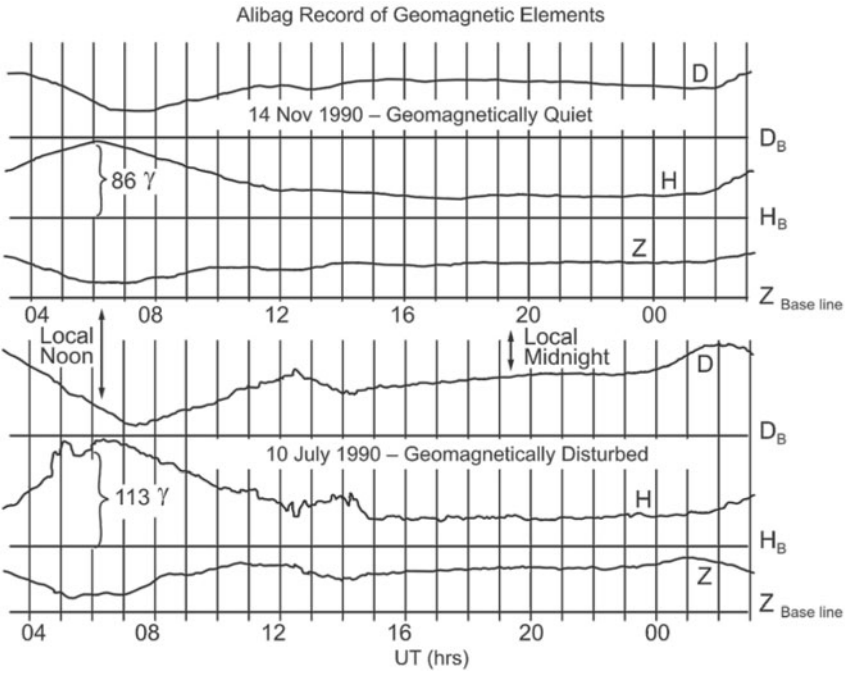

Figure 5.6. Records of the D, H and Z components of the geomagnetic field recorded at Alibag observatory, on 14 Nov 1990 (quiet day) and 10 July 1990 (disturbed day) (Rajaram and Pisharoty, 1998).

LT. Thereafter, it remains at almost the same level all night. This is the Sq (solar quiet) variation (e.g. Fig. 5.7b). It is caused by the fact that as Earth rotates, its gaseous atmosphere on the dawn side starts coming under the influence of solar extreme ultraviolet (EUV) radiation. This EUV radiation is selectively absorbed at different altitudes above 60–80 km by the gases, which comprise the Earth's upper atmosphere causing ionization of gases. Thus, a conducting medium of free electrons and ions (mainly positive at altitudes >90 km, negative at altitudes <90 km) is formed leading to electric current flow. This is the ionosphere, and the vertical profile of the observed electron density classifies it into the D, E and F (F1 and F2 by daytime) regions (Chapter 3). The Sq variation reflects the currents set-up in the conducting ionosphere and thermal tides rather than the gravitation tides caused by Moon. The Sq is assumed to have zero value near local mid-night, since the conductivity falls to nearly zero at this time. However, the mean Sq is not zero because of which daily mean differs from the midnight (baseline).

II. Lunar (L) Variations and Magnetic Field

These variations are brought about in the upper atmosphere by the tidal pull of the Moon caused by its gravitational attraction. This causes motion of the solar

EUV-ionized atmosphere across magnetic field lines, which sets up dynamo currents in the E region. The magnetic variations associated with currents of lunar tidal origin (L) differ from those of Sq origin in features of: (1) the amplitude of L variations is smaller than that of the Sq variations (hardly 0.1) because tidal forces caused by the Moon are far less powerful than the solar thermal tidal pulls, (2) period of L variation is found to be predominantly semidiurnal in contrast to the thermal solar diurnal variation, and (3) the lunar day exceeds the solar day by 50.5 min.

The dependence of lunar tides on the solar cycle, enhanced geomagnetic activity, lunar orbital distance (apogee and perigee) and polarity of the IMF are quantified using long series of Alibag data. The solar cycle influence on the lunar tides far exceeds the solar component in the summer. Enhanced geomagnetic activity modifies the amplitude of the phase-law tides depending on the station location in relation to the times of magnetospheric compression or expansion.

Quiet time variations of the EMF are associated with the equivalent Sq currents in the highly conducting E region of the ionosphere. Sq current system has an anti-clockwise current vortex in the northern hemisphere, and a clockwise current vortex in the southern hemisphere. Few examples of seasonal and solar cycle dependence of geomagnetic H and D variations demonstrate the influence of varying current systems even under quiet magnetic conditions. Dependence on longitude and month to month difference in the position and strength of Sq currents, are also seen.

III. Sq Day Variation near Focus of Current System

Magnetic variations associated with solar cycle have shown the latter depicts maximum events twice in the course of its length of ~22 years. During the first maximum, sunspot activity has its largest magnitude. Solar flares and sporadic magnetic activity are also largest during this period. The second maximum occurs 2 to 3 years after the first and the period is characterized by gradual commencement of storms and recurrent magnetic activity on Earth.

Figure 5.7b depicts hourly values of D, H and Z components from thirteen MOs (Fig. 5.7a), whose data are available in common with Gulmarg observatory. The mean pattern of daily variation in each of the components is obtained by averaging the hourly field values over all the international quiet (IQ) days of the year 1978. The mean Sq variation in D, H and Z for each of the stations is plotted as a function of 75°E meridian time (EMT) (Fig. 5.7b). Results reveal latitudinal difference pattern of daily variation. For example, D and Z variations in their latitudinal progression attain maximum close to Gulmarg, whereas H-variations diminish in magnitude. The diurnal as well as semidiurnal term phase shift in H is seen between Gulmarg and Tashkent approximating a reversal. This feature indicates Sq-focus being located close to the latitude of Gulmarg. Interestingly, as one moves northward from Ujjain, the near noon maximum of H-variation progressively shifts to a later hour until a reversed diurnal variation pattern registers at Tashkent.

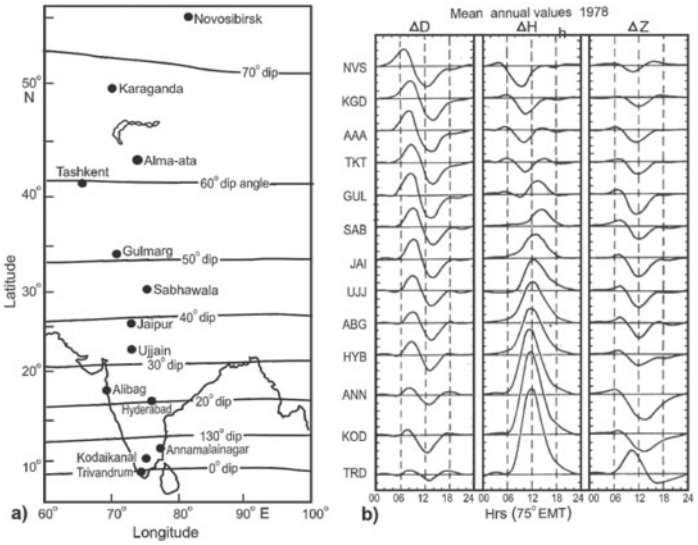

Figure 5.7. (a) Location of the magnetic observatories (named filled circle) in India and Russia. (b) Solar quiet-day variations in geomagnetic field components, D, H and Z at magnetic observatories along Indian longitudinal belt for the year 1978 plotted as a function of 75°E meridian time (EMT) (Patil et al., 1983). TRD – Trivandrum, KOD – Kodaikanal, ANN – Annamalainagar, HYB – Hyderabad, ABG – Alibag, UJJ – Ujjain, JAI – Jaipur, SAB – Sabhawala, GUL – Gulmarg, TKT – Tashkent, AAA – Alma-ata, KGD – Karaganda, NVS – Novosibirsk.

IV. Sq (H) Variation and Seasonal Parameters

Separate study of Sq variations at Gulmarg for the three seasons shows that daily variation of H during d-months (winter months of Jan, Feb, Nov and Dec) is predominantly diurnal in character with the maximum before noon (Fig. 5.8). During e-months (equinox months of March, April, Sept and Oct), and more so in j-months (summer months of May, June, July and Aug), daily variation of H-field is predominantly semi-diurnal in character with consistently minimum around 08-09 hr LT during 1978-1980. These features of Sq are suggested to be due to the deformation of current loops caused by the changing latitude of focus during the course of the day.

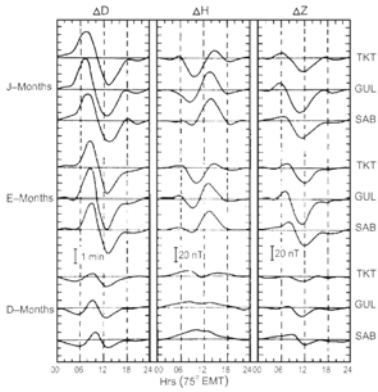

Figure 5.8. Mean seasonal quiet-day variations in D, H and Z at Sabhawala, Gulmarg and Tashkent for the year 1978 (Patil et al., 1983).

V. Sq (D) Variation and Seasonal Parameters

Seasonal and solar cycle dependence on the diurnal variations of ΔD (departure from the respective local night base), are examined for the period 1984 to 1989. Data sets are divided into three seasonal groups of three months, viz. winter d, equinox e, and summer j months. Dominant features of seasonal changes are positive (upward) variation over the night level indicative of an eastward directed field, and negative (downward) variation indicative of a westward field of the D component (Fig. 5.9). The focal meridian can be determined by the time at which Y or D changes sign (positive to negative, i.e. eastward to westward directed field in the northern hemisphere).

The abnormal seasonal characteristics of D when examined show that the diurnal variation for e and j months is on the expected pattern of a prominent eastward directed field in the morning hours and a westward field in the afternoon hours (Fig. 5.9). In contrast, the anticipated ΔD pattern in d-months of 1987 is systematically departed from the regular diurnal trend (Fig. 5.10). Dominance of a westward directed field is obvious during most of day hours at equatorial and low latitude stations. Prominent diurnal pattern compared to the semidiurnal variation at equatorial latitudes is a special feature observed during Feb 1987, with minimum occurring around 12 hr LT, unlike the normal d-seasonal minimum time between ~6 and 7 hr LT. This pronounced effect of the westward field is seen farther away from equatorial latitudes. The complex features seen in the d-months of 1987 could be due to the modification of the entire northern Sq current system, either by penetration of southern Sq system or by the prevailing wind conditions.

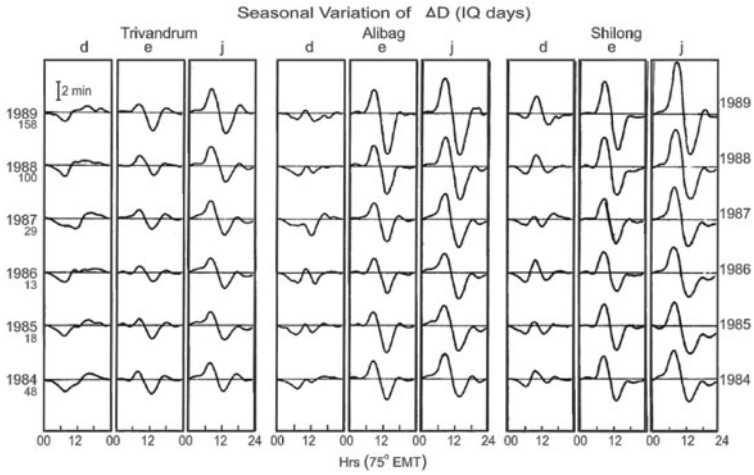

Figure 5.9. Average solar quiet daily variations of the declination component, D, at the equatorial station Trivandrum and the two non-equatorial stations Alibag and Shillong for the three (d, e, j) seasons (Alex et al., 1992a, b). Solar activity R_z value for each year is indicated below the year marking.

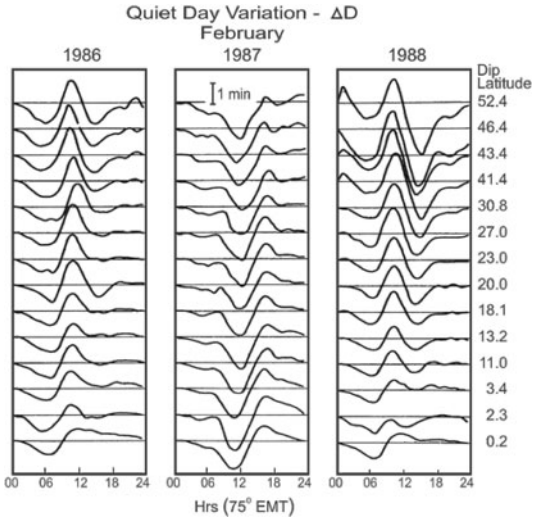

Figure 5.10. Complex variation of DD at 14 locations in the Indo-USSR longitude belt for February 1987 plotted as a function of 75°E Meridian Time (MT). Curves for 1986 and 1988 are also shown for comparison (Alex et al., 1992a,b). TRD – Trivandrum, KOD – Kodaikanal, ANN – Annamalainagar, HYB – Hyderabad, ABG – Alibag, UJJ – Ujjain, SHL – Shillong, JAI – Jaipur, SAB – Sabhawala, GUL – Gulmarg, TKT – Tashkent, AAA – Alma-ata, NKK – Novokazalinsk, KGD – Karaganda.

5.4 EQUATORIAL ENHANCEMENT AND GEOMAGNETIC FIELD VARIATIONS

Electrodynamics in the vicinity of the dip equator is more complex and enigmatic than in the middle latitudes. At auroral regions between ~65° and 75° latitudes in both the hemispheres, the dawn-to-dusk electric field maps into ionosphere to interact with Z component, and gives rise to strong E-W directed auroral electrojet currents. The mere horizontality of the highly conducting geomagnetic field lines generates large vertical polarization electric fields within ±5° of the dip equator (Fig. 5.11a, where the Z component and I are zero), and this produces a rather dramatic increase in the ionospheric currents resulting in the EEJ phenomenon. The electric fields associated with EEJ not only produce surface magnetic signatures but also drive the F-region fountain, which takes the plasma from the equatorial regions to the anomaly crest. The coupling between the plasma and neutral species transfers the momentum to the neutrals, forming the neutral anomaly. Good quality scalar and vector data are needed to yield vertical extent of the 3D current loop associated with EEJ.

I. Equatorial Electrojet

EEJ is the high concentration of ionospheric current flowing from west to east in a narrow belt flanking the dip equator in the Sunward hemisphere (Chapter

3). In the region of dip equator, magnetic lines of force are horizontal, as a consequence of which a large vertical polarization electric field called the Hall electric field (responsible for the enhanced eastward currents) is set up. Part of it is due to the highly enhanced electrical conductivity in the E region of lower ionosphere over the 100 to 130 km altitude range. This is the Cowling conductivity. The latitudinal position of the electrojet axis is dictated by the position of the dip equator at that longitude, while the Hall conductivity is sensitive to the magnitude of the magnetic field. These features are fairly well brought out by equatorial magnetograms in the form of highly enhanced H, which falls off rapidly with latitude (Fig. 5.11b). The difference in daily range in H between an equatorial and non-equatorial location can be as much as 80-100 nT. The EEJ is basically a daytime phenomenon which grows with the daytime Sq current, reaches a peak around noon, and decays towards evening. The understanding of the EEJ is very essential if it has to be used as diagnostic tool for the systematic study of upper atmospheric motions and currents.

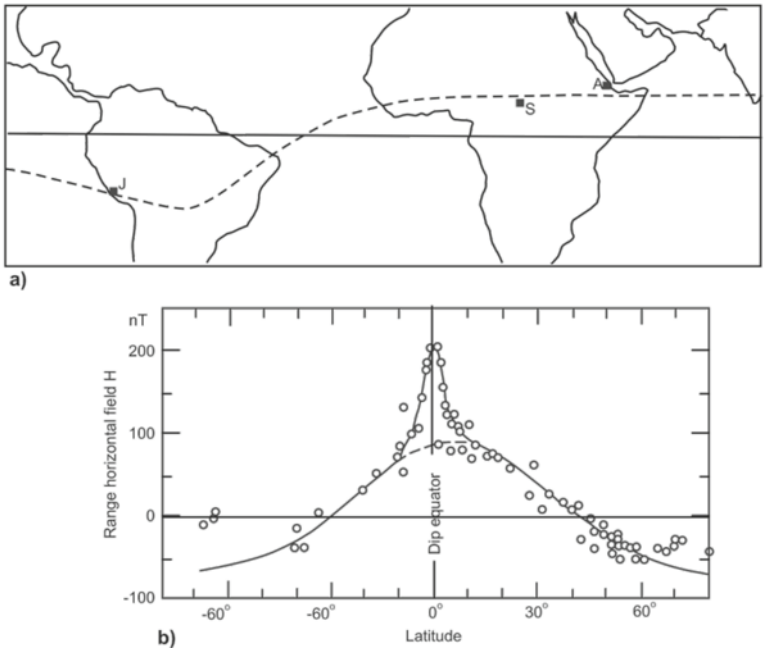

Figure 5.11. (a) World map showing the dip equator (- - - -) and the geographic equator (——). Jicamarca, Peru (J), Sarh-Fort Archambault, Chad (S) and Arta-Djibuti (A). (b) Variation of the daily range in the H-component of the geomagnetic field as a function of latitude. Note the highly amplified range within ±5° dip, which is due to the E-W flowing equatorial electrojet current (Rajaram and Pisharoty, 1998).

II. Counter Electrojet

On certain days, magnetograms recorded at equatorial regions show a noticeable dip in the H component for 2–3 hrs in the forenoon or afternoon hours. The minimum of the dip, occasionally, has a value below night values. This phenomenon is called the counter electrojet (CEJ). It often occurs on days which are classified as magnetically quiet, and at such times is not related to a magnetospheric disturbance. The CEJ is ascribed to a weakening of the eastward directed Cowling current which flows in the equatorial latitudes.

III. Equatorial Electrojet and Induced Effects

Variations in the EMF are caused by electric currents which flow at ~100 km altitude in the Earth's conducting upper atmosphere, mainly in the location of E region of the ionosphere. A small portion of the currents flows in the higher ionospheric and magnetospheric regions. While these atmospheric currents contribute to ~2/3 of the observed magnetic variations, the remaining 1/3 is caused by electric currents, which are induced by the ionospheric currents in the conducting upper layers of the Earth's crust.

Equatorial electrojet provides a strong non-uniform field for studying the electromagnetic induction in Earth. So far opinion differed even on the presence of currents induced by EEJ, but satellite data now strongly confirm the presence of EEJ induced currents. Indian MO data analysis shows that EEJ in the Indian region has an associated internal current. The induction effects are local features dependent on subsurface geology. Hence, they are spatially variable and therefore needed to be studied in great detail. The induction studies have implications on the modelling of global subsurface conductivity features.

IV. Equatorial Electrojet and Seasonal Parameters

The data generated at Travancore MO displayed a pattern strongly dependent on the time of the day, seasons and solar cycle. The declination between Nov and Feb was found to be exactly opposite to that observed between May and Sept. This kind of feature results because the boundary between northern and southern systems of the magnetic field crosses over the magnetic equator.

The geomagnetic data recorded by a network of MOs (Table 5.2) was examined to investigate the spatial structures of the EEJ compared to global Sq. Sq (H) variations, for each month of 1992, were derived using hourly values of selected quiet days with Ap≤7, where no single 3-hr Kp index exceeded 3_+. The monthly mean Sq variations are subjected to harmonic analysis to obtain amplitude and phase corresponding to periods of 24, 12, 8 and 6 hrs, respectively. Figure 5.12 shows the latitudinal profiles of the amplitude normalized with respect to the amplitude at Alibag. The amplitude-latitude profiles are shown for winter (Feb), spring (March), summer (July), and fall (Sept) seasons (Fig. 5.12). Consistent with the intense flow of eastward directed

EEJ currents, amplitude of all harmonics of Sq (H) are enhanced in the vicinity of the dip equator in relation to the amplitudes at low latitudes. The dip equator enhancement is confined to a narrow latitude range of ±4 dip latitude (Fig. 5.12), and does not show any systematic dependence on the period of fluctuating fields.

Spatial behaviour of variations from equator towards polar region reveal that magnetic fluctuations in equatorial region have bimodal origin related to ionospheric dynamo and magnetospheric process, wherein the latter results from almost instantaneous transmission of polar electric field to equatorial region (Fig. 5.12). When these two sources operate independently, the magnetic fluctuations in equatorial belt in relation to that at low latitudes are enhanced roughly by a factor of 4±1 due to enhanced Cowling conductivity. However, when the two mechanisms work in an interactively coupled manner, they account for the variability of equatorial enhancement seen in individual cases.

The difference in the fields of Thiruvananthapuram and Alibag is used to derive indices of EEJ and CEJ. The long series of MO data help in bringing out inverse correlation of CEJ with solar activity and peak occurrence in a given year in June and Jan. Also, the lunar semidiurnal tide is identified as one of the major sources of the CEJ.

Table 5.2. Geographic, geomagnetic co-ordinates and dip latitudes of geomagnetic observatories along 75°E meridian

Station name	*Station code*	*Geographic*		*Geomagnetic*		
		Latitude (N)	*Longitude (E)*	*Latitude (N)*	*Longitude (E)*	*Dip lat.*
Kanyakumari[a]	KAN	8.10	77.54	1.21	148.98	–0.23
Trivandrum	TRD	8.48	76.95	–0.88	148.24	0.28
Virudunagar[a]	VIR	9.61	77.94	0.26	149.52	1.61
Karur[a]	KAR	11.01	78.09	1.64	149.80	3.32
Annamalainagar	ANN	11.40	79.68	1.77	151.20	3.67
Bangalore[a]	BAN	12.98	77.60	3.64	149.52	5.72
Anantapur[a]	ANT	14.67	77.63	5.32	149.71	7.83
Alibag	ABO	18.63	72.87	9.64	145.39	12.96
Nagpur	NAG	21.15	79.08	11.64	151.74	15.74
Ujjain	UH	23.02	75.78	13.50	147.00	18.42
Tashkent	TKT	41.33	69.62	32.51	145.52	41.50
Alma Ata	AAA	43.25	76.92	33.69	152.21	43.50
Novosibirsk	NVS	55.03	82.90	44.92	159.07	58.90
Moscow	MOS	55.48	37.32	50.79	121.62	54.92
Uloroski	ULO	69.8	60.80	65.00	137.70	71.40
Karmakuli	KRM	72.40	52.90	67.40	133.00	72.14
Dixon	DIK	73.55	80.57	63.36	162.45	78.36

[a]IEEY stations.

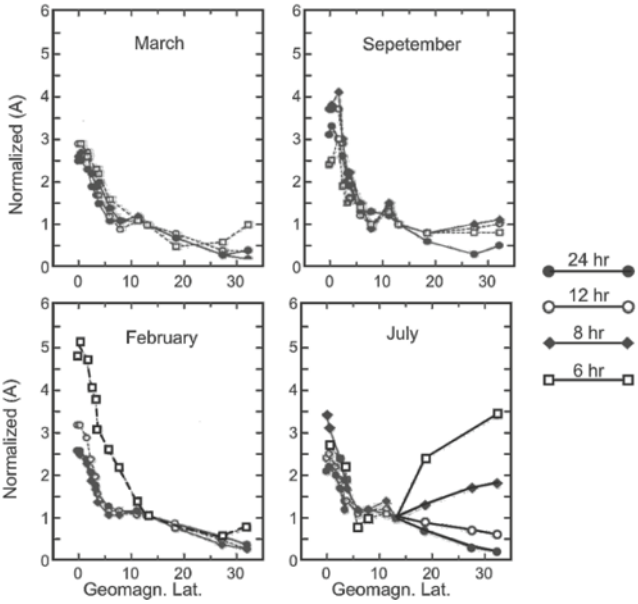

Figure 5.12. Plots showing equatorial enhancement of the different harmonics of the regular daily variations in horizontal component during different months of 1992. The latitudinal structure and equatorial enhancement factors do not show any regular dependence on the period of oscillating field, both of dynamo and disturbance origin (Arora and Bharadwaj, 2003). Amplitudes are normalized with respect to the value at Alibag observatory.

V. Longitudinal Inequalities of Equatorial Electrojet

The EEJ is studied using the surface and scalar data of the Pogo satellite. An empirical EEJ model including local time and longitude dependence is constructed based on the surface magnetic data recorded at 26 stations located in six different longitude sectors that were set up or augmented during the international equatorial electrojet year (IEEY) (Fig. 5.13). The model reproduces the characteristic signatures of EEJ associated with H and Z magnetic components at ground level. The model-predicted variations at the orbit of Pogo satellite are generally in good agreement with onboard magnetic signatures. The nature of difference suggests that the global scale magnetospheric or field aligned current systems may sometimes dominate the satellite data. The nature of longitudinal inequalities in EEJ strength indicates it to be strongest in South America (80° to 100°W) and weakest in the Indian sector (75°E) with a secondary minimum and a maximum centered respectively in the Atlantic Ocean (30°W) and in western Africa (10°E). The EEJ strength is shown to be inversely correlated with the main field intensity along dip-equator. The longitudinal differences in the EEJ are used as diagnostic tool for the systematic global subsurface conductivity probing in induction studies.

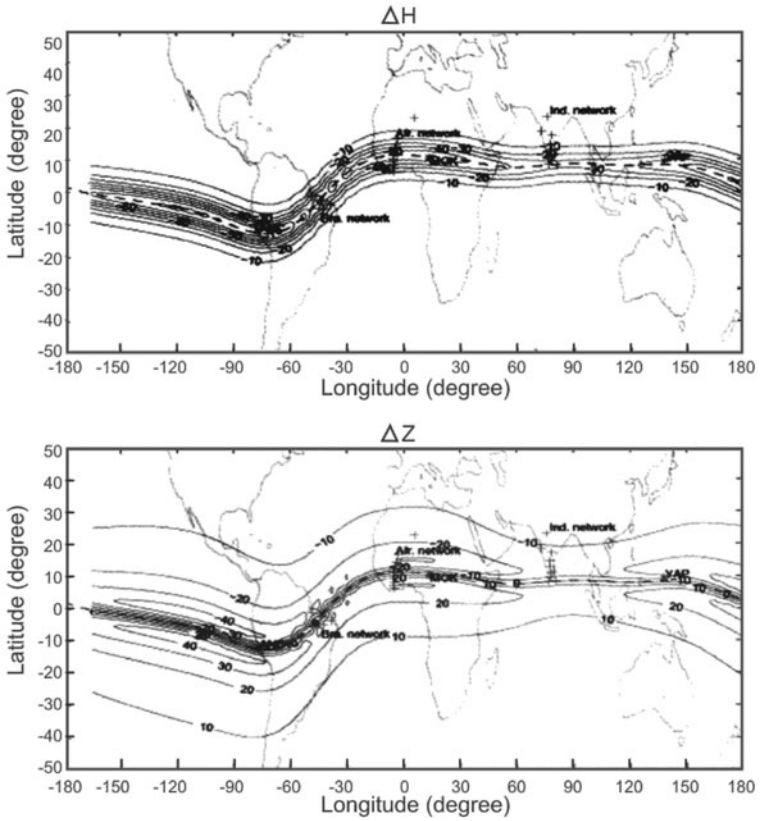

Figure 5.13. Global view of Sun-synchronous EEJ associated magnetic field (H and Z) at an altitude of 450 km as estimated from the empirical model constructed based on the surface magnetic data recording at 26 stations in different longitude sectors. The empirical model includes terms to define variations with latitude, longitude, local time and altitude (Doumouya et al., 2003).

VI. EEJ Phenomena using Oersted Observations

Data from ground MO as well as satellites are used to understand the structure of the EEJ. Analyses revealed that the equatorial enhancement varies by a factor of 3 to 10, and is strongly controlled by the nature of activity in the polar region. When there is an exaggerated geomagnetic activity in the polar region, there is a greater enhancement of EEJ. This is attributed to the almost instantaneous transmission of polar electric field to equatorial region. It also appears that EEJ acts as a simple amplifier that enhances any input electrical field by a factor of 3 to 5. One conspicuous feature of the width of the EEJ varies considerably with longitude. Studies show the fundamental understanding about the processes leading to formation of EEJ system and dissipation of its energy, signifying the fact that electrojet controls the electrodynamics of the entire low latitudinal ionosphere.

Analyses of magnetic field observations obtained from Oersted satellite underscore an excellent database for studying not only the longitudinal structure of the EEJ but also the sources responsible for its variations from day-to-day. An objective method is devised for identifying the signature of EEJ at satellite altitude and determining the parameters that define its basic structure. This method works very well in describing the surface manifestations of EEJ as seen in the observatory data.

(i) Preliminary treatment of the Oersted data: Detailed analysis of the scalar magnetic field data from Oersted shows that the width of EEJ varies considerably with longitude. Its axis (centre of EEJ) closely follows the dip equator at altitude of 106 km and there is a small departure that undergoes diurnal variation, with a minimum at noon (Fig. 5.14). The globally averaged EEJ amplitude follows expected diurnal pattern. Principal component analysis technique reveals that first four components can explain around two thirds of electrojet variability. The first component, which contributes over 30% to the observed variance, is identified with global variation of the EEJ emanating from day-to-day variability of migrating tides. The second and fourth components, which account for ~15 and 10% of the variance respectively, are driven by forces that depend on whether the location of the EEJ in that sector is in the northern or southern hemisphere. The third component provides maximum contributions wherever the geomagnetic and dip equators are sufficiently close, accounting for 12.5% of the variance. The remaining

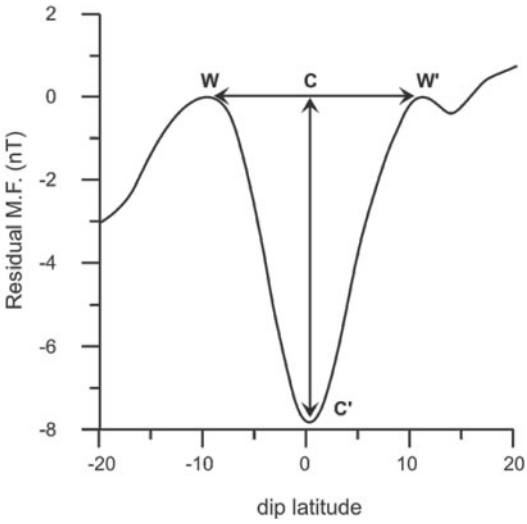

Figure 5.14. Latitudinal variation of residual magnetic field observed at Oersted satellite height for 135°E longitude pass on 2 August 1999, showing anomaly at dip equator (Jadhav et al., 2002a,b). CC'is vertical distance between dip and shoulders, a measure of the strength of the EEJ currents contribution, and WW'is horizontal distance between two shoulders, giving the width of signature of the EEJ current system.

components can be associated with contribution of non-migratory tides or other unknown mechanisms. Thus, besides conductivity, atmospheric tidal modes play an important role in defining the zonal variability of the EEJ current system.

(ii) Comparison between satellite and ground observations: The scalar data from 57 orbital passes on four representative quiet days, covering the forenoon to afternoon hours, provide a greater insight into relative importance of geomagnetic field structure and tidal control. The Oersted initial field model along with the earlier IGRF models is used to study secular changes in the global patterns of position and strength of EEJ. A northward drift in the location of dip equator (hence the position of the axis of EEJ) to the extent of 1° per decade is seen ~300°E. In contrast, in the Pacific, east of Australia, there is practically no drift. It is also observed that the largest secular variation in the Cowling conductivity occurs in South American sector with a possible 4% increase per decade for the same level of ionization in the E region. The Oersted main field model does not suggest any changes or reversal of these trends. A very significant result is that the magnetic field at the dip equator need not be perpendicular to the line of zero dip, and this deviation from the idealized scenario of the EEJ can result in significant contribution of EEJ to the D component. EEJ signatures in American and Indian sectors are shown in Fig. 5.15.

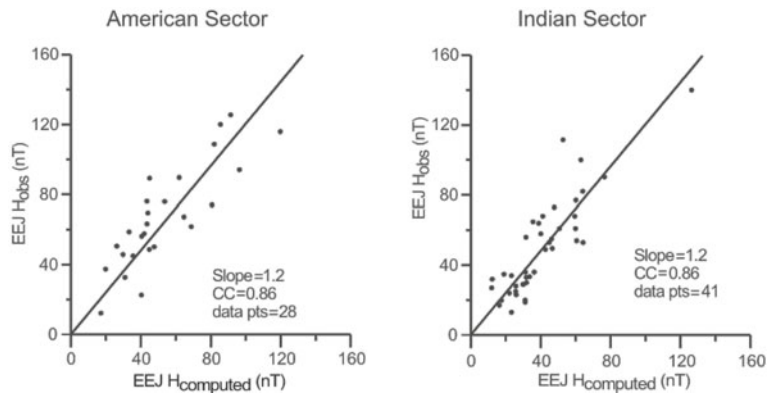

Figure 5.15. Scatter plot of EEJ H_{obs} from American and Indian MO data plotted against the EEJ $H_{computed}$ computed at the axis of EEJ from satellite based EEJ parameters (Jadhav et al., 2002a, b).

The daytime ionosphere is seen to introduce a shift in phase of the hydromagnetic wave impinging on it, wherein the phase shift is greater for higher frequencies and higher conductivity of the ionosphere. There are also significant phase differences in oscillations recorded at the centre of the electrojet and below the fringes of the electrojet. The equatorial enhancement is generally higher for lower frequencies as compared to the higher frequencies.

5.5 GEOMAGNETIC STORMS AND THE MAGNETOSPHERE

The extent of the geomagnetic field in near-Earth space defines the magnetosphere (Chapter 3). The magnetosphere is also described in terms of its constituent electric currents. The magnetopause is defined by a surrounding current that flows eastward near the equatorial plane. The magnetotail is understood in terms of a westward equatorial current sheet. The magnetospheric interior within ~3-6 R_E contains neutral plasma of 1 to 200 keV hydrogen and oxygen ions and lower energy electrons. These particles undergo a cyclotron motion around magnetic-field lines, bounce between mirror points in the northern and southern hemispheres, where field lines converge, and a slow migration across field lines takes place due to gradients in the magnetic field. As a consequence, ions drift westward and electrons eastward, a contrary motion that gives rise to a westward equatorial ring current. Along with solar wind, the interplanetary magnetic field controls the behaviour of the magnetosphere. Occasionally, abrupt ejections from the Sun push the magnetosphere into a highly dynamic, time-dependent state called a magnetic storm. This expression was coined by von Humboldt in 1808 to describe occasional periods during which ground-based measurements show large, rapid, and irregular variation of the geomagnetic field (Chapters 1 and 3).

I. Indices of Geomagnetic Activity

Magnetic indices are simple measures of magnetic activity that occur over a period of less than a few hours, recorded by observatories. Indices quantify the variations that have their origin in the Earth's ionosphere and magnetosphere. The planetary-scale magnetic activity is measured by the Kp index. Kp scale is a logarithmic one, hence it is necessary to have a linear scale for assessing the level of magnetic activity. This is provided by the a_p index (index of planetary amplitude), which is derived from Kp index. During magnetic storms, magnetic electric currents are diverted along field lines. To measure the auroral zone component of this circuit, Davis and Sugiura in 1966 defined the auroral electrojet index AE. The disturbance storm (Dst) index is commonly used to assess the strength of geomagnetic storms. The strength of the symmetric westward ring current, which encircles the Earth in the equatorial belt of roughly ±30°, is distinct during storm times. This ring current has a dipole moment, which is directed opposite to the Earth's natural magnetic field. The Dst index is calculated from four low latitude locations.

II. Geomagnetic Storms

Magnetic storms occur as a result of abnormal activities at the Sun that affect the intensity of the solar wind. These are most easily observed in low-latitude magnetograms as a depression in intensity of the H component of the magnetic

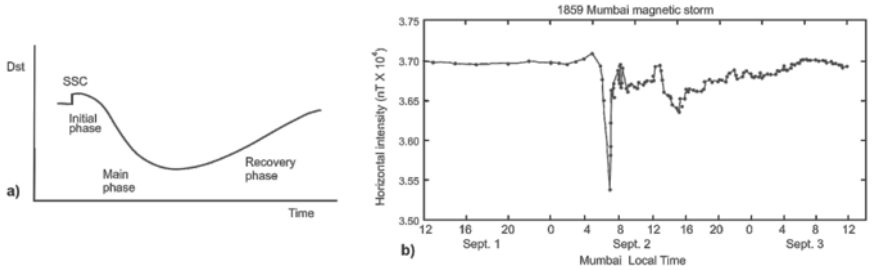

Figure 5.16. (a) A sketch representation of the Dst index during a typical magnetic storm (Lester, 2007). (b) The Colaba magnetogram for the 1-2 Sept 1859 geomagnetic storm. The peak near 0400 UT 2 Sept, is due to the storm sudden commencement caused probably by the shock ahead of the magnetic cloud. This was followed by the storm main phase which lasted for about one hour and a half (Tsurutani et al., 2003).

field. This decrease in H-component intensity is due to the increased population of energetic charged particles, which make their entry by the injection from the near-Earth magnetotail into the inner magnetosphere. The after-effects of magnetic storms on space environment surrounding the Earth are serious, hampering human activities in space and on the ground. Dst identifies a magnetic storm, based on the change in the H component measured at low-latitude stations separated in longitude. Figure 5.16a presents a schematic of the Dst index for an individual storm, which illustrates three of its specific phases, each having different timescales. The initial phase follows rapid enhancement in the Dst index, over a timescale of a few min referred to as storm sudden commencement (SSC) caused by rapid increase in solar wind pressure incident on the Earth's magnetosphere. The second main phase lasts 5–10 hours reducing Dst index to its minimum value as the ring current intensifies. This represents the period of the main energy transfer and storage into the Earth's magnetosphere. The final phase lasting 10–15 hours is the recovery phase during which the Dst returns to its pre-storm values. Thus, the timescale for the whole storm is typically 24–30 hours.

Coronal mass ejections (CME), solar flares, and coronal holes initiate magnetic storms. These phenomena create unusual conditions in the solar wind, leading to high values of the solar wind density and velocity (and hence pressure) and the interplanetary magnetic field (IMF). The orientation of IMF is central to the energy transfer from solar wind to the magnetosphere. When the IMF has a southward component, the energy transfer is most efficient, and occurs through the process of magnetic reconnection between the IMF and the geomagnetic field. During magnetic storms a large amount of energy is dissipated in the polar regions leading to profound changes in the global morphology of the upper atmosphere. An example of the solar flare/CME causing a big geomagnetic storm is shown in Fig. 5.17.

Substorms: Coinciding with the decrease in the field, a magnetic storm is generally accompanied by intense auroral brightening. Occasionally, the auroral

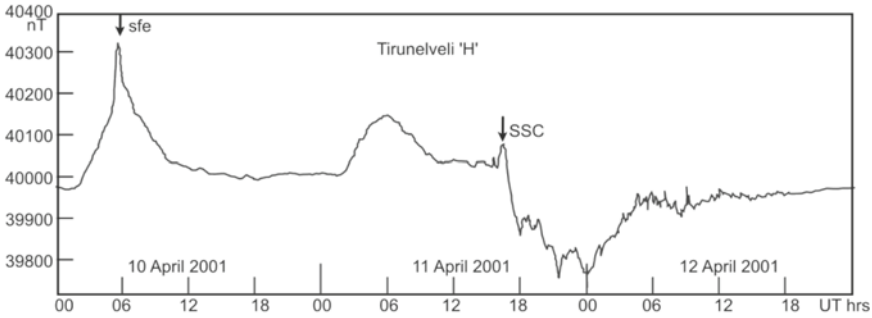

Figure 5.17. Magnetogram from Tirunelveli magnetic observatory showing the geomagnetic storm caused by a solar flare/CME [The effect of a powerful X-class solar flare that occurred on 10 April 2001 at ~0525 hrs UT modified the ionospheric current and affected the magnetic field within a few minutes as shown. The CME eruption following the flare led to an intense shock as observed by the ACE spacecraft on 11 April at 1520 hrs UT, after almost 34 hrs. The impact of the shock on the magnetosphere is seen as a sudden impulse on the magnetic record at ~1545 hrs UT. Subsequently, the development of the intense main phase associated with the westward ring current is evident] (Lakhina and Alex, 2002).

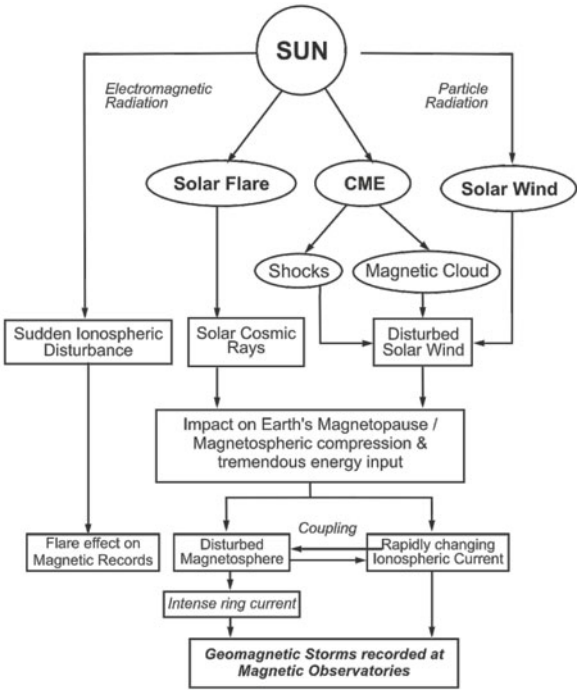

Figure 5.18. Flow chart representing schematically the chain of solar-terrestrial processes giving rise to space weather disturbances in the near-Earth's space environment.

ovals expand equatorward with the occurrence of auroral substorms or magnetospheric substorms. A magnetospheric substorm denotes phenomena that occur in the magnetosphere. Substorms consider part of the normal solar wind magnetosphere interaction, and comprise three separate stages: the growth, expansion, and recovery phases. The overall timescale of a magnetospheric substorm is typically 2–4 hours.

Severe magnetic storms are relatively rare. However, during magnetic storms, intense substorms are observed in the polar regions and subsequent development of intense ionospheric currents. Apparently, perturbations of solar origin form an important link in the complex chain of solar-terrestrial relations. A flow chart showing the chain of solar-terrestrial processes that are involved in causing magnetic storms is shown in Fig. 5.18.

Geomagnetic storms types: The Dst index profile of geomagnetic storms is used to characterize the geomagnetic storms into various types and categories. The sudden commencement (SC) storms are characterized by an abrupt increase in the horizontal magnetic field intensity shortly before the main phase (Fig. 5.19). This rise in magnetic field strength is caused by the interplanetary shock compression of the magnetosphere. The period between the SC and the main phase is called the initial phase. However, all magnetic storms do not have the initial phase. A geomagnetic storm not accompanied by a SC is called a gradual

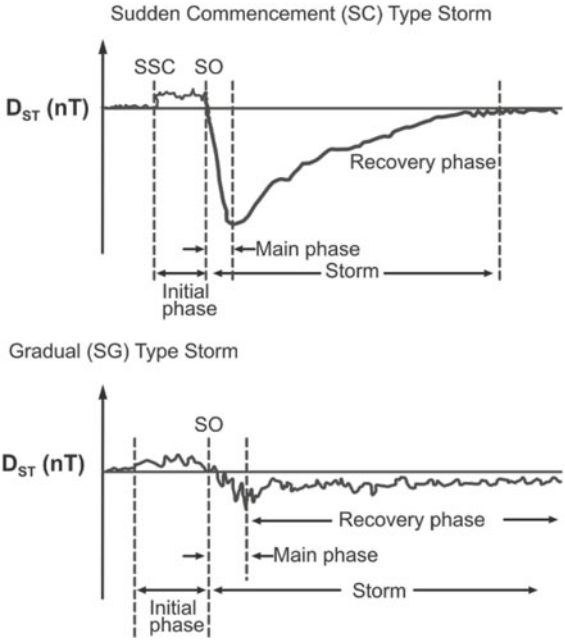

Figure 5.19. Schematics of magnetic storms (top) sudden commencement (SC) type driven by interplantery CMEs and (bottom) gradual (SG) type caused by corotating interaction regions (CIRs). All storms may not have initial phases (Tsurutani et al., 2006).

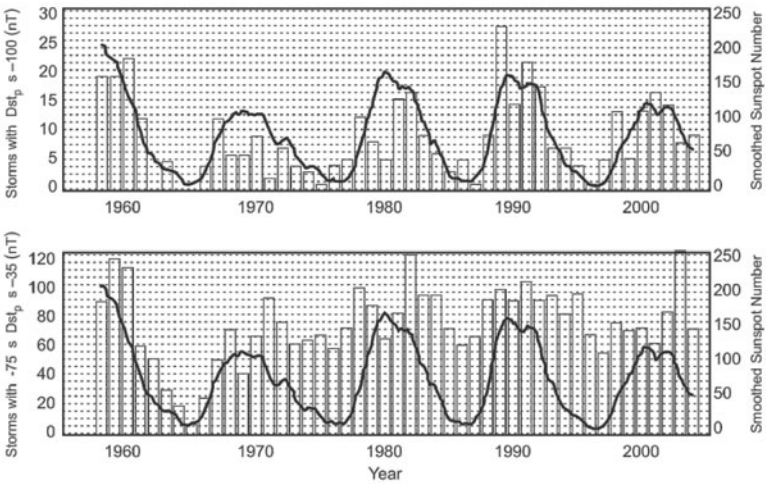

Figure 5.20. Annual occurrence of magnetic storms between 1958 and 2004. The number of magnetic storms/year with Dst<–100 nT are given at the top and those with –35>Dst>–75 nT on the bottom. The smoothed sunspot number is shown as a solid dark line. The number of major (Dst<–100 nT) magnetic storms follows the solar cycle sunspot number. There are ~15 to 20 major magnetic storms/year during solar maximum and only ~1 to 2 during solar minimum. The ratio is ~15 to 20. For weak to moderate intensity magnetic storms, there is much smaller solar cycle dependence. CIRs/high-speed streams are presumably responsible for most of the weaker storms (Tsurutani et al., 2006).

geomagnetic storm (SG) (bottom panel of Fig. 5.19). Magnetic storms having a single main phase, wherein the Dst decreases more or less continuously to a minimum value and then starts to recover, are called Type I or one-step storms. In Type 2 or two-step storms the main phase undergoes a two-step growth in the ring current in a way that before the ring current had decayed to a significant pre-storm level, a new major particle injection occurs leading to further build-up of the ring current and further decrease of Dst. Hence, there is a possibility of multi-step storms depending on the ring current injection events caused by interplanetary conditions.

The intensity of magnetic storm is measured by the Dst index at peak of the main phase. Magnetic storms are called weak when Dst>–50 nT, moderate when –50>Dst>–100 nT, and intense when Dst<–100 nT and super intense when Dst<–500 nT. Tsurutani and coworkers in 2003 deduced the super-intense geomagnetic storm of 1–2 Sept 1859 with a Dst ~–1760 nT. This large value of Dst is consistent with the decrease of ΔH=1600±10 nT recorded at Colaba observatory.

The SC type magnetic storms result from interplanetary shocks associated with CMEs, while the SG type are caused by corotating interaction regions (CIRs). Figure 5.20 shows the number of major (Dst<–100 nT) storms follow the solar cycle sunspot number. For weak to moderate storms, there is smaller solar cycle dependence.

III. Long-period Oscillations of External Origin

Long period geomagnetic oscillations such as quasi-biennial (QBO), annual (AO), and semi-annual (SAO) oscillations over Thumba (8.5°N) show considerable variation from year to year. Large series of data available for Thumba is used to quantify these inter-annual variations using the technique of complex demodulation. In spite of the large inter-annual variation, the height profiles of AO and SAO retain their basic characteristics. The inter-annual variations of AO amplitude at tropospheric heights are smallest (2sd ~5 m/sec, sd is standard deviation) and are well correlated with solar activity. Inter-annual variations of SAO near stratopause height are largest (2sd ~12 m/sec) and are inversely correlated with solar activity. The QBO period is noticed to show considerable height variation with largest value of ~31-month near 40 km altitude. An oscillation with a period of ~14-month is identified between 18 and 50 km. The characteristics of this oscillation tend to suggest it is an independent oscillation.

IV. Energy Budget of Geomagnetic Storms

Understanding geomagnetic storms in terms of energies involved in various associated processes has been a long standing problem. Availability of satellite measurements of various interplanetary plasma and magnetic field parameters related to the development of geomagnetic storms provides a unique platform for investigating the interplanetary causes of storms. Data used are nine intense magnetic storms (|Dst|>175 nT), for the period from 1998 to 2001, from hourly values of Dst index provided by Kyoto world data center, horizontal magnetic field variation data with 1-min time resolution from Alibag observatory, and the solar wind parameters such as wind velocity, density, temperature, and IMF components obtained from ACE satellite measurements downloaded from the internet (http://nsssdc.gsfc.nasa.gov).

The analyses of intense geomagnetic storms (|Dst|>175 nT) with ACE satellite measurements, and ground magnetic field values at ABO confirms the crucial role of southward IMF in triggering the storm main phase as well as controlling the magnitude of the storm. A sudden increase is observed in the solar density variations maximizing at 0230 UT, when magnetosphere boundary gets compressed to 6.5 R_E (Fig. 5.21). Next higher density impulse with magnitude ~45/cc around 0715 UT is seen during which the boundary moved further inward to 5 R_E. The main phase interval shows clear dependence on the duration of southward IMF. An attempt is made to identify the multi-peak signature in the ring current energy injection rate during main phase of the storm. In order to quantify the energy budget of magnetic storms, computation of different energy components by the solar wind, magnetospheric coupling, auroral and Joule heating and the ring current for each storm under examination is made. Calculation of the solar wind-magnetosphere coupling function considers the variation of the size of the magnetosphere, by using the measured solar wind ram pressure.

During the main phase of the storm, the solar wind kinetic energy ranges from 9×10^{17} to 72×10^{17} J with an average of 30×10^{17} J, the total energy dissipated in the auroral ionosphere varies between 2 and 9×10^{15} J, whereas ring current energies range from 8 to 19×10^{15} J. For the total storm period, ~3.5% of total solar wind kinetic energy is available for the redistribution in the magnetosphere, and ~20% of this goes into the inner magnetosphere and in the auroral ionosphere of both the hemispheres. It is found that during main phase of the storm almost 5% of the total solar wind kinetic energy is available for the redistribution in the magnetosphere whereas during the recovery phase the percentage becomes 2.3%.

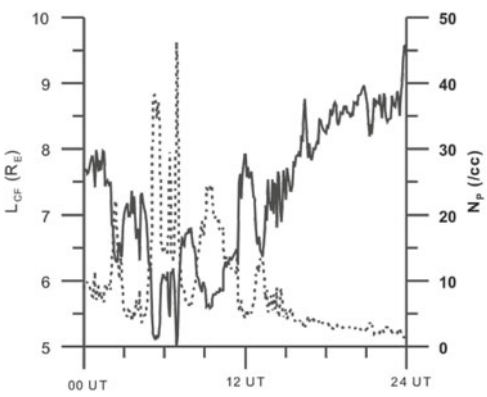

Figure 5.21. Variation of the magnetopause boundary (L_{CF}, solid curve) using ACE data, on 4 May 1998 along with the solar wind proton number density variations (N_P, dotted curve) (Vichare et al., 2005). LCF is Chapman-Ferro magnetopause distance.

V. Dependence of Main Phase Interval

The relationship between strength of the storm and main phase duration has not been adequately quantified. The main phase interval shows better linear dependence on the duration of the southward IMF rather than the strength of the storm. The plot of maximum deviation of Dst vs. magnitude of maximum southward IMF indicates the strength of the magnetic storm is directly proportional to the strength of southward IMF (Fig. 5.22).

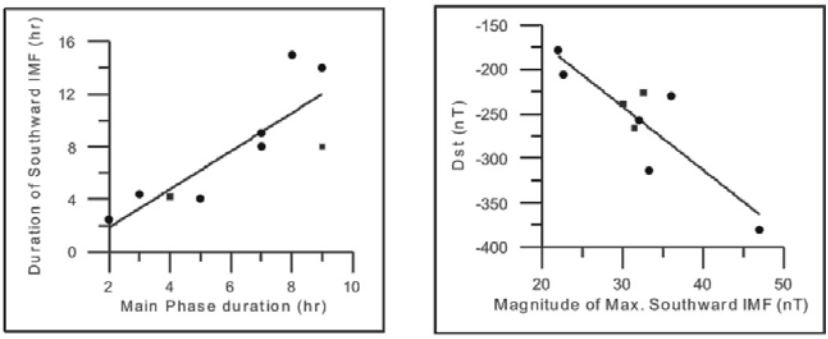

Figure 5.22. The strength of the magnetic storm is directly proportional to the strength of southward IMF (Vichare et al., 2005).

6

SOLID EARTH GEOMAGNETISM

One of the fundamental issues in geosciences relates to formation and evolution of the crust, whose understanding has increased many-fold with advanced geophysical techniques. The geological history spans from Archaean, 3.8 Giga years (1 Giga=10^9), to the present (Neogene). Geophysical methods and techniques investigate the structure, composition and physical state of the Earth by mapping crustal anomalies associated with mineral deposits, structural features, and hydrocarbons. Since these constituents lie hidden beneath the surface, geophysics has become a preferred tool of exploration compared to geological techniques. The present section deals with crustal anomalies, and deliberates on their form and detection using appropriate geophysical procedures.

Geophysical methodology is used to detect anomaly in the crust arising essentially due to differences in physical properties of rock materials (Fig. 6.1a), which are related to structural setting of subsurface geological features. The principle of geophysical technique, regarding observed anomalies of magnetism, gravity and electrical resistivity, is employed to investigate crust-mantle relationship.

In general, geophysical surveys fall into two categories: (i) natural field methods, which measure physical properties of the Earth, e.g. gravity, magnetic, radioactive and geothermal and (ii) artificial source excitation methods, which generate pertinent signals used as input into the Earth. The response of input signal is then measured and analyzed to characterize physical properties, e.g. electrical, electromagnetic and seismic of host material. Natural field surveys are passive and easier to conduct, since they do not require large equipment. These surveys delineate the structures to greater depth, but suffer from severe limitations with regard to spatial resolution. Artificial source surveys, on the other hand, are techniques designed and organized to image the structures to a desired degree of accuracy and resolution in an optimal fashion.

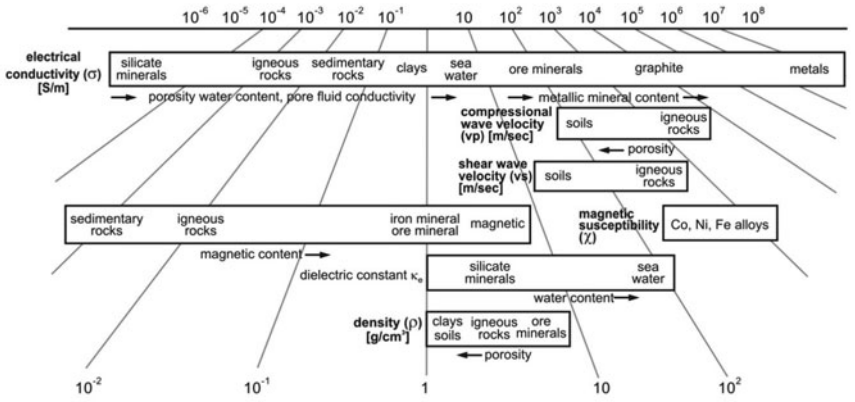

Figure 6.1a. The range of values for the physical properties that can be measured with the methods of applied geophysics (http://appliedgeophysics.lbl.gov/intro/figures fig_prop.jpg).

Seismic tomography with controlled resolution, for example, is a versatile technique capable to resolve complex structures in 3D. Among the various tomographic techniques, teleseismic wave tomography (TWT), local earthquake tomography (LET), and high resolution tomography (HRT) are commonly employed to delineate layered structure in association with seismic wave velocity perturbations. Wide angle seismic refraction and reflection data are acquired along several profiles using chemical explosions as artificial seismic sources. Analysis of teleseismic receiver functions of several P and S phase configurations produced by conversions at interfaces within the crust and upper mantle, using a large number of broad-band seismic stations, and azimuthally well distributed teleseismic sources, is more relied upon. The stacked receiver functions obtained essentially by waveform inversion give lithospheric structure with improved accuracy. The low velocity zones (LVZ) and plume conduits are also imaged well.

Geophysical surveys are carried out on land (magnetics and electromagnetics), at sea (ocean bottom magnetometry (OBM) and seismic reflection), and in air (aeromagnetics), over a range of scales: reconnaissance over 10 to >100 km, focussed mapping in 1 to 10 km range, and high resolution mapping (for finer details) in a few tens to few hundred metres range. The Indian subcontinent has been surveyed by a variety of geophysical tools and the data gained relate to analysis of ground, aerial and satellite potential field anomalies (gravity and magnetics), geoelectromagnetic inductive studies (geomagnetic depth soundings, OBM and magnetotellurics) on land and at ocean bottom, tectonomagnetism (repeat magnetometry for earthquake precursory changes and global positioning system for seismotectonics), rock and sediment magnetism (palaeomagnetic and mineral magnetics), and magnetic petrology. In this chapter, fundamental principles involved in the application

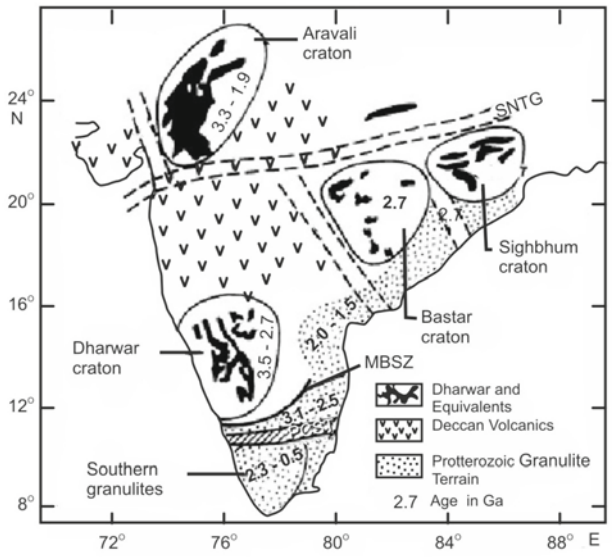

Figure 6.1b. Locations of Archean-Early Proterozoic cratons in the Indian peninsular shield. CG, SNTG, GG, MG, MBSZ and PCSZ refer to the Cambay graben, Sone-Narmada-Tapti graben, Godavari graben, Mahanadi graben, Moser-Bhavani shear zone and Palghat-Cauvery shear zone, respectively. Geologic ages are from S.M. Naqvi (pers comm) (courtesy: Pandey and Agrawal, 1999).

of these methods to the major tectonic and lithologic problems, are discussed with emphasis on comprehensive study of the Earth's interior.

The Indian shield is known to have grown through the nucleation of six widespread Archaean-early Proterozoic cratons separated by Gondwana rift valleys, sutures, and mega-lineaments (Fig. 6.1b). These distinct tectonic and lithostratigraphic assemblages differ in petrography, chemistry, thickness and seismic structures. The deeper structures beneath different geological provinces, which exhibit interesting cratonic formations, grabens with active and dormant geologic faults and shear zones are studied through geomagnetic methods and techniques.

Pure and applied geophysical studies: Geophysical methods employ natural and artificial sources. Earth's 'natural' signatures like gravity, magnetism and EM are employed for mapping anomalous structures in the Earth's deep interior, whereas induced electromagnetism involving geomagnetic deep sounding (GDS) and magnetotelluric (MT) techniques provide information supplementing the above methods. For example, the MT method is used in a large frequency or period range, which corresponds to a depth interval from the surface to some hundred km. The aim of exploration varies according to depth. In artificial source methods, the response of subsurface geological feature to artificial energization of the ground is attempted. Such approaches include artificial electrical, EM, seismic methods and microseismics.

Thus, geophysical studies have both fundamental and applied aspects, essential to enhance research and development in geosciences. These studies upgrade the basic understanding of regional tectonics, and considerably improve knowledge on the global geodynamical processes that drive the continents, control generation of energy, give rise to mineral deposits, earthquakes, volcanoes, and the like. A few of the applied aspects specifically relate to information on optimizing land-use, potential resource locations, and marking out earthquake prone areas by identifying active faults and conductive zones. However, both pure and applied aspects of a geophysical measurement are necessary to produce a holistic understanding of the dynamical processes at work in the Earth's interior. In this sense, they are complementary to each other.

6.1 GEOPOTENTIAL FIELD ANOMALY STUDIES

Geopotential field methods involve measurement of Earth's gravity and magnetic field to prepare anomaly maps. An anomaly is an abnormality, i.e. something different from the normal (theoretical value estimated from homogeneous Earth model) formed by spatial gravity and magnetic field variations, depending on the discrepancy in surface geology, and changes in composition, subsurface temperature, or thickness of the crust and mantle. Magnetic (gravity) anomalies are perturbations of the geomagnetic (gravity) field due to Earth structure. They are seen when one subtracts a regional magnetic (gravity) field from a series of observed readings.

I. Sources of Regional Anomalies

Many of the regional tectonic features of the study area appear coincident with satellite geopotential field anomalies. Sources for these anomalies may be generalized as lateral variations of the vertical integral of crustal density and magnetization. Hence, optimally reduced anomaly maps are used to detect these lateral variations. These variations in density and magnetization of the crustal column may in turn reflect petrological, structural, or thermal variations of the crust, resulting through active tectonic processes. Anomaly maps are used to constrain tectonic configuration of the lithosphere.

In general, long wavelength magnetic anomalies can be modelled by regional scale magnetization variations of the lithosphere, which lies between the surface and a lower boundary at which magnetic minerals do not occur. This boundary is defined as the topography of the Curie point isotherm of the crustal magnetic minerals. The location of this lower boundary is not unanimously agreed upon. Seismic velocities and analysis of upper mantle xenoliths indicate that lower crust is made up of granulite grade metamorphic rocks, and that the upper mantle is dominantly peridotite (Chapter 2). Mantle xenolith studies also indicate magnetite or serpentinized metals do not exist below the Moho, making it the magnetic basement except where a limiting Curie isotherm is above the Moho. Some invoke serpentinization as a source

of magnetic mineralogy below the crust extending the magnetic boundary to the upper mantle. However, the debate will continue till this problem is definitely sorted out.

Crustal conditions affecting regional scale magnetization generally involve variation in the amount, distribution, and magnetic properties of magnetite within the lower crust. The amount and distribution of magnetite are related to crustal composition and thickness, whereas the magnetic properties of magnetite are temperature dependent (Chapter 2). Thus petrologic, structural and thermal perturbations within the crust and upper mantle produce magnetization contrasts. These physical and lithologic variations often combine to produce anomaly superposition, and source ambiguity, which limits the interpretation of regional magnetic anomalies.

This is overcome by combining the gravity data. In general, gravity anomalies are related to density variations, formed from several sources. At satellite elevations, gravity signals with long wavelengths characterize crustal and upper mantle density contrasts due to regional variations in composition (bulk mineralogy), temperature or crustal thickness. Longer wavelength anomalies, which are of continental scale, commonly arise from deeper mass variations in the mantle and core, which occur below the magnetic lithosphere. The combined analysis of gravity and magnetic data is, however, more effective in bringing out crustal and mantle features, since they map the source fields at different depths. Hence, ground magnetic and gravity surveys are planned, wherein ground data can then be coupled with aeromagnetic and satellite data for a comprehensive subsurface picture.

II. Anomaly Contour Maps

The compilation of gravity and magnetic anomaly maps in this book are qualitatively presented in the form of contour maps (points having equal gravity and magnetic values). Presence of 3D bodies is suggested by more or less circular or elliptical contours, whereas elongated ones define the presence of 2D bodies. The contour map is then divided into zones of different magnetic characters, which are correlated with the known geology and these correlations are extrapolated to poorly mapped regions. The axes of the anomalies are usually drawn on the maps to derive information on major structural controls. Repetition of the contour pattern is suggestive of a folded sequence of sedimentary beds. Termination of the contours along a line, or the presence of flexures in the contours indicates a fault. Magnetic axes are also frequently displaced due to faulting. Individual bodies of the same rock type occurring within a single geological province show similar magnetic characteristics. Frequently, magnetite may be formed in some rocks due to effects of the adjacent igneous intrusives helping to outline the intrusive itself. A qualitative idea of the depth of the sources can also be obtained from some striking characteristics of the anomaly patterns; sharp anomalies indicate, for example, the anomalous bodies to be at very shallow depths.

III. Geopotential Problems

Solutions to geopotential problems are non-unique, and other available geophysical data are necessary to constrain the models. Hence, magnetic surveying is often done in conjunction with other geophysical techniques such as gravity, heat flow, seismic and MT to recognize different source field depths, and thereby help to reconstruct the plate history. Magnetic data together with integrated geophysical data have proved especially useful in studying several processes, such as intrusive bodies with different magnetization than the country rocks, the juxtaposition of crustal blocks of different magnetization through plate tectonics, and creation of the oceanic crust during different core field polarity periods.

IV. Ground, Aero and Satellite Magnetic Surveys

Magnetic survey is the measurement of EMF intensity or its components (such as vertical component) with the objective of measuring the magnetism over an area of interest. Magnetic measurements can be made from a variety of platforms (water, ground, air) and altitude (ocean bottoms to satellite heights). These measured magnetic data have contributions from source fields over several spatial scales. Due to the availability of the data at various scales and elevations (which generally represent geophysical variations at different depths), synergistic use of these data provides a unique opportunity to study similarities and variances of geologic and structural variations through the entire lithospheric column. Short-wavelength signal is generated by magnetic material that resides within the uppermost part of crust, medium-wavelength comes from materials at shallow depths, and long-wavelength component is generated from deep-seated structures. The ground data contain contribution from all these sources, but the air-borne data contain mostly medium and long wavelength components, basically limited by the size of the survey area. The satellite data, on the other hand, contain only long-wavelength module. As far as exploration of resources at exploitable depths is concerned, the ground data offer more information than the air-borne data. For pinpointing exact location of the geodynamic structure, long as well as medium-wavelength components derived from ground and air-borne data are subtracted.

Analysis of data for crustal magnetic anomalies is obtained from (1) satellite data of polar orbiting geophysical observatory (Pogo), and MAGnetic field SATellite (Magsat), (2) aeromagnetic maps, and (3) ground magnetic surveys conducted over petroliferous sedimentary basins of India.

6.2 SATELLITE MEASUREMENTS OF EARTH'S GRAVITY FIELD

Remote sensing of the Earth through satellites provides data to undertake studies that embrace virtually every aspect of the origin, dynamics and evolution of

the lithosphere. One of the earliest scientific uses of satellite technology has been the mapping of the Earth's gravity field and determining its shape (the Geoid). As early as in 1956, a new value for the flattening of the Earth was determined from tracking of Sputnik I. The gravity field is not easy to measure from air-borne sensors to an accuracy needed for a proper analysis of shallow subsurface structures. The gravity field is the result of mass and its distribution inside a body. Therefore, a spacecraft tracking, using its radio communication signal, determines its orbit or trajectory from which the gravitational field and a mass of the body can be inferred. For a proper analysis of shallow subsurface structures, gravity anomalies can be calculated from satellite orbital motions.

I. Satellite Free-air Gravity Anomaly Maps

This book uses free-air anomaly maps at ground level and 400 km height prepared by Rapp from the spherical harmonic analysis of the 1° by 1° averages of the measured free-air gravity anomalies and satellite tracking data. These maps are often called the satellite-derived free-air anomaly maps, or satellite gravity anomaly maps (Fig. 6.2). In essence, Fig. 6.2b is a downward continuation of Fig. 6.2a at ground level.

India is known for a thorough gravimetric coverage of its landmass, although major part of it still continues to be impervious to detailed geological and geophysical surveys. This is because of problems posed by the highly varying topography of Aravallis, Vindhyans, eastern and western ghats, Deccan plateau, and the Himalayas. The only recourse is satellite-based measurements, which can map surface and subsurface structures of the entire subcontinent,

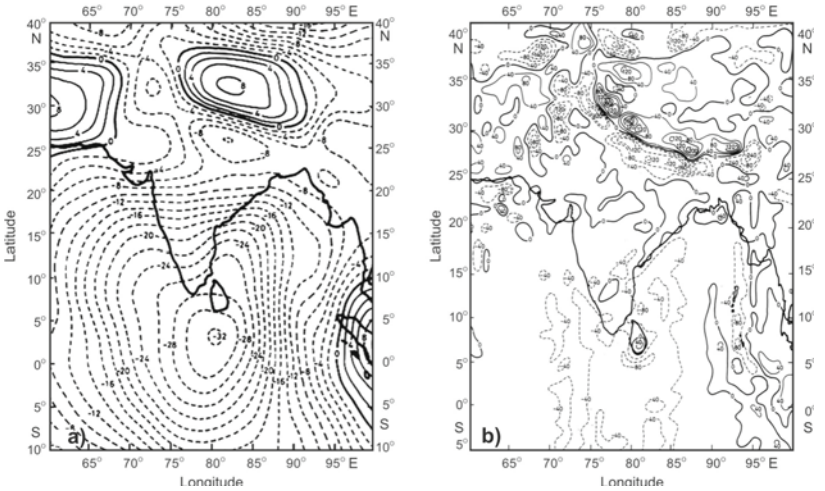

Figure 6.2. (a) Satellite free-air gravity field anomaly observed at a height of 400 km, contour interval 2 mgal. (b) Satellite free-air gravity field anomaly observed at ground level, contour interval 40 mgal (Singh et al., 1992a).

and its neighbouring oceanic realm; hence, satellite gravity anomaly maps are analyzed.

Satellite gravity anomaly, sources: Gravity anomalies are caused, in principle, by lateral density variations that can be located anywhere from the Earth's surface to the Earth's core. Anomaly components of a wide band of wavelengths are usually superimposed on each other on gravity anomaly maps. Generally, the Earth's gravity field can be considered to be distinctly composed of short-wavelength (a few to few tens of km), intermediate-wavelength (a few hundreds to few thousands of km), and long-wavelength (larger than described by spherical coefficients of degree and order 10) components. The short-wavelength anomalies, which are of interest in crustal studies are usually associated with the near-surface structures such as faults, intrusive bodies, sedimentary basins and others. In contrast, large-scale features such as mountain belts, isostatic processes, and inhomogeneities due to changes in composition, thermal state or thickness of the crust and mantle lead to long-wavelength anomalies. Short-wavelength anomalies overlap and dominate the ground gravity maps, making it difficult even to identify the trends of anomalies from deeper tectonic causes. However, anomalies measured at a few hundred km above the Earth's surface represent density variations at large depths only, since most of the short-wavelength components are automatically filtered out at these heights (Fig. 6.2a).

II. Ambiguity in Gravity Interpretation

Interpretation of gravity data means locating and determining various parameters of the sources responsible for the anomalies. A given gravity distribution on the ground surface can be explained by a variety of mass distributions at different depths. Following the theorem of equivalent stratum, the ground surface (or plane observation) can be replaced by a hypothetical mass distribution. The observed anomalies are actually continued downwards to different levels, and from these continued anomalies, a hypothetical mass distribution can be calculated at each level. Only one of these mass distributions is the correct solution to the observed anomalies, and this can be selected, if the depth to the mass distribution is known. In the absence of any outside information such as depth to the mass distribution, gravity interpretation is ambiguous, and no solution can be found that explains the observed anomalies uniquely.

To make the problem determinate, the unknown parameters must be reduced to a number less than the observations. This can be done in many ways, each pertinent to the problem in hand. The most important way of overcoming ambiguity is to assign a regular shape to the disturbing body, and to assume that the model has a uniform or uniformly varying density contrast. The important geometrical models very often used in gravity and magnetic interpretations are spheres, cylinders, faults, dykes, and others. A 2D fault structure, for instance, with a uniform density has only four parameters to be

determined from the gravity anomalies. These parameters are the density contrast, two depths (one each to the top and bottom interfaces), and the dip of the inclined face. The contour pattern of the anomaly map itself and the knowledge of local geology permit the assumption of the pertinent shape to the target.

III. Qualitative Interpretation of Satellite Gravity Anomaly Maps

The free-air anomaly map at 400 km height (Fig. 6.2a) shows only a couple of very broad highs and lows, formed by density variations at the boundary of the upper and lower mantle at 600 km. A major low over the southern part of India (specifically the Indian ocean low, IOL) and a high over the Kohistan-Himalaya high (KHH) are the two main prominent gravity features at satellite heights. The long wavelength of the IOL and its geographical coincidence with extreme geoidal minima of –104 m suggests the anomaly source to be in the crust or upper mantle.

On the other hand, the free-air anomaly at the ground level (Fig. 6.2b) is generally –40 mgal south of 15°N, and nearly zero over the northern portion of the peninsular shield. The latter observation signifies that the Indian peninsula is isostatically compensated. The region between 25° and 35°N is dominated by a strong negative anomaly reaching to <–120 mgal, and an equally strong positive anomaly north of it. These trends are attributed to the Himalayan mountain ranges and their overcompensation.

The free-air anomaly at the ground level shows several localized high and low anomaly values defining different blocks, which do not appear in 400-km height (Fig. 6.2a), since these anomalies have their roots in crust or upper mantle. For instance, the gravity high values up to 40 mgal, not seen at 400-km level, are associated with Sri Lanka and Shillong plateaus, Aravallis, Marwar and eastern ghats, suggesting their sources limited to the crust. Another significant feature of 90°E ridge gravity high does not reflect at 400-km level, implying a crustal anomaly. The long belt of negative anomalies of –40 to –80 mgal, covering the region between latitudes 5° and 18°N confined to 95°E longitude, corresponds to the trench system of Andaman Islands. These anomaly components are also missed at 400-km level. There is no obvious expression of Deccan traps, an extensive cover of the flood basalts, both at ground and at 400 km level.

IV. Anomalous Satellite Gravity over Himalayas and Its Isostatic Compensation

The satellite free-air gravity anomaly at ground level (Fig. 6.2b) is further used for studying the isostatic condition in many parts of Indian peninsula in general and the Himalayas in particular. The anomaly is consistently zero over

the northern portion of the peninsular shield, which implies major part of the peninsula being isostatically compensated. A strong positive free-air anomaly, initially trending NW-SE at 34°N and 75°E, and then turning E-W beyond 30°N and 80°E, correlates with the known trend of Himalayas (Fig. 6.2b). The high positive anomaly is bordered on the south by an equally strong negative anomaly. The Himalayas are generally considered isostatically overcompensated, and are expected to give rise to negative free-air anomalies. But, contrary to expectations, free-air anomalies over the Himalayas in satellite data are positive, ranging from 40 to 160 mgal. Some have explained this anomalous behaviour in terms of isostatically undercompensated processes.

To solve the riddle, free-air anomalies are calculated over typical models of trapezoidal topography depicting elevated masses and steep valleys following the local compensation theory of Airy-Heiskanen. The crust-mantle boundary outside the anomalous zone is assumed to be at 30 km depth. According to the Airy-Heiskanen system, a topographic height of 1 km increases the thickness of the crust by 6.67 km for a density of 2670 kg/m^3 of the topography and the universally accepted density contrast of 400 kg/m^3 at the Moho.

Figure 6.3 clearly indicates that free-air anomalies are positive over the topography, flanked by negative ones on either side, which are stronger on the flanks of a steep slope. This shows that the Himalayas are indeed overcompensated isostatically and it would be erroneous to presume that the positive satellite gravity anomalies over them prove undercompensation. It is also stressed that the true nature and extent of isostatic compensation of the Himalayas can only be decided by investigating both the positive and negative anomalies resulting from the mountains and their roots.

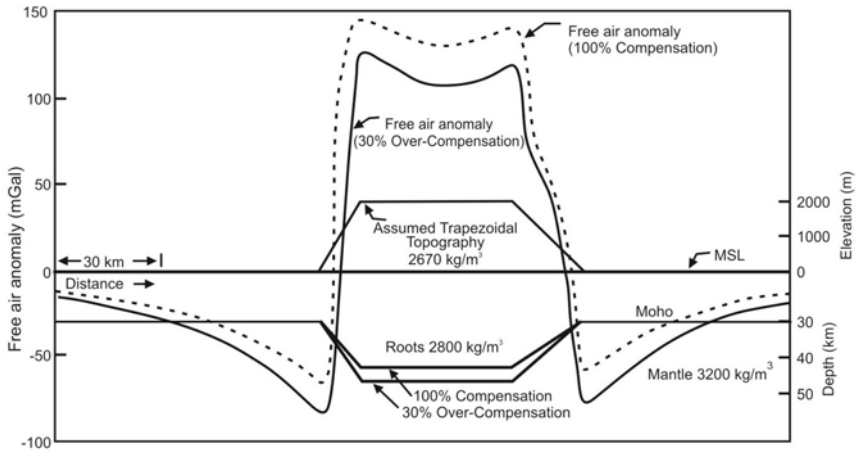

Figure 6.3. Calculated free-air anomalies over an assumed trapezoidal topography model depicting the Himalayas with an elevation of 2000 m and base width of 75 km for both cases of complete and 30% over-compensation (Basavaiah et al., 1991).

V. Preparation of Residual Free-air Anomaly Map

The anomalies at ground level (Fig. 6.2b) are composed of long-wavelength anomalies from distant deep sources, which are removed to study crustal and local features. The long-wavelength part estimated from the inversion of the gravity anomaly at 400-km level for an equivalent mass distribution at ~600-km depth is a fairly representative value for lateral heterogeneity in the upper mantle. Deep earthquakes have foci up to 600-km depth. The anomaly components due to such a mass distribution are used to recalculate the long-wavelength anomalies at ground level (Fig. 6.4).

It shows a pronounced minimum over the IOL, and three systematic maximum anomalies over Sumatra-Indonesia high (SIH), KHH and Baluchistan high (BNH). These anomalies are long wavelength components and are subtracted from Fig. 6.2b. The difference between observed total anomaly at ground level (Fig. 6.2b), and those calculated through the equivalent point source technique (Fig. 6.4) is called the 'residual anomaly'. Figure 6.5 shows the residual gravity anomalies, which give a better idea of sources at shallower than 600-km depth.

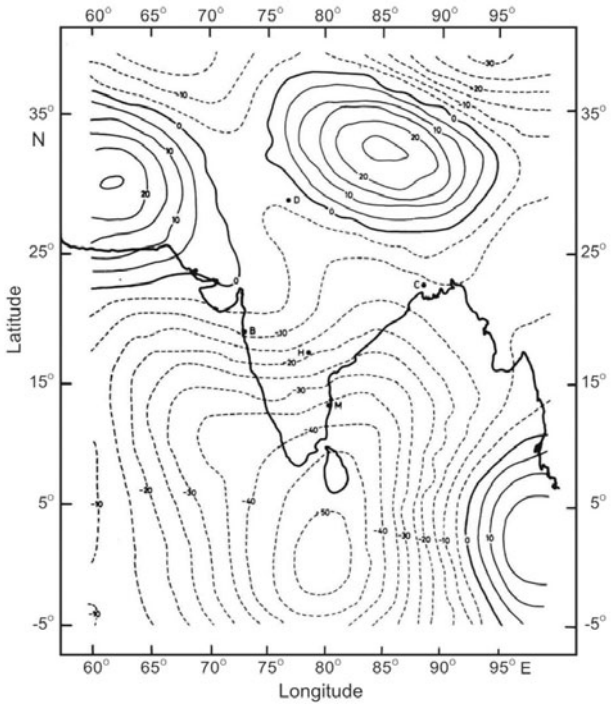

Figure 6.4. Gravity anomaly, in mgal, at the surface of the Earth recalculated from the equivalent mass distribution obtained by inverting gravity data at a height of 400 km, contour interval 5 mgal (Singh et al., 1992a).

VI. Residual Free-air Gravity Anomaly Map and Tectonic Implications

Figure 6.5 shows several highs and lows of different magnitudes, some extending to several hundred km, and others confined to small areas. The residual gravity map can identify geological lineaments, horst like structures, intra-cratonic basins, oceanic ridges, and transform faults that are caused by or associated with structures at the Conrad or Moho levels or both. Some localized closures characteristically identify the tectonic units. The high of 40 mgal near 25°N latitude defines the Shillong plateau (shown as SP in Fig. 6.5). Over Sri Lanka, a distinct positive anomaly closure is surrounded by negatives. The well-defined and isolated highs over Shillong plateau and Sri Lanka are due to their associated horst-like structures developed by deep faulting in Meso-Cenozoic time at Moho discontinuity. The Dharwar folding (DF) is also reflected on the residual map by a general NNW-SSE trending, partly superimposed by high grade granulites. The Cuddaph (CD) basin is seen as a major negative anomaly, indicating it to be the result of tectonic activity at deeper levels either

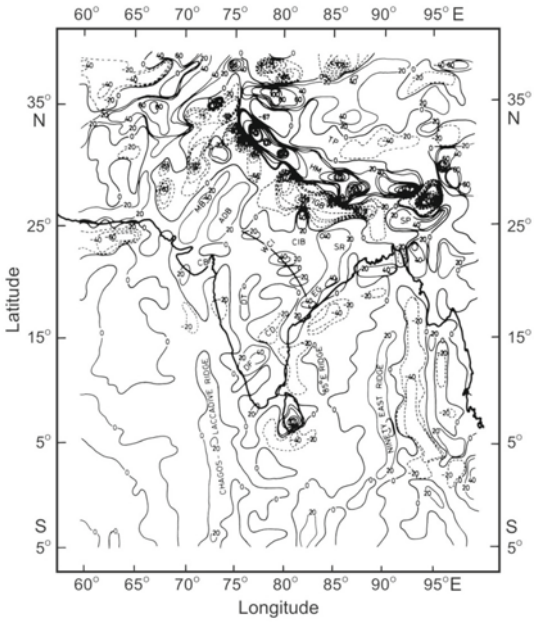

Figure 6.5. Residual gravity field anomaly, in mgal, after removal of the calculated long wavelength part due to sources in the upper mantle at a depth of 600 km from the observed gravity anomaly at the ground surface. Contour interval 20 mgal. DF - Dharwar Folding; DT - Deccan Traps; CB - Cambay Basin; MB - Marwar Block; ADB - Aravalli-Delhi Block; CIB - Central Indian Bijawars; SR - Singhbhum Region; EG - Eastern Ghats; CD - Cuddapah Depression; SP - Shillong Plateau; TP - Tibetan Plateau; HM - Himalayan Mountain ranges; IGB - Indo-Ganga-Brahmaputra basin, and WCI - West-Central Indian lineament (Singh et al., 1992a).

at Moho or Conrad or both. Importantly, Fig. 6.5 accentuates many features, which are not so obvious in Fig. 6.2b. Perhaps, the situation is unique for the Indian region, where sharp gradients of a strong long wavelength component masks the local features. The causative sources of all these residual gravity anomaly trends are wholly located within the crust.

In addition to long running anomaly closures, many localized closures are also seen to align in well defined trends that can be identified as lineaments. The most important ones are marked as Himalayas (HM), west-central Indian (WCI), eastern ghats (EG), and ridge features in the Indian ocean. Some of these lineaments coincide with or run parallel to the known major geological trends. The anomaly trends of the Himalayas, eastern ghats, Aravallis-Delhi block (ADB), Marwar block (MB), and 90°E ridge appear distinctly in the residual map, but are subdued in the ground map. In addition, this map brings out a few more important trends, and anomalies such as the Chagos-Laccadive ridge, 85°E ridge, west-central Indian lineament, Dharwar folding, and Cuddapah depression. It also gives clear demarcation of the Himalayas, Indo-Ganga-Brahmaputra basin and Tibetan plateau (TP).

VII. Residual Bouguer Gravity Anomaly Map and Crustal Thickness

A Bouguer anomaly map of India (Fig. 6.7) is prepared after removing the long wavelength component from the modified Bouguer gravity anomaly map (Fig.6.6). The calculated residuals are plotted in Fig. 6.7, and are used to estimate the thickness of the 'Indian' crust.

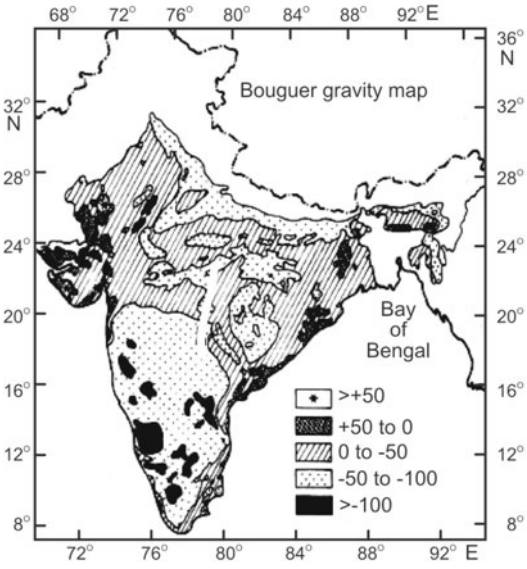

Figure 6.6. Modified Bouguer gravity anomaly map of India prepared by the National Geophysical Research Institute (1975). Contours are drawn at 50 mgal intervals.

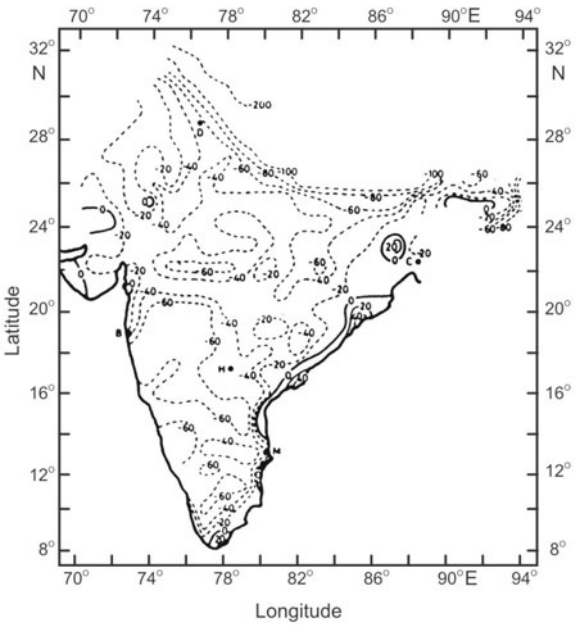

Figure 6.7. Residual Bouguer gravity anomaly map after removal of long wavelength component shown in Fig. 6.4 from Fig. 6.2b (Singh et al., 1989a).

Thin crust exists across the Delhi folding, Aravallis, the Bombay high, Cambay basin and eastern ghats (Fig. 6.7). The change in pattern and amplitude of anomalies is indicative of different crustal configuration along the east and west coasts. Although the data do not extend into the oceanic region on the east coast, closures of anomaly contours on the continental side are evident and a line of zero-anomaly coinciding with the coast line signifies a transition in the nature of the crust. The gravity pattern indicates a long linear trend along the eastern coast suggesting dimensional extent of the causative source. On the other hand, the contour loops on the west coast seem to continue into the oceanic side. These deductions of the continent-ocean boundary are corroborated using the satellite magnetic data.

6.3 SATELLITE MEASUREMENTS OF THE EARTH'S MAGNETIC FIELD

The Earth is heterogeneous in age from the land to ocean. Beneath oceanic realm, the crust is young, thin and layered. The continents, at places, have a crust as thick as 70 km (45 miles) with age up to 4,000 Ma. Research expeditions mounted through ingenious techniques such as seismic, geochemical, petrological and the like have been able to accumulate knowledge of its highly complex structure and composition. The continental crust is alternately seen to form and deform by the mechanism and processes that are still not well

understood. A new geophysical tool based on satellite measurements of the EMF (discovered almost by chance) offers a new avenue of testing models of the evolution and deformation of the continental, and to some extent oceanic crust. This methodology has already given some promising results in the exploration of cosmic bodies such as Mars or the Moon.

The first global EMF measurements encompassing all the sectors of the Earth were made by Cosmos (USSR) and a series of USA's Pogo 2, 4 and 6 satellites launched by NASA in the late 1960s. Cain and his associates in 1970 were the first to recognize long wavelength anomalies from the total field residuals obtained from Pogo data. Magnetic bodies of such magnitude were hard to predict, and difficult to conceive with the investigative tools at hand at those times. Scientists, then, were content with delineating micro-level features, and structures of the crust (fold/fault) as well as the compositional and temperature changes that were deciphered from rapid variations caused in the process of propagation of seismic waves.

The anomalies deciphered by Pogo were confirmed later by the Magsat satellite, launched by NASA in November 1979. This satellite had a lower and less elliptical orbit equipped with magnetometers that measured the Earth's magnetic field vector. NASA's Langel and his team were the first to publish new anomaly maps mounted from Magsat data, which were improved later by other groups. These long wavelength anomalies (product of Pogo and Magsat) gave newer insights into deformations and other tectonic imprints from innumerable areas that were inaccessible till then. Magsat has a unique place in global magnetic studies, since it churned out vector measurements. The total field measured by Cosmos and Pogo has a scalar component from which ionosphere components are difficult to separate out. Even for Earth resource survey, vector measurements are more potent than just the scalar ones. Because of this reason, Magsat data are extensively used by both space and geoscientists. The Magsat-like Oersted satellite launched in 1997 covered near-noon local time, and provided ideal conditions for studying ionospheric current systems. Such an effort is rewarding not only in an integrated use of Magsat data, but also in providing appropriate method for reduction of the data to be obtained through forthcoming missions.

Anomalies in the static part of the magnetic field as deduced from satellites establish the utility of space-borne measurements in studies of long wavelength anomalies, which originate largely within the lithosphere. Long wavelength anomalies are mostly recognized from near-Earth satellites at altitudes of 350-750 km, and these altitudes define the shortest wavelengths traditionally associated with such geomagnetic features. Virtually identical features have now been recognized in satellite magnetic field records from Pogo (1967-1971), Magsat (1979-1980), Oersted (1999-), CHAMP (2000-) and SAC-C (2004).

All masses contribute to gravity field, but only those materials that have a significant susceptibility contrast add to magnetic anomalies. The density variations of different layers within the lithosphere may change by less than one order of magnitude, but susceptibility variations contributing to

magnetization can change by three orders of magnitude, thus making magnetic data a very sensitive indicator of change within the lithosphere. With the advent of digital signal processing techniques, it is now possible to extract far greater information and gain accurate results.

I. Regional Magnetic Anomaly Map

Potentiality of satellite magnetic data in determining structure of geological significance and in identifying inhomogeneities in the lithosphere, has been proved beyond doubt. Identification of the Bangui anomaly in Africa from Pogo data is an excellent example of the importance of satellite magnetic data. The magnetic field residuals obtained from several passes of Pogo satellite over India reveal them to be positive over the southern part of India, and negative over the Himalayas. Boundary separating regions of positive and negative anomalies appear to be in line with the Narmada-Sone lineament, which extends from the western to eastern margins of Indian plate. To resolve the structural complexities of the Indian plate, regional geomagnetic reference field and magnetic anomaly maps are prepared using ground and Magsat data.

II. Magnetic Anomaly through Magsat

Data obtained during its passage over the Indian region (0° to 40°N geomagnetic latitude and 60° to 100°E longitude) with finer time resolution were used to draw anomaly maps. These data contain contributions from three sources: (1) Earth's core (~40,000 nT), (2) ionosphere-magnetosphere currents (up to 200 nT), and (3) geological structures within the crust (0 to 20 nT). Magsat data provide additional constraints to study oceanic basins and continental margins, besides giving an insight into deep crustal conditions, as well as providing useful framework for tectono-mineralogic analyses and synthesis along with surface and other satellite-based data. These datasets provide interesting information on the geodynamical structures and processes, which are discussed below.

III. Data Processing

Several processing and reduction procedures involving equivalent point source inversion modelling were synthesized and applied to satellite magnetic data. These yielded improved reduction techniques and better resolved anomaly maps suitable for geologic analysis. Observed satellite magnetic data came from the Magsat <2°> scalar and vector anomaly maps derived by Agarwal and his coworkers.

IV. Isolation of Crustal Origin Components and Reduction of Data

Data from Magsat measurements are reduced to isolate components of crustal origin of 10 to 20 nT. Considering that crustal component constitutes only

~0.5% of the total field, its isolation is an involved process. The normal procedure is to eliminate core field constituting ~99% of the main field through MGST (4/81) thirteenth order and degree spherical harmonic expansion. From the remainder, contribution of ionospheric-magnetospheric currents (which usually refer to as external field) is removed. The ionospheric contributions are neglected since Magsat orbits always confined to dawn-dusk meridian. The distribution of external field currents during disturbed conditions of magnetosphere is sufficiently complex to preclude a simple expression. However, when the magnetosphere is quiet, $P_1°(\cos \theta)$ is reasonably taken to represent the latitudinal dependence of external field, where P_1 is Legendre polynomial of 1° and θ is the dipole colatitude of the observation point. The data of 92 passes with $Kp<1_0$ are selected. Even after all these corrections, the residual data from overlapping passes show zero-level difference. This has been ascribed to lack of base-line control arising from the nature of measurements, which are made with a continuously moving magnetometer. To account for base-shift, a quadratic trend is subtracted. The residuals are then scrutinized, and values with magnitudes >20 nT are rejected. The remaining data are then isolated for 2° by 2° blocks, and data in each block are averaged. Values deviating by $>2\sigma$ (σ = standard deviation) from the block mean are rejected. A new average is then estimated, which represents the anomaly at the average height of 420 km for the block. The crustal part (often referred to as anomaly field): total (B), N-S (X), and vertical (Z) fields are shown in Figs. 6.8a, b.

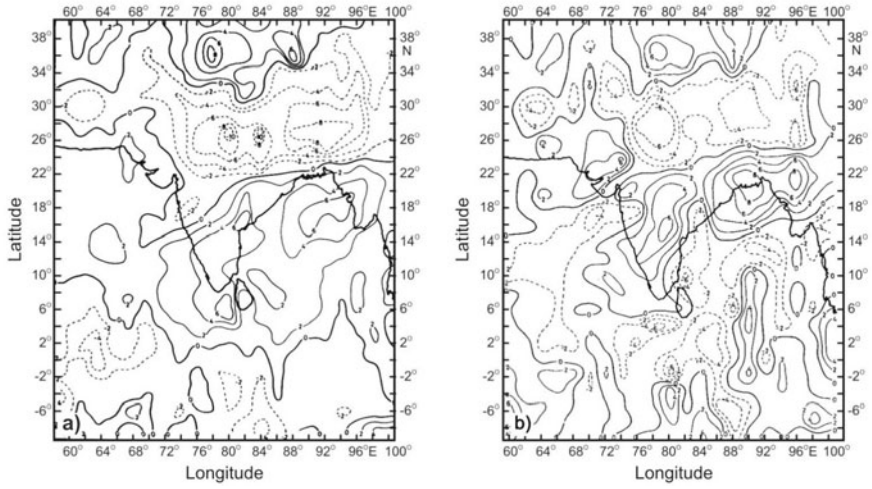

Figure 6.8. Data collected over the Indian subcontinet from the Magsat satellite are used to understand the crustal structure by determining crustal magnetic anomalies. Since the crustal component contributes only 0.05% to the total observed values, its isolation is a complex process. Here the anomaly shown is for: (a) vertical field (Z), and (b) scalar total field (B) computed from X, Y, and Z anomalies for an average Magsat height of 420 km. The values plotted are in units of nT (Agarwal et al., 1986).

The B-anomalies synthesized from X-, Y- and Z-anomalies are compared with B-anomaly estimated directly, and found the two to agree quite well. This gives credence to the data reduction technique, and at the same time establishes reliability of the anomaly maps.

V. A Tricky Magnetic Interpretation

Characterization of crust in terms of geological properties directly from the anomaly map is difficult, because the angle of inclination changes from zero over the southern end of peninsula to ~45° over the Himalayas. Apart from depending on the geological structure, the pattern of anomaly also depends upon the direction of magnetization. Hence, further reductions aimed at improving the resolution of geologically significant Magsat anomalies are applied. Most importantly, because magnetization of lower crustal and upper mantle sources are predominantly induced, the data are reduced for the variable geomagnetic field effects of inclination, declination and intensity to enhance geologic analysis.

The vector anomaly maps (particularly the X and Z) exhibit much larger amplitudes than the scalar anomalies, indicating that the scalar anomaly is not the total anomaly. Rather it is the projection on the direction of the main field. Thus, when the main field is wholly horizontal, the scalar anomaly can have no contribution from anomalies in vertical direction. Such a situation is seen over the southern portion of the Indian peninsula and the adjoining sea. Since the angle D over India is 1° to 2°, the scalar anomaly is independent of E-W direction anomalies. These regions have one or two components (X, Y and Z) as zero, hence utmost care should be taken when synthesizing models for geological structures from just total field measurement.

Further, geographical coincidence between the magnetic anomalies and various tectonic and geological structures need cautious interpretation. Because of the essential dipolar nature of the Earth's main field, the anomalies are not always directly above the sources. The position and character of a magnetic anomaly caused by a body of given geometry depends on its magnetization direction, which varies with latitude (Fig. 6.8 c-f). Thus a positive anomaly can be seen, if the source is at the pole (here the main field is vertical); a negative anomaly is encountered, if it is at the equator (here the field is horizontal) (Fig. 6.8 c-e). This problem can be overcome by either reducing the anomaly to the pole (Fig. 6.8 f), which deliberately aligns the anomalies with the sources, or by calculating the magnetization distribution. The latter is mostly adopted because it directly parameterizes the crustal characteristics. The transformation makes the anomalies overlie the sources, making it possible to correlate the magnetic anomalies over gravity and geological information (Fig. 6.11).

VI. Correctness of Anomaly Maps: Forward Modelling

Realizing the utility of magnetic field anomaly maps in numerical modelling of ground and aeromagnetic data, it is useful to examine the physical reality of

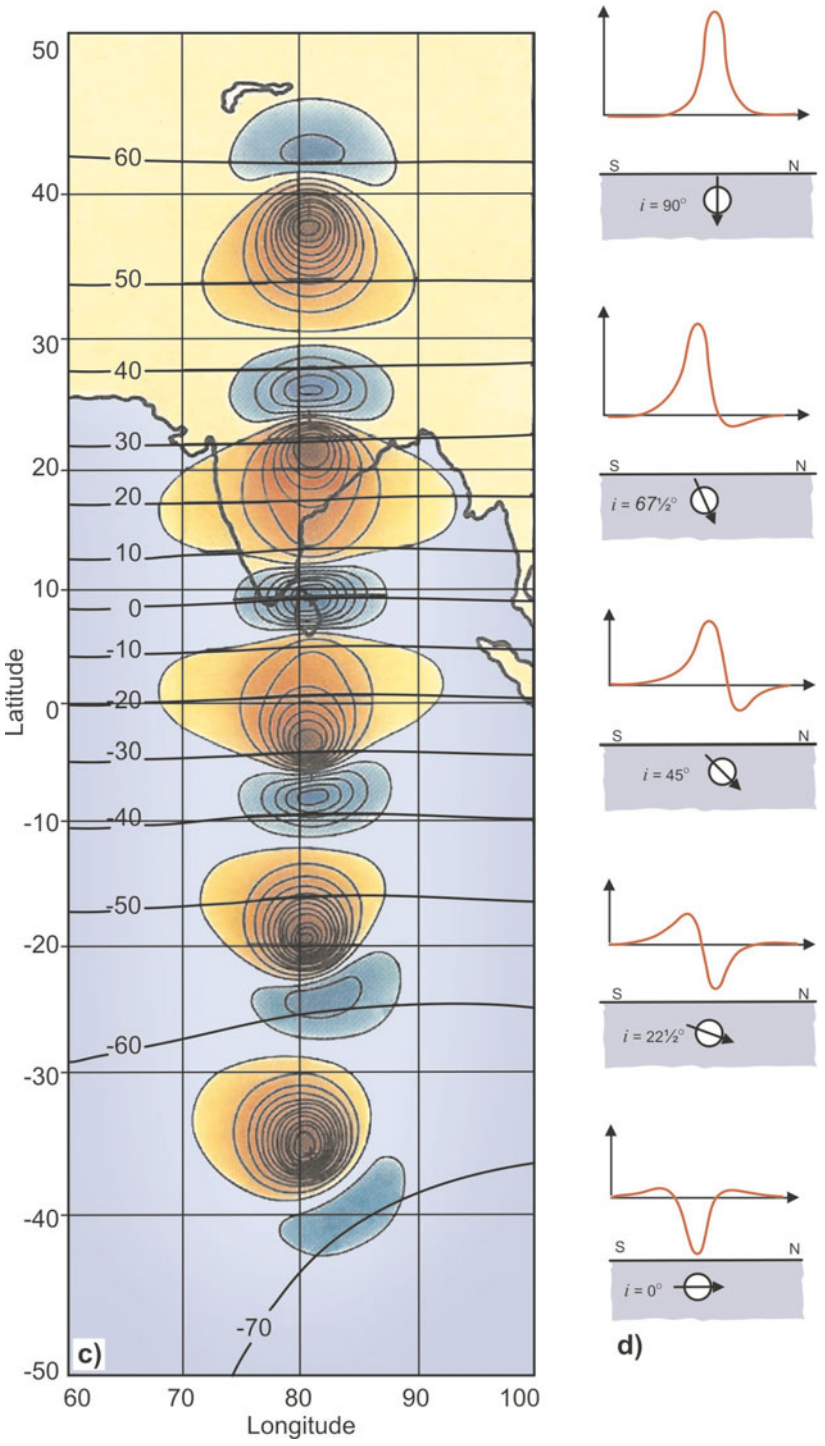
50
40
30
20
10
0
-10
-20
-30
-40
-50
Latitude
60
70
80
90
100
Longitude
60
50
40
30
20
10
0
-10
-20
-30
-40
-50
-60
-70
c)
S
N
i = 90°
i = 67½°
i = 45°
i = 22½°
i = 0°
d)

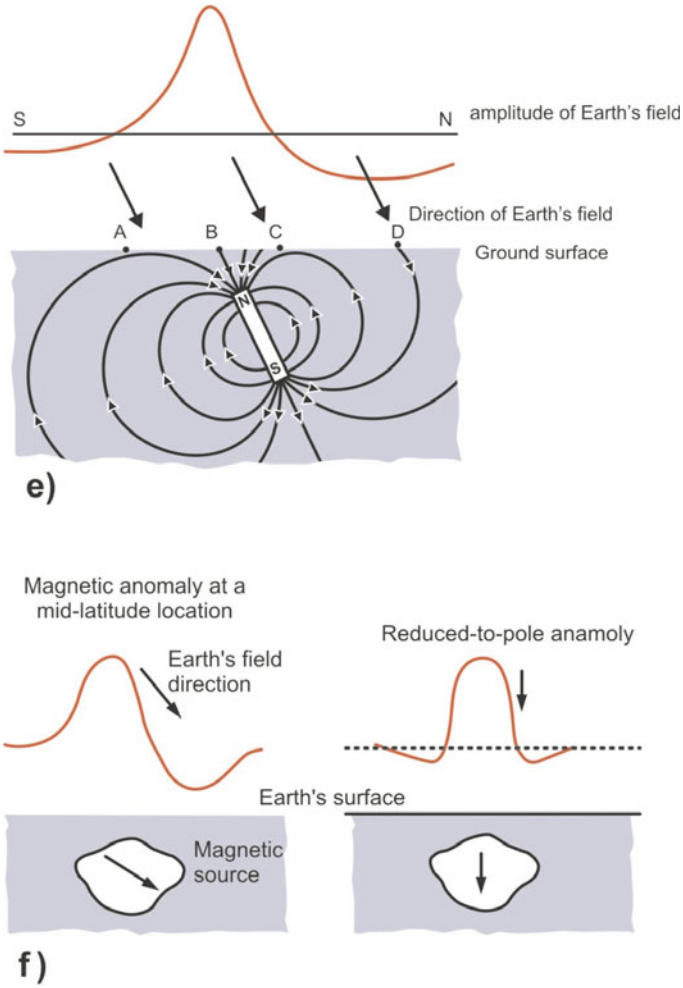

Figure 6.8. (c) The magnetic anomaly produced by a magnet of given dimensions (a point source marked by a + moving latitudinally), which always has two poles, one positive (red) and the other negative (blue), depends on the magnetic direction within the body. The main field is dipolar and its inclination is a function of latitude. The bold lines represent inclination of the main field. Note the position and shape of the poles of the magnetic anomaly produced by a point source depend on the latitude of the source (courtesy: Achache et al., 1988), (d) The variation of magnetic anomaly with (magnetic) latitude. I = inclination. The magnetized body is a sphere with all the magnetization induced, (e) The magnetic anomaly profile across buried ore body situated at a magnetic latitude of 60°N, in which magnetization is entirely induced. The magnetization in the body is dipping in the same direction as the EMF, at ~60°. The magnetic field measured at point A to D is a combination of the Earth's field (black) and the field induced in the body (red), and (f) Skewness of a magnetic anomaly due to a uniform arbitrarily magnetized source below the Earth's surface in an obliquely oriented EMF (left) and its reduced-to-pole expression in the vertical magnetization and vertical field condition (right).

the isolated crustal component. The forward model assumes: (1) the source field of the anomaly to lie within the crust, (2) only induced magnetization exists, and (3) the susceptibility is constant over the whole region represented by the dipole. Since there is little information on susceptibility and its variation with depth for the Indian region, a mean value of 0.0025 emu/cc (0.031 SI) is used for the model. For computation of the anomalies, the total region is divided into dipoles of 4° by 4° size with their depth of magnetization extending to the Moho discontinuity. This being the usual crustal thickness, is derived from the Bouguer gravity anomaly (Δg) maps using the relation $T = 32.0 - 0.08\Delta g$. By using this formula, the calculated values of crustal thickness are given in Fig. 6.9. As Bouguer gravity anomaly maps are not available in the deep sea region, thin oceanic crust of ~5 km is assumed.

With this information, the anomaly in total field (B_{an}) is calculated at Magsat 420 km height in spherical co-ordinates using the equivalent point source (EPS) distribution of magnetic dipoles. Evaluation of the anomaly is done numerically using the Gauss-Legendre quadrature integration method. The salient features of the calculated anomalies (Fig. 6.10b) show good agreement with observed Magsat anomalies (Fig. 6.10a). In particular, the zero contour line across central India and negative anomalies to its north of the observed map are well reproduced in the computed map. However, to the south of the zero line,

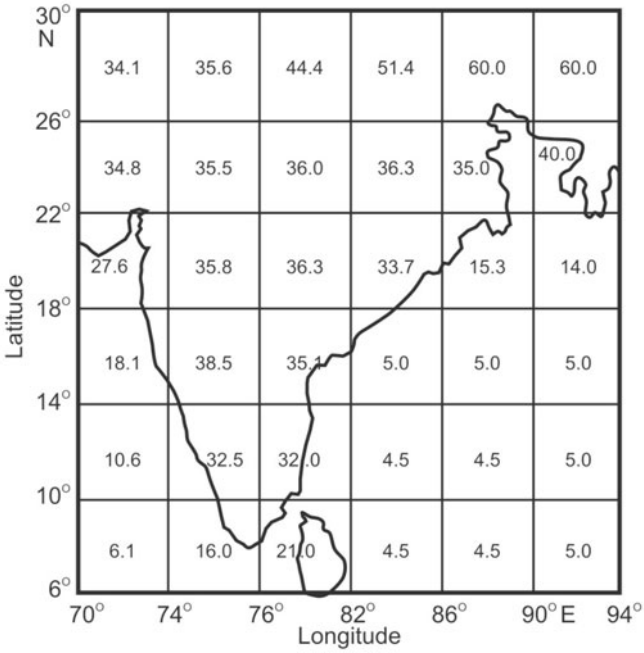

Figure 6.9. Average crustal depth values in 4° by 4° grid of the Indian region. Crustal depths have been derived from the Bouguer gravity anomaly maps (Rajaram and Singh, 1986).

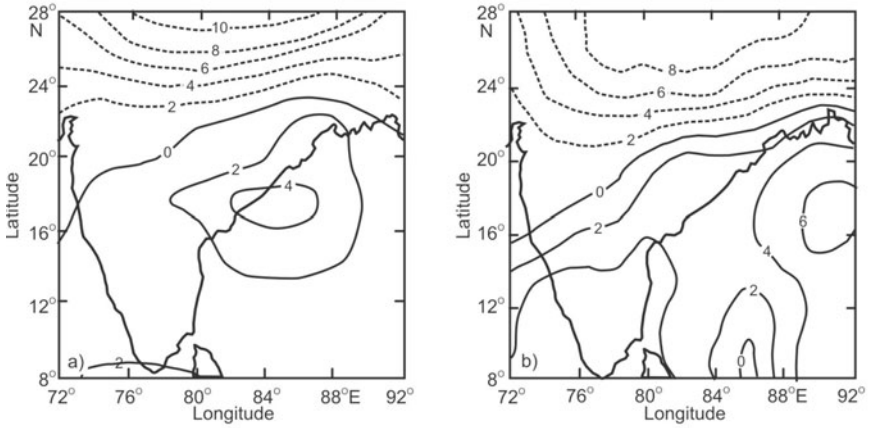

Figure 6.10. (a) Scalar magnetic anomaly map deduced from the MAGSAT data. (b) Scalar magnetic anomaly map deduced from spherical Earth model. The anomalies are contoured at 2 nT interval (Rajaram and Singh, 1986).

particularly over the Bay of Bengal, the agreement is not good because of the nonavailability of a good estimate of the crustal thickness. It is established that the crustal component of satellite data is accurately isolated. The details of anomaly features are then used to find lithological structures through inversion techniques.

VII. Ridge Regression in Inversion of Low Latitude Magnetic Anomalies: Crustal Magnetization Map

The approach adopted is to calculate moments of a set of dipoles over the surface of the Earth in such a way that they collectively reproduce the observed anomaly at satellite height in the sense of least squares. Magnetization being totally induced, dipoles are considered magnetized in the direction of the main field at their point of location. The moment, being directly dependent on the product of layer thickness and susceptibility, forms a useful parameter, and reflects well the depth of Curie isotherm. The inversion technique differs from the forward model calculation in the sense that dipoles of 2° by 2° size provide finer details of the crustal structure. First the gross feature of the anomaly is tested, and through inversion, the finer details of the Magsat measurements are used.

The ridge regression technique is used to stabilize EPS inversion over the low latitude equatorial regions. Anomalies averaged over 1° by 1° blocks form the input data, and the calculated moments are for dipoles representing magnetization of 2° by 2° crustal blocks. The whole region between –8°S and 38°N latitude, and 60° and 100°E longitude is treated as one 46° × 40° block. The magnetization of the crust derived by inverting the anomaly in Z-field is given in Fig. 6.11. The resultant crustal magnetization maps facilitated tectonic

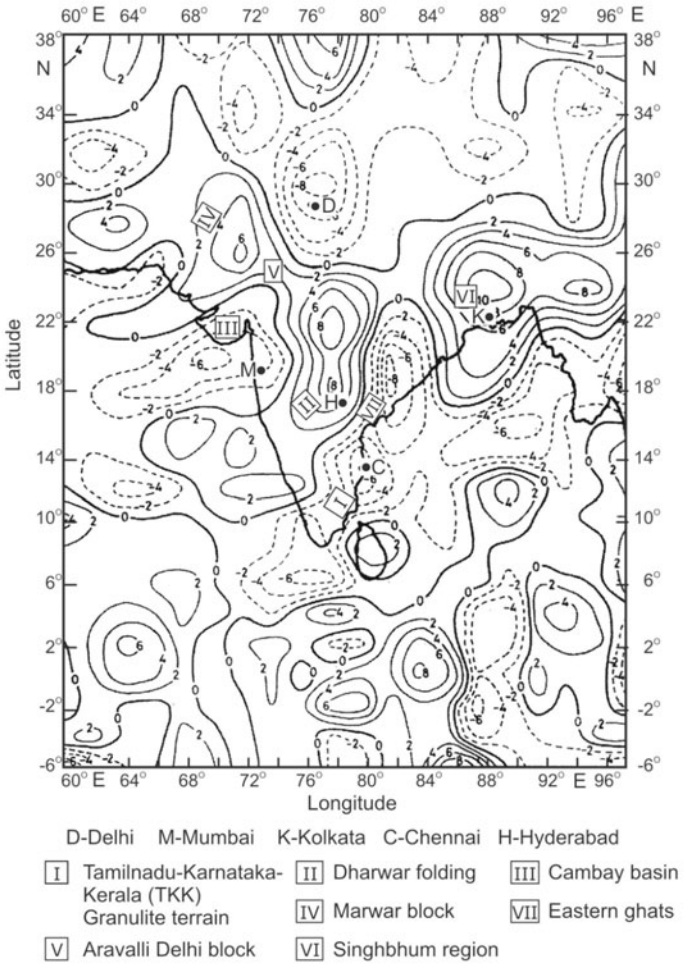

Figure 6.11. Lithospheric magnetic anomaly cannot be directly interpreted in terms of the geological properties of the crust. To circumvent this, anomalies are inverted using a ridge regression technique to calculate magnetization values. Magnetic moment (10^{14} Am^2) distribution of 2° by 2° blocks calculated by inverting anomalies in the vertical component of the magnetic field (Z) observed at MAGSAT height (contour interval $2\times10^{14}Am^2$). The magnetic moment is proportional to the product thickness of the crust and susceptibility of its material. In representation, a positive moment means a thick crust and a negative moment a thin crust (Basavaiah and Singh, 1997).

analyses of magnetic susceptibility variations within the lithosphere; mostly due to magnetization of the lower crust.

VIII. Geological Interpretation of Magnetization Maps

The magnetization map displays only relative magnetization levels that are correlated with the thickness and magnetic content of crust and depth of Curie

isotherm (Fig. 6.11). In this concept, negative magnetization represents a thin crust, crust containing weakly magnetic material, or a high subsurface temperature. On the other hand, for areas of positive magnetization, the geophysical situation is just reverse, i.e., thick crust, low temperature and high susceptibility. Therefore, the highs and lows on the magnetization map (Fig. 6.11) signify lateral variations in the magnetic crust. An overall correlation is noticed between magnetization and broad tectonic elements of the region, starting from I to VII.

The high values over four stable Precambrian blocks of the Indian landmass, namely Dharwar (II), Aravalli-Delhi (V), Marwar Craton (IV) and Singhbhum (VI) do conform to the high susceptibility of lower crust, since reflection seismic studies in several parts of the world have found the crustal mass underneath shield areas to be composed of alternating layers of mafic and ultramafic material. On the other hand, relatively low magnetization values are observed over eastern ghats, Kerala-Tamilnadu-Karnataka (KTK) granulite terrain, Panvel flexure and petroliferous Cambay basin. The low magnetization in KTK granulite correlates well with granites and some retrograded metamorphic rocks exposed in the region, while the low over a rift-type Cambay basin indicates a high heat flow. Likewise, over the Himalayas and Tibet plateau the low magnetization may have arisen from thermal state of the region. Seismic and gravity studies have inferred the crust to be thick beneath the Himalayas and Tibet plateau. The physical evidence that the triple junction of the western coast is characterized by low magnetization supports the presence of a small scale convection generated by hot spot activity. This heat transport has played an important role in the generation of hydrocarbon deposits found in Bombay High and also those expected in the Cauvery basin.

The magnetization pattern also correlates well with known variations in crustal thickness as estimated by gravity, seismic and heat flow data. Typical values for thickness of the crust from south to north are 35 to 40 km under the peninsula, 30 to 35 km under Indo-Gangetic plains and 60 to 80 km under the Himalayas and Tibetan plateau. Magnetization is negative under Indo-Gangetic plain, where the crust is thin, and positive on both sides where the crust is thick. Assuming that the oceanic crust is very much thinner than the continental crust, it is expected the former to have less degree of magnetization. Such a drop in magnetization, as one proceeds from continental realm to oceanic is clearly seen around the peninsula and Sri Lanka island (Fig. 6.11), where the magnetization changes from a positive to negative value.

In general, negative values are seen over the oceanic regions and features prominently over IOL (a structure which still remains to be fully understood). As expected, positive magnetization values are observed over Laccadives-Chagos and 90°E ridges. A special trait of interest is the transition from continental to oceanic crust and is seen to be sharp on the east coast, and gradual along the west. Positive magnetization contours (continental crust) extend into the northern portion of the Bay of Bengal. The fact that these patterns are seen

at satellite heights indicates their deep-seated origin and modelling may provide some unique information on the tectonic framework of the subsurface structures.

IX. Tectonic-anomaly between Magnetization and Residual Gravity

To constrain source characteristics of tectonic boundaries, and determination of their depths, satellite magnetic and gravity data are jointly analyzed in conjunction with geologic and other geophysical datasets of seismic, heat flow and petrophysical properties. This is done to understand the relationship between large-scale features and broad general patterns in the magnetization and residual gravity data. The joint analysis featured high gravity and low magnetization anomaly found across the eastern ghats can be modelled in terms of crustal thinning (as analogous to high heat flow). The SW and NE trending magnetic low contours over the Arabian Sea seem to centre near Mumbai—a region associated with local gravity high and also basic and ultrabasic dykes. Other known associated geological features with this axis of inverse correspondence between magnetic low and gravity high are the Konkan coast, hot springs, the Cambay rift and the Panvel flexure. Basic and ultrabasic post-Deccan trap volcanism, occurrence of mercury, carbonates and high heat flows that characterize this region suggest it to be a marginal aulacogen.

The other highlight is the occurrence of inverse correspondence between high gravity and low magnetization over petroliferous basins like the Assam oil field, Bombay High and Cauvery basin. This is related to a shallow Curie depth, consistent with high heat flow values, and a thin crust of gravity high. A comparison with the heat flow map of the region depicts zones with heat flow ~70 mWm^{-2} are areas of low magnetization with the exception of the central Indian region. An inverse relationship in the two anomalies over the Himalayas is due to higher thermal gradients that average beneath these high mountain ranges. Therefore, inverse correspondence between residual gravity and magnetization (Figs 6.5 and 6.11) can possibly be used to infer heat flow values. Nevertheless, with the availability of heat flow map for the country, Magsat results and gravity maps can be used more effectively.

The western region of India and the Rajasthan shield is associated with magnetic as well as gravity 'high'. Magnetically this region has similarity to the southern, rather than northern shield. The 90°E ridge in the Bay of Bengal is associated with a NS trending magnetic and gravity high, flanked by lows to the east and west. The IOL south of Sri Lanka finds an expression as localized closures.

The low magnetization (Fig. 6.11) and low mass distribution (Fig. 6.12) are consistent with the trans-Himalayan conductor and the Palk Strait conductor (Figs 6.32 and 6.33) identified by EM induction methods. This correspondence between the two suggests that both these conductors are associated with either high heat flow or low magnetic susceptibility and density. The anomalous

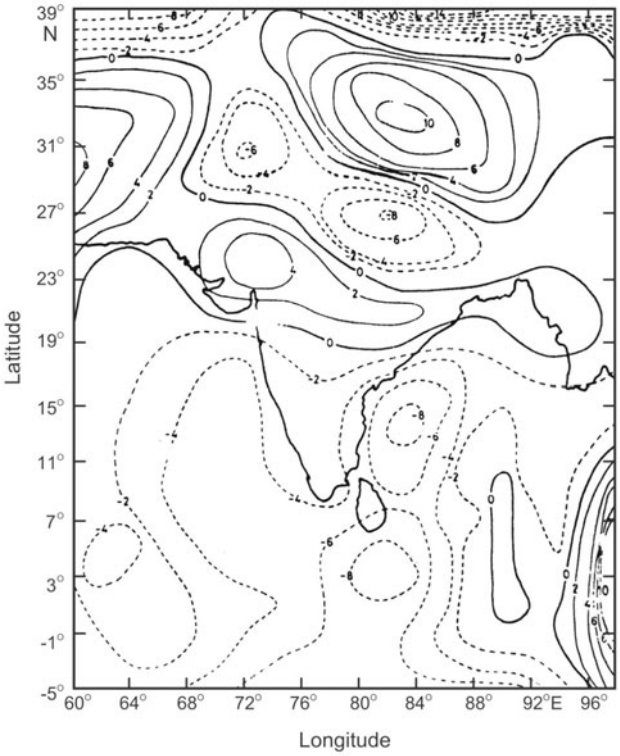

Figure 6.12. Anomalous mass distribution of 2° by 2° blocks calculated through inversion of satellite gravity anomalies at 400 km height (given in Fig. 6.1a) taking the location of equivalent point sources to be at a depth of 200 km. Contour interval 2×10^{19} g. Note two highly conducting regions in the Palk Strait and trans Himalayan area (Fig. 6.32) depict low mass distribution from satellite gravity data (Basavaiah, 1993).

character of the lithosphere immediately south of India has low magnetization anomaly, which reflects thin magnetic crust related to the rise of the Curie isotherm.

6.4 AIR-BORNE MAGNETIC SURVEYS

Magnetic surveys are carried out over several spatial scales and elevations. Aeromagnetic surveys are the most common component of reconnaissance appraisals conducted to estimate depth of the basement, or equivalently the thickness of the sedimentary basins. With an advent of aircraft-mounted magnetometer system developed mainly for submarine detection during World War II by Muffly in 1946, the areal magnetic coverage has expanded rapidly. Surface and subsurface information are gained in a relatively cheap way through aeromagnetic surveys, which also provide uniform coverage of inaccessible areas.

I. Survey Objectives

Aeromagnetic surveys are done for a variety of reasons, primarily for geological and structural mapping, mineral and oil exploration, environmental and ground water investigations. Most surveys are flown to aid in surface geologic mapping, where the magnetic effects of geologic bodies and structures are detected even in areas where rock outcrop is scarce or absent, and bed rock is covered by water, ice, sand or vegetation. Broad correlations are made between rock type and magnetic properties, but the relationships are complicated often by temperature, pressure and chemical changes. Nevertheless, the combined ground and aeromagnetic maps with available geologic information are effective for meaningful geological insights. Certain kinds of ore bodies may produce magnetic anomalies that are desirable targets for mineral exploration. Hydrocarbon deposits are not directly detectable by aeromagnetic surveys, but magnetic data can be used to locate areas that provide favourable conditions for oil/gas production and accumulation. Similarly, mapping magnetic signatures of faults and features within water-bearing sedimentary rocks provide valuable constraints on the geometry of acquifers and framework of groundwater systems.

The first aeromagnetic survey for geological properties was carried out in 1945 in Alaska and by the end of 1940s, it had a global sweep. Parts of India too have been aeromagnetically surveyed. These results are published in the form of total intensity contour maps in degree sheet format without incorporating corrections due to main field variations of the Earth, which can be acquired from GSI.

II. Quality Control

The magnetic effects of different heading directions and aircraft manoeuvres are first measured during a calibration flight in the absence of magnetic anomalies, and then subtracted in real-time during survey operation as magnetic anomalies are recorded. During survey operation, the recorded aircraft attitude is used to apply an appropriate correction to each reading of the magnetometer. The following tests are carried out periodically to demonstrate the success of compensation.

The 'clover-leaf' test for magnetic heading effect: The 'clover-leaf' test is designed to demonstrate that the aircraft and system have no significant 'heading effect', i.e. that the same magnetic field value is recorded at a given location in x and y, regardless of the direction in which the location is overflown (once corrections for temporal variations of the magnetic field are applied). A visible point on the ground in an area of few

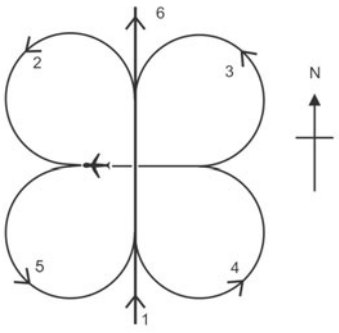

magnetic anomalies is chosen and overflown at survey altitude in, say, a northerly direction. The aircraft then turns and flies over the same point again in an easterly direction, then in a southerly direction, a westerly direction and finally in a northerly direction again to check for any diurnal variation since the first overflight.

Noise level monitoring: Noise experienced while recording a magnetometer profile can be divided into discontinuous and continuous noise. The former causes spikes to appear on the profile, which may be attributed to a plethora of sources, internal and external to the aircraft. These include lightning, DC trains and trams, power lines, radio transmission, electrical switching and so forth. Such effects usually demand manual elimination—or non-linear filtering—during data reduction. The continuous effects are largely eliminated by the compensation system in a modern installation, but there will be detectable residuals, which still set the limit to the sensitivity of the system.

Lag test for correcting the position (herringbone effect): The differing positions of magnetometer (or other) sensor within the aircraft and possible electronic delays in recording values are checked by overflying a magnetic object such as a bridge twice, the second time in the direction opposite to the first. The displacement between the two anomalies relative to the source is twice the shift that must be applied to bring magnetic and positional information into registration. A lag of 0.1 to 0.2 sec—equivalent to about 10 m on the ground—is not uncommon. Since survey lines are often flown alternately in opposite direction, i.e. after completion of flying one line E to W, the aircraft turns around and flies the next line W to E. Failure to correct adequately for lag can result in values being shifted systematically, e.g. E on lines flown E-W and W on lines flown W-E. This is one possible cause of the so-called 'herringbone' effect seen on contour maps of surveys, which are not reduced correctly. However, in modern surveys such effects are more often due to incomplete levelling of the flight lines.

III. Aeromagnetic Survey Operations and Processes

Usually oil exploration and regional surveys are flown at a constant elevation in order to provide a constant datum for the basement depth estimates. Mineral surveys are carried out with a constant ground clearance. The planning of survey operations consists of choice of magnetometer, aircraft, navigational aids, proper scales for base maps, and flight parameters such as flight line direction, spacing and flight elevation.

Magnetometers: Compared to the magnetometers used in the 1940s, the resolution and accuracy of recent magnetic field measurements have increased significantly (Chapter 4). The early fluxgate magnetometers had resolutions of ~1 nT, noise envelopes of 2 nT and suffered from appreciable drift of ~10 nT/hr. The fluxgate magnetometer can also be used as gradiometer, and it is therefore most sensitive to shallow magnetic sources. Proton precision

magnetometers have followed fluxgate magnetometers with a resolution of 0.1 nT, noise envelope of 1 nT and minimal drift. These are superseded by the cesium vapour magnetometers, which have a resolution of 0.001 nT and a noise envelope of 0.005 nT.

Single magnetometer aircraft configurations simply produce measurements of the magnetic field intensity in the direction of the EMF. By adding extra sensors, various other quantities can be measured. With increased sensitivity, three component systems at the wing-tips and tail are increasingly being used.

Aircraft motion, noise, attitude sensors: Magnetic noise caused by the survey aircraft arises from permanent and induced magnetization effects and from the flow of electrical currents. The permanent magnetization of the aircraft results in a heading error. Induced magnetizations occur due to the motion of the aircraft in the EMF. These effects are partially reduced by mounting the magnetometer either on a boom attached to the aircraft's tail or in a towed 'bird' attached by a cable. One serious disadvantage with the towed bird installation is that the motion of the bird in the EMF causes noise on the magnetometer record, and there is virtually no satisfactory way of compensating for the motion of the bird. A rigid extension of the airframe—usually in the form known as a stinger—solves many of these problems, but necessitates closer attention to the sources of magnetic effects on board the aircraft. The permanent magnetic field of the aircraft at the magnetometer sensor is compensated (backed-off) by passing appropriate DC currents through each of three orthogonal coils in the vicinity of the sensor. The induced component was offset by mounting pieces of highly permeable material close to the sensor in a position (found by trial-and-error) such that their magnetic effect is always equal and opposite to that of the engines. The eddy-current effects are similarly mimicked, but in opposite sign by coils of wire placed close to the sensor. Recently, active magnetic compensators have been developed to address these problems 'on-line' during survey flight. Once the survey is started, the aircraft's noise level is assessed repeatedly to ensure that the same level of data quality is maintained.

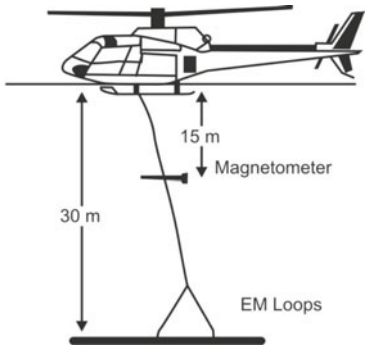

The choice of aircraft is a matter of economics and balancing costs against performance. The most common aircraft types include single-engine cessnas, twin-engine aircrafts, and larger model Dakotas.

Navigation, positioning: No matter what accuracy is achieved in the magnetic field measurements, the value of the final survey data is dependent on exact location of measurement points. Traditional methods of navigation rely largely on visual tracking using aerial photographs. The actual location of the flight

path is recovered manually by comparing these photographs with images from onboard video cameras. However, in areas of poor photographical features, navigational aids like Doppler or ANA (aircraft navigation using atomic standards) become necessary. These techniques are superseded by the introduction of GPS in 1990s. GPS relies on the information sent from an array of satellites, whose locations are known precisely. Signals from a number of satellites are used to triangulate the position of the receiver in the aircraft, so that its position is known for navigational purposes and to locate the magnetic field measurements. GPS brings a number of important benefits to aerial surveying. Firstly, the coordinates of the survey aircraft (horizontal and vertical) are provided on a continuous basis. This not only improves the quality of survey navigation and reduces its cost, it also eliminates to a large degree the tedious and error-prone manual steps inherent in flight path recovery from film or video. Secondly, GPS provides a reusable positioning system. Surveys flown at different times in the same area may be correlated in position, making it easy to repeat survey lines or to fly infill lines. Current surveys generally use real-time differential GPS navigation where the raw positional information is corrected as the data is being collected. Altimeter keeps track of the altitude.

Temporal effects: Monitoring of the EMF is an essential component of aeromagnetic surveys. The time-varying effects due to micropulsations, magnetic storms and diurnal variations are removed through base-station subtraction, tie-line levelling and microlevelling (decorrugation). One or more base station magnetometers are used to track changes in the field during survey operations. The smoothly changing diurnal variation is removed from the data using tie-line levelling. Simply subtracting this variation from the measured data is not sufficient, since diurnal changes may vary significantly over the survey area. Nonetheless, the recorded diurnal is used as a guide in the levelling process. Tie-line levelling is based on the differences in the measured field at the intersection of flight lines and tie-lines that run perpendicular to the flight lines. If the distance and time taken to fly between these intersection points is small enough, then it can be assumed that the diurnal varies approximately linearly and can be corrected for.

Micro-levelling (de-corrugation): Creating a grid is still less than satisfactory in that some line-related noise remains evident. This effect is described as corrugations and the standard procedure for its removal as de-corrugation or micro-levelling. The micro-levelling procedure used to remove line-related noise has become standard in recent years. It is essentially a filtering process, whose wavelength in the across-line direction is equal to twice the line spacing and in the along-line direction to the spacing between the tie-lines. The need for micro-levelling arises from the imperfections in the polynomials applied to hang the flight line data on the tie-lines. Micro-levelling is applied to gridded data and the adjustments made to improve the grid are then feed back as a correction to the original profile data so that, when next gridded, line-related noise will not be evident. Adjustments made in micro-levelling need to confine

to a few nT. The assumption in micro-levelling is that the near-DC component of each profile resembles that of its neighbour, i.e. that the 'regional' field varies only smoothly from line to line across the whole survey area. The danger is that genuine geological features can also follow flight lines and micro-levelling can remove these.

Example, aeromagnetic survey operations, data acquisition: Aeromagnetic surveys over the peninsular shield were conducted in distinct epoch and altitude ranges (Fig. 6.13). The flight lines, which are parallel lines flown in a regular pattern of equally spaced, are N25°E - S25°W, where the flight altitude is 7000 ft, and for the rest of the region, the flight lines are N-S. The line spacing for all these blocks was maintained at 4 km, except for the 'drape' survey over Cuddapah basin (altitude 500 ft) covered under 'operation hard rock', where the line spacing varied from 500 m to 1 km. It thus becomes inevitable to reduce data to a common barometric altitude to obtain an overall idea of magnetic response of the geological terrain in general.

IV. Data Display and Interpretation

The final product is a set of levelled flight line data that are interpolated onto a regular grid of magnetic field intensity values covering the survey region. These values can be displayed in a variety of ways, the most common being a colour map, where the magnetic field values based on their magnitude are assigned a specific colour. Similarly the values can be represented as a simple line contour map. Both kinds of representation can be used in a qualitative fashion to divide

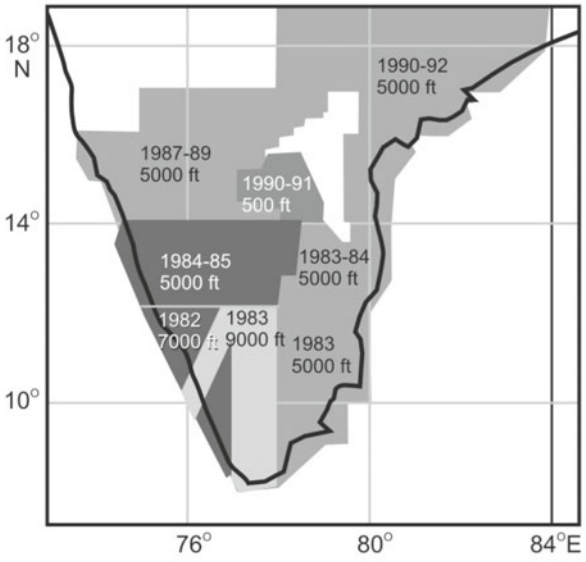

Figure 6.13. Sketch map depicting epoch and altitudes of aeromagnetic survey undertaken. Note different flight altitudes are indicated in different colours (Rajaram and Anand, 2003).

the survey area into sub-regions of high and low magnetizations. Since the data are available digitally, it is straightforward to use computer-based algorithms to modify and enhance the magnetic field image for the specific purpose of the survey. Transformation and filtering allow certain attributes of the data to be enhanced, such as the effects due to magnetic sources at shallow or deep levels, or occurring along a specified strike direction. More sophisticated methods may estimate the depths, locations, attitudes, and magnetic properties of magnetic sources.

Example, aeromagnetic anomaly map preparation: The GSI catalogue published in 1995 has details about the collection of aeromagnetic data. There, however, exists a data gap, as degree sheets are not available over a part of the Cuddapah basin, hence ground magnetic data collected over this basin at 10 km interval has been incorporated. The acquired degree sheet maps were machine digitized along contours. The observed digital aeromagnetic data for each block are corrected to remove the main field contribution using the 1980 and 1985 IGRF models interpolating appropriate date and altitude of observation. The data were then regrided at 2 km interval. IGRF removed data in different blocks are at different elevations, therefore all are continued to the same elevation of 5000 ft above msl and merged. The colour-shaded image of aeromagnetic crustal anomaly map, thus prepared is presented in Fig. 6.14. The red colour represents high and blue low values.

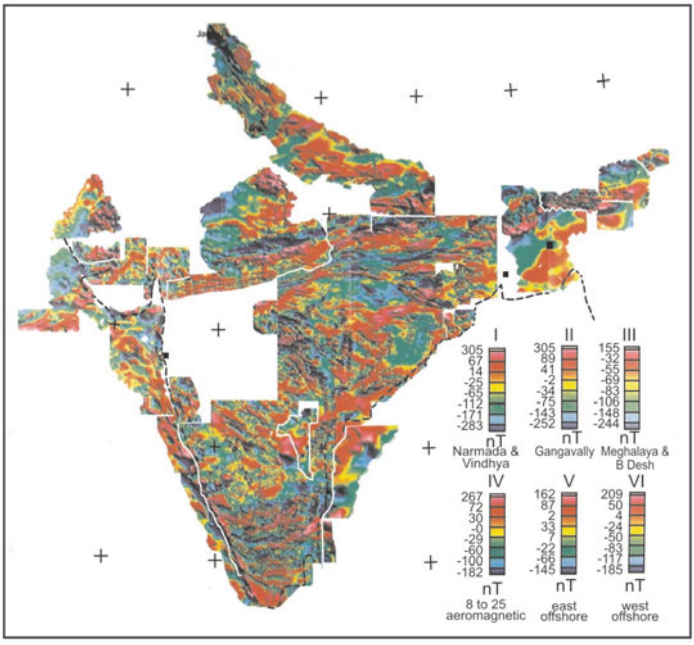

Figure 6.14. Composite aeroborne total intensity anomaly map. The aeromagnetic anomalies are used to understand tectonic elements and regional magnetic characteristics of the Indian peninsula showing a thin exhumed southern granulite crust with its lithological and mineralogical changes at ~22 km (Rajaram et al., 2006).

V. Geological Correlations of Crustal Magnetic Anomaly

The map (Fig. 6.14) clearly shows tectonic elements and regional characteristics of the peninsula. Superposed on it are short wavelength anomalies near surface features. A very striking element of the map is that north of 13°N, coinciding almost with the line of change of amphibolite to granulite facies, the trend of anomalies change from NNW-SSE in the north to essentially E-W in the south. The region between the line of change of facies and the Palghat-Cauvery shear zone exhibits east-west trending alternate high and low values. This striking contrast in gradients across the Moyar-Bhavani shear system is indicative of a change in magnetic sources.

Based on magnetic anomaly pattern (Fig. 6.14), the image map can be broadly classified into two distinct blocks, viz. block I covering area between 13° and 18°N latitude and block II between 8° and 12°N with a transition region between 12° and 13°N. Block I includes the Dharwar craton and block II comprises southern granulite terrain (SGT) and northern granulite block. Block I is heterogeneous and characterized by sparsely distributed broad anomalies, besides isolated 2D linear anomalies. A well defined 3D feature is much less common. In contrast, block II is fairly homogeneous and is characterized by a generally high density of anomaly distribution. This block is dominated by 2D linear anomalies trending mainly ENE-WSW to E-W and contains a localized 3D feature. Dense anomaly signature along the west coast between 8° and 14°N latitude represents post-Gondwana rifts and Cretaceous-Eocene magmatic activity.

The investigated area being in low latitude region, the inclination of the inducing main field increases the complexity of anomalies and makes the interpretation difficult. The analytic signal of total field reduces the magnetic data to anomalies whose maxima mark the edges of the magnetized bodies, thus helping in identifying the magnetic source distribution. The analytic signal map is represented in Fig. 6.15. The peaks (sources) of analytic signal within the Dharwar region represent intrusives/localized iron ore bodies. At 13°N parallel, the maxima align themselves along E-W direction parallel to the orthopyroxene isograd. The zone between Moyar-Bhavani-Salem-Attur faults and the Achankovil shear zone is characterized by many maxima representing extensive magnetic sources related to charnockites. Thus the analytic signal can be used to define change in grades of metamorphism. In fact, subsurface charnockites, and those in inaccessible regions like forests can be mapped using the analytic signal map. The west coast fault is also clearly visible. Surprisingly, no signature of khondalite belt is evident in this picture though they show clear highs in aeromagnetic anomaly map. This is because low gradients prevail over the khondalite belt in the aeromagnetic map, which has a lower susceptibility compared with charnockites.

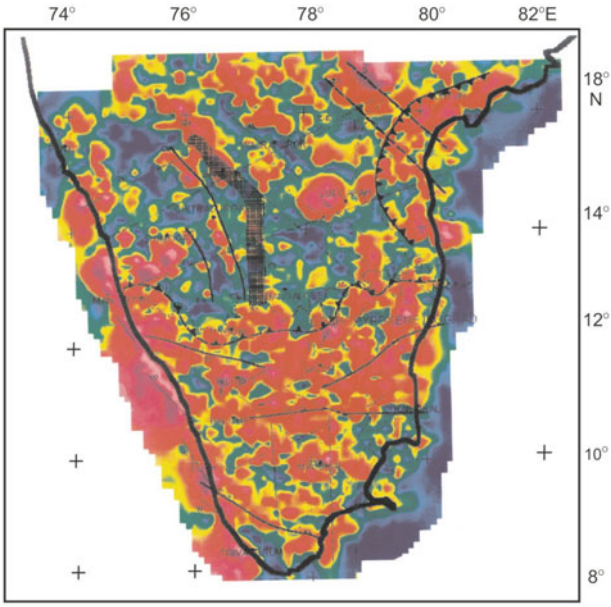

Figure 6.15. Analytic signal map of the aeromagnetic anomaly. Red colour represents magnetic sources (highs). Analytic structural trends, lineaments and faults identified are demarcated. Magnetic sources (highs) in the region south of 13°N are mainly charnockitic and that above 13°N are iron ore bodies of schist belts (Rajaram and Anand, 2003).

VI. Aeromagnetic Interpretation

The sources of magnetic anomalies over peninsular India are charnockites, intrusives, iron ore and trap flows. In the Dharwar craton, the NW-SE trends are deeper, older and are cut by several younger NE-SW shallow trends, the junction of which yields diamond-bearing kimberlite pipes. Chitradurga schist belt forms the dividing line between eastern and western Dharwar. The analytical signal map also reveals changes in metamorphic grades.

Magnetic crust below the high-grade terrain of SGT and all along the east coast is thin. Below the thin exhumed crust of SGT, there is a lithological/mineralogical change at ~22 km depth also seen as velocity change in deep seismic sounding (DSS) studies. The inverted magnetic data gave a crustal model along the existing Palani-Kolatur DSS profile. The model suggests that alteration of charnockites into hornblende-biotite-gneiss is more towards the north than south, wherein the process of retrogression is high but the exhumation of charnockites is more between Cauvery fault and Salem-Attur fault. Aeromagnetic anomalies on the east coast continue and merge gently with marine magnetic anomalies till the ocean continent boundary, but the west coast fault abruptly terminates the aeromagnetic anomalies towards the western offshore.

6.5 NATIONAL GROUND MAGNETIC SURVEYS

I. Data Acquisition and Total Field Anomaly Map

Aeromagnetic data in general and satellite surveys in particular regionalize the surface and subsurface geological characteristics, whose exact location is decoded by supplementing with ground survey data. Study of continental anomalies from a national magnetic anomaly map is being carried out extensively in USA. For such a study in India, SOI prepared total field anomaly map (Fig. 6.17) based on ground measurements at ~800 field and repeat stations, whose distribution is shown in Fig. 6.16.

II. Data Reduction and Processing

Based on these data, an analytical field representation is developed through a sixth degree polynomial as a function of latitude and longitude. This covers spatial variation of the field with wavelengths as short as 1000 km. The field values at stations corresponding to above model are subtracted from the observed field values, and residual values are used to compile the magnetic anomaly (Fig. 6.17), which can be considered free from anomalies >1000 km. The shortest wavelengths are ~80 km controlled by inter-station spacing.

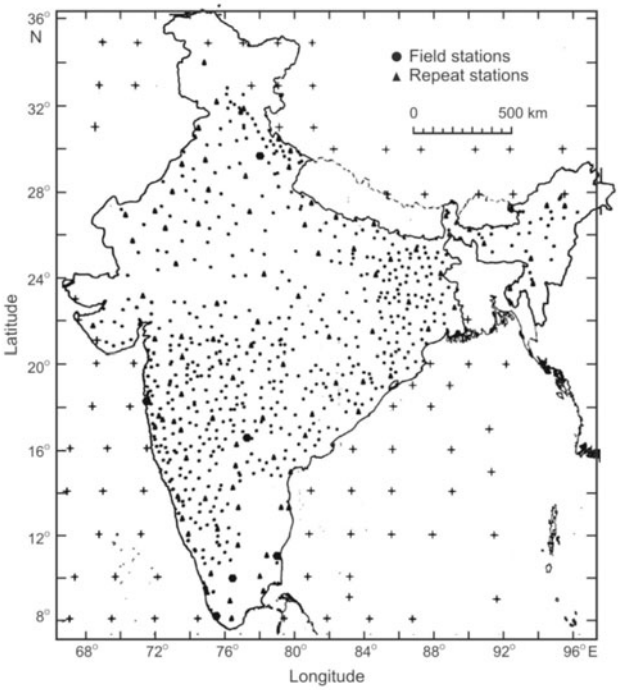

Figure 6.16. Location map of ~800 field and repeat stations installed by the Survey of India in order to collect the ground magnetic data used in the preparation of regional isomagnetic charts over the Indian region.

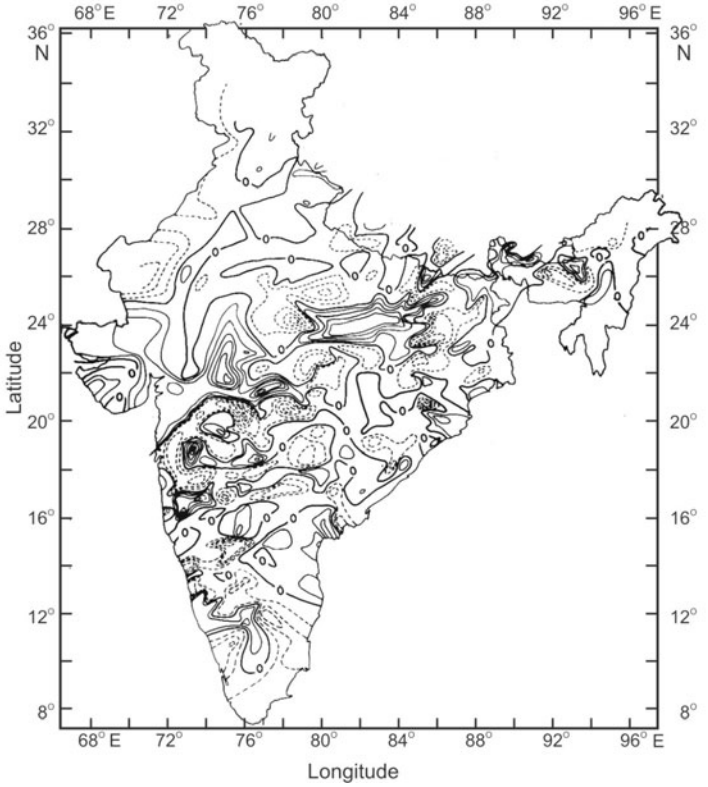

Figure 6.17. Residual total intensity anomaly map prepared after removing regional anomalies represented by a sixth degree polynomial model from the observed field values at stations in Fig. 6.16. These residual anomalies are considered to be free from anomalies of wavelengths >1000 km. The anomaly patterns are used to understand the crustal structure by comparing with an anomaly in total field as seen from the Magsat heights of 420 km. Contour interval 100 nT (courtesy: Survey of India).

III. Qualitative Interpretation of Anomaly Trends: Tectonic Features

The most conspicuous feature of total magnetic intensity anomaly map (Fig. 6.17) is the presence of a number of parallel to subparallel E-NE trending zones over central India that stretch right from west to east coasts. These anomalies correspond well with the Narmada-Sone lineament (NSL). NSL forms the boundary between the Vindhyans to the north and the Gondwanas to south and is known to be a prominent rift structure from gravity and seismic observations. To the north, anomalies are aligned in N-E direction corresponding to Aravalli mountain ranges. These mountain ranges represent rejuvenated uplifted block mountains resulting from tectonic activation of Indian shield. The whole of southern peninsula and Deccan trap region are characterized by small scale, large number of positive and negative anomalies, though Deccan

has blanketed the pre-existing topography over a considerable area. However, the presence of structures such as basins, rift valleys, fissure zones and dykes have been conjectured with scanty information from geophysical surveys. It would be interesting to examine whether the zones of positive anomalies characterize the fissure zones along which large lava eruption has taken place. The negative anomalies correspond to presence of pre-trappean sediments, primarily Mesozoic, which are also indicated from seismic surveys.

IV. Tectonic Correlations between Magsat and Ground Anomalies

In satellite anomaly maps due to natural filtering, many of the local features disappear because of which large scale regional features get sufficiently enhanced. When Magsat total field anomaly (Fig. 6.8b) is compared with ground data (Fig. 6.17), it is found that the ground anomalies cannot be distinctly separated in geological provinces. The conspicuous Magsat anomaly over the Himalayas is indecipherable in ground data. The general trend in Magsat data has a positive and negative anomaly over the southern and northern regions respectively, separated by a zero anomaly coinciding with NSL. The demarcation of NSL is not so clear in ground data. Perhaps, strong features of local extent mask the presence of this lineament. Other applications extend the existing analysis capability for knowledge of the conductivity of the upper mantle useful for inferring temperature, structural and compositional variations.

6.6 GROUND MAGNETIC SURVEYS

The magnetometer readings made at each observation point on ground surface represent a combination of main field, its temporal variation due to ionospheric current system and the relevant anomalous component due to lateral variations in magnetic parameters of the crust, mostly in the outer shell measuring 18 to 25 km thickness. Watchful evaluation and removal of extraneous contributions are essential to the attainment of a satisfactory picture of magnetic anomalies of small relief. Careful attention to various corrections to magnetometer reading corrections forms an important aspect in the application to oil prospecting in view of weak anomalies than to the exploration for iron ores, igneous intrusions, etc. where the anomalies are stronger. Table 6.1 shows different stages of magnetic data reduction in calculating crustal magnetic anomalies.

I. Plan of Conducting Ground Magnetic Surveys

The exact manner of conducting survey depends upon the purpose of the survey, the type of host region, the ease of transportation, and the type of anomalies expected. Regional surveys involve large areal extent (thousands of sq km) and can be for mineral or oil exploration. In contrast, detail surveys for minerals usually cover only a few km. Regional surveys are primarily intended to serve

Table 6.1 Typical example of reducing magnetometer data

Sl. No.	*time-F*	*obs-F*	*time-Z*	*obs-Z*	*H*	*Z*	*IGRF-F*	*ext.H*	*ext.Z*	*IGRF(F+ext)*	*Final-F*
1	8.45	40578	8.47	8478	2.5	4.1	40403	38109	18519	40027	551
2	8.55	40536	8.57	8546	2.6	4	40401	38111	18517	40024	512
3	9.05	40517	9.07	8426	2.6	3.9	40400	38111	18515	40024	494
4	9.12	40432	9.14	8332	2.8	3.8	40399	38114	18513	40020	411
5	9.18	40574	9.20	8525	2.9	3.6	40398	38116	18510	40020	555
6	9.25	40540	9.27	8440	3.1	3.4	40397	38119	18506	40017	523
7	9.35	40537	9.37	8373	3.2	3.2	40396	38121	18502	40016	521
8	9.42	40514	9.44	8343	3.4	3.1	40394	38124	18500	40012	502
9	9.48	40486	9.50	8336	3.6	3.1	40392	38128	18500	40007	479
10	9.55	40531	9.57	8466	3.8	3.1	40391	38131	18500	40003	529

the purpose of reconnaissance, to identify favourable ore environments or to understand geological or tectonic framework of a region. It helps to delineate major lithographic units favourable for specific type of mineralization or fault-fracture pattern of a region as a prelude to detailed work. Magnetic surveys for oil exploration over large sedimentary basins are primarily intended to know the thickness of sediments and the configuration of the underlying basement in order to locate structural oil traps. Regional surveys can be carried out on a regular grid pattern at 2 to 3 km interval or stations can be set up on all available roads and tracks so that an average station density of 2 to 3 km is achieved. 1:5000 scale maps are adequate for such a survey.

Detailed surveys for minerals are usually carried out on regular grid. The profiles are laid at right angles to the geological strike. A baseline along the strike of the body is fixed and profiles are set across the baseline. If L is strike length and w the width of the geological body, a profile interval of L/4 or L/5 and station interval of w/10 are adequate.

II. Surveyed Areas and Frontier Sedimentary Basins

The eastern continental margin of India (ECMI) has several sedimentary basins, which evolved following the dismemberment of Gondwanaland in Mesozoic (245 to 65 Ma) and formed between late Jurassic (200 to 130 Ma) and Miocene (23 to 5 Ma) as a result of southwesterly drainage associated with northward anticlockwise drift of India from southern latitudes to its present position. These basins were intracratonic, pull-apart type during their initial stage of formation, but after the break-up, became pericratonic. The intracratonic basin occurs on continental crust, either in the interior or at the crustal margins of old continental plates. They are caused by divergence and tension within the continental block and more often by subsidence along reactivated primordial faults. The pericratonic rift basins, on the other hand, form by subsidence of rifted trailing edges along extensional faults. Their basin axes are usually parallel to continental/oceanic crust boundary and sediments overlap into the oceanic crust. The common feature of east coast basins is subsidence along down-to-basement faults. The sedimentary fill, ranging in age from Jurassic to Pliocene, includes deltaic transitional marine sediments, carbonates, clastics, etc. In order to shed light on the evolution of ECMI and hence to reconstruct the configuration of Gondwanaland, knowledge of the structure, tectonics and sedimentation history of these sedimentary basins is very vital.

Ground magnetic survey was carried out over Deccan trap (Maharashtra), Cambay and Kutch (Gujarat), Khandwa (Madhya Pradesh), Mahanadi (Orissa), schist belts of Chitradurga-Holenarsipur (Karnataka), Krishna-Godavari (Andhra Pradesh), and the Proterozoic Cuddapah-Palar (spanning Andhra Pradesh and Tamilnadu) (Fig. 6.18). These surveys were carried out with point readings maintaining an average station interval from 5 to 10 km on a grid using indigenous PPMs (Chapter 4).

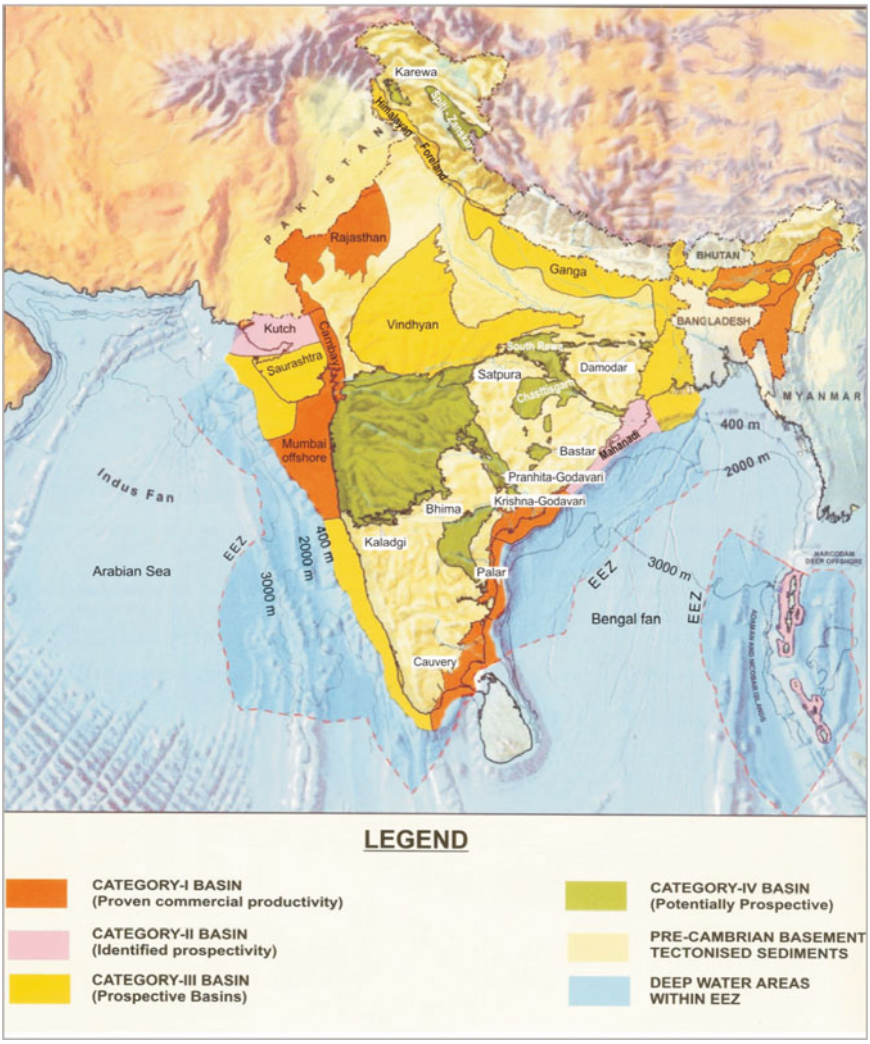

Figure 6.18. Generalized map of various sedimentary basins, which are categorized according to their hydrocarbon bearing potential (Biswas et al., 1993). These form the potential regions for carrying out ground magnetic surveys to understand the relationship between their magnetic characteristics and hydrocarbon bearing potential.

III. Reduction of Ground Magnetic Observations

To isolate crustal anomaly, spatial and time variations occurring in EMF over the period of surveying area are determined, and removed from the raw measurements. The EMF, however, varies rather uniformly over large distances of hundreds of km, and is thus easily predictable using IGRF. This, together with contributions from external current systems when subtracted from the observed field (obs-F in Table 6.1), leaves behind the magnetic anomaly.

(i) Diurnal corrections: These corrections are very important since the magnitude of diurnal variations of EMF is from 10 to 100 nT. There are three methods used for making diurnal correction: **(1) Observatory measurement:** Magnetic observatories make continuous records of magnetic measurements. Data are procured from the closest MO and corrections effected. But it has two roadblocks: (i) the data may not be available immediately, and (ii) the surveyed area may not be in the vicinity of observatory. **(2) Repeat observations:** Repeated observations at the same point during the course of the day can check for constancy of magnetic intensity. Any inconsistency in the readings will give out magnetic variation for the day. However, the daily variation curves show readings at an interval of even 2 hr can miss details of the daily variation of as large as 10 nT. Therefore, this method is inadequate, wherein a precision of a few nT is desired. **(3) Continuous recording:** In this method, an auxiliary base instrument is used, which records continuous curve of the daily variation at the base station. This curve is used for corrections, which is considered safe to effect corrections in field station curves within a perimeter of 80 km.

(ii) Normal corrections: This correction is made to remove normal variation of magnetic intensity over the Earth's surface. The magnetic field is determined from magnetic charts, since it cannot be represented mathematically in terms of the geographical coordinates; its direction, distance, and absolute value are also not normally known at the base. The corrections are made by drawing contours of normal variations at a convenient interval of 10 nT. For example, the N-S and E-W gradient can be evaluated from the isomagnetic maps published at five-year intervals by the world data centre. Knowledge of the NS and EW distance of the field station from primary base helps remove the normal variation (with proper sign) from the observed data. For example, for Indian latitudes, say ~20°N, the normal field gradient of the order of 5 to 6 nT/km along NS and ~1 nT/km along EW direction exists for 1985 epoch.

IGRF coefficients of a fixed epoch are used to calculate the response of main field at each observation point (IGRF-F). For quantifying period of external field variations of the survey area, data recorded at a nearby magnetic observatory are used. In Table 6.1, values of H and Z represent digitized data from magnetograms corresponding to the date and time of the recording done at field, while the ext.H and ext.Z represent horizontal and vertical magnetic field components, obtained by adding the baseline values after multiplying H and Z with their scale values. The baseline and scale values are supplied by the observatories along with the magnetograms. Ext.F is obtained by squaring and adding ext.H and ext.Z and taking the square root. The value of ext.F thus obtained is summed with IGRF value and deducted from the observed total field value to gain the final anomaly (final-F), which is further plotted against location co-ordinates. The total field anomaly map (F) thus prepared for different basins is shown in Figs 6.19, 6.20, 6.23 and 6.28 for Cambay, Mahanadi, Krishna-Godavari, and Cauvery basins, respectively.

IV. Transformation and Interpretation of Magnetic Anomalies

The varying amplitudes and wavelengths of the total field come from magnetic sources at different depths. To know certain characteristics of sources, anomaly maps are subjected to various transformations. Transformation and filtering allow certain attributes of the data to be enhanced such as the effects due to magnetic sources at shallow or deeper levels or those occurring along a specified strike direction. To resolve shallow sources, downward continuation and second vertical derivative transformations are done. Upward continuation and horizontal gradient of pseudogravity (HGPG) transformations are performed to isolate deeper sources. **(i) Magnetic field analytical continuation:** The continuation techniques transform mathematically the magnetic anomalies on to a plane either above or below the plane of observation. In the upward continuation, i.e. to a plane above the level of observation, the regional features are preserved at the cost of shallow sources and in the downward continuation, i.e. to a level below the level of observations, the shallower sources are enhanced and regionals suppressed. **(ii) Derivative technique:** In the magnetic data processing, derivative is generally used to denote the first or higher vertical derivatives of magnetic anomalies. These are used to enhance the anomalies of shallower sources. When the influence of overlapping sources or regional features is predominant, derivatives help to resolve the shallower sources better than the original field. Computation of even second, fourth, sixth derivatives, etc. is much easier in the space domain than the odd derivatives. Several procedures are in vogue now for the preparation of second derivative maps. **(iii) Reduction to the pole:** The magnetic anomaly observed over a particular source is dependent on its location and orientation. Usually, the magnetic anomalies constitute a pair of negative and positive peaks located on either side of the source. Instead of dipolar anomalies, a technique known as 'reduction to pole' centres the anomalies over the respective sources (Fig. 6.8f). This procedure does not create any confusion with respect to dipolar anomalies. Reduction to pole maps are generally used for quantitative interpretation, and for direct comparison of gravity and magnetic maps. **(iv) Apparent susceptibility mapping:** This is a data processing technique that converts a total field magnetic map to an apparent susceptibility map. This method involves such operations as downward continuation and reduction to pole; all conducted in the frequency domain. It has advantages such as overlapping of anomalies being reduced, areas of uniform susceptibility appear relatively flat, and level differences appear between units with different magnetic properties and contacts between rock types, are demarcated clearly. The application of the various techniques is discussed below.

1. Cambay basin: The anomaly trend is controlled by faults within the basin (Fig. 6.19) and outside on the NE; it depicts the Aravalli trend. The anomaly map also shows margin faults, ENE-WSW trending NSL, major faults and geological features. Also the expected residual gravity values are higher inside than outside the basin, while magnetic anomalies are low over the graben.

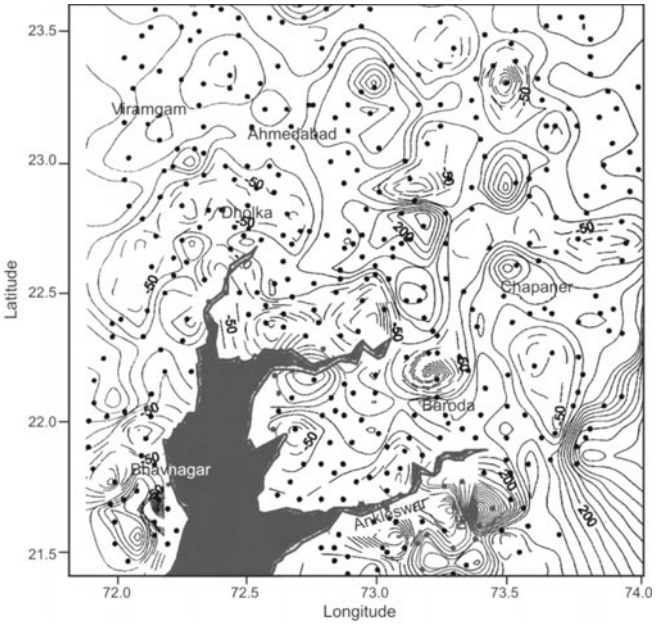

Figure 6.19. The ground magnetic data collected at ~5 km over petroliferrous Cambay basin. Data are used to prepare its total field anomaly map. Note the correlation between magnetic anomalies and tectonic structures in its basin evolution. Regions of high heat flow reveal negative magnetic anomalies and positive gravity anomalies indicating a thin crust beneath them.

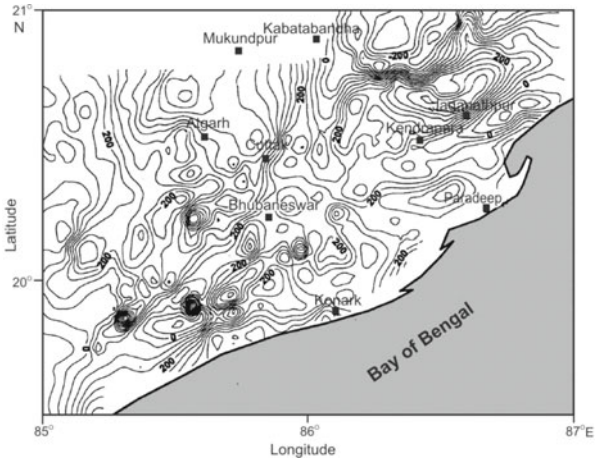

Figure 6.20. The correlation between total field anomalies and tectonic structures in the Mahanadi basin. Contour interval is 40 nT (Anand et al., 2002).

This is in line with the satellite gravity and magnetic anomaly interpretation of their inverse correspondence depicting high heat flow, resulting into this proven petroliferous basin.

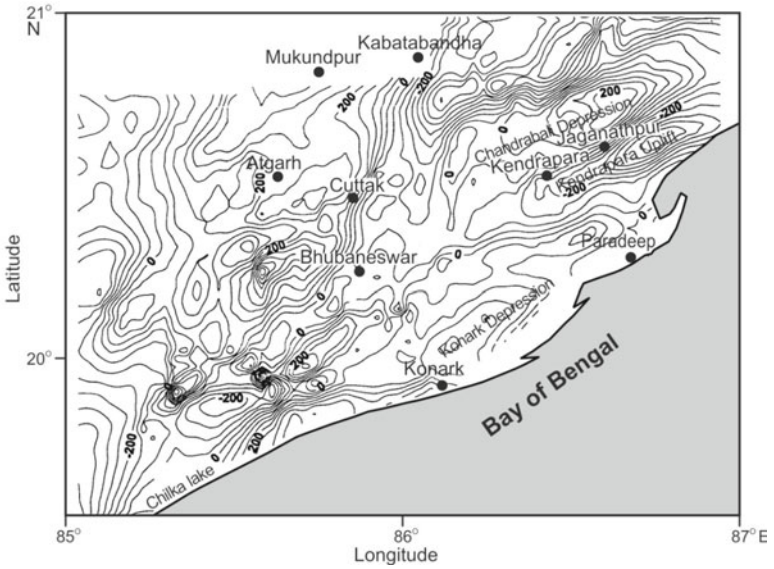

Figure 6.21. Second vertical derivative map of Mahanadi basin showing NE-SW to E-W trends associated with shallow features. Contour interval is of 50 nT/sq km (Anand et al., 2002).

2. Mahanadi basin: Ground magnetic surveys were conducted at 5 km interval over Mahanadi basin covering an area of 21,000 sq km. The total field anomaly map (Fig. 6.20) shows a combination of NE-SW, E-W and NW-SE trends.

Second vertical derivative map (Fig. 6.21) has enhanced the shallow NE-SW to ENE-WSW source trends, which are in conformity with eastern ghats rock exposures on the western side as well as the trend of the ridges and depressions within the basin. The thick band contours running NE-SW from north of Chilka lake to south of Kabatabandha, are the basin margin fault, which limits the basin to the west. This fault was not delineated by gravity studies. A geological contact is found further west.

The anomaly map continued to 10 km above msl reveals deeper features having NW-SE trends (Fig. 6.22). The observed NE-SW and E-W trends in second vertical derivative and downward continuation are related to shallow ridges and depressions of the coastal basin. However, the deeper features evidenced from upward continuation show NW-SE trends (Fig. 6.22), possibly associated with extension of Mahanadi graben under the coastal basin. The shallow trends of NE-SW to E-W seem to be superposed on deeper NW-SE ones formed prior to the breakup of Gondwanaland. Thus, this delta has two structural units, wherein the shallower one is associated with breakup of Gondwanaland and the deeper with formation of intracratonic Mahanadi graben.

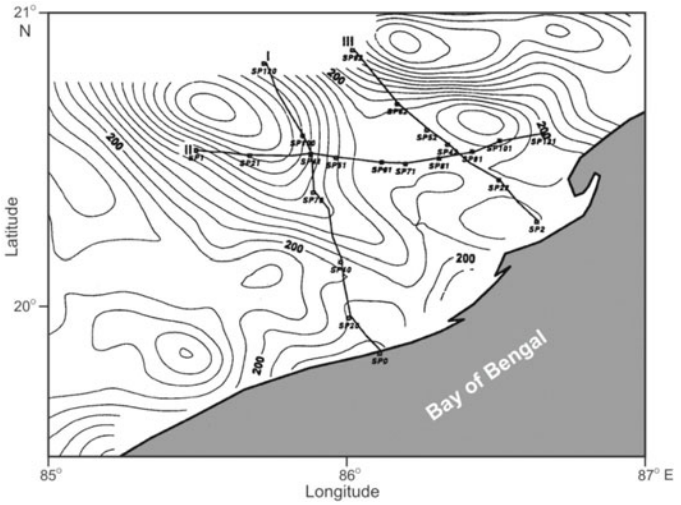

Figure 6.22. Anomaly map of Mahanadi basin continued upward to 10 km above msl, showing NW-SE trend of the deeper features. Locations of I, II and III are DSS profiles (Anand et al., 2002).

3. Krishna-Godavari basin: The prominent trends (Fig. 6.23) are in the NE-SW direction in accordance with subsurface ridges and depressions in this basin. The elongated negative anomaly initially runs NE-SW and later turns ENE-WSW aligning with Baptala, Tanuku and Kaza ridges. Some secondary NW-SE trends are terminated at the NE-SW ends. One such trend passes right on to the south of Rajamundry (RAJ) forming the eastern boundary fault of Chintalapudi sub-basin.

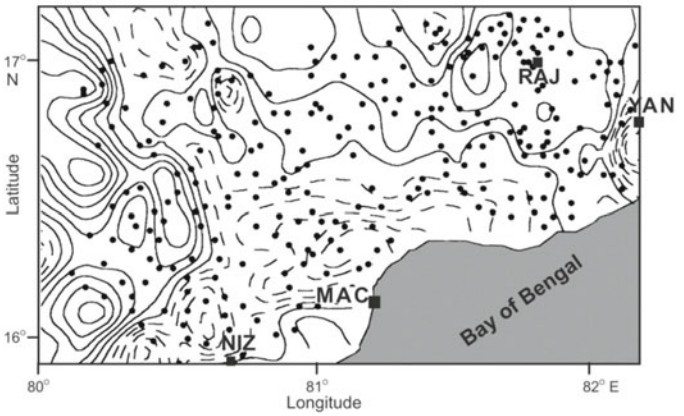

Figure 6.23. Map of total field anomaly over Krishna-Godavari basin prepared from the ground data. Data are interpreted in terms of its basement configuration and estimating the total thickness of sediments. Solid lines represent highs and dashed lines low. Contour interval 40 nT. NIZ: Nizamapatnam, MAC: Macchlipatnam, RAJ: Rajamundry (Rajaram et al., 2000).

Similarly, in the NW portion of the map, another NW-SE trend is found to match with Chintalapudi cross (CCS) trend. Several close anomalies south of CCS are associated with eastern ghats and charnockites.

West of Rajamundry (Fig. 6.23), the closed anomaly pattern is due to the basaltic exposures. The coastal basin has lower values, whereas the Archaean exposures of eastern ghats have relatively higher values. Like Mahanadi, NE-SW trends in KG basin are shallower and superposed on deeper N-S trends related to extension of Godavari graben.

The second vertical derivative map (Fig. 6.24) shows a combination of N-S, NNE-SSW and NE-SW trends. Towards the western side, trends of N-S to NNE-SSW are seen; the N-S to NNE-SSW trend is associated with eastern ghats and NE-SW trends reflect the KG basin. The ridges and depressions cannot be distinctly demarcated probably due to a large station spacing of ~10 km in comparison with the width of the structures.

Figure 6.25 shows the anomaly map continued down to 2 km from msl, which shows a combination of NE-SW and N-S/NNE-SSW shallow trends associated with coastal basin and eastern ghats, respectively.

Figure 6.26 presents 6 km upward continuation from msl. As the level of continuation increases, the NW-SE trends become more prominent. The most conspicuous feature of this map is the appearance of several NW-SE trends at the expense of dominant NE-SW trends, implying limited extent of KG basin, while sources related to NW-SE trends are at larger depth.

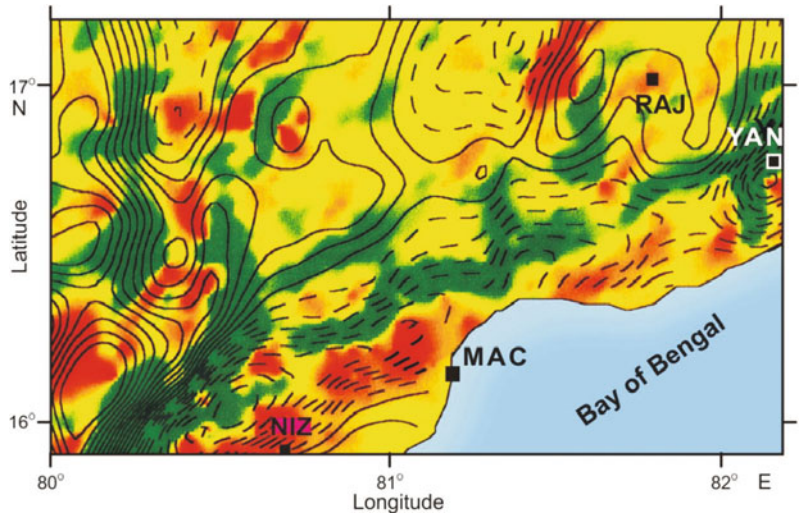

Figure 6.24. Second vertical derivative anomaly map of the ground total magnetic field superposed on the shaded relief map of the Krishna-Godavari basin to isolate the NE-SW trends (red depicts maximum reflectance decreasing to green). Contour interval is of 30 nT; solid lines represent high values and dashed lines low values (Rajaram et al., 2000).

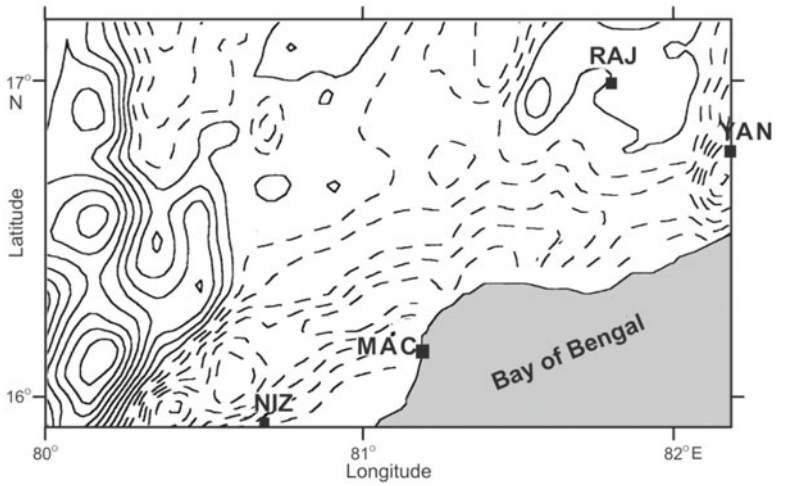

Figure 6.25. Anomaly map of the Krishna-Godavari basin continued downward to 2 km. Contour interval 200 nT (Rajaram et al., 2000).

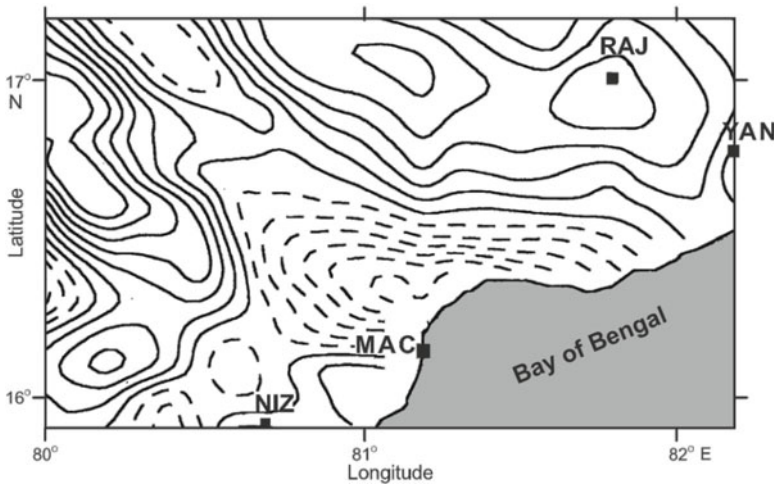

Figure 6.26. Anomaly map of Krishna-Godavari basin continued upward to 6 km. Contour interval 10 nT (Rajaram et al., 2000).

The total field magnetic anomaly is converted into gravity anomaly by replacing magnetization distributions with identical density distributions. This is the pseudogravity anomaly and is measured in pseudo mgal. The steepest horizontal gradient of gravity anomaly or of a pseudogravity anomaly caused by a tabular body tends to overlie the edge of the body. It amplifies the long wavelength components. This characteristic of pseudogravity anomalies is used to locate abrupt lateral changes in magnetization. The horizontal gradient tends to have a maxima located over the edges of pseudogravity sources, hence

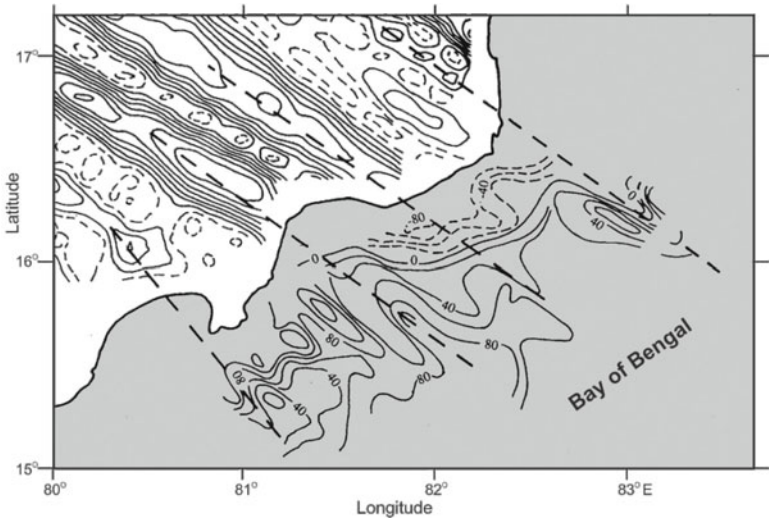

Figure 6.27. Composite HGPG map of ground F data (contour interval 0.5 mgal; solid lines represent highs and dashed lines low; all the values are positive) and the marine magnetic total field anomaly map over the KG basin and its offshore region. The continuation of the NW-SE trends into the offshore is marked on the figure as dashed lines (Rajaram et al., 2000).

horizontal gradient pseudogravity (HGPG) transformation is carried out. The composite HGPG anomaly map of ground data and the marine magnetic anomalies (Fig. 6.27) shows clear and direct continuation of onshore NW-SE trends.

The magnetic data reveal deeper features associated with Dharwar and Bastar cratons prior to the rifting of India from Gondwanaland. The superposed horst and graben structures are formed as a result of rifting and drifting of India from Gondwanaland. The deeper features and horst/graben structures belong to two different tectonic events. NE-SW trends associated with the coastal basin and N-S to NNE-SSW trends of the eastern ghats indicate shallower sources.

4. Cauvery basin: NW-SE anomalies are seen to dominate within the Cauvery basin (Fig. 6.28), which are constrained within the eastern ghats folding. Anomaly trends also show mixed high NW-SE, NE-SW and E-W anomalies over the charnockites. Regions of marine transgression also depict high anomalies. Interestingly, the Ariyalur-Pondicherry (AP) depression is associated with a NE-SW high on ground and aeromagnetic anomaly maps, while the gravity anomaly map shows a low over this depression. The gravity low is due to large sediment thickness of ~5 km, while the magnetic high is due to charnockite basement. The high associated with the AP depression extends offshore in NE-SW direction right up to the ocean-continent boundary.

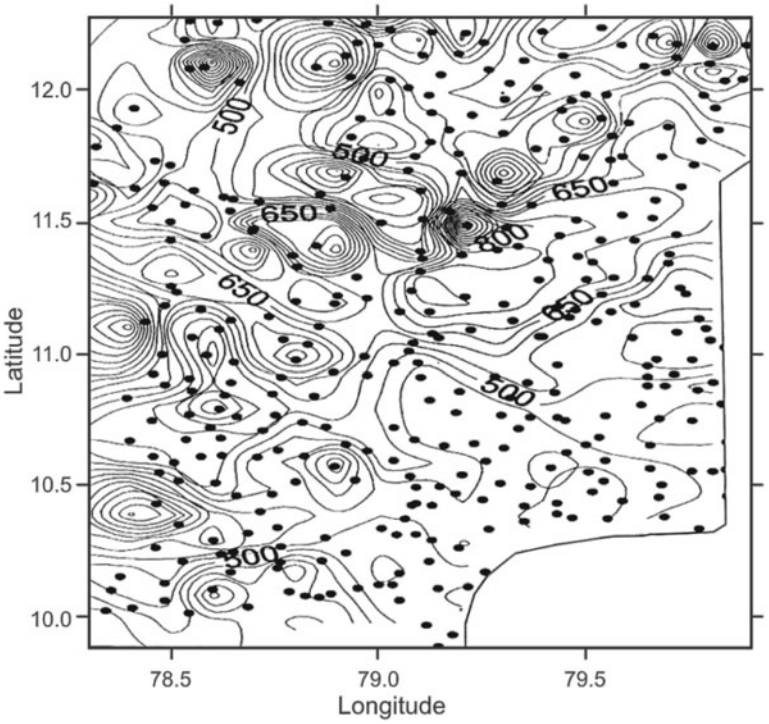

Figure 6.28. Total field anomaly map of the Cauvery basin. The anomaly trends are used to understand the influence of eastern ghat orogeny on its basin evolution and characteristics of ocean-continent boundary.

6.7 ELECTROMAGNETIC (EM) INDUCTION METHODS

Subsurface images of the electrical conductivity can be gained from two methods. The first is electrical technique, in which a constant electrical current is applied to the Earth. The second is EM induction, in which electrical currents are induced to flow in the Earth by a time varying external field. GeoEM induction maps the Earth's surface through to the mantle, where it delineates conductivity structures to improve upon the prevalent understanding of tectonic processes. These studies are carried out on local and regional scale of a few km to hundreds of km to get both lateral and depth extensions of the conductor. Local scale studies include active fault zones or volcanoes, while regional studies include investigations of subduction zones, orogenic belts, seafloor measurements, and mantle hot spots. EM induction studies are used to construct models of electrical conductivity variation in 1D, 2D or 3Ds.

EM induction methods are broadly categorized by the type of source field. If the source of the externally varying field is sufficiently distant from the location of measurement, the source is approximately plane wave, and is said to be 1D (varying in only one direction). On the other hand, if the source and

measurement are close, then it is 3D (varying in all spatial dimensions). This latter category can be further subdivided into techniques, (i) that use a continuously varying controlled source field, usually in the form of a sine wave, known as frequency domain EM, and (ii) those that require a source that abruptly switches on and off as a square wave, known as time domain EM or transient EM induction. Deep Earth conductivity is being traditionally demarcated either by geomagnetic depth sounding (GDS), or magnetotelluric (MT) methods. These two methods do not have any measurement limit, since they use the dynamic part of EMF temporal variations, unlike the static magnetic anomalies that can probe only up to Curie isotherm (~20 to 40 km). The data generated through these methods extend the existing knowledge on conductivity patterns, useful in inferring temperature, structural and compositional variations from the crust down to the lower mantle (~1500 km).

In gravity or magnetic fields, the anomalies are small perturbations over the normal field, but in transient variations they can be greater than the normal part by a few orders of magnitude. The causative process is the large electrical conductivity contrast of 13 orders of magnitude (e.g. dry crystalline rocks have conductivities $<10^{-6}$ S/m, while ores have conductivities exceeding 10^{6} S/m). Electrical conductivity is a sensitive parameter for saline fluids, carbon grain-boundary films, conducting minerals, high heat flow and partial melts (molten rocks or aqueous solutions). This parameter is extensively used in GDS, OBM and MT for mapping geoelectrical structures.

6.8 BASIC METHOD OF EM INDUCTION

A time-varying magnetic field induces currents in a neighbouring conducting medium in accordance with Faraday's law. An oscillating externally magnetic field of the wave generates electric currents in the Earth through EM induction, and the signal propagation becomes diffusive, resulting in signal attenuation with depth (skin depth). The induction process is governed by Maxwell's equations (Appendix 6.1). The factors that control the strength of induced currents are: conductivity distribution of the Earth's interior, and variation in time and space of the external field.

I. Earth's Natural EM Field

The source of natural currents flowing inside the Earth is definitely located outside of it. Periodic and transient EMF fluctuations are correlated with time varying solar emissions, which have a great influence on the ionospheric currents. The telluric currents are thought to be induced in the Earth by currents flowing partly in ionosphere and magnetosphere.

The currents are produced through complex interaction of EM radiation and particle flux radiated from the Sun with the EMF. The incoming EM radiation interacts with gases in the upper atmosphere producing distinct ionized layers at 40 to 400 km. These layers move across the EMF due to thermal

gravitational action of the Sun producing varying currents in the ionosphere. These variations depend on the Earth's position with respect to the Sun, hence have a periodicity of 24 hrs, which is the periodicity of Earth's rotation. The currents in the magnetosphere are due to complex interaction of solar wind, interplanetary field and EMF. These currents are situated around $4R_E$ to 10 R_E (Chapter 3). Below a frequency of 1 Hz, most of the signals originate in the magnetosphere as periodic external fields including magnetic storms, substorms and micropulsations. These signals are normally incident on the Earth's surface. Above a frequency of 1 Hz, the majority of EM signals flash out through lightning activity.

The inductive mechanism is an EM field propagated between the ionosphere and the Earth surface somewhat in the manner of a guided wave between parallel conducting plates. That is to say, it proceeds by bouncing back and forth between these boundaries, and hence has a large vertical component. At large distances from the source, this is a plane wave of variable frequency (10^{-5} Hz to audio range). Obviously, these MT fields can penetrate the Earth's surface to produce the telluric currents.

II. Principle of EM Method and Relations between Primary and Secondary Fields

If an EM field is produced on Earth's surface, currents flow in the subsurface conductors in accordance with EM induction laws. The natural electric field associated with these currents inside the Earth is of the order 10 mV/km. The 'primary' currents in the induction process are electric currents, which flow external to the Earth and change with time. As the solid Earth conducts electricity, 'secondary' currents (which are out-of-phase and of same frequencies with the primary current) are induced. In general, the resultant field recorded at the Earth's surface differs from the primary field in intensity, phase and direction, revealing the presence of subsurface conductors. In many instances, the primary fields are uniform and spatially uncorrelated from one induction event to the next; but the spatial patterns occurring systematically reflect spatial patterns in the secondary fields due to conductivity structures.

III. Determination of Nature of Conductivity (High/Low) of EM Anomalies

The EM field shifts in phase on encountering a relatively good conductor. In fact, the conductor becomes the source of a secondary field, which differs in phase from the primary field, while having the same frequency. In commonly used EM field method, the in-phase and out-of-phase components are measured. If the secondary field is 90° out-of-phase with the primary field, the subsurface conductor is a bad one. On the other hand, if the out-of-phase secondary field is 180° with the primary field, it is a very good conductor.

IV. EM Depth Sounding

It is used to study the variation of conductivity with depth. EM depth soundings are carried out either by change of frequency or change of transmitter to receiver (T-R) separation. Measurements may be in frequency or time domain. The sounding depth of any EM method depends on the frequency (time period) contents of the induced fields, and subsurface conductivity (skin depth). The EM signal diffuses to a distance into the Earth, defined as the skin depth, δ, in metres by $\delta = 503/\sqrt{\sigma f}$, where σ is the conductivity (S/m) and f is the frequency (Hz). The skin depth is inversely related to the frequency, and thus high frequency signals probe the shallow subsurface, while low frequency fields penetrate a much wider induction space and depth into the Earth. Depth persistence of the conductor or conductive overburden can be resolved by the use of two frequencies.

If the anomalous conductor is indicated by more than one T-R separation, it is assumed that the conductor persists with depth. If the same anomalies are indicated on the adjoining traverses (y-direction), the body persists along the strike direction also.

V. Advantages of EM Sounding Method

The major advantage of EM induction methods of GDS, MT and OBM is that the frequency can be varied to obtain different profiles for different frequencies. Such EM profiles then help in locating the target more clearly. Another advantage is that it requires no ground contact, and can successfully be used in sandy areas. Also, EM soundings have operational convenience even in highly resistive surface areas, where DC resistivity surveys are not feasible. In noisy environments, active EM methods like transient EM, and controlled source EM can be a good choice, but the sounding depth of these methods is restricted to the first few metres, but in favourable conditions perhaps a few km. For the really deep targets, one can only rely on natural source MT.

VI. EM Data Interpretation

If the Earth had ideal spherical symmetry, and its properties (including electrical conductivity) varied with the depth only, the observational analysis for structure determination is straightforward and is termed 1D. But for a 2D situation, the conductivity varies with two spatial parameters such as depth and one horizontal direction; while in a 3D situation the conductivity may vary in all directions.

Developments in modelling of EM induction data are closely parallel to those in other subsurface geophysical imaging techniques such as seismology. The forward problem of EM induction involves solution of Maxwell's equations in the electrically conducting Earth, excited by appropriate external sources. Inverse modelling of EM data reverses this process, using data generally observed on the surface to image conductivity variations within the Earth. For natural source methods such as GDS and MT, the frequency-dependent response

of the Earth to large-scale sources is determined by statistical estimation of transfer functions (especially local ratios of field components) from EM time series data.

Initial inverse modelling efforts were focussed on 1D interpretation, wherein data from one site are inverted to obtain information about the local conductivity-depth profile. Later 2D inversion methods were developed for profiles of data across a dominant geoelectric strike. Finally, as more powerful computational resources became available, methods for full 3D inversions evolved.

6.9 GEOMAGNETIC DEPTH SOUNDING (GDS)

The technique of detecting inhomogeneities in the subsurface conductivity with GDS has its origin in the pioneering works of Schuster in 1908 and Chapman in 1919, which was a popular natural source EM method between 1950 and 1980. The book by Rokityansky in 1982 covers all aspects of the GDS, while a detailed account of theory is given by Weaver in 1994. With the advent of more powerful computing facilities, MT took over from GDS, which was then somewhat ignored.

6.10 METHODOLOGY, OBJECTIVES OF GDS TECHNIQUE

I. GDS Survey Instruments

These instruments are different from MT since they employ only the magnetic, and not the electric field to investigate subsurface electrical conductivity distribution through an array of three-component magnetometers. Magnetic observatories provide the requisite periodicity data to map depths running into hundreds of km. But, because of their poor distribution, only the smoother fields can be defined adequately. In GDS profiles or arrays, three-component Gough-Reitzel or fluxgate magnetometers are left in position for periods of one to several months, during which time they record geomagnetic variations such as storms, bays, pulsations and the normal daily variation. These variations contain the external and internal parts. By mapping the patterns of induced currents, and using suitable analysis of the magnetic variations, theoretical models of the subsurface electrical conductivity structure are inferred. GDS is also known by the term magnetovariational (MV) method, since it uses the ever changing magnetic variations.

II. Sounding the Earth Using Natural Geomagnetic Variations

A slowly varying magnetic field inside a uniform conductor (conductivity σ and relative magnetic permeability μ) satisfies the induction equation: $\nabla^2 E = \mu\mu_0\sigma\delta B/\delta t$, the time varying field induces eddy currents in the conductor,

which flow so as to exclude the field from the deeper parts. The amplitude of a spatially uniform field of frequency ω falls to 1/*e* of the surface value at the 'skin depth': $Z_0 = (2/\omega\mu\mu_0\sigma)^{1/2}$. This expression provides a rough guide to the 'sounding depth', which might be expected of a particular frequency. The basis of sounding method is to measure the Earth response at a range of frequencies and/or source wavelengths.

6.11 ACQUISITION, ANALYSIS AND PRESENTATION OF GDS DATA

I. GDS Data Acquisition

The method involves collecting simultaneous records of N-S (X), E-W (Y), and vertical (Z) components of naturally time-varying geomagnetic field from a 2D array of magnetometers deployed in a regular grid pattern. The observed variations over the surface of the Earth have contributions from external currents as well as from induced currents. Over an infinitely conducting horizontally layered surface, the field due to spatially uniform external varying field and its induced counterpart interact with each other in such a way that they nullify the vertical component Z and enhance the horizontal components H or D of the observed field to an extent that it becomes twice the value due to external field only. Under this condition, if one observes Z over the surface of the Earth, it can be indicative of lateral heterogeneities of conductivity near the observation site.

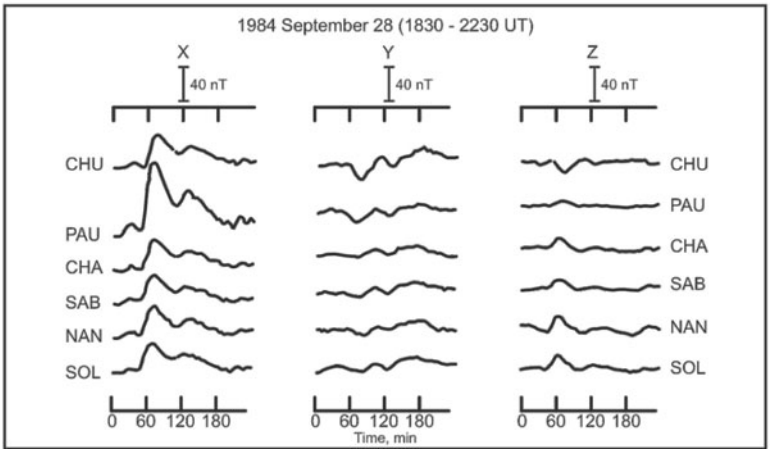

Figure 6.29. Stacked profile of substorm recorded on 28 September 1984 at some of the lesser Himalayas array stations. Note a marked enhancement of X and highly suppressed Z variation at PAU. But the two stations on its two sides show opposite Z variations, indicating the presence of a conducting zone beneath PAU.

II. Stack Plots

In the first instance, a sample stack plot of variations in the three components of the field is prepared by taking data recorded through an array of magnetometers from a disturbed period. An example of such a plot is given in Fig. 6.29 taken from array records of 28 September 1984. A reversal in sign of Z is seen between CHU (Chaukutia) and CHA (Champawat). The conductor is located between these two stations underneath PAU (Pauri). Therefore, the observed features of associated X, Y and Z variations are used to locate subsurface conductive zones. However, the observed variation over a site is due to combined response of different subsurface conductive layers. To achieve the proper estimates of contribution of each layer to the observed phenomena, data processing techniques given in section 6.12 are used.

6.12 DATA PROCESSING TECHNIQUES

The determination of the vertical variation of conductivity has two steps: (1) measurement of the response or transfer function, which links the input (external part of the magnetic field) to the output (internal part created by induced currents), and (2) inversion of the response for the conductivity, detecting conductivity from the response and its associated errors. For arriving at proper estimates of dimension, conductivity, depth and direction (strike) of the causative body, one or more of the Fourier transform maps, transfer functions, Parkinson's vectors, etc. are used.

I. Fourier Transform Maps

GDS data gathered in time domain are converted to frequency domain to map fields at selected periods. The spectral peaks of amplitude and phase exhibit EM response of structures in a particular depth range. It thus enables to isolate the response of layers of interest, and study their behaviour separately over the array area.

II. Transfer Functions

Transfer functions are more quantitative and frequency dependent. For calculating transfer functions, five or more events of almost same duration and with different intensity and polarization are selected to arrive at Fourier transforms, after removing the linear trend. Tables 6.2a,b and Appendix 6.2 present the procedural steps followed in processing the raw data to compute transfer functions.

III. Parkinson's Induction Vectors

The first task in interpretation is to determine the spatial pattern of conductivity without actually modelling the response. If there are a number of irregularly

Table 6.2a Information from time series raw data

Event date	*Period range, sec*	*X-Variations, nT*	*Y-Variations, nT*	*Z-Variations, nT*
1 April 2004	1-512	(-30) – (20)	(15) – (-12)	(-10) – (20)
30 March 2005	1-512	(-40) – (40)	(25) – (-15)	(22) – (17)

Table 6.2b Data in frequency domain after determination of transfer functions

Period, sec	*A*	*B*	*C*	*D*
256	(0.868, -0.016)	(0.033, 0.015)	(0.100, 0.060)	(0.796, -0.097)
90	(0.891, 0.037)	(0.051, 0.024)	(0.159, 0.017)	(0.708, 0.039)
60	(0.911, 0.042)	(0.067, 0.018)	(0.163, -0.019)	(0.708, 0.039)
40	(0.928, 0.039)	(0.077, 0.001)	(0.145, -0.055)	(0.708, 0.039)
30	(0.937, 0.035)	(0.076, -0.016)	(0.121, -0.017)	(0.708, 0.039)

distributed magnetometers, then induction arrows are plotted. Parkinson showed in 1964 that geomagnetic variation in the amplitude of Z-component mainly depends on the direction of horizontal field. The Z-response is maxima for a particular direction of horizontal field. Near a conductivity contrast, Parkinson vectors always point towards the zone of high conductivity.

IV. Complex Demodulation

Variation of field component with time represents gross response from subsurface layers. Complex demodulation method was introduced by Banks in 1976, which combines the time and frequency domain analysis. It provides variation with time of both amplitude and phase of selected frequency for the time duration of the event. Additionally, this procedure provides an accurate method for estimating the transfer function from a single storm's stretch of data, which has different directions of polarization.

V. Hypothetical Event Analysis

This method was developed as an analytical tool in the absence of simultaneous records from recording stations over a surveyed area. For each station, an estimate of A and B is made, and then the analysis proceeds to estimate the Z-response for hypothetical uniform source fields for selected direction of polarization. Contour plots and pseudo-sections of anomalous vertical fields estimated from the hypothetical event analysis on transfer functions are essential to characterize the orientation and dimensionality of electrical conductive structures of the region.

VI. Thin Sheet Modelling and Island Effect

The electromagnetic induction effects due to highly conducting sedimentary basins, seawater of variable depth (continent-coast interface, island effect) are

solved by assuming that these conductivity anomalies are confined to a thin layer. In such cases, mathematical model used comprises an infinitesimally thin sheet of varying surface conductivity materials. It is known as thin sheet because thickness of this sheet is negligible as compared to the skin depth of underlying layer. This condition ensures that electrical properties of the materials in the thin sheet itself are electrically linked to substratum so that at the period of interest, horizontal electric field remains constant over the thin sheet.

A number of records are generally analyzed to cover wide range of frequency bands, and different polarizations of incident waves. Electromagnetic impedance of ratio of vertical magnetic variation and most correlated horizontal component is estimated to gain transfer functions. The transfer functions are frequency dependent, and they provide induction arrows, and its variant hypothetical event analysis and Z/H pseudosections for various source field polarizations. All these data analyses methods are based on the fact that a time varying magnetic field tries to avoid a conductor.

6.13 GDS FIELD SURVEYS

Magnetic array studies provided valuable initial information on the conductivity structure of the crust and upper mantle all over the globe, especially in North

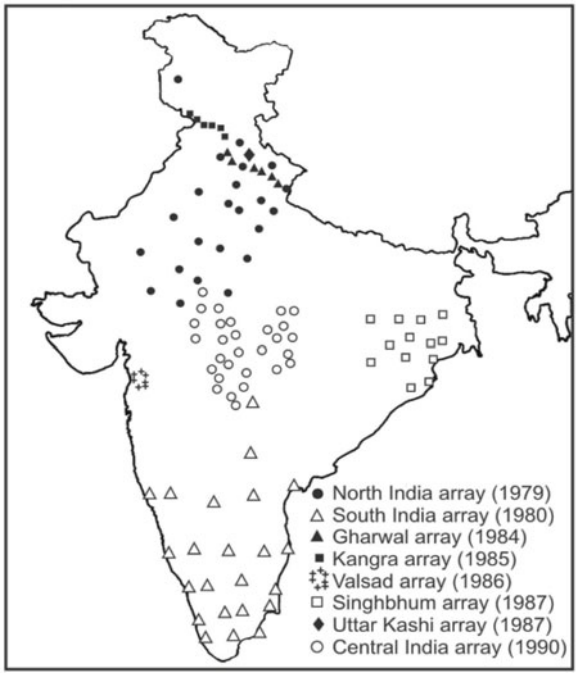

Figure 6.30. Location map of some arrays of magnetometer operated to understand the subsurface electrical conductivity of the Earth. The map shows where and over what periods these arrays operated.

America, Africa, Australia, and Europe. India, too, is not lagging behind in these studies. With the inception of two equatorial geomagnetic observatories at Annamalainagar and Trivandrum in the 1970s/1980s, an exciting era of induction studies was initiated. To account for anomalous behaviour in observed Z variations at these observatories, the phenomena of induced current perturbations was invoked. So, they were started in 1979 in India after which areas such as Garhwal, Kangra, Valsad, Singhbhum, Uttarkashi, central India and Ladakh-Leh regions were surveyed under different array campaigns. Figure 6.30 shows the station locations and some of the regions covered by these arrays.

6.14 MAGNETIC VARIATION MAPPING EXAMPLES

Large magnetometer arrays employed in different tectonic regimes imaged deeper structures of the crust and upper mantle. The observed conductivity anomalies have different causes and variable regional extents, which are presented below in the form of case studies.

I. Conductive Bodies below the Himalayas

A 'trans Himalayan conductor (THC)', running from the NE Indian shield to the foothills of the Himalaya was deciphered. The position of this conductor coincides with a localized high seismicity zone (Figs 6.32 and 6.58). This

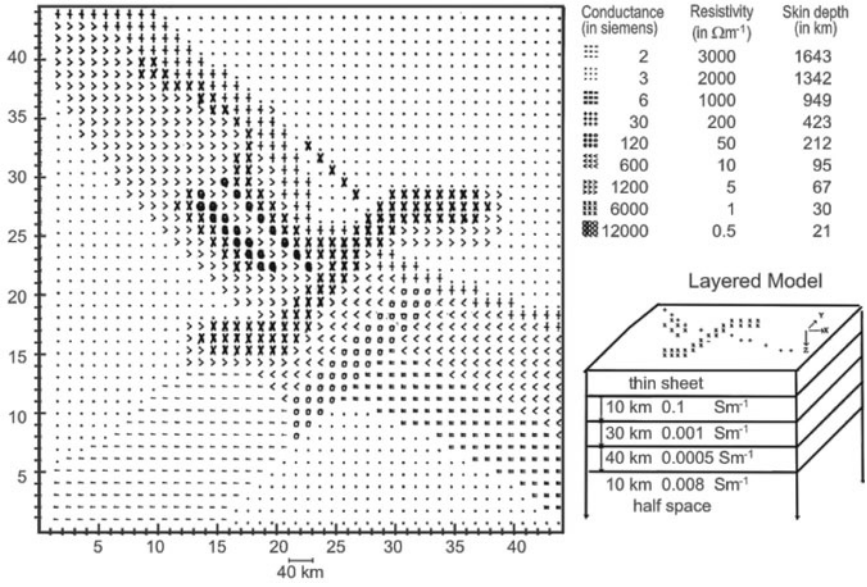

Figure 6.31. 3D view of the conductance map. The integral sign high conductance zone signifies eastward and westward extension of the THC. Also, note the furrowed type conducting zones paralleling the trend of Himalayan collision zone.

conductor is modelled as a 45 km wide, 85 km high protuberance from the asthenosphere into the lithosphere (Fig. 6.31). A resistivity of 2 ohm-m and background resistivity of 10^4 ohm-m were used in the modelling. Also, 'Garhwal Lesser Himalaya conductivity anomaly' was established along the Uttarkashi region (Figs 6.30-6.32). This mapped conductive zone in the epicentral track of 1991 Uttarkashi earthquake is viewed as a shallow but extended fracture zone above an obducted crustal block. Movement in the fracture zone to readjust compressive forces explains the correlation of this conductive zone with Garhwal Lesser Himalayan seismic belt and with recent Uttarkashi earthquake.

II. Conductance and Seismicity in Central and Western Parts of India

A plutonic body delineated near Valsad in south Gujarat is embedded in the upwarped asthenosphere along the western continental margin (Figs 6.32 and

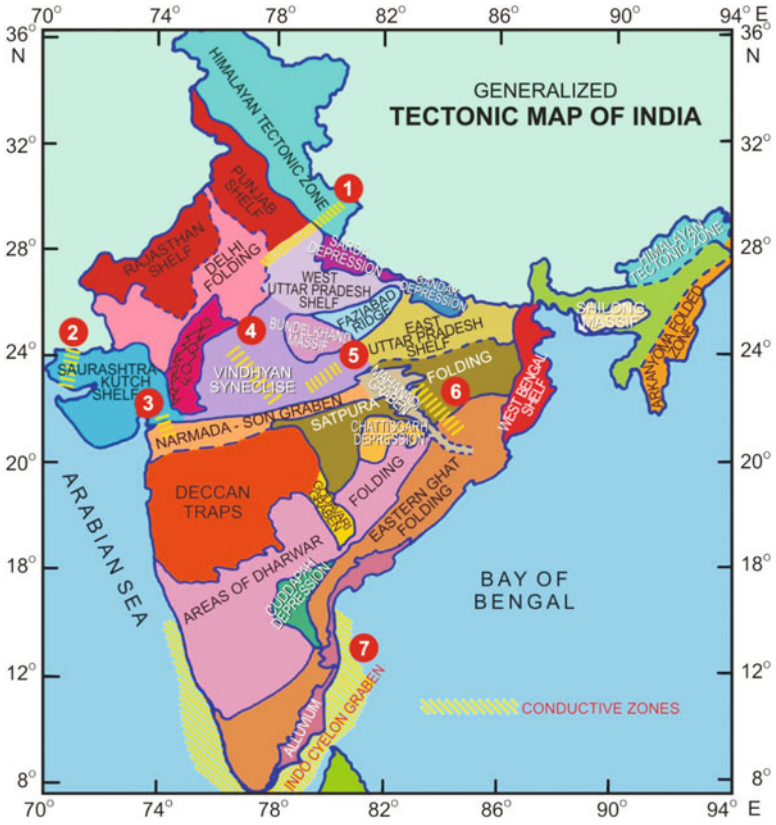

Figure 6.32. Generalized tectonic map of India and the different conductivity structures identified through GDS, MT and long-period MT probes. The numbers on the map are the following conductive structures: 1 - Trans Himalaya, 2 - Bhuj, 3 - Valsad, 4 & 5 - Central India, 6 - Singhbhum, 7 - South Indian offshore conductivity anomaly.

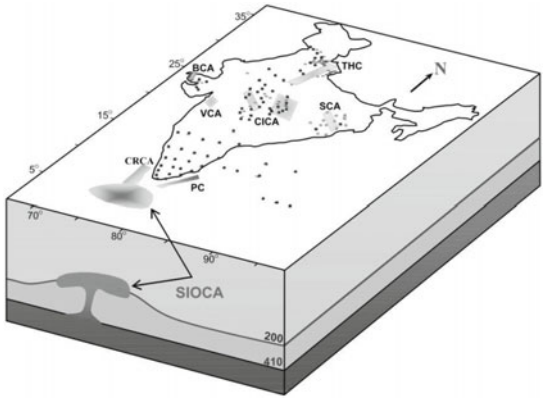

Figure 6.33. A composite map of different conductivity structures. THC - Trans Himalayan Conductor, BCA - Bhuj Conductivity Anomaly, VCA - Valsad Conductivity Anomaly, CICA - Central India Conductivity Anomaly, SCA - Singhbhum Conductivity Anomaly and PC - Palk-Strait Conductor. (Arora and Subba Rao, 2002).

6.33). This region has been experiencing earthquake swarms in recent years. Studies in seismically active Bhuj region point to the concentration of induced currents in thick sedimentary columns. The high conductance prevalent in western part of Kutch region, NW of Lodai is related to half graben formed due to the uplifted Wagad upland (Figs 6.32 and 6.33). An arcuate-shaped conductor at mid-crustal depth is also found beneath the Satpura ranges. This conductor coincides with Mandla gravity high. A geothermal anomaly is also observed in this area.

The Godavari graben is mapped up to the southern limit of NSL beyond which it is shrouded under the thick cover of Deccan traps (Figs 6.32 and 6.33). Electrical characteristics of the Bengal basin marginal fault and also the E-W trending conductor bordering the Singhbhum craton are well established (Figs 6.32 and 6.33). In Singhbhum region, a linear trend of conductivity anomaly extending in E-W direction is located to the north of Ranchi and Bokaro lying at greater depths. Its source is the Gondwana grabens of Damodar valley (Figs 6.32 and 6.33).

III. South Indian Offshore Conductivity Anomaly

The south Indian offshore conductivity anomaly (SIOCA) is associated with relics of the Marion plume outburst. The conductivity anomaly beneath Palk Strait is due to thermal interaction, when the Indian lithosphere passed over the Marion plume. However, the conductivity anomaly observed beneath Comorin ridge and a rift structure encountered along the west coast margin of India appear to be related to Reunion hotspot activity (Figs 6.32, 6.33 and 6.34).

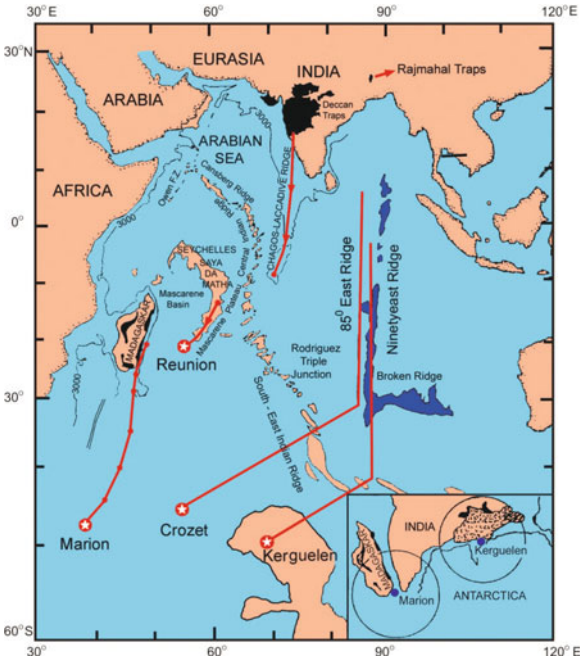

Figure 6.34. Locations of different hotspots (white stars) and volcanic ridges formed during the transit of the Indian plate over them. Inset: Areas affected by the outburst of Marion plume that led to the separation of Madagascar from India (Arora et al., 2003).

IV. Determining Electrical Conductivity from MO Data

The MOs spread over the globe collect time-series data of magnetic and electric fields. This data can be inverted to gain a profile of electrical conductivity with depth. For example, crustal conductors are modelled following finite difference and thin sheet approximation (3D modelling), providing important geoelectrical parameters of lithosphere. This MV data are important to study conductivity heterogeneities residing in the deep interior of 1000 km. Theoretical model on electrical conductivity structure of the upper mantle (~50 to 1200 km) is

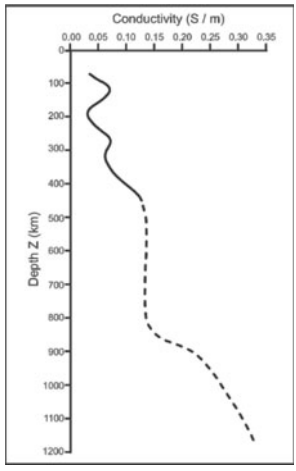

Figure 6.35. Conductivity distribution pattern with depth derived from continuous strings of geomagnetic field components recorded at Indo-Soviet chain of MOs (Chandrasekhar and Arora,1992).

developed using the continuous strings of geomagnetic field components recorded at Indo-Soviet chain of MOs. This model reveals alternate increase and decrease in the conductivity up to ~500 km from where it does not change up to ~900 km, beyond which a steady increase is seen (Fig. 6.35).

6.15 OCEAN BOTTOM MAGNETOMETER STUDIES

The ocean floor, with pressures of up to 600 atm (60 MPa), temperatures ~3°C and no possibility of radio contact with instrumentation, presents a particularly harsh environment for carrying out magnetic and electrical measurements. Furthermore, sea water is corrosive and a conductive fluid. However, with the availability of reliable underwater technology, electrical conductivity studies of the ocean bottom have now become a routine affair. This is done through ocean bottom magnetometers (OBMs), which are similar to GDS fluxgate units. They can enhance understanding the surface and subsurface structures of the ocean in conjunction with land-based geoelectrical studies. OBMs sit on the floor and measure the attenuation of magnetic field components between sea surface and seafloor. As magnetic field variations are difficult to measure on sea surface, nearest land station is taken as a reference station. OBM data are found to have increasing applications on seafloors to study mid-oceanic ridges, plate margins, subduction zones, hot spot trails and others.

6.16 OBM FIELD EXAMPLES

OBM arrays were set at Mariana trench back-arc spreading centre, Barren Island in Andaman Sea, 85° ridge, 90°E ridge in the Bay of Bengal, and off the coast of Cochin in the Arabian Sea. The latest trend in marine surveys is to gain improved depth resolution through MT methods using ocean bottom electrometers (OBE).

I. Conductivity (Resistivity) below Arabian Sea and Bay of Bengal

A long conductive structure aligned in a N-S direction at a depth of ~12 km below the Arabian seafloor was identified ~100 km off Cochin. The oceanic crust and upper mantle underlying the Bay of Bengal is more resistive than the crust and mantle below the Andaman arc region, because the Bay of Bengal crust is older than the Andaman arc region. The OBM results reiterated the subduction of Indian plate beneath the Burmese plate, providing a breakthrough for understanding mantle dynamics related to plate subduction (Fig. 6.36).

II. Barren Island Volcanism

Two different conductivity zones in depth ranges of 17-27 km and 80-100 km mapped beneath the Barren Island in Andaman Sea saw eruption of a volcano

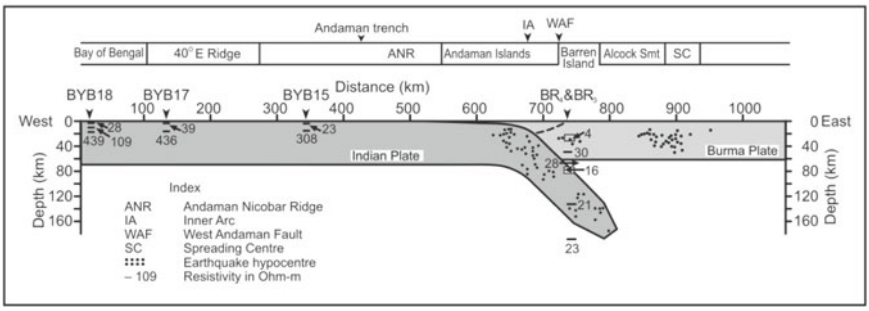

Figure 6.36. Map showing the subduction of Indian plate beneath the Burmese plate along with the resistivity values obtained from OBM array studies (Subba Rao et al., 2000).

in March 1991 (Fig. 6.36). Furthermore, the Andaman Sea experiment showed the spreading ridge significantly perturbs the regional current flow. A subsurface conductive channel is proposed between the mouth of the Irrawaddy River and Coco Island. No evidence of conductive plume or plug is noticed beneath the Narcondam or Barren Islands.

6.17 MAGNETOTELLURIC SURVEYS

Natural EM signals are used in magnetotellurics (MT) to image subsurface electrical structures. It is now routinely used in both commercial exploration and pure research. Its commercial applications include exploration for minerals, hydrocarbons and geothermal resources. Researchers use MT to study the continental subsurface structures and dynamics of plate boundaries. Most continents consist of Archaean cratons, which are enclosed by Proterozoic and Phanerozoic geotectonic belts and suture zones. Many of the old structures are covered today by huge sedimentary basins, whose position and structure can be unravelled through this method.

Excepting seismic method, greater depths of exploration are not attainable by other techniques. Hence, MT holds promise for deep exploration, forming an alternative to seismic in oil exploration and basement studies. Additionally, the method can be valuable for reconnaissance, especially in sedimentary areas, where highly insulating formations like salt, anhydrite and evaporite beds are involved. This is because the EM waves penetrate large depths, if the ground is highly insulating. Specifically, the Deccan volcanics provide an ideal geological setting for exploiting MT method. Here, the entire Precambrian formation is covered by Deccan basalts, and is thus not available for scrutiny through conventional geological methods. The basaltic cover forms a high velocity zone and a large number of reflections generated by these rocks make the seismic interpretation difficult. Hence, MT methods are useful in this terrain. Recently, the scope of MT studies has been extended to

map lithosphere-asthenosphere boundary by introducing long-period MT instruments called LMT measurements. These instruments measure very low frequencies ($1–10^{-4}$ Hz), and are used for imaging the lower crust and upper mantle.

Determination of Earth's conductivity by measuring the geomagnetic field and telluric currents was suggested by Taikhonov in USSR and Cagniard in France. Cagniard showed that if magnetic and electric fields comprising a plane EM wave travelling into Earth are measured, the resistivity of the Earth can be computed. Later on, considerable studies were carried out by Vanyan and other Soviet investigators regarding depth soundings by natural and artificially induced electromagnetic fields. Keller furnished English translation of these papers in 1967 which also gives an interesting historic account of the developments in this field.

6.18 METHODOLOGY, DATA ACQUISITION AND TIME SERIES PROCESSING

I. Basic Method of MT and Time Series Data Processing

MT method involves simultaneous measurement and analyses of five components of naturally existing EM fields of the Earth constituting two orthogonal electrical and three orthogonal magnetic fields. In this method, oscillations of the electrical and magnetic fields are recorded normally in two or three frequency bands in the range of 10^{-4} to 10 Hz. Though Earth's natural EM fields contain a wide spectrum of frequencies originating from different causes, frequencies <1 Hz originating from interaction between EMF and flow of plasma of the Sun (solar wind) are of interest to MT. Hence frequencies higher than a few Hz originating mainly due to sources of meteorological and man-made power lines are not considered.

II. MT Data Collection and Penetration Depth

An example of recorded time series (variation of field amplitude with time) of the five electrical and magnetic field components is shown in Fig. 6.37. The total recording for a MT sounding is ~5 to 7 hrs. MT time series data are processed to yield frequency domain estimates of apparent resistivity and phase. Modern processing schemes compute fast Fourier transform of subsections of the time series. In MT data collection, time series data are recorded simultaneously at several locations to allow for the removal of noise at the measurement location through the remote reference method.

In MT, the skin depth δ (km) for a period T (hrs) in a half-space of conductivity σ (S/m) is calculated using the same formula as given in GDS section, i.e. $\delta = \sim 30.2 \times (T/\sigma)^{1/2}$. The better the conduction and higher the frequency are, the smaller is the skin depth or penetration depth.

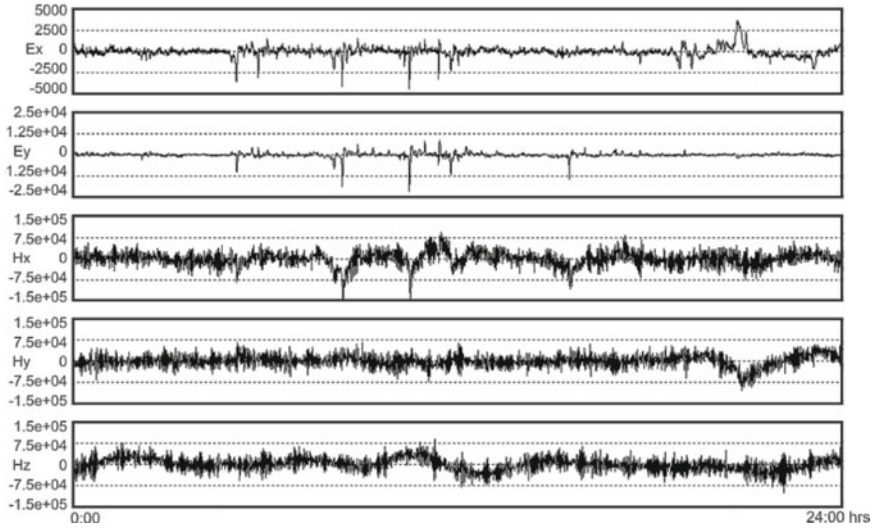

Figure 6.37. The measured time series of the five components (Ex, Ey, Hx, Hy and Hz) at a MT sounding site.

III. Instrumentation and Field Technique

MT soundings measure tangential components of both the electrical and magnetic fields on the ground surface so as to determine their ratio as a function of frequency. A typical field set-up of MT data acquisition is shown in Fig. 6.38 which basically consists of the following components: (i) two electric sensors that are normally two pairs of grounded non-polarizing electrodes connected to suitable amplifiers for measuring electric components Ex and Ey, (ii) three highly sensitive magnetic sensors for measuring the three magnetic components Hx, Hy, and Hz. The magnetic sensors are normally induction coil type or more recently super conductivity magnetometers (Chapter 4). Highly resistive fluxgate type magnetometers can also be utilized when low frequencies are of main interest, (iii) suitable post amplifier units for five field components, Ex, Ey, Hx, Hy and Hz, (iv) digital data acquisition system for recording and analyzing the data by computer, and (v) a five-channel analog strip chart record for monitoring the field data.

Presently, there is a clear tendency for a large number of recording instruments to operate simultaneously, and with much denser site spacing. Another development has taken place in 3D MT wherein instruments are distributed over an area or aligned in a grid instead of simply following profiles.

IV. Basic Theory

For developing the basic theory for MT method, an isotropic Earth of a plane surface and plane EM waves are assumed near the site of measurement. A homogeneous isotropic Earth has no real significance in exploration geophysics,

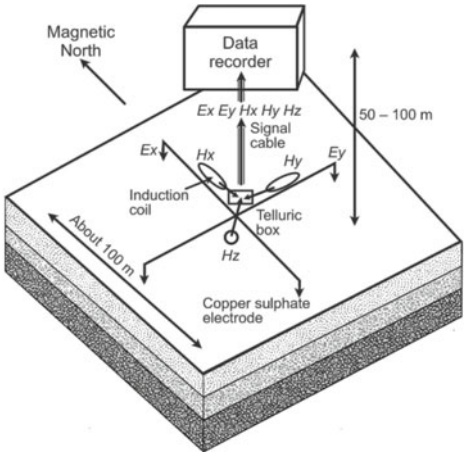

Figure 6.38. A pictorial representation of the field set-up for MT sounding. (http://science.jrank.org/article_images/science.jrank.org/ magnetotelluric-prospecting.1.jpg).

but the response of such a model can be utilized to define an apparent resistivity. Since the theory is concerned with EM fields, any material medium can be described by the three physical parameters, viz. electrical conductivity (σ), magnetic permeability (μ) and dielectric constant (ε). Starting from the Maxwell's EM equations (Appendix 6.1), it can be shown that impedance is a characteristic of the electric properties of the medium of propagation and the frequency of the EM field. The impedance is calculated by taking the ratio of the amplitudes of electric field and the associated orthogonal magnetic field (E_X/H_Y or E_Y/H_X) for a given frequency. The subscript X and Y denote the direction of the measurements. The frequency provides an extra dimension to the measured ratios, which permits deduction of the frequency variations of the apparent resistivity similar to that obtained at various electrode separations in DC resistivity method. By determining the impedance elements at various discrete frequencies, the conductivity of the Earth as a function of depth is obtained. Appendix 6.2 reports calculation of elements of a 2×2 impedance tensor Z.

In MT analysis, initially four impedance values of ZXX, ZXY, ZYX and ZYY are determined from the measured electrical and magnetic field components. In the case of a horizontally stratified Earth model, both ZXX and ZYY are equal to zero and ZXY = – ZYX. When a structure is present, such as fault, both ZXX and ZYY are nonzero. In this case the impedances in various directions are mathematically determined by rotating the coordinates of the measured impedances. When one of the rotation axes becomes parallel to the strike direction, the quantity Z'XX + Z'YY will become minimum, while the quantity Z'XY + Z'YX will become maximum (here Z'XX, etc. are the

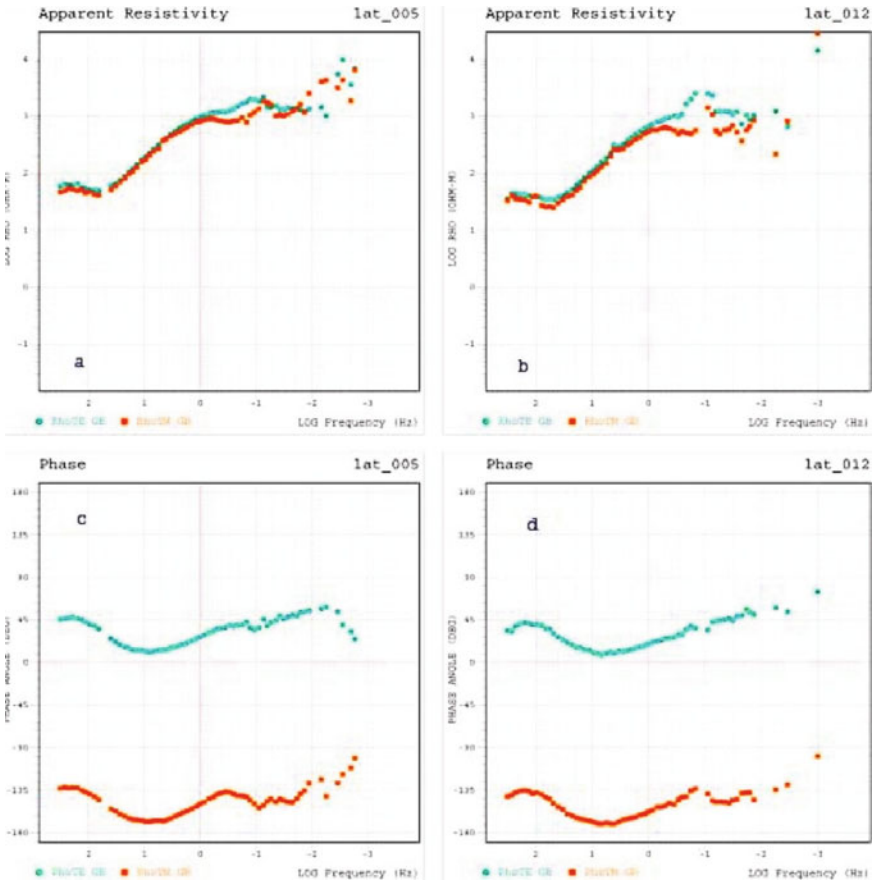

Figure 6.39a-d. An example of MT sounding curves of the apparent resistivity (and phase) vs. frequency.

rotated impedance values). This property of the tensor impedance is utilized to determine the values of Z'XY and Z'YX—known as principal impedances. One of the principal impedance elements is either parallel (transverse electric, TE or E-polarization) or perpendicular (transverse magnetic, TM or H-polarization) to the strike of the structure or formation. The rotated data, with respect to the strike direction, are used to calculate the apparent resistivities (ρ_a) in the principal directions, i.e. parallel and perpendicular to the strike from

$$\rho_a(T) = 0.2\ T\ |Z'|^2$$

where T is the time period and Z' is the subsurface impedance of the stratified Earth either in TE or TM mode. After calculating the apparent resistivities, the data are presented as MT sounding curves by plotting apparent resistivity values versus time period and apparent resistivity versus phase. Examples of frequency

versus resistivity, and frequency versus phase curves at a site in two different directions (both for raw and rotated data) are shown in Figs. 6.39a-d.

V. MT Data Interpretation

Based on various Earth response functions obtained from processed data like skew, tipper, induction arrows and polar diagrams, the data are analyzed for dimensionality (1D/2D/3D) and directionality of the subsurface conductors. Before modelling or inverting MT data, it is vital to understand its dimensionality. Tensor decomposition is a common approach and determines well the measured MT impedance data fit to a 2D geoelectric model and gives an estimate of the geoelectric strike direction. Once the dimensionality is understood, and distortion for static shifts addressed, MT can be forward modelled or inverted in 1D, 2D or 3D to recover a model of subsurface electrical conductivity. Thus, analysis of MT signals yields apparent resistivity, and phase as a function of frequency. The interpretation involves deducing subsurface geometry from quantitatively interpreting true resistivities, depths of geoelectric layers and postulating the possible geological structures. The basic technique of MT interpretation involves comparing field results with those obtained from computed models.

6.19 PRINCIPLE OF MT METHOD AND ITS UTILITY

The MT method involves a comparison of the amplitudes and phases of the electric and magnetic fields associated with the telluric currents. It can be shown that the surface electric and magnetic fields E and H respectively are horizontal and orthogonal. Their amplitudes are related by

$$\rho = 0.2\, T\, |E/H|^2$$

where ρ is in ohm-m, E in mV/km and H in nT. Their phases differ by $\pi/4$, H lagging behind E. If, then, E and H are measured at a definite frequency, the first indication of the non-homogeneity of the Earth is that the phase difference θ will not be $\pi/4$. Secondly, ρ calculated from measurements at different frequencies is the same. However, apparent resistivity ρ_a can always be defined by the above equation. On determining ρ_a and θ as functions of frequency by actual measurements, MT sounding curve analogous to electrical resistivity sounding curve is obtained.

GDS and MT are considered to be two complementary geophysical methods. The former has a better lateral (horizontal) resolution, while the latter has a better vertical resolution. For some years now, MT measurements have added substantial information to that gleaned from GDS observations. For example, MT soundings conducted along the foothills of Kumaon Himalayas have not only confirmed the presence of the trans-Himalayan conductor (Figs 6.32 and 6.33) postulated by GDS, but also provided support to earlier estimates

of its depth and lateral extent. The effectiveness of MT data to provide constraints on the tectonic configuration under study increases on synthesizing its information with gravity, seismic wave velocity and heat flow data.

While the theoretical aspects of MT method are dealt with exhaustively, there are scanty publications on practical applications from the subcontinent. Now however more and more scientists and organizations are planning to put this technique to enhance its practical use. Furthermore, efforts are on to compile all the available 'Indian' EM data generated so far to derive a comprehensive electrical conductance model to demarcate thermally favourable zones of hydrocarbon deposits and to provide a better insight into the seismic pattern of the region.

A few more EM induction methodologies are: (i) audio-frequency magnetic field (AFMAG) or audio-frequency MT (AMT) based on measurement of natural magnetic field originating in thunder storms at frequency 100–500 Hz. The method is said to be useful to explore large deep seated conductive zones, faults, shear zones, and water bearing fissures of appreciable extent and (ii) very low frequency EM method (VLFEM) which utilizes EM fields in the range 15–25 Hz radiated by powerful radio stations meant for military communications.

6.20 APPLICATIONS OF MT IN GEOPHYSICAL PROSPECTING

In geophysical prospecting, MT is used in a very large frequency range, which corresponds to a depth interval from the surface to some hundred kms. The aim of the exploration varies according to depth. The method is widely used in Russia, and has been developed further in USA, Canada, and Germany. In India, MT studies were initiated in 1984 with the procurement of a conventional band (4 to 4096 sec) MT system; presently the Indian geoscientists are working with three wide band (300 to 0.002 Hz) MT systems.

Analysis of the MT signals yields the apparent resistivities, phases and various other parameters as a function of frequency. These data are interpreted into a geoelectric section of the subsurface from which inferences are drawn regarding the geoelectrical structures. The main applications of the MT method are in the evaluation of large sedimentary basin and Earth deep interior. It is a complement and often as alternative to seismic method. The results presented here come from MT measurements made on various geological and tectonic settings, such as the Deccan traps, Vindhyan and Siwalik sedimentary regions, Precambrian crust of Rajasthan and Dharwar, the Himalayas, etc. These campaigns (Fig. 6.40) yielded some major findings, not amenable for studies with other techniques.

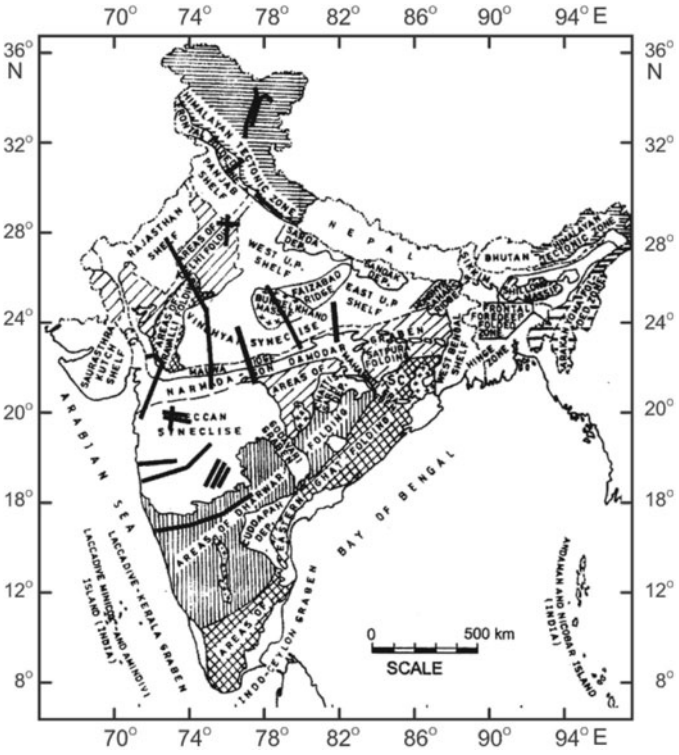

Figure 6.40. Geological map of India showing locations of the MT profiles over the period 1984-2003 (Gokarn, 2003).

I. Geoelectrical Structure below the Dharwar Craton

From studies on granite-greenstone formations over Dharwar craton, a shallow and deep sections (Figs 6.41 and 6.42) of the geoelectric structure are inferred that constitute a high resistive (2000 ohm-m) upper crust and a deep crustal conductor (DCC) between the depths of 5 and 25 km. Variations in Bouguer gravity are attributed to the undulations of DCC. From joint analysis of MT and seismic data, an anticline is delineated in the region of Closepet granite. However, the Closepet granite, which is assumed to be a major crustal divide, has only a weak signature in the geoelectric cross-section.

II. Electrical Conductivity Image from Seismic Regions of West and Central India

A conducting fluid filled ductile layer is identified in the depth range of 10 to 17 km in the earthquake-affected region of Bhuj. It is conjectured that this ductile layer prevented accumulation of stress within this section of crust, leading to earthquake hypocentres being concentrated either in the brittle upper crust above or in the lower crust below this conducting layer. Indications are obtained regarding the prevalence of compressional tectonics regime prior to

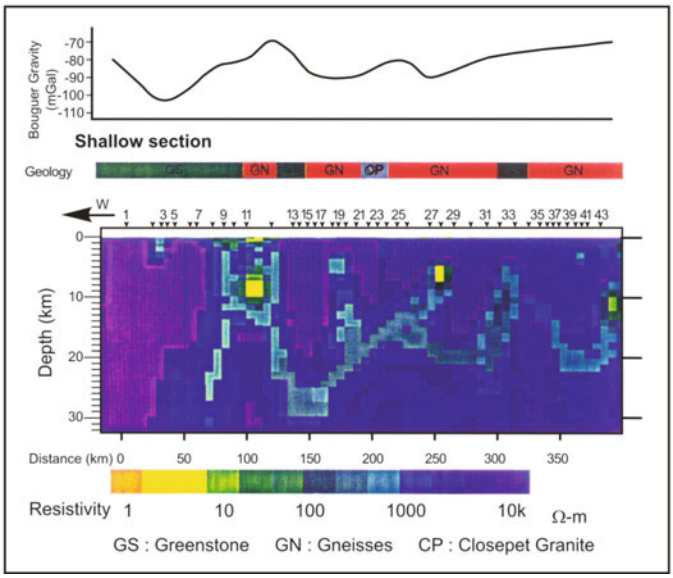

Figure 6.41. Shallow crustal structure in the Goa-Raichur region. Also shown are the Bouguer gravity variations along the MT sounding profile. The geology along the profile is also shown on the top of the crustal section (Gokarn, 2003).

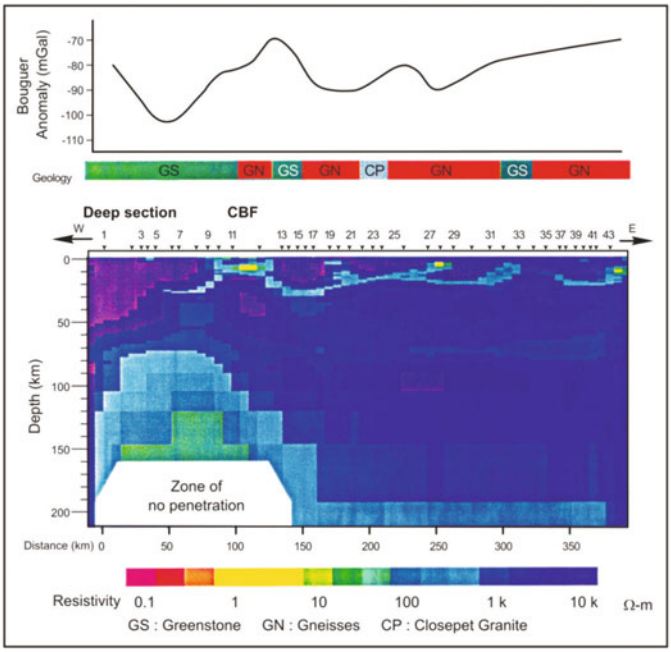

Figure 6.42. Deep section of the geoelectric model over the Goa-Raichur profile. The important geological units along the survey profile and the Bouguer gravity along the profile are shown on the top (Gokarn, 2003).

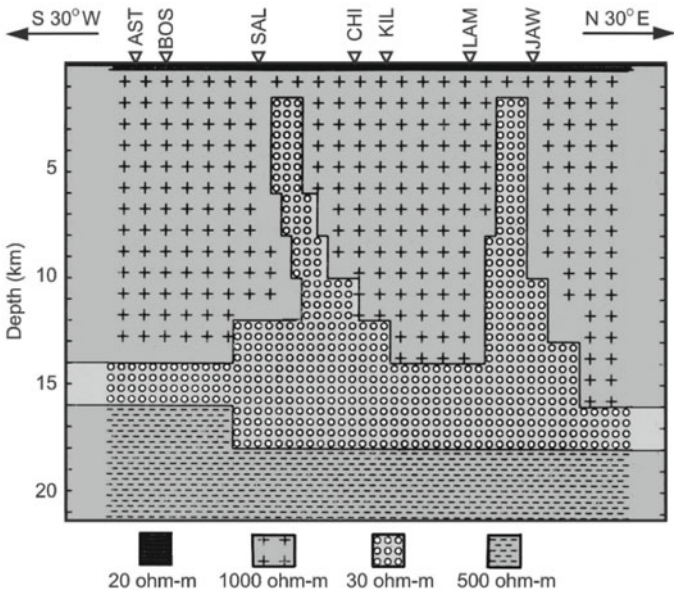

Figure 6.43. MT data were collected at seven stations along a linear profile of ~100 km across a part of Kurduvadi rift. 1D analysis revealed a four-layered conductive structure in the region surveyed. AST -Astha, BOS - Bosga, SAL- Salegaon, CHI - Chincholi, KIL - Killari, LAM - Lamjana and JAW - Jawli (Gokarn et al., 1992).

Deccan volcanism near Nasik, and conversely an extensional tectonic regime around Koyna. At Koyna, existence of a resistive block has been suggested in vicinity of the epicentre of the earthquake that rocked it in 1967. MT has also revealed a mid-crustal conductor across the Kurduvadi rift in Solapur region (Fig. 6.43) at a depth of 15 to 20 km at the Concord discontinuity, allowing interpreting the gravity low in this area to be not due to a rift-type structure but rather due to undulations in the crustal thickness. MT campaigns have delineated NW-SE trending high conductivity (100 ohm-m) structure at a depth of 60 km below the Panvel flexure (Fig. 6.44). This flexure extends to south and goes beneath the Dharwar craton and has been attributed to the passage of Indian plate over the Reunion hot spot (Fig. 6.34)

A lower crustal intrusive body that rises from below Jabalpur to shallow depths of ~2.4 km is dentified. This study is important in terms of understanding the cause of recent earthquake that occurred on 22 May 1997 with a magnitude of 6.0 on the Richter scale. The epicentre of this earthquake is located 20 km SE of Jabalpur. Furthermore, MT studies have yielded a strong lateral resistivity contrast (Fig. 6.45) near the great boundary fault along the Kota-Kekri profile and also similar formations in the Katangi-Jabalpur region separating the Precambrian upper and lower Vindhyan sediments on the north and the Deccan basalts on the south as well as other regions south of Mandla. A 10 km thick conductive layer of oceanic crust is also identified along a 400 km long profile in the NW Rajasthan shield area.

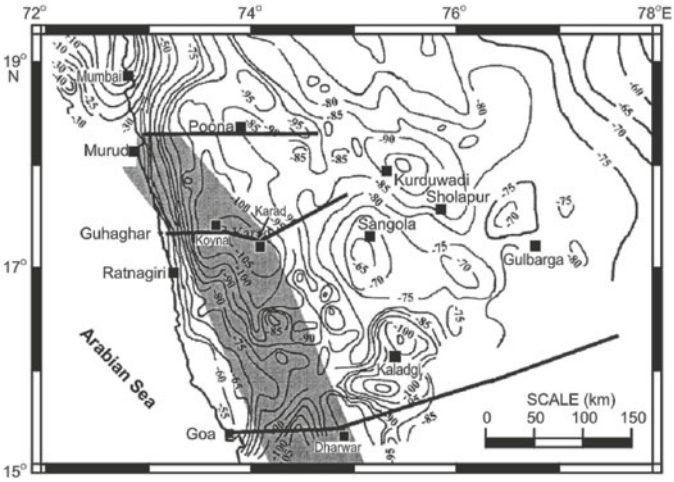

Figure 6.44. The Deccan trap volcanic region is experiencing mild to severe seismicity, necessitating its investigation at several closely-spaced sites in this region. The low resistivity feature in the lithospheric mantle is the shaded portion, superimposed over the Bouguer gravity map of the Deccan volcanic province and the northern part of the Dharwar craton.

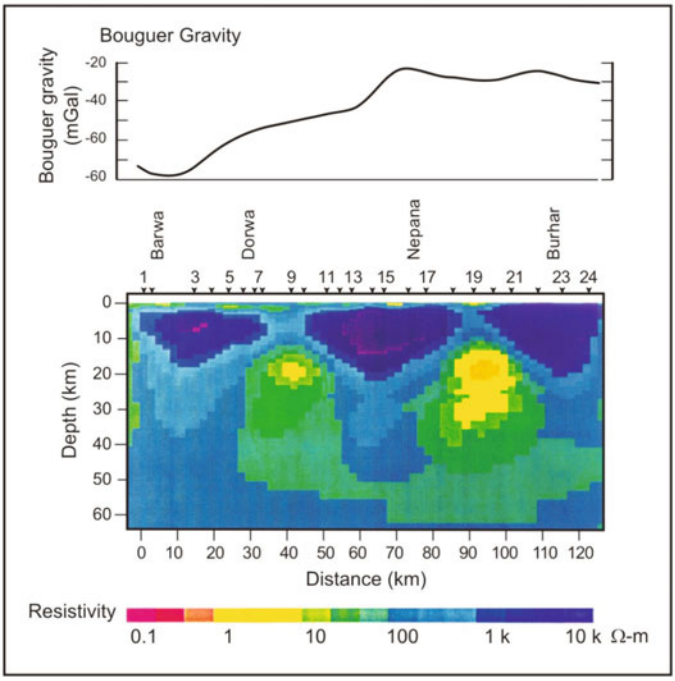

Figure 6.45. Deep geoelectric structure in the Satpura region. The Bouguer gravity variation is shown on the top of this figure (Gokarn, 2003).

III. Electrical Image of Siwalik Sediments

Thickness of Siwalik sediments is ascertained over 150 km long profile in the Mohand-Ramnagar region. This geoelectric structure is predominantly four

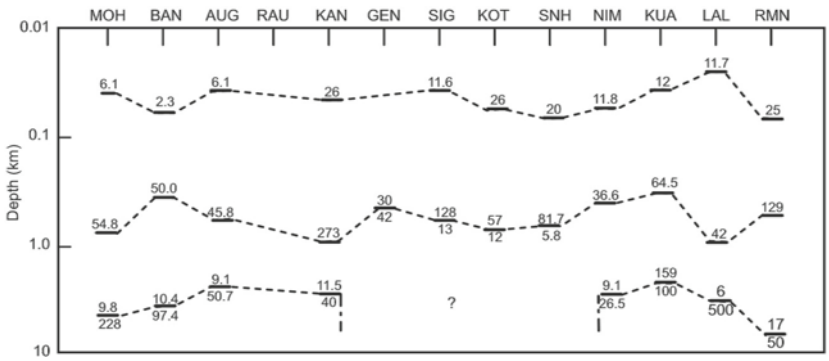

Figure 6.46. MT data were collected at 13 stations along a ~100 km long linear profile in the Mohand-Ramnagar region. 1D analysis showed a four-layered geoelectric cross-section at different sites. Note the break in the delineation of resistive basement between stations GEN and SNH, broadly coinciding with the width of the THC identified by GDS. MOH - Mohand, BAN - Bandarjudh, AUG - Aurangabad, RAU - Rauli, KAN - Kangri, GEN - Gendikhata, SIG - Siggadi, KOT - Kotdwar, SNH - Sanch, NIM - Nimgot, KUA - Kuakhera, LAL - Laldhang and RMN - Ramnagar (Gupta et al., 1994).

layered (Fig. 6.46) and is explained by presence of three layers of sediment overlying the resistive basement. The top layer (50 m thick) is due to the alluvial and post-Siwalik sediments deposited over a more resistive upper Siwalik layer with a thickness of 700-1000 m. The third layer is ~3 to 4 km thick and is believed to be of middle and lower Siwaliks. The resistive basement is delineated below the middle and lower Siwaliks at depths of 5 to 8 km from the surface.

IV. Transects along the Himalayan Collision Belt

In NW Himalaya, MT deep sounding studies are carried out to obtain information on the position and structure of deep crustal blocks over the Himalayan collision belt under the HimProbe project, as part of deep continental studies. Two high resistive blocks of Ladakh and Chushul batholiths (Figs 6.47 and 6.48) with a depth extent of 12 km are delineated to the north of Indus Tsangpo suture (ITS) zone. A vertical low resistivity zone (500 ohm-m) demarcates the Ladakh and Chushul batholiths.

The use of MT as a tool for geoexploration is on the rise because of its many advantages: a number of national and international groups are using this technique to explore various geological and tectonic settings, not amenable with other techniques. In fact, Indian scientists have already ventured into the Himalayan collision belt, where topographic effects are rather strong. Recently, MT studies were conducted in the syntaxial belt of NE Himalayan region and

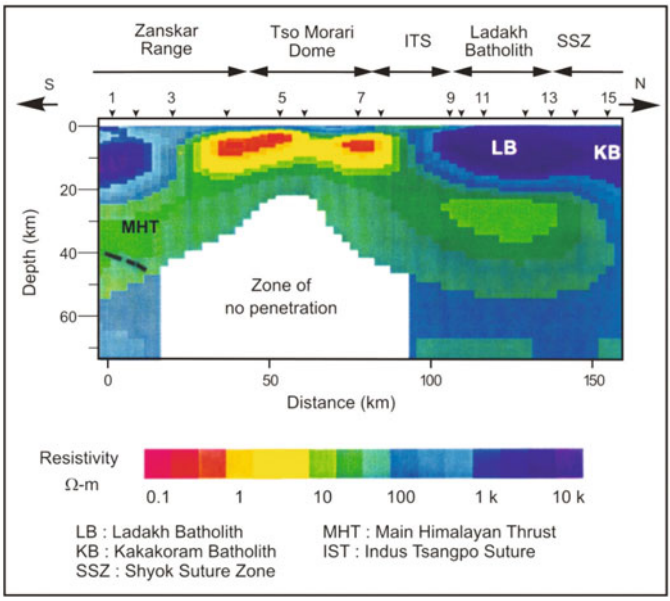

Figure 6.47. Geoelectric structure over the Bara la Cha la Panamic profile. The major structural features are marked on the top part of the figure (Gokarn, 2003).

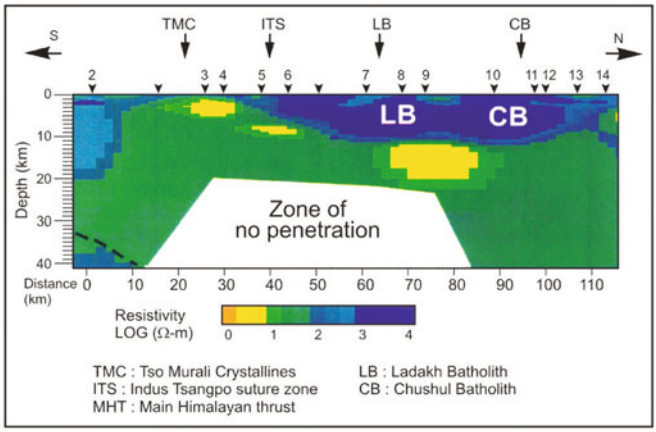

Figure 6.48. Geoelectric structure over the Pang-Phobrang profile. The major structural blocks are marked on the top of the figure (Gokarn, 2003).

also in Andaman Nicobar islands. Also a major thrust is needed towards understanding the complex nature of crust below the Vindhyan sediments and a complex pattern of rift valleys prevalent in the basement below the Deccan basalts. Precambrian tectonics and crustal evolutionary processes will also be carried out by MT technique.

6.21 EARTHQUAKES: CAUSATIVES AND MEASUREMENTS

Earthquakes are the outward manifestation of Earth's internal dynamism and occur where tectonic deformations are active, i.e. mainly along the boundaries of mobile crustal blocks, where portions of the crust are either scraped or generated or destroyed. They also occur, when fluvial migrations leave behind a hollow.

All the current hypotheses acknowledge that when stress exceeds the material strength of crustal rocks, a fracture occurs across the weak planes releasing large amount of accumulated strain energy. The release can be in almost one go or in successive stages through the violent breaking of rocks. This energy travels through Earth in the form of vibrations called seismic waves consisting of P (primary), S (secondary/shear/transverse) and surface (Love/ Rayleigh) waves (for their characteristic features, refer to Chapter 2). Seismic waves move out from the focus (the place where the rupture begins) of the earthquake in all directions. The intensity and position of earthquakes, seismicity (frequency of earthquakes) of an area, type of fault in the rocks and the velocity of the waves (mainly P (Vp) and S (Vs) waves) in different rocks, reveal different properties of the Earth (Chapter 2). Surprisingly, people on the surface feel tremors, but those in caves in the same area do not. This is because ground motions on the surface are induced by Rayleigh waves, which are seldom felt below 65 m depth. The great 1934 Bihar earthquake brought disaster to coal mines due to wrenching along fault planes. Thus, caves and mines are wholly not immune to earthquakes. It is generally accepted, ground motion decreases with depth during an earthquake.

Changes in crustal stress are seen to precede as well as occur simultaneously with earthquakes. Magnetic properties of crustal rocks are sensitive to stress and this leads to the possibility of monitoring it using magnetic measurements. Local changes in geomagnetic field due to any kind of tectonic activity are termed 'tectonomagnetism' and the study which specifically relates to earthquakes is called 'seismomagnetics'. Location of faults and their extent is deciphered on sharp magnetization and resistivity contrasts in subsurface layers. The prediction is done through analyzing changes in the intensity of magnetization and resistivity that follows an earthquake cycle.

Seismic activity prevalent across the Indian subcontinent is attributed to underthrusting of Indian plate below the Eurasian plate, although convergence is considered as not the sole process responsible for its seismicity. Seismic studies were earlier concentrated in Himalayas to the exclusion of the stable peninsular shield, which is also regularly shaken by violent Earth tremors at Koyna, Latur, Jabalpur and Bhuj. According to plate tectonics, seismic energy dissipates only along the plate boundaries. Since neotectonic movements are leading to catastrophic earthquakes in the peninsular region, installation of wide band sensitive seismographs (instrument recording ground motion) in a

closer grid within critical areas (Fig. 6.60) is being made a priority. Also, integrated geological and geophysical investigations are carried out to supplement seismic studies. This will help in carrying out large scale structural and deformational studies as well as mapping the stress accumulation and release phenomenon (Fig. 6.49) occurring in the Indian plate.

Seismic deformation: A fault rupturing causes two types of deformations (strain)— static and dynamic. Static deformation, unlike dynamic, is permanent displacement of ground due to a rupture event. The earthquake cycle progresses from a fault that is not under stress to a stressed one, as tectonic motions driving the fault slowly proceed to split during an earthquake and form a newly relaxed but deformed state fault (Fig. 6.49)

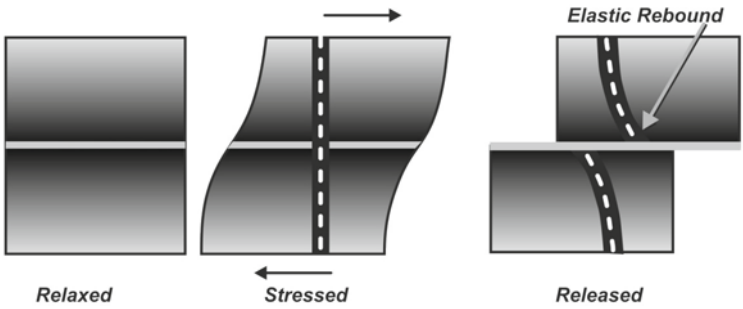

Figure 6.49. Simplified schematic representation of a fault rupture.

Richter Magnitude

The magnitude (M) of an earthquake, represented by Richter scale (RS), is a measure of the amplitude of the largest seismic wave recorded at the time of an earthquake and the amount of energy released. It calculates the strength of an earthquake from seismograph data. The dynamic and transient seismic waves released by any earthquake propagate throughout the globe, and are recorded by sensitive detectors. Nuclear test-ban treaties, in effect, rely on the ability to sense underground nuclear explosions equivalent to an earthquake of magnitude 3.5 (M3.5) on Richter scale.

In early twentieth century, earthquake intensity was measured on a 12-point scale devised by Guiseppe Mercalli. This scale was later modified and called the modified Mercalli (MM) scale. In 1935, Charles Richter, after analyzing data of earthquakes in southern California, proposed an alternative scale, where each point corresponded to 10 times the intensity or 30 times the energy. The MM scale with 12-divisions of intensity is based on the amount of damage caused to various types of structures. The RS has 8-divisions of magnitude, and allows making more uniform comparison of quakes world over. In this scale, the amplitude of the surface waves is measured on a standard instrument called the Wood-Anderson type seismograph.

Under Richter scale, earthquakes M<3 are called microquakes, which are not even felt by people living in the area and are detected only by sensitive seismographs. Earthquakes of M4 can be detected globally and stack up to thousands everyday. Up to M5 are moderate quakes, while M7 are major, and those of M8 or more are the great quakes. The Richter scale has no upper limit (it is open ended), but the largest known quakes fall in magnitude range of 9.0 to 9.5. Earthquakes with M9 and higher, are not possible on RS because rocks are not sufficiently strong to store energy without breaking at higher stress.

Though Richter proposed the 'logarithmic' scale (where the difference between the values of successive points keep increasing), others too have contributed to its refinement. Gutenberg proposed an alternate method in which he used 'body waves', unlike the 'surface waves' utilized by Richter. Actually, the difference in the reported magnitude of earthquake (by different agencies, institutions and countries) arises due to different measurement methods used. For example, the US, Japanese and many other countries use 'surface' waves (M_s mode) for large earthquakes, while it is a common practice to make use of 'body' waves (m_b mode) at large (teleseismic) distances. Thus, magnitudes differ when the method of calculation alters. Magnitudes calculated in the 'local' mode (M_L) are quite different than those calculated in the M_s mode or the M_w mode (moment magnitude). Apart from different methods of measurement, there are also different units in circulation like 'intensity', 'magnitude' and 'energy'. There are several relationships connecting different types of seismic magnitudes. Few of them are well calibrated and therefore universally standardized based on which it is possible to convert one type of magnitude into the other depending on the requirement. A generalized expression for determining magnitude is given by the following empirical equation:

$$M = \log (A/T) + xf(\Delta, h) + y$$

where A is maximum amplitude of a wave in microns, T – wave period in seconds, Δ – distance from the point of measurement of signal amplitude at observing station to the epicentre, in degrees of an arc of meridian (great circle arc), h – focal depth in kilometers, x and y – constants determined empirically and f is the function obtained through study of empirical and theoretical results.

The magnitude scale patterned after the RS is logarithmic and measures the energy (E) released by earthquakes in ergs. Its relation with the magnitude of earthquakes is expressed by the formula: $\log E = 12.24 + 1.44\ M$ for M>5. The use of the scale is explained in Table 6.3 that compares magnitude to the seismic energy yield released in terms of TNT explosive equivalent. For example, the M8.4 Bihar earthquake of 1934 is calculated to have released 2.04×10^{25} ergs of energy, while 1952 Assam quake of M8.7 released an energy equivalent to ~6,000 times that of the atom bomb dropped over Hiroshima. For every unit of increase in magnitude on the RS, there is roughly a 30 fold increase in the energy released by an earthquake. For instance, an M2 earthquake releases 30 times more energy than an M1 earthquake. On the same scale, the

Table 6.3 Richter scale used to compare magnitude with seismic energy yield

Magnitude	*Amount of TNT for energy yield*	*Example (approximate)*
-0.5	6 ounces	Breaking a rock on a lab table
1.0	30 pounds	Large blast at a construction
1.5	320 pounds	-
2.0	1 ton	Large quarry or mine blast
2.5	4.6 tons	-
3.0	29 tons	-
3.5	73 tons	-
4.0	1,000 tons	Small nuclear weapon
4.5	5,100 tons	Average tornado
5.0	32,000 tons	-
5.5	80,000 tons	Little skull mountain
6.0	1 million tons	Double spring flat
6.5	5 million tons	Northridge
7.0	32 million tons	Ryogo-Ken Nanbu
7.5	160 million tons	Landers, California, quake, 1992
8.0	1 billion tons	San Francisco, California, quake, 1992
9.0	5 billion tons	Anchorage, Alaska, quake, 1964
9.5	32 billion tons	Chilean quake, 1960
10.0*	1 trillion tons	San Andreas-type fault circling the Earth
12.0*	160 trillion tons	Fault dividing Earth in half through centre, or Earth's daily receipt of solar energy

* Hypothetical examples

ratio of the energy released between earthquakes of magnitudes M3/M1 is 900 times (30×30).

6.22 MAJOR EARTHQUAKES OF THE WORLD AND INDIA

The earliest earthquake recorded in a catalog occurred in China in 1177 BC, which has description of several dozen large earthquakes from then onwards. Earthquakes in Europe find mention as early as in 580 BC, but the one for which some description is available, occurred in the mid sixteenth century. The earliest known earthquakes occurred in Mexico were in the late fourteenth century and in Peru in 1471. The descriptions of the effects, however, are not well documented for any of these quakes. By seventeenth century, depictions of the effects of earthquakes, exaggerated or distorted, were published around the world (Fig. 6.50).

Earthquake prone areas of the Indian subcontinent: Indian subcontinent is replete with seismic prone areas (Fig. 6.51, Appendix 6.4), the most well known being the Himalayan region, which is a part of worldwide zone of earthquakes running from the Alpine belt through Indonesia, Mynamar, Himalaya (of India,

Date	Place	Magnitude	Deaths	Date	Place	Magnitude	Deaths
① Apr 4, 1905	Kangra, India	8.6	19,000	⑫ Dec 26, 1939	Erzincan, Turkey	7.8	30,000
② Aug 17,1906	Valparalso, Chile	8.2	20,000	⑬ Oct 5, 1948	Ashgabat, Turkey	7.3	110,000
③ Dec 28, 1908	Messina, Italy	7.2	100,000*	⑭ May 31, 1976	Peru	7.9	66,000
④ Jan 13, 1915	Avezzano, Italy	7.5	29,980	⑮ Feb 4, 1976	Guatemala	7.5	23,000
⑤ Dec 16, 1920	Gansu, China	7.8	200,000	⑯ Jul 27, 1988	Tangshan, China	7.5	655,000*
⑥ Sep 1, 1923	Kanto, Japan	7.9	143,000	⑰ Dec 7, 1988	Spitak, Armenia	6.8	25,000
⑦ May 22, 1927	Tsinghai, China	7.9	200,000	⑱ Sep 29, 1993	Latur, India	6.2	9,748
⑧ Dec 25, 1932	Gansu, China	7.6	70,000	⑲ Jan 26, 2001	Gujarat, India	7.7	20,023
⑨ Jan 15, 1934	Bihar, India	8.1	10,700	⑳ Dec 26, 2003	Bam, Iran	6.6	26,200
⑩ May 25, 1935	Quetta, Pakistan	7.5	60,000*	㉑ Dec 26, 2004	Sumatra, Indonesia	9.0	283,106**
⑪ Jan 25, 1939	Chiltan, Chile	8.3	28,000	㉒ Oct 8, 2005	Muzaffarabad (PoK)	7.8	N.A.

How many earthquakes occur worldwide each year? **Estimated* *** Including deaths from Tsunami*

Description	Great	Major	Strong	Moderate	Light	Minor	Very Minor
Magnitude	8 & higher	7 - 7.9	6 - 6.9	5 - 5.9	4 - 4.9	3 -3.9	2 - 2.9
Annual Average	1	17	134	1319	13,000 *(Estimated)*	130,000 *(Estimated)*	1,300,000 *(Estimated)*

Source : The United States Geological Survey

Figure 6.50. Map of the world showing the locations and the time of the known major earthquake occurrences (http://earthquake.usgs.gov/earthquakes/world/historical.php/).

Nepal, Tibet, China), Afghanistan, Iran and Turkey to the Mediterranean Sea. This belt has been the seat of great many earthquakes in the past resulting in massive destruction. Peninsular shield made of Dharwar, Aravalli and Singhbhum protocontinents was considered seismically less hazardous. Yet the disastrous earthquakes at Koyna (1967, M_w= 6.3), Killari (1993, M_w= 6.1), Jabalpur (1999, M_w= 5.8) and Bhuj (2001, M_w= 7.7) disprove this myth. The intra-plate earthquakes, unlike the plate boundary shakings, are less frequent but kill more people. Reservoir induced seismicity (RIS) caused the Koyna quake, but the 1819 Rann of Kutch earthquake (M~8.0) was due to intra-plate events that produced a surface scarp of ~100 km long. During 35 years between 1963 and 1998, Koyna and its adjoining areas have faced 102,715 tremors, of which 79 were above M4.0, and seven were above M5.0. Seismologists

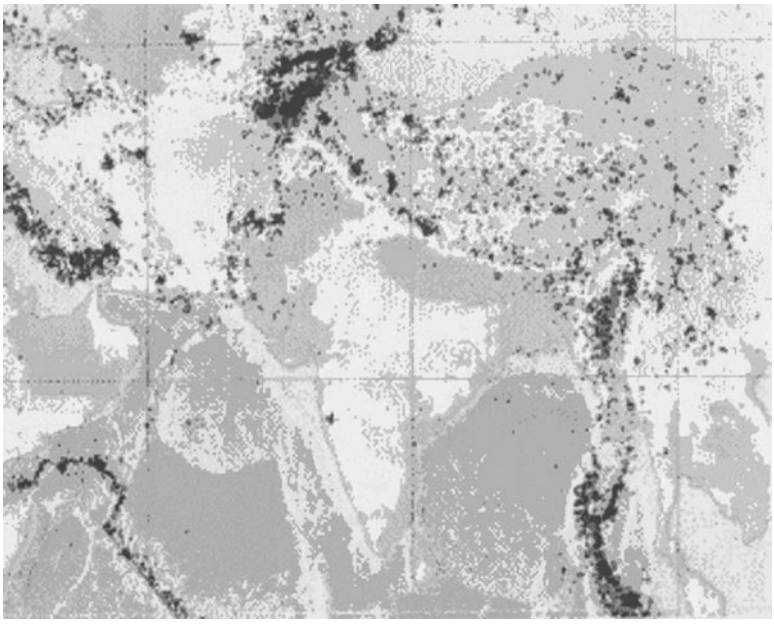

Figure 6.51. Seismotectonism of the Indian subcontinent. Note the seismic prone areas in the subcontinent; the most well known being the Himalayan region, which is a part of worldwide zone of earthquakes running from the Alpine belt through Indonesia, Mynamar, Himalaya (of India, Nepal, Tibet, China), Afghanistan, Iran and Turkey to the Mediterranean Sea (http://www.cessind.org/ earthquakes_inindia.htm#eqindian).

conclude that Killari (Latur, M6.4) type of disasters can occur on discrete faults in regions generally presumed to be aseismic.

Data recorded at Indian and international permanent seismological observatories are analyzed to model the structure and tectonic setting of Indian subcontinent. For example, P and S wave analysis led to estimating seismic velocity structure below the Indian region. Tomographic analysis of tele-seismic P wave residuals over the Deccan trap and adjoining area revealed the existence of 600 km long and 350 km wide NS trending anomalous high-velocity zone (2 to 5% contrast) at a depth over 100 km. Also, focal depth, faulting mechanism and moment tensor estimations are made for several other earthquakes.

6.23 HIMALAYAN TECTONICS AND ITS EFFECT ON PENINSULA

Seismicity in the Himalayan belt is attributed to movements along the main boundary thrust (MBT) and main central thrust (MCT). The MBT is the intracrustal boundary along which the Indian plate is sliding down. In the Himalayan region, seismic activity largely results due to building up tectonic stress from continuous movements along the faults and thrust zones. The

Figure 6.52. Generalized schematic map of major rift zones of Indian subcontinent and their association with seismic activity. The seismicity in peninsular India is found mostly restricted mainly along NE-SW and NNW-SSE trending faults and fractures.

resultant pressure has upwarped the peninsula at many places, and reactivated ancient rifts (Fig. 6.52). The seismicity in peninsular India is found mostly restricted mainly along NE-SW and NNW-SSE trending faults and fractures. The Coimbatore earthquake in 1900 (M6) is attributed to a NNW-SSE fault. The Bhadrachalam earthquake of 1969 (M5.7) is thought to have been caused by movement along a graben fault. The earthquake that shook up Bharuch in 1970 was located at the intersection of the boundary faults of the Narmada and Sabarmati grabens. Movements along faults in a NNE-SSW direction delimiting the Aravalli ridge are considered to have given rise to earthquakes in the Delhi region. 1993 Latur earthquake occurred due to the rubbing together of landmasses on two sides of the 400 km long Kurduvadi rift having 40-60 km width and spreading from SE of Solapur and ending in the north of Pune (Fig. 6.52).

The Himalayan collision zone witnessed four great earthquakes (1897 Assam, 1905 Kangra, 1934 Bihar-Nepal and 1950 Assam) in a span of 53 years. The quantitative seismicity map of the Himalayan terrain shows high seismicity (M5-6) in the Kashmir valley, Doda in Jammu, Spiti, Nepal and Bhutan. Seismicity in the northern part of the Tibetan plateau and adjacent regions is attributed to strike-step movements along E-W trending transcurrent faults. The frequent moderate earthquakes and the infrequent great earthquakes suggest ongoing episodic slippage. These processes also imply future great earthquakes in the unruptured 'gaps' of the Himalayan front, with uncertainties attached to their recurrence interval. Recent destructive earthquakes from India are described below.

I. 1991 - Uttarkashi (Almora) Earthquake

The 1991 moderate Uttarkashi earthquake (M~6.5) attracted a lot of attention due to its proximity to the high Tehri dam in Garhwal Himalaya. The epicentre of the earthquake was found to lie in Almora, but the maximum damage to buildings and human life took place in Uttarkashi and Chamoli. This damage can be attributed to the incohesive condition of soils and the weak structure of buildings. This earthquake occurred because of slippage along the MCT, a major tectonic boundary, which also divides lesser Himalayan terrain in the south from the snow-clad mountains in the north. Some environmentalists fear that the construction of the Tehri dam across the Bhagirathi river may lead to reservoir induced seismicity. The fear is compounded by the fact that the area is normally prone to seismic activity. From the engineering point of view, it is considered that the proposed dam can withstand earthquakes with magnitude up to 7.2.

In 1995, a pair of telluric and resistivity sounding dipoles and PPM were set up at Rohtak and Jhajjer region (Haryana) to monitor the electric and magnetic precursors to earthquakes in parts of Garhwal Himalaya. Three ultra-low frequency (ULF) stations were also installed in 2001-2002 in Uttarkashi region in Garhwal Himalaya.

II. 1999 - Chamoli Earthquake

The Garhwal region was rocked by M6.8 earthquake on 29 March 1999. The main tremor was followed by after-shocks with magnitudes between 4.9 and 2.0. The focus of the earthquake lay at a depth of 30 km. The death toll and injury in and around Chamoli and Rudra Prayag were at least 100 and 300 people, respectively. The earthquake occurred in zone V in the inner Himalayas. Tremors were reported from adjoining Himachal Pradesh, Jammu and Kashmir, Haryana, Rajasthan and Delhi.

III. 1819 - Kutch Earthquake

The 1819 earthquake (M~8.0) at Kutch generated a 100 km long fault scarp, popularly known as Allah Bund, meaning the wall of God. Mapping the scarp morphology, trenching excavations near Allah Bund and developing age constraints are some of the studies in progress.

IV. 1967 - Koyna Reservoir Induced Seismicity

Seismicity associated with Koyna dam is one of the classic examples of reservoir induced seismicity, whose seismotectonics are governed by a large water load. Remarkable correlations are observed between seismicity and water filling cycles of Shivajinagar lake, Koyna. This is attributed to the pore pressure changes induced by the reservoir load, which reduces the strength of the rocks in the vicinity of the dam, leading to fault failure. Globally, Koyna is among

the four well documented RIS cases, where earthquakes in excess of M6.0 have been generated. An earthquake of M6.5, and many aftershocks of M>5, occurred at Koyna on 10 Dec 1967. There is an alternate theory. This earthquake might have resulted from Earth movement over a 10 km stretch long N10°E-S10°W trending fault below the Deccan traps. Because of this, the region is under tensional stress leading to record tremors of different magnitudes. Migration of seismic activity due south of the clustered Koyna events, is reported in recent studies.

V. 1993 - Latur Earthquake

The painful consequences of Killari earthquake felt over ~110 sq km area in the Latur and Osmanabad, Maharashtra are highlighted by the loss of 10,000 lives and several razed villages. The M6.3 Latur earthquake of 30 Sept 1993 is the world's most devastating stable continental region (SCR) earthquake, whose epicentre lies in an aseismic region. After the earthquake, several fractures in the ground are observed (Fig. 6.53), and high concentration of helium over the fractures is also detected. With a shallow focal depth of <10 km, this earthquake is similar to other moderate events in the Australian and Canadian shields. The repeat time of moderate SCR earthquakes is at the order of hundreds and thousands of years. Lack of historical documentation makes their strikes a total and unexpected surprise. Latur event gave a new perspective and urgency to initiate seismic hazard assessment in peninsular India leading to strengthening of seismic networks and upgradation of several existing facilities.

Figure 6.53. The Latur earthquake generated a surface rupture that was traceable for about 2 km. The maximum height of the scarp observed near Killari was about one metre (http://www.cessind.org/ earthquakes_inindia.htm#eqlatur).

VI. 1997 - Jabalpur Earthquake

The M6.0 earthquake of 22 May 1997 at Jabalpur was recorded by newly installed broadband digital stations in the shield region. This earthquake not just caused widespread devastation, but also generated great deal of data helping to understand the response of various types of residential and commercial structures to seismic waves. This offered valuable guideline in the design and construction of earthquake resistant buildings. Later, tectonomagnetic studies were initiated in areas adjoining Jabalpur. Figure 6.54a shows the layout map of ground geomagnetic repeat surveys undertaken using PPM. Repeated yearly surveys of 2003 to 2007 show secular changes in total geomagnetic fields concentrating locally (Fig. 6.54b). It also shows the anomalous geomagnetic field SVs in a range of ±0.06 to ±9.54 nT at separate stations across the profiles. These SV are related to anomalous accumulation of tectonic stresses, and tensions on the fault zones and crustal blocks due to recent geodynamic processes along the NSL.

VII. 2001 - Bhuj Earthquake

The Bhuj earthquake (M~7.7) in Gujarat that occurred on 26 Jan 2001 is historically the most catastrophic, whose epicentre is located 20 km NE of Bhuj (Fig. 6.55a). Seismic data from an aftershock array suggested south dipping thrust with a surface projection at ~23.8°N, near the central Rann of Kutch. Aftershocks were unusually deep (up to 30 km). The earthquake severed the lithosphere leaving ~20,000 people dead and ~200,000 injured. Nearly 400,000 houses were destroyed and twice as much damaged. Although damages of such proportion were astonishing, the occurrence of the event itself was not surprising, considering the geologic and seismic history of the region. The

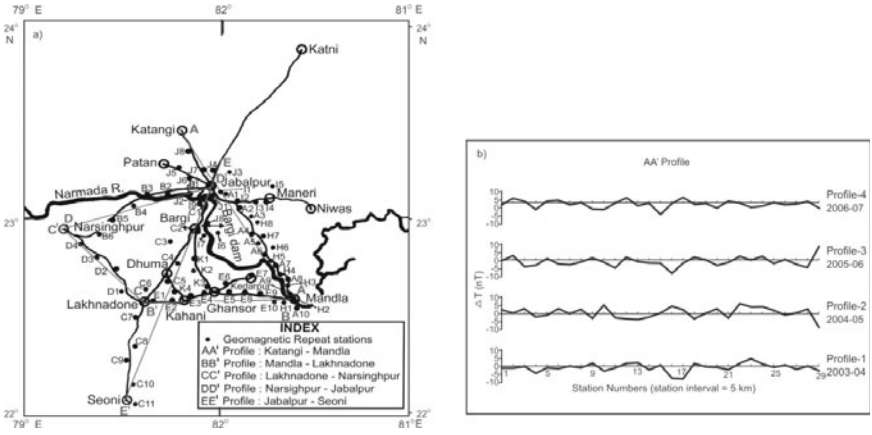

Figure 6.54. (a) Layout map of Jabalpur repeat survey. (b) Secular change of the geomagnetic field T along AA' profile in (a) (Waghmare et al., 2008).

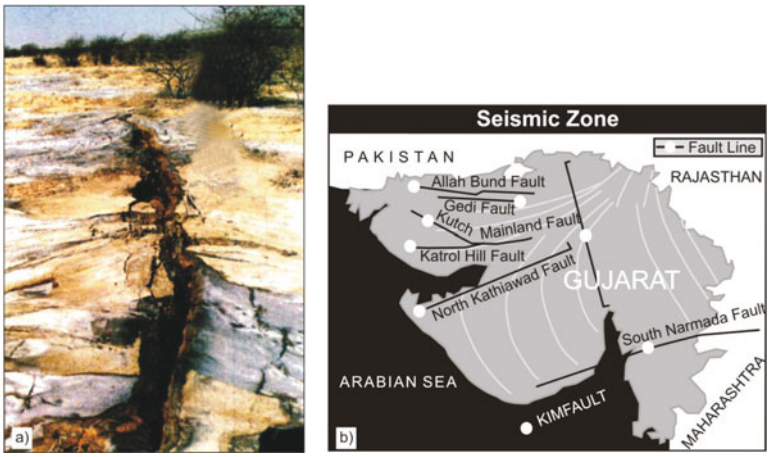

Figure 6.55. (a) The crack at Dhang-Godai village near the epicentre. (b) Simplified criss-cross faults within Gujarat exposing it to seismic activity.

Kutch forms a part of Mesozoic rift system and has been noted for occurrence of large earthquakes since historic times. For example, this area has been experiencing above normal levels of microseismicity throughout the past 200 years, and probably for many more millenia. Damaging earthquakes occurred in 1845, 1846, 1856, 1857, 1869 and 1956 in the same general region as the 1819 and 2001 earthquakes.

After the 2001 major quake, a substantial increase in tremors is seen since Gujarat is located over the south Narmada fault and attributed to its reactivation. Apart from this fault, there are scores of other major fault systems in Gujarat making the region extremely vulnerable to seismic activity (Fig. 6.55b).

6.24 SEISMIC ZONATION MAPS AND SEISMIC HAZARDS

Seismic zonation map (Fig. 6.56) is a guide to the seismic status of the region and its susceptibility to earthquakes. The Bureau of Indian Standards introduced the seismic zoning concept in 1962, and revised it from time to time on the basis of accumulating seismic data. India was earlier divided into five zones with respect to severity of earthquakes, but in the latest version these have been scaled down to just four with zone I getting the axe. Each seismic zone corresponds to a particular 'seismic coefficient' that has to be incorporated in the design of large civil engineering structures. According to the 'seismic gap' theory, the 2400 km long seismic belt of the Himalayas is divided into three major segments (Fig. 6.56b). Future earthquake shocks are likely in the gaps. Unfortunately, the Tehri dam is located on the longest stretch (300 km, between Hardwar and Tanakpur). The validity of the seismic gap theory is questioned, since it is based on circum-Pacific belt, which cannot be applied to the Himalayan terrain. In the circum-Pacific area, continental plates interact with

oceanic plates, but the Himalayan terrain occupies continent-continent collision zone.

Of all the seismic zones, zone V is seismically the most active where earthquakes of M8 or more can occur. In case of shield type earthquakes, historic data are insufficient to plug them in higher zones because their recurrence intervals are much longer than the recorded human history. This gives a false sense of security. Occurrence of the damaging earthquake at Latur, falling in zone I (according to old seismic zonation map) is a typical example of this situation.

However, within a single seismic zone not all structural faults and thrusts, and not even all elements of single fault, are identically active. Furthermore, in the task of preparing seismic zoning map of the region, which lends support to determining the long-term predictability of earthquakes, the structures of the zone in which tectonic stresses cause faults are often not considered. Physical basis of long-range earthquake occurrence patterns cannot be effective without elucidating the deep structures of seismically active regions. Therefore, the emphasis of geophysical research in these regions should be the study of crustal structures to a depth of several tens of km, discrimination of inhomogeneities in terms of structures and physical properties, clarifying their characteristics and distinguishing seismically active areas from relatively inactive ones.

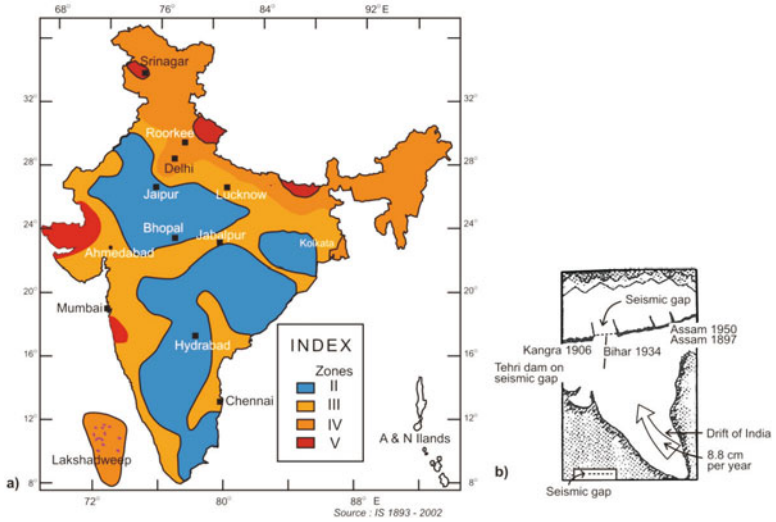

Figure 6.56. (a) Seismic zones of earthquake vulnerability in India at macro-level. Zone II to Zone V show increasing magnitude; Zone V is of the highest seismic intensity, zones IV and III are relatively of moderate damaging intensities for well built structures and dangerous for poor buildings and Zone II is light to minor shaking regions. Within the zones, earthquakes of more or less same intensity may be expected. (b) Himalayan seismic gap.
(http://www.earthscrust.org/earthscrust/science/transects/india.html)

Seismically active areas should intensively be monitored for stress induced changes effected in a host of physical parameters.

6.25 GEOPHYSICAL STUDIES IN SEISMICALLY ACTIVE REGIONS

Lack of geophysical data inhibits understanding into the subsurface linkages of tectonic features with the contemporary seismicity of the region. This necessitates examination of crust from its surficial levels to the lithospheric depths, for which gravity and magnetic (GDS, MT) investigations are recognized as effective tools. Thus, areas rocked by earthquakes are investigated by geological and geophysical (magnetic, GDS and MT) methods for evaluating their long-term seismicity.

GDS and MT can probe the deep interior. They are quick, inexpensive and used as proxy tools to explain spatial-depth distribution of seismicity, identifying zones of strain accumulation, layering, and for constraining tectonic evolution model. These techniques map zones of sharp conductivity contrast associated with fault planes, whose depth and dimension are estimated later on. For example, the noted correlation between mapped structures by GDS, OBM and MT, and high seismicity underlines the role of fluids in current tectonic processes. For instance, consideration of space-time pattern in seismicity in relation with high conductive zone helps infer the nature of electrical conductivity distribution. This can be a sensitive pointer towards the reactivation of subsurface structures that lead to earthquakes. This subsurface structural mapping provides better insight into the seismicity pattern and cycles of stress accumulation and release in the Indian plate. Towards this end, two broadband seismic observatories are established at Rewa and Kolhapur. Few examples from regions in the Himalayas (Nazibabad-Satpuli profile and Trans-Himalayan conductor) and peninsular India are discussed below.

I. Nazibabad-Kotdwar-Satpuli Line

Spatial variation of magnetic field along Nazibabad-Kotdwar-Satpuli in the Himalayas is examined for earthquake precursory signals. Two pronounced anomalies associated with large susceptibility contrasts correlate with Amri thrust and Nayar fault (Fig. 6.57). The magnetic anomalies are explained in terms of intrusion of basic material along the thrust and associated fault plane.

II. Trans-Himalayan Conductor, NW India

GDS experiments over NW India and Garhwal Himalayas discovered a major conductivity structure running across Ganga basin into the foothills of Himalayas following the strike of Aravalli mountain belt of the Indian shield. The overall geometry of this conductivity structure can be approximated as an asymmetric domal upwarp in the middle and lower crust located between Delhi-

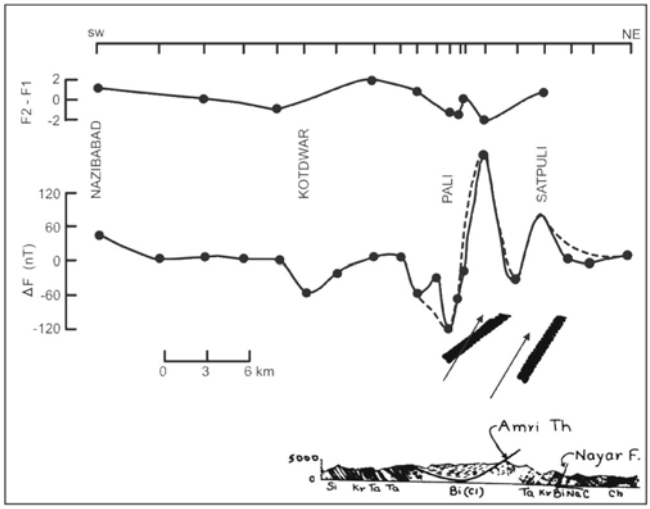

Figure 6.57. Trend-free magnetic anomalies associated with large susceptibility contrasts are shown to correlate with Amri thrust and Nayar fault. Two pronounced anomalies are interpreted in terms of intrusion of magnetic material along Amri thrust and Nayar fault (Singh et al., 1986).

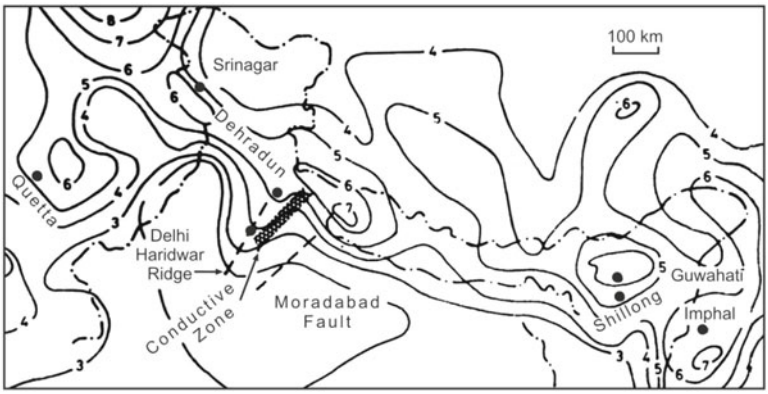

Figure 6.58. Position of trans-Himalayan conductivity structure identified by GDS studies (Arora and Mahashabde, 1987), superimposed on the quantitative seismicity contour map of the Himalayas (Kaila and Narain, 1976).

Hardwar ridge on the NW and Moradabad fault on the SE. The position of the conductive zone is shown in Fig. 6.58, overlain on quantitative seismicity map of the region. A zone of high seismicity characterizes this region, containing the electrical conductivity anomaly. The correlation suggests that this conductivity belt is associated with either present tectonic activity or with ancient tectonic structure, which is now reactivating.

III. Rohtak Region

In the 1960s and 1970s, Delhi and surrounding regions were frequently rocked by earthquakes. The temporary seismic network set up then recorded ~100 shocks of varying magnitudes for ~10 years duration. During Dec 1995, MT data were collected at 18 stations in Bahadurgarh-Jind region covering the epicentral cluster west of Delhi. The results indicate a deep NS trending ~5 km wide conductive feature located below Rohtak and Jind. Microearthquake data indicated deeper microseisms foci in the vicinity of this conductive zone, and the depth of foci to be decreasing away from it. Thus the conductive feature was proposed to be an active fault leading to the earthquakes.

IV. Khandwa-Jabalpur Region

The region surrounding Khandwa has been seismically active, where the earthquake swarms increased between Aug and Sept in 1998. Subsequently, MT surveys were undertaken and data collected at 30 stations along the 250 km long NS trending Burhanpur-Khandwa-Barwaha profile. The results indicated a conductive deep crustal intrusive ~50 km south of Khandwa, which was associated with the EW aligned Malwa ridge. The earthquake epicentres are located on the northern flank of this ridge. MT studies in the Damoh-Jabalpur-Mandla region delineated a similar deep crustal intrusive ~30 km SE of Jabalpur, which is again due to the Malwa ridge. This occurrence along with the enhanced seismic activity in the Khandwa region is indicative of the fact that the north flank of the Malwa ridge is seismically reactivated.

V. Nasik-Dalvat Region

The magnetic (GDS) and deep resistivity (MT) studies conducted in the Nasik-Dalvat region indicated a complex rift pattern in the basement, which is covered by 500 to 700 m thick Deccan volcanics. MT showed a NS aligned rift valley passing through Nasik, extending almost up to Dalvat on the Maharashtra-Gujarat border. Another rift valley was identified perpendicular to the Nasik–Dalvat rift near the village Vani ~30 km north of Nasik. Further investigations are needed to get a detailed picture of the rift pattern in this region.

VI. Koyna Reservoir Region

Spatial behaviour of residual magnetic field around the Koyna reservoir was monitored in four phases between May 1978 and October 1980. Figure 6.59 gives the residual field for three phases of measurements reckoned with respect to the field level of phase I (May 1978). The residual field pattern for phase III (May 1980) is quite different from those obtained during phase II and IV (January 1979 and October 1980). The characteristic pattern of phase III is explained in terms of electrokinetic effect suggesting water diffusion along NS fault running parallel to Koyna river in response to high pressure exerted

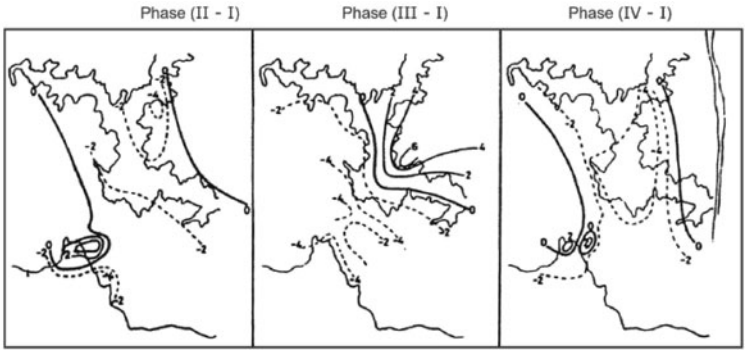

Figure 6.59. Contour map of temporal changes in residual geomagnetic field for three phases of measurements around Koyna reservoir (Arora, 1988).

by the reservoir. These results indicate that geomagnetic measurements in continuous mode can provide effective means of detecting precursory signals of earthquakes from Koyna region.

6.26 CO-SEISMIC INVESTIGATIONS—MAGNETIC AND ELECTRICAL ROCK PROPERTIES

Increased manifestation of Earth tremors both in seismic and aseismic areas makes it imperative to study this phenomenon more intensely. Magnetic and electrical properties of rocks are subjected to change with the stress imparted by impending earthquakes. Continuing worldwide efforts have shown that, from among the variety of geophysical precursors, geomagnetic and geoelectrical forewarnings lend good support to prediction programmes. Geomagnetic repeat surveys with high sensitive magnetometers in dense network configuration have proved effective in delineating long term (>few years) precursors.

Considering the recurrence of earthquakes in different parts of India including the seismically active Himalayan belt, and to isolate seismic precursors, an augmented plan has been put in place to monitor geomagnetic and geoelectrical parameters. Specifically, an increase in density of geomagnetic repeat stations, establishment of more digital geomagnetic observatories, electrical resistivity dipole and telluric current recordings supplemented by monitoring ionospheric parameters obtained from digital ionosonde (digisonde) and VHF receivers like ball antenna, form useful earthquake precursory experiments.

More frequent observations of magnetic field changes show better understanding of secular variation and help in delineation of stress induced changes in geomagnetic field. Noting that SV trend is locally distorted in seismic areas due to accumulating stress, a close network of repeat stations, as in Jabalpur, can be set up in other such areas. Efforts would need to transmit data

in real time by radio telemetry system to a centralized recording station where rapid on-line computerized analysis is organized for detecting short-term premonitory signals preceding an earthquake.

6.27 PREDICTING EARTHQUAKES

The goal of prediction is to issue warning of potentially damaging earthquakes early enough to allow appropriate response to the disaster for minimizing loss to life and property. The aim is to increase earthquake probability estimates within reasonable spatial and temporal accuracy. Earthquake probabilities are estimated in two ways: by studying the history of large earthquakes, and the rate at which elastic strain builds up in the rocks.

The frequency of past earthquakes is a pointer to future shocks. For example, if a region has experienced four M7 or larger earthquakes during 200 years of recorded history, and if these shocks occurred randomly in time, then it is assigned a 50% probability (just as likely to happen, as not to happen) to the occurrence of another M7 or larger quake in the region during the next 50 years.

But in many places, the assumption of random occurrence with time may not be true, because when strain is released along one part of the fault system, it may actually increase on another part; this reasoning is open to debate and controversy. For instance, four M6.8 or larger earthquakes and many M6.0-M6.5 tremors shook the San Francisco bay regions for 75 years between 1836 and 1911. For the next 68 years (until 1979), no earthquake of M6 or larger took place. Beginning with a M6 shock in 1979, earthquake activity in the region increased dramatically between 1979 and 1989, wherein four earthquakes of $M \geq 6$ struck, including the M7.1 Loma Prieta earthquake. This sort of clustering of earthquakes led scientists to estimate the probability of an M6.8 or larger earthquake to occur during the next 30 years in the San Francisco bay region to be ~67% (twice as likely as not).

Another way to estimate the likelihood of an impending earthquake is to study the rate of strain accumulation. When plate movements build the strain in rocks to a critical level, like pulling a rubber band too tight, the rocks suddenly break and slip to a new position. Scientists measure the amount of strain accumulating along a fault segment in a given time, say each year, the time passed since the last earthquake along the segment, and the quantity of strain released during the last earthquake. This information is then used to calculate the time required for the strain to build to the level capable of triggering an earthquake. This simple model is complicated by the fact that such detailed information regarding dynamic behaviour of faults is rare. Only the San Andreas fault system has adequate records for using this prediction method.

6.28 EARTHQUAKE PRECURSORY CHANGES

Forecast of earthquakes falls broadly in two categories: long and short range. For long range forecasting, a map showing all epicentres with spatio-temporal patterns of seismic activity is compiled. Figure 6.60 presents such a map along with major tectonic features and significant earthquakes (M ≥ 5) that helped identify main seismic belts in peninsular India. Statistical techniques are also employed to assess earthquake risks. The technique of short range forecast includes observation of foreshocks, space-time variation of earthquake activity, changes in seismic wave velocity, geomagnetic anomalies and others.

Some earthquakes in Russia, Japan, China and USA have been successfully predicted, though systematic precursory observations are very few. The science of earthquake prediction is still in its infancy. The current approach is to collect

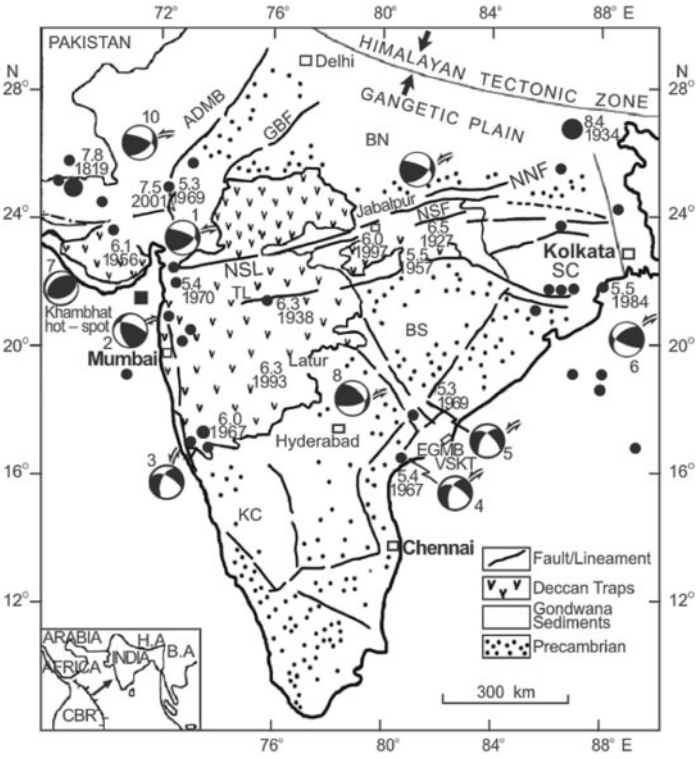

Figure 6.60. Epicentres of the major tectonic features and the significant earthquakes (M~5) in peninsular India; the recent damaging earthquakes are shown by star symbols. Preferred fault-plane solutions are shown by beachball symbols (1-6: after Chandra, 1977; 7: Chung and Gao, 1975; 8-10: USGS); the dark area indicates the zone of compression, and the blank area zone of dilatation, the fault movement is shown by arrows. NSL: Narmada Sone Lineament, NNF: Narmada North Fault, NSF: Narmada South Fault, TL: Tapti Lineament, KMF: Kutch Mainland Fault. Inset: Indian plate movement from theCarlsberg ridge (CBR), HA: Himalayan arc, BA: Burmese arc (Kayal, 2003).

data on all possible parameters and investigate possible correlations. This includes monitoring variations in seismic wave velocity, magnetic field, electrical resistivity, water level in wells, porosity/permeability, emanations of odours/gases and determination of ground deformation through tilt/strain measurements. In some cases even animal instincts (abnormal behaviour of certain animals) are reported to be helpful. For example, the Asian tsunami came as a complete surprise to humans, but the animals in the area had gone to higher ground hours before the tidal waves unleashed their wrath.

The physics of earthquake precursors is commonly described in terms of dilatancy-diffusion (DD) or crack-avalanche (CA) models. Non-universality of premonition signals is related to the diverse nature of earthquakes; shear-rupture or strike-slip motion. Because of limited information available on the nature of faults and lack of theoretical understanding of the growth, coalescence and recovery of fractures, the strategy for prediction depends upon observation of precursory changes. Delineation of active faults and knowledge of their

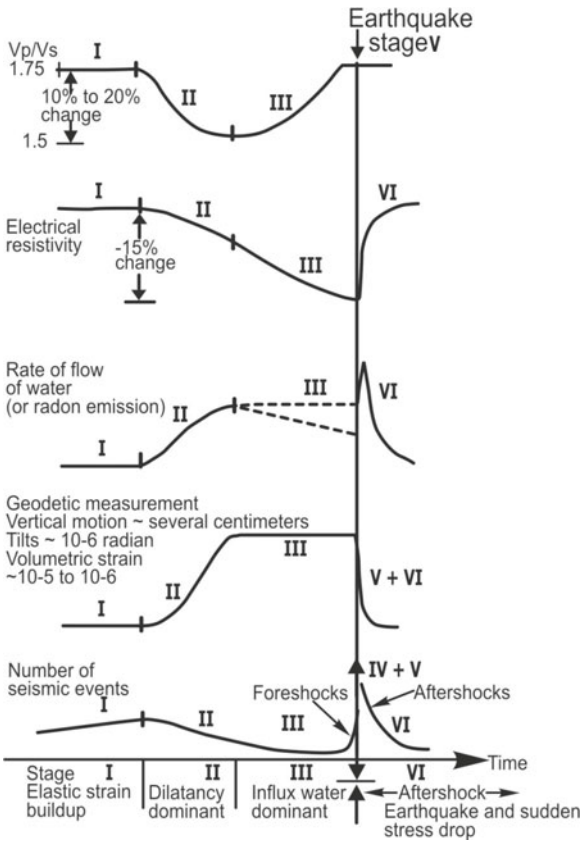

Figure 6.61. Predicted systematic changes in the rate of dilatancy, resistivity, volume, water flow and the number of seismic events as a function of time during earthquake cycle based on the dilatancy-diffusion model (Scholz et al., 1973).

stress distribution are of great help in optimizing forewarning observational networks.

The DD model developed experimentally by Scholz and his coworkers explains many of the premonitory phenomena (Fig. 6.61). They found that dilatancy is produced by the formation and propagation of cracks within the rock and these cracks begin to appear when stress level reaches nearly half of the fracture strength giving rise to changes in physical properties of rocks, such as permeability and electrical resistivity. This can be clearly seen from Fig. 6.61, which shows changes in Vp/Vs, electrical resistivity, radon emission, volumetric strain and number of seismic events (foreshocks). Stage I corresponds to the period of strain accumulation. This phase sees a steady increase in stress levels leading to an increase in volume of crustal rocks. During the phase of stage II, resistivity of rocks drops considerably due to an increase in the number and dimension of cracks and fluid flow into the dilatant zone. On the occurrence of an earthquake, there is a reduction in stress because of which cracks close and water flows out of the source region, resulting in the return of resistivity to its earlier values.

The CA model is also somewhat similar to DD model. In this model, physical properties change only slightly, marking the onset of phase I. After a certain critical density is reached, there is a marked increase in oriented fracture formation. There is thus an avalanche like rapid growth signifying the presence of phase II. The stage III begins with a further rise in strain accompanied by a drop in stress in the narrow zone of the future macro-fault. This also causes reduction in the stress throughout the volume of rock, dividing the area into two parts with differing properties. This model allows one to explain the relation between precursor times and the magnitude of impending earthquake.

The piezomagnetic theory explains the effect of stresses on magnetization of crustal rocks that causes anomalous changes in geomagnetic field in relation to seismic activity. The effects of stress on magnetic susceptibility and remanent magnetization are well understood. In general, the compression axis decreases while the transverse susceptibility tends to increase. The electrokinetic phenomenon, on the other hand, is based on the effect of water diffusion into newly created cracks in the dilatant region. The underground water, because of the effect of stress, is forced through the porous medium which creates a streaming potential inducing electric current flow. This current is strong enough to produce detectable variations in the electrical as well as magnetic fields at the Earth's surface.

6.29 EARTHQUAKE PRECURSORY CASE HISTORIES

Geomagnetic and geoelectric precursors have played a significant role in the prediction of earthquakes, for example in China, Greece and other parts of the world. The nature and duration of premonitory changes from its first appearance

till the time of earthquake suggest these two have large potential in medium and short-term, as well as in immediate prediction of earthquakes. However, the spatial extent and precursory time are seen to vary from one seismic zone to other. Inclusion of this aspect into earthquake prediction strategy in conjunction with other seismological and geophysical precursors would put these studies on a better footing from diagnostic (probabilistic) to prognostic (deterministic) level.

I. International Status

Secular variation anomaly in geomagnetic field prior to a large earthquake in Japan is given in Fig. 6.62, where station A is treated as a magnetic benchmark. Here the rate of SV during the decade of 1950-60 was ~7 nT/yr compared to the normal 2 nT/yr recorded at stations B and C. This anomalous behaviour disappeared after earthquakes of M6.1 and M6.4 close to station A, which showed up several years before and persisted up to the time of earthquake occurrence. A relation between the spatial extent of anomalous area and magnitude was obtained by Rikitake as: $\log r = 11.4 + 1.1\ M$, where r denotes the radius of the anomalous area in cm and M the magnitude.

Another example of short-term precursory change in geomagnetic field (Fig. 6.63) was detected in association with M5.2 earthquake on 28 Nov 1974 along an active fault in California. The plot gives the temporal variations in local geomagnetic field obtained by differencing the simultaneously observed field at two pairs of stations. In this process, the temporal variations associated

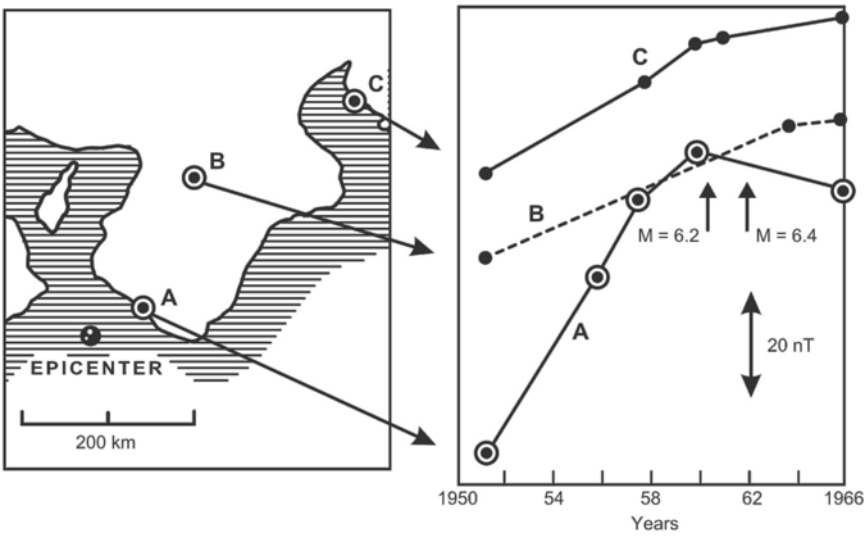

Figure 6.62. Typical example of anomalous behaviour of large secular variation in the geomagnetic field intensity observed in association with two earthquakes in Japan. Note secular change foreruns large earthquakes (Tazima, 1968).

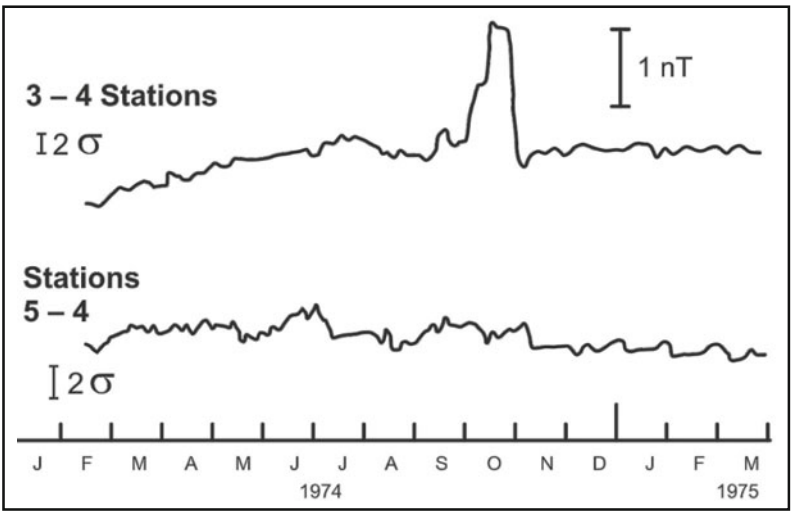

Figure 6.63. An example of mid-term precursory change in geomagnetic field detected in association with a magnitude 5.2 earthquake on 28 November 1974 along an active fault in California. Note a clear bay-shaped change in residual geomagnetic field intensity preceding the earthquake (Smith and Johnston, 1976).

with ionospheric and magnetospheric currents are effectively eliminated, leaving behind the component of tectonic origin. The plot shows a clear and distinct bay-shaped anomaly preceding the earthquake. It was seen that an increase in magnetic field began seven weeks before and returned to normal four weeks prior to the earthquake. The epicentral distance of this site was 11 km. Another place located only a few km away did not record any change. Such examples of precursory changes are many, but there are also instances, where no discernible change preceding an earthquake has been found.

The most popular techniques employed in China, Russia and USA for earthquake prediction are the measurement of telluric current, Earth potential and resistivity. In an experiment in China, electric potential difference between two pairs of electrodes aligned in NS and EW directions were measured daily, where potential difference between NS electrodes showed a sharp drop of 100 mV during ~2 to 3 days prior to the earthquake (M7.3) at Haicheng on 4 Feb 1975 (Fig. 6.64). At another station in the same region, but located at epicentral distance of 145 km, the NS component of telluric current had showed a 40 μAmp decrease ~10 hrs before the earthquake (Fig. 6.64). The anomaly lasted for 7 hrs and then the telluric current intensity recovered to the previous level, 3 hrs before the shock. Kamchatka in Russia is another area, where anomalies in telluric current forerunning impending earthquakes have been observed very often, which have now become one of the regular parameters for making short term predictions of earthquakes.

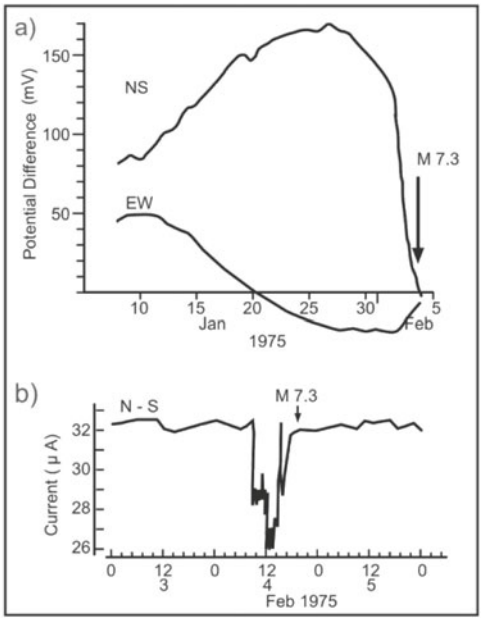

Figure 6.64. (a) Variation in self-potential differences between the NS and EW electrode pairs recorded in association with Haicheng earthquake at a station about 25 km from epicentre. Potential difference showed a sharp drop of >100 mV about 2–3 days before the earthquake. (b) Abrupt changes in electric current observed a few hours before Haicheng earthquake at a station located about 145 km from epicentre. Telluric current showed a 40 μA decrease about 10 hrs before the earthquake (Raleigh et al., 1977).

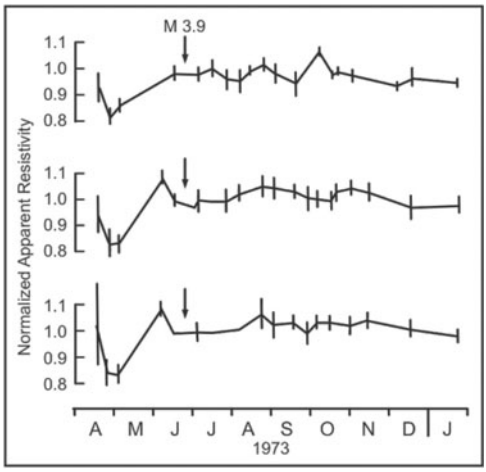

Figure 6.65. Changes in apparent resistivity observed in association with earthquake in the San Andreas fault region. Note a precursory change in resistivity amounting to 15% and lasting for 60 days before an earthquake of magnitude 3.9 (Mazzella and Morrison, 1974).

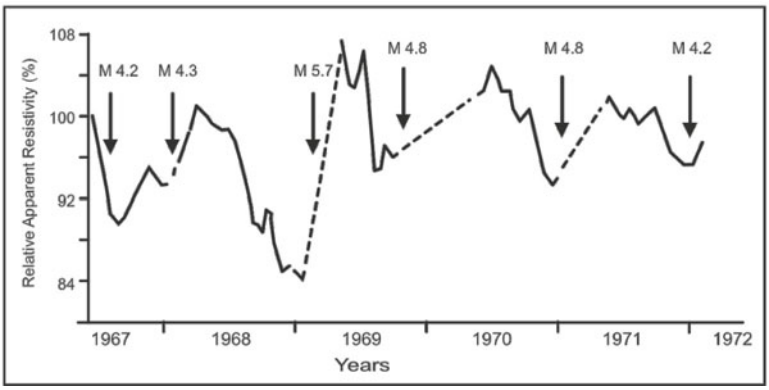

Figure 6.66. Temporal variation in apparent resistivity observed at Garm, central Asia and earthquake occurrence times of M>3. A strong correlation is evident between minima in electrical resistivity and earthquake occurrence time (Barsukov, 1974).

A strong correlation between minima in electrical resistivity and earthquake occurrence (Figs 6.65 and 6.66) is also found. A decrease in electrical resistivity is observed up to 20% for large/near earthquakes and up to 10% for small/distant earthquakes. The precursory time is seen to vary from ~2 to 7 months for earthquakes of M4.2 to M5.7, and it tends to be longer for larger earthquakes.

II. Results from Shillong, NE India

Geomagnetic field variations at Shillong, a place located in an intense seismic region, are examined for possible association with the felt earthquakes in its

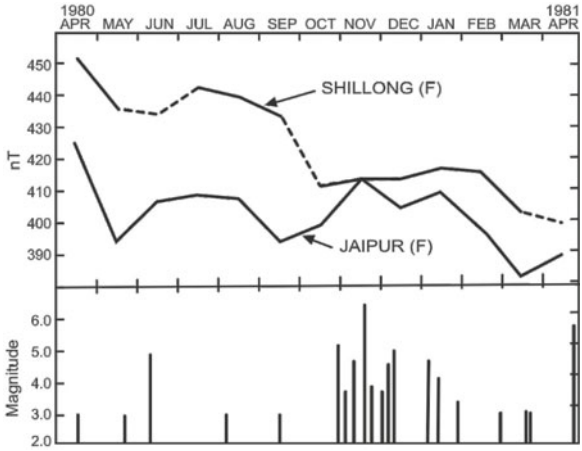

Figure 6.67. Changes of geomagnetic total field (F) at Shillong and Jaipur. The frequency of felt earthquakes during April 1980 to April 1981 is shown at the bottom and monthly variation in F (total geomagnetic field intensity) is shown at the top. Note the tectonomagnetic effect showing a systematic decrease in magnetic field at Shillong prior to earthquake during Sept to Oct 1980 (Chakrabarty, 1984).

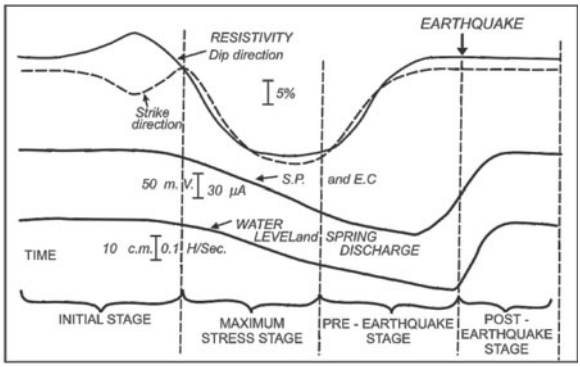

Figure 6.68. General trend of variation of geophysical (electrical resistivity, self potential and Earth current) and geohydrological (water level and spring discharge) parameters with the different stages of earthquake activity associated with M4.2 earthquake on 9 March 1980 near Shillong in NE India (Nayak et al., 1983).

vicinity. The results are compared with Jaipur, a station along the same latitude as Shillong, but differing in LT by one hour. It revealed a depression of the geomagnetic field prior to the shock, when epicentre of the earthquake is not too far away from Shillong (Fig. 6.67). The field change is most likely due to alteration in the crustal stress generated by NE Himalayas.

The geomagnetic field intensity curves for Jaipur and Shillong apparently display similar signatures (Fig. 6.67). However, a significant change in the total geomagnetic field intensity 'F' is observed at Shillong between Sept and Oct 1980. During this period Shillong shows –22 nT change, while Jaipur shows +5 nT change. The anomaly at Shillong is directly attributable to the earthquake occurrences during this interval (Sept-Oct 1980), which includes the largest M6.5 earthquake. Similar changes are also observed during other months as well. These observations thus reveal changes of regional geomagnetic field due to magnetization changes in subcrustal rocks.

Figure 6.68 gives changes in geoelectrical and geohydrological parameters such as electrical resistivity, self potential (S.P.), Earth current (E.C.), spring discharge and water level in dug wells recorded in association with 9 Mar 1980 earthquake (M~4.2) at a site near Shillong. Although precursory changes in all these measured parameters were seen preceding many earthquakes, the strongest precursory change was registered in resistivity, which gradually decreased by 25%. The precursory time in various parameters varied from 7 to 20 days.

III. Sunspot Activity and Earthquakes

Sunspot activity is also monitored to predict the occurrence of an earthquake. The sunspot hypothesis suggests certain changes in Sun-Earth environment affect the EMF that can trigger earthquakes in areas prone to it. During sunspot

activity, a huge mass (or energy) from the outer periphery of the sunspot is hurtled towards the Earth (Chapters 3 and 8). This disturbs the magnetic field and brings about changes in the atmosphere, ionosphere and geosphere. The changes associated with sunspot activity are known to take place typically ~24 to 36 hrs before a moderate earthquake and hence can be utilized to predict earthquakes. Such a change, for example, occurred on 24 Jan 2001 and two days later, a large earthquake measuring M7.7 hit Gujarat (Bhuj; on 26 Jan 2001).

6.30 PALAEOSIESMOLOGY: QUASI-EMPIRICAL EARTHQUAKE PREDICTION TECHNIQUE

'Palaeoseismology' is the study of prehistoric earthquakes in terms of their location (fault dislocation), timing (date) and size (magnitude). The probability of a future earthquake can be worked out, but not accurately predicted. To circumvent this lacuna, geoscientists study earthquakes of the geological past. The instrumental, historical and geological records reveal major quakes to recur after a gap of 100 years or more. The seismographs are not more than century old, which precludes the possibility of instrumental record beyond that timeframe. Historical earthquake records are scanty and do not go beyond 500 years. Religious scriptures have mentions of older earthquakes, but their veracity is difficult to confirm. But the earthquakes that go long back in time have left behind definite tell-tale marks, the study of which forms part of a comparatively new science called 'palaeo-seismology'. These signs are in the form of active faults, shifting of river courses, tilting of rock beds, displacement of strata, liquefaction of sediments (as sand dykes and sand blow), sudden change in sedimentation pattern in lakes and co-seismic land slides.

I. Methodology and Palaeoearthquake Studies

Sedimentary formations are normally deposited as layers and these are deformed if an earthquake occurs. While searching for past earthquakes, geoscientists search for clues that locate and identify deformational features called 'seismites'.

The study and methodology of palaeosiesmology involve identification of seismites, trenching and collecting relevant material for dating, and also cataloguing of stratigraphic sequences. Past earthquakes may generate a series of faults, hence it becomes necessary to ascertain the number of displacements (indicative of past earthquakes), which is done by excavating the trenches across the fault zone. The magnitude of a palaeoquake is judged by the amount of relative fault displacement. The age of the sediments displaced by the fault is then determined using various dating techniques. For example, the sample overlying the undeformed strata gives the minimum age, since it postdates the event. On the other hand, organic material deposited at the time of seismic event along with the deformed strata provides the coeval age, i.e. age pertaining to the palaeoseismic event. ^{14}C dates are then related to the geological signatures

to constrain the time of seismic occurrence along with measurement errors (uncertainties). Relative dating method of magnetostratigraphy is also undertaken to complement direct dating techniques.

Palaeoseimology also involves approximating probable magnitude, apart from estimating the timing of seismic event. The recurrence period of large earthquakes is then reconstructed from a set of events identified in a given area. This information helps in estimating the extent of areal threat experienced by the region in historical past, and serves to make realistic projections to mitigate the hazards.

II. Indian Palaeoseismological Studies

Palaeoseismological studies have recently started in India. An earthquake induced fault in Nainital was dated to 40 ka. Deformational structures (seismites) are mapped from Shillong plateau. The faulting due to M8.7 Shillong earthquake of 12 June 1897 shifted the course of Krishna river. Dated liquefied structures coincided with this earthquake timing. Studies also suggest the area quaked with similar magnitude 500, 1000 and 1500 years BP (1950 is taken as a reference year), suggesting recurrence period of 500 years. Similarly, a few notable studies show Latur was not just rocked for the first time in 1993, but damaging earthquakes had taken place in the area some 200 years ago too. Allah Bund is another palaeoseismological signature due to 1819 Kutch earthquake. Geologists investigating the 2001 Bhuj earthquake found a number of liquefaction features in the form of sand blows, ground fissures, mud craters and subsidence craters. Earthquake occurrences even much before the collision of the Indian and the Asian plate, some 120 Ma ago, have been found in deformational structures from the rocks of Chaibasa formation (2100 to 1600 Ma) of eastern India.

Since instrumental records are short and historical records sparse in India, it is necessary to understand the mechanism responsible for producing

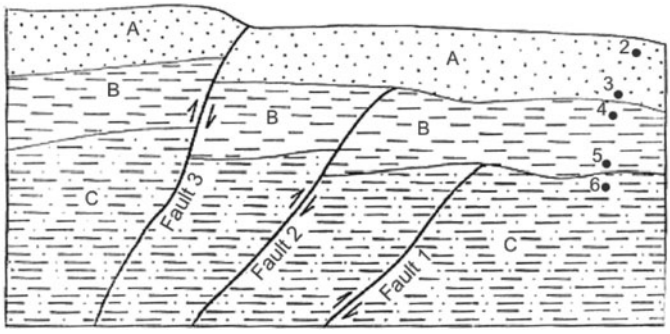

Figure 6.69. Dating faulted deposits. Trench exposure showing displacement of sand and gravel deposits. Fault 1 displaces only unit C, Fault 2 displaces B and C and Fault 3 displaces A, B, and C. Samples of 2, 3 (UB), 4, 5, and 6 (LB) are used for age estimation. UB - Upper bound, LB - Lower bound (Keller and Pinter, 1996).

catastrophic earthquakes and their repeat times from sedimentary sequences. Thus, palaeoseismological studies are of global relevance. Examples of palaeoearthquake age determination and an array of seismites are shown in Figs 6.69-6.72.

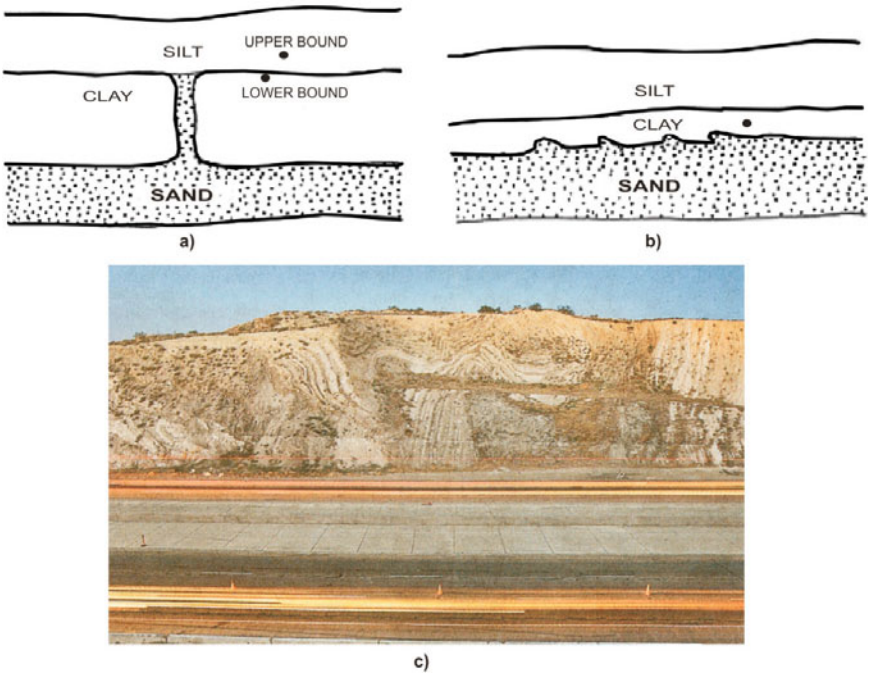

Figure 6.70. Dating of liquefaction features: (a) In case of sand dykes, (b) Penecontemporaneous event, and (c) Layers of earthquake-twisted ground seen at the San Andreas.

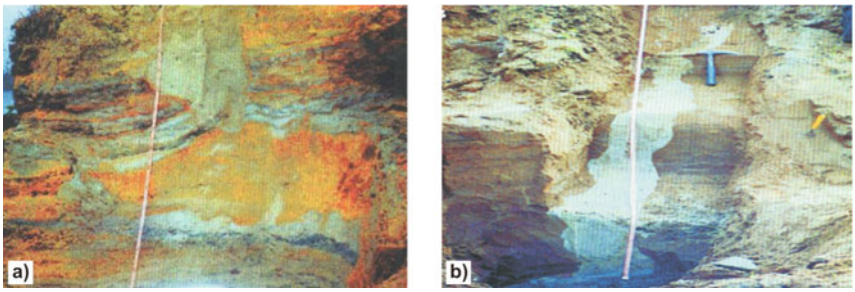

Figure 6.71. (a) Palaeoliquefaction feature at Nayapara site along the Krishna river, Shillong plateau, India. (b) A trench at Beltaghat meander showing multiple sand dykes originating from the sand bed below (Sukhija et al., 1999 a,b,c).

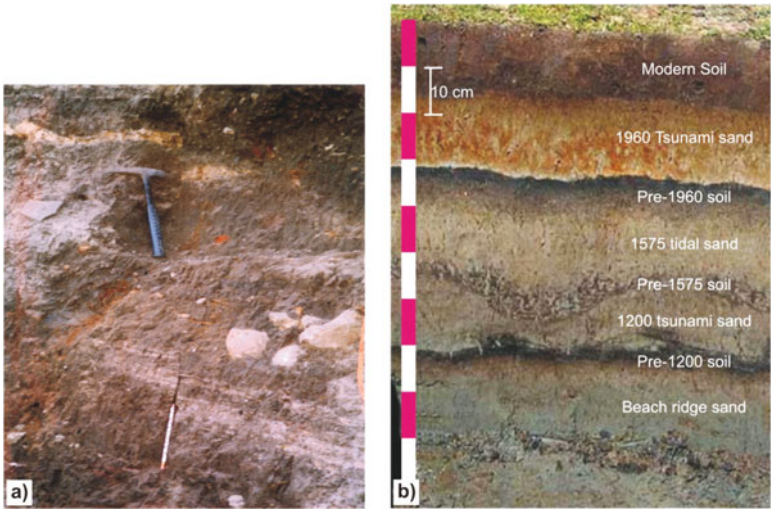

Figure 6.72. (a) A fault observed with a displacement of about 15–25 cm at Ther village, along Terna river. (b) Geological records of tsunamis from lithological field observations at Andaman Nicobar islands. Note that the sediments carried by the tsunami waves have an admixture of offshore and onshore material and are mainly composed of fine to medium sand layers.

6.31 GPS MEASUREMENTS AND GEODYNAMICS

The global positioning system (GPS) designed for military and civilian navigation has become a preferred method to study a wide range of geophysical phenomena. GPS measurements are now used to determine the motion of tectonic plates, deformation around active faults/volcanoes and to measure crustal isostatic adjustments in response to changes (past and present) in the mass of sediments/ice sheets. It is also used in combination with tide gauges to monitor global sea level changes. Because GPS signals are measurably delayed as they pass through the Earth's atmosphere, they are even able to contribute to atmospheric studies.

The tremendous growth in GPS research can be attributed to several reasons. It provides 3D relative positions with the precision of a few mm to a cm over baseline separations of hundreds of metres to thousands of kms. The 3D nature of GPS measurement allows to determine vertical as well as horizontal displacement at the same time and place. Previously, horizontal measurements were often made by trilateration and vertical measurements by spirit levelling. The two data types are almost never collected at the same time and place considerably complicating the analysis. Furthermore, the collective vertical and horizontal information often place more robust constraints on physical processes than do either data type alone. GPS receivers and antennas are portable, operate under essentially all atmospheric conditions, and do not require intervisibility between sites. The level of precision and accuracy are enhanced by using a combination of precise GPS satellite orbit information, dual-

frequency GPS receivers, advanced software packages for post-processing the GPS observations, and multipath-mitigating antennas, to name a few. With such a remarkable development, GPS found its way in the field of geophysics for studying crustal deformation.

GPS technology started out as a military tool. It was initiated in 1970s by the Department of Defense (DoD), and developed later to provide an invaluable navigational service in an alien terrain to save soldiers' time and life. In 1980, this utility was opened to civilian use as well. The remarkable development in space technology, radio science, and the experience with very long baseline interferometry (VLBI) greatly facilitated its development.

I. The GPS Constellation

The first of 24 satellites GPS network called NAVSTAR was launched in 1978. The cluster of NAVSTAR satellites orbits the Earth every 12 hours (twice a day), and emits continuous signals irrespective of weather conditions. These satellites run in a specific orbit, that is ~20,000 km above the ground, and travel as fast as 14,000 km/hr. The satellite orbits are distributed such that a set of at least four satellites are always visible from any point on the Earth at any given instant (with up to 12 visible at one time). Each satellite carries with it an atomic clock that 'ticks' with an accuracy of one nanosec (one billionth of a second). With proper equipment, any user can receive these signals to calculate time, location and velocity. Receivers have been developed for use in aircraft, ships and land vehicles. Portable ones are also available for hand carrying.

The navigation system uses radio frequencies that are sent out by the satellites to locate a transmitter. In this sense, signals transmitted from the satellites are 'trapped' by the GPS receivers, and then the time a signal was transmitted by a satellite is compared with the time it was received. The time difference, if any, tells the GPS receiver its distance from the satellite. With distance measurement from a few more satellites, the receiver determines the user's position and displays it on the unit's electronic map. In order to calculate latitude and longitude, receivers need information from three satellites. But if it has to determine altitude as well, then it has to receive information from four or more satellites. In addition, GPS can also provide other information such as sunset time.

GPS technology has now matured into a resource that goes far beyond its original visualized goals. These days scientists, sportsmen, farmers, soldiers, pilots, surveyors, hikers, delivery drivers, sailors, dispatchers, lumberjacks, fire-fighters, and people from many other walks of life are using GPS in ways that make their work more productive, safer, and sometimes even easier.

II. Principle

GPS satellites transmit synchronized signals on their position and real time (t) to the ground based receiver. The ground receiver however receives the signals

from a given satellite at a time ($t+\delta t$), where δt is the transmission delay between the satellite and the ground station. This delay at ground station is different for signals arriving from different satellites positioned at different places in space. The ground station processor uses these delays to compute its location with reference to the four 'best' satellites. The set of four satellites helps determine the four unknown parameters at the ground station, viz. the three position coordinates in space and the fourth, time. The error of measurement of these parameters is governed by various external parameters, such as the error in the position and time coordinates transmitted by a satellite, the constellation (spatial distribution of the satellites at the time of measurements), the topospheric refraction of the electromagnetic signals, etc.

III. GPS System and Sources of Errors

The GPS system has been designed to be as accurate as possible. But, it still gives out some errors. These errors, when compiled together, cause a deviation of ±50 as 100 m from the actual GPS receiver position. The source of errors is many, but the most significant ones are discussed below:

Atmospheric conditions, also known as ionosphere and troposphere, delay causing an inaccuracy due to reduced speed of propagation. Radio signals travel with the velocity of light in the outer space, but are slower through the ionosphere and troposphere. The GPS system uses a built-in model that calculates an average amount of delay to partially correct for this type of error.

Signal multipath occurs when the GPS signal is reflected off objects such as tall buildings or large rock surfaces before it reaches the receiver. This increases the travel time of signal, thereby causing errors. It is difficult to completely correct multipath error, even in high precision GPS units. Hence, this error has become a serious concern.

Satellite orbits: Although the satellites are positioned in very precise orbits, slight shifts are possible due to gravitation forces. The resulting error is very low, which is not >2 m.

Receiver clock errors: A receiver's built-in clock is not as accurate as the atomic clocks onboard the GPS satellite. Therefore it may have very slight timing errors.

Satellite geometry/shading refers to the relative position of the satellite at any given time. Ideal satellite geometry exists when the satellites are located at wide angles relative to each other. Poor geometry occurs when the satellites are located in a line or in a tight grouping.

6.32 OBSERVATIONAL PROCEDURE

GPS receivers and antennas: The ground-based GPS equipment is only a receiver, without any transmitting capability. The satellites do not contain any

Figure 6.73. GPS unit at Shillong.

database about their location or other parameters. They are equipped with only highly precise atomic clocks that generate some codes, which are transmitted to the Earth. The GPS receiver gets that code from multiple satellites which is slightly time shifted due to difference in the distance to the satellites. Using this difference, the receiver precisely calculates the geographic longitude and latitude of its own position. Indian scientists use both Trimble and Leica GPS receivers for data collection.

A GPS site is chosen such that it has exposed bedrocks with unobstructed view of the sky and a non-reflective environment. About 1 cm diameter and 6 cm deep hole is made into strong and sturdy bedrocks and a non-magnetic stainless steel pin is rigidly driven into the hole. A fine dot of 0.5 mm is made on the pin to aid accurate measurements (Fig. 6.73). Later, 2-channel dual frequency receivers are used in re-occupation mode. Microstripped omni directional (with 9 cm internal ground plate) GPS antenna is placed over the marks (fine dot made on the pin) using tripods. The sampling interval and cut-off angle of elevation (to receive signals from the orbiting satellites) are then fixed at 30 sec and 15^{o}, respectively. However, the sampling interval and cut-off angle of elevation can be changed according to the requirement and needs of the purpose.

6.33 METHODOLOGY, DATA ACQUISITION AND ANALYSIS

GPS satellites transmit signals on two carrier frequencies: the L1 carrier and L2 carrier. L1 carrier is 1575.42 MHz, used for civilian purposes and the L2 carrier is 1227.60 MHz used for more precise military purposes. These signals

travel by line of sight, i.e. they pass through clouds, glass and plastics, but cannot go through most solid objects such as buildings, mountains, etc. In every transmission the satellite sends three types of information: *Pseudo-random code* is an I.S. code that identifies which satellite the information is being sent from. *Ephemeris data* tells the receiver, where the satellite should be at any given time of day. The *Almanac data* is the part that is essential for determining the user's position. Almanac data is constantly transmitted by each satellite, and it contains important information about the status of satellite (healthy or unhealthy), the current date and time.

GPS methodology follows three different approaches: (i) *Estimating the strain field* in seismic zones using GPS receivers: Precise measurement of baselines between well defined ground markers is made. The methodology is such that the changes in position coordinates and baseline lengths in three orthogonal directions (coordinates)—computed with GPS data during two or more visits to the same place or during successive reoccupations—enable to assess crustal deformation in the survey region. Four to five sets of observations are required to estimate the strain field. In addition to the observed strain field, attempts are made to compute strain field for hypothetical stress distribution either by the method of least-square collocation or finite element method. This enables to relate the GPS results to the seismotectonics of the region. (ii) *Establishing certain prerequisites* in high precision geodesy, and (iii) *Establishing the ability of synthetic aperture radar (SAR) interferometry* for deformation measurements: SAR is a new technique in which the phases of two SAR scenes are made to interfere to generate interference fringes which relate to terrain elevations. This technique promises to revolutionize the study of active tectonics by providing high precision deformation measurements carried out remotely from space.

The GPS data is normally organized into 24 hrs covering Greenwich Mean Time (GMT) day. The data are processed using the GAMIT post-process software to produce estimates, and associated covariance matrix of station positions for each session. The site coordinates are constrained by surrounding International GPS Service for Geodynamics (IGS) stations. To get a combined solution for site positions and velocities, all such covariance matrices are input to GLOBK software, which is essentially a Kilman filter that gives the coordinates and velocity vectors at each site. Figure 6.74a shows the horizontal component of the velocity vector with 95% confidence error ellipses. The horizontal components of these velocity vectors are further used to estimate the horizontal strain field by least-squares prediction method in which two empirically deduced local covariance functions (corresponding to E-W and N-S components of horizontal crustal movement in Gaussian form) are used.

6.34 GPS: REPEAT CAMPAIGNS, PERMANENT SITES AND CASE STUDIES

I. Survey Design

GPS networks are operated all over the world to estimate crustal displacements. Permanent networks like CIGNET and the IGS network have proven their utility to the geodetic community for orbit determination, and have also been used for plate tectonic studies. India started GPS in 1995 and since then taken up campaign-style repeat surveys over a period of time in seismically active regions, viz. western Maharashtra, Bhuj, Chamoli, North-East India, Andaman & Nicobar Islands, and Antarctica (here focus is on glacial movements). Continuous GPS (or permanent GPS) monitoring is an essential complement of seismological observations (time unit: sec), and geological (time unit: a ka or a Ma). It is the only technique that can directly measure displacements about a few mm/year over distances of several hundred kms. In view of this, a network of 13 permanent GPS sites are established in different parts of the Indian subcontinent, four in Andaman-Nicobar Islands, and two in east Antarctica region. The GPS data obtained at these stations are used to detect ionospheric TEC perturbations associated with large vertical ground movements related to earthquakes.

II. Seismological Device

Before describing some results obtained with GPS data, its general role of crustal deformation measurements in the study of earthquakes is discussed. Measuring long term current displacements of the crustal blocks in an active zone of deformation like the Himalayas allows to know the amount of energy which accumulates at the active faults, which could be released during earthquakes. These measurements are complementary to seismological data because they document the full earthquake cycle, including interseismic and transient postseismic processes, as well as coseismic deformation. To directly monitor crustal deformation between (interseismic), during (coseismic) and after (postseismic) earthquakes, there are several well established and recognized space-borne geodetic (geodesy is the science of surveying and mapping the Earth's surface) techniques such as VLBI, satellite laser ranging (SLR), SAR interferometry, and GPS. Compared to these techniques, GPS is more widely used in deriving crustal displacement, velocity and strain distribution because its receivers are cost-efficient and highly portable allowing their deployment in large numbers and also in frequently repeating modes as warranted by the deformation status of a particular region. Apart from these factors, post-process softwares, which circumvent purposeful degradation of GPS signals by the DoD to reduce the accuracy and precise orbits from International GNSS Service (IGS), make it ideal to use GPS for geodynamic studies.

GPS data are used to accurately determine horizontal as well as vertical movements to characterize active fault regions, and to determine the position of centroid of the deformation zone. GPS records serve as equivalent tools to very low frequency seismograms. Recently, many countries have developed a way to use GPS satellites to monitor the environment, which could lead to better weather prediction models. They are also trying to develop a system using GPS signals to image things on the ground, measuring soil moisture, and the thickness of ice on the Earth's surface. Few GPS applications in studies of the weak crustal motion, geodynamics (velocity and strain field), and glacial movement are discussed here.

III. Plate Motions and Plate Boundary Deformation

The success of the GPS investigations depends to a large extent on the speed at which the crustal movements occur. In the absence of any significant movements in the crust, the GPS studies may not be conclusive. At present, the Indian continent is subducting below the Eurasian continent at a rate of 4 to 5 cm/yr. This fact has been established by the GPS studies, which have shown that the distance between Bangalore and Hanley (Ladakh) is decreasing at the rate of 4 to 5 cm/year. Thus, GPS data are vital to understand the compressive effects and estimate strain within different crustal blocks, which is possible by taking a NS trending profile across the entire Indian subcontinent.

It is instructive to examine geological and tectonic evidences after the 26 December 2004 Andaman-Sumatra giant earthquake. GPS data from Andaman & Nicobar Islands, nearby IGS sites, and some sites from the Indian subcontinent indicated thtat the south Indian shield shifted towards east by ~1.5 cm, and all the baselines cutting across the India-Burma interface have been shortened by 2-4 cm.

IV. Crustal Deformation in Deccan Trap Region

From GPS data, 2D strain field is estimated and modelled for crustal deformation. GPS has brought out an extensional regime along the western coast of Maharashtra including south of Koyna and Warna reservoirs, which transcend into a region of compressive strain towards the interior of the shield area. The extensional strain regime coincides with the west coast geothermal province, and intersecting fault system south of Koyna-Warna reservoirs. The crustal deformation strain rate has been estimated to be in the range of 40 to 60 mm/year (Fig. 6.74a) with an average of 51 mm/year in N47°E and compressive strain of ~0.4 μ-strain/year (Fig. 6.74b). Strain pattern in the Deccan trap region is a reflection of the transmitted stress field caused by northward continental collision between Indian and Eurasian plates along the Himalayan arc in NS to NNE-SSW direction (Fig. 6.74a).

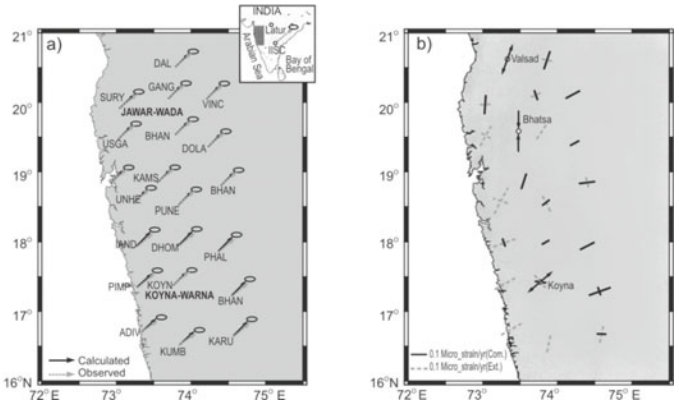

Figure 6.74. (a) Observed and calculated horizontal velocity vectors at 21 sites in Deccan volcanic province. The velocity vector for IGS site IISC (Bangalore) is shown in the inset. (b) Principal axes of strain at GPS sites corresponding to the dilatation strain rate. Note the axes of compressional and extensional strain rates (Reddy et al., 2000).

V. Crustal Deformation in Bhuj Region

Bhuj earthquake affected region is investigated for evaluation of seismotectonics of the region. A compressive strain of ~0.1 μ-strain/year in the epicentral region is established, and the crustal deformation strain rate is estimated to be about 50 mm/year in N-NE direction (Fig. 6.75). The residual velocity of 11.62 mm/year in N-NW direction and 5.24 mm/year towards south is seen at sites south and north of the epicentre. This indicates localized ongoing convergence in the epicentral region. The results also suggest ongoing transpressional deformation across the area with a blocked structure embedded between the north and south Wagad fault. This deformation is believed to be

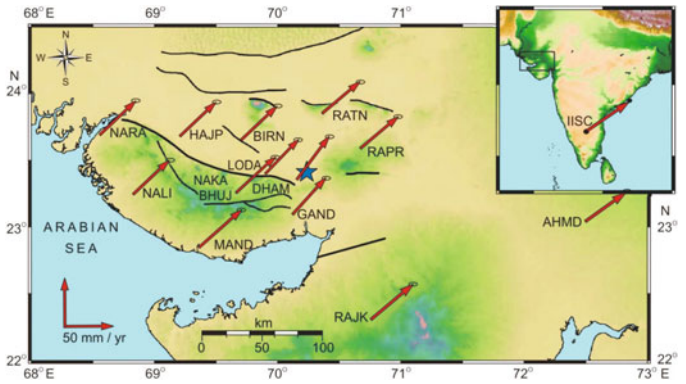

Figure 6.75. GPS derived velocity vectors in ITRF2000 estimates from Bhuj. Star (blue coloured) indicates the 2001 earthquake. The study region and velocity of IISC (IGS site) are shown in inset.

related to the present neotectonic compressive stress regime of the Indian plate due to its NNE movement against the collision front in the north, and its proximity to the triple junction in the western continental margin of the study area.

VI. Antarctic Schirmacher Glacier Movement

GPS studies on ice-sheet dynamics of the Schirmacher glacier (east Antarctica) have revealed that the magnitude of horizontal velocities of the glacier sites lie between 1.89±0.01 m/year and 10.88±0.01 m/year to the N-NE with an average velocity of 6.21±0.01 m/year. The velocity and strain-rate distributions across the GPS network in Schirmacher glacier are spatially correlated with topography, subsurface undulations, fracture zones/crevasses and the partial blockage of the flow of nunataks and the Schirmacher oasis (Fig. 6.76).

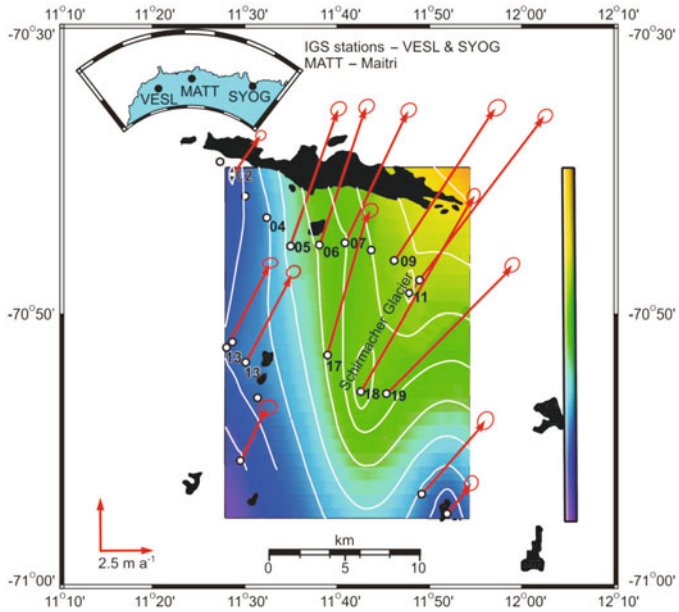

Figure 6.76. Horizontal velocity vectors (with 95% confidence ellipses) for the GPS network on Schirmacher glacier, superposed on a shaded relief velocity–distribution map with 1 m contour interval obtained from the GPS velocity field. The scale represents the glacier flow rate corresponding to the velocity shaded relief (m/yr). The black patches indicate the Schirmacher oasis and nunataks (Sunil et al., 2007).

APPENDIX 6.1

Maxwell's Equations

To understand the propagation and attenuation of electromagnetic waves, it is necessary to use Maxwell's equations relating to electric and magnetic field vectors.

Name	*Differential form*	*Integral form*
Gauss's law	$\nabla \cdot \mathrm{D} = \rho$	$\oint_s \mathrm{D} \cdot d\mathrm{A} = \int_v \rho d\,\mathrm{V}$
Gauss' law for magnetism (absence of magnetic monopoles)	$\nabla \cdot \mathrm{B} = 0$	$\oint_s \mathrm{B} \cdot d\mathrm{A} = 0$
Faraday's law of induction	$\nabla \times \mathrm{E} = -\frac{\partial \mathrm{B}}{\partial t}$	$\oint_\mathrm{C} \mathrm{E} \cdot d\mathrm{I} = -\frac{d}{dt}\int_s B \cdot d\,\mathrm{A}$
Ampère's law (with Maxwell's extension)	$\nabla \times \mathrm{H} = \mathrm{J} + \frac{\partial \mathrm{D}}{\partial t}$	$\oint_\mathrm{C} \mathrm{H} \cdot d\mathrm{I} = \int_s \mathrm{J} \cdot d\,\mathrm{A} + \frac{d}{dt}\int_s \mathrm{D}$

Symbol	**Meaning**	**SI Unit**
E	electric field	V/m
H	magnetic field also called the auxiliary field	A/m
D	electric displacement field also called the electric flux density	C/m^2
B	magnetic flux density also called the magnetic induction also called the magnetic field	Tesla or Wb/m^2
ρ	*free* electric charge density, not including dipole charges bound in a material	C/m^3
J	*free* current density, not including polarization or magnetization currents bound in a material	A/m^2

APPENDIX 6.2

Transfer Function Estimates

The transfer functions showing the relationship between seafloor station horizontal components (X_{SF} and Y_{SF}) and land station horizontal components (X_L and Y_L) are estimated from the magnetic storm and sub-storm (bays) by using tensor analysis. The relationship between the horizontal field components and transfer function is given by

$$X_{SF} = A\,X_L + B\,Y_L$$
$$Y_{SF} = C\,X_L + D\,Y_L$$

where the subscripts SF stands for seafloor station while L for land reference station. The analysis has been carried out in frequency domain. A, B, C, and D are thus the frequency dependant complex numbers and are known as transfer functions, for the north and east components of geomagnetic field variation between land and seafloor station. Transfer functions are computed by using tensor analysis technique. Single station vertical transfer functions are calculated from

$$Z = Txx\,X + Tyy\,Y$$

where X, Y and Z are time varying magnetic fields observed at that particular station. The following assumptions are made in order to calculate the transfer functions: (i) The normal inducing field (X_n,Y_n) is nearly equal to the observed field X and Y, i.e. (X_n,Y_n) = (X,Y) and (ii) in low and middle geomagnetic latitudes the normal Z-component is zero and hence total recorded Z can be taken as wholly anomalous, i.e. $Z_a = Z$.

APPENDIX 6.3

Trembles that Shook Mumbai in the Past

Year	*Month*	*Intensity (MMI)/Magnitude (RS)*
1618	May	IX
1832	Oct	VI
1906	March	VI
1929	February	V
1933	July	V
1951	April	VIII
1966	May	V
1967	April	4.5
1967	June	4.2
1993	September	6.4
1998	May	3.8
2005	March	5.1
2005	June	3.7
2005	August	4.1

APPENDIX 6.4

Major Earthquakes in the History of the Indian Subcontinent

Year	*Location*	*Magnitude*	*Intensity*	*Death Toll*
1618	Mumbai	-	-	2000
1720	Delhi	6.5	-	2000
1737	Bengal	-	-	3000
1803	Mathura	6.5	-	Hundreds, shock felt up to Calcutta
1803	Kumaon	6.5	-	200-300
1819	Kutch, Gujarat	8.0	XI	Thousands, chief towns of Tera, Kathara and Mothala razed to the ground
1828	Srinagar, Kashmir	6.0	-	1000
1833	Bihar	7.7	X	Hundreds
1848	Mt.Abu, Rajasthan	6.0	-	Few people killed
1869	Assam	7.5	-	Affected an area of 2,50,000 sq. miles
1885	Srinagar, Kashmir	7.0	-	1,600
12 June 1897	Shillong	8.7	XII	1600
4 April 1905	Kangra, Himachal	8.0	XI	20,000
1906	Himachal Pradesh	7.0	-	Heavy damage
1916	Nepal	7.5	-	All houses at Dharchula in Pithoragarh, India collapsed
8 July 1918	Assam	7.6	-	Heavy damage
1930	Dhubri, Meghalaya	7.1	IX	Heavy damage in Dhubri
15 August 1934	Northern Bihar-Nepal	8.3	XI	20,000
1935	Quetta, Pakistan	7.5	IX	25,000
26 June 1941	Andaman Islands	8.1	X	Very heavy damage
1947	Dibrugarh	7.8	-	Heavy damage
15 August 1950	Assam	8.6	XII	>1,500
1952	Northeast India	7.5	-	Heavy damage
1956	Bulandshahar, Uttar Pradesh	6.7	VIII	Many killed
1956	Anjar, Gujarat	7.0	VIII	Hundreds of people killed
1958	Kapkote, Uttaranchal	6.3	VIII	Hundreds of people killed

(Contd.)

Year	*Location*	*Magnitude*	*Intensity*	*Death Toll*
10 December 1967	Koyna, Maharashtra	6.5	VIII	200, Koyna Nagar razed to ground
1969	Bhadrachalam, Andhra Pradesh	6.1	I	Moderate damage
19 January 1975	Kinnaur, Himachal Pradesh	6.2	-	42
1980	Dharchula, Uttaranchal	-	-	Heavy damage
1980	Jammu, J&K	-	-	12
1986	Dharamshala, H.P.	5.7	VIII	Heavy damage
1988	Almora, Uttaranchal	-	-	1000
1988	Assam	7.2	XI	Few people killed
21 August 1988	Bihar- Udaypur (Nepal)	6.5	VIII	Large number of people killed
20 October 1991	Uttarkashi, Uttaranchal	6.6	VIII	768, heavy damage to property
30 September 1993	Latur, Osmanabad, Maharashtra	6.4	VIII	>9,000, heavy loss of property
22 May 1997	Jabalpur, Madhya Pradesh	6.0	VIII	40, heavy damage to property
29 March 1999	Chamoli, Uttarakhand	6.8	VIII	100, heavy loss of property
26 January 2001	Bhuj, Gujarat	7.7	X	>20,000, huge devastation
25 October 2005	Mujaffarabad, Pakistan and Kashmir, India	7.6	X	73,000 dead including both countries. Heavy loss of property

7

EXPERIMENTAL GEOMAGNETISM

Experimental geomagnetism deals with experimental observations and their potential applications of palaeomagnetic and environmental magnetic investigations. Palaeomagnetism is a specialized study, which has provided positive evidence of continental drift and development of the hypothesis of plate tectonics. The other major contributions relate to understanding of the generation of EMF, palaeointensity, relative movements of continental blocks, concept of tectonostratigraphic terrains and magnetostratigraphy as a dating tool. All these varied research activities require the development and use of extremely sensitive instruments.

Palaeomagnetic studies, therefore, are of special significance to students of geology and geophysics. The deciphering of India's flight northwards is largely dependent on the acquisition of palaeomagnetic data and their interpretations. The first section covers theoretical aspects as well as experimental details of both rock magnetism and palaeomagnetism. Few examples of application of these techniques are reviewed enabling to understand apparent polar wandering path of the continents, how the magnetic minerals register the palaeolatitude and pole position and how one can de-convolute them in the laboratory.

Initially, the study of magnetism implied certain standard types of measurements such as magnetic susceptibility and remanent magnetization. With the progress in understanding of microscopic processes in natural materials of soils, sediments and rocks, the study of magnetism has considerably diversified leading to new exciting areas like the environmental geomagnetism. It is in this context that the second section of this chapter is devoted to discuss exclusively the rock and environmental geomagnetism, which constitutes one of the major subjects in modern Earth Sciences. The environmental geomagnetism, particularly for the Quaternary studies (last 2 Ma), is considered to be a powerful technique to ascertain the past climate, erosion and pollution. Results obtained from potential applications of magnetic properties or

parameters through investigations of such subjects as the magnetic and chemical constitution of different rocks, sediments and waters from streams and lakes, the measurements of impurities in the atmosphere and water bodies and the reconstruction of environmental and climate change, are discussed in detail here.

7.1 PALAEOMAGNETISM AND GEOMAGNETIC FIELD IN GEOLOGICAL PAST

Even a weak Earth's magnetic field (50 μT) can make a lasting impression on rocks, baked materials and sediments. The fossil magnetism naturally present in a rock is termed the natural remanent magnetization (NRM), whose NRM directions help in recovering EMF history. This forms the subject matter of palaeomagnetism, which started to take up shape in the early 1950's. By 1960, however, it evolved into two separate disciplines referred to as rock magnetism and palaeomagnetism. By producing information about the location and orientation of continents relative to the Earth's magnetic pole, palaeomagnetism has played a significant role in understanding the Earth processes, particularly with regard to continental drift, polar wandering and the development of plate tectonics. As currently practised, palaeomagnetism includes topics related to age dating, stratigraphy and magnetic anomaly interpretation together with traditional topics like tectonics, polar wander, and historical evolutionary EMF studies.

Palaeomagnetic studies suggest EMF has frequently changed and the polarity reversals occurred 24 times during the past 4.5 Ma. It is tentatively concluded that a complete reversal of the EMF takes place in 10^3–10^4 years. The changing pattern of convection currents in the Earth's outer core is generally considered the reason for polarity reversals.

An approximate coincidence of the magnetic axis with the axis of rotation is seen to exist. Accordingly, when there is dislocation of magnetic poles, there is a change in the position of the Earth, and its outer layers with respect to the axis of rotation. Thus, the dislocation of magnetic poles takes place simultaneously with the dislocation of the geographical position, and dislocation of the geographical location influences the climatic regimes of the Earth. The slow variation of EMF at any given place, and also a slow shift in the geographical position of magnetic poles, which are roughly cyclic with a period of ~500 years, is called secular variation. By means of repeated magnetic observations from time to time made at any stations, and MOs, maps and tables can be prepared showing the annual rate of change of geomagnetic field.

I. Direct Measurements and MOs

Magnetic observatory measurements reveal EMF as a transient phenomenon. The field is subject to periodic fluctuations in direction and intensity with rates of change varying from second to thousands of years. At present, the average

annual value of the field is undergoing a regular change known as secular variation (SV), leading to a decrease in its total intensity and inclination. The first known instrumental measurement of declination was carried out by the Chinese, which was far from comprehensive. Global chain of MO measurements is used to determine EMF's past and future changes. Spherical harmonic models are created using data from MOs, satellites and ancient marine logs. There are now models based on direct measurements of geomagnetic field, e.g. London and Paris MOs that extend from ~400 yrs ago to the present (Fig. 7.1). This time span is well short of that required to obtain a valid time-averaged magnetic field, the characteristics of which must be incorporated into any valid theory for the origin of the geomagnetic field.

When SV of the geomagnetic field is averaged out over several thousand years, the field can be modelled as a geocentric axial dipole, i.e. a dipole at the centre of the Earth aligned along the Earth's rotational axis. If this was true throughout the geological past, then palaeomagnetic measurements can be related to geographic position, provided that results are averaged over a sufficiently long time range. This assumption is fundamental to the application of palaeomagnetism to geological and geophysical problems, and is therefore important to examine the characteristics of SV in the geological past and determine its effects on palaeomagnetic measurements. The two techniques, which are used to investigate the SV during pre-observational times, are: (1) archaeomagnetism and (2) palaeomagnetism.

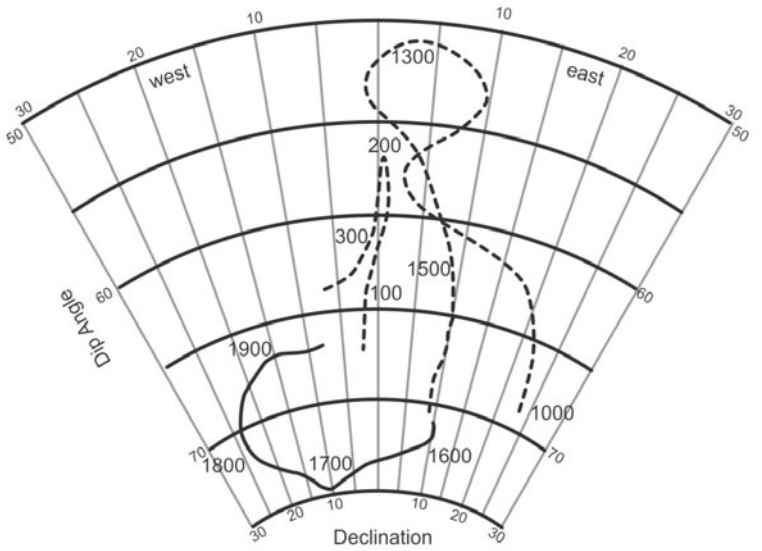

Figure 7.1. A stereographic projection of secular variation of declination and inclination since 1000 at London from observatory (solid curve) and archaeomagnetic (dashed curve) data (*courtesy:* Jacobs, v1, 1987).

II. Historical Indirect Measurements and Archaeomagnetism

As observatory studies of the geomagnetic field only extend back for 400 years, it is only relatively recent 'magnetized' material that can be dated by direct comparison with observatory record. The extension of such records over archaeological time, therefore, requires archaeomagnetic observations based on well-dated magnetized materials. Measurements of the SV during historic time are made using archaeomagnetism; the palaeomagnetism of archaeological specimens. Pottery, kilns and pots acquire thermoremanent magnetization (TRM) parallel to the geomagnetic field existing at the time they are fired. The TRM is the magnetization acquired by magnetic minerals as a result of cooling from a higher temperature ($>T_C$ of the mineral than the normal temperatures). Such magnetization is stable against mechanical, thermal and other external influences. If the objects are found at the actual position of firing, then both the declination and inclination of the palaeomagnetic field can be determined. If the objects are pottery or bricks, not in the position of firing, then only the inclination can be found. By dating the hearths, and hence the magnetizations archaeologically or by radiocarbon methods on associated material, archaeomagnetic measurements yielded results about the properties of the geomagnetic field during the last 30,000 years and a SV pattern up to ~2,000 years for southern India (Fig. 7.2).

Since archaeological materials normally record events such as firing at a specific point and time, most archaeomagnetic records are intermittent in both space and time. Over the past few thousand years, many world civilizations have produced artifacts such as kilns, helping to record the EMF at the place, and time they are baked (Fig. 7.2). However, it is not possible to extend the observations back in geological time using artifacts because such well dated materials closely spaced in time are not available.

III. Geological Past Indirect Measurements and Palaeomagnetism

The history of geomagnetic field can be extended into the geological past through the study of NRM, since natural material can record its ancient direction and intensity. If one can find such materials, reconstruct their palaeo-orientation, measure their remanent magnetization, and date the time of acquisition of the magnetization, then one can trace the geomagnetic field in the past. Palaeomagnetists have assembled a remarkable picture of the ancient geomagnetic field using such fossil remanent magnetizations from many parts of the world, and for ages ranging back to those of the very oldest rocks found on Earth. The materials studied are the youngest lava sequence, sedimentary sequence and rocks.

(i) Remanent magnetism of lava sequences: Volcanic rocks are heated well above the T_C, so the magnetization is free to align with the external magnetic

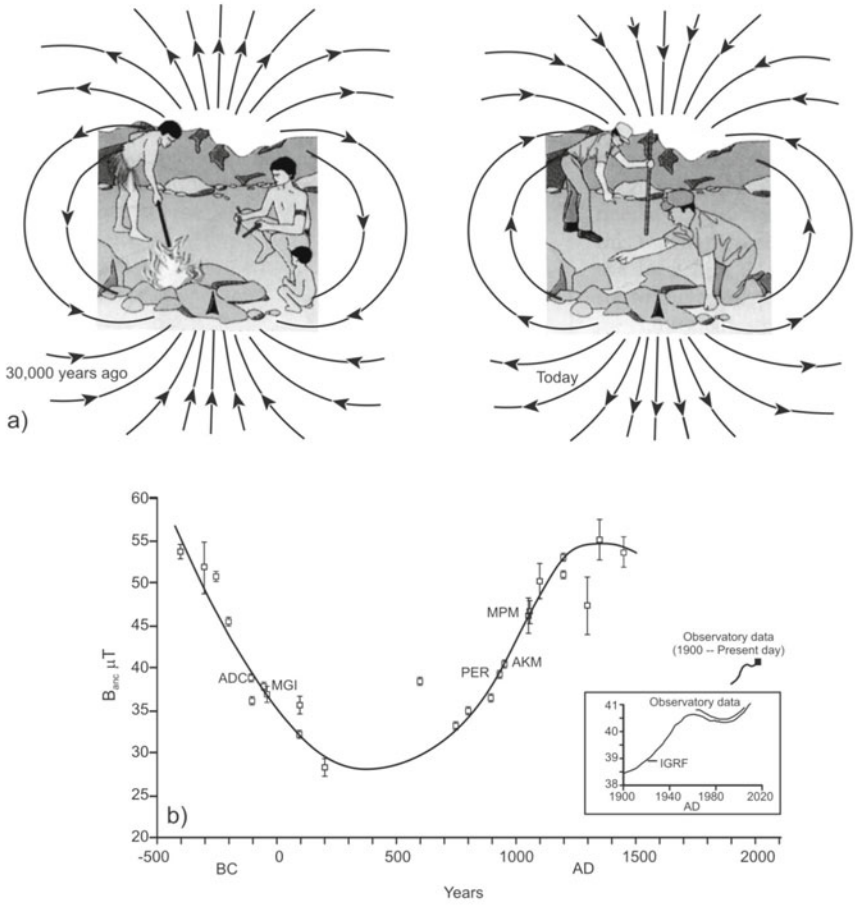

Figure 7.2. (a) Sketch showing reversed and normal patterns of Earth's magnetic field over 30 ka and present times (Press and Siever, 2002). (b) The Tamilnadu palaeointensity secular variation curve estimated using Thellier and modified Shaw methods. Error bars give the standard error of the mean for each site. Inset shows yearly mean intensity of EMF calculated from Annamalainagar and Pondicherry MOs data from 1964 to 2005 together with IGRF model since AD 1900. The horizontal dashed line indicates the present day field intensity (*courtesy:* Ramaswamy and Duraiswamy).

field, and retains it as the rock cools. The processes by which lavas become magnetized are well founded in the theory of TRM. Secular variation of the geomagnetic field may be reflected in small differences in the remanent magnetism of sequential lava flows. The results of measurements on historically dated lavas are used in conjunction with archaeomagnetism for the extension of observatory data. Dating lava flows of the remote past involve errors, which are large in comparison with the SV time scale; therefore in such cases only the sequence of geomagnetic directions can be determined.

(ii) Remanent magnetism of sediment sequences: The magnetic particles of sedimentary rocks align themselves with their magnetic axis parallel to the ambient magnetic field during their process of deposition, and give rise to detrital remanent magnetization (DRM). The magnetization acquisition process is still not well understood, and the role of the complex interplay of processes occurring during deposition, water-sediment interface processes, burial, and compaction requires further analysis (Fig. 7.3a). The magnetic polarity positions of sediments (normal and reversed) represent changes in the direction of EMF at the time of deposition of particles of the sediments. The speed of deposition of marine sediments is estimated to be 0.5 to 3.0 mm/ka. If the rate of sediment deposition is slow, then the DRM of a small sediment sample indicates the geomagnetic field at one instant on the SV timescale. If the deposition is continuous, SV may be represented by an upward variation in remanent magnetism of the sediment sequence. For most sedimentary rocks, as with lava flows, it is difficult to establish an accurate timescale. In the case of varves, however, it is generally assumed that one pair of laminae correspond to the annual deposit. Studies of lake sediments produce palaeomagnetic picture extending the historical documented observations of the geomagnetic field further back in time. The palaeomagnetic directions have discovered field reversals of SVs, possessing periods of 10 ka, and also revealed the essentially dipolar character of the geomagnetic field throughout the time span covered by the geological record. Correlation of $\delta^{18}O$ records with the marine isotopic stages can provide high-resolution age control through a reversal. Such records provide information regarding the age, timing, and duration of polarity transitions.

(iii) Remanent magnetism of rocks and origin of palaeomagnetism: Rocks of all ages with ancient fields 'fossilized' into them are significant sources of palaeomagnetism. The fact that rocks acquire the ambient magnetic field at the time of their formation was recognized by Gilbert in 1600. When solidification process passes through temperature ranges below T_C, magnetic minerals acquire permanent magnetization in the direction of the ambient field (Chapter 2). Magnetite, for instance, acquires magnetization below its T_C (Fig. 7.3b), and this is the 'spot reading' of the Earth's field. This is because the time needed for magnetic minerals to crystallize out of the magma through different temperature ranges is short compared to the time needed for significant changes to occur in the core-generated main field. A series of such extrusive rocks give a series of 'spot readings' of the field. In general, the field recorded this way is the geomagnetic field at that site, and the differences noted between individual 'spot readings' are a measure of the amount of change in the geomagnetic field.

Some researchers have inferred correlations between changes in Earth's orbital parameters, and geomagnetic field variations. The outstanding question concerns the very ancient geomagnetic field. The field is known to have existed for 3.5 Ga, suggesting it is continuously regenerated. However, polarity reversals are documented from as early as 1.5 Ga.

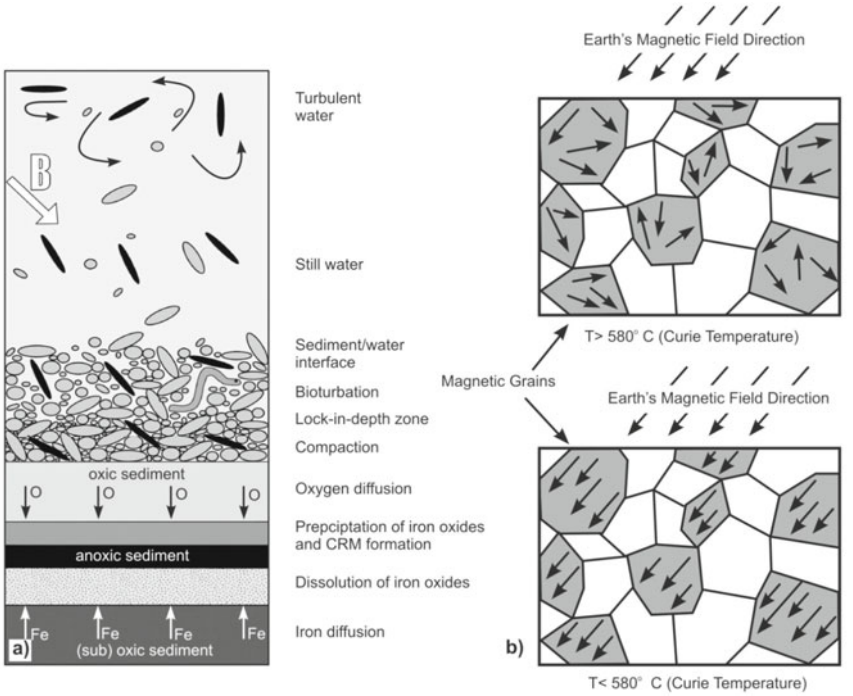

Figure 7.3. (a) Magnetization resulting from sedimentation process referred to as depositional or detrital remanent magnetization (DRM), and chemical remanent magnetization (CRM). (b) Above the Curie point (here for magnetite), atoms take random directions unlike below the Curie point in the presence of an external magnetic field, where domains line up (http://www.phys.uu.nl/~sommer/master/geopotential%20fields/).

IV. The Pioneers Who Shaped Palaeomagnetism

Humboldt was the first to describe magnetism of rocks from a serpentinite outcrop in Germany. Later in 1848, Joseph Fournet wrote a summary entitled 'Glimpses on the magnetism of ores and rocks and on the causes of some anomalies in terrestrial magnetism' providing all experimental procedures and description of magnetic ores and rocks. He prognostically suggested avoiding crystalline rocks in favour of limestone terrain to locate the MO since they affect the instruments and the readings. Delesse experimentally analyzed the magnetism of rocks and minerals, and defined for the first time in 1849, the notion of coercivity. He found coercivity depending on chemical composition, and was zero for soft iron, which increased through the addition of O, S, P, Si, and C to iron. He also deciphered shock sometimes increased magnetic power, and asserted recent lava flows are uniformly magnetized in alignment to the local EMF.

Macedonio Melloni built a very sensitive astatic magnetometer, and established permanent magnetization of 108 different species of volcanic rocks.

According to him, to study the intensity of EMF, the magnetic state of a specimen is important, and not the amount of material. He also explored the origin of TRM by heating and cooling fragments of lava to propose in 1853, 'the general law of permanent magnetization of lavas'. Later on, Sidot in 1868 announced that the direction of magnetization coincides with that of the applied field, and not the crystallographic axes of the material.

Giuseppe Folgheraiter followed Melloni, and showed that Melloni's inferences on Vesuvias lavas can be extended to other rock types also. He in 1894 was the first to distinguish between permanent and induced magnetization, and also first to recognize viscous remanent magnetization (VRM). He showed that on heating, material remagnetizes and transforms hematite to magnetite. He also laid down the foundations of archaeomagnetism by displaying the variations of inclination between 800 BC and 100 AD from Greek and Etruscan vases.

Later, Bernard Brunhes and Pierre David worked on natural bricks baked by overlying lava flow to find their magnetization to be homogeneous, but different from the recent field orientation at the site. This magnetization, they believed to be the EMF at the time when the volcanic flow transformed the clay into brick. Brunhes and David then turned their attention to lavas, since baked clays besides being rare were found to be strongly magnetic, had similar directions, and gave less homogeneous results. From a Royat quarry, they discovered two flows sandwiching a clay layer, wherein the flow at the bottom had a different direction from the overlying clay and flow layer. David also studied trachyte-made flagstones at the temple of Mercury on top of Puy-de-Dome, and found from several samples taken from the same slab dissimilar D, but identical I, helping locate the quarries from where the slabs had been extracted throwing up an archaeological application.

Brunhes discovered magnetic reversals in 1905, when he studied together: (1) an outcrop of basalt flow, and (2) baked clay under that flow near Pontfarein in Cantal, France, to find both having same negative I of –75°. The rocks collected some 100 m away from them, though had different magnetization. He reasoned that the long horizontal layer of metamorphic clay could not have turned upside down, because the lava that cooked it would have found below, and not above, leading conclusively to the concept of magnetic reversals.

Pierre Curie discovered in 1895 that magnetic susceptibility varied inversely with absolute temperature. The fact that TRM in lavas was much more intense than isothermal remanent magnetization (IRM), was discovered in 1909 by George Allen. Paul Langevin published his theory of paramagnetism in 1910, and the theory of ferromagnetism was published in 1911 by Pierre-Ernst Weiss. Further in 1926, Mercanton insisted on the stability of reversed magnetizations for past geological ages in both the hemispheres leading to the understanding of magnetic poles undergoing 'enormous displacements'. This is the first clear statement that workers in the field of palaeomagnetism could demonstrate and measure polar wander, and/or continental drift. He also described the first

magnetostratigraphic section of three reversals in Tertiary lavas. Raymond Chevallier determined SV of D in Sicily based on some 100 blocks from 10 distinct lava flows for the time-frame between 1200 and 1900 AD. Motonori Matuyama of Japan showed for samples from Manchuria and Japan that their magnetizations were arranged in two groups, a Pleistocene being normal (N), and pre-Pleistocene, reversed (R). In 1933, Johann Koenigsberger showed the importance of magnetite and maghemite as carriers of natural remanent magnetization (NRM), and proposed the first theory for TRM that led to formulation of techniques to ascertain confidence in palaeomagnetic measurements.

Emile Thellier's lasting contribution to rock and palaeomagnetic laboratory practice was the development of cleaning methods, and palaeointensity determinations which revealed the differences in behaviour of IRM versus TRM. Thellier used astatic magnetometer to measure the induced and remanent magnetization of baked and unbaked clays as far back as 1932. He also was the one to propose his famous sampling technique for large rocks or archaeomagnetic samples using a cover or 'hat' of Plaster of Paris. He also established the existence of VRM in basalts. Lake sediment studies of palaeosecular variation were undertaken by many scientists like Gustaf Ising who found SVs of 10° in D, and 20° in I when studying lake varves in Sweden dated from a period of ~350 years. Juliette Roquet, in 1954, performed the first systematic study of grain size dependence of TRM. Louis Néel wrote his first paper on ferromagnetism in 1949, and in the same year, John Graham introduced field stability tests, like fold and conglomerate tests. Along the same time, Graham and Torreson developed a very sensitive spinner magnetometer able to measure very weak magnetization.

V. Sampling, Laboratory Experiments and NRM Measurements

The palaeomagnetic method involves: (1) collecting oriented samples, (2) determining their direction of remanent magnetization, (3) confirming the stability of remanence, (4) establishing ChRM, (5) ascertaining characteristic components related to the EMF direction during rock formation, and (6) determining age of ChRM from established palaeomagnetic data with reliable radiometric absolute ages.

(i) Primary and secondary remanence: When magnetic grains alter by oxidation to, for example, hematite, or by oxidation and hydration to minerals such as goethite, the original magnetization is replaced by a later or 'secondary' magnetization in a process called remagnetization. Often, such alteration or weathering leaves some original magnetite untouched, and surrounded by younger oxides or oxyhydroxides. The resulting magnetization is now a composite of ancient ('primary'), and secondary components. In sediments, the primary remanence is usually a DRM acquired when ferromagnetic particles

are aligned in the geomagnetic field during deposition. In sedimentary rocks, dewatering during the prolonged process of lithification usually has enhanced the alignment of these grains with the geomagnetic field to produce a post-depositional detrital magnetization (PDRM). Lightning reaching the ground is capable of inducing magnetization in rocks in a very strong, essentially instantaneous magnetic field. This is called isothermal remanent magnetization (IRM), and can completely obscure the primary remanence. Meteorites are extraterrestrial samples that can acquire a secondary shock remanent magnetization (SRM), both in the event that excavated the material from the parent body, and during impact at arrival on Earth.

(ii) Isolation of NRM components using demagnetization: A major task in all palaeomagnetic investigations is to identify and separate the magnetic components in the NRM using a range of demagnetization and analysis procedures. Hence, the laboratory measurements and the Zijderveld plots arise from the need to separate these different components from each other in a process called stepwise demagnetization. Such alternating field or thermal demagnetization is done in a zero magnetic field, provided by a shielded room, lest the samples acquire a new magnetization during treatment (Fig. 7.4a,b). The MAgnetic VACuum System (MAVACS) used for thermal cleaning, which produces magnetic field free space in a 5-litre volume to an accuracy better than 2 nT is shown in Fig. 7.5. The characteristic remanent magnetization (ChRM) is the earliest acquired component of magnetization that can be isolated. Interestingly, a secondary magnetization need not be thought of as totally useless. In certain situations, a secondary magnetization's direction can be compared with known directions for the geological past, and allows one thereby to date the event that caused the rocks to acquire a secondary component of magnetization. Hence, both primary and secondary components in a rock can record geological events, e.g. the time of formation, metamorphism, or an impact

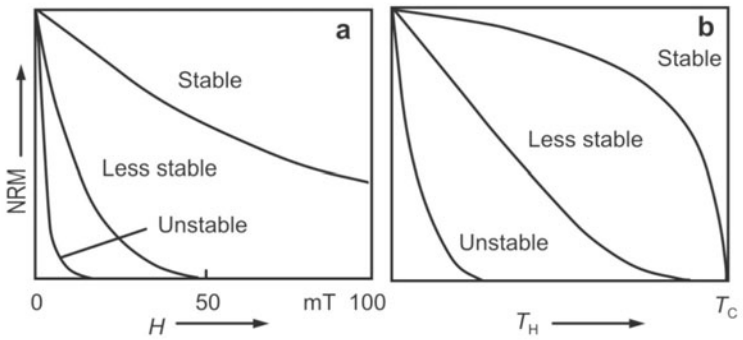

Figure 7.4. Schematic behaviour of a remanent magnetization during: (a) AF (alternating field) demagnetization, and (b) thermal demagnetization. H: maximum intensity of the alternating magnetic field, T_H: maximum heating temperature, T_C: Curie temperature (*courtesy:* Soffel).

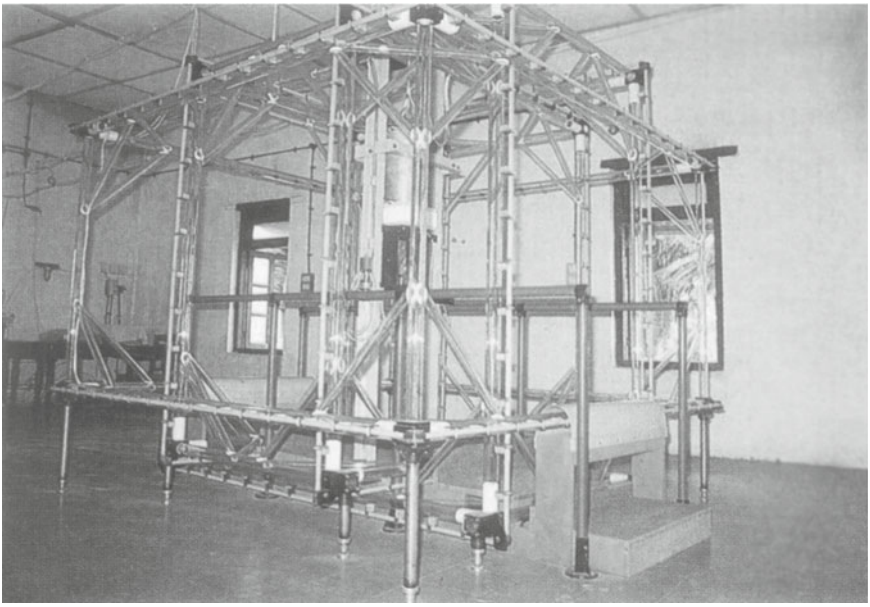

Figure 7.5. The magnetic vacuum system (MAVACS) that creates a 'magnetic vacuum' in which thermal cleaning is carried out to get at the 'primary component' to infer the direction and intensity of the ancient magnetic field.

event, and are of interest in unraveling the geological history. Depending on the intensity, and duration of the events responsible for secondary magnetizations (also known as overprints), the secondary component may partly or completely reset the primary magnetization.

Typically there is also significant effort put in to date the magnetizations so that not only the detection of the magnetic field at that particular sampling site is known, but also the time when the field was in that direction. Many of the successful applications of palaeomagnetism are derived from an effective partnership with geochronology.

(iii) Reliability and improvements in palaeomagnetic analysis: Geological processes like metamorphism during geological history of rock formation may cause remagnetization resulting in the reset of initial magnetization at younger age than the age of rock formation. This leads to erroneous age dating interpretations. A number of tests exist that can constrain the age of magnetization. If a baked contact next to an intrusion has a magnetization that is the same as that of the intrusion (because this baked margin was thermally re-magnetized at the same time as the intrusion was emplaced), and if the host rock far away from the intrusion carries a different magnetization, then this 'positive' contact test provides evidence that the magnetization of the country rock is older than the magnetization in the intrusion. Similar (fold-,

conglomerate-) tests exist in other geometrical situations, and collectively such tests provide several key poles with a high reliability factor. This factor is an invention of Van der Voo, who in the late 1980's felt the need to come up with a parameter that quantified the relative reliability of a given result. It has since become a widely used quality component.

Another assessment method involves the use of electron microscopy. Knowledge about the minerals that are potential carriers of the magnetization is tremendously important as palaeomagnetists try to decide how and when the magnetization was acquired. For magnetite, for instance, its primary nature may be revealed by its titanium content, whereas its magnetic stability can be deduced from the grain size. Grains that are larger than several micrometres (μm) are usually not able to preserve an ancient remanent magnetization. Instead, it is the fine magnetic grains of ~0.05 μm that are important. Such grains cannot be seen with an ordinary microscope, but with scanning and transmission electron microscopy, it is possible to build up the magnetization history of a large variety of rock types. Combined with modern rock magnetic research, these studies have been truly pioneering and promise to become a standard component in future studies.

VI. Palaeomagnetic Data from India

The Indian sub-continent has a northward drift, which can be understood precisely by measurement of stable remanent magnetization of well dated rocks. Palaeomagnetic study of Indian rocks was first carried out by Cleg, Deutch and Blackett. Subsequently, palaeomagnetic measurements of a few Precambrian rocks, Tertiary-Mesozoic formations (Deccan and Rajmahal traps), and Gondwana sediments were carried out. The geographical distribution of various formations studied, and the approximate sampling locations are shown in Fig. 7.6, and their palaeomagnetic data are given in Appendix 7.2.

The scarce data show that there is room for rectifying anomalies regarding: (1) Precambrian results with lack of reliable radiometric ages, (2) large gap of ~45 Ma in the Indian Cretaceous palaeomagnetic data between Rajmahal Traps (110 to 115 Ma), and the Deccan Traps (65 Ma), (3) the precise age, duration, and extent of Deccan magmatism, (4) detailed magnetostratigraphy of Cretaceous basins of the western and eastern parts of India for delineating accurate ages, (5) lack of palaeomagnetic data across different cratons of the Indian sub-continent, (6) establishing Indian sub-continent to be an amalgamation of smaller plates, or a single unit, (7) synclinal rotation of the Himalayas in the NE region, and (8) tectonic and orogenic upliftment of the Himalayas, and the effect on monsoon initiation. In order to address several neglected palaeomagnetic issues, few laboratories were established especially at Allahabad and Navi Mumbai, which are operated by IIG.

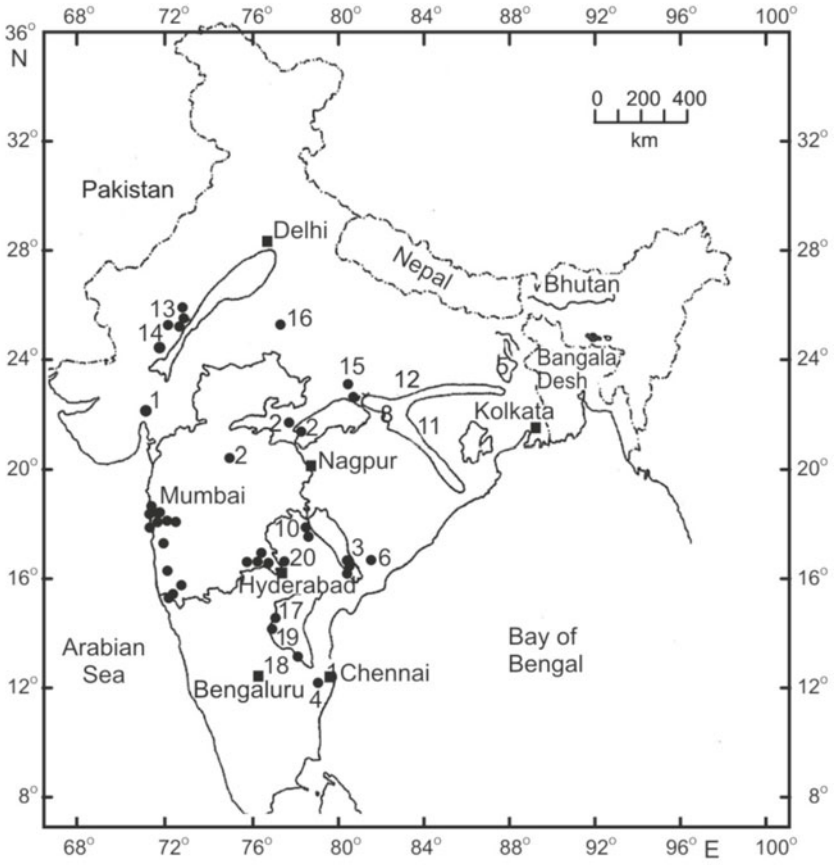

1. Pavagadh
2. Deccan traps
3. Tirupathi sandstones
4. Satyavedu sandstones
5. Rajmahal traps
6. Rajmahendri traps
7. Sylhet traps
8. Dykes from Palamau etc.
9. Parsoa sandstones
10. Kamthi sandstones
11. Himgir sandstones
12. Vindhyan sandstones
13. Malani rhyolites
14. Mundwara complex
15. B.H.Q. and B.H.J.
16. Bijwal traps
17. Veldurti hematites
18. Chitlor dykes
19. Cuddapah sandstones and shales
20. Hyderabad dyke

Figure 7.6. Geographical distribution of the various geological formations used in palaeomagnetic studies and the approximate locations of sampling sites. The sites are classified into Tertiary-Mesozoic volcanic activity, sedimentary rocks belonging to Gondwana system and Precambrian formations based on the ages of rocks studied and the dispersion in their magnetic directions shown in Appendix 7.2 (*courtesy:* Athavale and his coworkers).

7.2 PALAEOLATITUDE, POLE POSITION, APPARENT POLAR WANDER PATH

I. Geocentric Axial Dipole Hypothesis

Palaeomagnetic data analysis mainly deal with: (1) obtaining ChRM related to ancient EMF of a particular sampled rock formation, (2) gaining statistically significant data, (3) determining age of ChRM component, and (4) expressing magnetic field directions in geographical coordinates. For this purpose, some constant feature associated with the geomagnetic field is required to provide a reference system on a geological timescale. This reference system then forms the basis for comparing the palaeomagnetic results obtained from different landmasses. Based on numerous studies on rocks of ages ranging from recent to ~5.0 Ma, it has been found that EMF averaged for a period of 10 ka or more, can be assumed to be due to a geocentric axial dipole (Fig. 7.7a) coinciding with the geographical N-S axis of the Earth. Thus at any point on the surface of the Earth, the time-averaged palaeomagnetic latitude (λ) is equal to the geographic latitude (Fig. 7.7b). This is the most important assumption in palaeomagnetic studies, which enables to compare the pole position of different continental masses of a given age for the reconstruction of their relative orientations in the geological past. This assumption of the existence of geocentric dipole is in contravention to the one made in geomagnetic studies. In geomagnetic studies, the axial dipole field is known to make an angle D. Therefore, palaeomagnetic studies allow the determination of the palaeolatitude of the sampled area from inclination and orientation of the ancient pole (palaeomagnetic pole) from declination and inclination.

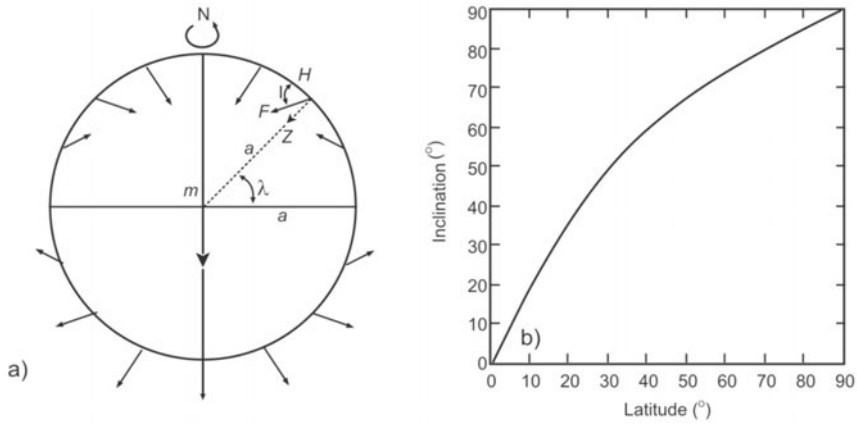

Figure 7.7. (a) The field of a geocentric axial dipole (where m - magnetic moment, a - Earth's radius, H, Z, F - horizontal, vertical components and total field at latitude λ). (b) Variation of inclination with latitude for a geocentric dipole (*courtesy:* McElhinny).

II. Palaeolatitude

The remanent magnetization acquired by either TRM of igneous, CRM of metamorphic or DRM of sediments is parallel to the ambient EMF at the time of their formation. Palaeolatitude can be calculated from the mean inclination of NRM. To find out the latitudinal location, and the polarity of geomagnetic field (N or R) at the time of rock formation (Fig. 7.7c), the equation ($\tan \lambda_s = 0.5 \tan I$) is used. In this equation, λ_s denotes palaeolatitude of the sampling site, and I is the mean inclination of the magnetization acquired in that particular rock formation.

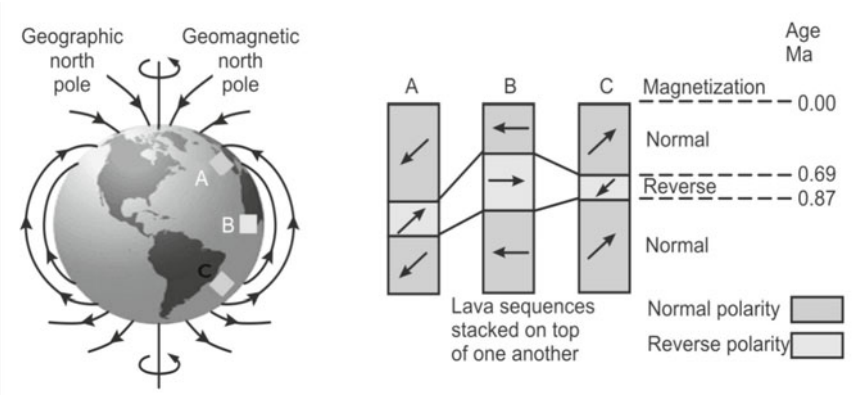

Figure 7.7c. Sketch of lavas (A-C) located at three different latitudes showing normal and reversed magnetizations (http://www.phys.uu.nl/~sommer/master/geopotential%20fields/).

By pooling together the inclination values of the remanent magnetization of Deccan rock samples with those of the dipolar field in Fig. 7.8a, the ancient geographical latitude of India can be determined. For instance, the NRM directions (D and I) of Deccan traps, particularly in terms of their mean inclinations, display variations: 64° upward in Jurassic, 60° upward in Cretaceous, 26° upward in the early Tertiary, and 17° downwards in middle Tertiary (Fig. 7.8a). It must be noted that the upward inclinations indicate the sampling site in the southern hemisphere, whereas downward inclinations suggest the site to be in the northern hemisphere with respect to the present day normal polarity, which can be related to the distribution of inclination of dipolar field at various latitudes of the Earth (Fig. 7.8a). In Fig. 7.8b, the dotted arrow represents the inclination value for Jurassic basalt in India, while the solid arrow represents that of the dipolar field. In order to make the two arrows coincide, one must place India around point *J* in the southern hemisphere. If Mumbai is taken as the reference point, which is today located at 19°N, obviously this must have been located at 40°S in the Jurassic as revealed from Fig. 7.8b. The ancient latitudes for India for four geological periods (Jurassic, Cretaceous, early Tertiary and middle Tertiary) are computed and displayed in

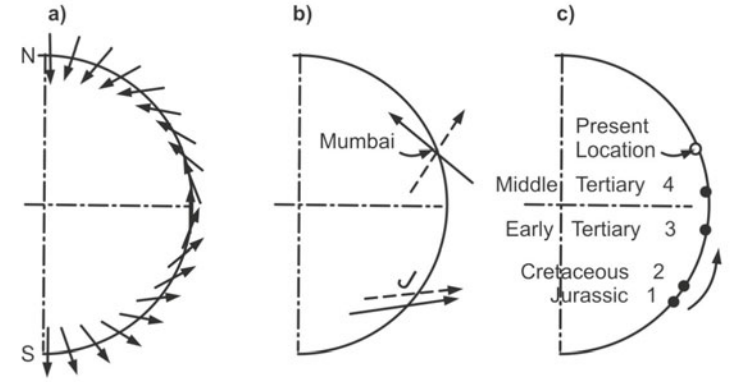

Figure 7.8. (a) Inclination values of the NRM of the dipolar field at various latitudes of the Earth. (b) The dotted arrow represents I value of the Jurassic basalt in India, while the solid arrow represents that of the dipole. In order to make the two arrows coincide, one needs to place India around point J in the southern hemisphere. If Mumbai is taken as reference point which is today located at 19°N, obviously this must have been located at 40°S in the Jurassic. (c) Ancient latitudes for India for other geological periods are computed. Mean inclinations display variations: 64° upward in Jurassic, 60° upward in Cretaceous, 26° upward in the early Tertiary and 17° downwards in middle Tertiary (*courtesy:* Deutsch).

Fig. 7.8c, which clearly shows that India moved northward for ~700 km, perhaps at the rate of a few cm/year since Jurassic.

III. Palaeomagnetic Poles and Apparent Polar Wander Path

The basic criteria for a key palaeomagnetic pole are: (1) *Age of the palaeopole:* The palaeopole should be demonstrated to be primary and the rock-unit precisely and accurately dated. (2) *Quality of the palaeopole:* The primary palaeomagnetic remanence needs properly isolated, secular variation averaged out, and where necessary, correction made for tilting. When the angles of D and I are measured, the position of the palaeomagnetic pole can be calculated (see Appendix 7.1). Table 7.1 shows formation mean directions and calculated pole positions for four sites from A to D. Palaeomagnetic measurements are made on rocks of different geological ages and continental areas with their mean pole positions given in Table 7.2. If palaeomagnetic pole positions are obtained from rocks of different ages on the same continent, these poles can be plotted. Such a plot is called an apparent polar wander path (APWP) (Fig. 7.8d-g) and shows how the magnetic pole moved relative to that continent. If such APWPs from two continents coincide, then the two continents cannot have moved relative to each other during the times shown. However, if the paths differ, there must have been relative motion between the continents. This is because these continents have drifted with respect to each other, as well as relative to the rotation axis of the Earth. Each of the several continents has its own APWP

Table 7.1 Formation mean directions (A to D) and their computed pole positions

Site ID	*Natural Remnant Magnetization (NRM)*				*Site positions*		*Pole positions*	
	Before AF demagnetization		*After AF demagnetization*		*Latitude* λ_s	*Longitude* ϕ_s	*Latitude* λ_p	*Longitude* ϕ_p
	Declination	*Inclination*	*Declination*	*Inclination*	*N*	*E*	*N*	*E*
A	151.3	51.6	155.1	48.7	16.37	73.84	38.0	281.6
B	356.9	–39.8	351.2	-52.5	15.95	74.02	40.2	263.7
C	132.9	68.1	161.8	39.1	19.25	74.83	45.0	279.0
D	317.3	–55.0	300.5	-54.7	20.91	77.86	10.4	303.6

Table 7.2 Position of the north magnetic pole in different periods as determined by palaeomagnetic studies

		North America	*Europe*	*Russian platform*	*Siberian platform*	*Africa*	*South America*	*Australia*	*India*
Tertiary	U	87N, 140E	80N, 157E	78N, 191E	66N, 234E	87N, 152E	82N, 62E	77N, 275E	
	L	85N, 197E	75N, 151E	68N, 192E	57N, 152E	85N, 186E		70N, 306E	
Cretaceous		64N, 187E	86N, 0E	66N, 166E	77N, 176E	61N, 260E	78N, 236E	53N, 329E	22N, 295E
Jurassic		76N, 142E	36N, 50E	65N, 138E		65N, 262E	84N, 256E	48N, 331E	
Triassic		62N, 100E	45N, 143E	51N, 154E	47N, 151E		80N, 71E		20N, 308E
Permian		46N, 117E	45N, 160E	44N, 162E	34N, 144E	27N, 269E	60N, 180E		7S, 304E
Carboniferous	U	37N, 126E	38N, 161E	43N, 168E		46N, 220E		46N, 315E	26S, 312E
	L			22N, 168E		26N, 206E	43N, 151E	73N, 34E	
Devonian		29N, 123E	0N, 136E	36N, 162E	28N, 151E			72N, 174E	
Silurian				28N, 149E	24N, 139E			54N, 91E	
Ordovician		28N, 192E	10N, 176E		25S, 131E	24S, 165E	11S, 143E	2N, 188E	
Cambrian		7N, 140E	22N, 167E	8N, 189E	36S, 127E				28N, 212E

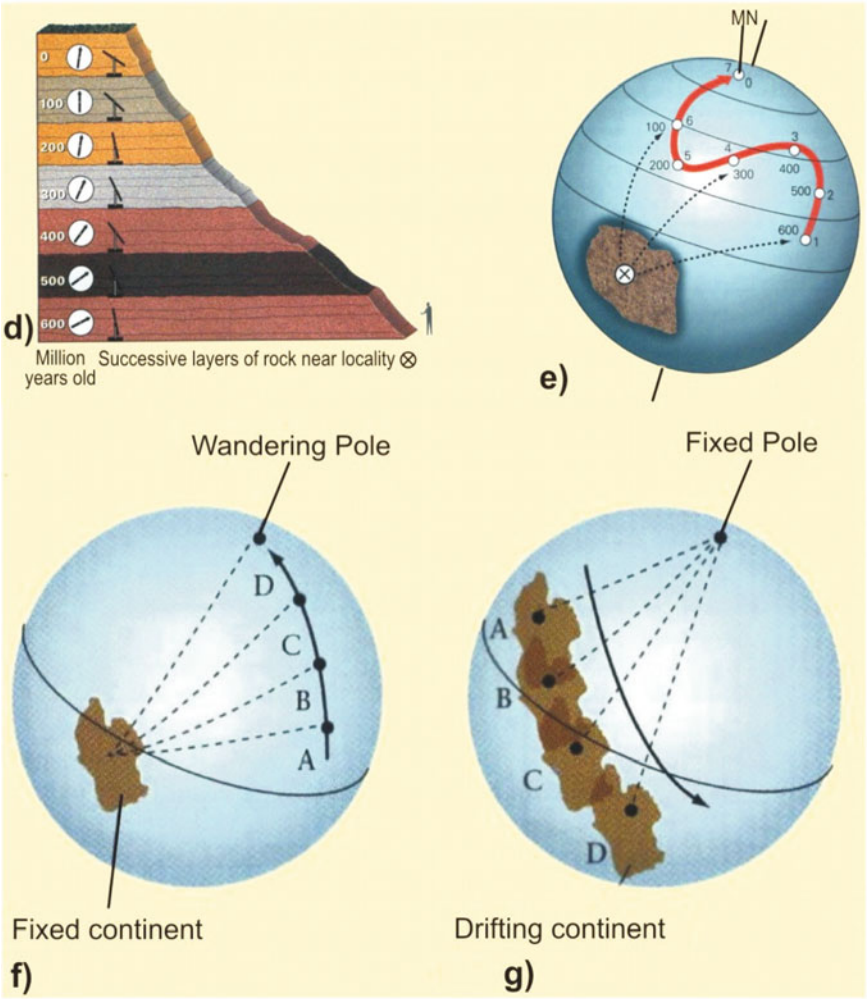

Figure 7.8. (d) Successive rock layers. (e) Movement of poles from 600 Ma to present. (f) APWP derived fixing the continent. (g) Continental drift keeping pole position fixed (http://www.phys.uu.nl/ ~sommer/master/geopotential%20fields/).

curve altogether different from that of other continents, but all converging at the present-day pole. The only plausible alternative, therefore, is that the continents have migrated their position during the geological period. Comparison of APWPs from different continents enables observation of their ancient juxtaposition. Their reconstructions can be compared and improved using palaeontological, geochronological, geomorphological and structural data.

IV. Plate Tectonics

Plate tectonics views the whole Earth as a dynamic system in which internal heat drives lithospheric plates in relative motion with respect to each other

(Chapter 2). Palaeomagnetism enables to view continental movements in the past, viz. changes in latitude and orientation relative to the geographic poles. The worldwide efforts led to the discovery of polarity reversals of the EMF over geological history and thus the realization that the seafloor acts as a tape recorder of the Earth's magnetic reversals and polar wandering (Chapter 2). In particular, the polar wandering is the interpretation given to the observation that the magnetic pole (and the geographic pole) has moved extensively in the geologic past.

According to the GAD model, when averaged over time, magnetic north is geographic north. There are simple relationships between the geographic latitude and the angle I of the EMF, which are applied to plate reconstruction and palaeogeography. Palaeomagnetic data can be used to find latitude and N-S orientation of the palaeocontinents. Palaeolatitude changes calculated from palaeomagnetic data are consistent with palaeoclimatic changes; the distribution of various palaeoclimatic indicators is latitude dependent. Although it is not possible to assign longitudinal position to the palaeocontinents, the relative positions of the continents around the globe can often be pieced together by matching the shapes of APWPs.

There are two principal ways of summarizing palaeomagnetic data for a given region. One approach is to construct palaeogeographic maps of the region for different geologic periods. A much simpler way is to plot successive positions of palaeomagnetic pole for a given continent from epoch to epoch on present latitude-longitude grid. By careful gathering the available palaeomagnetic, geological and geophysical data and integrating them, Earth scientists are testing new hypotheses about smaller scale, intracontinental deformation. It is important to realize the crucial role that palaeomagnetic studies have played in providing the tectonic framework that guides geological investigation and interpretation.

7.3 MAGNETOCHRONOLOGY

Palaeomagnetic dating and graphic correlation methods take advantage of the fact that the EMF varies over time and this variation is recorded by the rocks. The magnetic field has two stages, normal and reversed. One of the most fascinating characteristics of the EMF is that the dipole undergoes complete polarity reversals a few times every million years on average. The intervals between reversals have a stable normal or reversed polarity and are called subchrons, chrons, and superchrons, depending on their duration. Analysis of rocks of increasing age allows to trace the history of the magnetic field and palaeomagnetism can be used as a chronological tool: the polarity, direction and intensity are compared with reference curves and the rock's relative age is derived. Methods and techniques differ according to the age and thus the time resolution needed as described below.

I. Secular Variation Magnetostratigraphy

Earth's field can be divided on a broad spectrum of time variations as shown in Fig. 7.9a. The horizontal scale represents a temporal change, whereas the vertical line height gives relative magnitudes of each type of magnetic field contribution. These temporal intensity and directional changes are due to internal and external sources of field (details in Chapters 1 and 3). Changes in geomagnetic direction useful for dating are of two types; generally assumed to be caused by fluid motion in the core reflecting antiparallel directions (180° of D and opposite sign of I). The first type relates to polarity reversals having periods on the order of 10^6 years, and these polarity intervals are called chrons. There are also short N and R intervals, whose duration lies between 10^4 and 10^5 years, called subchrons. During a polarity reversal, the intensity of the field drops to ~10 to 20%, then increases again. The last one occured ~780 ka ago (Chapter 2, Fig. 7.12). The second type is called secular changes, whose periods are from 10^2 to 10^3 years. These are minor (fleeting) changes in the nondipole part of the field, whose D and I changes to the extent of ~30°, and are recognizable over regions of 'continental extent'.

SV master curves provide rapid means of dating sediment sequences by matching the fluctuations with a previously dated SV record. This approach, however, is much more difficult to apply than that of polarity reversals because: (1) geomagnetic secular variations are not uniformily global, (2) SV records are generally based on lake sediments, which are exceedingly difficult to date

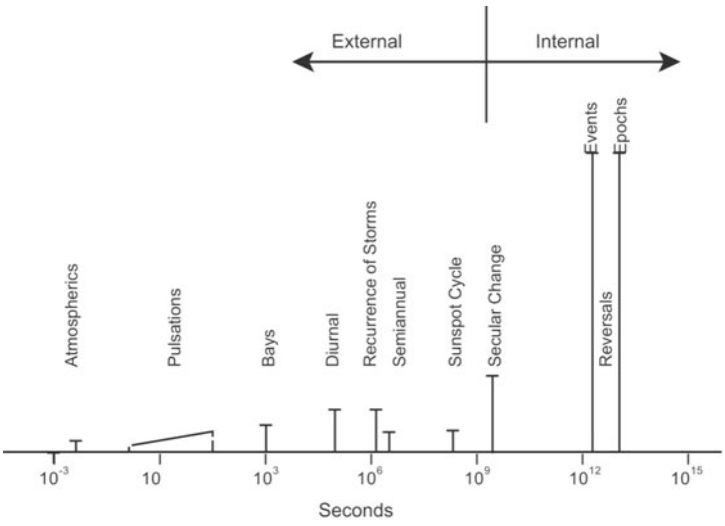

Figure 7.9a. Internal and external temporal changes in the magnetic field observed on the surface of the Earth are represented in this figure. The amplitudes of the shorter-period changes are exaggerated relative to the secular change and reversals (http://www.grisda.org/origins/10018.htm).

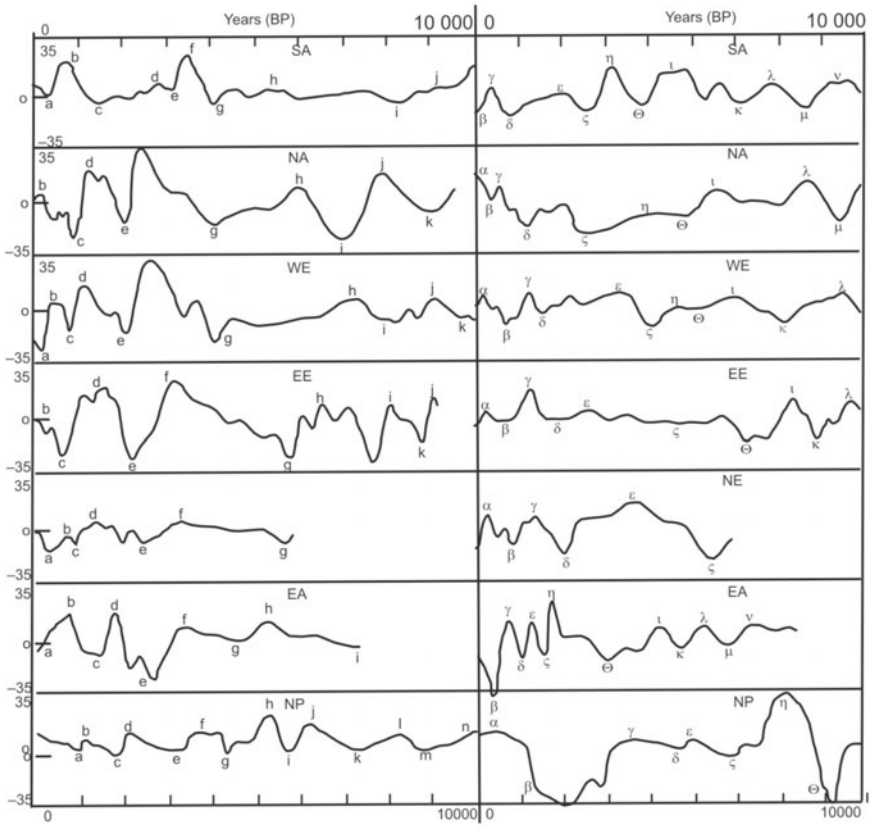

Figure 7.9b. Regional Holocene declination and inclination master curves for South Australia, SA; North America, NA; western Europe, WE; eastern Europe, EE; Near East, NE; East Asia, EA and north Pacific, NP. Curves based on data from different sources given in Thompson and Oldfield, 1986.

with better than 10% accuracy, and (3) SV patterns with amplitudes of ~20° are more susceptible to noise than polarity changes of 180°. Secular I fluctuations are large and significant at low latitudes, whereas secular D changes are prominent at high latitudes, hence are used for dating purposes in the respective regions (Fig. 7.9b, Table 7.3). The SV records of both D and I from seven regions of the world (Fig. 7.3b) are useful for dating applications of magnetostratigraphy within the past 10 ka. These patterns of SV can be used as master curves for dating newly acquired palaeomagnetic records.

Sediments and volcanic rock record several types of magnetic archive of interest to palaeolimnologists. At the longest timescales, a record of polarity reversals is preserved and identified in lake deposits, providing absolute age information. However, the binary nature of magnetic reversals (N or R) implies that some independent means need to be employed to infer polarity transition in a particular sequence of lake beds. In practice, this is usually done by cross-

correlation with some other source of age information such as biostratigraphical or radiometric dates (Table 7.3).

Table 7.3. Ages of magnetostratigraphic features (Thompson and Oldfield, 1986)

	*SA**	*NA*	*WE*	*EE*	*NE*	*EA*	*NP*
Declination							
a[Ψ]	300	-	140	160	220	0	900
b	680	100	450	300	700	700	1100
c	1300	750	600	600	850	1200	1800
d	2000	1200	1000	1400	1300	1650	2150
e	2800	2000	2000	2200	1900	2200	3200
f	3500	2400	2600	3100	2100	3100	3900
g	4500	4000	4900	5700	2400	4400	4400
h	5500	5900	7100	6500	3200	5100	5300
i	8300	7000	8300	7600	5600	7300	5600
j	9000	7900	9100	8000	-	-	6000
k	-	9000	10000	8700	-	-	8350
l	-	-	-	9000	-	-	8900
Inclination							
α	-	50	240	300	300	-	200
β	-	420	650	600	550	400	2150
γ	400	750	1150	1300	700	760	3500
δ	900	1200	1650	1900	900	1000	4700
ε	1900	2300	3100	2600	1400	1300	5100
ς	2600	2900	3800	4600	2000	1550	5800
η	3200	3700	4300	5500	3600	1750	7000
θ	3600	4400	5000	6400	5300	2800	8200
ι	4600	5300	6000	7200	-	4100	8950
κ	6000	6600	7100	7800	-	4600	9800
λ	6800	7700	8300	8600	-	5100	-
μ	7900	8400	8800	-	-	5600	-
ν	8600	9600	9700	-	-	6600	-
ξ	10000	-	-	-	-	-	-

* SA South Australia (35°S 140°E) based on Barton and McElhinny (1981)
NA North America (45°N 90°W) based on Banerjee et al. (1979)
WE Western Europe (55°N 05°W) based on Turner and Thompson (1981)
EE Eastern Europe (60°N 30°E) based on Huttunen and Stober (1980)
NE Near East (30°N 35°E) based on Thompson et al. (1985)
EA Eastern Asia (35°N 140°E) based on Horie et al. (1980)
NP North Pacific (20°N 155°W) based on McWilliams et al. (1982)

[Ψ] a to l declination turning points. α to ξ inclination turning points. Ages tabulated in calibrated ^{14}C years BP. The EA ages are rather poorly known, based here on a linear interpolation between the basal tephra layer and the archaeomagnetic features preserved in the upper sediments. Errors in ^{14}C ages at all the sites possibly amount to several hundred years. Labelling of the palaeomagnetic features is purely for convenience of reference. Any likenesses in ages or in shapes of similarly labelled features are probably chance occurrences, unlikely to be duplicated in other parts of the world.

II. Magnetostratigraphy and Geomagnetic Polarity Timescale (GPTS)

Magnetostratigraphy refers to the description, correlation, and dating of rock sequences by means of magnetic polarity reversals. Remanent magnetic moments measured on field-oriented rock specimens along sedimentary strata enable to determine polarity reversals of EMF during the time interval of deposition of those particular sedimentary strata called magnetostratigraphy. One of the most fascinating characteristics of the EMF is that the dipole undergoes complete polarity reversals a few times every million years on average. The intervals between reversals have a stable normal or reversed polarity and are called subchrons, chrons, and superchrons, depending on their duration. They define characteristic pattern of polarity zones through time and, as such, form a fundamental tool for dating of the geological record: the geomagnetic polarity time scale (GPTS).

In a sequence of rock formations, each polarity intervals are called magnetozones. Magnetozones of alternating polarity yield magnetic polarity stratigraphy. This form of magnetostratigraphy plays an important role in the construction of GPTS. The association of radiometric ages with key biostratigraphic stage boundaries, which are correlated by magnetostratigraphy to the marine polarity record, yields a dated GPTS.

Exact stratigraphic correlation of normally, and reversely magnetized strata from all over the world assumes significance. The potassium-argon (K-Ar) technique has made it possible to precisely date volcanic rocks of known polarities helping to compare polarity patterns in a stratigraphic column to define its age. This is therefore an indirect dating method, since recognition of polarity reversals alone does not provide an estimate of age. Palaeontological analyses based on ammonites, foraminifera, or nanofossils define a biostratigraphy that is tied to the magnetostratigraphy.

Since continental volcanic activity is essentially an intermittent process, a continuous sequence of the entire history of polarity changes is not possible. However, marine magnetic anomalies at the mid-oceanic ridges give a continuous pattern, and order of polarity reversals from Mesozoic (~200 Ma) to the present. The age of polarity reversals is determined from the sea-floor spreading model, and age of marine magnetic anomalies on the basis of hypothesis of Vine and Matthews. The extrapolation of this timescale enables isochrons to be drawn on the ocean floor up to 2000 to 3000 km from the ridge axis. This permits correlation of anomalies of specific number, and age from one ocean to the other helping to erect a Mesozoic-Cenozoic polarity timescale.

Microfossils also help in establishing polarity timescale. For example, to test the polarity chron 25 (this pertains to marine magnetic anomaly numbering system) of early Palaeocene age, a core is drilled through the sediment containing marine magnetic anomaly 25. This core when studied should contain microfossils of the same age (early Paleocene) as determined from magnetic

anomalies. Palaeontological dating of deep sea sediment cores puts a strong constraint on the polarity timescale. A polarity superchron for Phanerozoic and Proterozoic is given in Fig. 7.10.

To use a geomagnetic timescale to date the oceanic plates, it is necessary to recognize specific anomalies. The prominent anomalies up to age 83 Ma are numbered from one to thirty-three. For ages 125-162 Ma, they are labelled with the prefix M (M standing for Mesozoic). Particularly prominent is the long magnetic quiet zone in the Cretaceous (83-124 Ma numbered C34), during which no reversals occurred. Information for construction of GPTS is lacking for older periods (oldest oceanic crust that still exists is ~200 Ma), and hence determination of polarity timescale beyond 200 Ma has to be done through palaeomagnetic studies from the continental rocks alone. Nevertheless, several attempts have been made to set up polarity timescales of earlier periods including the Precambrian. The best known features of the polarity timescale for the Paleozoic are the Permo-Carboniferous R-superchron, R-superchron in the Devonian, and N-superchron in the late Ordovician and early Silurian (Fig. 7.10). Schmidt and Embeleton recognize that a common APWP can be drawn

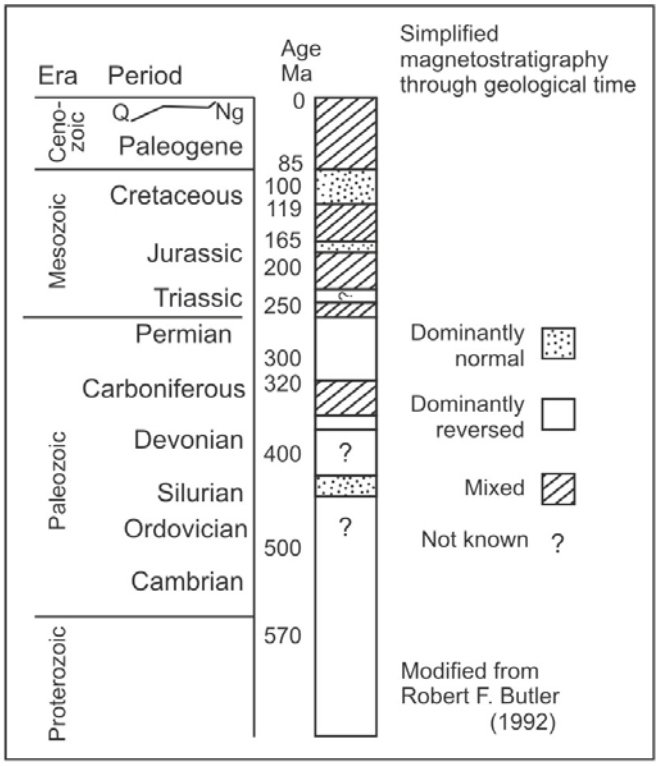

Figure 7.10. Simplified magnetostratigraphy through geological time scale modified from Butler, 1992. This is used to understand the pattern of polarity reversals from the Paleozoic and Proterozoic eras.

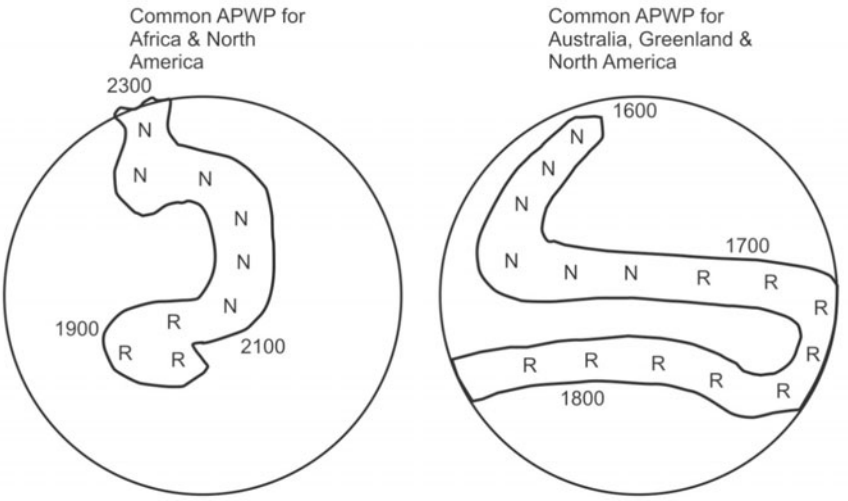

Figure 7.11. Simplified figure from Schmidt and Embleton (1981). N-poles with normal polarity, R-poles with reversed polarity.

for Africa, Australia, Greenland and north America. They have shown that the N-polarities predominate from 2300 Ma to ~2100 Ma (Fig. 7.11). From 2100 to ~1650 Ma, the R-polarities are common. N-polarities again become the norm from 1650 Ma onwards. Halls in 1991 reported from Matachewa dyke swarm of Canada, the oldest known magnetic reversal to have occurred at 2452 Ma ago.

III. Application of GPTS for the past 6.0 Ma

The polarity timescale of the last ~5.0 Ma has been established by compiling palaeomagnetic data of known K-Ar or biostratigraphic ages. Allan Cox and Richard Doell have built a well defined polarity timescale comprising epochs and events (Fig. 7.12). The optimum GPTS is the CK95 timescale, which adjusts for Earth's orbital variations and climatic responses published in 1995 by Cande and Kent. Significant periods of time marked by consistent orientations of the EMF are called epochs (it is the same term used for the smallest division of the geological timescale, e.g. Pliocene epoch). Epochs come in two states (Fig. 7.11) of N and R. Unfortunately, it is impossible to extend the polarity timescale beyond 4.5 Ma, because of inaccurate dating. Within the Brunhes normal polarity epoch, which began 0.78 Ma ago, many have identified temporary reversals and major polarity fluctuations, termed excursions such as 272 ka (Biwa II), 187–192 ka (Biwa I), 110–120 ka (Blake), 40–45 ka (Laschamp), 25–30 ka (Mono lake), 10 to 12 ka (Gothenburg) and ~2.8 ka (Starno). Short-term variations of the magnetic field are also used for dating during the last few hundred ka.

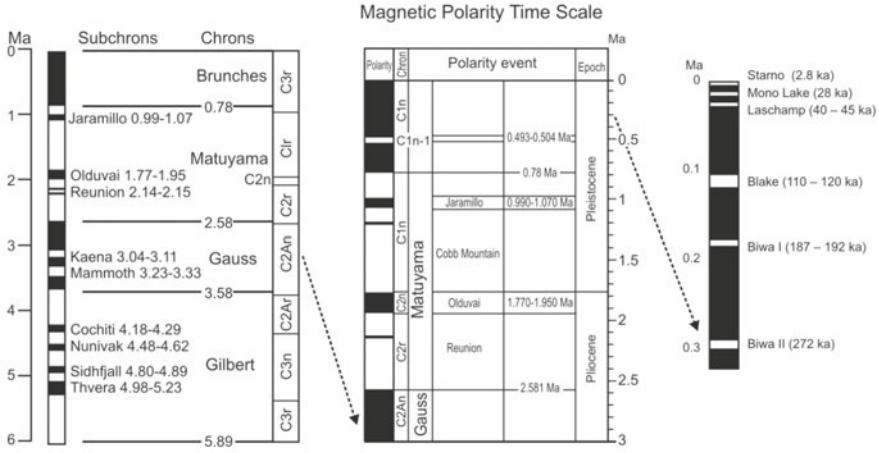

Figure 7.12. Details of the recent reversals of the Earth's magnetic field as determined from detailed radiometric dating of continental and oceanic island lavas and palaeomagnetism of marine sediments. Simplified geomagnetic polarity time scale with focus on Quaternary magnetostratigraphy (Cande and Kent, 1995). Epochs (chrons) have been named after prominent scientists (e.g. Gilbert, Gauss, Bruhnes, Gauss) and events (subchrons) are named after their location found (e.g. Olduvai George, Tanzania, the site of early hominid discoveries of Leakey; Mammoth, California, USA and Jaramilo creek, New Mexico, USA). This scale may not yet be completed; many short events remain to be firmly established.

7.4 IMPLICATIONS OF PALAEOMAGNETIC RESULTS

Study Areas: Palaeomagnetic studies have been carried out (on): (1) dyke swarms of the Deccan volcanic province (~65 Ma) in the Dhule district of Maharashtra, (2) magmatic rocks occurring in Kutch rift basin, Gujarat, (3) middle to upper Cretaceous (~100 Ma) sediments of the Bagh group in the Man valley of Madhya Pradesh, (4) dolerite dykes and Closepet granite in the Archaean terrain of south India, (5) Eocene (~55 Ma) sediments of the Tapti river section in the Cambay basin of the Gujarat, and (6) magnetostratigraphy of Tertiary sequence of Machhial-Neri river section, Himachal Pradesh. Magnetostratigraphic screening of sedimentary formations covering the entire Cretaceous period in the western part of Narmada basin infers their magnetization/remagnetization ages, and related tectonic and geophysical implications. The salient features of the studies are as follows:

I. Dyke Swarms of Deccan Volcanic Province

Dykes present south of Narmada river and Mumbai region have yielded pole positions similar to the Deccan Super Pole (40°N, 79°W) shown in Fig. 7.13a. These intrusions are affiliated to the massive Deccan extrusion that took place ~65 Ma ago, which spanned a short duration of just <0.5 Ma. The studies also

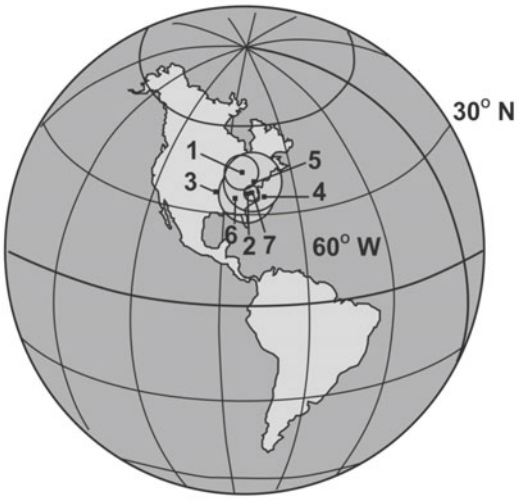

Figure 7.13a. Palaeomagnetic pole positions of the Deccan trap related dykes and the Deccan Super Pole. Note dyke intrusions are affiliated to the Deccan extrusion, which spanned a short duration of just <0.5 Ma. (1) Murud dykes, (2) Dhadgaon dykes, (3) and (4) Mandaleshwar dykes, (5) Goa dykes, (6) North Kerala dykes and (7) Deccan Super Pole.

indicate post-trappean dyke swarms which possibly coincide with the opening of Arabian sea, and rifting of the Seychelles-Mascarene oceanic plateau.

II. Tholeiites and Alkali Basalts of the Kutch Rift Basin

Palaeomagnetic results of 30 magmatic bodies of Kutch, Gujarat yielded a VGP pole at 33.7°N and 81.2°W (d_P/d_m= 5.81/9.18), which is statistically concordant with that of the Deccan Super Pole (36.9°N and 78.7°W). The magmatic rocks of the Kutch basin are broadly contemporaneous straddling 30N-29R-29N chrons. It is suggested that the magmatic rocks of Kutch were generated by the impact of the Reunion plume on the Kutch lithosphere under extensional setting (Fig. 7.13b).

III. Cretaceous Bagh Group Sediments: Pervasive Deccan Remagnetization

The mid to upper Cretaceous intra-trappean Bagh sediments in the Man river valley of Narmada basin in Dhar District, Madhya Pradesh have their pole position near the late Cretaceous segment of the Indian APWP (Fig. 7.14a). It is concordant with other poles reported from the Deccan basalt flows, and also with dated deep sea cores of the Indian ocean. The study has further revealed that these sediments were subjected to large scale remagnetization due to igneous activity of Deccan basalt effusion. Since Andaman sediments are far away

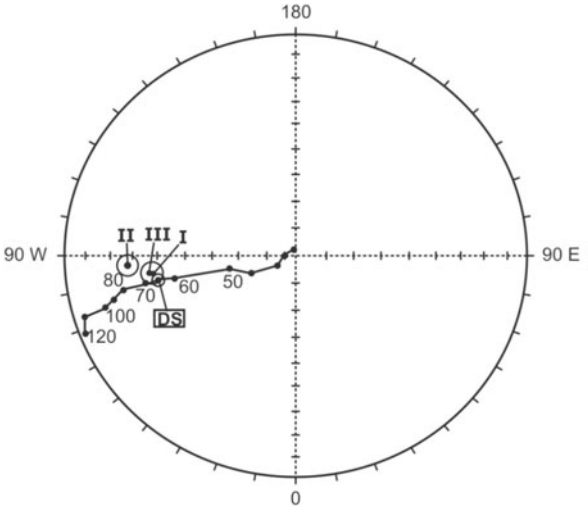

Figure 7.13b. Groups I, II and III Kutch magmatic bodies, and Deccan Super pole (DS) virtual geomagnetic poles (VGP) are plotted along with synthetic APWP for India. Group I: Tholeiites and gabbroic dykes of Kutch mainland, Group II: Alkali basalt plugs of Kutch mainland and Group III: Magmatic rocks of northern Island belt (*courtesy:* Paul et al.).

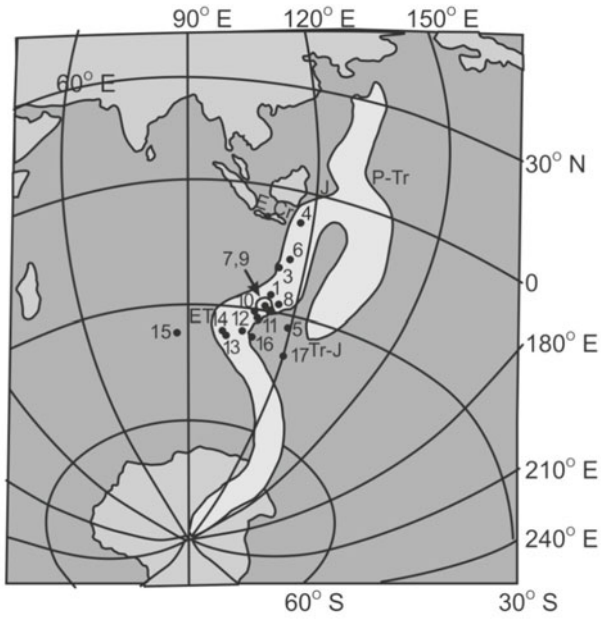

Figure 7.14a. Palaeopoles obtained for different rocks of Cretaceous age. The swath, in greyish white, is the APWP suggested for India and Pakistan (*courtesy:* Prasad et al.).

from the Deccan influence, Bagh sediments can give reliable palaeomagnetic and magnetostratigraphic results in Cretaceous period for the Indian subcontinent. The results also revealed that the Indian subcontinent experienced counterclockwise rotation by 13°±3° and a latitudinal northward drift by 3°±3° during Deccan volcanism.

IV. Eocene Sediments of the Cambay Basin

The middle to upper Eocene sediments of Tapti river section near the village of Bodhan (21°18′ N; 73°3′ E), in Gujarat showed a mismatch with Tertiary part of the standard APWP. Two pole positions are displaced east of the APWP, which suggests a clockwise rotation of ~65° of the sampled area. The two rotated poles are almost coincident, and agree reasonably well with the APWP, the displacement being 10° towards the younger side of the polar path. The discrepancy arises due to steeper inclinations observed in the rock samples, than was expected at the sampling locality according to the relevant portion of the APWP.

V. Proterozoic Dykes of the South Indian Granulite Terrain

Palaeomagnetic results on Proterozoic dolerite dykes from the granite greenstone terrain (GGT) are similar to the adjacent Tiruvannamalai dykes from the adjoining south Indian granulite terrain (SIGT). Thus, there was no relative movement, at least since 1600 Ma ago, between the GGT and SIGT. The palaeomagnetic directions of basement rocks to these dykes showed an age of ~1100-1000 Ma due to partial remagnetization/streaking that occurred probably during eastern ghats orogeny (EGO). Anorthosite rocks at Oddanchatram from SIGT have yielded two magnetic components: (1) corresponding to ~1100 to 1000 Ma reflecting the vestiges of EGO, and (2) ~550 Ma corresponding to the Pan-African thermal event that has prominently affected part of the SIGT.

VI. Magnetostratigraphy of the Tertiary Sequence

The magnetostratigraphic investigations on the ~5-km thick sedimentary sequence of Himachal Pradesh Machhial-Neri section yielded 12-N and 12-R polarity magnetozones. The graphical comparison of prepared magnetic polarity scale (MPS) is compared with standard GPTS within chrons 5AAr to 6r. The sediment deposition is found to have occurred within a span of ~7-Ma, ranging in age from 20 to ~13 Ma with an average sedimentation rate of ~63 cm kyr^{-1}.

VII. Magnetostratigraphy of the Karewa Palaeolake Sediments

The Karewa (in Kashmir) lake deposits are in the northwest Himalaya, which is an intermontane basin presently experiencing rapid uplift along its southwestern margin. Karewa sediment profile contains a unique climatic record

of a series of climatic oscillations, comprising glacials, interglacials and interstadials. Rock magnetic studies reveal titanomagnetite, magnetite and hematite are the main carrier of characteristic remanent magnetization.

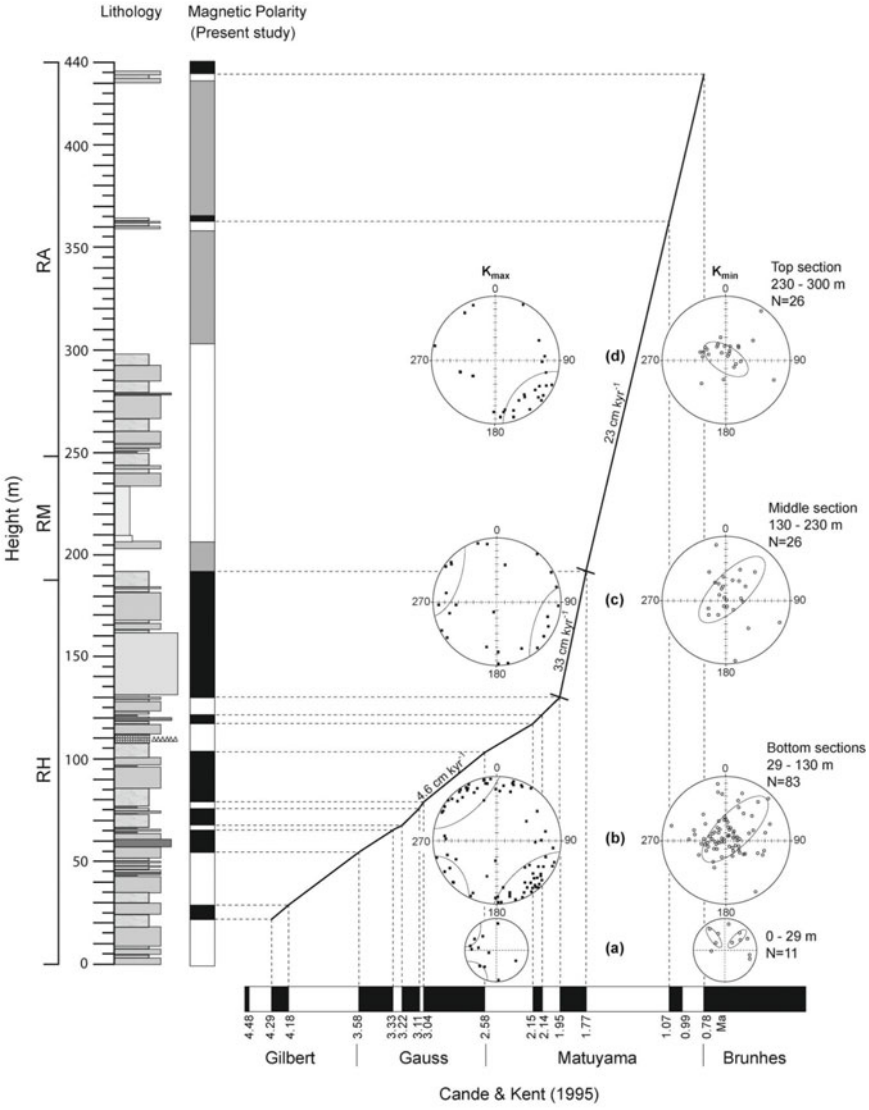

Figure 7.14b. Age vs. stratigraphic thickness plot of Kashmir paleolake sediments showing the sediment accumulation rate (SAR) deduced from polarity sequence and anisotropy of magnetic susceptibility (AMS). Note an increase in sedimentation rate from 4.6 cm/kyr to 33 cm/kyr at Plio-Pleistocene boundary coinciding the onset of westerlies in the Kashmir valley, thereby reducing the influence of SW monsoon (Basavaiah et al., 2010).

Detailed magnetostratigraphy has been investigated from 250 sites collected at 435 m thick Romushi section of lower Karewa deposits, which records a chronometrically constrained volcanic ash. The ChRM directions obtained through AF demagnetization procedure are used to calculate the virtual geomagnetic pole (VGP) positions. VGP latitudes were plotted against the stratigraphic level to obtain the magnetic polarity time scale (MPTS). A total of eight normal and eight reverse polarities are deciphered in Romushi sediments. MPTS of Romushi formation is well correlated with standard GPTS (Fig. 7.12). The samples collected from Romushi river section gave an age of 0.79 to 4.68 Ma and sediment accumulation rates (SAR) range from 32 to 4.6 cm kyr^{-1}. The revised magnetostratigraphy delineates chronological depositional processes influenced by both climatic and tectonic factors. For example, the low SAR of 4.6 cm kyr^{-1} indicates a calm sedimentation regime prevailed until the Pliocene/Pleistocene boundary. The rapid increase in SAR after ~2.0 Ma, is either due to local or regional tectonic event, or by strengthening of the monsoon reported for ~2.6 Ma.

7.5 ENVIRONMENTAL GEOMAGNETISM

Rocks, baked materials and sediments owe their magnetization/magnetic properties to Fe oxides, oxyhydroxides, sulfides and solid solution components present in them. Recent developments in electronics and computing have helped manufacture sensitive instruments for magnetic measurements, enhancing/establishing a now familiar study area called environmental geomagnetism (also called mineral magnetism). The rock magnetic techniques investigate nondirectional magnetic properties of natural and synthetic materials to delineate environmental or climatic controls on accumulation of the parent material (rocks, glacial till, eolian and alluvial deposits), and its microstructural and chemical alteration (pedogenesis) with time. Basically, environmental geomagnetism employs the experimental approach to identify/characterize the mineralogy, concentration, grain size, morphology and composition of the magnetic mineral phases present.

Magnetic grains with their distinctive assemblages are virtually omnipresent and their type, size and concentration change relative to their source and depositional history. The sensitivity and detection of magnetic attributes (even in ppm to ppb concentration ranges) by environmental instrumentation make the methodology relatively inexpensive, easy, and rapid compared with other types of mineralogical analysis. This methodology has a nondestructive trait, wherein the same samples can be used for any additional and complementary investigations. In multidisciplinary studies, one small diameter core is generally sampled for pollen, diatom, ostracode, isotope, geochemistry, mineral magnetism, carbon, radiocarbon, lead isotope and amino acid dating. Consequently, the researchers run out of sample before they run out of ways to examine it. Thus, the nondestructive method of environmental geomagnetism

stands to be a great asset. Most importantly, it enables comparison of different records across thousands of kilometres. Magnetic analyses thus help a great deal in producing spatial as well as temporal record of ambient climatic, environmental and post depositional processes. Environmental magnetists use the magnetic properties to isolate natural and human-induced changes in climate and environment on both spatial (site-specific and regional scales) and temporal (contemporary and geological timescales) level.

7.6 ENVIRONMENTAL GEOMAGNETISM VS. PALAEOMAGNETISM

Environmental geomagnetism is a distinct scientific entity, which studies intrinsic magnetic characteristics of the mineral types within nonoriented samples such as magnetic susceptibility (χ), frequency dependent susceptibility (χ_{FD}), anhysteretic remanent magnetization (ARM) and isothermal remanent magnetization (IRM). Some of these properties (χ and χ_{FD}) are measured in the field, while others are measured as a remanent response to a series of externally applied and artificially induced magnetizing fields of different kinds (AC, DC) and magnitudes (ARM, 0.1 T and IRM up to ~9 T) in the laboratory. The magnetic properties of sediments are entirely independent of the EMF and are largely a function of mineralogy and grain size that provide insights into the mode of transport, deposition and changes in their properties caused by different processes of iron mineral authigenesis, diagenesis and dissolution. Thus, this branch is independent of palaeomagnetism, which primarily determines the directional nature of remanent geomagnetic field, wherein oriented samples are an absolute necessity. In mineral magnetic research, however, samples are not required to be measured in situ or to have their original orientation noted. It involves measuring 'bulk' magnetic properties complementing other techniques such as geochemical or micropalaeontological studies, to name just a few.

Environmental geomagnetism also has palaeomagnetic applications which focus on: (1) correlation of palaeomagnetic signals in sediment cores, (2) development of astronomically calibrated age model, (3) testing the hypothesis of orbital forcing of the EMF, and (4) determining the origin of the palaeomagnetic signal. In essence, environmental magnetic measurements allow detection of quantitative as well as qualitative variations in magnetic minerals as an aid to environmental data interpretation, rather than the geomagnetic directional properties. Thus, palaeo and rock magnetists use magnetic measurements to identify which magnetic minerals are responsible for acquiring a record of the Earth's magnetic polarity at their time of formation. Environmental geomagnetists seek to identify causal links between magnetic properties and climatic and environmental histories/origins.

7.7 ENVIRONMENTAL MAGNETISM: OBJECTIVES AND EVOLUTION

Environmental magnetism largely relies on the sensitivity of Fe compounds to physicochemical changes, and on their tendency to persist as diagnostic 'tracers' over long periods of time. Magnetic properties of the natural materials are largely connected with the element Fe, its valency, concentration, and partitioning. This methodology can be applied to many areas of study such as soil forming processes, slope and evolution, basin erosion/sedimentation, sediment source tracing, historical/contemporary particulate pollution, differentiation of atmospheric dusts/aerosols, stratigraphic correlation of a wide range of temporal/spatial/depositional sites, archaeological studies of pottery/soils, interpretation of palaeoclimatic records, diagenetic changes and authigenic sulphide formation. Besides, the growth of biomagnetism as a major field has run parallel to the above developments.

Environmental magnetism has evolved on three principal objectives: (1) characterizing spatial variability in physical properties of the shallow subsurface (soils, sedimentary sequences) environment, wherein the information is used to model palaeoclimate and palaeoenvironment, (2) environment pollution characterization based on the fact that atmospherically transported magnetic particulate material makes a significant contribution to the iron (hydr)oxide particle content of many sedimentary deposits/soils and (3) biomagnetism, where the research programme aims to provide information about the environmental control variables (temperature, rainfall, pH, as well as microbial type and concentration) for the process of Fe^{3+} to Fe^{2+} reduction and challenges posed by environmental magnetic observations of biomineralized nanophase (1–100 nm) materials. The most fascinating examples of investigation come from magnetotactic bacteria found in diverse environments playing a role in fine magnetic particle (submicron size) studies.

I. The Beginnings

Gustav Ising first used magnetic minerals as a proxy in 1926. He collected annually laminated glacial lake sediments from Sweden and measured their χ and NRM, which varied seasonally and with distance from the source. He found lake sediments deposited in the spring time were more magnetic than those deposited in winter. He interpreted it in terms of detrital input and higher density of magnetic minerals. Forty years later, John Mackereth used magnetic measurements on lake sediments from Windermere to investigate the magnetic mineral source.

In 1950s, the study of soil magnetism was pioneered by Le Borgne, who unraveled the phenomenon of magnetic 'enhancement' (increased χ) in natural top soils (humus rich horizons), and ascribed it to in situ conversion of a proportion of the weakly magnetic forms of iron (hydr)oxide to a strongly magnetic form of secondary ferrimagnetic oxides (maghemite, magnetite). But

the process controlling the enhancement of χ was then poorly understood. Thompson and Oldfield later invoked a mechanism based on Mullin's hypothesis to explain the postulated formation of microcrystalline maghemite or magnetite from weakly magnetic iron (hydr)oxides through the redox cycles, which occur under normal pedogenic conditions. An alternate hypothesis proposes soil bacteria to grow small chains of stable single domain (SSD) magnetite crystals within their cells resulting into the enhancement observed as normal part of pedogenesis.

Frank Oldfield, in the mid 1970s, was inspired by a demonstration by Mackereth of the use of palaeomagnetic secular D measurements for dating Holocene lake sediments. He found χ had striking similarity between cores of the Lough Neagh sediments, which became the first attempt of core correlation. He and his coworkers in late 1970s put forward the concept of using magnetic properties as proxy parameters. Thompson and his team's article in '*Science*' in 1980 formally announced environmental magnetism to be a sub-discipline, and extended the use of rock magnetic methods in soil, sediment, peat and atmospheric dust studies. It has now become a rapidly expanding research methodology (see review articles and books by King and his associates, Thompson and Oldfield, Oldfield, Maher and Thompson, Walden and his associates, Evans and Heller and Basavaiah and Khadkikar).

II. Environmental Impacts on Magnetic Minerals

In an environmental system, the magnetic minerals found in descending order are iron oxides (hematite, magnetite, maghemite), iron oxyhydroxides (ferrihydrite, goethite, lepidocrocite), iron sulphides (greigite, pyrrhotite) and manganese (rhodochrosite, vivianite) minerals (Chapter 2), which are commonly scattered within the nonmagnetic matrix of the natural materials.

The nature of Fe compounds, their presence, environmental sensitivity and variable stability make magnetic measurements widely adaptable to many environmental fields. For instance, majority of magnetic minerals, which cycle in environmental systems, originate from the Earth's crust and pass through the atmosphere, hydrosphere and biosphere in varied ways (Fig. 7.15). Only a small part of atmospheric magnetic dust is derived directly from the Earth's interior, via volcanic eruption, whereas extra-terrestrial inputs are found to be very limited. Magnetic minerals in unweathered parent rock material or those which survive largely unaltered in weathered contexts are characterized as primary minerals. Those formed by chemical/physical processes or biogenic effects associated with weathering, pedogenesis, diagenesis or authigenesis are secondary. Human intervention also leads to some of these processes such as fossil fuel combustion and soil erosion (Fig. 7.15).

Chemical transformation can lead to Fe conversions among paramagnetic, ferrimagnetic and antiferromagnetic forms giving rise to environmental 'finger prints', which become significant indicators in environmental tracing investigation. Also, fire and soil forming processes enhance top soil magnetic

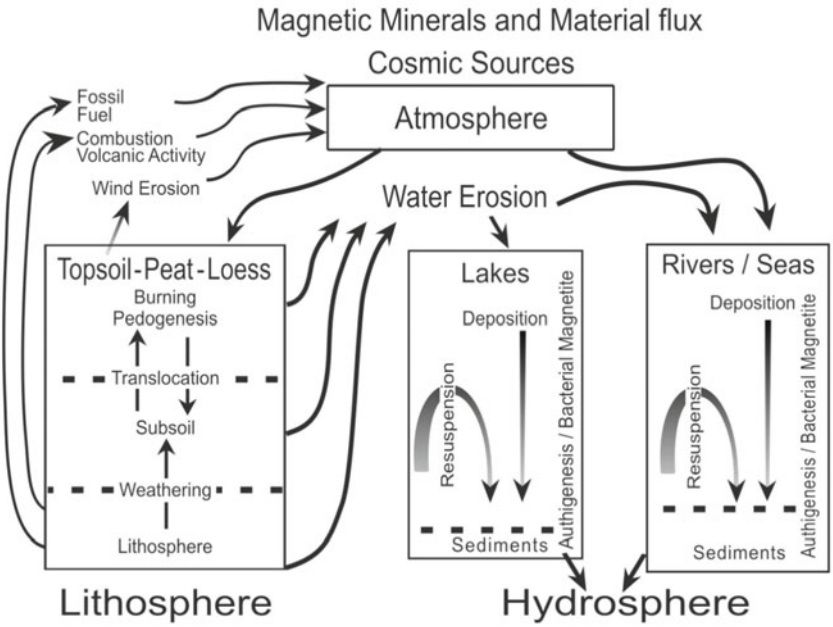

Figure 7.15. Major sources and cycles of magnetic minerals within the environment. Magnetic minerals can be produced, modified, transported and deposited by a range of environmental and anthropogenic processes. Environmental geomagnetism can be applied to identify/differentiate/characterize principal sources of magnetic minerals displaying ferromagnetic behaviour within the environment of soils and sediments. These include detrital minerals derived from rocks, sediments or soils (transported by water or wind), authigenic/diagenetic production, volcanic ash, in-situ pedogenic processes, cosmic sources (important near sites of meteor impacts), anthropogenic pollution and magnetic bacteria. Examples of major areas of application of environmental geomagnetism include environmental change, past climates, sediment sourcing and mapping of particulate pollution (Thompson and Oldfield, 1986).

material by converting nonferrimagnetic minerals to fine ferrimagnetic grains. These secondary magnetic oxides differ, both in crystal form and size, from the primary magnetic oxides present in the underlying substrates; both of primary and secondary minerals are eroded and incorporated in river and lake sediments. Thus, differences in primary and secondary magnetic minerals form the basis for sediment source identification. Alternatively, chemical transformation can make the environmental interpretation of magnetic data more difficult. Diagenesis or authigenesis, for example, may distort the magnetic 'signals' from source materials preserved in sediments, which can mislead the analysts.

Physical processes usually perform the function of simply removing and redepositing magnetic mineral assemblages. These processes are relatively conservative of magnetic minerals, but the magnetic properties can still be

affected through the following mechanisms: (1) magnetic grain size reductions and crystal shape changes, (2) regrouping of mineral assemblages, and (3) vertical rearranging of magnetic assemblages. However, these minerals are found to persist unaltered in a wide range of transport and deposition contexts. Hence, appropriate mechanism needs to be taken into consideration, when specific EMM study is finalized. For instance, particle size based magnetic study should be harnessed to reduce the effect of sorting in sediment source tracing. Sediment source identification can be established in a catchment system (if) (1) some weathering and soil formation have taken place and the types of source materials can be characterized by magnetic measurements, (2) the timescale over which erosion and sedimentation are being studied is substantially shorter than the rate at which the assemblage of metastable Fe oxides is being transformed in the potentially eroding soil and (3) sediment diagenesis or authigenesis have not affected the magnetic properties of the sediments.

III. Magnetic Mineralogy as a Proxy

Natural as well as anthropogenic influenced climatic and environmental changes have occurred innumerable times in the past. In a fundamental sense, the discernment of past changes (and future ones) requires a database that goes long back in time and space. This information is contained in historical records of meteorological observatories, ship-logs, personal records, etc., as also in religious texts and epics which volunteer detailed descriptions of floods, droughts and such other natural disasters. They are, however, allegedly considered short on reliability. But, the 'proxy' indicators of climatic alteration, unlike historical records, go a long way back in time (Ma), and their distinguishing feature is their ability to characterize the natural system, or part thereof in an approximate manner. They are also easily and quickly 'measured' at a competitive cost, enabling rapid measurement of large number of samples; a key advantage in obtaining high-resolution spatial and temporal environmental data.

Climate proxies are generally used as signs of past climatic processes, which include physicochemical properties and isotopic compositions of minerals, fluids or gases. The other contenders are the anatomical assemblages of certain fossil plants, animals, and presence (or absence) of index fossils. On land, climatic variables used as proxies include temperature, precipitation and evaporation. In the ocean, the key variables include currents, temperature, salinity, nutrient availability, productivity and redox chemistry. Biodiversity patterns, continental weathering rates, winds and storms also come in handy as climatic proxies.

The use and reliability of different proxies are established by comparing the present day values with some record of the past, e.g. the tree-ring thickness or the isotopic composition of water. Here, the present is used as a key to the past. When scientists understand how tree rings change their thickness in recent

wet and dry periods, the information (or an assumption) gained is then extrapolated back in time to make a reliable (nearer to truth) estimate of a climate or an environmental change. The assumptions, however, involve some amount of uncertainty. The conjecture that under different climatic conditions, a marine organism grew most vigorously during the same season and at the same water depth as in the modern environment, has a tinge of chaos and uncertainty to it. To circumvent this problem, multiple proxies, about whom few suppositions are made, are used in the decision making process to increase the reliability of palaeoclimate reconstruction. The physical proxies like old air extracted from bubbles in ice cores, old water from pore spaces in seabed sediments or continental rocks, concentration of noble gases found dissolved in old groundwater provide direct evidence of past climatic compositions. In the category of direct evidences are also included sand dunes, and glacially polished bedrock.

Many cross checks are used when interpreting proxies for climate changes. Marine isotopic stages (MIS) deduced from alternate warm and cool period of the Earth's past climate are used as one of the tallies. Based on carbon and oxygen isotopes from the marine sediments/organisms, these stages are chronologically arranged as MIS1, 2, 3, 4, etc. (Fig. 7.16). It is based on the fact that physical and chemical characteristics of atoms of differing isotopic mass increase with decreasing temperature of the medium. For example, the carbonate shells growing in water typically favouring isotopically heavy oxygen tend to become isotopically heavier at lower temperatures. The growth of ice sheets removes isotopically light water (ordinary water) from the ocean, forcing the organism to use isotopically heavy oxygen from water in their carbonate shells, which then provide information on the presence (or absence) of ice sheets over time. To quote another example, a few chemicals are always common in the environment, but the organism may use only a typical 'favoured' isotope. A shortage of this chemical may force it to use another 'less favoured' isotope. Also, marine photosynthesis increasingly favours a lighter isotope of carbon as CO_2 becomes more abundant. This allows estimation of changes in CO_2 concentration from the isotopic composition of organic matter in oceanic sediments. The change in ocean isotopic composition can be estimated independently from the composition of pore waters in sediments, whereas the change in temperature can be estimated from both the abundance of cold or warm loving shells in sediments. Concentrations of noncarbonate ions substituted into calcium carbonate shells provide further information. Reversals of the EMF have helped to provide a timescale for changes in oxygen isotopes, giving it a chronology that could be used to understand the frequency of glaciations and rates of change (Fig. 7.16).

It is important to consider the quantum of time when interpreting climatic change. Four major timescales are generally considered, which include: Long-term (hundreds of Ma), medium-term (one Ma), short-term (~160 ka), and modern period (hundreds of year). This is important because climate has both

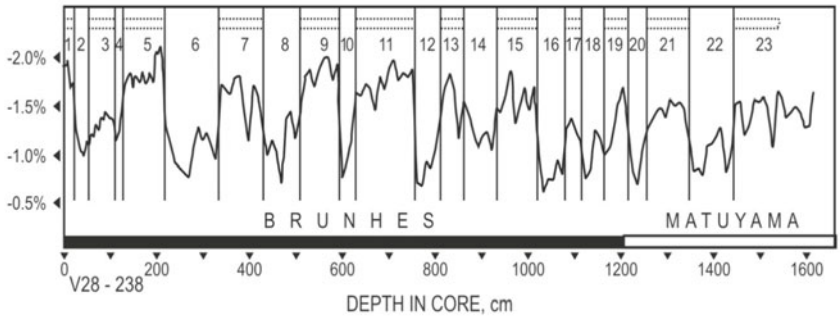

Figure 7.16. Climatic oscillations during the last 870 ka based on oxygen isotopic measurements of marine foraminifera from the sea core V28-238 (*courtesy:* Emiliani).

long-term trends and short-term variability. Long-term datasets provide the observer with a sense of 'big picture' of the climatic trends, when major shifts such as ice ages are easily recognizable. Short-term variations like a colder than average month, can exist within longer pattern of warming trend. The coexistence of short and long-term trends complicates the climate change signal. But, the magnetic proxy is able to tackle and discern the complex trends in a far better and cogent way than the other proxies.

The oceanic sediments are a mix of terrestrial and atmospheric constituents. The rivers of the Himalayas and the peninsular India drain tonnes of detrital material into the Bay of Bengal and the Arabian Sea, where the typical rate of sedimentation is much higher for the former than the latter. Lake sediments, on the other hand, have the potential of yielding high-resolution palaeoclimatic fluctuations, especially from proglacial lakes, which may have annual laminations (varves) that are deposited in the higher central Himalayas. The time resolution achievable from these lakes depends on sedimentation rate, sampling interval, and methods of dating. In general the temporal resolution is ca. 100 years. For high resolution in time, cores are retrieved from areas, where sedimentation rate is higher, but for a longer history with poorer temporal resolution sedimentary cores are raised from regions where sedimentation rate is slower. These sediments are studied for understanding long-term dynamics of the monsoon and climatic fluctuations. However, the chemical and biological proxies are limited in spread and strongly depend on the local climatic and environmental conditions. Index fossils thrive in particular locations and particular climatic umbrella only (their growth is also a function of a number of other variables). Hence, their use in tying up loose ends connected to climate, environment, stratigraphy and correlation remains equivocal.

Magnetic proxy parameters do not have this limitation, and so reliable results can be obtained from them. To begin with, relationships are found to exist between χ and oxygen isotope ratios, elemental constituents, and foraminifera instilling confidence in using it as a quantified and calibrated proxy. The carriers of magnetic properties of samples generally result from the

uppermost layer of crust (sediments), which is prone to many physical (erosion, weathering) and chemical (oxidation, reduction) processes governed by atmospheric, oceanic and terrestrial system changes (Fig. 7.15). Precipitation, in excess or deficit, has some chemical (change in redox environment) and physical (increased or decreased detrital input) influence on the lake, ocean and terrestrial sediments. In case of terrestrial sediments, the variable degree of water saturation alters the redox states leading to the formation of magnetite during periods of enhanced rainfall, whereas the formation of hematite/goethite is made possible through oxidative processes during periods of reduced rainfall. This interpretation has been experimentally verified and established. Fe-oxide system is found to be capable of carrying out a few interconversions between its different phases. In favourable conditions, almost every Fe-oxide can be converted into at least two others. Under oxic conditions, goethite and hematite are found to be the end members of many transformation routes, since thermodynamically, they are the most stable compounds. Although thermodynamically unstable (in the presence of oxygen), magnetite and maghemite are widespread in the environment. It is seen that at RT, magnetite very slowly oxidizes to maghemite. But at higher temperatures, magnetite metamorphoses to hematite. The oxidation of magnetite to maghemite is thus a significant environmental process, and is a topotactic reaction in which the original particle morphology is maintained throughout. Experiments have also shown ultrafine magnetite crystals (100 to 300 nm) to change to maghemite at RT, but in some cases, small particle sizes, of a couple of hundred nm, failed to initiate oxidation even after one year. Some experiments show that for ~9 nm nanocrystals at 24°C in water, oxidation is detectable after a few hours and completed in ~3 months.

These experimental reactions are replicated in natural environment. In an actual environmental setting, thermal transformation of magnetic polymorphs caused by natural or man made fires is seen to be widespread. The frequent occurrence of maghemite in surface soils of the tropics and at localized burning sites around the world, is due to the presence of organic matter which directs the transformation of goethite or ferrihydrite during heating to maghemite, whereas in the absence of organic matter, hematite is formed. Reductants such as zinc powder or elemental sulphur lead to maghemite formation, and it is assumed that the transformation proceeds via magnetite. In fact with higher amounts of reductant, e.g. sucrose, and/or lower O_2 supply, magnetite is formed instead of maghemite.

This establishes the veracity of magnetic proxy evidences for palaeoenvironmental interpretation. Palaeoclimatic history from magnetic properties is reconstructed by determining the magnetic framework of the sedimentary material. The next step involves ascertaining the basic aspect of the climate (physical-chemical), which predominantly has control over the magnetic signature. Finally, the magnetic measurements reveal the parameters (especially χ, ARM) most sensitive to climate change. In all this, it becomes

essential to identify space and time characteristics of climate/environment and magnetic minerals and ascertain their relationship with each other. However, in some situations, this magnetic proxy can be nonunique and noisy, to circumvent which independent and complementary analyses are adopted to compare the magnetic data with other environmental proxies, e.g. pollen, carbon isotopes or geochemistry.

IV. Mineral Magnetic Data of Resolving Ambiguity

In studies of environmental magnetism, often the recourse is to use only magnetic properties as analytical probes. In such cases, data interpretation becomes difficult since measurements are of bulk properties, comprising contributions from the entire gamut of magnetic minerals, rendering it to be nonunique. Hence, their scales are generally utilized in a relative sense. To get around this problem, many a times, ratios of several parameters are used to reduce nonuniqueness. In the process, interpretation of a ratio may change depending on the absolute values of numerator and denominator. Hence, the analysis may vary from one depositional environment to another or sometimes within similar kinds of environment as well. Proper comprehension of a mineral magnetic dataset, therefore, requires expert training and a feel for potential variability in the databank. The compilation of existing theoretical and experimental data derived from known sample sets enables to narrow down the ambiguity in interpretation and also reveals several ways of plotting the results. As a consequence, the inferences of sample 'interrogation' can be related to all the information available for the samples enabling to search causes of variability of magnetic properties. In the light of this, mineral magnetic data is interpreted confidently without resorting to use of other proxy data. Also, the results enumerated ahead and compiled from different sources can indicate the type of information obtained from the qualitative study of the magnetic and complementary parameters. The rock magnetic components listed in Appendix 7.3 provide an overview of the measurements undertaken in rock and environmental magnetism research.

V. Mineral Magnetism: Theory and Measurement

All substances demonstrate some degree of magnetic behaviour determined by: (1) interactions between electron spins, and (2) nature of their alignment in B_{ext}. In order to allow interpretations of bulk magnetic measurements, the phenomenon of magnetism is usually discussed on the subatomic scale, and then in ascending scales of reference in terms of atoms, subgrains, grains and grain assemblages (Fig. 7.17).

Basic magnetism: Minerals consisting of ions without an intrinsic magnetic moment are diamagnetic (Chapter 2). Minerals with an intrinsic magnetic moment are either ferro-, ferri- or antiferro-magnetic, where there exists exchange interaction between these ions, or paramagnetic, when there is no

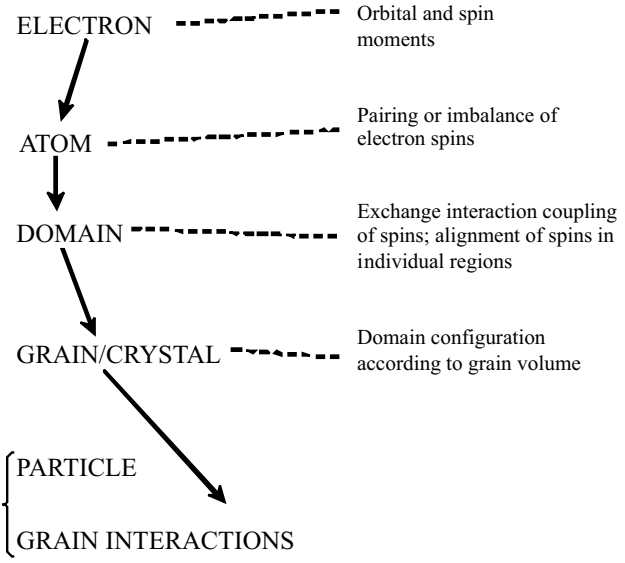

Figure 7.17. Scales of magnetic order.

interaction. For the existence of an intrinsic magnetic moment in an ion, presence of unpaired electrons in the electron's outer shell is necessary. Different magnetic measurement techniques respond to different properties of a mineral assemblage, e.g. paramagnetic and diamagnetic minerals have an effect on only the susceptibility measurements, but SIRM measurement reacts to minerals, which retain remanent magnetism. Table 7.4 summarizes the magnetization and remanence characteristics of main types of magnetic behaviour.

Magnetic granulometry is the determination of the effective grain-size of magnetic materials, based on the discrimination between magnetic relaxation effects (SP and SD particles) and domain processes (MD grains). In rock magnetism, magnetic grains are divided into SP, SD (stable SD), PSD and MD according to their magnetic properties, and domain states (Chapter 2, Fig. 7.18). The approximate magnetic grain size (distinct from sediment particle size) boundaries for magnetite are: SP (20–25 nm), SD (25–80 nm), PSD (80 to ~10–15 nm), and MD grains (>10–15 μm) (Chapter 2). Basically, there are two types of magnetic parameters that are strongly dependent on grain size: (1) magnetic hysteresis and (2) remanence properties. Also it is based on measuring some of these same magnetic parameters as a function of temperature either low temperature or high temperature, below or above RT. Figure 7.18 illustrates relationships between the magnetic parameters and the mineral grain size.

An approximate method, known as the Lowrie-Fuller test, compares the AF demagnetization spectra of ARM and SIRM to distinguish fine grains

Table 7.4 Main types of magnetic behaviour.

Substance	*Ferrimagnetic*	*Antiferromagnetic*	*Paramagnetic*	*Diamagnetic*
Definition	These substances are strongly attracted by the magnet		These substances are weakly attracted by the magnet	These substances are repelled by the magnet
Nature of alignment	Part of the atoms line up in one direction, the other part oppositely with net moment	Electron spins alternate atom by atom, thus cancelling out each generated moment	Align with the applied field	Align in opposite direction to the applied field
Field	+	+	+	-
Susceptibility (χ)	Large and positive	Small and positive	Small and positive	Small and negative
Magnetization	Strong	Weak	Weak	Very weak
Remanence	High	Low	None	None
Temperature effect	$\chi \propto 1/T$	$\chi \propto 1/T$	$\chi \propto 1/T$	Independent of temperature
Examples	Magnetite Maghemite Greigite	Hematite Goethite	Ferrihydrite Lepidocrocite	Quartz Calcite

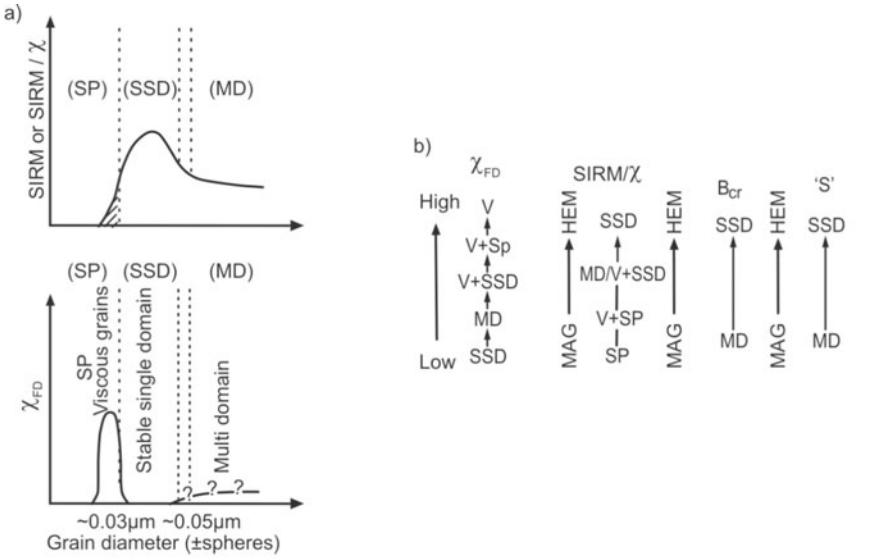

Figure 7.18. (a) The relationships between SIRM (SIRM/χ) and χ, and mineral grain size, showing approximate ranges of miltidomain, SSD and viscous grains. (b) A summary of the general influences on χ, SIRM/χ, B_{Cr} and S ratios of mineral grain size (MD, SSD, SP) and mineral type: magnetite (MAG) and hematite (HEM) (*courtesy:* Dearing and his coworkers).

(<20 μm) from coarse grains (>20 μm). Banerjee and his coworkers in 1981 argued that the ratio of anhysteretic susceptibility (χ_{arm}) to magnetic susceptibility (χ) can be used as a proxy for grain-size changes in magnetite. This reasoning is based on the fact that ARM is enhanced in the fine-grained SD fraction, whereas χ is relatively independent for the coarse grained PSD and MD fractions. The ratio, therefore, varies inversely with grain size. Furthermore, as pointed out by King and his coworkers in 1982, χ_{arm} is a strong function of concentration, so caution is warranted. Nonetheless, it is clear that susceptibility is virtually independent of grain-size, while χ_{arm} is a strong function of grain size, so changes in χ_{arm} normalized by χ in fact reflect changes in grain-size. Later, Maher and Oldfield have proposed variations of this method using χ_{arm}/SIRM or χ_{arm}/χ_{FD} to discriminate SP from MD particles.

Application of magnetic granulometry: The determination of effective grain sizes is useful for various geological and geophysical problems such as detection of climatic and cultural signatures left in natural sedimentary materials and formation/erosion of soil on bed rock. Grain size determinations are extremely valuable to identify origins of the various components in environmental samples. Since the data have contributions from all magnetic grain sizes, including detrital/pedogenic components, some magnetic properties, particularly coercivity and remanence, vary greatly with particle size. It is therefore possible

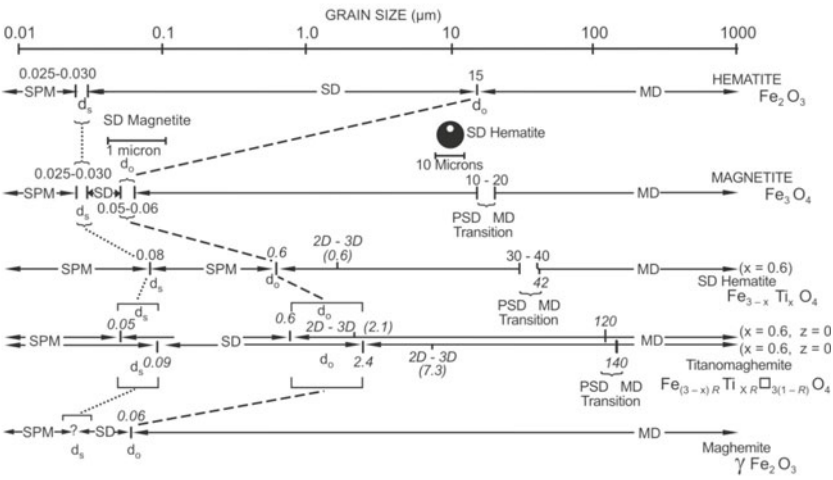

Figure 7.19. Theoretical and experimentally determined critical grain size transitions in some common iron oxide minerals (*courtesy:* Dunlop).

to categorize grain-size by the study of remanence. It is widely accepted that the coarse MD fraction is predominantly detrital (eolian), while the ultrafine SP grains are mainly authigenic or pedogenic in origin. An increasing body of evidence supports the dominance of in situ formation of ultrafine magnetic minerals, which enhance the susceptibility of soil layers. The critical grain size boundaries, which divide the various types of size-dependent magnetic behaviour are shown in Fig. 7.19. Moving from the finest to coarsest grain sizes, the boundaries d_s and d_0 separate those particles, which display SP to SSD and to PSD through MD behaviour.

7.8 PRIMARY MAGNETIC MEASUREMENTS—MAGNETIC PROPERTIES

Magnetic measurements do not just reveal the nature of magnetic material, but also signify its structure through anisotropy and its history through palaeomagnetism. To comprehend the relationship between magnetic parameters, and distinctive features of magnetic grains (e.g. chemistry, size, shape, defects and origin), a number of smart and effective techniques have been developed. To bring out the practical facets, and its realistic applications, a brief description of magnetic parameters and the basis that lies behind the methodology and interpretation of data is described.

I. Low-field Magnetic Susceptibility (χ)

This type of susceptibility is the ability of a given substance to get magnetized, i.e. it grows an induced magnetization that dissipates after the external field is

removed. There are several valid definitions in vogue, but the one given by Encyclopedia Britannica defines magnetic susceptibility as 'a quantitative measure of the extent to which a material may be magnetized in relation to a given applied magnetic field'. Thus χ is studied by applying magnetic field (H) and measuring the magnetization (M) induced in the material. There exists a relation connecting M and H: $M = \chi_V H$, which yields $\chi_V = M/H$, where v denotes 'volume'. χ is specified either by volume (κ) or mass (χ) ($=\kappa/\rho$, here κ is replaced by χ_V and ρ is density). Thus, χ is used to classify materials in terms of their response to B_{ext} as diamagnetic, paramagnetic and ferro(i)magnetic, making it an attractive magnetic characterization tool.

If ultrafine SP particles are present, the frequency of applied AC field has significant effect in terms of applied magnetic field. At higher frequencies, energy of thermal fluctuations reduces the alignment effect of the applied field, and consequently χ measured at higher frequencies is always equal or lower than that measured at lower frequencies. By measuring at different frequencies, the frequency dependent of magnetic susceptibility $\chi_{FD\%}$ can be expressed as (Fig. 7.18a):

$$\chi_{FD\%} = (\chi_{LF} - \chi_{HF}/\chi_{LF}) \times 100$$

χ_{FD} is particularly sensitive to grain sizes spanning the SSD to SP boundary, often referred to as fine viscous (Fig. 7.18a), because these grains show a degree of time dependent loss of remanence. Hence, this is a proxy for the relative amount of SP grains. It has strong implications with regard to delineating source type, since mineral assemblage exhibiting χ_{FD} is rare in unweathered rocks, volcanic ashes or fossil fuel derived sediments, but is characteristic of soils in which secondary magnetic minerals form as a result of pedogenesis and fire. Thus, natural susceptibility of sediment needs to be measured at two or more different frequencies to gain information about the amount and grain size of magnetite. For instance, while ultrafine magnetite (<0.03 μm) is formed in soils giving high (>8%, <16%) χ_{FD} percentages, relatively larger magnetite (MD ranges) is usually eroded out of rocks. While χ_{FD} depends on grain size, χ itself depends mostly on magnetic mineralogy and its concentration.

Pedogenesis and/or intense weathering induce hematite-magnetite transformation and reduction in effective grain size. This change is reflected in χ and χ_{FD}, which display higher susceptibility for magnetite. Simultaneous χ and χ_{FD} measurement discriminates active enhancement of ferrimagnetic minerals during pedogenesis from the passive enhancement caused by the leaching away of nonmagnetic components in the humus-rich horizon. Thus, a parallel increase of χ as well as χ_{FD} points to secondary origin, whereas variations of χ not associated with corresponding variation of χ_{FD} indicate contribution of ferrimagnetic minerals of primary origin. Therefore, χ and its frequency dependence are used to determine the intensity of weathering, and hence climatic changes in different environments.

High-field magnetic susceptibility: Hysteresis loop is used to determine χ at fields higher than the EMF. The field strength H_{MAX} relating to χ_{MAX} is practically independent of the percentage magnetite, but is connected with the grain size. The greater the grain size, the smaller is H_{MAX}. For pure crystals of magnetite, H_{MAX} will be 2 mT or even smaller. The ratio of χ_{MAX} to χ at the EMF does not appear to vary with the grain size, but is dependent on the percentage of magnetite by volume. Generally, the reversible high field susceptibility (χ_{HIGH}) is measured as the gradient of the magnetization slope between 800 and 1000 mT, indicating paramagnetic and antiferromagnetic component of a material minus the diamagnetic component.

Factors affecting susceptibility: Magnetic susceptibility is influenced by the type of magnetic minerals, their shape, size and the geological history. It decreases as a rule with decreasing grain size. Layered rocks always exhibit magnetic anisotropy, i.e. the susceptibility ($\chi_{||}$) along the layers is greater than the susceptibility across the layers ($\chi_{\perp}$). The magnetic anisotropy of a rock is defined by the ratio $\chi_{||}/\chi_{\perp}$. This ratio can be as high as 3.0 and is dependent on the percentage of magnetite content. This observation does not, however, apply to the susceptibilities obtained in situ. One of the main interests in the determination of the low field anisotropy of magnetic susceptibility (AMS) is its value as a petrofabric indicator. In magnetite, for example, shape anisotropy is dominant, as crystalline anisotropy is weak. Thus, for an elongate (nonspherical) magnetite grain, susceptibility measured in a magnetic field parallel to the grain's long axis would be greater than the susceptibility measured in the same field if that field is applied normal to the grain's long axis. AMS studies are useful in delineating individual flow directions of Deccan basalts, tectonic and metamorphic events of south Indian highly deformed rocks.

Curie temperature susceptibility, χ-T graphs: Low-field susceptibility is controlled by the internal forces acting in a grain. These in turn are determined by mineralogy, crystal structure, shape, and size of the grains. These parameters may vary with temperature as thermal energy of the system is increased or decreased. Magnetocrystalline anisotropy is particularly sensitive to temperature, and is dependent on crystal structure and composition only. High-temperature (high-T) and low- temperature (low-T) susceptibility were studied from liquid nitrogen temperature (–196°C) to 700°C. Measurements on natural and synthetically produced magnetites of known sizes have helped to define the major changes in χ with crystal size and domain, which are shown in Fig. 7.20.

The presence of minerals and domains is detected from the shapes of the χ-T curves and distinctive transition points. Figure 7.20 summarizes the more common features in low-T and high-T curves. The lack of irreversible change and the presence of several diagnostic transitions mean that low-T curves are easier to interpret than their high-T counterparts.

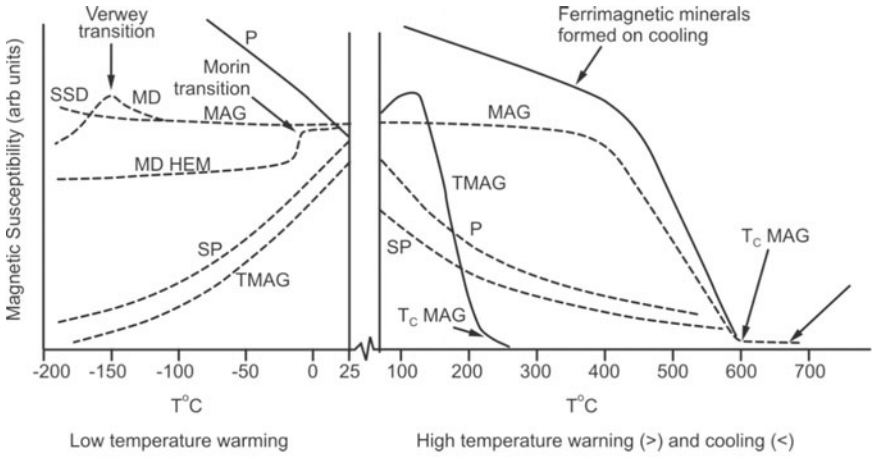

Figure 7.20. Schematic trends and transitions of κ_{lf} values from -196°C (liquid nitrogen) to 700°C for different minerals and domains; SP, SSD, MD, paramagnetic (P), magnetite (MAG: T_C 580°C), titanomagnetite (TMAG: T_C 250°C) and hematite (HEM). Susceptibility axis not to scale (*courtesy:* Dearing).

II. Anhysteretic Remanent Magnetization (ARM)

This parameter, independent of hysteresis effects, is measured by subjecting a sample to an increasing, then decreasing alternating field in the presence of a weak DC bias field, which serves to impart a magnetization in a known direction. Typical values for the peak alternating field (H_{AC}) are 100-300 mT, whereas the bias field varies between 30 and 100 μT. All ferrimagnetic minerals with a coercivity ≤ H_{AC} are remagnetized.

The ARM intensity is a function of the bias field, for low bias fields (<100 μT), it scales linearly. Hence by dividing the ARM intensity by the bias field value, a field-independent parameter is created, referred to as anhysteretic susceptibility (χ_{ARM}) through its analogy with χ. Some instruments allow the field to sense particular coercivity windows and such ARMs are referred to as partial ARM (pARM). ARM is considered to be a good analog of TRM created by cooling through the T_C in a small magnetic field. In particular, stable SD domain grains are sensed by ARM.

Anhysteretic remanence shows grain-size-dependence in magnetite (Fig. 7.21), such that SSD to PSD grains (0.02 to 0.1 μm) have a higher remanence than larger MD grains. It is suggested that IRM_{20mT}/χ_{ARM} ratios provide a simple way to discriminate between a ferrimagnetic mineral assemblage dominated by SSD or MD grain sizes (ca. >1 μm), aiding to clarify the dominant control upon χ_{ARM}. Also, the effects of SP or large MD grains which can dominate the χ are minimized. Ultrafine grains ranging from SSD to SP of ferrimagnetic minerals formed by pedogenesis give rise to characteristic χ_{ARM} and χ_{FD}.

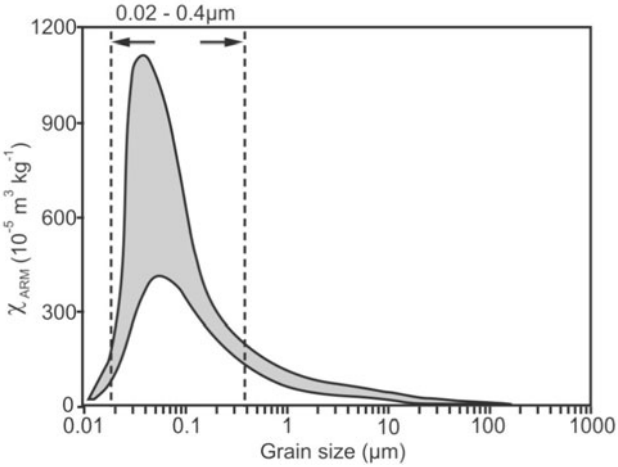

Figure 7.21. Variation of χ_{ARM} values with magnetic grain size in the 0.02–0.4 μm range for magnetite. With ferromagnetic grain sizes both above and below this range χ_{ARM} values drop quite dramatically (*courtesy:* Maher).

ARM is used in a variety of applications: (1) estimate absolute palaeointensity from igneous rocks, and relative palaeointensity from lake and marine sediments, (2) characterize magnetic carriers, and determine domain state/grain size, (3) detect magnetic fabrics in rocks/sediments, and (4) study the fundamental aspect of magnetism.

III. Isothermal Remanent Magnetization (IRM)

As indicated by the name, IRM is a remanent magnetization acquired without the aid of changes in temperature. The term IRM denotes a remanence resulting from the application and subsequent removal of a pulsed DC field. Beyond the threshold of χ measurements, magnetic substances magnetized in a direct field (H_{IRM}, generally >10 mT) follow a magnetization acquisition curve to a point of saturation (Fig. 7.22b). All ferro(i)magnetic grains with a coercivity ≤ H_{IRM} are remagnetized in the applied field direction. Since IRM is a strong-field remanence, the imparted magnetization is not linearly related to H_{IRM}.

Saturating IRM (SIRM) is the maximum IRM a sample can obtain, and is determined by recording IRM in progressively higher magnetic fields (Fig. 7.22b). On reaching saturation, IRM does not increase further regardless of strength (high) of the magnetic field. The saturation field depends strongly on the type and to some degree on the grain size distribution of magnetic mineral(s). For minerals such as hematite and goethite, magnetic fields larger than a few Tesla are required for saturation. Nevertheless, some laboratories with limited magnetic 'power' at their disposal still call IRM_{1T} as SIRM. Figure 7.23a shows grain-size dependence of SIRM for (titano-)magnetite, hematite and pyrrhotite. Thus, magnetite and hematite give out characteristic 'curves' when subjected

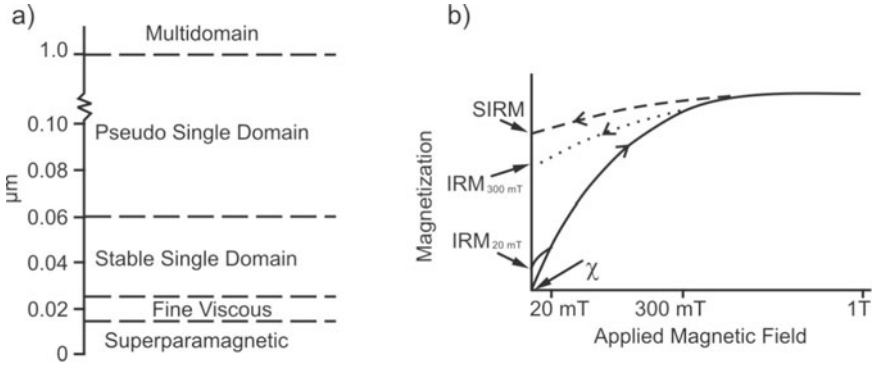

Figure 7.22. A sketch of: (a) Magnetic grain size boundaries and (b) IRM acquisition curve (*courtesy:* Oldfield).

to the entire spectrum of IRMs with an increase in induced field (Figs 7.24 and 7.25).

Low-field IRMs are not fully representative, because they are mainly influenced by magnetically 'soft' ferrimagnetic grain sizes. But, IRMs imparted in fields >300 mT reflect signatures of all remanence holding minerals, including canted antiferromagnetic and 'hard' and 'soft' ferrimagnetic minerals. A general linear relationship between SIRM and χ (Fig. 7.23b) can also be used to characterize the maximum possible range of magnetic mineral assemblages.

Further, a combination of magnetic parameters including the forward IRM acquisition curve, SIRM, coercivity, B_{CR}, IRM demagnetization curve and S-ratio are used to determine sediment sources.

IRM acquisition in forward and back-fields: Recently, researchers have started to measure IRM acquisition curve (remanence vs. log of the applied

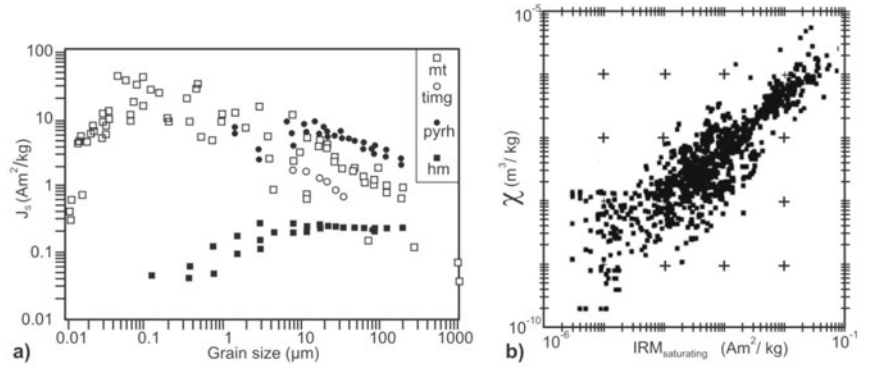

Figure 7.23. (a) Variation in intensity of Saturation IRM in different magnetic minerals as a function of grain size (*courtesy:* Jackson, 1991). (b) Log-log plot of 1000 natural samples (Thompson and Oldfield, 1986). The IRM is imparted in a magnetizing field strong enough to saturate magnetite.

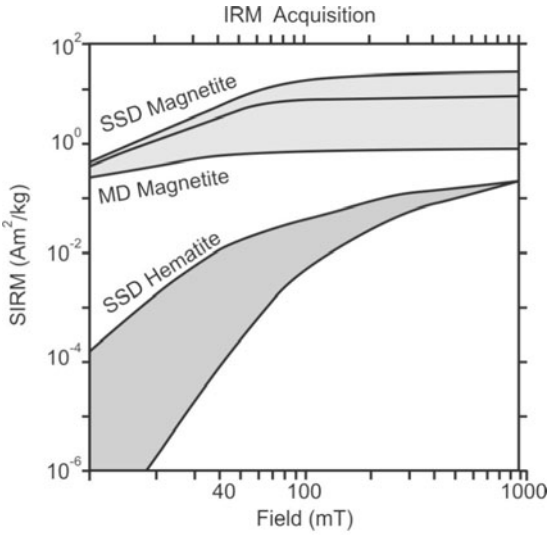

Figure 7.24. Acquisition of isothermal remanent magnetisation with increase in inducing field strength. Magnetite crystals have curves of acquired remanence that plot in the stippled area, whereas hematite crystals plot in the cross-hatched area (*courtesy:* Thompson).

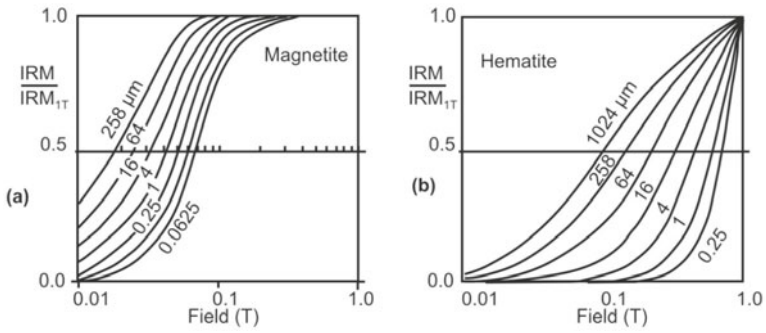

Figure 7.25. Empirically derived, idealized, normalized acquisition of isothermal remanent magnetization curves for magnetite (a) and hematite (b) of different grain sizes (*courtesy:* Thompson).

field); the gradient of this curve is the IRM coercivity spectra. In this process, a sample is demagnetized after ARM measurement, and then exposed initially to small fields (~20 mT), later on subjecting to a set of increasing magnetic fields, say in the range 0–4 T. All these fields are applied in the same direction and are commonly referred to as 'forward' fields. After each field is applied, the sample magnetization is measured. These values represent total combined vector for each field and can be termed as the 'raw' data. A typical IRM acquisition analysis requires a selection of a series of the following forward fields (all in mT): 20, 40, 60, 80, 100, 200, 300, 500, 600, 800 and 1000.

Such a progressive field produces IRM acquisition data, which can easily be compared with theoretically derived IRM acquisition data (Figs 7.24 and 7.25). Also, once the sample is saturated, a number of backfields may be used; the following set of fields is sufficient (all in mT): 20, 40, 100 and 300.

To understand/appreciate the form of raw data, a sequence of hypothetical measurements for four samples is listed out in Table 7.5. Note the data for samples 1 and 2. This is considered to be a 'good' one, since for the forward fields the remanence acquired becomes gradually greater and is always positive. It reaches a maximum at 1000 mT, and thereon when the backfields are applied (–20, –40, –100 and –300 mT), the SIRM at 1000 mT goes on reducing to eventually become negative. The data for samples 3 and 4, show errors at 300 and 100 mT forward reading, respectively. The 1000 mT forward field reading for sample 3 is slightly smaller than the 800 mT forward field reading. Also, for sample 4, the 300 mT backfield reading is in error, since it is larger than the saturation achieved by 1000 mT forward field. For possible errors in measurements, there are a number of explanations: (1) small calibration errors, (2) small differences in the orientation of the sample within the magnetometer, (3) movement of grains within the sample pot, and (4) delay between magnetization in the pulse magnetizer and the remanence measurement in the magnetometer.

Partial IRMs: Partial IRMs and their ratios are widely used for sediment characterization in environmental (rock) magnetism. For example, the hard fraction, HIRM, is determined by substracting the IRM acquired in 300 mT (IRM_{300}) from SIRM, to estimate the contribution of antiferromagnetic minerals (e.g. hematite and goethite) to the saturation remanence. HIRM is an absolute

Table 7.5 Hypothetical raw data for four samples generated using the combination of pulse magnetizer and magnetometer

Fields		*Sample 1*	*Sample 2*	*Sample 3*	*Sample 4*
20	forward (mT)	65.3	3.3	190.2	65.3
40		140.6	19.5	260.2	160.6
100		1025.7	70.6	792.4	–1095.7
300		1534.0	140.3	62.5	1634.0
500		1601.1	166.4	4112.3	1701.1
600		1606.3	185.3	4263.5	1706.3
800		1607.3	190.2	4302.6	1707.3
1000		1608.5	195.4	4296.5	1708.5
20	back (mT)	1200.6	140.3	2200.7	1300.6
40		800.6	26.4	–3.9	600.6
100		–792.3	–95.2	–1024.4	–992.3
300		–1554.6	–165.0	–2684.9	–1754.6

Values represent total combined vector taken from the magnetometer for each field (*courtesy:* Walden)

concentration-dependent parameter. The soft fraction is quantified in relative terms through S-ratios, calculated from measurements of SIRM and of the IRM subsequently acquired in backfields of 100 mT (IRM_{-100}) or 300 mT (IRM_{-300}): $S_{100} = -IRM_{-100}/SIRM$ and $S_{300} = -IRM_{-300}/SIRM$. These ratios range from –1 for samples containing only hard antiferromagnets to +1 for samples dominated by soft ferrimagnets. These parameters are frequently used in palaeoceanographic and environmental applications because they are sensitive to changes in magnetic mineralogy. Table 7.6 shows a hypothetical example of this process for an individual sample. In effect, it normalizes the data for each sample for its overall concentration of magnetic minerals, as indicated by SIRM. The advantage of this exercise is that it aids in comparing different samples and exhibits the proportion of remanence acquired by each one of them at relatively low or high fields helping to identify the relative proportions of magnetically 'soft' and 'hard' mineral species.

Component analysis of IRM coercivity spectra: In contrast to magnetic susceptibility, the remanent magnetization is carried only by ferro(i)magnetic minerals. The ability to retain a remanent magnetization is a coercivity parameter and is dependent on grain size, temperature, and an applied field. Information about the remanence carriers can be obtained by analyzing IRM coercivity spectra. The coercivity of grains is governed by their volume, shape, stress, oxidation state and impurity content. Therefore, an attempt can be made to separate and quantify different magnetic components according to their coercivities. Another way to quantify mixed magnetic mineralogy is the IRM component analysis, the decomposition of a measured IRM acquisition curve into several components with the use of model analysis. Initially, cumulative log-Gaussian curves are used to closely conform to measured IRM acquisition

Table 7.6 Processing of a raw data set to produce mass specific IRM data for each forward field and IRM/SIRM ratios for both the forward and back fields

Sample weight = 10.09 g			*Forward field only*	*All fields*
Field used		*Raw data (total combined vector × 1.29)*	*Mass specific IRM*	*IRM/SIRM ratio*
20	forward (mT)	57.7	5.72	0.25
500		199.3	19.75	0.86
600		217.8	21.59	0.94
1000		230.7	22.86	1.00
20	back (mT)	83.9		0.36
100		–143.6		–0.26
300		–204.8		–0.89

Hypothetical data for an individual sample. The raw data values represent the total combined vector taken from the magnetometer (*courtesy:* Walden)

curves. Recently Kruiver and her coworkers proposed the use of the F-test (and t-test) to judge upon the number of coercivity fractions required for the optimal fit.

IV. Demagnetization Parameters

Demagnetization techniques test the stability of the magnetic minerals that carry the remanent magnetization, and provide information on their properties. Starting from the SIRM state, application of successively larger backfields causes the net remanence first to decrease, and then to grow in the reverse direction eventually reaching the negative SIRM state. This process is often termed DC demagnetization (Figs 7.26 and 7.27), and is similar to a part of the isothermal remanent hysteresis cycle.

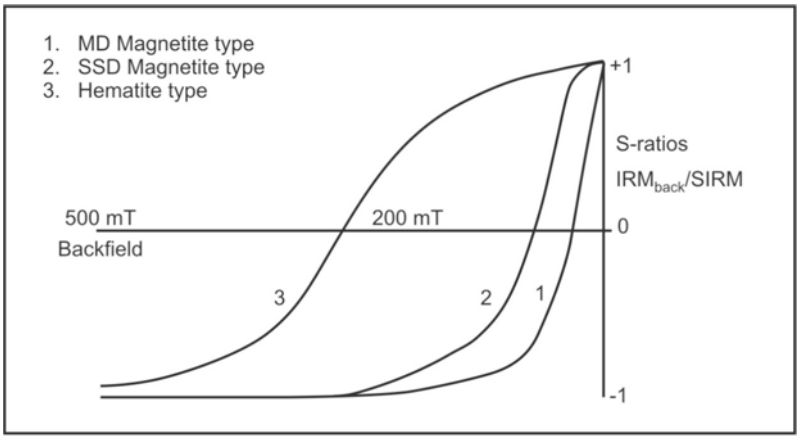

Figure 7.26. Typical coercivity spectra plots for MD magnetite, SSD magnetite and hematite.

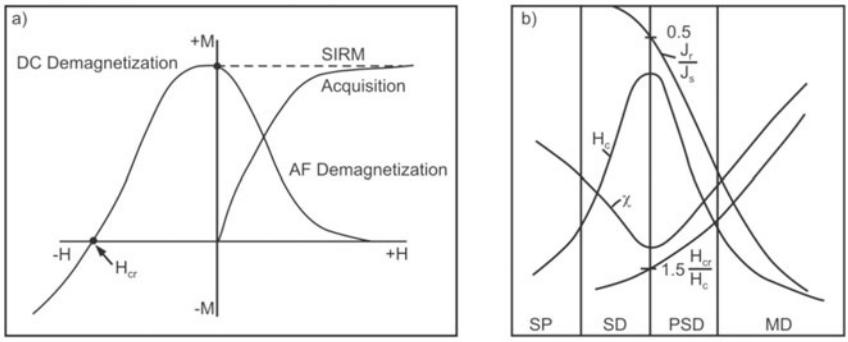

Figure 7.27. (a) Comparison of DC demagnetization, IRM acquisition and AF demagnetization. (b) Magnetic properties of small particles: H_c coercive force, χ susceptibility, M_{rs}/M_s and H_{cr}/H_c (*courtesy:* Soffel).

Assemblages dominated by MD and SP grains exhibit 'soft' demagnetization behaviour, because they easily relinquish the induced alignment of their moments, through domain relocation and thermal disordering. Characteristically, concave demagnetization curves result with low H_{CR} (backfield at which the IRM equals zero) values and reverse saturation attained in low field strengths (Fig. 7.27b). A slightly more resistant curve arises from the harder response of SSD grains, giving a convexity in the upper part of the curve due to initial resistance in the lower fields before realigning at slightly higher intensities. Coercivity curves derived from canted antiferromagnetic minerals contrast with those typically characterizing ferrimagnetic minerals (Fig. 7.26), e.g. convexity of the curve indicates the extreme magnetic 'hardness' of the material giving high (>60 mT) values of H_{CR}, which only attain reverse saturation at maximum backfield intensities. Coercivity is thus seen to sensitively discriminate between natural samples, even where the curves are composite results of mineral and grain size mixtures.

The two parameters of the coercivity spectra, simplified S-ratios ($IRM_{-0.1T}/IRM_{1T}$) and Y-percentages [$(IRM_{-0.3T}/IRM_{1T} \times 2) \times 100$], are useful to discriminate between 'hard' and 'soft' magnetic minerals (Fig. 7.26). A sample's coercivity spectrum is estimated by plotting the ratio of IRM to $IRM_{0.8T}$ for a range of backfields (5–500 mT). High H_{CR} suggests 'hard' or 'hematite type' behaviour. Intermediate and low values indicate SSD and MD 'magnetite type' behaviour, respectively.

With AF demagnetization, the peak AF is increased until magnetic minerals with the highest coercivity are demagnetized (Fig. 7.27a). It is important to note that coercive force values are concentration-independent. To a first-order description, this is warranted in many natural situations. Under this condition, values of magnetizations and various remanences scale linear with the concentration of the magnetic minerals. By dividing two concentration-dependent parameters, a concentration-independent ratio is obtained that contains information on grain size or the oxidation degree of the magnetic mineral.

V. Hysteresis and Remanence Coercivity

Most of the fundamental magnetic properties used in environmental magnetism studies can be illustrated and defined with reference to a hypothetical hysteresis loop (Fig. 7.28) for an assemblage of randomly oriented ferro(i)magnetic grains ranging in size from MD through to SSD and SP.

The induced magnetization rises (shown by [a] on the apparent curve) when a small magnetic field is applied (Fig. 7.28). On removal, however, the magnetization intensity returns to 'pre-magnetized' state. This linear and reversible response is produced by the combined reactions of the constituent magnetic grains: (1) in MD grains, reversible movement of domain walls causes enlargement of domains, whose moments are aligned closest to the field direction. Conversely, slight rotation of the nonaligned moments also takes

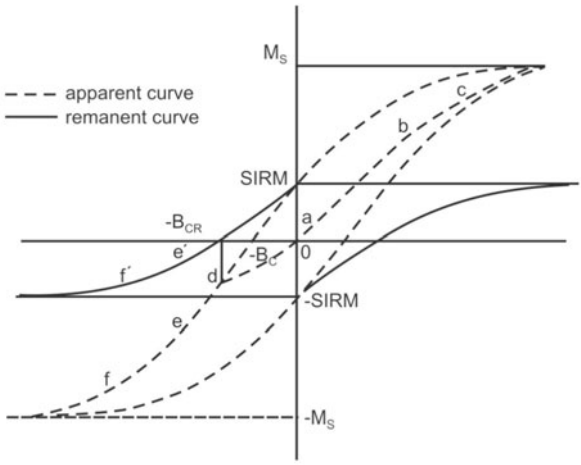

Figure 7.28. The hysteresis loop of a magnetic material. Various symbols are explained in the text (*courtesy:* Dankers).

place, (2) in SSD grains, there is slight domain rotation towards the field direction, whereas (3) SP grains spend a proportionally longer time aligned within the field. The gradient of the curve (a) gives the χ of the sample. The χ is the magnetization observed in low field, which is equivalent to the Earth's field (50–100 μT).

Subsequently, when the applied field intensity is increased, magnetization again increases, but now non-linearly (part [b] of the apparent curve), and the process is no longer reversible. When the applied field is removed, the induced magnetization does not return to its origin, but merely relaxes towards a level of remanent intensity defined as IRM. This non-reversible magnetization process is produced by contributions from MD and SSD grains. In MD grains, it is caused due to irreversible domain wall movements, while in SSD it is by irreversible flipping or rotating of the previous easy axes of magnetization. SP grains do not contribute to remanence, since their in-field alignment is lost through thermal disordering immediately upon removal from the field. Further increase in applied field intensity induces increased in-field and remanent magnetization. But, a point is reached where no further in-field magnetization is attained despite continued field increase. This point represents the largest magnetization the assemblage can attain with maximum alignment of: (1) the domains of the larger grains (achieved through energized wall movement), (2) the individual domains of the small grains (which have all been flipped and/or rotated), and (3) the individual SP grains. This maximum magnetization is termed the saturation magnetization (M_S on the apparent curve), which relaxes to the saturation IRM (SIRM, on the remanent curve). M_S is measured in the laboratory by applying a magnetic field over 1 to 2 T.

The amount of viscous magnetization loss undergone by a sample from its M_S to its SIRM is dependent on the grain sizes present with the moments of

MD and to a lesser extent SSD grains. These tend to readjust and relax towards their inherent easy axes of magnetization, while the SP grains totally lose their imposed in-field magnetic order. The ratio of SIRM to M_s for an assemblage of randomly oriented SSD grains has been theoretically calculated as 0.5 for magnetite and Ti-magnetite, PSD grains give a ratio between 0.1 and 0.3 for magnetite and 0.05 for Ti-magnetite, and MD and SP grains tend towards a ratio of zero. Thus, the viscous loss is greatest for SP and MD grains and least for the SSD configuration (Figs 7.29, 7.30 and Table 7.7).

Having attained forward saturation of the sample, a series of fields is then applied in the opposite direction to identify DC demagnetization behaviour of mineralogy and grain volume. This is attained by verifying the degree of ease (or difficulty) with which the induced forward magnetization can be reduced and then reversed. The point (d) on the remanent curve reveals the SIRM to have been reduced to zero. The field intensity required to achieve this is the parameter of remanent coercivity (B_{CR}). At this point, half of the remanent magnetization is directed opposite to the original remanent saturation direction.

Table 7.7 Magnetic hysteresis properties of some pure samples of known narrow grain size

Sample	*Domain state*	M_S 10^{-6} *A m*^{2}	M_{RS} 10^{-6} *A m*^{2}	M_{RS}/M_S	B_C *mT*	B_{CR} *mT*	B_{CR}/B_C
Magnetite	fine PSD	2.32	0.92	0.397	38.4	57.7	1.5
Magnetite	PSD	1.80	0.29	0.162	8.7	18.6	2.1
Magnetite	MD	9.07	0.08	0.008	1.2	14.4	12.0
Magnetite	MD	7.67	0.09	0.011	1.4	12.0	8.8
Hematite	SD	1.98	1.19	0.602	150	230	1.5
Greigite	SD	0.81	0.45	0.557	53.8	69.4	1.3

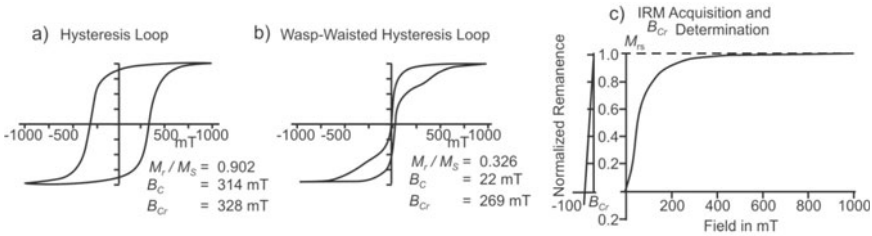

Figure 7.29. Examples of magnetic hysteresis loops (a, b). (a) Hysteresis loop of an ensemble of SSD, characterized by square hysteresis loops; loops of PSD and MD are increasingly slender and have inclined slopes hysteresis loop for hematite. (b) Example 'wasp-waisted' hysteresis loop. The central section is smaller than the outer parts. Wasp-waisted loops are typically of mixed phases with contrasting coercivities: either a mixture of two magnetic minerals (magnetite and hematite in the present case) or a mixture of SP and MD of the same mineral. (c) Determination of an IRM acquisition curve and the remanent coercive force (*courtesy:* Dekkers).

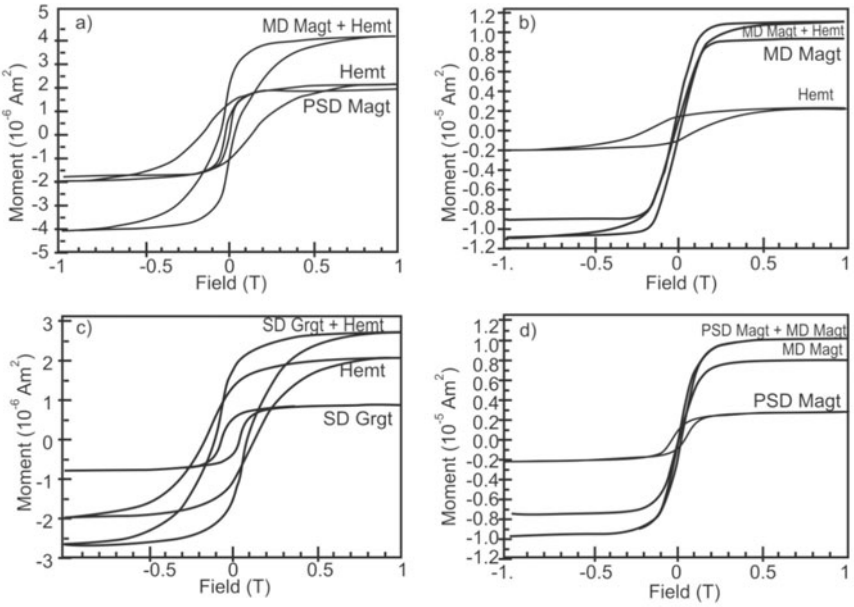

Figure 7.30. Hysteresis loops for two pure samples of known grain size, shown with the composite loop obtained by measuring both samples together. Loops are listed from lowest to highest moment: (a) PSD magnetite, hematite, PSD magnetite + hematite; (b) hematite, MD magnetite, MD magnetite + hematite; (c) SD greigite, hematite, SD greigite + hematite; and (d) PSD magnetite, MD magnetite, PSD + MD magnetite. The hysteresis parameters for these samples are listed in Table 7.7 and can be matched by comparing M_s values (*courtesy:* Roberts).

These two directional moments being 'equal but opposing' cancel each other thereby producing a zero net moment. On the apparent curve, the coercive force B_C (Fig. 7.28) occurs, where in-field forward and reverse magnetizations are 'equal and balanced'. Continued increased intensity of the reverse fields past the B_C and B_{CR} points causes the induced magnetization to follow the paths (e) to (f) and (e') to (f') on the apparent and remanent curves, respectively. The cycle of hysteresis is then completed with the attainment of reverse saturation and remanent magnetizations (M_S and –SIRM). A reverse field of 300 mT corresponding to point (f) on the curve, denoted by IRM_{-300} is given by (Of'). The ratio IRM/SIRM at a specific reverse field is denoted by [S-ratio] (Fig. 7.28). For hematite, B_{CR} is >0.2 T; for magnetite it is ~0.05 T. Values of S–ratio (~IRM_{-300}/SIRM) of ~1 indicate a high proportion of magnetite, whereas the lower values indicate an increasing proportion of hematite and goethite.

Day plot and hysteresis loops: If there is only one magnetic mineral, and it is known to be magnetite or titanomagnetite, the grain size can often be estimated from the plot of two ratios between magnetization (M_{rs}/M_s), and coercivity (H_{cr}/H_c). It is called the Day plot obtained from bulk hysteresis parameters.

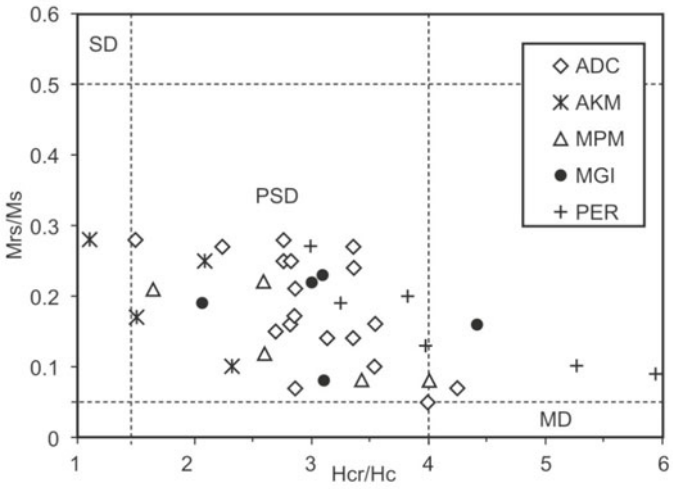

Figure 7.31. The data of Indian archaeological samples as shown on 'Day plot'. ADC - Adhichanallur, AKM - Azhagankulam, MGI - Mangudi, MPM - Mamallapuram and PER - Perur. M_S = saturation magnetization, M_{rS} = saturation remanent magnetization, H_c = coercivity, H_{cr} = remanent coercive force. The plot is usually divided into regions: SD for $M_{rS}/M_S > 0.5$ and $H_{Cr}/H_C < 1.5$, MD for $M_{rS}/M_S < 0.05$ and $H_{Cr}/H_C > 4$ and PSD.

Figure 7.31 illustrates how SSD, PSD and MD grains can be recognized through their magnetization and coercivity ratios in the Indian archaeological samples, where identification of SSD magnetic grains is important in absolute paleointensity studies.

7.9 SECONDARY MAGNETIC PARAMETERS: INTERPARAMETRIC RATIOS

Concentration independent parameters: These reflect relative proportions of magnetic minerals of different types and/or grain sizes and are thus mainly unaffected by bulk concentration of magnetic material in a sample. These are inter-paramagnetic quotients (or ratios) primarily influenced by either the mineralogical or granulometric composition of the sample's magnetic assemblage rather than its bulk concentration. The most important concentration-independent parameters include S-ratio, SIRM/χ, χ_{arm}/χ, χ_{arm}/SIRM, χ_{fd}%, HIRM%, SIRM/M_S, B_{CR}/B_C and M_{RS}/M_S.

Rock magnetic parameters and their ratios: In routine environmental studies, about a dozen magnetic parameters and ratios are used to characterize magnetic materials, which basically relate to four main aspects of mineral magnetic properties (Table 7.8). These are: (i) the concentration of magnetic minerals, (ii) the stability of the magnetization (measured by the hysteresis loop width; goethite and hematite have high stabilities, hence low S-ratios), (iii) the

squareness of the hysteresis loop (related to steepest gradient of the hysteresis loop; goethite and hematite show square loops that can be identified by IRM/χ ratio), and (iv) the type of magnetic interactions between crystals as chains (Table 7.8).

Table 7.8 Four important mineral magnetic properties

Characteristic	*Hysteresis loop*	*Remanence*
Concentration	Height	IRMs
Stability	Width	S ratios or ARM demag
Ease of magnetization	Squareness	SIRM/χ or ARM/χ
Grain interactions	Steepness	ARM/SIRM

Figure 7.32 presents a flowchart which shows how a few magnetic measurements can be used to discriminate between the major magnetic constituents. The flowchart uses magnetic ratios rather than individual magnetic properties, because individual remanence or magnetization measurements predominantly reflect just magnetic concentration, and not magnetic mineralogy. In the flow chart, four types of magnetic ratio have been listed to aid in mineral discrimination. They are: (i) S-ratios which relate to IRM acquisition, (ii) IRM/χ and ARM/χ ratios, measure of the shape/squareness of hysteresis loop, (iii) ratio A_{-40}, a measure of the stability of the anhysteretic remanence and (iv) ratio ARM/SIRM, which is related to the strength of grain interactions. Table 7.9 summarizes typical values of these four types of ratio for a range of natural magnetic minerals. A biplot of magnetic stability against squareness (Fig. 7.33) graphically reveals these differences for a range of magnetic minerals, grain sizes and morphologies.

Table 7.9 Typical magnetic ratios of natural minerals (*courtesy:* Maher and Thompson)

Mineral	*SIRM/χ (kA m^{-1})*	*S_{40}*	*S_{100}*	*A_{-40}*	*A/S*	*ARM/χ (kA m^{-1})*
Magnetite (soft)	1.6	0.83	0.97	0.001	0.02	0.03
Magnetite (hard)	55	0.26	0.85	0.5	0.005	0.3
Titanomagnetite (soft)	10	0.5	0.82	0.24	0.004	0.5
Titanomagnetite (hard)	60	0.08	0.34	0.9	0.04	2.4
Hematite	400	0.005	0.003	Low	0.001	0.01
Ilmenohematite	320	0.02	0.13	0.9	0.004	19.0
Greigite	92	0.03	0.38	0.8	0.01	0.9
Pyrrhotite (soft)	90	0.8	0.95	0.04	0.018	1.6
Goethite	70	0.005	0.02	Low	0.01	1.0
Iron	40	0.4	0.8	0.5	0.01	0.4

S_{40}: proportion of SIRM grown in a forward DC field of 40 mT
S_{100}: proportion of SIRM grown in a forward DC field of 100 mT
A_{-40}: proportion of ARM remaining after partial demagnetization in a peak alternating field of 40 mT
A/S: ratio of ARM to SIRM

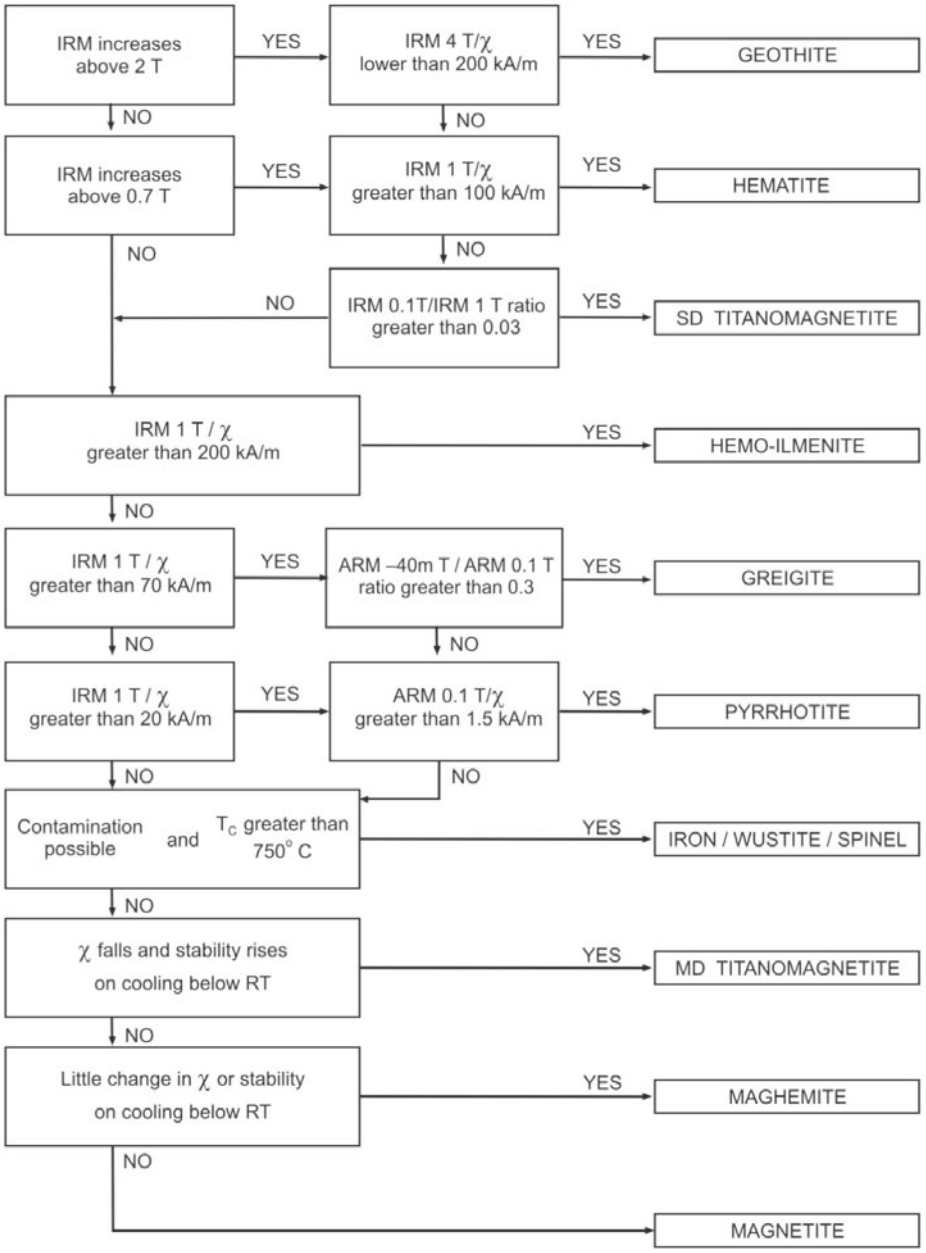

Figure 7.32. A flowchart indicating utility of few magnetic measurements to discriminate between the major magnetic minerals found in environmental samples. Note few magnetic measurements are sufficient to identify major magnetic constituents in the samples (Maher and Thompson, 1999).

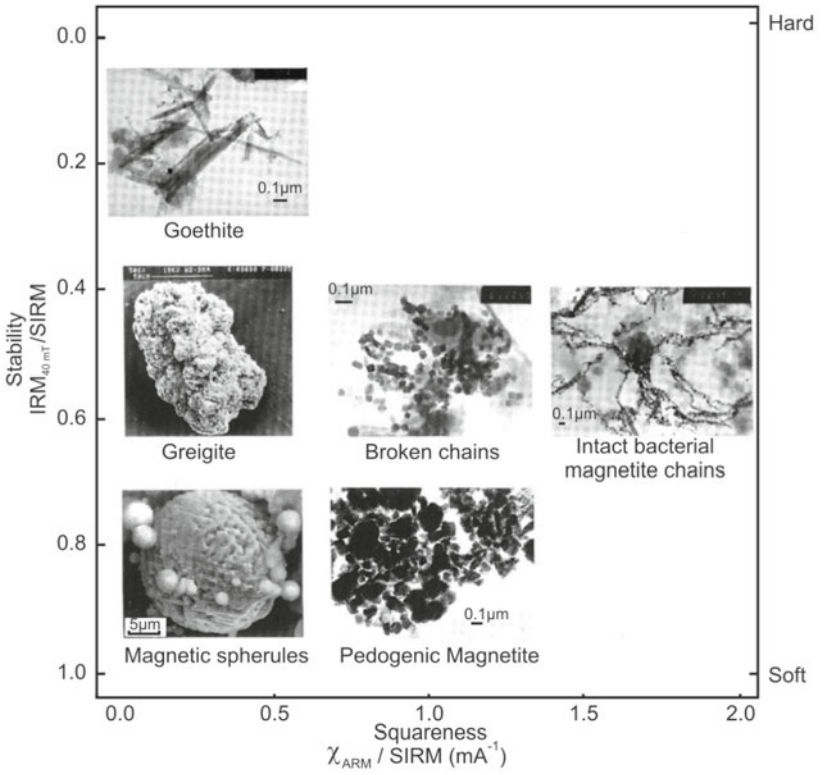

Figure 7.33. A biplot of magnetic stability vs. squareness showing six examples of different magnetic minerals, grain sizes and morphologies (*courtesy:* Maher and Thompson).

7.10 MAGNETIC STUDIES, COMPLEX ISSUES

Magnetic method is a powerful tool to reconstruct environmental history, though it is restricted in its application by the potential complexity of relationship between sediment sources and sinks. A catchment has several magnetically distinguishable sources, because of which determining relative source contributions become mathematically and statistically complicated.

A significant impediment to use of lake and marine sediment records is the post-depositional chemical changes in magnetic mineralogy. Dissolution is a diagenetic process that involves initial loss of the finest magnetic fraction and later on the coarser magnetic minerals. In such cases, the assumption of an entirely detrital origin becomes erroneous, because it requires the presumption that magnetic properties are conserved during transport from the source to the sink.

Apart from the chemical reduction of magnetite, marine and freshwater bacterium are also found capable of dissolving and reducing magnetite. Iron sulfides such as greigite, and fine grained (SSD) biogenic magnetite are reported

to have authigenically grown in lacustrine and marine sediments. These minerals are produced intracellularly and to some extent extracellularly. Magnetic bacteria have also been found in soils as well. Thus, biogenic ferrimagnetic minerals can make a contribution to the assemblage of magnetic minerals in sediments, although this contribution is likely to be more significant in depositional environments that favour the growth of magnetotactic bacteria.

An important issue associated with sediment transportation processes is the complex relationship between sediment particle size and magnetic properties. The highest χ values occur in the <125 μm fraction of river bed sediment, implying downstream increase in particle sorting, which makes the sediment progressively finer. However, this relatively simple setting is complicated by other processes that come into play in the form of abrasion, particle breakage or the selective deposition of heavy minerals that contain a high proportion of magnetic minerals (like magnetite). To reduce ambiguity associated with sediment transport, it thus becomes necessary to conduct tracing studies on well defined (laboratory sorted) particle size fractions. This may, however, not eliminate magnetic mineral dilution or enrichment by fluvial sorting processes.

I. The Mixing and Unmixing Problem

Rocks and sediments inevitably contain mixtures of magnetic minerals of different grain sizes and weathering states. Most environmental (rock) magnetic techniques rely on a set of parameters, designed to interpret in terms of mineralogy, concentration and domain state of magnetic minerals. In some cases, however, such interpretation of natural samples can be misleading. A more reliable approach to magnetic mineralogy models is based on the analysis of magnetization curves, which are decomposed into a set of elementary contributions characterizing specific set of magnetic grains with unimodal distribution (component analysis) of physical and chemical properties. Magnetic components are then related to specific biogeochemical signatures, not characterized as just SSD magnetite. This unconventional approach opens up a direct link to the interpretation of natural processes on a multidisciplinary level. Despite these advantages, component analysis has not yet come into wide use for three reasons: (1) lack of quantitative magnetic models for natural, non-ideal magnetic grains, and/or the statistical distribution of their properties, (2) intrinsic mathematical complexity of unmixing problems, and (3) need of accurate measurements that are beyond the usual standards.

Since magnetic components rarely occur alone in natural samples, unmixing techniques and rock magnetic models are interdependent. Recently, efforts have been initiated to verify the basic properties of magnetization curves, and obtain useful/reliable solutions to the unmixing problem. It has already resulted in collection of a few hundred magnetic components from various natural environments. The properties of these components are controlled by their biogeochemical history, regardless of the provenance of the hosting sediment.

For example, the coercivity of all detrital magnetites is tuned by the transport mechanism (air/water) and the ARM of biogenic magnetites is controlled by their (paleo)redox condition. The consistency of these results supports the linear additivity principle upon which all current magnetic unmixing methods are based. Once the rock magnetic properties of individual components and their statistical distribution are known, the solution of unmixing problems provides important benefits. One of the major benefits pertains to making the whole process simple, thereby making it accessible to even the non-specialized users. Simplified unmixing algorithms are robust, and are capable of delivering reliable results based on relatively fast measurements.

II. Ternary Diagram and Thermomagnetic Curves

In the context of mineral magnetic studies, it is those minerals spanning the solid solution series between magnetite (Fe_3O_4) and maghemite (γFe_2O_3), which are most important. In addition, the various Ti substituted compositions of these two minerals called titanomagnetite and titanomaghemite often dominate much of the magnetic information gained from the bulk sample measurements.

Three solid solution series on Fig. 7.34 have a characteristic crystal form, but vary in their composition, especially the Fe/Ti ratio (Chapter 2). As the material oxidizes, it moves across a constant Ti/Fe ratio line signifying increase in its oxygen concentration. The titanomagnetites solid solution series are usually found in basic igneous rocks with a movement towards the magnetite end of the series as rocks become more acidic. The ilmenite-hematite solid solution series are usually found in more oxygen-rich environments. For example, hematite can be formed by the oxidation of titanomagnetites or by inversion of maghematite (>350°C). The minerals of pseudo-brookite solid solution series are all paramagnetic above liquid oxygen temperature (Chapter 2). At low latitudes, weathering in the form of low temperature oxidation (LTO) of titanomagnetites yields ferro(i)magnetic mineral as a product through the process of maghemitization. Pyrrhotite (FeS_{1+x}, $0<x<0.15$) when present also contributes to LTO.

Thermomagnetic analysis determines the compositional diagnostic T_C for different minerals by monitoring high-field magnetization M_S-T, and low-field susceptibility (χ-T) during heating to a maximum of 700°C (Figs 7.20 and 7.34). This together with results of chemical analyses plotted on ternary diagram, can be diagnostic of the chemistry of magnetic minerals. Two points in the ternary diagram represent chemical composition of the magnetic mineral between Fe-Ti oxides. Curie temperatures change with oxidation degree of the magnetic mineral according to its position in ternary diagram and Ti content. Thermal alteration frequently occurs, when the magnetic mineral is heated. Alteration temperatures and thermomagnetic behaviour of the alteration products provide further information as to the initial mineralogy of the sample. Use of magnetic measurements at cryogenic temperatures for characterizing magnetic mineralogy is becoming a valuable new tool in rock magnetic and

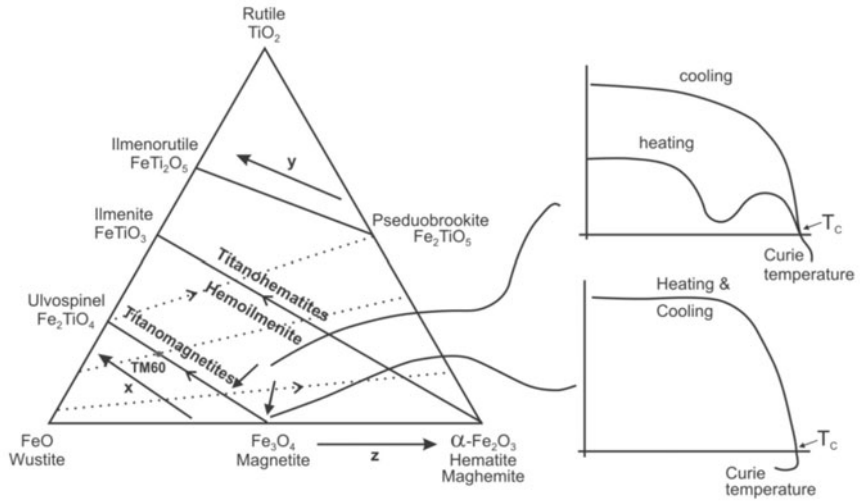

Figure 7.34. Ternary diagram for iron oxides. Solid lines are solid solution series with increasing titanium concentration (x). The dashed lines with arrow indicate the direction of oxidation (z). Two typical examples show compositional relationships (*x* or *y*) and Curie temperatures of Fe-Ti oxide minerals (http://magician.ucsd.edu/Essentials/WebBook162x.png).

environmental magnetic investigations. This is because low-T magnetometry has the potential to complement conventional high-T methods, while offering an advantage of avoiding chemical alteration in magnetic mineralogy during heating.

The various enviromagnetic parameters and their combinations discussed here are employed for the purpose of answering three broad questions: (1) Composition (i.e. which magnetic minerals are present?), (2) Concentration (i.e. how much of each one is present?), and (3) Granulometry (i.e. what are the dominant grain sizes present?).

7.11 ENVIRONMENTAL MAGNETISM—ITS APPLICATION TO THE INDIAN DEPOSITIONAL SETTINGS

Mineral magnetic variations, depending on the environmental context, are used as an aid towards elucidation of a diversity of problems. Several Indian research groups are working diligently to reconstruct palaeoclimate over the subcontinent, and its contiguous oceanic realm. These studies offer considerable potential to correlate marine and terrestrial sequences. However, only a few investigators have used rock magnetic and environmental magnetic properties to extract palaeoclimatic and palaeoceanographic information, which has been presented in the next sections.

Depositional environments under investigation: Indian subcontinent has many sedimentary basins, which are investigated for a complete perception of

the sources and processes to understand subcontinental environmental and climatic changes. In this attempt, use of other techniques such as X-ray diffraction (XRD), scanning electron microscope (SEM), and transmission electron microscope (TEM) is undertaken to confirm rock magnetic interpretation.

Mineral magnetic measurements have been performed on core and hand specimens collected from India encompassing depositional environments of varying type and provenance, viz. ~>4.0 Ma Kashmir Karewa palaeolake sequence; ~10 ka to ~30 ka old palaeolake sequences in the central higher Himalayas at Goting, Pipalkoti, Burfu and Garbayang; ~12 ka shallow playa lakes of Thar desert in Rajasthan; Nalsarovar lake in Gujarat, which is almost ~6.0 ka; ~5.0 ka Mastani lake near Pune; ~500 years old Powai and Tulsi lakes in Mumbai city; near shore deltaic/estuarine environments like those of Godavari, Krishna, Cauvery and Iskapalli situated on east coast and Mandovi on west coast; ~25 ka Himalayan loess deposits, ~25 ka, ~50 ka and ~120 ka terra rossae palaeosols of Saurashtra, and beach samples of Maharashtra, Karnataka and Goa. Figure 7.35 shows the locations, from where sedimentary samples have been collected for environmental magnetic investigations.

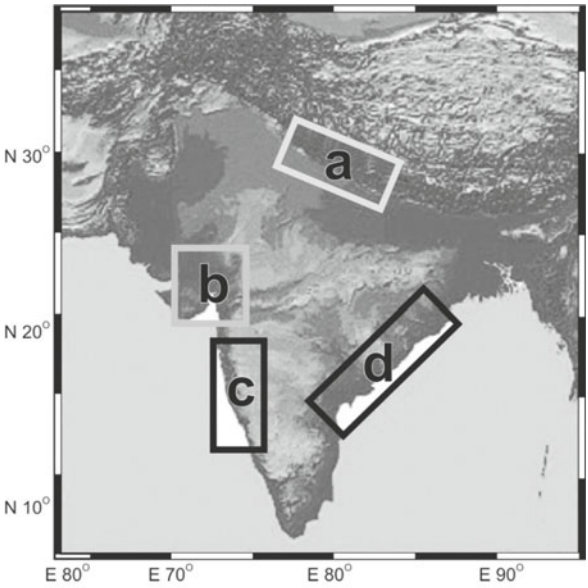

Figure 7.35. Location map of the samples collected for environmental mineral magnetic studies. Digital elevation model based on 1-arc sec resolution (~0.03 km) GTOPO30 data. (a) Proglacial lake deposits from central higher Himalayas, (b) Thar desert lakes and playas, Gulf of Kutch coastal deposits and continental deposits in Mainland Gujarat, (c) Mumbai lakes and Konkan belts covering estuaries in Goa and mangroves along the west coast and (d) East coast deltas, viz. Mahanadi, Krishna, Godavari, Cauvery and Pennar. In these regions stress is being given on mangrove deposits as they are ideal sites for using the mineral magnetic approach.

7.12 MAGNETIC SUSCEPTIBILITY AND DEPOSITIONAL ENVIRONMENTS

How stable are Fe oxides in a given set of environmental conditions, and modify with a change in chemical and physical ambience are discussed earlier. Since they have the diagnostic ability at interconversions between different phases, magnetic minerals are used as a quantified and calibrated proxy. The premise is based on the fact that magnetic mineralogy reflects the course of environmental (climate) changes by recording evidence of associated modifications in sedimentation, weathering and pedogenic regimes. In all, magnetic susceptibility is found to be a valuable tool that accurately plays back the original signals entrenched in the sediments.

I. Magnetic Susceptibility and Mangrove Sediments

In India, mangroves are unevenly distributed along the east and west coast regions. Because of major deltas along the east coast, the mangroves here are better and well developed compared to those along the west coast. Factors such as geomorphology, climate, tidal amplitude/duration and quantity of freshwater inflow determine the mangrove distribution, wherein the sedimentation is influenced by interaction between the mangrove root systems and sediment laden tidal waters.

Indian climate is dominated by two monsoon seasons, and the rate of rainfall varies considerably from one place to the other. Holocene monsoonal and environmental changes are stored in mangrove swamps, where high rate of sediment accumulation takes place. Accordingly, the mangrove swamps develop into good storage sites with a huge pile of fine black clays and silts ideally suited for high-resolution palaeoclimatic study. Natural events and man-made changes have significant impact on the climate, which in turn affects the vegetation, and these signatures are reflected in the subsurface sediments of mangroves. As of now, there is hardly any input of environmental magnetism from the mangrove swamp sediments of India, and hence there is tremendous scope to utilize this technique.

In sediments of Deccan basalts, the magnetization is due mainly to large-grained (titano)magnetite grains of high χ. But, when the rock or sediment weathers by the passage of water through cracks, it results in oxidized grains such as hematite that has a much lower χ. The core logs of χ are used for two studies: (1) to see if different outcrops could be characterized for their similar or dissimilar origins and (2) to use weathering profiles to differentiate diverse depositional sequences.

The transition or variation in χ is governed by a change in the depositional environment. For example, the characteristic feature of mangrove sediments is the display of very low and consistently invariant χ values, which discriminate these deposits from others (Figs 7.36 and 7.37). The section from the base to 40 cm depth, where there is a change in environment, is dominated by very

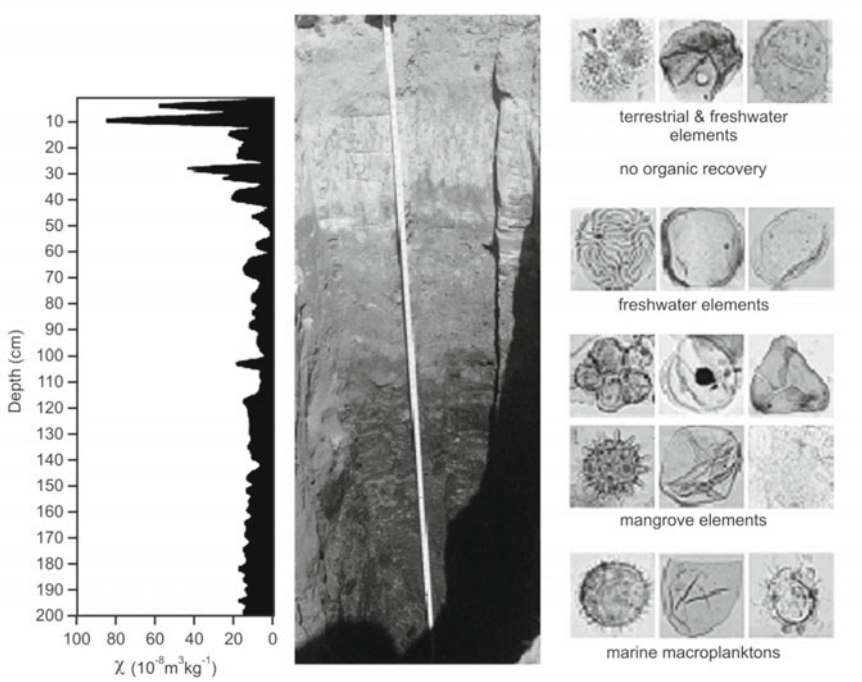

Figure 7.36. The Hadi mangrove sediment core with representative microfossil assemblages at different species and corresponding magnetic susceptibility curve. The low and invariant χ values correspond to the dark clays of mangrove origin. Magnetic susceptibility together with palynoflora enables to recognize marine, estuarine, freshwater aquatics, sandy beach and terrestrial or hinterland ecological complexes (Kumaran et al., 2004).

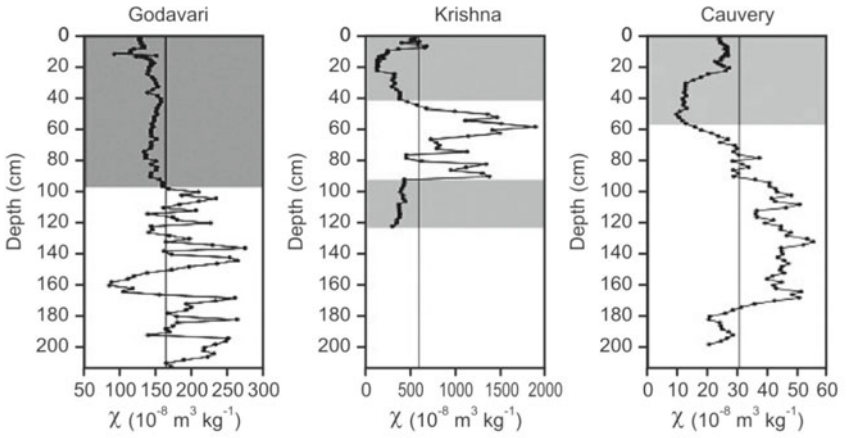

Figure 7.37. The mangrove sediments from east coast deltaic vibra-cores exhibit low and invariant magnetic susceptibility values. The χ logs across three major east coast deltaic basins distinguish depositional mangrove environments from non-depositional ones in a relatively more reliable and inexpensive manner (Seetharamaiah et al., 2004).

low χ variation reflecting mangrove elements (Fig. 7.36). The terrestrial and freshwater sediment input increase χ values significantly towards the top.

The major peninsular rivers like Godavari, Krishna and Cauvery have built large deltas on the eastern coast of India over a total area of ~19,187 sq km. The initiation of these modern deltas is believed to have begun ~8.5–6.5 ka and the rivers bring in a total sediment load of 28×10^9 tonnes annually to the Bay of Bengal. These deltas are characterized by the presence of extensive mangrove swamps along their seaward margins. Low χ variation of the shaded portion (Fig. 7.37) is the repository of mangrove sediments, whereas the highly fluctuating χ indicates more vigorous detrital environment from eastern India deltaic environments of Godavari, Krishna and Cauvery. The ^{14}C ages obtained are: Godavari mangrove delta (2.1 to 1.7 cal ka at 83 cm depth), Krishna mangrove (4.3 to 3.7 cal ka at 95 cm), and Cauvery mangrove (2.3 to 2.0 cal ka at 126 cm).

Generally, sediments from various environments have different χ values. But, the mangrove results indicate that even in a similar environment, ferrimagnetic mineral concentrations vary vertically from one delta to another. The χ values range between 10 and 2000 with the highest ferrimagnetic mineral concentrations in Krishna mangrove swamp followed by Godavari and Cauvery. In the upper part of the cores, there is a steady decrease in χ. High fluctuations in χ occur below 100 cm depth in Godavari, and ~40 to 60 cm depth in Krishna and Cauvery delta mangroves, indicating a change in sequence evolution of deltaic environments during the late Holocene in these regions. It is argued that fluctuations in Holocene χ records reflect climatic change in sediment provenance areas.

II. Magnetic Susceptibility and Flood Plain Sediments

Floods are usually local, short-lived events that happen suddenly across a part of moving or still water body because of intense precipitation that produces more runoff than an area can store or a stream can carry within its normal channel. Rivers can also flood when dams fail, when ice jams or landslides temporarily block a channel or when snow melts rapidly depositing detrital components in the nearby areas giving rise to flood plains. In a broader sense, normally dry lands can be flooded by high lake levels, by high tides or by waves driven ashore by strong winds. Thus, these sediments contain history of climatic changes in the form of flooding and nonflooding events.

The sediments of the Mahi floodplain cover a considerable part of western India, which were formed within the time span of 30 to 10 ka. Rapid oscillations in the intensity of SW monsoon during the last glacial phase have been deciphered from magnetic and calcrete proxy records. Alternating strong and weak monsoon events identified from Mahi river basin in Gujarat, suggest impact of glaciation and glacier melting to have occurred on regional and global scale.

The values of χ and χ_{FD}% vary from 12 to 21 SI and from 0 to 1.2%, respectively. Here both allogenic and authigenic processes (pedogenesis and early diagenesis) occurred together, to differentiate which χ records were compared with opaque magnetic heavy mineral percentages. As can be seen from Fig. 7.38, increase in χ_{FD}% follows an increase in opaque magnetic heavy mineral concentration pointing to heavy detrital input on account of flooding. As opposed to this phenomenon, when there is an increase in χ_{FD}% accompanied by a decrease in opaque magnetic heavy minerals, it is suggestive of pedogenesis. The secondary enrichment of ferrous/ferric Fe due to pedogenesis is captured by simultaneous converging or diverging trends in χ_{FD}% and magnetic heavy mineral concentration. Based on these two collective parameters, four pedogenic horizons are delineated. Seven flood and non-flood periods are also identified, reflecting strong and weak monsoonal phases at a time scale of a few thousand years.

III. Mineral Magnetism and Foraminiferal Assemblage in Mudflat Sediments

Mudflat is an intertidal sedimentary area formed by deposition in low energy coastal environment, like an estuary, whose sediment consists mostly of silts and clays with a high organic content. It is also characterized by high biological productivity and abundance of organisms, but has low diversity with few rare species.

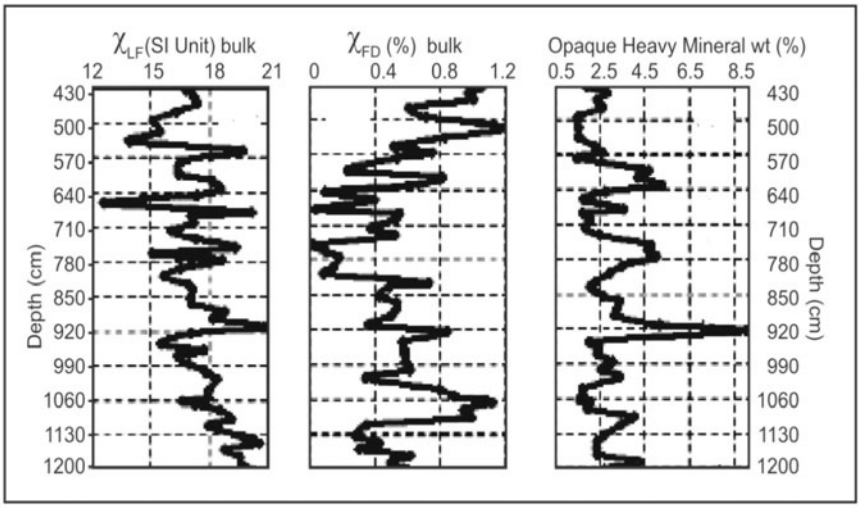

Figure 7.38. Variation of magnetic susceptibility, frequency dependent susceptibility and opaque heavy mineral percentage along depth profile for the sediment sequence at Bhimpura, where the Roman numerals indicate flood events. Simultaneous measurements of χ and its frequency dependence coupled with heavy minerals can be used to identify flood periods and nonflood periods, reflecting indirectly strong and weak monsoon phases (Sant et al., 2006).

The samples of Navlakhi mudflat, whose organic matter was subjected to carbon dating, gave an age of ~11 calibrated ka years before present (cal years BP). A combination of foraminiferal and magnetic analyses was used to reconstruct the depositional environment of clays from a 3.5 m shallow core of the mudflats of the Gulf of Kutch (Fig. 7.39), wherein samples of two levels, viz. 140 cm and 200 cm yielded ^{14}C dates of 9,390±140 years (cal 11,040 to 10,430 years) and 8,720±200 years (cal 10,150 to 9,530 years).

Wet periods of monsoonal reinforcements occurred at the early and middle (°) Holocene, which has been suggested by: (1) overall reduction in magnetic grain size reflected in higher values of ARM/SIRM, (2) low hematite content inferred from high S-ratio, (3) higher (lower) values of S-ratio correlate well with higher (lower) numbers of *Elphidiidae* and *Nonionidae*, which seemed to be governed by the increasing (decreasing) degree of salinity, and (4) increase in percentage abundance of the micro-fauna of *Elphidiidae* and vice versa. The relation of these magnetic parameters to climate change is through discharge variations across time. For example, low variations in the S-ratio, which relates directly to the presence of hematite, indicate changes in fresh water influx in this environmental setup. As this hematite is derived from erosion of oxidized soils of the catchment during drier periods, low values in S-ratio can directly be related to low discharge conditions (weaker monsoons). On the other hand, high S-ratio values reflecting more titanomagnetite in the sediments reveal increased fresh water influx during wet periods of monsoon reinforcement.

IV. Magnetic Susceptibility and Rajasthan Playa Sediments

Playas are enclosed shallow depressions in desert basins, tectonic lows, interdune flats and abandoned channels, which contain deposits and evaporites

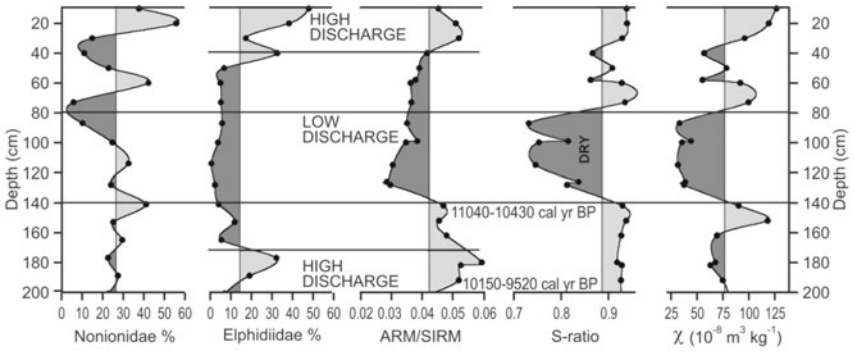

Figure 7.39. Downcore variations of magnetic susceptibility and remanence measurements and their quotients together with foraminiferal from the Navlakhi mudflat core. Interpreted values of low and high discharges are marked across the plots. The study demonstrates magnetic parameters coupled with foraminifera provide useful insights into climate related salinity changes. Note S-ratio together with ARM/SIRM suggests the influence of fresh water resulting in salinity variations (Rajsekhar et al., 2004).

from the impoundment of episodic stream flow or near-surface groundwater. These can be entirely dry or seasonally filled with water, where the sediment load carried into a playa from streams or blown in by wind includes clay, silt and fine grained sand. Evaporation of water from playas leaves exposed surfaces of the resident material, which can be any mix of clay, silt, fine sand and salt. Episodic streams may enter the playa from runoff during or shortly after rainfall in distant watersheds. Water may also appear due to rising groundwater in localities, where the basin floor or a channel intercepts the water table.

The playa sediments carry both the history of past climates and hydrology. In a desert, changes in water level, water chemistry and rate of sedimentation are all controlled by the climate. A dry phase of climate means dessication and shrinkage of the lake leading to increase in salinity. A wet climate leads to more vegetation around the lake filled with water. The pollen of steppe type of vegetation has been reported for Didwana. However, from 8.1 to 6.3 ka and 4.6 to 2.0 ka the landforms were unstable, and the climate was dry and arid, during which maximum influx of sediments took place in the lake.

Bap-Malar and Kanod lakes are in the arid Thar desert of Rajasthan, where climatic records for the past ~12 ka have been preserved. χ values at Kanod and Bap-Malar show progressive decrease down the profile and are interpreted in light of the changing hydrology of the lakes. During periods of high lake levels or rise in groundwater table, sediment composition is governed by the presence of paramagnetic minerals brought into the playa either by eolian or

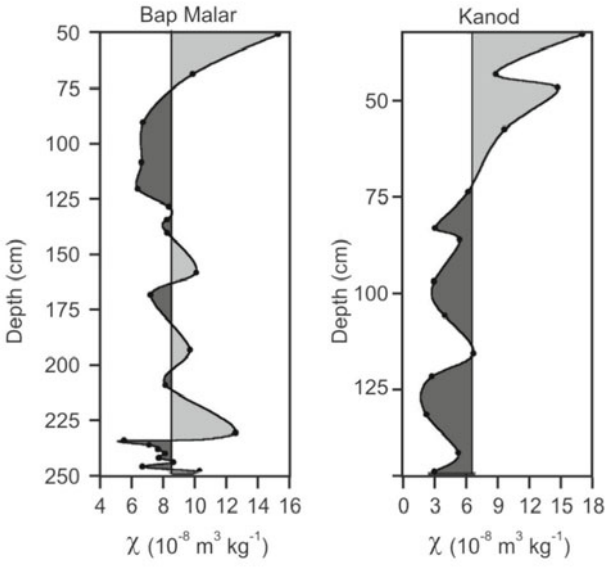

Figure 7.40. Variation in magnetic susceptibility in the Bap Malar and Kanod playa lake sediments. Variations in χ reflect changes in the lake hydrology, leading to dilution of χ through increases in diamagnetic evaporitic minerals. Higher χ values occur when aeolian detrital fluxes increase onto the playa surface (Deotare et al., 2004).

wind activity. When the lake evaporates and groundwater tables go down, the precipitation of evaporites and carbonates suppresses χ. With progressive aridity and simultaneous drying up of the lake, precipitation of evaporite and carbonate minerals decline. Subsequently, eolian sediments rich in hematite deposited onto the lake surface increase χ values.

V. Magnetic Susceptibility, FTIR Record and Civilization Collapse

The world has witnessed gradual as well as abrupt civilizational growth and collapse. The decline has been because of any one or a combination of factors such as war, drought, natural disaster, disease, overpopulation and economic disruption. In India, past settlements and old civilizations occur along most of the lakes and river basins, barring few of the inhospitable terrains. Palaeoclimatic fluctuations are known to coincide with changes in cultural stages in Palaeolithic sites of Rajasthan and Gujarat.

Lothal in Gujarat is a fascinating remnant of ancient Harappan civilization and little is known about the climate that prevailed before, during and at the terminal phase (3.5 ka ago) of this grand culture. Hence, collective proxy studies were carried out to ascertain critical palaeogeographical and palaeoclimatological issues. The magnetic record is jointly interpreted with remote sensing and Fourier transform infrared spectroscopy (FTIR) studies. FTIR was employed to know the relative abundance of carbonate with respect to silicate in order to see the effect of any dilution on the χ values.

Three different levels of χ in the sediment trench record (Fig. 7.41) display changing depositional environments from coastal realm at the lower part to

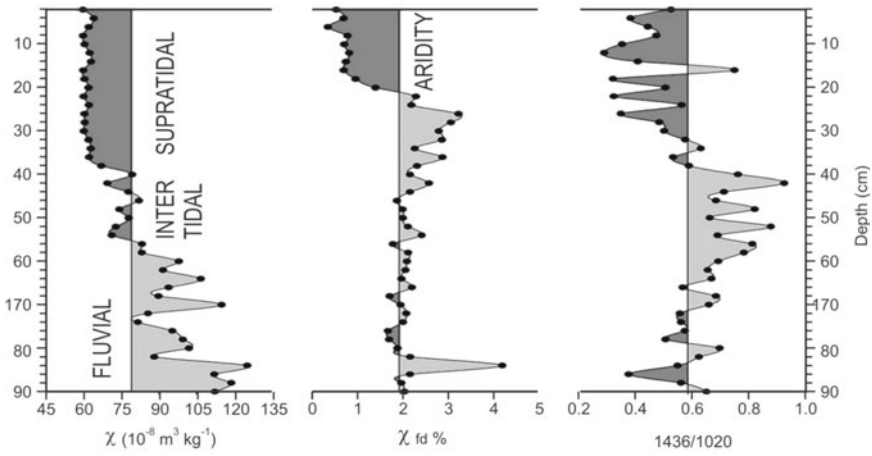

Figure 7.41. Down profile changes in χ and χ_{fd}% compared with variations in relative percentage of carbonate with respect to silica in the sediment. χ and carbonate concentration show fluctuations that are governed by changes in the depositional environment. A marked drop in χ_{fd} is observed towards the top implying a reduction in soil generating processes (Khadkikar and Basavaiah, 2004).

intertidal at the centre, and supratidal at the top. The uppermost part of the sediment record is characterized by low χ. This is not matched with χ_{fd}%, showing high values till ~26 cm after which a fall is observed at 18 cm. This low χ_{fd}% implies reduced monsoon rainfall accompanied by high sea levels witnessing collapse of Harappan civilization. When Lothal was inhabited, the weathering processes in the provenance area were subdued.

VI. Magnetic Susceptibility and Terra Rossae

Late Quaternary aeolinites occur along the coast of Saurashtra in Gujarat, western India. They show a wide array of epikarst and red soil (Terra Rossa) events making them typical formations to study the manner and character of aeolinite weathering under a monsoonal regime (Fig. 7.42). Karst is derived from a German word meaning crag or stone. In geomorphological terms, it refers to limestone terrains, and describes locales with distinctive characteristics

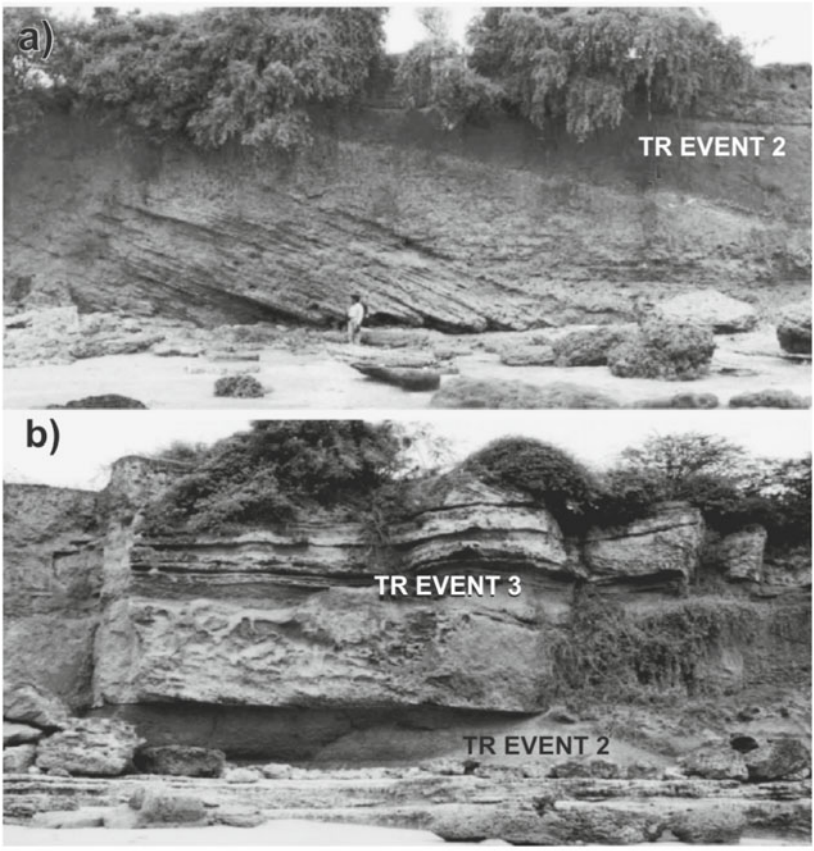

Figure 7.42. Terra Rossae inter-stratified with aeolianites at the classic exposure of Gopinath along with their event stratigraphy and notations (Khadkikar and Basavaiah, 2004).

of relief and drainage arising primarily from a higher degree of rock solubility in natural waters than is found elsewhere. The term also refers to dissolution features found pervasively developed in aeolinites, like in Gujarat. 'Karst' is essentially a variant of solution pipes that are vertically oriented, sometimes interconnected to form honeycomb network or appear as an irregular surface dominated by cavities and channels. Most of the variants of karst are 'epikarst'. These are solution features that have developed near the surface within depths extending to a few metres only. Terra Rossa, on the other hand, are red soils commonly developed on limestones under a Mediterranean type of climate. These are also reported from tropical regions. The Terra Rossa soils are understood to have formed by leaching and residual accumulation of limestone. Alternatively, it has also been suggested that the dust from Sahara gave rise to these soils.

Three Terra Rossae events were observed along the coast of Saurashtra, which placed the age of lower Palaeolithic in western India at ~30 to 100 ka. Of the three Terra Rossae events, event 2 was formed during the last interglacial period and the older event correlates with 170 ka event similar to MIS-3 during which time the Earth entered into interstadial. These Terra Rossae events were formed during periods of interglacial style of climates that were also durations of increased SW Indian monsoon rainfall.

The down-profile changes in χ, χ_{FD} and ARM (Fig. 7.43) are complex, and are related to changes in concentrations of SSD and SP magnetite, siliciclasts, carbonate, and hematite. Seasonal wetting in the monsoon months formed SSD and SP magnetic grains by the breakdown of MD magnetite, whereas formation of hematite was restricted to dry hot summers through oxidation of magnetite. The formation of SSD and SP magnetite and hematite are linked genetically to weathering of the aeolianite that formed Terra Rossa.

VII. Magnetic Susceptibility and Beach Sands

Beaches are by far the most widely distributed of any of the coastal sedimentary environments. The actual shape and orientation of the beach is apparently dependent on a number of variables, including the direction of wave approach, the material comprising the beach, the overall shape and composition of the coast. Beach sediment is the unconsolidated debris produced from the weathering of rocks. Since beaches are prone to erosion or deposition of sediments and are used for recreational purposes, their study forms an important public utility service.

Magnetic proxy measurements can serve as a fast and efficient tool for screening anthropogenic heavy (magnetic) mineral accumulation in soils and sediments. Beach samples from Vengurla (Fig. 7.44) were collected in the three seasons of the year from 2002 to 2005. Magnetic measurements (χ) were carried out to understand sediment movement along the beaches, and to test the validity and efficacy of this technique to collect rapidly and reliably the initial data on sediment movement. The study found that magnetic minerals

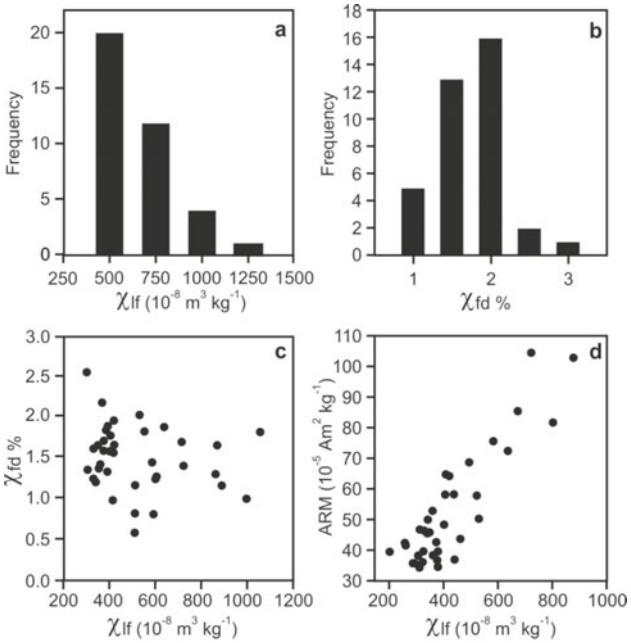

Figure 7.43. Histogram showing the frequency distribution of (a, b) low and frequency-dependent susceptibility (χ_{lf} and χ_{fd}). Both these parameters do not covary as shown in (c). (d) Bivariate plot of ARM and magnetic susceptibility χ_{lf} which shows that they are positively correlated, implying a genetic relationship (Khadkikar and Basavaiah, 2004).

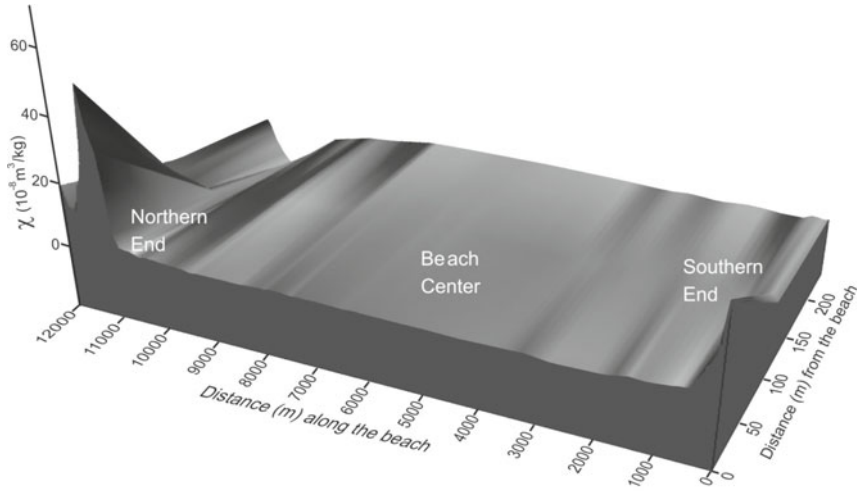

Figure 7.44. Magnetic susceptibility changes delineating magnetic mineralogy and sand migration along beaches of Redi, Aravali and Vengurla, of Sindhudurg district, Maharashtra, India. It can be seen from the diagram the prevalence of magnetic minerals at the extreme ends of the beaches denoting the migration path of beach sediments and the morphotectonic features of longshore currents (Gawali et al, 2010).

across the beach are mostly of ferrimagnetic and antiferromagnetic type concentrated more towards the northern and southern ends of the beaches (Fig. 7.44). But stations situated at the centre of the beaches are distinguished by exclusive presence of antiferromagnetic and/or paramagnetic minerals. The studies also revealed that concentration of magnetic minerals is more during the monsoon season than in pre-monsoon and post-monsoon because of the increased detrital influx from both land and sea. The main source or provenance of these magnetic minerals is the Deccan basalts, laterite and iron ores present along this stretch.

VIII. Magnetic Susceptibility and Himalayan Lake (Vanished) Sediments

The great Himalayan mountain range as a highland emerged by middle to late Miocene (11 to 7.5 Ma); it became a mountain barrier high enough to disrupt W–E flow of winds and push low-pressure area over northern India, which attracted moist summer winds from the Indian ocean. Palaeoclimatically, the uplift of Himalaya and Tibet exerts profound influence on regional and global climate in several ways.

Since the ascent of the Himalayas, the region has undergone several climatic vicissitudes experiencing glaciation for ~18 ka. Such events have devastating effect. For example, the slopes of the Alaknanda valley are loose and fissile phyllitic rocks prone to landslides, which temporarily block the river from a few days to several thousand years. The filled up reservoir is unable to withstand pressure from the stored water causing flash floods in its wake. Landslides of the recent past blocked scores of the Himalayan rivers, inducing scientists to look for evidences of ancient and pre-historical blockades. The presence of ancient river streams and lakes is confirmed by the respective presence of sand and clay/silt at the bottom. Two palaeolakes were thus identified at Goting and Garbayang (Fig. 7.45) in the higher central Himalayas, where sampling was carried out for detailed analyses like mineral magnetics, geochemical and optically stimulated luminescence studies (OSLS).

These palaeolakes contain signatures of glaciation within the timeframe between 40 and 10 ka. The higher central Himalaya is a narrow strip of mountainous terrain between the great Himalayan range and the Indo-Tibetan water divide. Garbayang lies in a transitional zone between dry steppe (Tibetan plateau) and the sub-humid (Himalayan) climate zone. Here the SW monsoon is the dominant source of precipitation which accounts for 80% of the total precipitation, a part of which falls as snow. During Nov to Feb, the westerly disturbances (winter monsoons) contribute the remaining 20% of the precipitation. Goting basin, on the other hand, represents the dry steppe climate of the adjoining Tibetan plateau. At Garbayang, deposition occurred in a proglacial lacustrine environment. These deposits formed in a lake blocked by terminal moraine after the retreat of the main valley glacier. The base of the

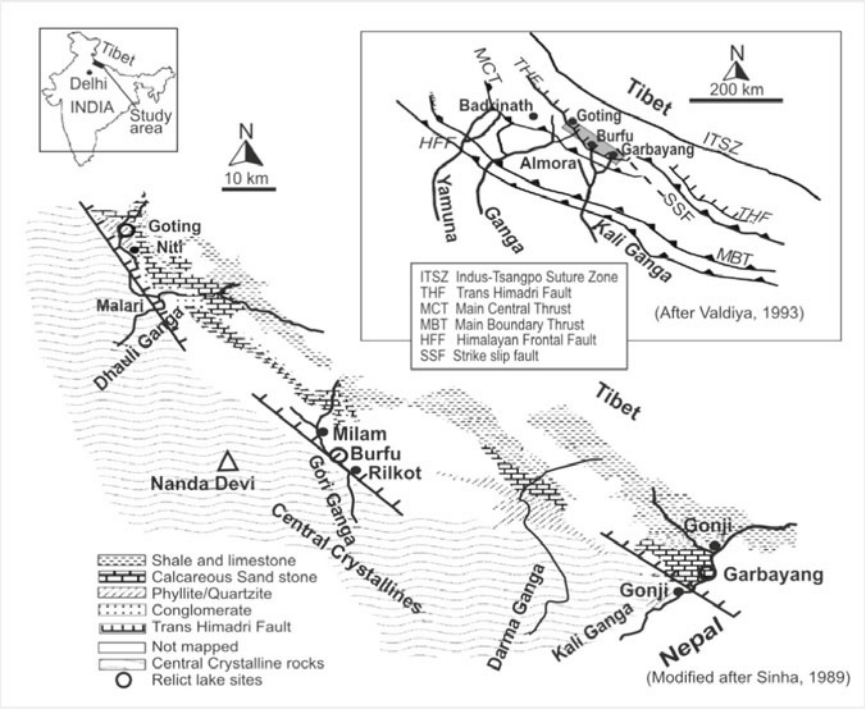

Figure 7.45. Lithology and structure between Garbayang (NE) and Goting (NW). Central crystalline rocks (wavy symbol) are south of the trans-Himadri fault (THF). Open circles are the relict lake locations. An inset indicates a synoptic view of major structures in the region.

palaeolake at Garbayang and Goting has been dated to 20±3 and 29±3 ka, respectively (Fig. 7.46).

Garbayang varve lake deposits: Environmental magnetism can extract valuable insights from physical and biogeochemical lake processes and can characterize lake systems 'prior to' and 'post' significant anthropogenic impacts. Variations in magnetic mineral concentration, grain size and mineralogy are used in the Himalayas to identify changes in environmental conditions that include deglaciation, Younger Dryas cold and arid events during the early and mid Holocene. Younger Dryas represents the 'big freeze' between 12.7 and 11.5 ka. This was a global phenomenon during which time apparently everything remained frozen.

The Swiss launched the first scientific expedition to the remote Himalayas in 1930s, when Heim and Gansser discovered varve-like deposits at Garbayang. Varves (Swedish varv) are fine clays deposited in layers, each representing a year (summer/winter) of glacial melt. Melting of ice increases with the advent of summers, which bring in more detrital input forming thicker layers whereas during winters due to reduced snow melt, the layer of sediments are thinner.

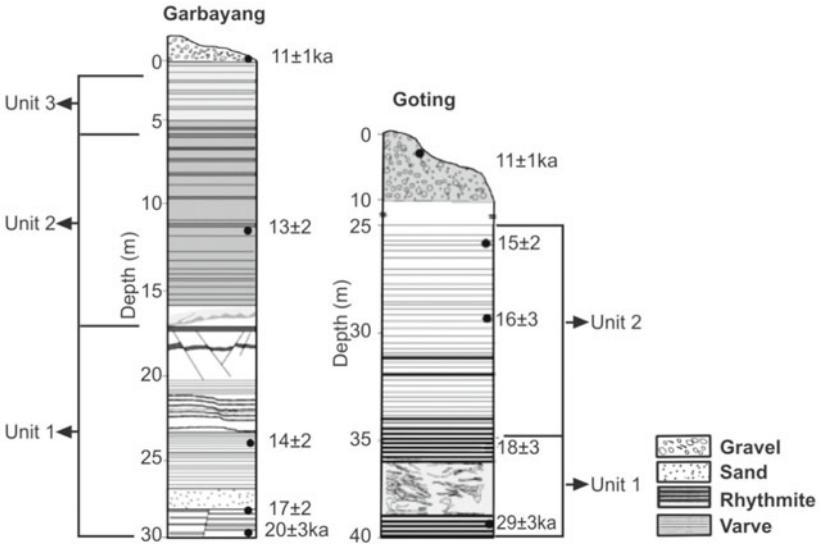

Figure 7.46. Stratigraphy and luminescence chronology of Garbayang and Goting deposits.

One can count such varves with ease and decipher the number of winters and summers the area witnessed in the past.

The Garbayang sediments are equivalent to MIS stage 4 and are estimated to be ~100 m thick. However, the steep cliffs make most of the succession inaccessible and only the top 28 m accessible part is studied. The varves at Garbayang are typical of layered deposition in a placid and calm lake already formed, while the glacier existed (Fig. 7.47). This fact was confirmed by the terminal moraine that proved to be much older than the lake sediments.

Mineral magnetism and palaeoclimate in Garbayang lake deposits: Garbayang deposits reveal high frequency, but low amplitude fluctuations from the base to the top (Fig. 7.48). The provenance of this lake is weakly magnetic precluding the chances of high magnetic material entering the lake. Elemental data was obtained for the upper 8 m of the sequence, which agrees well with the magnetic data (Fig. 7.48) underscoring the immense utility of this technique of being fast, inexpensive and reliable. The salient features of the study are: (1) Dominance of varves and a decline in susceptibility values between 20±3 and ~18±3 ka represent LGM, (2) Magnetic susceptibility and sedimentalogical data suggest that the period between 18±3 and ~13±2 ka witnessed high frequency/low amplitude climatic oscillations, (3) A sudden drop in magnetic susceptibility and elemental concentration of layers dated at 12–11 ka suggests cooling associated with Younger Dryas, and (4) A 1.7 m thick sand body reflects enhanced melt water discharge.

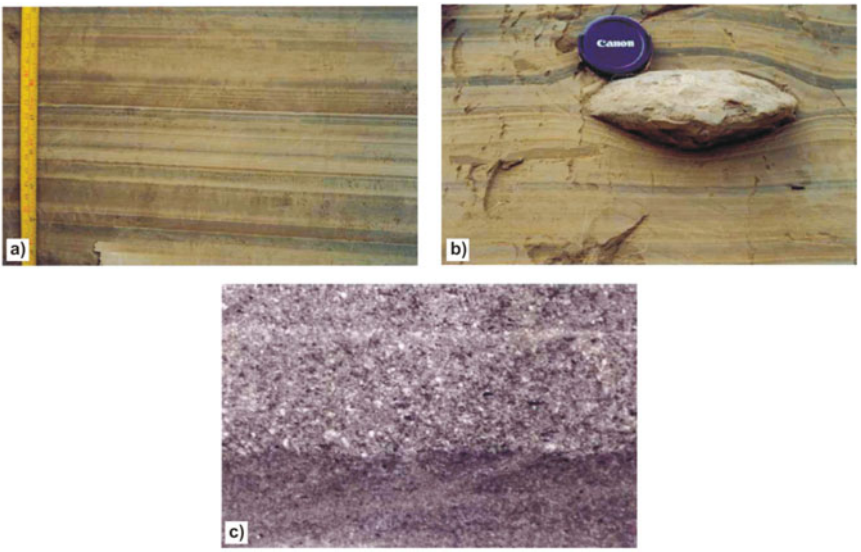

Figure 7.47. (a) Varve like laminations, scale is given alongside. (b) Dropstone (~10 cm horizontal axis) embedded in varve-like laminations. (c) Photomicrograph showing dark winter and light summer lamina, horizontal scale at the bottom is 12 mm (Basavaiah et al., 2004).

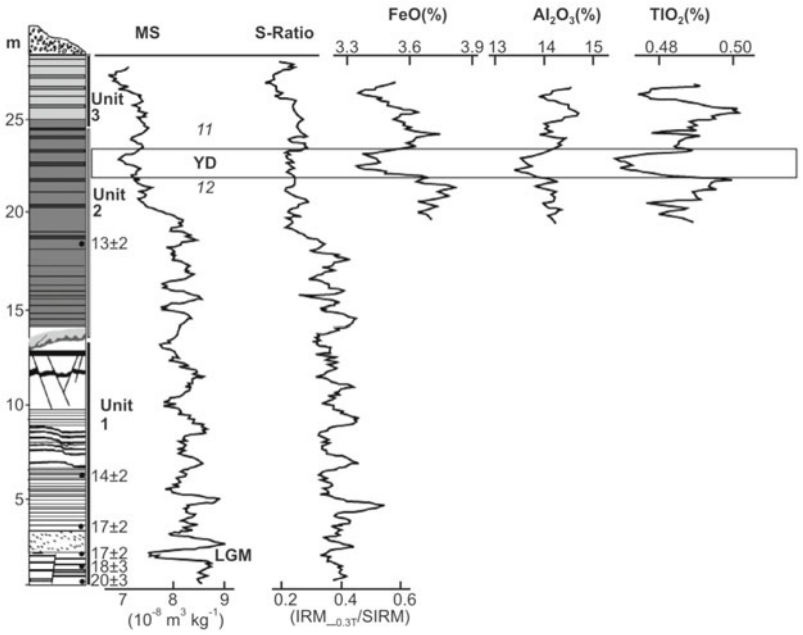

Figure 7.48. Magnetic susceptibility, S-ratio and elemental data plotted against the litholog. Infrared stimulated luminescence (IRSL) ages are shown along side the susceptibility curve. The IRSL ages of 12 ka (22 m height) and 11 ka (25 m height) are interpolated ages (Navin et al., 2004).

Magnetic mineralogy and climate linkages in lake sediments: The property of magnetism is temperature dependent and to exactly identify magnetic minerals following techniques are employed: (i) low and high temperature (–196° to 700°C) dependence of magnetization and magnetic susceptibility, (ii) hysteresis parameters (saturation magnetization M_S, saturation remanence M_{RS}, coercivity remanence H_{CR}, and coercivity H_C) and resistance to AF or thermal demagnetizations. Based on stepwise thermal demagnetization of SIRM, the Himalayan Garbayang lake sediments are found to contain Ti-rich titanomagnetites with varying titanium content and pure hematite (Fig. 7.49a,b). It is suggested that low temperature oxidation (LTO, maghematization) is more advanced in samples (e.g. GB-854 in Fig. 7.49a) of drier phases (decreased rainfall) expressed by alteration (oxidation) of titanium-rich titanomagnetite to hematite. Samples (e.g. GB-906 in Fig. 7.49b) from wetter spells (increased rainfall) show that LTO is less pronounced and titanomagnetites are still preserved. The changes in magnetic mineralogy confirm its suitability in climate related studies.

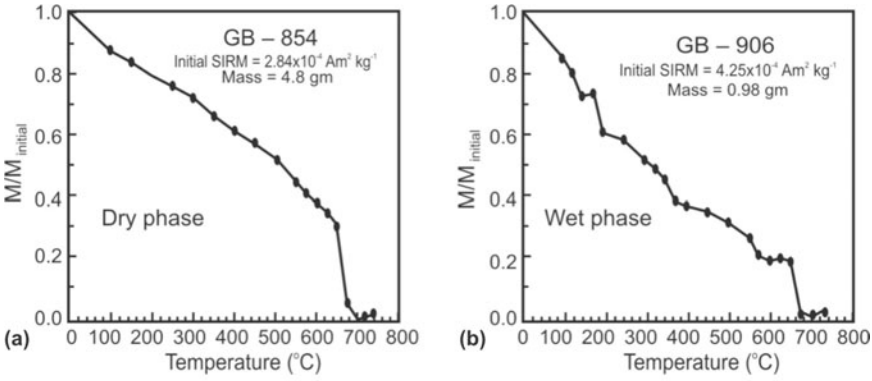

Figure 7.49. Typical thermal demagnetization curves of the normalized SIRM values of the Garbayang lake sediments: (a) GB-854 sample shows a sharp decrease in magnetization at ~675°C suggesting dominance of hematite. (b) Sample GB-906 indicates three magnetic phases, i.e. Ti-rich titanomagnetite, magnetite and hematite (Juyal et al., 2004).

Mineral magnetism and palaeoclimate in Goting lake deposits: Sedimentological evidences indicate the prevalence of two distinct climatic regimes at Goting by infrared stimulated luminescence (IRSL) dating between 29 and 18 ka. The lower unit-I suggests enhanced sediment supply (dominated by titanomagnetite) and higher surface water temperature, whereas the overlying varve dominated unit-II indicates cooler condition punctuated by frequent warm oscillations (Fig. 7.50). The Goting samples are characterized by χ values between ~11 and 17.5 (10^{-8} m^3/kg). Warm condition prevailed with less frequent oscillations between 29 and 18 ka; LGM is identified at ~18 ka (depth 34 m).

IX. Mineral Magnetism and Palaeoclimate in the Himalayan Loess (Silt Deposits)

Loess is a glacial rock flour blown by wind and deposited thousands of miles away from its place of origin. These are homogenous because winds can carry particles of a particular size only. On deposition, the carbonate content binds them together to form huge deposits. Loess sediments are commonly found in China and midwestern USA and are also a hall mark of several European countries. India has very few loess deposits, and the first to identify them was R.K. Pant from Kashmir valley in 1978. Subsequently, in 1984, R.J. Williams and M.F. Clarke reported loess from Sone valley in central India. Pant and his team were lucky to strike loess once again at altitudes ranging from 1800 to 2500 m in the central Himalayas at Dhakuri in Bageshwar district in Pindar river basin and Chopta in Chamoli district in Alaknanda river basin of Uttarakhand (Fig. 7.51).

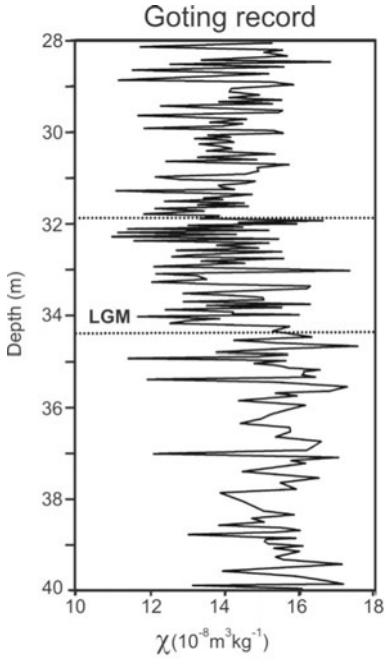

Figure 7.50. Magnetic susceptibility of Goting varve deposits. Note a marked low representing LGM in a saw tooth pattern. LGM - last glacial maximum (Basavaiah et al., 2004).

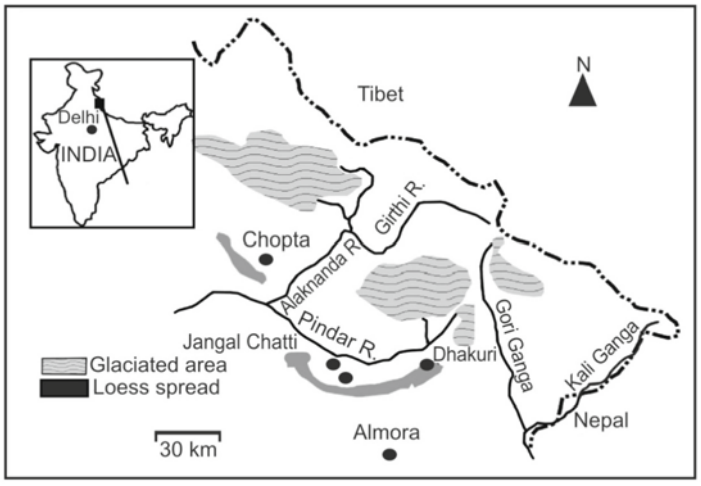

Figure 7.51. Map of the central Himalaya showing distribution of loess deposits south of the glaciated terrain (Pant et al., 2005).

To estimate the age and duration of loess accretion and soil formation episodes, IRSL and ^{14}C techniques were used. IRSL determines the time elapsed since the loess mineral grains were last exposed to sunlight. As the fine sediments carried by the winds are deposited layer after layer, year after year, the sunlight to older sediments becomes dearer. The IRSL ages ranged from 20±4 ka for loess at 200 cm depth and 1±0.3 ka at 20 cm depth (Fig. 7.53). Dhakuri has a higher magnetic content and the anticipated source area is postulated to be a granite terrain. However, granites are poor in Fe content; hence, it is conjectured that they come from a far away place. Some have obtained loess from the sea floor drill-cores. Alternatively, oxidation could have enhanced the magnetic content, as the results suggest. Thermomagnetic χ-T runs between RT and 700°C and unblocking temperatures (SIRM-T) reveal inflection in the heating curves at ~350 and 300°C, which are attributed to the formation and destruction of maghemite due to oxidation (Fig. 7.52). The magnetic properties of the sequences seem to be dominated by magnetite and maghemite in palaeosols, whereas magnetite as well as hematite (with additional maghemite) dominates the loess (Fig. 7.52).

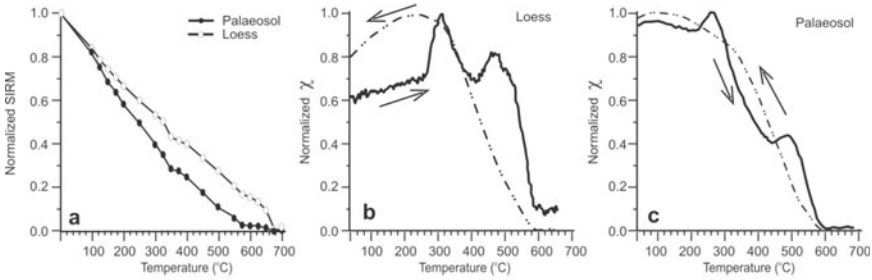

Figure 6.52. (a) Thermal demagnetization of saturation isothermal remanent magnetisation (SIRM) for palaeosol and loess samples. Normalized susceptibility versus temperature curves for loess (b) and palaeosol (c) samples. Thick (broken) lines represent heating (cooling) curves (Pant et al., 2005).

Variations in mineral magnetic properties (Fig. 7.53a-c) are in good agreement with loess stratigraphy, where palaeosols S1 and S2 have higher χ and χ_{FD}% indicating secondary formation of ultrafine grained SP ferrimagnetic minerals (maghemite and possibly magnetite). Lower χ and χ_{FD}% and S-ratio corresponding to loess indicate higher contribution of hematite. Variations in χ are attributed to pedogenic enhancement by inorganic and biogenic processes. Loess accumulation and pedogenesis (soil formation) occur alternatively because loess accumulation is greater during cooler and drier conditions, whereas pedogenesis occurs during wetter conditions. These episodes are interpreted in terms of changes in the strength of the Indian SW monsoon. Thus, magnetic measurements reveal changes in mineralogy and concentration of dominant magnetic minerals between the loess and palaeosols. Geochemistry also corroborates magnetic data (Fig. 7.53d-e).

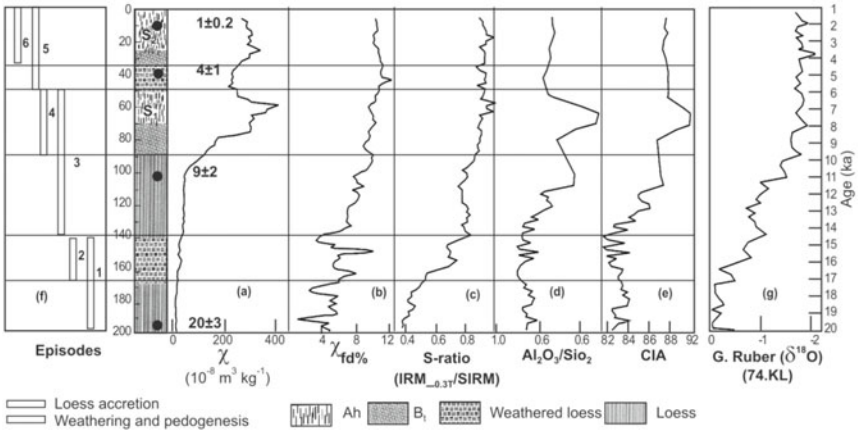

Figure 7.53. Plot of mineral magnetic parameters (a)–(c) of magnetic susceptibility (χ), frequency-dependence susceptibility (χ_{fd}%) and a simplified S-ratio and geochemical data (d)–(e) of Al_2O_3/SiO_2 ratio and chemical index of alteration (CIA). In 2 m loess-palaeosol sequence, six episodes have been identified (f), odd numbers (white vertical bars) represent periods of loess accretion and the even numbers (shaded vertical bars) represent episodes of weathering and pedogenesis. A close correspondence between loess-palaeosol sequence and the oxygen isotopic data (g) obtained on *Globerinoides ruber* from the Arabian Sea (core 74KL, Sirocko, 1996; Pant et al., 2005).

This study allows the following conclusions: (i) loess-palaeosol sequences in the central Himalaya mimic changes in the regional climate including SW monsoon variability over the last 20 ka, (ii) the region experienced a drier and dustier climate from 20 to >15 ka, 12 to 9 ka and 4 to >1 ka, suggesting these to be phases of weaker SW monsoon and (iii) enhanced SW monsoon existed between ~16 and 12 ka and even stronger monsoon conditions existed during 9 to >4 ka, facilitating pedogenesis of loess.

Figure 7.54 reports a synthesis of monsoonal variability in the Indian subcontinent. Loess accretion between 24 and 12 ka is reported from central India, whereas the southern margins of Thar desert experienced enhanced dune building activity during this same period (Fig. 7.54). The period 11 to 7 ka saw the emergence of microlithic culture in the southern margin of Thar desert, and the Ganga plain witnessed channel activity due to the strengthening of the SW monsoon.

7.13 MAGNETOMINERALOGICAL S-RATIO AND PALAEOCLIMATE IN SEDIMENTS

The foregoing sections and case studies prove the effectiveness of mineral magnetic parameters like susceptibility and remanence, revealing climate and environmental change features that are unresponsive to other proxy parameters. Magnetic proxies are very effective in basaltic terrain, especially the S-ratio.

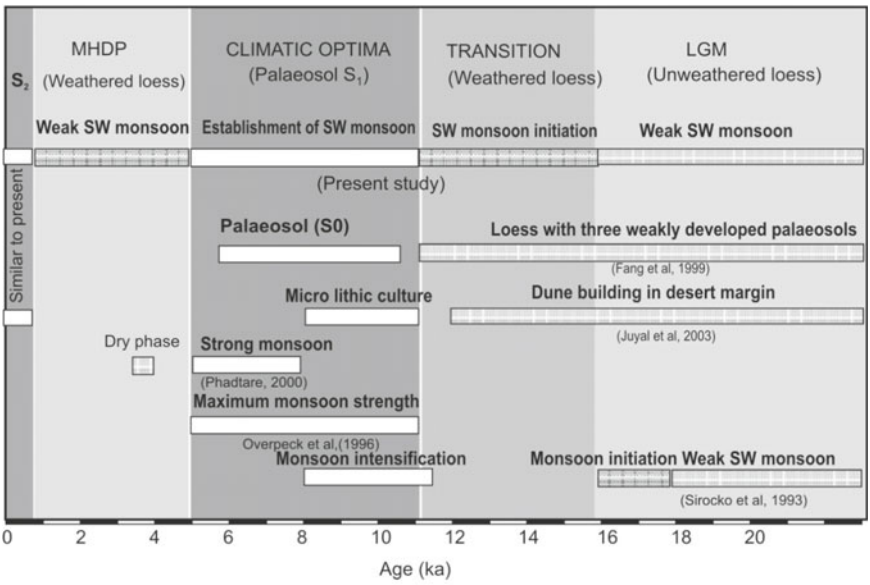

Figure 7.54. Synthesis of marine and terrestrial records of monsoon variability since past 20 ka from Indian sub-continent (*courtesy:* Navin Juyal).

S-ratio is defined as the ratio of laboratory induced backfield IRM and SIRM in fields of 300 mT and 1.5 T, respectively. An example of the use of mineral magnetic lithostratigraphy in late Pleistocene and Holocene studies is shown in Fig. 7.55, where S-ratio is plotted against depth for several sediment cores and profiles covering peninsular and extra-peninsular regions. The mineral magnetic fluctuations of the last 20 ka in S-ratio can be correlated with different environmental (climatic) variations.

High (low) S-ratios occur in warm (wet) sediments indicating higher proportions of 'magnetite' as opposed to 'hematite' minerals in cold (dry) climates. This parameter essentially documents changes in the relative abundance of two ionic states of Fe^{2+} and Fe^{3+}. For example, the oxidation state in magnetite is Fe^{2+}, while that in hematite is Fe^{3+} (also see Fig. 7.49). These oxidation states are primarily governed by weathering and water saturation of soils, which in turn are sensitive to mean annual rainfall. That is, during periods of reduced rainfall, the somewhat weaker magnetic rhombohedral hematite (αFe_2O_3) forms due to oxidation of magnetite (Fe_3O_4) and Ti-rich titanomagnetites. When there is increase in precipitation the opposite is true.

Extensive studies of sedimentary sequence in the Deccan trap region have revealed that S-ratio has a low variation. For example, the S-ratio derived for Godavari (Fig. 7.55) ranges between 0.90 and 0.96 attributed to different stages of oxidation states of (titano)magnetite having varying amounts of Ti oxide. To infer climatic events affecting the entire Indian subcontinent, one need to have composite and multiple maps which can be relied upon more intimately than on single or isolated maps of localized extent (Fig. 7.55). S-ratio has enabled in identifying key events hitherto unreported from the Indian monsoon.

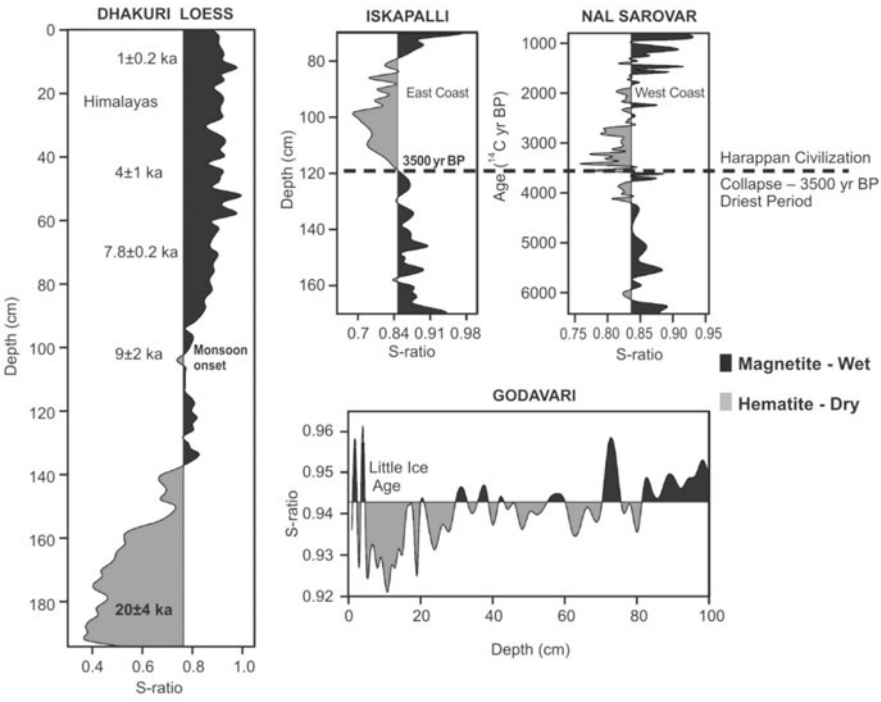

Figure 7.55. The stacked S-ratio as an accurate proxy of palaeomonsoon rainfall. Variation of mineral magnetic S-ratios with depth in sediment cores from the entire Indian subcontinent. High magnetic ratios corresponding to high 'magnetite to haematite' ratios occur in the wetter spell sediments and vice versa. Himalayan Dhakuri loess S-ratio clearly outlines key climatic events over the past 20 ka revealing step-wise improvement in SW monsoon since last glacial maximum, culminating in its establishment around 9 ka (Basavaiah and Khadkikar, 2004).

These include identification of Younger Dryas, YD (11 ka), little ice age, LIA (1780 AD) and reduced monsoon during 4000–3000 cal year BP.

Composite S-ratio map and palaeoclimate: Studies till date establish S-ratio to be an effective tool in decoding the past monsoonal characteristics of the peninsular and to a limited extent, the extra-peninsular region of India. For example, the S-ratio record of Dhakuri loess site in the central higher Himalayas clearly outlines key climatic events over the past 20 ka revealing step-wise improvement in SW monsoon since LGM, culminating into its establishment ~9 ka (Fig. 7.55). The S-ratio trend depicts a prolonged dry spell along the eastern (Iskapalli) and western (Nalsarovar) coast of India at ~3.5 ka back, effectively bringing about the downfall of Harappan civilization (Fig. 7.55). Little ice age from ca. 1400 to 1850 AD is sort of a repetition of the earlier ice ages but with a smaller geographical extent and is identified from the analyses of Godavari mangrove vibra-core samples. Also, a globally known cooler event, the LGM, that occurred ~20 ka ago is identified from Goting/Garbayang

palaeolake sediments and Dhakuri loess sequences (Fig. 7.55). Environmental geomagnetic studies have also identified YD cooling event that occurred ~11 ka back from the Himalayan lake sequences of Garbayang. Since these events are global in nature, it is envisaged that the central higher Himalayan climate was influenced by the northern hemispheric glaciation.

Also, a link between LTO of titanomagnetite and monsoon rainfall is proposed from lake sediment studies of Thar desert playas, Tulsi, Mastani and Nalsarovar. The ability of S-ratio to sensitively documents palaeomonsoonal changes, especially reduction of monsoon rainfall in time with higher latitude climate events of LGM, YD and LIA, imparts a great deal of confidence in establishing its efficacy as an accurate proxy of climate change.

7.14 FUTURE STUDIES

I. Magnetotactic Bacteria

Biogenic processes are an important source of magnetic minerals. Bacterial magnetite (BM) contribution is found in lacustrine, brackish and marine sediments, rivers, salt marshes, ponds, terrestrial soils and stratified ocean waters. For example, the importance of BM contribution in sediment cores can be gauged from the Chatham Rise, SW Pacific Ocean which has documented higher χ and increased concentration of SD magnetic grains for interglacial periods. It is interpreted that low productivity during interglacial periods favoured oxic conditions at the sea bottom for longer periods producing more magnetite, when compared to glacial periods. Small water bodies normally have high nutrient levels and rates of productivity, hence the sediments are commonly organic-rich and reducing. This is usually the case in temperate climate water bodies as well as in saline playas of arid areas. Under such conditions diagenetic destruction of bacterial magnetite is likely. The abundance and distribution of magnetotactic bacteria are dependent on four environmental factors, viz. organic matter, iron, oxygen and sulphide. It is very difficult to identify magnetotactic bacteria or their extracts for the simple reason that they are very tiny and elusive.

The magnetic particles formed by magnetotactic bacteria may contribute significantly to the magnetic properties of sediments. Their presence can be used as an indicator of microaerobic conditions that point to the oxic and anoxic conditions, as well as the EMF direction, intensity and the environment at the time of their existence. Also, any palaeoenvironmental or palaeoclimatic signal that may be encoded by BM is determined by the ecology and subsequent degree of preservation of the fine grained magnetite in the sediments indicating the palaeoecological and palaeoredox conditions. Bacteria that produce equant magnetosomes are abundant under more oxic conditions, while those that produce elongate magnetosomes are more tolerant of less oxic conditions. Some have also found greater abundance of magnetosomes in interglacial sediments, because of thicker oxic zone enabling the magnetite-producing bacteria to colonize for a longer period.

II. Mineral Magnetism and Pollution Studies

All particles are magnetic, though their individual intensity differs considerably. Hence, nearly all atmospheric fall-out dusts, whether of natural or anthropogenic origin, contain magnetic spherule particles. Spherules are formed through transformation of iron impurities within the fossil fuel and appear to be characterized by presence of both magnetite and hematite phases and relatively large (>SP/SD) magnetic grain size. In urban and industrial areas, during combustion of the coal, pyrite may be decomposed into elemental sulphur and pyrrhotite and the latter will further break down into sulphur and iron. Finally, the iron oxidizes to form a microscopic sphere of magnetite. Besides the combustion processes, magnetic particles can also originate from road traffic and also get deposited on the top surface of tree leaves. The distribution of the pollutants depends on the direction and speed of the wind, atmospheric humidity, precipitation, topography and vegetation. It is frequently possible to distinguish between anthropogenic and natural dusts with regard to its origin. The industrial dusts contain magnetic spherules that can be easily identified using thermomagnetic and microscopic analysis. Compared to the magnetic properties of natural dust, industrial dust that includes these magnetite spherules show high values of SIRM/ARM ratio, low levels of frequency dependent χ, low ARM and dissociation from finer, clay sized components of the soil. This provides an effective way to use magnetic methods to identify industrial pollution. Pollution history (back in time) can be revealed from measurements of depth profiles of soils and/or sediments.

III. Secular Variation Master Curves

Characteristic patterns of secular variation changes occur on a regional scale, e.g. on the spatial scale of North America or Europe. These changes can be recorded in rapidly accumulating lake sediments. The technique relies on radiocarbon dating of lake sediments. These enable to date earlier SV changes and can then be applied to other SV records from lake sediments in the same region. It is envisaged to develop dated secular variation 'master curves' for India. Also a study will be made to construct magnetostratigraphy for a wide range of sediment sequences from the Cretaceous through the Quaternary to the recent.

IV. Archaeomagnetism Studies

India has a rich cultural history which extends back more than 4500 years. There are extensive Neolithic and Palaeolithic cultural sites which may extend back more than 100 ka. Magnetostratigraphic studies will be undertaken to better date archaeological sites, especially those with a stratigraphic sequence of several cultural levels. The advantage of archaeomagnetic studies to palaeomagnetism is the addition of new time series of magnetic field variation for the South Asia over the last 4000 years.

V. Palaeoseismological Studies

Mineral magnetic investigations supplemented with particle size analyses will be made towards the study of palaeoseismic record by analyzing stratigraphic sections of fluvio-lacustrine sedimentary sequences. This work is expected to yield useful data on earthquake recurrence intervals and develop quasi-empirical techniques for earthquake predictions.

VI. Lonar Lake Magnetism

Lonar Lake has become a focal point of intense debate regarding its origin (Fig. 7.56a). A section of Earth scientists and geophysicists feel it to have formed by an impact of meteorite while others assign to it a volcanic origin. Both these groups have strong evidences to back their claims. However, the work carried out on Lonar is decades' old and it needs to be revisited equipped with state-of-art equipment and a new thought process (Fig. 7.56b). An integrated approach is required to understand its geomorphological, geological and geophysical characteristics. The entire basaltic terrain is formed by fissure-type volcanic activity and Lonar study is taken up to provide a unique insight into the magmatic extrusion on such a massive scale. Its impact origin provides an opportunity to study extra-terrestrial material enhancing the knowledge about the origin as well as the fundamental understanding of the universe. The planned Mars and Moon expeditions will greatly benefit from these studies.

The Lonar Lake can play a major role in studying the modern and past climatic conditions prevalent in central Indian region. This is the only lake in central India with a long pre-anthropogenic record and therefore essential for documenting the human impact on natural climate change. Further, the crater has accumulated within its lake sediments of ~50 ka. It is thus a rich repository of climatic and environmental change signatures that can be studied to understand the monsoonal pattern. In conclusion, latest developments in sedimentology, mineral magnetism, and geochemistry, especially the use of microfacies analyses, XRF (50-μ resolution) and stable isotope (on microfossils and organic compound specific isotope investigations) researches have made seasonal scale climate reconstruction possible, necessitating the raising up of lake bottom sediment cores from Lonar Lake.

Figure 7.56 (a) The magnificent Lonar Lake. (b) Mini boat and 1.2 m pneumatic Mackereth sampler for recovering under water sedimentary cores from the Lonar Lake.

APPENDIX 7.1

Calculation of Geomagnetic or Palaeomagnetic Pole Position

Suppose that D_m and I_m be the site-mean magnetic field direction which is located at geographic latitude λ_s and geographic longitude Φ_s. Here, D_m and I_m may be direct measurements of the field or may refer to the ancient field recorded by a rock.

Let λ_p and Φ_p be the geographic latitude and longitude respectively of the geomagnetic or palaeomagnetic pole position. From the knowledge of spherical trigonometry the magnetic colatitude p (i.e. the angular distance between site and pole) is

$$p = \cot^{-1}(\tan I_m/2)$$
$$= \tan^{-1}(2/\tan I_m)$$

Since p is the angular distance, it should be positive. If it comes negative, then it should be added with 180°.

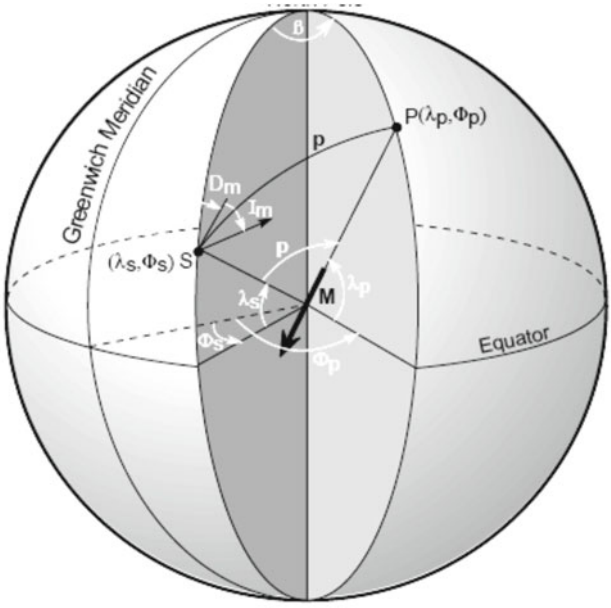

Now pole latitude is given by $\lambda_p = \sin^{-1}(\sin\lambda_s \sin p + \cos\lambda_s \cos p \cos D_m)$

The longitudinal difference between site and pole i.e. $\beta = (\Phi_p - \Phi_s)$ is related as

$$(\Phi_p - \Phi_s) = \sin^{-1}(\sin p \sin D_m/\cos\lambda_p)$$

At this point in the calculation, there are two possibilities for pole longitude.

If $\cos p \geq \sin\lambda_s \sin\lambda_p$

Then $\Phi_p = \Phi_s + \beta$
If $\cos p < \sin \lambda_s \sin \lambda_p$
Then $\Phi_p = \Phi_s + 180° - \beta$

Refer to Table 7.1 for calculation of VGP of site A. Its λ_s and Φ_s are 16.37°N and 73.84°E respectively. The mean characteristic direction i.e. obtained after magnetic cleaning are $D_m = 155.1°$ and $I_m = 48.7°$.

The magnetic colatitude $p = \tan^{-1} (2/\tan I_m)$
$= 60.35°$

Pole latitude $\lambda_p = \sin^{-1} (\sin \lambda_s \cos p + \cos \lambda_s \sin p \cos D_m)$
$= -38.08°$ (i.e. in southern hemisphere)

The longitudinal difference β between the site and pole
$= \sin^{-1} (\sin p \sin D_m / \cos \lambda_p)$
$= 27.67°$

As $\cos p > \sin \lambda_s \sin \lambda_p$, hence $\Phi_p = \Phi_s + \beta = 73.84°$ (E) $+27.67°$ (E) = 101.51° (E)
Since $\lambda_p = -38.08°$ thus gives the position of the pole in the southern hemisphere. Conventionally palaeomagnetist calculates the north geomagnetic or palaeomagnetic pole position. Thus the dipole magnet is rotated by 180° to obtain the north geomagnetic pole.
Thus the pole longitude is

$$\Phi_p = \Phi_p + 180°$$
$$= 101.51° \text{ (E)} + 180°$$
$$= 281.51° \text{ (E)}$$

Thus the VGP of the site A is 38.1° (N) and 281.5° (E).

Palaeomagnetic Data from India

Sl. No.	*Geological formation and locality*	*Age (m. yr)*	*Co-ordinates*		*Sampling details*		*Mean remanents magnetic direction*		*Polarity*	α_{95}	*Palaeolatitude of Nagpur 21°N, 79° E*	*Palaeomagnetic*	
			Lat. (N)	*Long. (E)*	*No. of sites*	*No. of specimens*	*D*	*I*				*Lat.*	*Long.*
1.	Pavagadh acid tuffs	20-35	22° 28′	71° 33′	2	15	355	+17	N	7°	6° 30′N	75°N	89°W
2.	Pavagadh basic	50-60	22° 28′	71° 34′	8	69	351	-16	N	8°	9° S	58°N	91°W
3.	Upper Deccan Traps												
3A	Mahabaleshwar	55-75	17° 55′	73° 38′	7	175	339	-57	N				
3B	Amba	55-75	16° 59′	73° 46′	3	54	355	-26	N				
3C	Nipani	55-75	16° 26′	74° 22′	3	74	338	-32	N				
3D	Gargoti	55-75	16° 19′	74° 10′	2	35	11	-46	N				
3E	Ajra	55-75	16° 3′	74° 3′	1	22	35	-70	N				
3F	Alandi dykes	55-75	16° 34′	73° 35′	2	41	346	-53	N				
3G	Panchmarhi	55-75	16° 27′	78° 26′	2	25	338	-47	N				
3H	Mumbai	55-75	16° 58′	72° 49′	3	71	328	-47	N				
3.	Mean Upper Deccan Traps (8 localities)	55-75			23	497	345	-44	N	10°	25° 30′S	42°N	87°W
4.	Lower Deccan Traps												
4A	Mahabaleswar	70-90	17° 55′	73° 38′	20	339	157	+52	R				
4B	Khandala	70-90	18° 45′	73° 22′	16	233	147	+58	R				
4C	Linga	70-90	21° 58′	78° 55′	4	195	164	+48	R				
4D	Amba	70-90	16° 59′	73° 46′	5	109	144	+60	R				
4E	Nipani	70-90	16° 26′	74° 32′	2	44	168	+60	R				
4F	Neral dykes	70-90	18° 57′	73° 19′	5	65	139	+43	R				
4G	Neral flow	70-90	18° 57′	73° 19′	1	11	148	+40	R				
4H	Alandi	70-90	18° 34′	73° 53′	1	12	141	+66	R				

(*Contd.*)

Palaeomagnetic data from India (*Contd.*)

Sl. No.	*Geological formation and locality*	*Age (m. yr)*	*Co-ordinates*		*Sampling details*		*Mean remanents magnetic direction*		*Polarity*	α_{95}	*Palaeolatitude of Nagpur 21°N, 79° E*	*Palaeomagnetic*	
			Lat. (N)	*Long. (E)*	*No. of sites*	*No. of specimens*	*D*	*I*				*Lat.*	*Long.*
4I	Buldhana	70-90	20° 33′	76° 12′	2	20	149	+53	R				
4J	Panchamarhi	70-90	22° 27′	78° 26′	4	52	156	+50	R				
4K	Kalyan	70-90	19° 13′	73° 07′	1	15	164	+56	R				
4L	Gargoti	70-90	16° 25′	74° 14′	1	28	159	+56	R				
4M	Chincholi	70-90	17° 29′	77° 28′	1	59	153	+62	R				
4N	Gulbarga	70-90	17° 19′	76° 56′	1	69	145	+58	R				
4O	Vikarabad	70-90	17° 22′	77° 30′	1	48	140	+60	R				
4.	Mean Lower Deccan Traps (15 localities)	70-90			65	1299	154	+53	R	10°	30° 30′S	34°N	78°W
5.	Tirupati sandstones												
5A	Janam Peta	90-120	16° 46′	81° 8′	1	94	157	+51	R				
5B	Peddavegi	90-120	16° 48′	81° 8′	1	38	329	-59	N				
5C	Peddavegi	90-120	16° 48′	81° 9′	445	1	26	154	+62	R			
5D	Peddavegi	90-120	16° 49′	81° 13′	1	31	145	+55	R				
5E	Nayanapalli	90-120	16° 50′	81° 12′	1	47	153	+56	R				
5.	Mean Tirupati sandstones (5 localities)				5		153	+56	R	4°	34°S	28°N	73°W
							329	-59	N				
6.	Satyavedu sandstone	90-120	13° 30′	80°	1	13	321	-58	N	4°	33°S	26°N	67°W
7A	Sylhet traps	155-170	25°	91°	-	80	332	-59	N	7°	35° 30′S	16°N	60°W
7B	Sylhet traps	155-170	25°	91°	-	20	243	-60	N	16°			
8.	Rajmahal traps	155-170	25°	87° 51′		120	323	-64	N	4°	44°S	13°N	69°W
9.	Rajmahendari traps												
9A	Rajmahendari traps	155-170	17°	81° 46′	-	30	310	-53	N				
9B	Rajmahendari traps	155-170	17°	81° 46′	1	11	305	-45	N				
9C	Rajmahendari traps	155-170	17°	81° 46′	1	9	305	-44	N				

9.	Mean Rajmahendari traps					50	307	-47	N	4°	25°S	22°N	48°W
10.	Dykes from Palamau Satpura and Surguja												
10A		155-170	23°	83°	6	81	158	+52	R				
10B		155-170	23°	83°	4	59	338	-33	N				
11.	Parsora sandstone	215-230	23° 26′	81° 06′	2	113	318	-40	N	2.5°	23°S	28°N	54°W
12.	Kamthi sandstone												
12A	Jaipuram	245-260	18° 52′	79° 35′	1	55	303	-44	N				
12B	Jaipuram	245-260	18° 52′	79° 35′	1	87	306	-53	N				
12C	Rallapet	245-260	19° 7′	79° 30′	1	65	309	-47	N				
12.	Mean Kamthi sandstone				3	207	306	-50	N	2°	29°S	18°N	53°W
13.	Himgir sandstone	245-260	22°	84°	1	31	332	-44	N	6°	22°S	30°N	58°W
14.	Vindhyan sandstone												
14A	Upper Vindhyan sandstone	540-580	24° 37′	83° 6′	1	143	0	+30	N	6°	13°S	82°N	103°W
14B	Upper Vindhyan sandstone	540-580	24° 37′	83° 6′	1	38	186	-30	R	7°			
15.	Malani Rhyolites	580-735	26°	73°	9	170	353	+56	N	10°	31°S	78°E	45°W
16.	Mundawara complex, basic rocks	650-850	25°	73°	1	25	329	-24	N	21°			
17.	Banded Hematite quartzites, Porkhra	750-950	24°	81°	1	5	270	-12	N	7°	9° 30′S	2°N	3°W
18.	Banded Hematite Jasper, Parkhuri	750-950	24°	81°	1	5	289	-9	N	7°	7°S	15°N	25°W
19.	Bijiwar traps, Gwalior	750-950	26°	78°	11	25	70	+3	R	18°			
20.	Veldurthi Hematite	900-1200	15° 36′	78°	4	170	133	-37	R	14°	24° 30′N	45°N	3°W
21A	Chitloor dyke	1100-1200	14° 36′	79°	1	3	146	+11	R	19°			
21B	Chitloor dyke	1100-1200	14° 36′	79°	1	3	296	-32	N	3°	14°S	20°N	36°W
21C	Chitloor dyke	1100-1200	14° 36′	79°	1	3	264	-29	N	4°	9° 30′N	9°N	25°W
22A	Cuddapah shales	1400-1600	15°	78°	1	5	295	-10	N	5°	2°S	23°N	23°W
22B	Cuddapah sandstone	1400-1600	15°	78°	1	24	294	-6	N	8°		22°N	20°W
23.	Hyderabad dyke		17° 23′	78° 28′	1	26	44	-3	N	5°	3°S	43°N	173°W

APPENDIX 7.3

Palaeo-, Rock- and Environmental Magnetic Parameters

HYSTERESIS PARAMETERS

Instrumentation: Molspin Vibrating Sample Magnetometer (VSM); Princeton Measurements Alternating Gradient Force Magnetometer (AGFM)

Saturation Magnetization M_s [mAm^2kg^{-1}]	Maximum induced magnetization at 1T and is calculated by extrapolating the high field magnetization curve to the y-axis
Saturation Remanent Magnetization M_{rs} [$mAm^2\ kg^{-1}$]	Magnetization retained even after complete removal of magnetic field following magnetization at 1T and in theory the same as SIRM on the Molspin spinner
Coercive Force, H_c [mT]	The backfield that makes magnetization zero
Coercivity of Remanence, H_{cr} [mT]	Measured as larger backfield strength required than H_c to return M_{rs} to zero
Reverse low field (χ_{low}) or initial magnetic susceptibility χ_{in} [$10^{-6}\ m^3kg^{-1}$]	The slope of magnetization curve at the origin of a hysteresis loop within a small magnetic field and is reversible, i.e. no remanence is induced
High field susceptibility χ_{hf} [$10^{-6}\ m^3kg^{-1}$]	Measured as the high-field slope of a hysteresis curve between 800 mT and 1 T. χ_{hf} refers to paramagnetic susceptibility χ_{para} and is used to calculate the ferrimagnetic component χ_{ferri} in the total magnetic susceptibility χ_{total}

MAGNETIC SUSCEPTIBILITY

Instrumentation: MS2 Bartington Susceptibility Meter and Dual Frequency Sensor (noise level $3 \times 10^{-9}\ m^3kg^{-1}$); Agico KLY-2 Kappabridge (noise level $2 \times 10^{-10}\ m^3kg^{-1}$)

Volume Susceptibility κ [dimensionless]	Defined as $\kappa = M/H$, M being volume magnetization induced to intensity of magnetizing field H
Specific susceptibility, χ [$m^3\ kg^{-1}$]	Measured as the ratio of volume susceptibility to density $\chi=\kappa/\rho$

Frequency dependent of susceptibility χ_{fd} [percentage or $m^3\ kg^{-1}$]	Variation in χ between low (0.47 kHz) and high frequencies (4.7 kHz). χ_{fd} indicates viscous grains at the superparamagnetic/stable single-domain boundary

MAGNETIC REMANENCE

Instrumentation: Molspin Spinner Magnetometer (noise level 0.1 × $10^{-5}Am^2kg^{-1}$); Agico JR-6 Spinner Magnetometer; 2G-Enterprises SQUID Magnetometer (for 10 g samples, noise level 3 × $10^{-9}Am^2kg^{-1}$); Magnetic Measurements MMPM9 Pulse magnetizer, Molspin Pulse Magnetizer

Natural Remanent Magnetization NRM [mAm^2kg^{-1}]	Acquired in the Earth's magnetic field either by cooling of a mineral through its Curie (blocking) point, crystal growth through the blocking volume or deposition and 'fixing' of detrital particles
Viscous (time-related) remanent magnetization,VRM [mAm^2kg^{-1}]	Acquired on exposure to a new magnetic field and is time-dependent magnetization unrelated to Earth's magnetic field
Anhysteretic remanent magnetization ARM [$10^{-5}Am^2kg^{-1}$]	An ideal magnetic remanence for being free from hysteresis and is imparted in a peak 100 mT AF that smoothly decreased to zero in a small DC field's presence. ARM allows estimation of concentration and presence of finer ferrimagnetic minerals. For example, SSD particles have high ARM intensities per unit mass compared to MD particles
Susceptibility of ARM, χ_{ARM}[m^3kg^{-1}]	Normalized ARM for the strength of the steady field
Isothermal remanent magnetization IRMs [$10^{-5}\ Am^2kg^{-1}$]	Acquired in different DC forward and back fields (10 mT to 2 T or even up to 9 T) at a given temperature, commonly at room temperature
Saturation isothermal remanent magnetization SIRM [$10^{-5}Am^2kg^{-1}$]	Measured as the highest volume of magnetic remanence that can be produced in a sample by application of a very high field (usually >1 T). SIRM relates to both mineral type and concentration
'Soft' IRM, IRM_s [Units are same as for SIRM]	Remanent magnetization after a magnetization either in a relatively low forward field of 20 mT, 30 mT, 40 mT or 50 mT or reverse fields 'back IRMs'
'Hard' IRM, IRM_h [Units are same as for SIRM]	Difference between SIRM and IRM measured after magnetization in a field of 300 mT or difference between SIRM and IRMs in a reverse field of 300 mT, i.e. HIRM = SIRM-IRM_{-300mT}

(*Contd.*)

Palaeo-, rock- and environmental magnetic parameters (*Contd.*)

USEFUL PERCENTAGES AND QUOTIENTS (RATIOS): INTERPRETATION OF RESULTS	
χ_{fd}[%]	~10% or 5-10% would indicate a large fine viscous (magnetite) component of SP range
SIRM/χ	Useful to distinguish between different types of magnetic behaviour. For example, if both χ and SIRM are low, but SIRM/χ is relatively high, there may be a large amount of hematite. If χ is positive but there is little or no remanence, then the magnetic minerals in the sample will probably be mostly paramagnetic minerals
SIRM/χ; ARM/χ & ARM/SIRM	High SIRM/χ, ARM/χ and ARM/SIRM values denote significant SSD (magnetite) grains
ARM/SIRM	Low ARM/SIRM values indicate a large MD (magnetite) component
Backfield IRM/SIRM or S-ratio;	S-ratio defined here as $IRM_{-0.3T}$/SIRM recognizes samples with hematite to magnetite proportions
High field remanence HIRM	because ferrimagnets are expected to saturate in fields below 0.1 T. Larger high field remanences, HIRM are due to proportionally high imperfect antiferromagnetic components such as hematite and goethite
M_{rs}/M_s ratio	Indicator of magnetization state of a sample; ratio values of 0.5 represent SSD grains; less than 0.1 for MD and still lesser values for SP grains.
H_{cr}/H_c ratio	Provides magnetization state of a sample; uniaxial SSD grains have ratio of 1.09, MD grains around 4.0 and SP grains in excess of 10.0

8

UPPER ATMOSPHERE STUDIES

The Earth's atmosphere occupies some million times greater volume than the solid Earth. In this huge system, the charged plasma particles react strongly to electric and magnetic fields. Hence, electrical processes in one part of the system can influence the electrodynamical processes in another distant part. The redistribution of the charged particles in turn can modify the existing electric and magnetic fields in the atmosphere. Hence, an investigation of electrodynamical processes in various regions of the atmosphere and their coupling is very important for understanding the state of electrical environment of the Earth's atmosphere.

The region-wise electrodynamical study of the Earth's atmosphere is not feasible. The electric fields and currents do not care for human-designated boundaries such as tropopause, stratopause, mesospause and ionosphere. They propagate from one region to another and affect the entire electrodynamical processes, hence cannot be studied in isolation. An integrated approach using satellites and modern sophisticated instruments is required to advance the knowledge about dynamics of the near-Earth environment. This approach provides a framework for exploring interconnections and coupling of various regions and also for explaining the solar-terrestrial-weather relationships. Some of the important findings over the past few decades are reported in this chapter.

Little is known about the need for Earth to generate a large scale magnetic field to shield it from the high-energy radiation and wind from the Sun. However, it is now well known without the magnetic field, the atmosphere would be exposed to ionization and erosion by the charged particles in the solar wind. Thus, any form of early life would have been irradiated by the intense X-ray and high-energy UV emission from the Sun (Fig. 8.1a). The principal components of geomagnetic variations recorded by ground observations are due to currents and fields in the near-Earth space starting from ~80 km from the surface to the magnetopause and beyond. These are even intimately related to the electric fields at much lower heights, where meteorological features

predominate. Thus, the purpose of upper atmosphere studies is to address the phenomena occurring in the ionosphere, magnetosphere and beyond.

The Earth's atmosphere extends up to the magnetopause, which acts as a boundary between the Earth and the interplanetary medium and between the solar wind and the magnetosphere (Fig. 8.1b). Here, the solar wind dynamic pressure is balanced by the geomagnetic field pressure. The EMF is more or less confined inside the magnetopause boundary. A schematic of the 2D view of the magnetosphere (Fig. 8.1b) is correlated to 3D (Fig. 8.1c), which is the view obtained by an observer from outside the magnetosphere. It shows various important plasma regions, current systems and several effects due to the interaction of the solar wind with the EMF. The EMF is pushed back by high pressure solar wind into a characteristic shape known as the magnetosphere (Chapter 3). A bow shock is formed ~3-4 R_E ahead of the magnetopause, a boundary inside which EMF is contained because of solar wind pressure. Some particles of solar wind are captured by the EMF and are forced into a system of radiation belts called Van Allen radiation belts that girdle the Earth. Other familiar geomagnetic phenomena such as polar auroras and the communication disrupting ionospheric disturbances associated with magnetic storms arise due to the complex interplay between the solar wind and the Earth's atmosphere (Fig. 8.1a). Studies bear out that the radiation of Van Allen is highest over the geomagnetic equator and diminishes towards the poles. Auroras occur most frequently in concentric rings around the geomagnetic poles and diminish in frequency towards the equator.

In recent times, there has been keen interest in understanding Sun-Earth connection events. Magnetic storms are perhaps important components of space weather effects on Earth (Fig. 8.1). Super-intense magnetic storms have the largest societal and technological relevance, causing life-threatening power outages, satellite damages, communication failures and navigational problems. Thus, research on historical geomagnetic storms aids to create a good database of preceding and imminent intense and super-intense magnetic storms. Such study is carried to answer some basic questions: (1) how many super-intense magnetic storms have occurred in the last 160 years and what were their probable solar and interplanetary causes? (2) frequency of occurrence of super-intense storms and under what circumstances? (3) is a prediction of certain number (say 3) most severe magnetic storm during a solar cycle possible? (4) can the possible damaging effect of super-intense magnetic storms on the modern society be predicted in advance? and (5) what is the energetic effect of eruptive phenomena on Sun and Stars. The correlations between selective features on the Sun and surface magnetic field changes enable to predict the possibility of the occurrence of violent geomagnetic disturbances.

The investigation of various processes in Earth's magnetosphere responsible for the generation of large scale electric field with the focus on magnetic reconnection at the magnetopause and in the tail region is carried out analytically as well as numerically. The study advances the knowledge about magnetic

reconnection, a basic plasma physics process, which converts magnetic energy into the plasma heat and flow energy. Generation of geomagnetic pulsation and their propagation to low latitude ground stations are investigated. Numerical

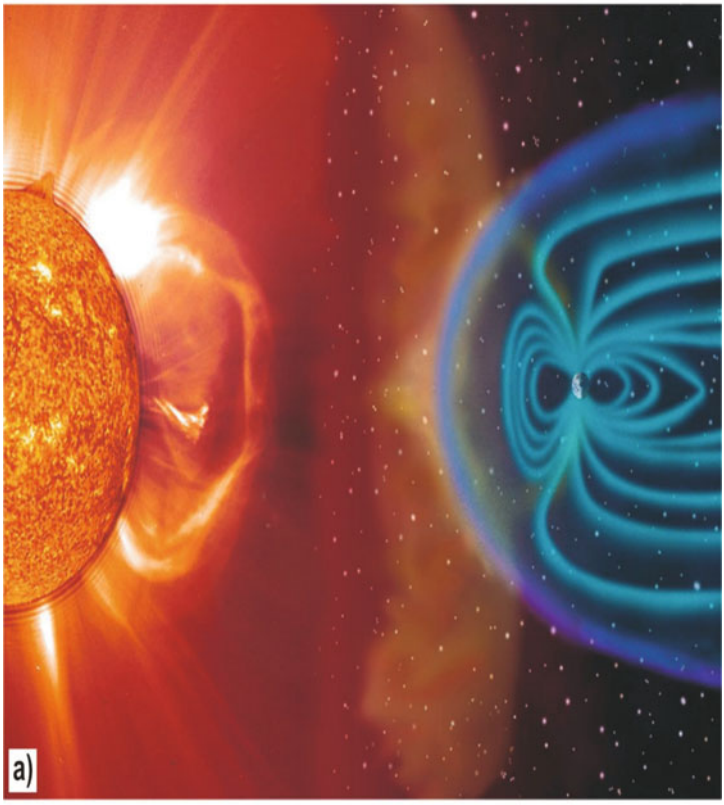

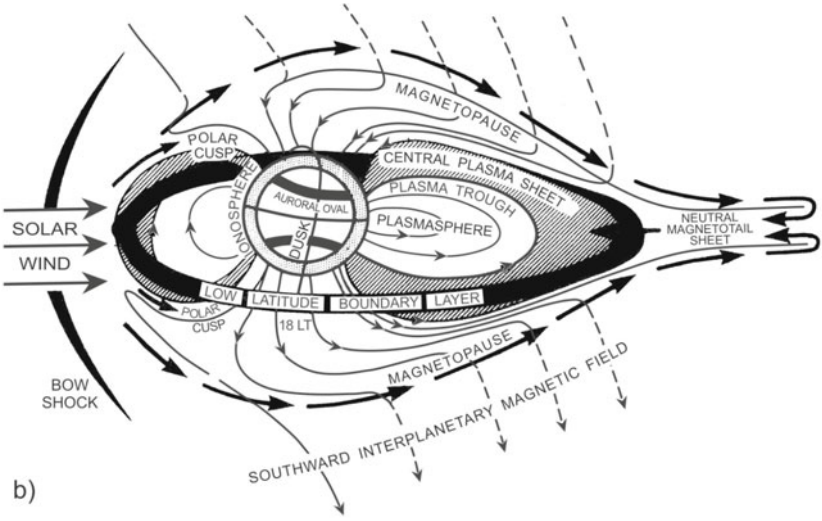

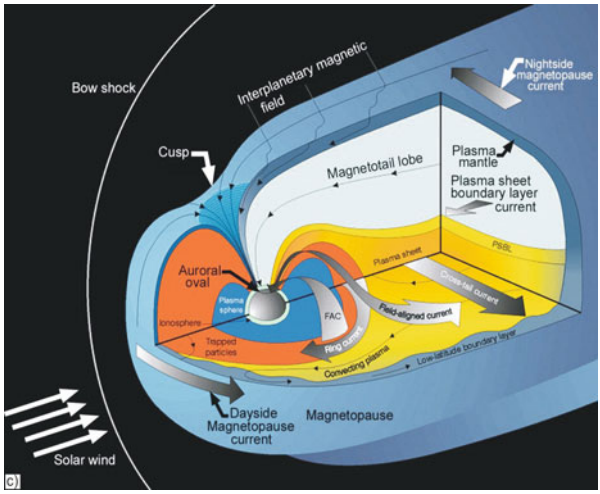

Figure 8.1. (a) Shelter from the storm. Clouds of hot gas called coronal mass ejections (CEMs) are often ejected by the Sun, when there is a large solar flare. It takes ~3 days for them to reach the distance of Earth's orbit. If they collide with Earth, the impact compresses and buffets Earth's protective magnetic field and can produce spectacular aurorae (Jardine, 2010). (b) Schematic polar cross sectional view of the Earth's magnetosphere, with its bow shock and the outflow of solar wind and interplanetary magnetic field from the Sun (Rajaram and Pisharoty, 1998). (c) An overview of different magnetospheric currents, which are setup in different regions by the charged particles flow (http://image.gsfc.nasa.gov/ presentation/cua_talk/sld004.html).

simulation codes are developed to study reconnection in 2D and 3D configurations. Magnetic topologies containing magnetic nulls are most susceptible to instabilities leading to reconnection.

I. International Magnetospheric Study

Upper atmospheric studies are not just restricted to the ionosphere, but extend to far-off space as well. Two essential ingredients for the formation of the magnetosphere are the EMF and the solar wind. The continuous flow of solar plasma is blocked by the EMF, confining it to magnetosphere. This process is vital to the existence of life on this planet. At the same time, this magnetic cavity filled up by tenuous plasma offers an excellent natural laboratory, helping throw up exciting new details by the world scientific community. Much is learnt about the dynamic plasma region over the past 40 years from the direct measurements by various spacecrafts (Chapter 3).

The solar wind carries the solar magnetic field out into space. Due to its extremely large electrical conductivity, solar wind plasma and solar magnetic field are tightly coupled, which means that the magnetic field is frozen into the plasma flow. At Earth orbit, the mean magnetic field strength is of the order of

7 nT. As the Earth rotates underneath the magnetosphere, a ground based observer sees different parts of the magnetosphere. Since the magnetosphere varies in time and space, the separation of temporal and spatial effects is not possible from a single location. Time variations are considerable and the magnetosphere never reaches a complete equilibrium because of continual flowing by solar wind. All models represent at best an interpretation of the time-averaged quiet magnetosphere. Measurements on the magnetosphere at different locations both in space and on surface are undertaken so that spatial and temporal effects are resolved and optimum use made of data.

More useful information about the temporal variability of solar magnetic activity is gained by the use of proxy data. Magnetic fields in the solar wind modulate the cosmic ray flux entering the Earth's atmosphere. These high-energy particles lead to the production of radioisotopes including ^{10}Be and ^{14}C, and so the abundance of these isotopes becomes a measure of solar magnetic activity; the abundance is anticorrelated with solar activity. The isotope ^{10}Be is preserved in polar ice-cores and its production rate together with the sunspot number is shown in Fig. 8.2. The figure clearly shows presence of the Maunder minimum and that, although sunspot activity is largely shut off during this period, cyclic magnetic activity continued with a period of ~9 years. The ^{10}Be record extends back over 50 ka and analysis of this record clearly shows

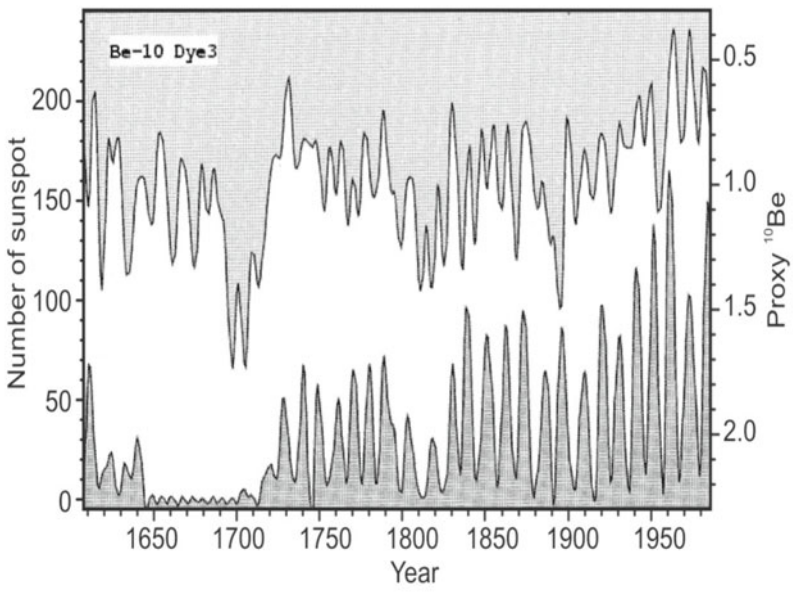

Figure 8.2. Comparison of the proxy ^{10}Be data from the Dye3 ice core (measured in 10^3 atoms/g) filtered using a low pass (6 year) filter, with the filtered (6 year) sunspot group number as determined by Hoyt and Schatten (1998). Note that the ^{10}Be is anticorrelated with sunspot activity (Tobias, 2007).

continued presence of the 11-year solar cycle. Analysis also indicates that the Maunder minimum is not an isolated event, but a regularly spaced minima (termed grand minima) interrupting the record of activity with a significant recurrent timescale of 205 years. The variations in ^{14}C production confirm this pattern of recurrent grand minima with a time scale of ~200 years. Moreover, both of these radioisotope records show significant power at a frequency that corresponds to roughly 2100 years. It appears as though grand minima occur in bursts.

Particles, substorms, whistlers: The basic understanding of the magnetosphere, combined with availability of high quality detectors for charged particles, waves and fields, on rockets and satellites of high reliability and with good telemetry, makes it timely to study numerous phenomena quantitatively.

One major area of study is the transfer of charged particles and energy from the solar wind into the magnetosphere. The major mechanism of energy transfer from solar wind to the Earth's magnetosphere is magnetic reconnection (Fig. 8.3). If the interplanetary magnetic fields (IMFs) are directed opposite to the EMFs, there is magnetic erosion on the dayside magnetosphere (by magnetic connection) and magnetic field accumulation on the nightside magnetotail region. Subsequent reconnection on the nightside leads to plasma injection at these local times and auroras occurring at high latitude nightside regions. As the magnetotail plasma gets injected into the nightside magnetosphere, the energetic protons drift to the west and electrons to the east, forming a ring of current around the Earth. The ring current causes a diamagnetic decrease in the EMF measured at near-equatorial magnetic stations. The decrease in the equatorial magnetic field strength is directly related to the total energy of the ring current particles and thus a good measure of the energetic of the magnetic storm.

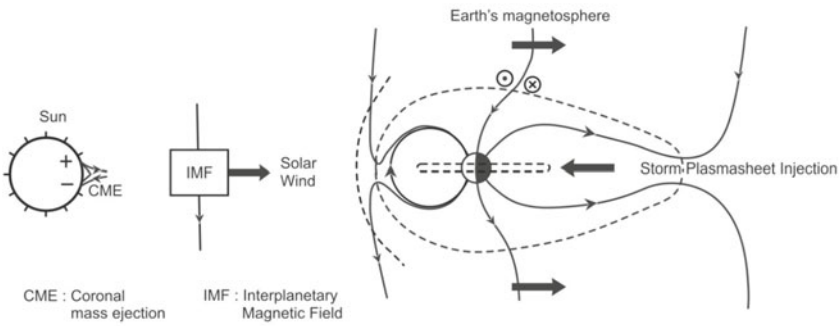

Figure 8.3. A schematic showing the magnetic reconnection process.

The storage of particles in the reservoirs of the plasmasphere and the plasma sheet and dynamics of these regions is another area of study. Propagation of very low frequency (VLF) whistlers enables the plasmapause to be identified and its movement followed. The substorm is an important natural perturbation of the magnetosphere. Magnetic energy accumulated in the tail is suddenly released and dumped in the auroral regions by charged particles. Substorms can either occur in rapid succession at the rate of several an hour as part of a magnetic storm (usually caused by solar flare induced effect) or separated by several days. It seems that a substorm may be triggered by the IMF turning southwards. During growth phase, the dayside boundaries are moved inwards towards the Earth and thus project to lower latitudes (Chapters 3 and 5).

Wave particle interactions are also of importance in the magnetosphere. The threshold electron energy for cyclotron resonance as a function of radial distance in the equatorial plane is shown in Fig. 8.4. In the cyclotron resonance, low energy waves propagating in the whistler mode resonate with trapped electrons of the appropriate cyclotron frequency; the wave amplitude can increase and the particles suffer pitch angle scattering so as to align their motion more along the field and so down to the atmosphere where they are lost by collision. While this theory of wave-particle interactions is incomplete, it does demonstrate that very high energy particles may be unstable everywhere and

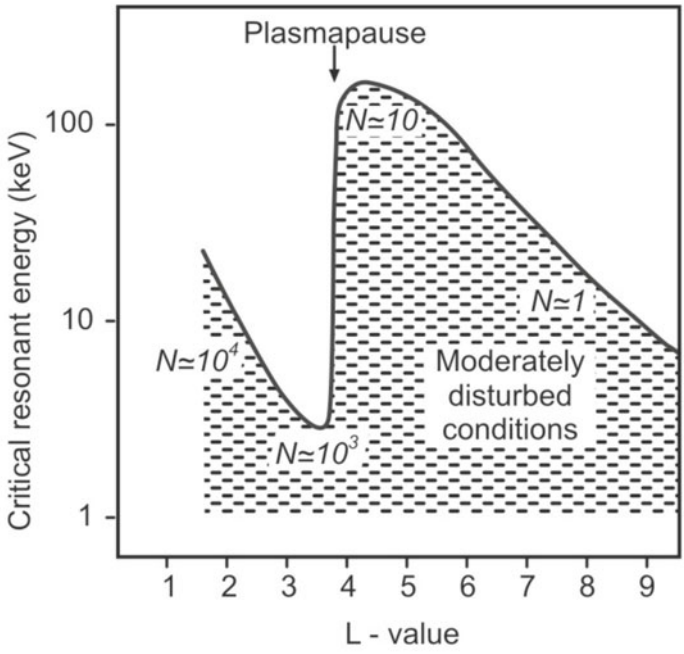

Figure 8.4. Threshold energy for unstable cyclotron resonance plotted against radial distance in the equatorial plane in Earth radii (L). N is the plasma density in particles/ cm^3 (Woolliscroft, 1978).

that electrons with over 10 keV are stable in the radiation belt. The transfer of magnetospheric energy down to the ionosphere and the atmosphere with possible effects on the weather is also studied.

Satellite use: Central to the success of the international magnetic study (IMS) are about a dozen dedicated satellites, of which the most important is the European space agency's GEOS satellite. GEOS is making valuable measurements on the magnetospheric plasma and waves. In particle terms the significance of electrostatic waves is now apparent. Complimentary to GEOS is the ISEE (international Sun-Earth explorer) spacecraft, apart from a number of other satellites such as Hawkeye and S3-2 and 3, which are making relevant measurements. Surface magnetic field measurements are also a valuable tool to study the magnetosphere. Continuous monitoring of the magnetosphere with magnetometers, unlike optical measurements, does not depend on the weather and is relatively cheap and reliable. The magnetospheric current systems, thus can be determined unambiguously with existing networks of high resolution magnetometers in addition to the ~200 magnetic observatories. In a similar manner, ground-based networks of ionosondes, riometers, low-frequency radio wave receivers and optical instruments aid magnetospheric study.

Two equatorial flights in April and Sept 1998 launched from the Indian low-latitude station SHAR detected plasma bubbles restricted to a narrow longitudinal extent. Plasma parameters are measured under two different conditions in the post-sunset ionosphere, when the F layer is moving upward (19:21 IST launch) and when the F layer is stationary (20:41 IST launch). Low altitude bubbles during upwelling of the F region in pre-reversal current enhancement phase are characterized by turbulent non-Maxwellian regions. Transitional scale waves with $k = 3.6$ are observed in the bubbles. This flight also detected strong sharp E layers during down leg and an intermediate layer at 170 km. Night-time bubbles during almost stationary F layer conditions show turbulent Maxwellian features with moderate cooling compared to the undisturbed environment. Transitional scale in the bubble region shows a spectral index $k = 3.1$. The spectral power is reduced by ~20 dB compared to the sunset flight.

II. Boundary Layer Waves and Auroras

Plasmas are generally far from their thermodynamic equilibrium states, and hence contain some amount of free energy, which can generate several kinds of plasma modes in the magnetospheric boundary layers such as magnetopause boundary layer, plasma sheet boundary layer, polar cap boundary layer (PCBL) and others (Fig. 8.5).

Polar observations indicate the presence of intense broadband plasma waves nearly all of the time (with ~96% occurrence frequency) near the apogee of the

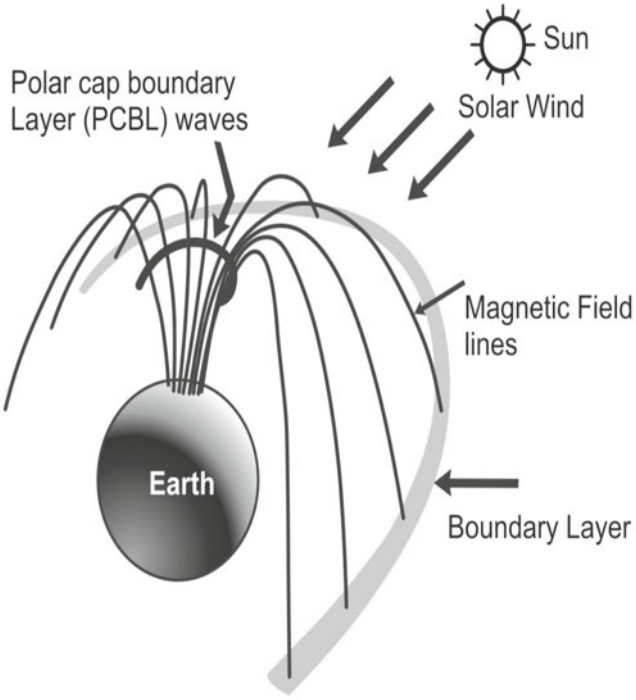

Figure 8.5. A northern polar view of the mapping of polar cap boundary layer waves to the low-latitude boundary layer (Tsurutani et al., 2003).

polar trajectory (~6-8 R_E). The region of wave activity bounds the dayside (0500-1800 LT) polar cap magnetic fields, and thus these waves are called PCBL waves. The waves are spiky signals spanning a broad frequency range from a few Hz to more than 20 kHz having a rough power law spectral shape. The wave magnetic component appears to have an upper frequency cutoff of the electron cyclotron frequency. The electric component extends well beyond the electron cyclotron frequency. The waves are possibly a mixture of obliquely propagating electromagnetic whistler mode waves and electrostatic waves. There are no clear intensity peaks in either the magnetic or electric spectra, which can identify the plasma instability responsible for generation of PCBL waves.

The wave character (spiky nature, frequency dependence and admixture of electromagnetic and electrostatic components) and intensity are quite similar to those of low-latitude boundary layer (LLBL) waves detected at and inside the low-latitude dayside magnetopause. Because of the location of PCBL waves just inside the polar cap magnetic field lines, it is natural to assume that these waves occur on the same magnetic field lines as the LLBL waves, but at lower altitudes, where the most likely scenario is that field-aligned currents

or current gradients locally generate the waves. A strong relationship is found between the presence of ionospheric and magnetosheath ions and the waves near the noon sector. These waves may thus be responsible for ion heating observed near the cusp region. Anti-sunward convection of these freshly accelerated O^+ ions over the polar cap during intense wave events (occurring during southward B_z events) might lead to enhanced plasma sheet O^+ population. For magnetic storm intervals, this mechanism leads to a natural delay between the main phase onset and the appearance of oxygen ions in the ring current.

High time resolution waveform observations by plasma wave instrument onboard the Geotail, Polar and FAST spacecrafts have shown broadband high frequency plasma waves consisting of a series of bipolar solitary pulses. Various models based on solitons/double layers and phase space holes are developed to explain the characteristics of these solitary structures.

III. Ionosphere-magnetosphere Coupling Studies

One of the outstanding questions of magnetospheric physics is associated with ionosphere-magnetosphere coupling. Ionosphere and magnetosphere are closely linked together via magnetic field lines, e.g. cold ionospheric electrons and ions (e.g. O^+) drift into the Earth's magnetospheric regions, namely plasmasphere, plasma sheet and tail lobes. The change in magnetospheric ion composition (especially increased O^+ ions) can have large effects on some important magnetospheric processes. The two missions, active magnetospheric particle tracer explorers (AMPTE) and the combined release and radiation effects satellite (CRRES) showed ionized oxygen escaping from the upper atmosphere could play a critical role in electromagnetic processes in the near-Earth space.

Several plasma instabilities are studied in presence of O^+ ions in the Earth's plasma sheet and ring current region. A theoretical model is developed to study Kelvin-Helmholtz modes driven by O^+ in the Earth's plasma sheet region (Fig. 8.6). The role of these modes is investigated in magnetosphere-ionosphere coupling processes, namely magnetic storm and substorm, and low-frequency turbulence. It is found that the presence of ionospheric-origin O^+ ion beams with anisotropic pressure can excite helicon mode instability in near-Earth plasma sheet region, provided their Alfvenic Mach numbers lie in certain range. The helicon modes are easily excited under the conditions when the usual long wavelengths fire-hose modes are stable. It is shown that the anisotropic O^+ ions in the ring current can excite low-frequency quasi-electrostatic waves (Fig. 8.7). The scattering of ring current particles by these low-frequency electrostatic waves could lead to ring current decay and thus provides a mechanism that is complimentary to charge exchange.

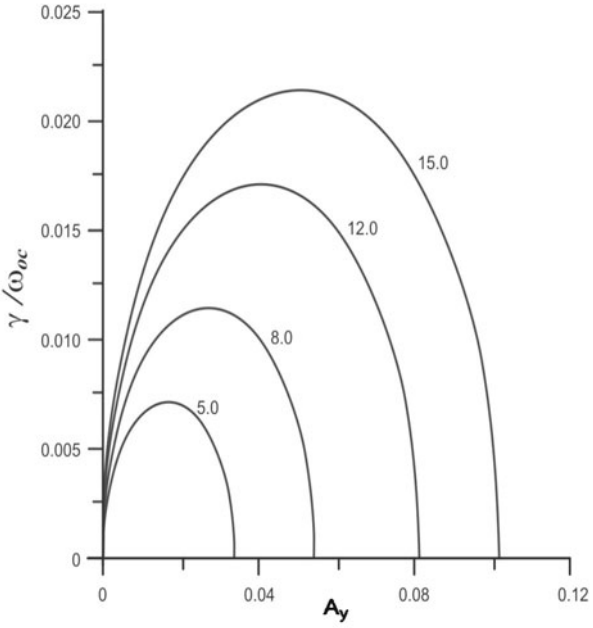

Figure 8.6. Variation of normalized growth rate γ/ω_{oc} with normalized parallel wave number A_y for the shear flow instability driven by O^+ ions in the plasma sheet region, for the parameters; normalized wave number $A_y = 600$, ratio of proton to oxygen density e = 2.0 and normalized shear S = 5, 8, 12, 15, $A_y = 600$, e = 2.0 (Kakad et al., 2003).

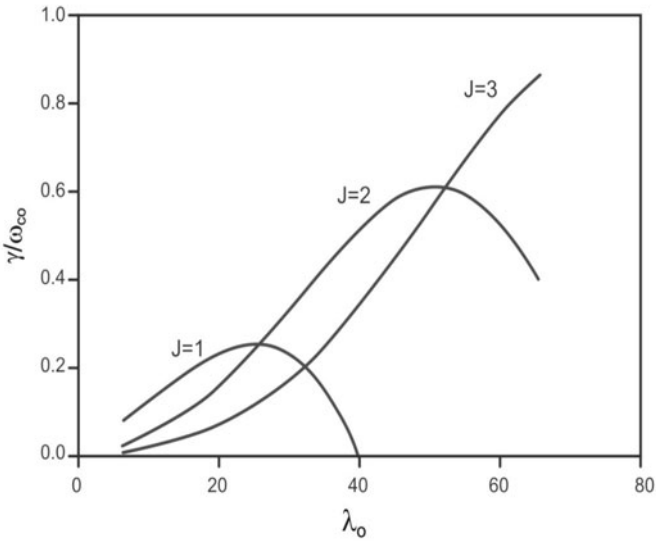

Figure 8.7. Comparison of growth rates for anisotropic index J for low frequency waves (Singh et al., 2004).

IV. Numerical Modelling

Global studies have opened innumerable observations that need to be established on theoretical platform. This can only be done through numerical modelling by incorporating various complex parameters in the code explaining observations in terms of associated physics related to transport of energy, momentum and mass transfer between the solar wind and magnetosphere. Plasma instabilities during sub-storm, which give rise to anomalous resistivity leading to generation of parallel electric fields, are being numerically modelled. The magnetosphere-ionosphere coupling during magnetospheric storms and substorms as well as the generation mechanisms of magnetic pulsations and their propagation to low latitudes is under close scrutiny (Fig. 8.8). Efforts are also directed towards developing magnetohydrodynamic simulation codes for investigating magnetotail dynamics that result in large scale electric fields in the magnetosphere.

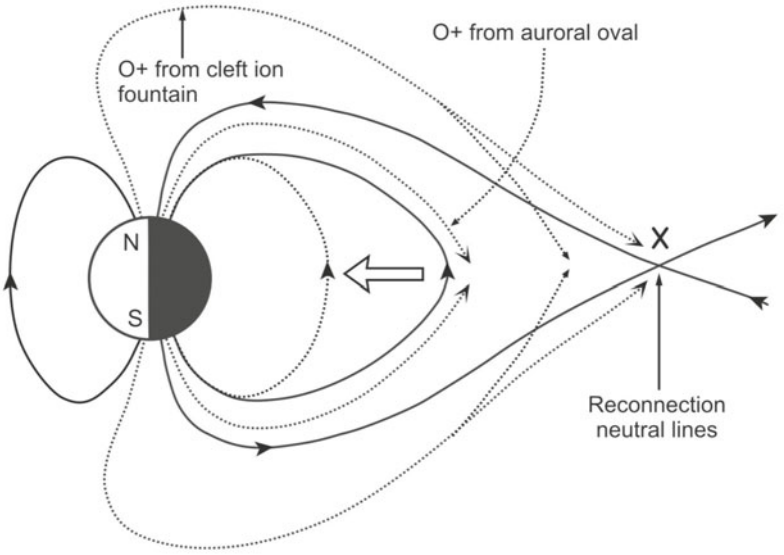

Figure 8.8. A schematic illustration of the respective paths into the magnetosphere of oxygen ions from the dayside cleft and the nightside auroral ionosphere (Gazey et al., 1996).

8.1 SPACE WEATHER EFFECTS

Modern society relies on technology, which is affected by conditions in space environment. Space weather refers to conditions between the Sun and Earth encompassing the solar wind, interplanetary space, magnetosphere, ionosphere and thermosphere. These conditions can influence the performance and reliability of space-borne and ground-based technological systems and can endanger human life or health.

Space weather disturbances caused by enhanced stream of solar plasma during solar flares and CMEs are known to disrupt communications, endanger satellite payloads and introduce severe errors in a variety of tracking and positioning systems (Fig. 8.12). The phenomena of geomagnetic storms are the most obvious features of space weather disturbances. Consequently, the geomagnetic response to differing solar conditions also varies to a wide extent. Some of these effects noticed during the intense magnetic storms are described in Figs 8.9–8.11.

I. Proton Flux Characteristics and Space Weather

Solar flares are the manifestations of the tremendous eruptions in the solar atmosphere, producing sudden energy release. The magnitude of magnetic energy thrown out in the solar chromospheres and corona during intense flares range between 10^{28} and 10^{34} ergs, energizing electrons and ions up to MeV and GeV respectively. During the high solar activity periods, active regions produce large fluxes of energetic flare particles to CME related shocks, which accelerate the solar energetic particle (SEP) events. Mass ejections play a dominant role in driving large geomagnetic storms by causing sudden commencements on the magnetic records produced by transient interplanetary shocks. Geoeffective nature of the solar disturbances and the energy transfer mechanism of the solar wind energy into the magnetosphere through the reconnection of IMF, are seen to take place.

A major solar flare eruption (Fig. 8.9) occurred at 1620 UT on 4 Nov 2001 followed by strong solar radiation storm and proton event. This was recorded

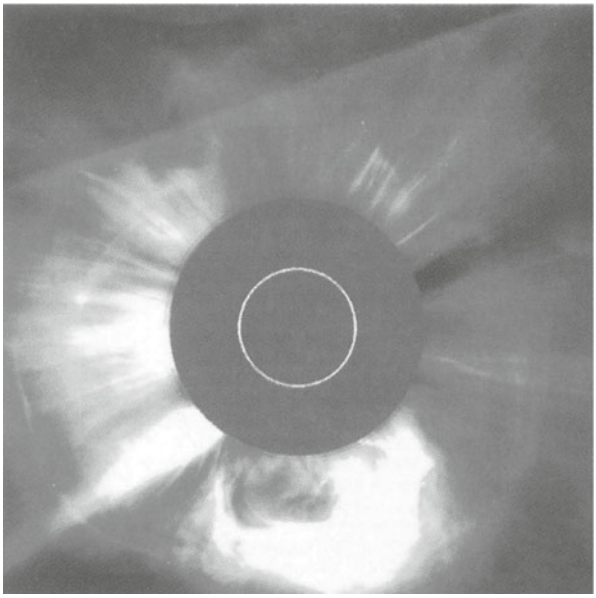

Figure 8.9. Coronal mass ejection or solar flare (http://www.nasa.gov/vision/universe/watchtheskies /july7_cme.html).

by SOHO and other interplanetary satellites. CME associated with the flare event triggered an interplanetary shock, which affected the geomagnetic field after ~33 hrs. The shock impact was quite intense to produce SSC magnitude of ~100 nT in H in low latitude ground magnetic records followed by sharp and deep main phase ($D_{ST} < -250$ nT) in the first stage, following the density (N_P) enhancement. High time resolution digital data from the equatorial and low latitude stations in India analyzed the influence of various interplanetary

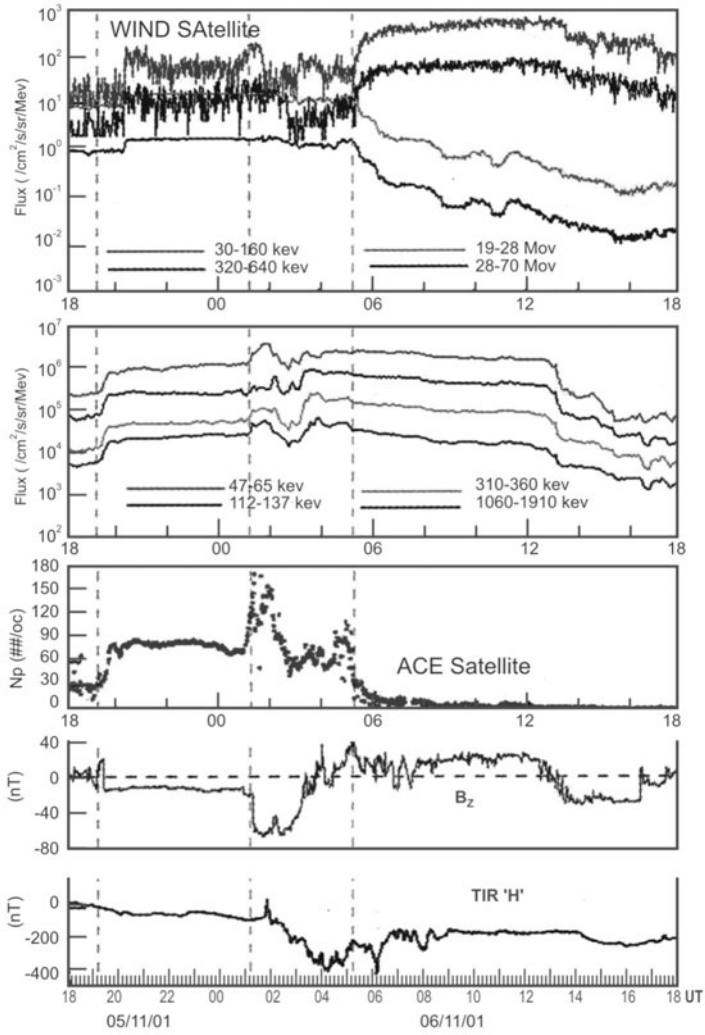

Figure 8.10. Proton flux intensities, as recorded by the ACE and WIND spacecraft, proton density N_P, IMF component B_z (ACE) and the variation in the H component at Tirunelveli (TIR) during 5-6 November 2001. Three dashed vertical lines shown represent the time corresponding to intense proton density enhancements (Alex et al., 2005).

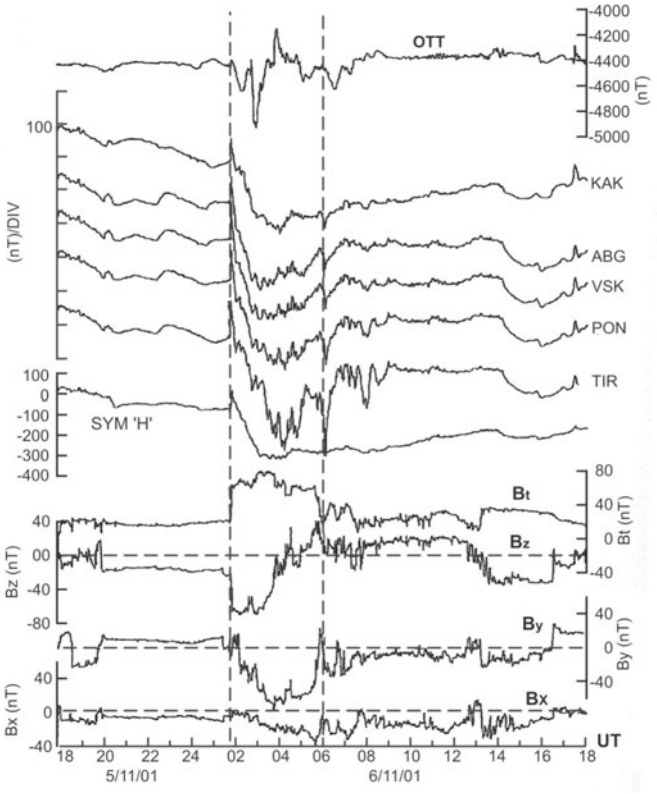

Figure 8.11. Shock effect in the equatorial, low and mid latitude digital magnetic records, seen as the sudden commencement (~80 nT) at 01:50 UT on 6 November 2001. Formation of intense main phase corresponding to the large B_Z of magnitude -70 nT is the salient feature of the event. Satellite data in time is shifted by 35 min. The first vertical line corresponds to the SSC onset and the second one indicates the peak time of development of substorm (Alex et al., 2005).

parameters on the intensity and duration of the magnetic storm. A double step storm was found to be in progress caused by multiple injections. During the period of recovery, after a lapse of 8 hrs, a third stage of depression in ground magnetic field was set in, which corresponded to the southward directed B_Z.

In order to understand the emission features of the particle energy accompanying the solar energetic proton event of 4 Nov 2001, proton flux of various energy levels from the ACE and WIND are given in the topmost panel of Fig. 8.10. Vertical dashed lines are marked against the recurring trend of enhancements in the particle flux densities during 5-6 Nov 2001. Following the strong X-ray flare at 16:20 UT on 4 Nov, proton flux showed sharp increase at all the energy levels as observed by WIND and ACE satellites (Fig. 8.10). The N_P as recorded by ACE satellite is considerably low on 4 Nov and a gradual increase is seen in the early hours of 5 Nov. Around 19 UT, a sudden jump in density is quite evident coinciding with second in N_P flux.

Figure 8.11 brings out the shock effect and magnetic storm characteristics as recorded from the interplanetary parameters by ACE and ground digital magnetic data records from the equatorial, low and mid latitude locations for 5-6 Nov 2001. The arrival of shock is conspicuous at all the locations from the SSC magnitude of ~80 nT, in the equatorial, low and mid latitude digital records. The ring current intensity parameter 'symH' (WDC, Kyoto) indicated that the symmetric component of ring current had a maximum magnitude of the main phase intensity ~–300 nT. The magnetic variation at mid latitude station Ottawa (OTT) given in the topmost curve, showed maximum negative deviation ~500 nT corresponding to the main phase period at the low latitudes. Second vertical dashed line shown at 06:20 UT of 6 Nov, marks the second minima during the recovery phase, which coincides well with the peaked positive value of ~20 nT in B_Y with a lag of ~20 min.

II. Geomagnetic Storm Effects on Technology

The following are the space weather effects on the technological systems:

(i) Solar eruptions directed towards the Earth are potentially harmful to advanced technology. Advancement in technology has been immense in communication, navigation and space-borne satellite systems. Modern instruments and links around the globe are increasingly dependent on electricity and electronics. Technological systems in space and on the Earth's surface are subjected to adverse effects from geomagnetic disturbances. During such events, the magnetospheric compression by the solar wind forces the magnetospheric boundary inward past the geostationary satellite position (Fig. 8.12).

(ii) Geosynchronous communication satellites orbiting the Earth are many in number. A large geomagnetic storm enhances the electrons and ions hitting these satellites, leading to intense spacecraft charging that damages the spacecraft.

(iii) Enhanced levels of solar radiation associated with intense flare activity on the Sun also cause heating and expansion of neutral atmosphere and increase the amount of atmospheric drag that a satellite experiences in an unpredictable manner.

(iv) Auroral activity and intense substorm disturbances cause dropouts and changes in paths of HF communication and increased scintillation degradation of radio signals at high frequencies and disrupt surveillance tracking of the satellite.

(v) The disturbance also induces extra currents in the wires of electrical power grid, producing temporary overload. Such severe geomagnetic disturbances induce DC currents in power lines and can cause destruction of power station transformers.

(vi) Geomagnetically induced currents and voltages can also damage long pipelines and communication cables. These currents affect the conductors used for telecommunications.

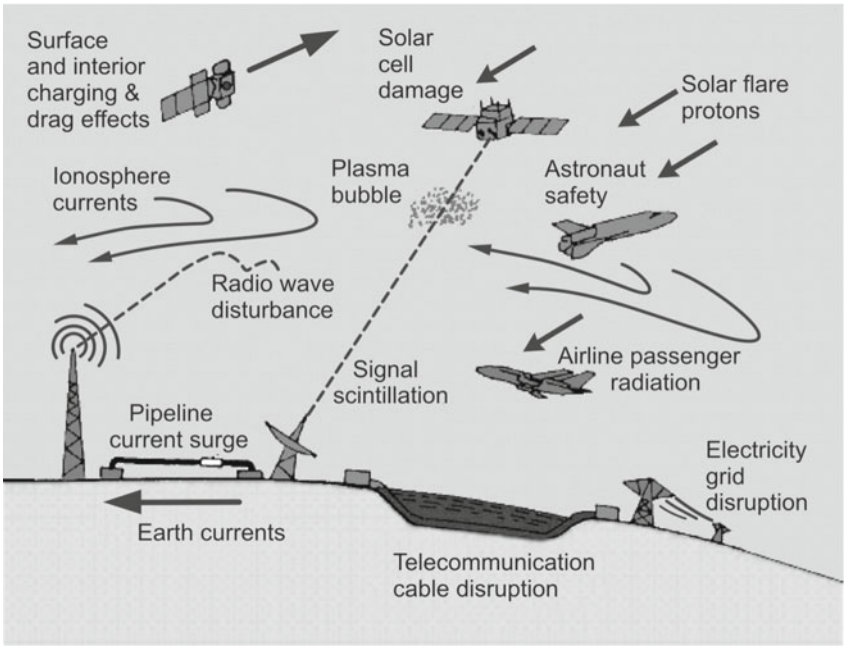

Figure 8.12. Space weather effects on the technological systems ranging from disruption in satellite communication to the destruction in power lines and underground cable (Lakhina and Alex, 2003).

(vii) Very high energy (~1 MeV) charged particle fluxes released during storms and substorms pose a serious retardation health hazard for astronauts. Chapter 9 provides details for items (i) to (vii).

III. Infrastructure for Space Weather Research in India

Several institutes and university departments are participating on various programmes associated with solar physics, interplanetary plasma and magnetic field, magnetospheric physics, ionospheric physics and atmospheric physics that form the backbone for space weather programme. Most of the scientists utilize solar, interplanetary and magnetospheric data from various NASA missions from 1970 onwards for modelling the medium and for the study of dynamics and instabilities in the regions. On the experimental side, expertise for HF Doppler radar, VHF, MST and partial reflection radars exists. Several ionosonde and airglow experiments provide data to understand the ionospheric irregularities. Excellent facilities for monitoring the Sun exist at solar observatories in Udaipur, Ooty and Kodaikanal. A brief summary of the existing infrastructure in India for space weather-related research activities is given in Table 8.1.

Table 8.1 Infrastructure available for space weather-related activities

Organizations/Universities	*Experiments*	*Investigations/activities*
Andhra University, Waltair	Airglow photometer; Digital ionosonde; HF Doppler radar	Ionosphere-thermosphere study; E- and F-region dynamics
Banaras Hindu University	Fabry-Perot spectro-photometer; Dual frequency microwave radiometer; ELF, VLF experiments by Whistler observations	For measuring thermospheric temperature and winds, air pollution; Whistler studies; Ionosphere magnetosphere dynamics
Baraktulla University, Bhopal	Radio beacon studies; Whistler measurements	Plasma irregularities; Ground-based technique for probing the inner magnetosphere
Bhabha Atomic Research Centre, NRL, Trombay	Cerenkov telescope at Mt.Abu	Study of gamma ray sources and the cosmic ray mass composition
Indian Institute of Astrophysics, Bangalore	Digital magnetometer; Digital Ionosonde	Ionosphere-thermosphere coupling; Solar-terrestrial relationships
Indian Institute of Geomagnetism, Mumbai	Network of 11 magnetic observatories; Digital fluxgate magnetometer set-up at six observatories; MF (1.98 MHz) radars at Tiruneveli and Kolhapur; Radio beacon experiments; Scanning photometer; Tilting photometer; All sky imaging camera at Kolhapur; TEC deduced from GPS measurements; CRABEX Experiment	Solar-Terrestrial physics; Magnetic storms and substorms; Secular variations; Geomagnetic activity; Forecasting and space weather; Theoretical and simulation studies on storm-substorms phenomena; Mesosphere winds, tides and planetary waves; Plasma irregularities; Monitoring nightglow emissions at different wavelengths; Atmospheric gravity waves and F-region irregularities; Ionosphere-thermosphere dynamics and Ionospheric tomography
ISRO Satellite Centre, Bangalore	Scanning sky monitor (SSM) for Indian Astronomy satellite; Solar X-ray spectrometer for GSLV: CRABEX	To study the long-term variability in bright X-ray sources for studies of variable stars; To study X-ray flux from Sun over 2 keV to 10 MeV energy range; Ionospheric tomography
Kerala University	HF Doppler radar data	To study the ionospheric plasma drift
National Geophysical Research Institute	Magnetometers at two locations	Studies related to low latitude magnetic variations

National MST Radar Facility (NMRF), Tirupati	MST (53 MHz) radar at Gadanki; Rayleigh lidar system	Studies of long period atmospheric waves, ionospheric irregularities; Temperature profiles at 5-85 km altitude range
National Physical Laboratory, New Delhi	Digital ionosonde; GPS, Radio beacon studies; RPA experiment on SROSS-C2; SASCOM Data Centre Lidar: Laser heterodyne system	Ionospheric plasma parameters and plasma irregularities; Total electron contents; Dissemination of data for global change related studies; Measurements of ozone, water vapour. etc.
Osmania University, Hyderabad	Ionospheric scintillation experiment	Ionospheric irregularities
Physical Research Laboratory, Ahmedabad	High resolution IR Fabry-Perot spectrometer; Ionosonde; All sky imaging camera; Fabry-Perot spectrometer at Mt. Abu; Coherent radio beacon experiment; Nd:YAG backscatter lidar at Mt. Abu	Observations of bright diffuse nebulae associated with star forming regions; Ionospheric plasma properties and ionospheric irregularities; Measurement of neutral thermospheric temperature and wind; Total electron content (TEC), ionospheric tomography; Vertical structure of atmospheric density and temperature around 90 km
Survey of India, Dehradun	One permanent magnetic observatory at Sabhawala	For studying the low latitude current system, Secular variation pattern
Tata Institute of Fundamental Research (TIFR), Mumbai	Ooty radio telescope; GMRT	Observations of high resolution interplanetary scintillations; Probing of inner heliosphere from 0.2-0.8 AU by IPS
Udaipur Solar Observatory of PRL, Ahmedabad	GONG telescope; Sun photometer; Solar X-ray spectrometer; Full disk telescope	To probe interior of the Sun using helioseismology; To study solar eruption processes, the solar flares, CMEs, etc.; Observations of soft X-rays from the Sun; Hα synoptic observation of solar activity
University of Rajkot, Gujarat	ELF, VLF measurements; Radio beacon experiments	Electromagnetic wave propagation in the ionosphere and magnetosphere; Ionospheric irregularities
Vikram Sarabhai Space Centre, Trivandrum	HF and VHF Doppler radar; Digital ionosonde; Langmuir probe measurements; Rayleigh lidar	Measurements of Doppler velocities and spectral width to study the ionospheric irregularities; Ionospheric E- and F-region parameters; E-region plasma properties; Vertical structure of atmospheric density and temperature from 5 to 85 km

8.2 IONOSPHERIC ELECTRODYNAMICS: SHORT PERIOD FLUCTUATIONS

The ionosphere has day-to-day weather that affects technologies in navigation and communication. A space weather modelling capability is useful for mitigating technology impacts. Observations of the ionosphere are sparse. The sparseness does not allow for a full ionospheric specification from data only. Empirical models are based on rough averaging of these sparse data. But the dynamic character of the ionosphere causes large differences between the empirical model result and observations. Ground-based observations on ionospheric scintillations, geomagnetic pulsations, partial radar and airglow experiments are discussed below.

The solar radiation is capable of splitting the neutral atmospheric constituents into ions and electrons leaving the atmosphere in an ionized state. The ionization affects short wave radio communication. The free electrons in the ionosphere are not uniformly distributed but form layers (Chapter 3). Furthermore, clouds of electrons (known as travelling disturbances) may travel through the ionosphere and give rise to fluctuations in the signal. The effects include scintillation, frequency change, and micropulsations. All these effects decrease as frequency increases. This ionized air moving across the EMF favours a dynamo to generate daytime electric currents. Typical altitude profiles of the mid-latitude electron density at day and night for years of minimum and maximum solar activity are shown in Fig. 8.13.

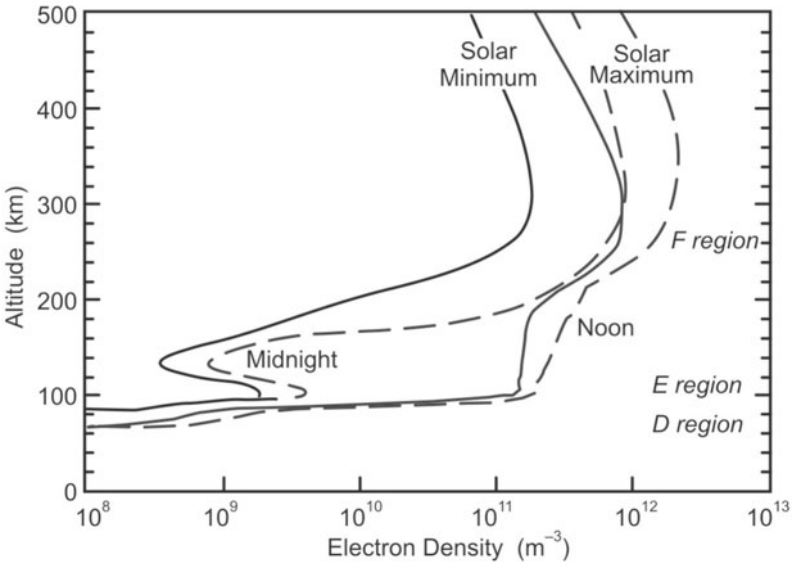

Figure 8.13. Altitude profiles of electron density at 18°N, 67°W, September equinox, representative of noon and midnight, solar minimum (solid lines) and solar maximum (dashed lines), with F, E and D regions indicated (Richmond, 2007).

The ionosphere refracts, reflects, retards, scatters and absorbs radio waves depending on wave frequency. Around the Earth, communications are possible by utilizing ionospheric and ground reflections of waves at frequencies below ~3–30 MHz (10 to 100 m wavelength), depending on the peak electron density. However, frequent collisions between electrons and air molecules in the D region remove energy from radio waves, leading to partial or complete absorption. At higher frequencies, radio waves penetrate entirely through the ionosphere allowing radio astronomy and communications with spacecraft. Nevertheless, such signals can still be degraded by refraction and scattering off small scale density irregularities. In case of GPS geolocation signals, variable ranging errors are introduced by ionospheric signal retardation. The retardation is proportional to the total electron content (TEC) or height-integrated electron density. A typical global pattern of TEC is shown in Fig. 8.14, which shows TEC larger in winter than in summer, because of slower chemical loss in winter.

Radio waves of frequencies in the very high frequencies (VHF) or higher ranges transmitted from satellites and received on the Earth, often encounter ionospheric irregularities in their path. The intensity pattern produced on the ground as a result of scattering of radio waves by the irregularities, results in temporal variations or scintillations in intensity of the signal recorded by the receiver. The phase of the wave also undergoes scintillations. Study of ionospheric scintillations provides a relatively inexpensive tool for monitoring the development of equatorial ionospheric irregularities in the equatorial spread F (ESF), which has its origin in plasma instabilities. There is a great deal of

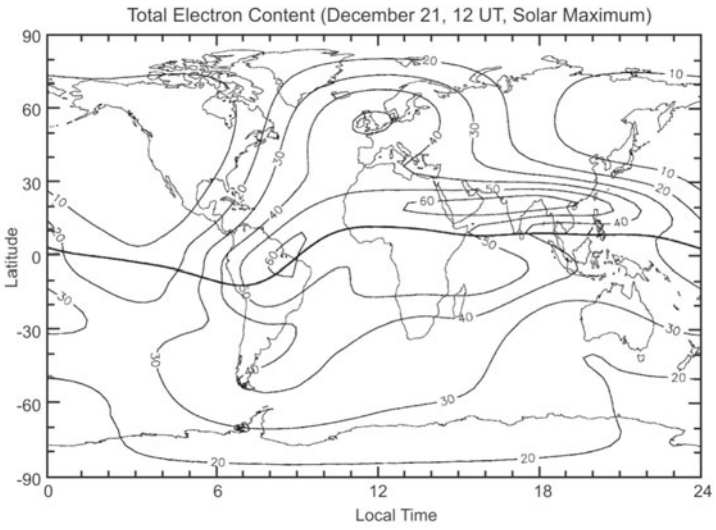

Figure 8.14. Global map of TEC at 12 UT, December solstice, solar maximum. Local time increases with longitude as shown on the bottom scale. Contours are spaced at intervals of 10×10^{16} electrons/m^2. The thick solid line is the magnetic equator (Richmond, 2007).

interest in the prediction of ESF which affects satellite communications and cause loss of phase lock for GPS satellites, particularly in a period around sunspot maximum (Chapter 9).

I. Ionospheric Irregularities and Radio Wave Scintillation

Ionospheric scintillations are variations in the amplitude, phase, polarization, or angle of arrival of radio waves. They are caused by irregularities in the ionosphere, which change with time. The main effect of scintillation is fading of signal. The fades can be quite severe, and they may last up to several minutes. They impose hazards on communication system through degradation in analog and bit rate errors in digital communications. The equatorial region comprising ±20° about the magnetic equator is particularly prone to scintillation activity after sunset. The basic purpose of scintillation studies is to extract irregularity parameters like amplitude of the density deviation, scale size and its distribution, drift, anisotropy and spatial distribution of the irregularities. This knowledge is used in developing models to minimize the problems due to fading of signals, and provide sufficient signal margins.

A chain of VHF polarimeters and scintillation recorders are used to study generation and movement of the ionospheric plasma irregularities, which cause radio scintillation. The radio source used for these studies is the 244 MHz signal from the ETS-2 satellite at 136°E for measurement of total ionospheric electron content. Three-channel PC based data logger capable of sampling data at 10 Hz is used in acquiring scintillation data. Typical scintillation records are shown in Fig. 8.15.

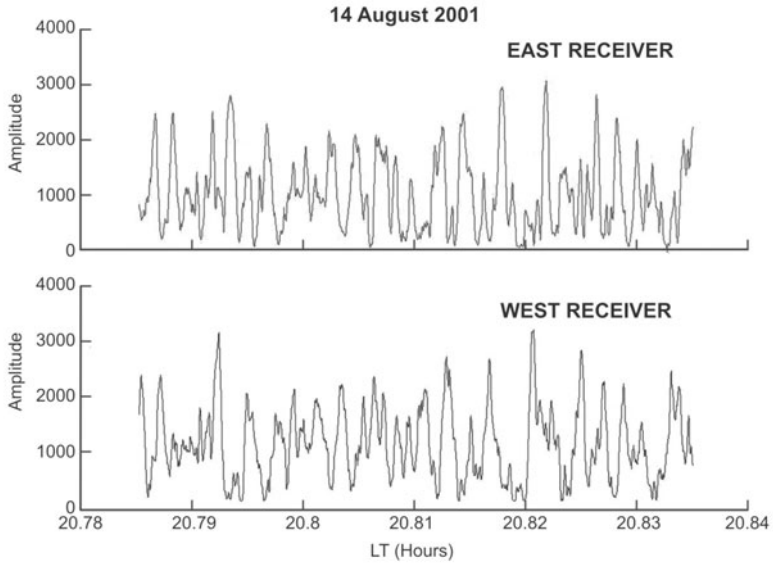

Figure 8.15. Scintillation records collected at Tirunelveli on 14 August 2001.

Daytime scintillation associated with E region irregularities are generally weaker than nighttime scintillations due to F region irregularities (range or frequency spread-F). Nighttime scintillations are continuous near the dip equator, but discrete patches of varying durations are seen at stations far off from it. Figure 8.16 shows the onset of scintillation recorded at Tirunelveli, Pondicherry and Mumbai on the night of 2 Dec 1995. A delay in onset time is seen when one moves away from equator. Equatorial scintillations are inhibited with increase in magnetic activity and this effect also shows seasonal and solar activity.

Figure 8.17 shows effect of sunspot activity on the morphology of the occurrence of scintillation. With an increase in sunspot number, mean percentage occurrence of scintillations increases at both equatorial station and at temperate station Mumbai. During low solar activity period from 1993 to 1996, percentage occurrence is higher at Ujjain than at Mumbai due to mid-latitude generation. Low-latitude scintillations can be either inhibited or triggered during storms depending on the phase of storm and its local time of occurrence.

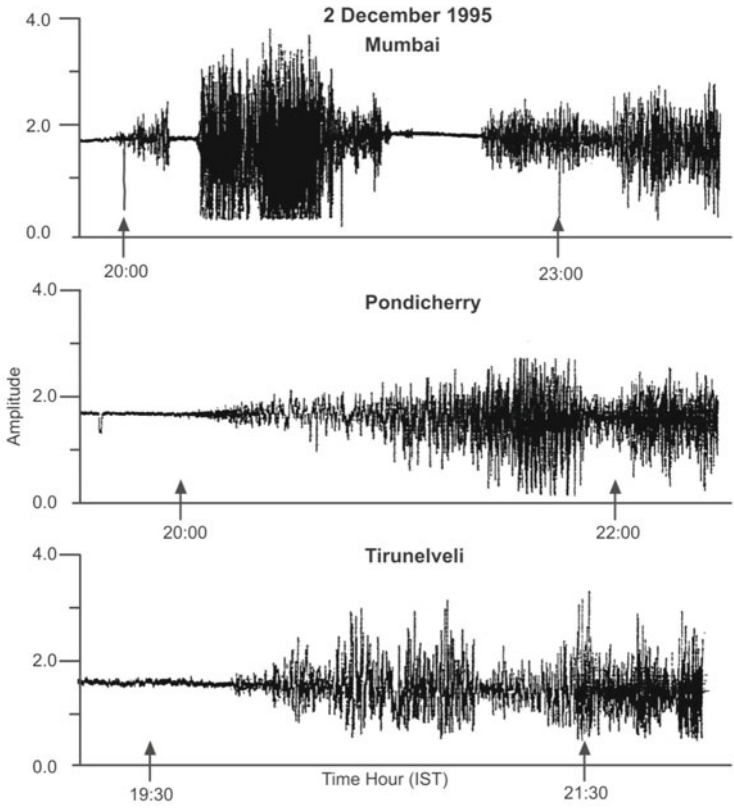

Figure 8.16. Example of scintillation onset on 2 December 1995 for three stations situated at different latitudes (Banola et al., 2005).

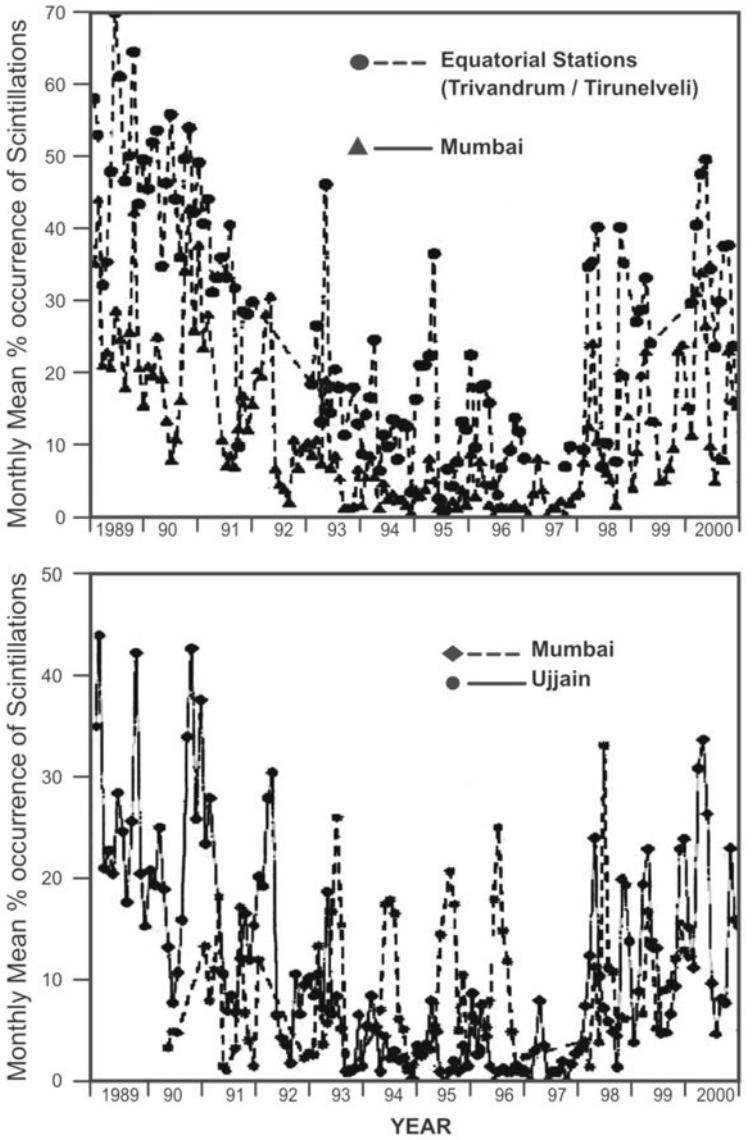

Figure 8.17. Effect of solar activity on the occurrence of scintillations at equatorial stations, Mumbai and Ujjain.

Fresnel frequencies deduced from the power spectra show transverse drift velocities of irregularities to vary between 40 and 118 m/sec, while decorrelation distance varied from 68 m to 188 m for the Indian region. Spectral indices vary in the range from 2.9 to 6.21 with a mean spectral index of 3.4 corresponding to scale sizes of 20–1000 m.

Boundary of equatorial scintillation is defined as dip latitudes, at which the occurrence of scintillation is reduced to half of its value at the magnetic

equator. This is estimated for solar cycle 1989–2000 using analog scintillation record of equatorial stations Trivandrum-Tirunelveli, Pondicherry-Karur and Mumbai-Ujjain. The latitudinal extent of this belt is higher during d- and e-months compared with that of j-months. There is a positive correlation between the width of the belt and solar activity. Geomagnetic control on the width of the scintillation belt is studied from latitudinal variations of scintillation occurrence separately for geomagnetic quiet (Q), disturbed (D) and normal (N) days and also for the groups of days with low, medium and high Ap values (Fig. 8.18). It is observed from Table 8.2 that with increase in geomagnetic activity, width of the scintillation belt decreases.

Table 8.2 Belt variation with geomagnetic activity

Year	*Sunspot number*	*Q*	*D*	*N*	*Ap ≤ 5 Low*	*5<Ap≤ 20 Medium*	*A >20 High*
1991	144	15	11	13.5	15	12	11
1996	8	9.5	6.5	7	7	7.5	6

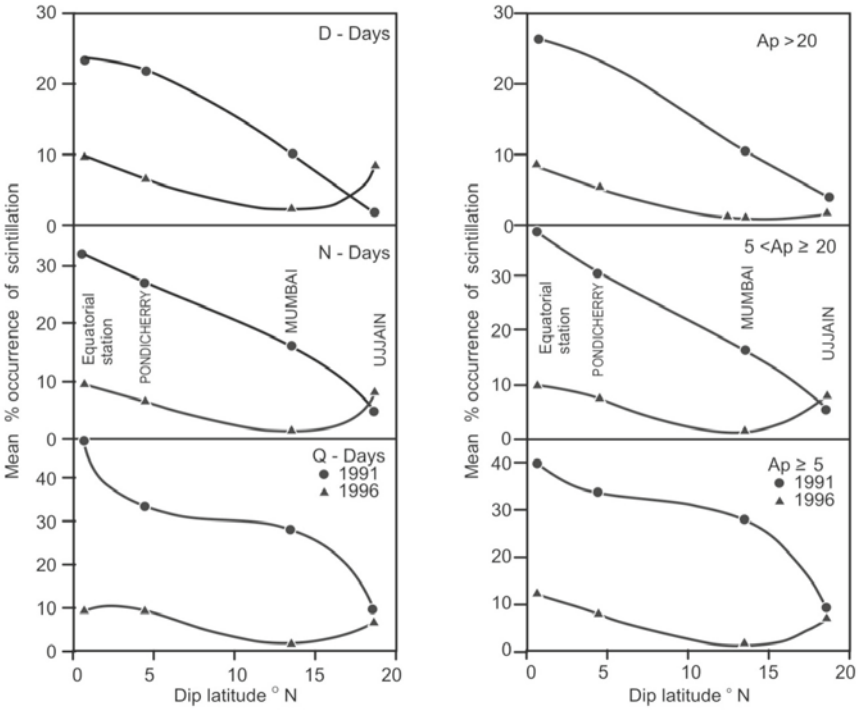

Figure 8.18. Scintillation belt variation as a function of geomagnetic activity recorded at different stations in 1991 and 1996.

II. Geomagnetic Pulsations

Geomagnetic pulsations or micropulsations are ultralow frequency (ULF) plasma waves in the Earth's magnetosphere. These waves have frequencies in the range 1 mHz to >10 Hz and appear more or less as regular oscillations in records of the geomagnetic field (Fig. 8.19). Geomagnetic oscillations or ULF pulsations as they are also called can be identified in electric field measurements in the ionosphere, magnetosphere and those made onboard spacecraft.

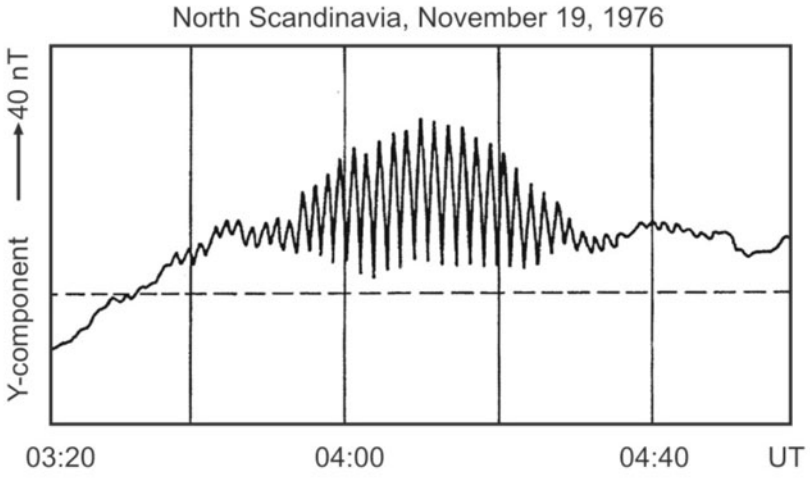

Figure 8.19. Geomagnetic pulsation of the Pc4 type, recorded at a magnetic observatory in North Scandinavia. The Y-component of the geomagnetic field is displayed relative to a quiet day period (Glaßmeier, 2007).

The lower frequency pulsations have wavelengths comparable to typical scale lengths of the entire magnetosphere. They are also interpreted as eigen oscillations of standing waves in the magnetospheric systems. The higher frequency waves are usually identifiable as proton ion-cyclotron waves in the magnetospheric plasma. The amplitudes of the lower frequency pulsations can reach several tens to hundreds of nT in the auroral zone while the higher frequency waves reach amplitudes of the order of a few nT.

Geomagnetic pulsations are classified into seven different types based on their oscillation period and appearance in magnetograms as almost continuous and more irregular pulsations (Table 8.3). The two classes, continuous pulsations (Pc) and irregular pulsations (Pi), are usually divided into subclasses. Micropulsation study is carried out to understand the mechanism by which they appear at low latitudes and also to know the speed and density of the solar wind and various characteristics of the ionized material present in the far away regions of space where EMF continues to retain its identity and exerts its influence in the magnetosphere. The study will provide clues to how the solar wind, the Earth's magnetosphere and its ionosphere are coupled with each

other on a global scale. These natural variations of the geomagnetic field can also be used for exploring the electrical conductivity distribution within the Earth to a depth of ~10 km.

Table 8.3 The IAGA classification of geomagnetic pulsations

Name	*Period range (sec)*
Continuous	
Pc1	0.2–5
Pc2	5–10
Pc3	10–45
Pc4	45–150
Pc5	150–600
Pc6 (during substorms this is known as Ps6)	>600
Irregular	
Pi1	1–40
Pi2	40–150
Pi3	>150

Some micropulsations seem to be caused by resonance of the field lines in response to Alfven waves with certain frequencies which are generated in the space environment even during quiet times. Examples of such pulsations from the Indian Antarctic station are shown in Fig. 8.20. Other pulsations notably Ps6 and irregular pulsations of the Pi type originate in the ionospheric and

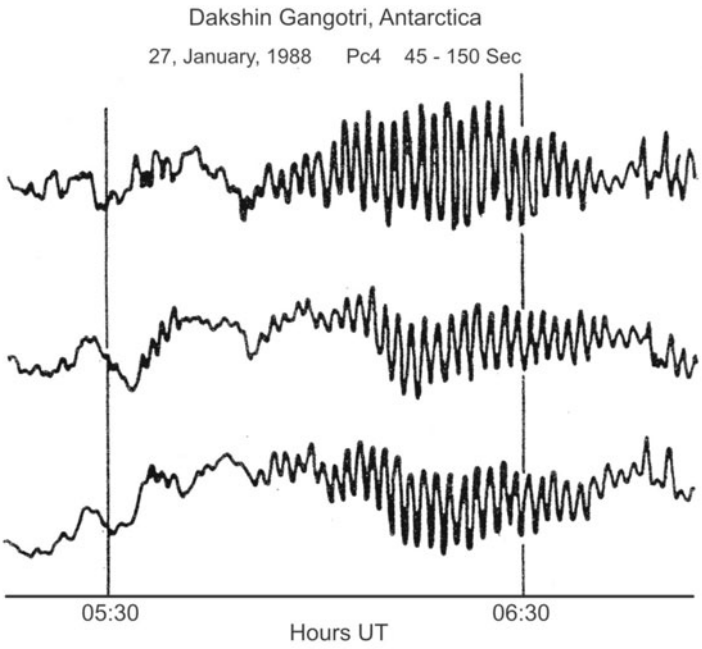

Figure 8.20. Pc4 magnetic pulsation seen on magnetic records from the Indian Antarctic station Dakshin Gangotri on 27 Jan 1988 (Rangarajan and Dhar, 1988).

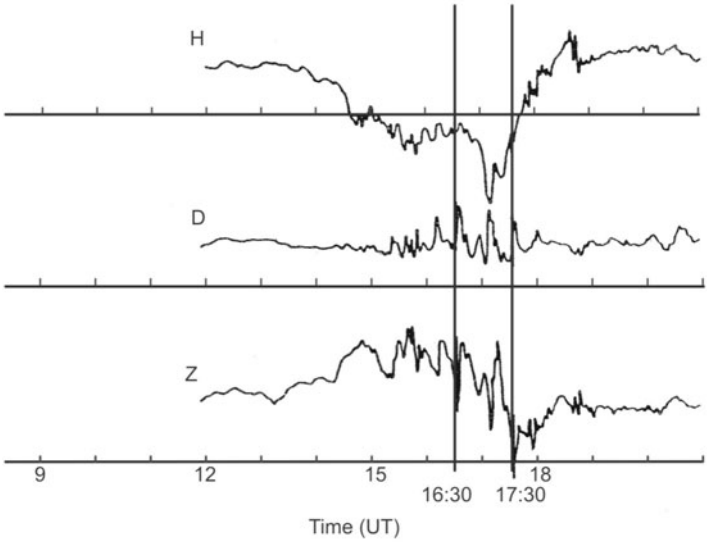

Figure 8.21. Ps6 pulsation event in the H, D and Z components of the geomagnetic field at auroral location Yellowknife on 16 Mar 1978 (Rajaram et al., 1990).

field aligned substorm currents which flow in the auroral regions during magnetically disturbed conditions. Shown in Fig. 8.21 is an example of the substorm associated Ps6 pulsation.

8.3 EQUATORIAL-LATITUDE ELECTRODYNAMICAL COUPLING AND ATMOSPHERIC STRUCTURE

The influence of geomagnetic activity is felt on the weather and climate. Though most of the currents associated with the geomagnetic field flow at altitudes far above the regions which control the weather, intriguing results have emerged from the studies of solar features, geomagnetic activity and meteorological parameters like the circulation patterns, temperature, drought conditions, rainfall, glaciations, etc. Scientists are working to identify a suitable catalyst that enables transfer of energy from the Sun and interplanetary space through the upper atmosphere to the lower regions. The mesosphere-stratosphere-troposphere (MST) radar facility at Tirupati in south India measures neutral winds (Table 8.1) and waves to high altitudes 80–10 km and even to 300–1000 km for studies of partial reflection radar (PRR).

I. Partial Reflection Radar

The partial radar (PR) operating in the medium frequencies (MF) yields useful information on mean winds, planetary waves, tides and gravity waves in thermosphere and lower atmosphere (60–100 km) region. The MF radar data provide quantitative information on the spaced antenna parameters, namely,

the fading time, the lifetime of the ground pattern, the pattern scale and pattern axial ratio.

The MF radar operating at Tirunelveli yields data on winds in the mesosphere and lower thermosphere in the altitude region (68–98 km) since 1992. Simultaneous data on geomagnetic field variation available from the nearby station, Trivandrum are made use to ascertain the range in the H component, which is a measure of the strength of the total ionospheric current flowing above the magnetic equator (Fig. 8.22a). The daytime (0700-1700 hrs) zonal winds between 84 and 98 km as determined by the MF radar for the days, 23 Dec and 26 Dec eastward winds are observed at all times except in the pre-noon hours at altitudes above 90 km (Fig. 8.22b). In the afternoon hours eastward wind speeds in excess of 20 m/sec are observed at an altitude of 88 km. On 26 Dec westward speeds exceeding 90 m/sec around noon at altitudes 96 and 98 km are noticed (Fig. 8.22c). In less than 6 km, the velocity is observed to change by more than 60 m/sec. Measurements on days with different electrodynamical conditions as noticed in the ground geomagnetic field variation indicate the influence of the equatorial current on the drifts measured by partial reflection MF radar.

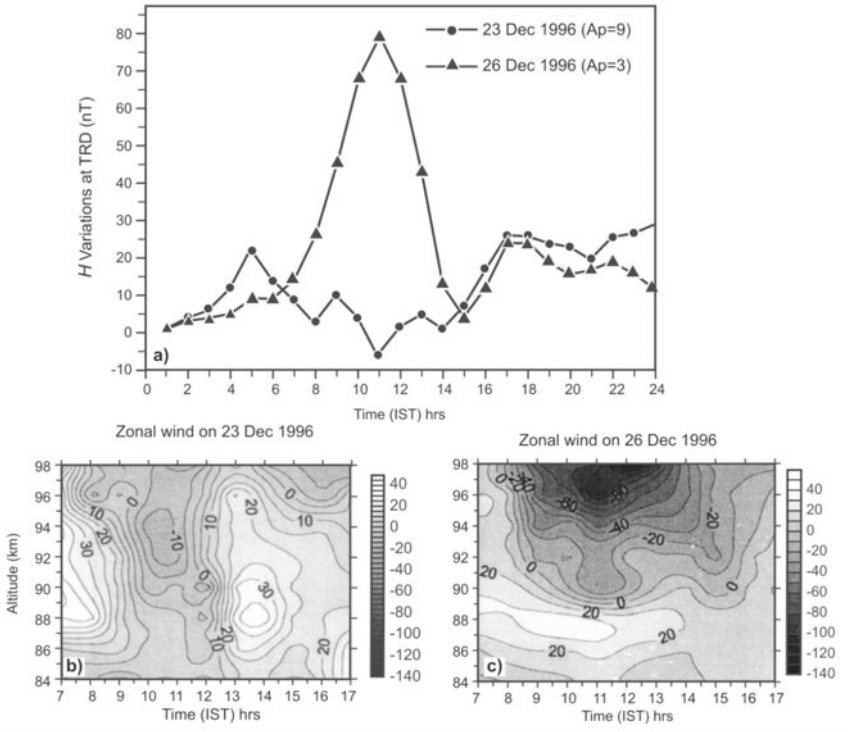

Figure 8.22. (a) Temporal variation of the horizontal component of the geomagnetic field as measured on ground at the equatorial station, Trivandrum (TRD), on 23 and 26 Dec 1996. (b, c) Daytime (0700-1700) radar zonal winds between 84 and 98 km on two days 23 December and 26 December 1996 (Gurubaran and Rajaram, 2001).

Further, PR data revealed a relationship between the tidal characteristics and the occurrence of afternoon CEJ. A clear anti-correlation is seen between the afternoon electrojet strength and amplitude of semi-diurnal tide in solstitial months of June and July 1995. It also revealed the presence of 3.5-day ultra-fast Kelvin (UFK) wave in mesopause region, at 84–98 km. Also, medium frequency radar observations of 3.5-day UFK wave in 84–98 km mesopause region over Tirunelveli for a period of ~3 years are monitored, wherein the UFK wave revealed semi-annual variability at heights (~85 km) where the mesopause semi-annual oscillation in the mean wind peaks. Large-amplitude wave events preferentially occur during westward flow regimes of the background wind. Mean eastward winds and their shears are qualitatively shown to be associated with bursts of waves with moderate amplitudes. Vertical wavelength estimates agree with earlier estimates based on satellite temperature retrievals for a wave number 1 UFK wave.

II. Airglow Experiments

Airglow measurements are complementary to the partial reflection radar since it yields mesospheric rotational temperatures at ~85 km during moonless clear nights. The mesopause region acts as an interface between the mesosphere and the lower thermosphere. It also represents the transition zone dominated by photochemical processes (lower atmosphere) and transport processes (upper atmosphere). One of the manifestations of this sort of transitional character is the multiple airglow emitting layers situated close to one another. The three most important airglow emissions from the mesosphere are: (1) vibrational rotational bands of hydroxyl radical (OH), (2) atomic and molecular oxygen emissions and (3) emissions from metallic atoms like sodium, magnesium, etc. The main energy source is the solar UV radiation, which dissociates the molecular oxygen into atomic oxygen, which in turn becomes chemically active. Transport effects enable the downward flux of O towards mesopause where O_3, OH and active O_2 are formed.

The technique uses measurement of the relative intensities of rotational lines in the hydroxyl vibration rotation band at wavelengths of 733.7 and 740.2 nm using tilted filter assembly. The tilting filters enable correction for background levels and provision is made for three additional filters that can be used for other wavelengths like 630 nm, 557.7 nm and 589.6 nm so that wave dynamical processes that modulate airglow intensities at different heights can be studied. The optical photometer is used to study crucial problems dealing with dynamical heating of the mesopause region through planetary waves, tides and gravity waves. By monitoring airglow emissions from the ground, a variety of quantitative information regarding chemical composition, wind velocity and temperature of the upper atmosphere during quiet and disturbed period is gained.

i. Mesosphere thermodynamics: Temperature of the mesosphere is an important physical parameter in remote sensing investigations of the mesopause thermodynamics and chemistry. At these latitudes, due to chemical reactions in atmospheric constituents, airglow emissions are produced. These emissions, if measured from ground-based instruments, infer the photochemistry and dynamics of the respective regions. Simultaneous measurements of several airglow emission lines from mesopause region provide important information related to the propagation of gravity waves, since these emission layers are situated between 80 and 100 km.

Measurements of hydroxyl rotational temperature for the (8,3) Meinel band are reported from observations of the ratio of relative intensities of $P_1(2)$ and $P_1(4)$ lines of the OH (8,3) band at Kolhapur (16.8°N, 74.2°E, dip lat 10.6°N) during the period 1 Nov 2002 to 29 April 2003 using tilting-filter photometers. Mean values of rotational temperature are computed for 60 nights. The monthly mean value of temperature lies in the range 194±11 to 208±18K. The mean rotational temperature obtained from all the measurements is found to be 202±15K. The results agree with other low latitude measurements of rotational temperature using photometric airglow techniques. Quasi-periodic fluctuations with ~1 to 2 hrs period are prominent on many nights. Furthermore, the results show a general agreement between observations and model (MSIS-86) predictions.

ii. Monitoring of gravity waves using all-sky imager: With the development of cooled charge-couple device (CCD) detector, it is possible to detect spatial and temporal variation of small-scale structures in airglow emissions more accurately. The night airglow observations were carried out from Kolhapur and Panhala (17.0°N, 74.2°E; height above msl 3200 ft) during Jan and Feb 2001, using tilting-filter photometers (630 nm and OH) and a CCD based multi channel all-sky imager, respectively, on clear and moonless nights. The multi-wavelength airglow imaging enables to study horizontal structures of small-scale gravity waves at various heights in the region of emissions and to investigate propagation of those waves in detail. Hydroxyl and OI 557.7 nm images on the night of 18 Feb 2001 showed row-like structures moving from north to south direction spanning over 500 km in the sky. The observed horizontal phase speed of ~50 m/sec, wavelength ~25 km and wave period of ~8 min of the atmospheric gravity waves were determined from a set of sequential images of OI 557.7 nm at 97 km and OH at 86 km observed at Panhala (Fig. 8.23). These are the first observation of the signature of atmospheric gravity waves using an all-sky imager in Indian region showing perturbation in density in the 80 to 100 km mesospheric region. Signatures of gravity waves are also seen at Kolhapur (Fig. 8.24).

Monochromatic imaging of large scale F-region plasma depletions associated with equatorial bubbles present during ESF occurrence shows simultaneous signature of depletions observed in OI 630 nm, OI 557.7 nm and

OI 777.4 nm. Also, the signature of midnight temperature maximum in OI 630 nm airglow is seen. An all-sky image (Fig. 8.24) depicts intense enhancement in OI 630 nm intensity on the night of 7 Feb 2000 ~23:45 hrs during the main phase of magnetic storm with minimum geomagnetic activity index D_{st} reaching at –41 nT.

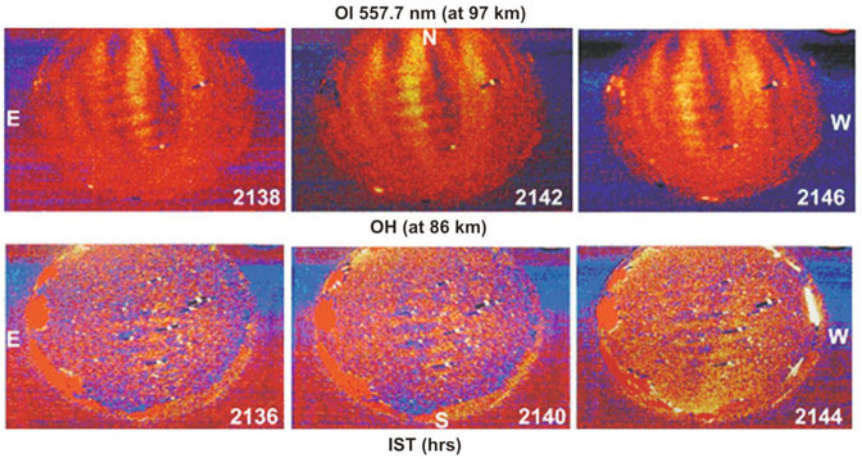

Figure 8.23. Signature of gravity waves observed by an all-sky imager at Panhala on 18 February 2001 (Mukherjee, 2003a,b).

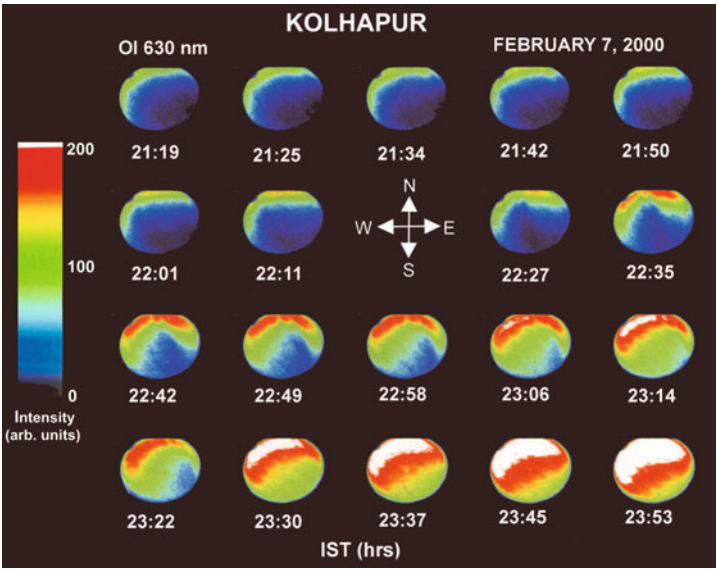

Figure 8.24. Signature of gravity waves observed by all-sky imager at Kolhapur on 7 February 2000 (Mukherjee, 2003a,b).

8.4 ANTARCTIC MAGNETIC DATA

To establish its place in the global arena, Indian scientists are carrying out a number of diverse experiments in Antarctica. India has been launching scientific expeditions to the Antarctic continent since 1981 and has permanent magnetic stations at Maitri and Dakshin Gangotri. The stations at Maitri and Dakshin Gangotri, where the experiments are conducted, are at latitude 70°S and longitude 12°E. Magnetic experiments are carried out to: (1) study the magnetospheric influences on terrestrial magnetic field in the continent on a long-term basis and to carry out systematic magnetic field variation, (2) establish a link between the magnetic field variation in the polar and equatorial regions, and (3) examine subsequently the subsurface structures of the continent using magnetic field variations.

The magnetic field in the polar region gets directly connected to the IMF and solar wind fluctuations, which are most easily communicated to these regions. The diurnal variations in the magnetic field in the polar regions are used to monitor the sector polarity of the IMF. At the same time, sector polarity effects are discernable in low latitude magnetic field variations. Thus the equatorial and polar magnetic field variations can be correlated or studied in tandem for similar features. Also, since the fluctuations in the interplanetary medium are communicated to the auroral ionosphere, these can be stored in the magnetic records.

Direct deposition of solar wind energy occurs at latitudes exceeding 60° geomagnetic latitudes, i.e. auroral and higher latitudes. The lower latitudes, however, are shielded from such direct energy deposition by the closed magnetic field configuration. It is the higher latitudes too, which experience the direct effect of the Earth's geomagnetic response to changes in the direction of the solar magnetic field (the IMF) from northward to southward and vice versa.

The magnetic field variations are also used in natural resource exploration. The rapidly dwindling resources of other oceanic and continental landmasses necessitate delineation of these prized resources on the Antarctic continent, though any exploitation of such resources is banned through many international treaties. However, such probing is also important in understanding the geological history of the Indian subcontinent. India broke away from the Antarctic continent only about a hundred million years ago. Thus, the two have a shared geological history, which can be unearthed by depth sounding along relevant coasts and interior of the two continents. Initially only the total magnetic field was measured using a PPM, but later on till 1989, a single-station fluxgate magnetometer recorded variations in X, Y and Z components.

I. Geomagnetic Studies at Antarctica

The MO at Maitri yields information on physical processes at work in the distant magnetospheric regions. Daily variations and pulsations (Pc2 and above) in the X, Y and Z components at the stations show time lags. These are used to

derive the velocity and direction of the auroral current systems. Magnetograms from the Maitri are used to understand the dependence of HF radio communication on the electromagnetic state of the Earth's ionosphere-magnetosphere system. Also the local time and seasonal variations of the Pc3, Pc4, Pc5 and Pc6 pulsations are studied.

II. Secular Variation Studies at Antarctica

The secular variation of the internal geomagnetic field at Maitri is currently causing a very rapid drop in total field F (~120–150 nT/yr), and at the south magnetic pole (~50 nT/yr). Specifically, studies on the characteristics of secular variation in total F at Antarctica for the interval 1960-1995 are carried out using contour plots of magnetic field variations. The period under investigation is grouped into 5-yr intervals and the average field magnitudes were computed and studied for each of these 5-yr zones (Fig. 8.25). The characteristics of average dipole, quadrupole and octupole fields are determined and their contribution to the total field variation is studied.

Antarctica shows absence of westward drift, which is a prominent feature of secular variation at some other locations. A region of peak decrease in total F lying in the Antarctic region is seen to be stationary. The rate of decrease of this feature is in the vicinity of ~100 nT/yr and the magnitude of this decrease is itself falling since 1980. The dipole field variation contributes less than 40% to this feature and the quadrupole and octupole fields contribute to an increasing

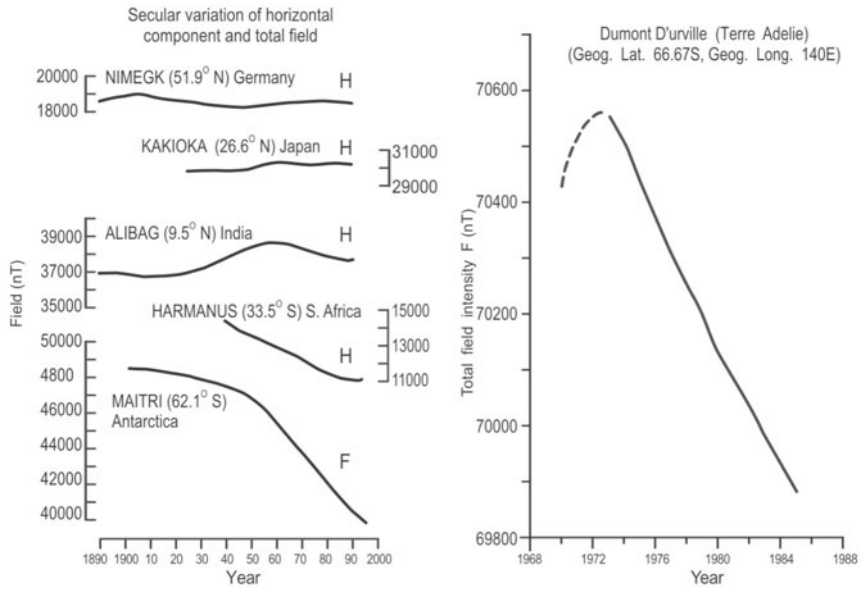

Figure 8.25. Secular variation changes observed at Antarctica and different places over the globe.

field in this region. This implies that a large geomagnetic contribution comes from localized region. Recent studies of secular variation at the core-mantle boundary have postulated that flux expulsion resulting from fluid upwellings could be a cause of secular variation features in the southern hemisphere high latitudes. The northern hemisphere also has a long-lived region of decreasing total magnetic field, but this is located at the mid latitudes. This northern hemisphere feature has a significant contribution from the decreasing dipole field.

III. Magnetic and Atmospheric Measurements

Monitoring the changes in the geomagnetic field on a continuous basis yields information on the electromagnetic state of the near and far space environment of the Earth. Magnetic recordings are a comparatively inexpensive method to monitor the signatures associated with large-scale currents generated in the ionosphere and magnetosphere.

The atmospheric global electricity is provided by a difference in electrical potential (~300 kv) between the highly conducting ionosphere and the Earth's surface, with the total current flow between the two of $\sim 10^6$ A. The air-Earth current is one component that links electric fields and currents flowing in the lower troposphere, ionosphere and magnetosphere and is part of a giant global electrical circuit. The integrated approach provides a good framework for exploring inter-connections and coupling of various regions of the atmosphere and also for explaining the solar-terrestrial relationship. The results from such studies will generate relationships between climate and solar sunspot cycle, and also between solar wind and short-term weather changes.

Ground-based measurements of electrical parameters pose difficulties in interpreting them in terms of the global air-Earth current since they are essentially the superposition of currents from various sources, namely, conduction current linked to the existence of vertical electric field, convection current density, diffusion current due to the movement of charged particles, lightning current due to rapid lightning over the measuring site and precipitation current associated with showers. The sum of these currents is called the Maxwell current. Different types of sensors are used for the measurement of air-Earth current like Wilson plate, spherical sensors, and the horizontal long wire antenna. Magnetometer and riometer data in both analog and digital form exists for the study of a wide spectrum of polar geomagnetic problems.

Air-Earth Maxwell currents and atmospheric electric fields, which require very clean conditions free from anthropogenic pollution, are measured at Antarctica to study the global electrical circuit. It extends the understanding of magnetosphere-ionosphere electrical coupling to the troposphere, an area most important because of its relevance to solar-weather relations. Figure 8.26 depicts Maxwell current density for a selected fair-weather day in the month of Feb 2002 observed at Maitri.

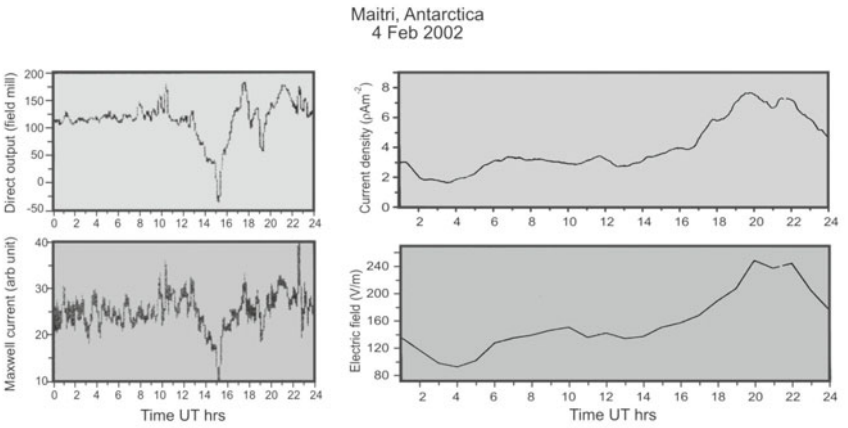

Figure 8.26. Air-Earth Maxwell currents observed at Maitri, Antarctica.

IV. Crustal Magnetic Anomalies

Studies of subsurface electrical conductivity and magnetic susceptibility from the Antarctic data are a little difficult because the inducing source field of the auroral electrojet is a sharply-bounded, non-uniform one. In the early years, a PPM was used to carry out a ground magnetic survey along six profiles, each 10–15 km long. Contours obtained of the magnetic field values show a pronounced magnetic low in the vicinity of the Indian Antarctic locations with axis in the N-S direction; and this is interpreted as the continuation of a rift valley below the ice-shelf.

9

USEFULNESS OF GEOMAGNETIC RESEARCH

Geomagnetism has applications in navigation, communication, space travel (manned or unmanned), power generation, in the search for minerals and hydrocarbons, in dating rock sequences and in unravelling past geologic movements such as plate tectonics. For studies related to different fields, suitably located MOs are operated throughout the country (Fig. 1.14) and worldwide (Fig. 5.1) to record strength, intensity, and direction of the geomagnetic field. It varies spatially and temporally on a very wide frequency spectrum of signals, whose characteristic times extend from geological to historical to millennial to centuries to subsec intervals (Figs 5.3b and 9.1). The longer timescales, typically those occurring over decades to millennia, are relevant to discern planetary magnetism. The long-period SVs of the main field are used for studying the dynamo action in Earth's core and the overlying mantle as well as CMB. Short-term variability finds several important applications related to Sun-Earth connection as well as geophysical prospecting of the Earth's deep interior. The transient type of short-period variations are used for studying the mantle and the crust (see EM induction methods). The small-scale anomalies which ride on the expected magnetic field give information about the crust of the Earth and the presence of petroleum and mineral deposits within it. The metal ores are concentrated in rocks rich in magnetites that are highly magnetic. Geomagnetism provides the cheapest geophysical exploration tool, but lacks the precision of seismic methods. The discovery of EM induction provided yet another technique for exploring the Earth's interior. The experimental methods which are employed for this are discussed in Chapters 6, 7 and 8. Variations on timescales of second to many years also occur due to dynamical processes in the ionosphere and magnetosphere (Figs 5.2 and 5.3).

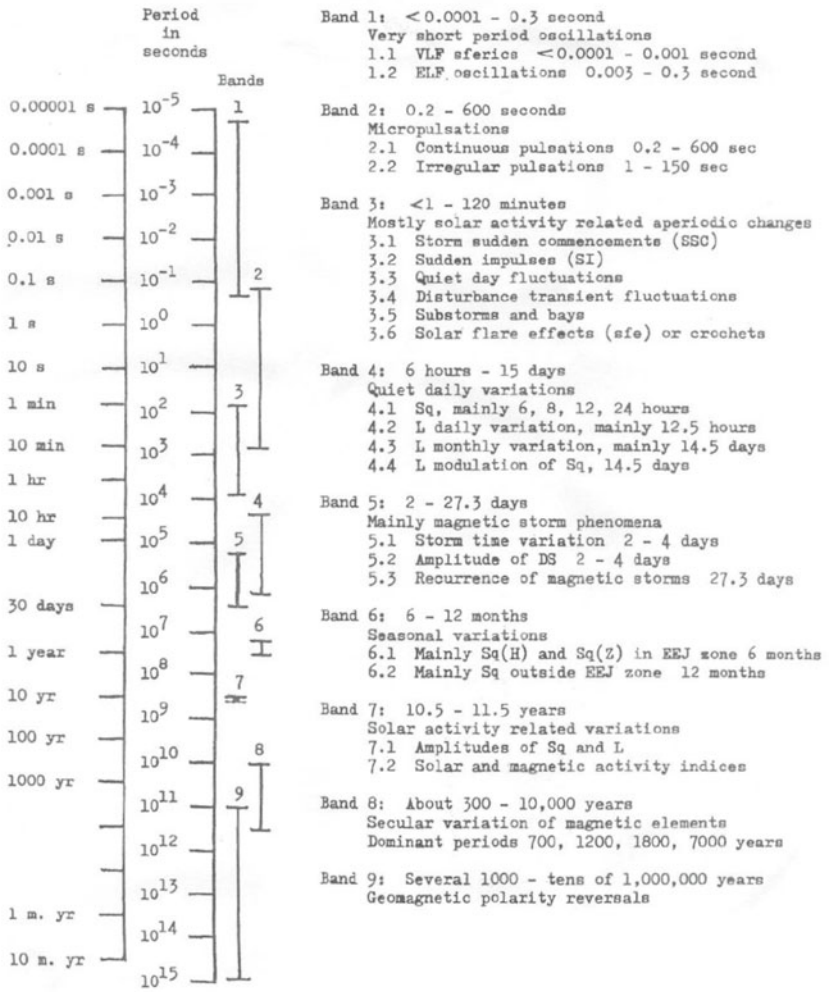

Figure 9.1. Spectrum of the periods of characteristic geomagnetic field variation from 1/100,000 sec to 100,000,000 years (courtesy: Onwumechili, 1997).

9.1 OBSERVATORIES AND DATA ANALYSIS

The geomagnetism programme deals with monitoring of the EMF through a network of MOs and conduct scientific analysis on the data collected (Chapters 1 and 5). Magnetic observatories in India have been running for more than 180 years. This network is ideal for studying equatorial, low and mid-latitude geomagnetic phenomena (Chapter 5) and space weather (Chapters 3 and 8). Geomagnetism is a cross-disciplinary science, hence observatories are run by a wide variety of institutes, whose interests range from geology, mapping, geophysics (including seismology and earthquake prediction), meteorology to solar terrestrial physics and astronomy. The practical use of MO includes help

in space, ground navigation systems and monitoring earthquake activity. The data at Shillong observatory are found sensitive to local earthquakes, providing useful clues for earthquake precursory studies (Fig. 6.67). The data generated at the observatory are passed through a series of quality control measures that involve data processing. Final observatory products of 1-min means, hourly means, annual means and K-indices are produced and disseminated by year-books and CDs. The Indian geomagnetic observatory in Antarctica closely reflects the history of the exploration of this mysterious and barely accessible continent. Its data are particularly useful for southern auroral and polar cap studies as well as tracking changes in the main field in this region (Fig. 8.25).

The geomagnetic field measured at MOs is a sum total of several fields having source both internal to the Earth (main and crustal fields) and external non-dipole field related to electric currents high in the Earth's atmosphere. Annual means of the geomagnetic elements recorded at observatories and those determined at repeat stations contain a solar cycle related variation, which is used to better describe individual observatories as regards the magnetic and electric properties of the Earth's interior; characteristic to the site with possible consequences in improving the SV and the main field models.

I. Application in Communication

Magnetograms recorded at MOs give information on the relationship between solar-terrestrial interaction and the geomagnetic fluctuations (Chapter 5). The daily variations in the EMF allowed Stewart (Chapter 3) to postulate a conducting layer (ionosphere) in the upper atmosphere. Since then, geomagnetograms are used to monitor and even forecast the state of the ionosphere and therefore possible disruptions in radio communication (Chapter 8). In the first half of twentieth century, radio communication was mainly through wavelengths, which are grouped as long and medium waves (frequency in kHz) and short wave bands (frequency in MHz). Such communication is greatly dependent on the EM state of the Earth's environment. Since the satellite era of the 1960s, much of the international communication (both audio and video) depends on the ultra-short wavelength band (frequency in GHz range). Even satellite communication, which is less dependent on the EM state, is affected by phenomena in the geo-atmosphere, e.g. plasma irregularities which produce scintillation and which are governed by the structure of the geomagnetic field and the upper atmosphere.

II. Application in Fundamental Research

The combination of data from magnetic survey satellites such as Magsat, Oersted and CHAMP and observatories worldwide is providing a rich resource for research into core processes. The observatory data are of great importance because of information they give on the SV, providing the basis for estimation of future values of the geomagnetic field at a given location. Observatories

also provide data on interactions that arise between the solar wind and magnetosphere as well as the ionosphere of the Earth, generating EM fluctuations with frequencies ≤1 Hz. Also, oscillations of the magnetosphere generate small, almost sinusoidal variations of the geomagnetic field called geomagnetic pulsations (Chapter 8). Inductive and magnetohydrodynamic interactions between the ionosphere and magnetosphere modify these fluctuating fields before they reach the Earth's surface. The largest geomagnetic field variations up to the order of a few hundred nT occur during magnetic storms (Chapters 5 and 8). These frequency ranges are very effectively used to arrive at the subterranean structure of the Earth (Chapter 6).

The EMF to a large extent resembles that of a central dipole. On the Earth's surface, the field varies from being horizontal with a magnitude of ~30,000 nT near the equator to vertical with ~60,000 nT magnitude near the poles; the root mean square (rms) magnitude of the vector over the surface is ~45,000 nT. The internal geomagnetic field also varies in time on a timescale of months and even longer, though yet unpredictable manner. Although this SV has a complicated spatial pattern with a global rms magnitude ~80 nT/yr, some evidence exists that these changes are cyclic with a period of 500 years. Consequently, any numerical model of the geomagnetic field has to have coefficients, which vary with time. These models also help to distinguish the magnetic field contribution of internal source from the external ones.

Also, models like IGRF based on global magnetic data give a reasonable approximation near and above the Earth's surface to that part of the EMF, which has its origin below the surface. However, errors in the coefficients lead to errors in the resulting model field. Because of the time variation of the field, really good models can only be produced for times when there is global coverage either by satellites or through ground magnetic surveys and establishment of MOs measuring the vector field. Appendix 9.1 gives the locations of north and south dip poles and geomagnetic poles that are computed from the eleventh-generation IGRF.

III. Application in Navigation and Geomagnetic Activity Index

Magnetic observatory serves as a singularly important site in a global network of observing stations, whose combined data define the planetary magnetic field and help track its secular change. Ground stations act as controls for field modelling by harmonic analysis. They are essential reference stations for airborne and satellite surveys and absolute calibration locations for field survey instrumentation. They are also essential for a number of applications such as production of angle D charts for navigation, removal of background fields from magnetic survey data collected from ground, aeromagnetic and ship-borne surveys and calculation of field lines and conjugate points for ionospheric and magnetospheric studies, etc. The MOs often provide backup support for temporary field stations and for purposes of calibration of field instruments.

The ionospheric and magnetospheric disturbance fields indicative of space weather conditions are characterized by various geomagnetic activities. Each of the Indian observatories provides data for the computation of the Kp-index. Data generated at different observatories are also used to arrive at various geomagnetic indices like the Dst, AU, AL, EEJ, Kp, AE, aa, PC, MT and so on, to characterize the geomagnetic activity at a particular location.

IV. Other Applications

The data collected at MOs are often sent to the air-force, marine and military installations for use in their operational models characterizing Earth's near-space environment as well as to scientific/technological establishments around the world. These institutions actively produce models of the EMF that are used in host of applications, including GPS receivers, military/civilian navigational systems and in research for studies of the effects of geomagnetic storms on the ionosphere, atmosphere, and near-space environment. India shares its geomagnetic data with a legion of international agencies based in USA, Canada, Japan, France, Brazil, UK and others as part of InterMagnet. The data are made available to the worldwide community via www.wdciig.res.in. Also, calibration of compasses the world-over is carried out at the MOs to account for any changes in angles D and I of a particular region.

9.2 SOLID EARTH GEOMAGNETISM

The extraordinary wealth of information collected in the last few decades has totally transformed our view of the Earth. The earlier notion of a static and placid globe has been replaced by a dynamic Earth, whose core is rotating, mantle convecting and crust drifting. The Earth's crust forms at the spreading mid oceanic ridges and floats on the convective mantle, making it amenable to collisions with each other (Fig. 2.49). The study of this motion helps understand plate tectonics, earthquakes, volcanic activity and even emplacement of natural resources. The mantle is studied, although indirectly, through magnetic field measurements. For at its bottom, the mantle is coupled to the liquid core and at top to the crust. The liquid core kinetically produces the magnetic field, whereas the crust is a repository of potential magnetic field. Both these fields can be measured easily and accurately from land, ocean and space because of which their magnetic properties can be harnessed for understanding multidimensional processes operating inside and outside the Earth.

Studies carried out through the spectrum of geomagnetism have three aspects. The first pertains to the basic urge to know the structure of planet Earth. Second relates to increasing need of the industrialized society for critical estimate of natural resources, to know which, the dynamics of the Earth's interior and the mechanism of resource emplacement need to be understood. Third, the nature of EMF and its variation with time give an opportunity to learn more of the structure of other planets and also of stars.

The geomagnetic field has two internal sources: one due to electric currents in the liquid (outer) core and the other from the crustal magnetization. The former is dynamic and changing, whereas the latter is static and unchanging. The crust has mainly induced magnetization and its magnetic field is often referred to as crustal anomaly, which is caused by nonuniform distribution of magnetic material. The detection of these anomalies forms an important practical application of geomagnetism. Large-scale magnetic anomalies (extending over some hundreds of km) are obtained from satellites, whereas smaller scale anomalies are detected through ground and aeromagnetic surveys. Mathematical and experimental techniques (discussed in Chapters 2, 6 and 7) help determine the contributions from subsurface structures in the observed magnetic records.

I. Interdisciplinary Geomagnetic Techniques and Earth's Interior

The technological impediments in reaching physically down to depths of mantle and core are partially removed by the access to this domain through different instruments (Chapter 4). Certain properties (density, temperature, velocity of seismic waves and so on) depend on physical characteristics, which are used in arriving at many (and diverse) interpretations of the physicochemical realm of the interior of the Earth, leading to an improvement in understanding the formative processes of this planet. Thus, without going down to the core or mantle, the composition of the core is deduced to be mostly Fe and Ni. The dynamo processes are also well understood with an improvement in instrumentation and computer simulation capabilities (Figs 2.40 and 2.45).

Earth's inner realm is consistently under investigation through seismology, terrestrial magnetism and geology. Seismology studies the propagation of seismic waves and is the only method effective enough to delineate principal inner subdivisions of the Earth. The nature of each of its units is identified by its ability to propagate (or block) shear waves (Fig. 2.12). Large fractures and polarity reversals of magnetization all along the mid oceanic ridges have formulated concepts relating to plate tectonics, ocean floor formation and continental drift. Induced and remanent magnetizations reveal polar wandering (Fig. 7.8) and associated theories of crustal movement (Figs 2.50–2.52).

Traditionally, geology has been closely associated with the study of tectonics through mapping (aerial photography) fold, fault trends and geomorphological characteristics. In such cases, however, the dependence is on surface expression of deep structural units and the picture obtained is therefore incomplete.

Some geotectonic aspects are novel to India, like the drifting of Indian plate, its subsequent docking with Eurasian landmass, associated Himalayan orogeny and opening of the Indian ocean, extensive continental flood basalts of the Mesozoic (Deccan and Rajmahal traps) and a complex geoelectric structure (SIOCA) at the dip equator. Also, the physical, morphological, geochemical environment of the peninsular and extra peninsular region give

an opportunity to study the 'contrast' in order to quantify magnetic and gravity fields, global warming, climate change, monsoon variations and other interesting topics.

Geophysics has injected the precision of exact sciences and methods of mass data processing into geology and physics, making feasible the studies related to seismology, geotherm, tectonophysics, structural and general geology. Applied geophysics, on the other hand, has the character of an applied science, which helps determine the micro and macro geological structures of the crust and upper mantle, delineates raw material deposits and characterizes geological activities pertaining to engineering geology, environmental geology, hydrology and others. Applied geophysics is divided into individual disciplines depending on field surveyed. The gravity field is studied by means of gravimetric methods, the magnetic field by magnetometric methods, the geoelectric field by geoelectrical methods, the field of elastic waves by seismic methods, the radioactive field by radiometric methods and the thermal field by geothermic methods.

The Earth's crust is an inhomogeneous medium with different physical properties of rocks and tectonic blocks (density, magnetic susceptibility, resistivity, radioactivity and nuclear properties, electrical and thermal conductivity and elastic parameters). The changes in the physical fields of the Earth are used to determine crustal inhomogeneities (structure, occurrence of raw-material deposits, etc.).

Geophysical data are interpreted through direct and inverse means. The solution to a direct problem is sought by determining the effect of a disturbing body of known size, shape, depth and physical properties on the corresponding physical field (e.g. the effect of a regular geometric body of known differential density and susceptibility on the gravity and magnetic field of the Earth). This problem has a unique solution. There is no ambiguity. But the inverse problem is usually ambiguous. In an inverse problem, one seeks to determine the disturbing body corresponding to an anomaly in a physical field. This problem is usually ambiguous. Hence to render it unique, several geophysical methods or supplemental geological information are combined together.

Apart from academic research, magnetic and EM methods find practical applications in: (1) locating mineral and hydrocarbon deposits, (2) in understanding the evolution of the Earth's crust and the dynamics of the mantle, and (3) possible prediction of earthquakes through the effect of tectonic stress within rocks. The potential uses of geophysical data are described below.

II. Geopotential Field Anomalies and Configuration of Crust

Configuration of the Earth's crust is done by using principles of geomagnetism. Changes in composition, subsurface temperature and thickness of the crust and mantle cause magnetic anomalies, by identifying which internal Earth features such as hot spots, rifts, seismic zones and tectonically active regions (Figs 6.5 and 6.11) are isolated. Magnetic anomalies also map Curie isotherm

depth (a proxy for heat flow), delineate different metamorphic zones and reconstruct tectonic evolution.

What satellite gravity and magnetic data sees: To build a model of the Earth's interior through magnetic measurements, the data are necessary to be global in extent. Satellites provide global uniformly accurate data and since their observation time is brief, secular drift corrections are not needed to apply. Satellite measurements are made with a remotely placed sensor, hence these data are extremely useful in bringing out large wavelength features of size ~1000 km. Remote observation has an advantage and a disadvantage as well. The advantage is that small-scale features present in the ground data, which make isolation of large-scale features difficult, get completely suppressed when observations are made from space. The disadvantage is that the crustal signatures get significantly reduced due to the great distance of the point of observation. To get finer details of the structural blocks, space observations are supplemented with ground, oceanic and aerial surveys.

Magsat satellite anomaly: Magsat anomaly maps (Figs 6.8a,b) have outlined major geological and geophysical structures in the subcontinent. In general, the anomalies depend primarily on the product of the magnetic susceptibility and layer thickness (i.e. 400 m of material with a susceptibility of 0.05 gives rise to almost the same magnetic anomaly as 2 km of material with a susceptibility of 0.01). Further, the geological properties of the Earth's crust cannot be directly derived from magnetic anomaly maps because they are masked by the changing inclination of the main magnetic field responsible for induction. The anomaly is inverted to obtain the depth of the magnetic crust. The crustal depths thus obtained are correlated with major geological lineaments/faults and tectonic features (Fig. 6.11), especially to study similarities and differences between continental and oceanic crusts.

The peninsular shield, the Ganga basin and the Himalayas are three different geotectonic blocks, clearly reflected in the crustal magnetization maps (Fig. 6.11). A thick magnetic crust under Aravalli, Singhbhum and Dharwar suggests these are comparatively stable. In general, seismic, gravity and heat flow data agree characteristically well with the magnetization estimates. It also delineated the cause for unique features of steep rise and fall of the anomaly, the depth structure of many geologic features (Figs 6.5 and 6.11) and the continuation of continental type of crust for some distance on the west coast as well as into the northern portion of Bay of Bengal (Figs 6.7 and 6.11). Magnetic signatures are variable and they appear to depend on the age and conditions of intrusion. The other applications include the creation of updated models of internal EMF and study of fields due to ionosphere and magnetosphere currents. These uses can be enhanced by acquisition of data from MOs and repeat stations at the Earth's surface.

Satellite gravity and isostasy: The satellite free-air gravity anomaly at ground level (Fig. 6.2b) is used for studying the isostatic condition in many parts of

Indian peninsula in general and the Himalayas in particular. These studies revealed that the peninsula is isostatically compensated, whereas the Himalayas are isostatically overcompensated (Fig. 6.3). This result contradicts the positive satellite gravity anomalies. It is stressed that the true nature and extent of isostatic compensation of the Himalayas can only be decided by investigating both the positive and negative anomalies resulting from the mountains and their roots.

Satellite residual gravity and magnetic anomaly: Stable cratonic areas like shields, platforms and flexural basins including the Himalayan foredeep, are overlain by relatively positive magnetic anomalies and negative free-air gravity anomaly values (Figs 6.5 and 6.11). This combination of anomalies reflects displacement of dense nonmagnetic mantle material by thick crustal material. Rifts, aulacogen and rift related basins are generally associated with relatively positive free-air gravity anomalies reflecting the presence of denser material in the crust. High gravity and low magnetization anomaly over the eastern ghats are modelled in terms of crustal thinning (as analogous to high heat flow). Magnetic low values over the Arabian Sea seem to centre near Mumbai—a region associated with local gravity high and also basic and ultrabasic dykes. Other geological features with the axis of inverse correspondence between magnetic low and gravity high are the Konkan coast, hot springs, the Cambay rift and the Panvel flexure. Pinpointing exact locations of these tectonic blocks requires that the satellite study be backed by aeromagnetic and ground survey.

Aeromagnetic studies: Long wavelength (regional) anomalies derived from satellite magnetic and gravity data normally give information about the lower crust. To better understand the overall geodynamics, aeromagnetic (wherever available) and ground surveys are combined. Aeromagnetically limited surveyed areas of the peninsula (Figs 6.13-6.15) show a thin exhumed southern granulite terrain crust, which has a lithological/mineralogical change at ~22 km depth. The inverted crustal model suggests alteration of charnockites into hornblende-biotite-gneiss. This alteration is more towards the north than south, wherein the process of retrogression is high. The exhumation of charnockites is more between Cauvery fault and Salem-Attur fault.

Ground magnetic studies: Compared to Magsat data, ground magnetic anomaly maps (Fig. 6.17) are not able to separate the geological provinces. The distinct Magsat anomaly over the Himalayas and Narmada-Sone lineament are indecipherable in ground data. This is because the strong features of local extent mask the regional features. The results of three basins, viz. Mahanadi, Krishna-Godavari (K-G) and Cauvery (Figs 6.20, 6.23 and 6.28) gave useful information on the breakup of India from Gondwanaland. Curie isotherm depth calculations for Cambay and K-G basins allowed inferring their hydrocarbon bearing potential. A few magnetic-cum-gravity profiles provided information on the basement configuration and the total thickness of sediments to pencil out areas for further intensive studies by electrical resistivity, seismic and EM methods.

III. EM Induction Methods

In gravity or magnetic fields, the anomalies are small perturbations over the normal field, but in transient variations they can be greater than the normal part by a few orders of magnitude. The causative process is the large electrical conductivity contrast of 13 orders of magnitude (e.g. dry crystalline rocks have conductivities $<10^{-6}$ S/m, while ores have conductivities exceeding 10^{6} S/m). Electrical conductivity is a sensitive parameter for saline fluids, carbon grain-boundary films, conducting minerals, high heat flow and partial melts (molten rocks or aqueous solutions). This parameter is extensively used in GDS, OBM and MT for mapping geoelectrical structures.

The EM method of GDS and MT types is found to be invaluable tool in probing subsurface conductive structures from measurements carried out in a selected band of frequencies (normally 10^{3} to 10^{-4} Hz). A time-varying EM field generated by thunder storm activity, micropulsations, polar substorms and solar activity induces current in the conducting medium to give rise to an associated secondary magnetic field. When the period-dependent spatially anomalous EM fields are isolated, they are used to image structures and lateral conductivity contrasts. For lower frequencies (long-periods), the depth of penetration is more and for higher frequencies (short-periods), the depth of penetration is less. Hence, by measuring the field at different frequencies (time periods), the subsurface information at different depths is obtained.

Applied EM methods map conductivity patterns, which indirectly infer temperature, structural and compositional variations from the crust down to the upper mantle and help in understanding the Precambrian tectonics, crustal evolutionary processes (Figs 6.41, 6.42) and the seismicity. GDS and MT are two complementary geophysical methods; the former has a better lateral (horizontal) resolution, while the latter has a better vertical resolution. The effectiveness of MT data to provide constraints on tectonic configuration under study increases on integrating its information with gravity, seismic wave velocity and heat flow data (e.g. Fig. 6.45). Seismic methods fail to reveal the desired subsurface information in complex sedimentary basins (Fig. 6.18). At such places, MT methods are applied to locate hydrocarbon deposits hidden beneath them. For example, MT methods are useful in Deccan volcanic (Figs 6.43 and 6.44), where the conventional geophysical and seismic methods fail because of high velocity basaltic cover.

The data pooled from GDS and MT studies (Figs 6.30, 6.32, 6.33, 6.40 and 6.44) can synthesize electrical conductance distribution map for the entire subcontinent, which not just demarcate thermally favourable zones of hydrocarbon maturation, but also provide better insight into the seismic patterns. Subsurface electrical structures below the ocean floor are mapped by OBM array studies. The oceanic crust/upper mantle underlying the Bay of Bengal is found more resistive than the one underlying Andaman arc region. This is because the former is older and latter younger.

The Earth's conductivity is also studied with the help of satellites (Magsat). The apparent resistivity of the American and Pacific regions is similar, but it differs in the European-African sector. The oceanic and continental apparent resistivities are seen to differ most at short periods, indicating a possible influence of induction in oceans. The apparent resistivities of the southern hemisphere are significantly higher than those of the northern hemisphere at all periods. This is an unexpected result, since the southern hemisphere is dominated by oceans, and analyses of ocean bottom data with the Z/H method and MT indicate lower resistivity of the oceanic mantle. In the Indian context, magnetization and mass distribution (Figs 6.11 and 6.12) maps prepared from satellite data are found to be consistent with the trans-Himalayan conductor and the Palk strait conductor (Figs 6.32 and 6.33) identified by EM induction methods. This correspondence between the two suggests that both these conductors are associated with either high heat flow or low magnetic susceptibility and density. The anomalous character of the lithosphere immediately south of India is also indicated as low magnetization anomaly, reflecting thin magnetic crust due to rise of the Curie isotherm.

Magnetic field changes originating in the Earth's core cannot reach the surface if their periods are much shorter than one year. Sudden geomagnetic core events called jerks occur at the high-frequency end of the SVs. They last only for ~1 year or so and are clearly observable at the Earth's surface and from satellites. Based on ground observations of the jerks, conductivities of lower mantle are found between 1 and 10^3 S/m (Fig. 6.35).

IV. Earthquakes: Causes and Measurements (GPS Receivers)

Understanding earthquake generating processes, seismic character and seismotectonics are the present topics of research. The ultimate aim and objective however are to forecast earthquakes, since both society and economy are impacted. Seismic zonation map (zones II to V) of India (Fig. 6.56) lists seismic status of the areas and their susceptibility to earthquakes.

The major earthquakes, by and large, are associated with marked crustal movements that lead to volumetric and mass changes aggravating build-up of tectonic stresses. Observations of crustal movements (vertical and horizontal) and deformations are done by GPS satellite receivers (Figs 6.74 and 6.75). GPS data are also supplemented by ground magnetic and gravimetric data to chart models regarding the earthquake preparation processes.

Build-up of tectonic stresses along faults and weaker zones lead to dilatancy and diffusion of fluids; piezomagnetic effect induces temporary changes in magnetic characteristics of rocks and sediments. These are few clues to an impending earthquake (Figs 6.61-6.68). Continuing research showing geomagnetic and geoelectrical precursory signals play pivotal role in earthquake prediction programmes (Figs 6.32, 6.44 and 6.58). Repeat magnetic surveys map distortions in SV trend (Fig. 6.54) in seismic areas due to accumulation of

stress. For example, magnetic anomaly contours (Fig. 6.59) in Koyna region represent patterns showing displacement of magnetic rocks by faults and thrusts. In geoelectrical investigations, GDS and MT surveys delineate lateral and radial distribution of the subsurface structures, e.g. fault planes (e.g. Figs 6.58 and 6.60).

Past seismic activities also leave behind tell tale signs of their occurrence in soft sediments in the form of seismites and other cataclysmic features (Figs 6.69 to 6.72). These signs, with the help of palaeomagnetic methods, are deciphered to date the relative time of their occurrence. Since earthquake activity (in some cases) is seen to occur in time bound episodes, the dates acquired by magnetostratigraphy can put a qualitative constraint on future occurrences of seismic episodes at a particular locality.

V. Palaeomagnetism and Continental Drift

Palaeomagnetism revealed significant data about the geomagnetic field's past behaviour and many other aspects of geology and Earth history (Figs 7.1-7.3). From NRM directions, the palaeolatitudes are worked out (Fig. 7.7), giving the probable geographical location of sampling site in the past. The knowledge has validated the hypothesis of continental drift. Alternatively, the position of the pole in the past is calculated to account for the observed direction of magnetization, establishing the theory of polar wandering (Fig. 7.8). Palaeomagnetic studies show that the EMF has been prevalent for at least last two billion years.

Magnetic reversal dating and magnetostratigraphy: Earth's history is chronicled through different methods like radiometric, isotopic, stratigraphic and so on. The joint development of measurements of oceanic anomalies and magnetic stratigraphy, both on oceanic piston cores and on land sections, produced GPTS (Chapter 7). It is the first great synthesis of an absolute chronology for the last 200 Ma in the history of the Earth (Figs 7.10-7.12). Determination of polarity of the remanent magnetism in rocks compared to the present magnetic field provides better scope to date dyke-intrusions in Deccan traps (Fig. 7.13). The GPTS (magnetostratigraphy) documents the changing configuration of continents and oceans as well as is an important method to establish timeline for significant tectonic and geologic episodes. This gives an advantage to date in relative terms the environmental or climatic patterns down the geological ages (Fig. 7.14). Over past three-and-a-half million years, the Earth's magnetic poles shifted approximately nine times. Scientists do not know how or why the magnetic poles reverse, nor do they know exactly what effect this will have on life. The magnetic poles of the Earth reverse on an average every 250 ka, but the intervals between such reversals vary from 10 ka to some Ma. But the Sun reverses its magnetic poles fairly routinely: essentially every 11 years.Studies are also carried out to map details of the magnetic field during polarity transition. Systematic departures from a simple dipolar structure during

a reversal are discovered. The non-dipolar character of the transitional field is widely recognized as direct consequence of the systematic drop of dipole intensity. A temporary reduction in the strength of the magnetic field allows the Earth's atmosphere to be less protected from the Sun's lethal radiation. This may cause climatic disruption, destruction of satellites, and eventually loss of life, though not to the extent of extinction, since our ancestors have successfully survived these flips (see Chapters 3 and 8).

Palaeomagnetists recently investigated the progressive evolution of palaeomagnetic directions in two transitional lava flows. Each lava unit recorded a complete sequence of directions going all the way from that of the underlying flow to the direction of the overlying flow. These features are interpreted in terms of very fast geomagnetic changes of 10° and 1000 nT/day. For comparison, values typical of the present-day SV are of the order of 0.1° and 50 nT/yr, i.e. some 10^4 times slower. Recent data reveal that the slow variation of the EMF and also a slow shift in the geographic position of the magnetic poles are roughly cyclic over a period of 500 years. Syntheses of palaeomagnetic records in the past decade yielded some controversial observations like the existence of preferred longitudinal bands for VGP paths over the Americas and eastern Asia, possibly in relation with the cold circum-pacific regions in the lower mantle, outlined by seismic tomography. Such features imply some form of indirect control of the reversal processes by the mantle, generating heterogeneous fluid flow at the core-mantle boundary.

Palaeomagnetic studies have definite relevance for India, which happens to be a fragment broken away from Antarctica and drifted northwards from Gondwanaland (Figs 2.46 and 2.48). These studies yield evidence for or against this hypothesis and these constitute one of the geological investigations taken up by the Indian expeditions to Antarctica. On a much smaller time-scale (a few ka), there is a steady drift of the magnetic north pole. The direction of the magnetic field is frozen in pieces of pottery made at those times. That knowledge is used to 'date' the pottery in archaeological studies; this aspect is called archaeomagnetism, namely the study of the magnetic field in historic times (Fig. 7.2).

AMS technique: The anisotropy of magnetic susceptibility (AMS) is a valuable tool to decipher changing environmental conditions because it reflects various accumulation regimes, e.g. variations of pathways and/or source regions (Fig. 7.15). The AMS allows to discern reworked material from a suite of material whose magnetic mineral content grew in situ. This new technique along with observations of satellite imagery and structural geology is successfully applied on the small Lonar crater (~1.8 km diameter) to evaluate the projectile path of its impactor. The AMS data suggest that the target basalt ~2 km west of the crater is highly shocked due to oblique impact from the east compared to the unshocked target basalt from an equal distance in the east (Fig. 9.2).

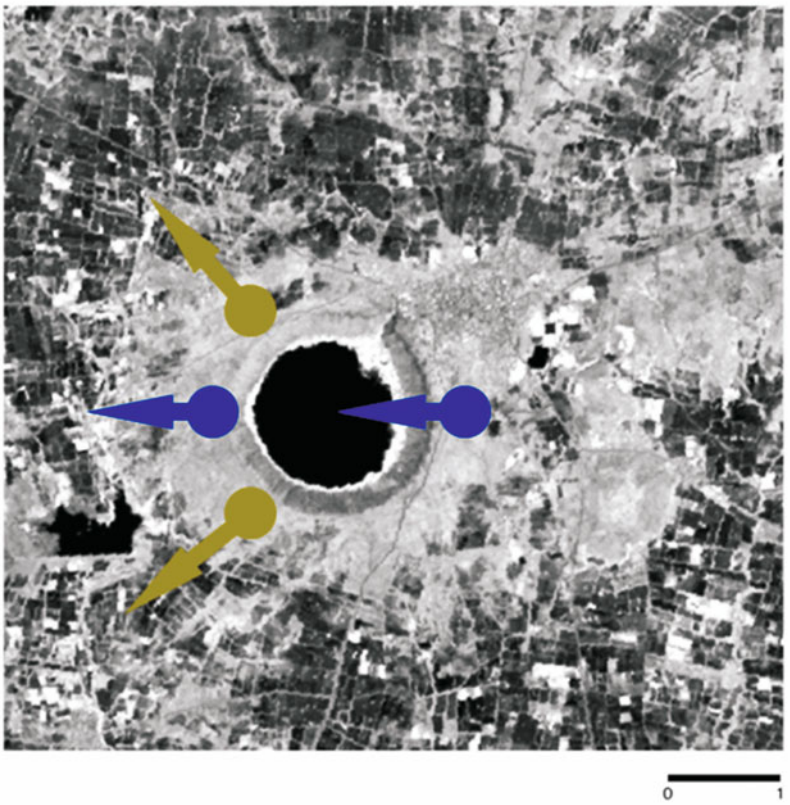

Figure 9.2. Satellite map of Lonar crater showing distribution of impact stress. The result is obtained by AMS study showing impactor direction from east and it had trifurcated into southwest, west and northwest directions after the impact (Saumitra et al., 2009).

VII. Geomagnetic Environmental Change

In recent years, laboratory-based environmental geomagnetism is fast catching up with other established geophysical streams. This uses hysteresis cycle (Chapters 2 and 7) of lumps of sediment, to obtain the parameters of coercivity (remanence), and saturation (isothermal) remanence magnetization of the ferri(o)magnetic component of the sediment. These parameters yield information on the 'domain' structure, and hence are able to determine the level of natural processes and human activity, which occurred over the years at the site of the sediment.

Extreme cases of environmental disturbances such as floods in Mumbai, hurricanes off the coast of America, heavy rains in south India and other similar cases are all a manifestation of increased precipitation due to warm atmosphere. Short-term climatological factors like the El Nino effect (periodic warming of the Pacific waters) could influence seasonal climate even in regions far away

from the Pacific waters. The question whether global warming is to be blamed for the vagaries of nature is debated. However, CO_2 levels are substantially higher now than at any time in the last ~800 ka, according to the latest study of ice drilled out of Antarctica. As fears grow over global warming, modelling and predicting climate change has become more important than ever. Such issues of climate change and environmental processes (environmental change and pollution) can be studied using environmental geomagnetism techniques. The approach essentially links the magnetic properties of rock and soil with changes in climate and the environment of natural and anthropogenic type.

In environmental geomagnetism, samples from lakes (wet and dry; spanning ages from ~50 ka to present), sea, land and atmosphere are used, where rock magnetic properties are tested with respect to their palaeoclimatic (temperature and humidity) implications. India has diverse climatic and environmental zones; the samples from which have improved understanding of how the subcontinent's complex climate (monsoon) system works and deciphered the elements sensitive to change. The research has also played a key role in predicting future climatic trends.

Rock magnetic properties can evaluate the remanence acquisition processes, since magnetic minerals are both stable and unstable, though not at the same time. Under a given set of physicochemical environment, magnetic mineral remains stable and unchanged. However, exposure to the atmospheric realm brings about transformations in them which enable palaeoenvironmental/palaeoclimatic reconstruction (Figs 7.36–7.41; 7.43, 7.44 and 7.48–7.55). Magnetic investigations also provide lithostratigraphy in addition to chronostratigraphy, besides offering considerable potential for studying correlation between marine and terrestrial sequences.

In some environmental contexts, there are strong links between the magnetic properties of a sediment and pollution levels. It helps in finding out the provenance of sediments (Figs 7.36–7.41) and performs studies on historical and contemporary particulate pollution in storm water sewers, estuaries and other coastal contexts. It is also a valid tool that brings out differentiation of atmospheric dusts to aerosols and the historical records of their deposition into lakes and mangrove sediments. By detecting magnetic materials within mudflat/peat sediments, it has been possible to obtain detailed records of industrial pollution over the last 200 years in a rapid and economical way.

9.3 UPPER ATMOSPHERIC STUDIES

With advancements in science and technology, the visit to Mars and other planets is increasingly possible. But, there is a need to understand the Earth-Sun connections to safely move out into space and inhabit other planets. Hence, different experiments are designed to explore the fundamental physical processes involved with the Sun, Earth, and other planets by collecting

information about the flow of energy within the solar system (Figs 8.1 and 9.3). The research will thus allow to prepare for the harsh effects the solar environment can have on life and technology. Advances in technology help to look deep into the internal workings of the Sun and understand how magnetosphere and EMF work and respond to solar activity (Chapters 3 and 8).

Magnetograms recorded at MOs provide information on how solar plasma interacts with the Earth's upper atmosphere above 100 km, which is also a plasma. The effects of this interaction appear as fluctuations in the magnetic records (Chapters 1, 3, 5 and 8). Data from instrumented satellites together with physical insight indicate the relationship between the solar-terrestrial interaction and the geomagnetic fluctuations. Thereafter, the magnetic records are used to monitor radio communication and even forecast space-weather, i.e. the interactions of the solar and terrestrial plasmas in space (Figs 3.7, 3.13–3.15, 5.5–5.22, 8.6–8.23). Forecast of such interaction, notably during periods of storms in space is likely to assume great importance in coming years. Evidence is gradually mounting that not only radio communication, which is affected during such space-storms, but the pervading energetic wave and charged particle radiations are also capable of causing total power breakdown in auroral regions (Figs 9.4 and 9.5) and of causing corrosion in long pipelines through their ability to induce electrical currents in long conductors on the Earth. These radiations also present health hazards to astronauts and equipment aboard satellites in geospace and in the interplanetary environment (Figs 9.6 and 9.7).

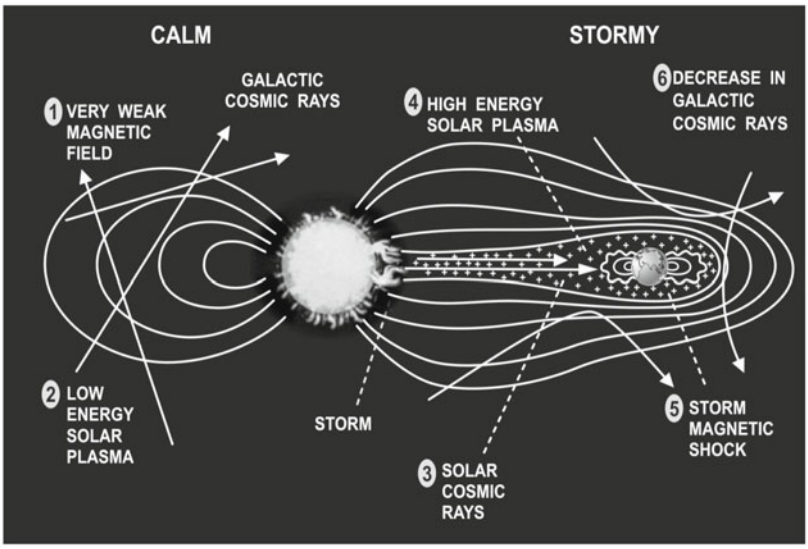

Figure 9.3. Early NASA photo showing just some of the elements in the EM spectrum. The atmosphere blocks harmful waves.

I. Sunspots and Terrestrial Phenomena

The importance of research dealing with solar-terrestrial physics is immense. Monitoring and prediction of the sunspot activity is being carried out for radio communications. Sunspots and solar activity are studied to understand the transfer of energy from the Sun to the Earth's atmosphere (Chapters 3 and 8).

The number of sunspots is strongly related to the occurrence of number of auroras (and violent magnetic storms in EMF) and variations in ozone concentration. An inverse correlation is established between air-Earth conduction current density and the sunspot cycle. The state of the ionized layer in the upper atmosphere is affected very critically by solar activity (sunspot number). The Sun's role in altering the Earth's weather and climate is a subject of popular and practical interest. From historical records, the Maunder minimum from 1645 to 1715 coincides approximately with the 'Little ice age'. This high latitude climatic event is also found in magnetic proxy records (Fig. 7.55) of the mudflat sediment cores. Furthermore, a recurrent period of ~22 years is identified in the pattern of droughts in the western US coinciding with the 22 year magnetic cycle (i.e. two 11 year sunspot cycles) of the Sun. These correlations suggest that the sunspot activity can be used to predict changes in electrical, magnetic and meteorological environment of Earth. Even the satisfactory working of the communication satellite depends critically on the solar activity.

II. Magnetic Storms and Society

The modern society is relying more and more on technology that is affected in some way by conditions in the space environment. Magnetic storms form a major component of space weather. The most dramatic events on the Sun are solar flares and coronal mass ejections during solar maximum (Figs 8.9–8.11). Intense and super-intense geomagnetic storms create hostile space weather conditions that can generate many hazards to the spacecraft as well as technological systems at ground (Figs 8.11–8.12). Several NASA missions reported loss of instrument data and damage of two spacecraft instruments during 30–31 Oct 2003 storms. The Swedish power grid reported failure of transformer at some stations for several hours. Adverse space weather conditions during intense magnetic storm can pose threat to astronauts and jetliner passenger due to both high radiation dosage and loss of contact with the ground station. Several trans-polar flights were cancelled during Oct–Nov 2003 intense magnetic storms. There can be malfunctioning or even permanent damage to spacecraft, e.g. one Japanese spacecraft was probably damaged beyond salvage during Oct–Nov 2003 magnetic storms. The geomagnetically induced currents (GICs) during intense magnetic storms can damage power transmission lines and corrode the long pipelines and cables.

How GIC affect power systems: Geomagnetically induced currents are driven by electric fields produced by magnetic field variations that occur during a

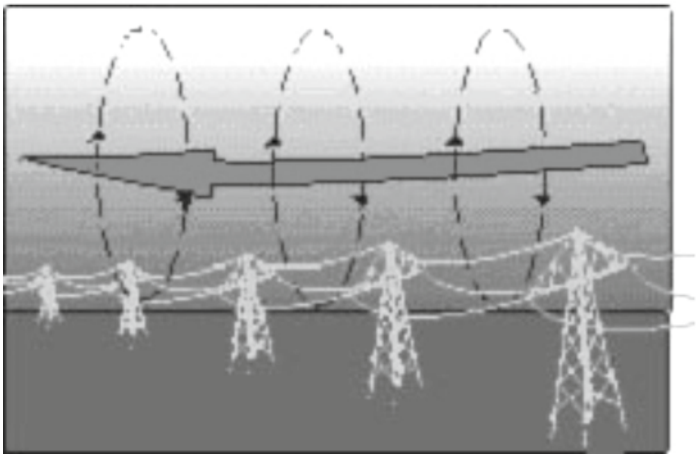

Figure 9.4. GIC flowing through the transformer winding (http:/ www.spaceweather.gc.ca/effects_e.php).

geomagnetic disturbance. Because of their low frequency compared to the AC frequency, the GIC is reckoned by a transformer as a slowly varying DC current. GIC flowing through the transformer winding produces extra magnetization during the half-cycles and can saturate the core of the transformer (Fig. 9.4). This results in a very spiky AC waveform with increased harmonic levels that can cause misoperation of relays and other equipment on the system and lead to problems ranging from trip-outs of individual lines to a total collapse of the whole system.

Continental cable systems: On 4 Aug 1972, an outage of the L4 coaxial cable system in the mid-western US occurred during a major geomagnetic disturbance. An examination of this disturbance showed that at the time of the outage, the EMF was severely compressed by the impact of high speed particles from the Sun. The resulting magnetic disturbance had a peak rate of change of 2200 nT/min and a rate of change of the magnetic field at the cable location estimated at 700 nT/min. The induced electric field at the cable was calculated to have been 7.5 V/km, exceeding the 7.4 V/km thresholds at which the line would experience a high current shutdown.

Transformer heating in power systems: Saturation of the transformer core produces extra eddy currents in the transformer core and structural supports which heat the transformer. The large thermal mass of a high voltage power transformer means that this heating produces only a negligible change in the overall transformer temperature. However, localised hot spots can occur and cause damage to the transformer windings (Fig. 9.5). Also, extra harmonics generated in the transformer produce unwanted relay operations, suddenly tripping out power lines. The stability of the whole system can also be affected as compensators switch out of service. Such a sequence of events led to the

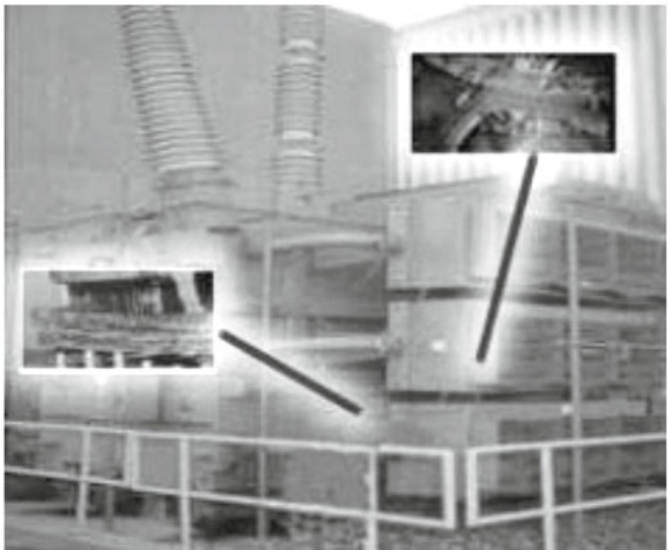

Figure 9.5. Damaged transformer (http://www.spaceweather.gc.ca/effects_e.php).

Quebec blackout of 13 March 1989, which left the whole province without power for over nine hours.

III. Geomagnetic Hazards

The geomagnetic hazard to technology results from the strengthening of magnetospheric and ionospheric current systems by the solar wind and by CMEs. A common theme that emerges from a study of geomagnetic hazards is a need for accurate geomagnetic storm forecasting in terms of onset time and duration, maximum amplitude, and variation period (Chapter 5). The close connection of geomagnetic hazard with solar activity is also clear. Some practical applications of geomagnetic variations will clearly benefit from a thorough physical understanding of the Sun-Earth magnetic interaction and in particular accurate prediction of geomagnetic variations. For instance, the response of the EMF to solar conditions is useful in investigating Earth structure using MT (see magnetotellurics in Chapter 6), but it also creates a hazard. This geomagnetic hazard is a risk to technology, rather than to health (Chapters 3 and 8).

Space weather effects on technology are far reaching and diverse as also expensive. Astronauts are definitely at risk from bursts of ionizing solar energetic particle radiation. Astronaut protection involves appropriate spacecraft shielding relative to Sun. Modelling and predicting the changing morphology of the geomagnetic field is important in determining, where charged particles may enter into the lower atmosphere (Chapters 3 and 8). The overall space weather effects can be summarized through Fig. 8.12.

IV. Satellite Operation, Navigation and Radio Communication

The ionosphere plays a significant role in VLF through to HF radio communication and in navigation systems. Ionospheric conductivity is partly affected by geomagnetic storms but more significantly by solar UV and X-ray control of the ionospheric D, E and F layers (see Chapters 3 and 8). Solar flares cause signal-phase anomalies and amplitude variations to occur (fades and enhancements) and conditions can persist for minutes to hours. Solar flares and CMEs are also important as sources of solar energetic particles, affecting radio communications at high latitudes. Ultrahigh-frequency (UHF) radio signals are central to the GPS that utilizes satellites in Earth orbit for precise ground position determination.

Space weather effects on GPS: UHF waves pass largely unattenuated through the ionosphere but the system accuracy is sensitive to variations in the TEC in the path between ground and satellite. The TEC determines the signal propagation delay. Varying propagation delays cause errors in the determination of the range (or distance), or 'range errors' (Fig. 9.6). TEC variation occurs during geomagnetic storms and these particularly degrade the accuracy of GPS equipment. Geomagnetic storms also produce ionospheric irregularities and scintillations. Ionospheric scintillation may cause problems such as signal power fading, phase cycle slips, receiver loss of lock and degraded quality of satellite navigation systems (Chapter 8).

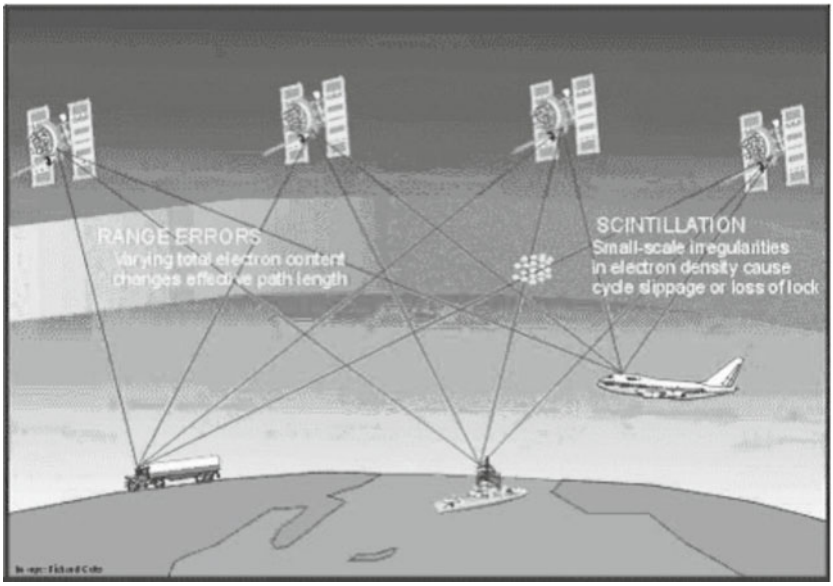

Figure 9.6. Space weather effects on GPS (http://www.spaceweather.gc.ca/effectsgps_e.php).

Another GPS technique uses carrier phase tracking. In this technique, the phases of individual cycles of the carrier waves are compared. However, if the TEC along a signal path from a satellite to a receiver changes very rapidly as a result of space weather disturbances, the resulting rapid change in the phase of the radio wave causes difficulties for the GPS receiver in the form of 'loss of lock'. Temporary loss of lock results in 'cycle slip', a discontinuity in the phase of the signal. Scintillations (<15 sec) are particularly troublesome for receivers that are making carrier-phase measurements, resulting in inaccurate or no position information. Code-only receivers are less susceptible to these effects.

From another viewpoint, the GPS system provides continuous routine measurements of the TEC along the multitude of varying signal paths to each receiving station in a regional or global network. These measurements permit the mapping of variations in the ionospheric TEC over a region. Such information can be useful for studying space weather phenomena.

Effects on satellites: Low Earth orbit satellites and space stations (up to ~1000 km altitude) experience increased air drag during geomagnetic storms. Satellites operate in an environment filled with charged particles (Fig. 9.7). These particles can affect satellites in a variety of ways, either directly by penetrating into the satellite electronics, or indirectly through spacecraft charging with the resulting discharge causing problems. For example, these processes can result in dummy commands, damage to electronic devices, loss of control, and even satellite failure.

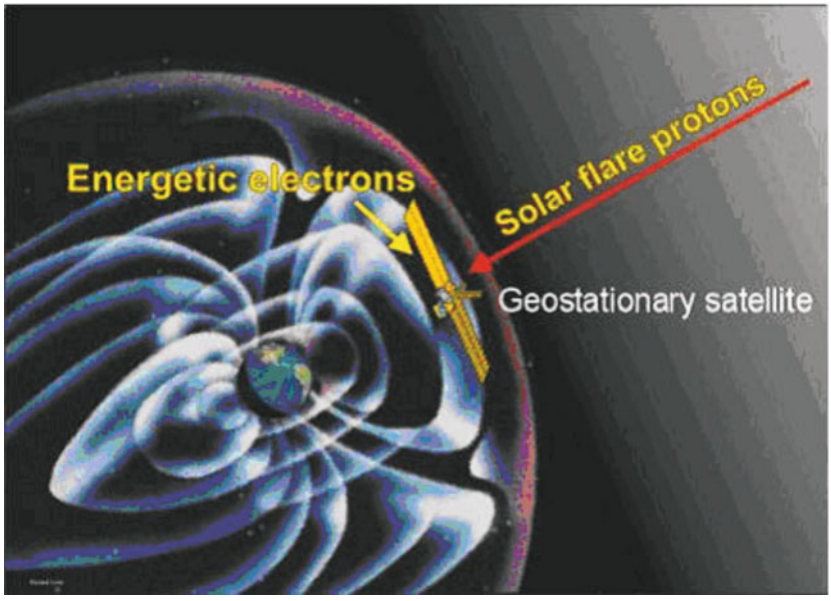

Figure 9.7. Geostationary satellite swamped by charged particles.

Several satellites are disrupted since high energy particles (solar wind) flow through sections of the satellites and damage their sensitive electronic devices. For instance, in 1979, the Skylab space station prematurely re-entered Earth's atmosphere due to a malfunction caused by increased solar activity, and consequently rained debris over the Indian ocean and parts of western Australia.

Solar proton effects: When high velocity ions (Fig. 9.8) plough through semiconductor devices of the satellites, they produce a large number of electrons and holes that carry currents within these devices. Large numbers of electron-hole pairs introduced into sensitive regions like memory cells can alter information and result in phantom commands. Effects can be devastating if ion impacts occur in control systems or decision-making circuits. In addition, these impacts degrade semiconductor lifetimes.

Surface charging: Surface charging of spacecraft in a synchronous orbit can occur due to incidence of a large incoming flux of electrons in the absence of sufficient charge drainage by mechanisms such as photoemission. 'Hot' electrons with energies in the range of several keV are mainly responsible for surface charging. Intense fluxes of these electrons are closely related to substorm activities. Hence, surface charging occurs more often in the midnight to dawn period. The differential charging of spacecraft surfaces can give rise to destructive arc discharges, causing satellite operational anomalies.

Internal charging: The occurrence of highly energetic electrons with energies >2 MeV represents adverse space weather conditions hazardous for geosynchronous satellites. When this happens, there is an internal charging of satellite components by energetic electrons with possible electric discharges, resulting in malfunction of the satellite. Such an event was the likely cause of a number of satellite operational anomalies in January 1994.

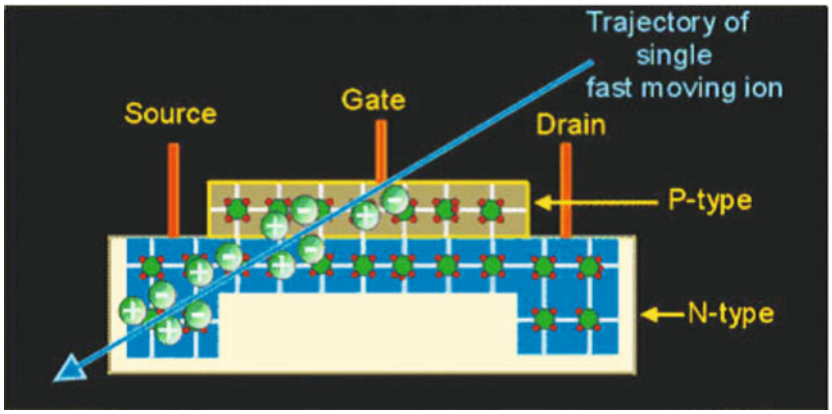

Figure 9.8. Solar proton effects on satellite devices (http://www.spaceweather.gc.ca/satellites_e.php).

V. Magnetism in Power Generation

The use of magnetic and electric fields for power generation is likely to become widespread in coming years. Such power generators are called magnetohydrodynamic (MHD) devices. In these devices, energy of thermal or kinetic nature is directly transformed into electricity. Magnetohydrodynamics is the behaviour of electrically conducting fluids in electric and magnetic fields at high temperature. Most of the MHD devices are still under research and at present are used for small power requirements, but applications have already commenced. There was recently a report of a ship having been developed in Japan to operate on MHD power.

It was mentioned in Chapters 3 and 8 that the Earth's magnetospheric tail is a site, where energetic solar wind particles rush at very high speeds (few hundred km/sec) through time-varying electric and magnetic fields. A NASA satellite made several attempts to tap this power, which is dormant in distant space. The idea is as follows. A space shuttle was to drag along with it a satellite tethered to it by a 20 km long electrically conducting cable. As the cable traversed the Earth's magnetic field lines, an electric potential of ~5,000 V will setup between shuttle and satellite—this attracts free electrons from the ionosphere to the satellite. In order to close the circuit, astronauts were to fire an electron gun from the shuttle to the ionosphere and an electric current flow through the circuit. This is schematically illustrated in Fig. 9.9. Unfortunately, the tether got stuck at a distance of 260 m from the shuttle and for fear of losing the satellite, the astronauts reeled it back. As the whole setup is intact, it is fairly certain that after a check-up, this experiment for generating power

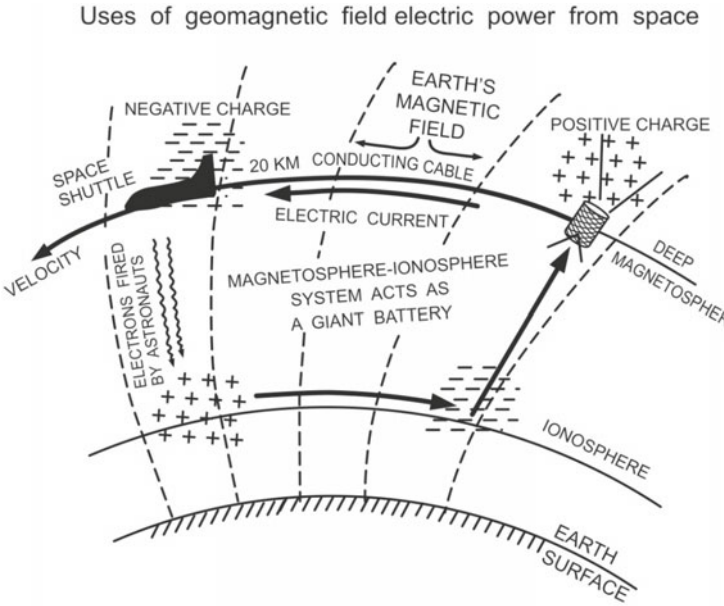

Figure 9.9. Tapping power which lies dormant in distance space is likely to become reality in the near future (Rajaram and Pisharoty, 1998).

from geospace will be flown again in the near future. If the idea should indeed work, the possibilities for power on Earth are limitless.

VI. Conclusions

The household applications of magnetism are too numerous to be pointed out here: the door-bell, the telephone, the television set, audio tapes, video cassettes. The list is endless. Indeed much of today's world just would not work if it were not for magnets and magnetism. Our emphasis in this chapter has been mainly on the applications of geomagnetism.

To conclude, it can be emphatically stated that geomagnetic studies are not at all 'ivory tower studies'. As shown in the foregoing sections, they have very wide and useful applications. What a society can derive from such studies, for economic and societal welfare, partly depends upon the degree of the nation's development in science. It also depends on the ability, mutual cooperation and the attitude of the scientists and planners involved. The required attitude is a cultural one. Geomagnetism also has many applications in defense especially in missile technology. It is the intention not to elaborate on this aspect here, since science and technology should be used for the benefit of humankind, not for its destruction.

Medical applications: It is shown that many degenerative diseases are connected with the disruption of normal iron homeostasis in the brain. Nanoscale magnetic biominerals (primarily magnetite and maghemite) may be associated with senile plaques and *Tau* filaments found in brain tissue affected by these diseases. These findings have important implications for our understanding of the role of iron in neurodegenerative diseases as well as profound implications for their causes. In addition, the presence of biogenic magnetite in affected tissue should also provide improved mechanisms for early detection through modification of magnetic resonance imaging (MRI) pulse sequences.

Recent evidence points to magnetic technique being more sensitive in assessing lung contamination than the traditional methods like radiography. Magneto-pneumography has been successfully applied to meet the needs of many workers employed in places like shipyard and foundry, where metal work is done. Nowadays, the magnetocardiogram is used as a supplement to electrocardiogram. MRI has become a preferred tool over other traditional methods like X-rays. MRI or NMR, nuclear magnetic resonance, is a technique that involves subjecting certain atomic nuclei to very strong stationary magnetic fields and then observing how they selectively absorb VHF radio waves. MRI is a relatively hazard-free, non-invasive way to generate visual images of thin slices of the body by measuring the characteristic magnetic behaviour of specific nuclei in the water and fats of the body. MRI images show great sensitivity in differentiating between normal, diseased and damaged tissues. This technique works better in imaging brain, heart, liver, kidneys, spleen, pancreas, breast and other organs. Thus, the applications and utilities of geomagnetism are many (Appendix 9.2).

APPENDIX 9.1

Locations of the North and South Dip Poles and Geomagnetic Poles

	North dip pole		*South dip pole*		*North geomagnetic pole*		*South geomagnetic pole*	
Epoch	*Latitude*	*Longitude*	*Latitude*	*Longitude*	*Latitude*	*Longitude*	*Latitude*	*Longitude*
1900	70.46	-96.19	-71.72	148.32	78.68	-68.79	-78.68	111.21
1905	70.66	-96.48	-71.46	148.55	78.68	-68.75	-78.68	111.25
1910	70.79	-96.72	-71.15	148.64	78.66	-68.72	-78.66	111.28
1915	71.03	-97.03	-70.80	148.54	78.64	-68.57	-78.64	111.43
1920	71.34	-97.39	-70.41	148.20	78.63	-68.38	-78.63	111.62
1925	71.79	-98.00	-69.99	147.63	78.62	-68.27	-78.62	111.73
1930	72.27	-98.69	-69.52	146.79	78.60	-68.26	-78.60	111.74
1935	72.80	-99.34	-69.06	145.77	78.57	-68.36	-78.57	111.64
1940	73.30	-99.87	-68.57	144.60	78.55	-68.51	-78.55	111.49
1945	73.93	-100.24	-68.15	144.44	78.55	-68.53	-78.55	111.47
1950	74.64	-100.86	-67.89	143.55	78.55	-68.85	-78.55	111.15
1955	75.18	-101.41	-67.19	141.50	78.54	-69.16	-78.54	110.84
1960	75.30	-101.03	-66.70	140.23	78.58	-69.47	-78.58	110.53
1965	75.63	-101.34	-66.33	139.53	78.60	-69.85	-78.60	110.15
1970	75.88	-100.98	-66.02	139.40	78.66	-70.18	-78.66	109.82
1975	76.15	-100.64	-65.74	139.52	78.76	-70.47	-78.76	109.53
1980	76.91	-101.68	-65.42	139.34	78.88	-70.76	-78.88	109.24
1985	77.40	-102.61	-65.13	139.18	79.04	-70.90	-79.04	109.10
1990	78.09	-103.68	-64.91	138.90	79.21	-71.13	-79.21	108.87
1995	79.09	-105.42	-64.79	138.76	79.39	-71.42	-79.39	108.58
2000	80.97	-109.64	-64.66	138.30	79.61	-71.57	-79.61	108.43
2005	83.19	-118.24	-64.55	137.85	79.82	-71.81	-79.82	108.19
2010	85.01	-132.66	-64.43	137.32	80.08	-72.22	-80.08	107.78
2015	86.07	-153.27	-64.30	136.74	80.36	-72.62	-80.36	107.38

Locations are computed from the 11th generation IGRF. (http://www.geomag.bgs.ac.uk/poles.html)

APPENDIX 9.2A

Day-to-day Applications of Magnetic Force

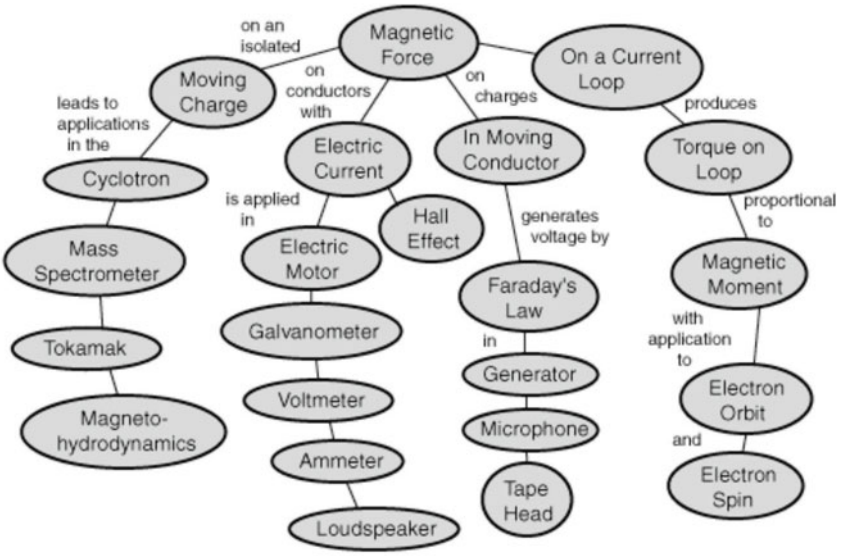

(http://hyperphysics.phy-astr.gsu.edu/hbase/magnetic/magforcon.html#c1)

APPENDIX 9.2B

Day-to-day Applications of Magnetism and Electricity

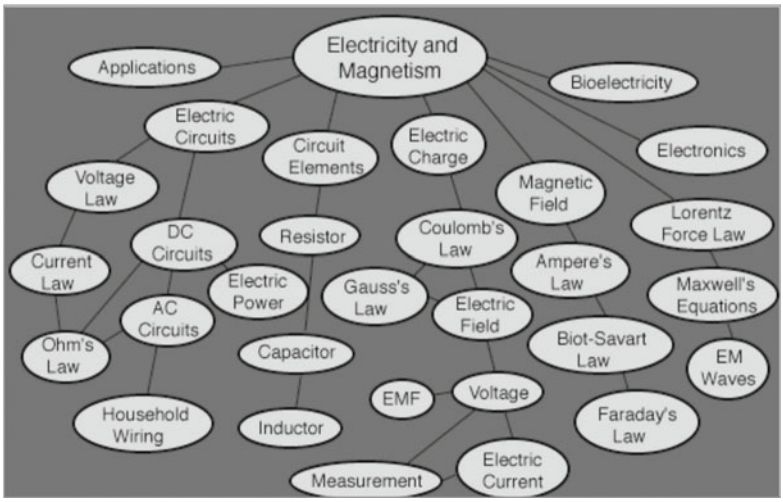

(http://hyperphysics.phy-astr.gsu.edu/hbase/emcon.html#emco)

10

PERSPECTIVE

The genius of people like Norman, Gilbert, Faraday, Oersted, Ampere and Maxwell gave geomagnetism a strong footing to tackle fundamental problems related to Earth and interplanetary space. These discoveries whetted the curiosity of the inquisitive mind to unravel the causative agents and look for inter-relationships between the Earth, the Sun and other planets or satellites and use this knowledge to predictive purposes. Intricacies of changes in the geomagnetic field are studied because they change over several timescales from few million years to fraction of a second in several spectral bands. Each band of frequencies is a goldmine of information indicative of various causative mechanisms with sources in the Earth's interior, near space or far space environment as outlined in Chapters 1 to 8. Specifically, Chapters 5 to 8 list out applications of geomagnetic measurements to understand the chemical, physical and dynamical characteristics of the atmosphere and the interior of the planet Earth. In virtually every case presented in this book, there is considerable scope for further development in exploratory techniques, analysis, interpretation and application. Prospects for the future, lie in further extension and refinement of established approaches used in magnetic observatory, upper atmospheric and solid Earth studies.

I. The Observatory

Most of the Indian MOs are equipped with digital magnetometers from where the data are transported in real time to the central node and to the GINs. It is expected to increase density of MOs to cover more latitudes and longitudes of globe/India. Density of MO is to be particularly increased in the southern region for Sq, EEJ and CEJ studies and in the north for Sq focus and seismotectonics. The Shillong MO data are found sensitive to local earthquakes. This has offered clues to undertake the installation of seismometers at all other planned and existing MOs. This colocation of magnetic and seismic instruments will

gainfully allow execution of timely response needed in earthquake monitoring studies. This would mandate inclusion of geomagnetism as a national programme. Ground-based data acquired at MOs together with data from magnetic survey satellites will provide ample opportunities for undertaking the investigations related to: (1) regional magnetic anomaly and reference field maps, (2) 'secondary effects' on Sq field, (3) induced currents associated with EEJ, (4) transient variations and (5) low-latitude 'bay' structure.

II. Antarctic Magnetic Data

After analysing the experiments carried out at Antarctica, the book can recommend widening of the scope of experiments to study: (1) magnetospheric influences on terrestrial magnetic field on a long-term basis and to record systematic magnetic field variation, (2) establish link between the magnetic field variation in the polar and equatorial regions, and (3) subsequently examine subsurface structures of the continent using magnetic field variations. Magnetic measurements at Maitri confirmed a decreasing trend in geomagnetic field, which needs to be incorporated in models depicting magnetic reversals. This will also have a bearing on the role octupoles and quadrupoles play during a reversal, since they are conjectured to maintain a semblance of geomagnetic field, when the dipole field is vanishing. The high latitude continent is an ideal place to study air-Earth Maxwell currents to extend understanding of the magnetosphere-ionosphere electrical coupling. Permanent GPS stations are setup for geodynamic meteorological and ionospheric studies. They also monitor glacier and iceberg migration. Study on Antarctic climate and environmental variability is initiated by conducting mineral magnetic studies on core samples collected from the basinal features of Antarctica and its adjoining regions. These can be correlated with subcontinental monsoon features for establishing teleconnections in weather patterns of these far off continents.

III. Space Environment

The entire range of phenomena in the field of equatorial aeronomy and its global connections between troposphere, stratosphere, magnetosphere and interplanetary space form a part of space environment research. Beginning with ground-based radio and optical probing of the upper atmosphere, the research has developed into an integrated programme that combines ground-based data with those obtained from balloons, rockets and satellites using a variety of payloads. Satellites carry onboard radio beacons to monitor and study ionospheric irregularities. Airglow measurements for wind and temperature parameters need to be continued. Recommended programmes include: the study of solar-terrestrial coupling, spread-F phenomena, EEJ/CEJ current systems, trace gases/minor constituents of the middle atmosphere, role of plasma in different interplanetary zones and space weather conditions. To learn about the mechanism/origin and development/decay of spread-F,

ground-based magnetometers, ionosondes, Fabry-Perot interferometers (for 6300 Å airglow radiation) and beacon satellite scintillation studies, are recommended. The measurement of atmospheric electric fields/conductivities needs to be carried out using balloon and satellite-borne equipment to study stratospheric electrodynamics and global electric circuit.

Magnetosphere: Considerable work has been done on the exchange of energy between solar wind, magnetosphere and its subsequent transport to various parts of the magnetosphere-ionosphere system. The physical mechanism of many of these phenomena, however, remains elusive. The coupled magnetosphere-ionosphere system is highly complex/nonlinear and it is impossible to construct realistic analytical models for the various properties exhibited by this system. The advent of new generation fast computers and subsequent progress in numerical analysis methods has offered a powerful tool of computer simulation technique. Computer simulation techniques are now an integral part of space plasma research. It is recommended to do computer simulations to understand the: (1) role of ionosphere in substorm dynamics, (2) energy transfer, (3) substorm dynamics, (4) effect of energetic particles on spacecrafts, (5) auroral acceleration processes, (6) ionosphere, (7) ionospheric irregularities, (8) ionosphere-neutral atmosphere interaction and (9) simulation of geodynamo.

Sun, magnetic storms: The intricate picture of the connection between the Sun and the Earth's space environment has been uncovered in the last few decades. However, understanding of the physical processes, which drive and couple this complex plasma system, is still far from complete. Magnetospheric substorms and major geomagnetic storms produce intense surges in energetic particle populations that can adversely affect the functioning of modern satellites, GPS and power grids on the ground. An outstanding problem in solar-terrestrial physics pertains to predicting the evolution of physical processes within the magnetosphere and Earth's space environment. The space environment is a natural plasma centre, where accurate in situ measurements can be carried out. The validity of theoretical models and assumptions regarding plasma dynamics can be tested on time and spatial scales far greater than available in the laboratory. In fact, this knowledge can be applied to the study of magnetospheres of other celestial bodies like planets, comets, pulsars and the like.

Sun, interplanetary medium: Although it has long been suspected that sporadic geomagnetic disturbances are due to eruptive events on the Sun, it is only recently that research on the solar corona and interplanetary medium has indicated the mechanism by which it occurs. This knowledge poses a further challenge to understand the timing and location of solar eruptions and establish whether individual solar events are likely to cause geomagnetic storms. Success in forecasting a storm a day or more in advance will also depend on improved knowledge and better monitoring of the Sun and the interplanetary medium. A

research project is proposed to study solar-terrestrial relationship as a comprehensively coupled system that starts from the Sun, goes through the interplanetary medium, magnetosphere, high/low latitude ionosphere, mesosphere, stratosphere, troposphere down to the boundary layer and the surface. This system also continues down into the shallow interior of the Earth, where induced currents are produced by electric currents, which come in handy for probes launched through electromagnetic induction studies.

10.1 SOLID EARTH GEOMAGNETISM

Improvements in instrumentation accelerated magnetic surveys: EM surveys became routine affair, proton magnetometers are towed behind ships (air/water) and satellites go to phenomenal heights with magnetometers. The sensitivity and accuracy of instruments needed to monitor and record magnetic field in the material domains of solid, liquid and gas (plasma) are getting better by the day. These days, geomagnetists have automated laboratory equipments at their disposal by virtue of which in a single day they can make more measurements of the absolute palaeointensity of magnetic materials such as ceramics and basaltic rocks than pioneer Thellier could do in a life time. Considerable emphasis needs to be put on developments of inversion techniques and models from the data gathered from MT, OBM, MOs, satellite data on plasma and EM field, etc. Joint inversion of gravity and magnetic satellite/ground anomaly data, incorporating constrains from laboratory density/susceptibility measurements should be undertaken to estimate depth of the source field. The satellite data will have to be inverted to better understand the lithospheric dynamics.

The recommended thrust areas are: (1) probing the lithosphere through the features of regional scale magnetic anomalies using ground, aeromagnetic and satellite data, (2) delineating subsurface electrical conductivity features using GDS and MT methods, (3) pool in all available MT-GDS survey data and conduct additional surveys wherever necessary to prepare a 'conductance map' for the country, (4) use OBM/OBE for MT/GDS studies on the ocean floor in the adjoining seas, (5) palaeomagnetic and petrographic studies, (6) reconstruct magnetostratigraphy of the sediment/rock sequences, (7) characterize geophysically the Indian terrain to model folds, faults, lineaments and suture zones, (8) develop methodology for identification of geomagnetic and geoelectric precursors associated with earthquakes, (9) use of GPS for precise baseline measurements in selected areas for monitoring crustal deformation, (10) take up challenging topics in emerging areas like environmental geomagnetism, archaeomagnetism, biomagnetism, and (11) take up EM (conductivity) study through laboratory scale experiments.

I. Lithosphere Study through Magnetic Anomalies

Potentiality of remote sensing through satellite in determining structure of geological significance and in identifying inhomogeneities in the lithosphere

has been proved beyond doubt. Identification of seismically active zones, hotspots, rifts, tectonically active belts due to mantle convection and resultant stress changes that followed the collision of the Indian plate with the Eurasian plate from Magsat magnetization map is an excellent example of the importance of satellite magnetic data. Low magnetization is encountered under Indo-Gangetic plains and positive on either side of it. Inverse correspondence between high gravity and low magnetization over petroliferous basins like the Assam oil field, Bombay High and Cauvery basin, is also identified. Joint inversion of gravity and satellite/ground magnetic anomalies incorporating constrains from density/susceptibility laboratory measurements should be undertaken to estimate depth of the source field. The satellite data need to be inverted at both the global and regional (Indian subcontinent) level to be able to better understand the lithospheric dynamics. This will entail massive data matrix inversion requiring sophisticated computing facilities.

Recommendations to enhance the geologic utility of satellite geopotential anomalies include: (1) Magsat data with <2°> anomalies had limited resolution. Use of improved magnetic anomaly data may provide better anomaly maps for crustal analysis, (2) obtain additional geophysical data to establish better constraints on tectonic interpretations. This may include seismic or geothermal data or gravity data that reflects improved areal coverage, (3) correlation analysis conducted is qualitative. Quantitative correlations could be used to further constrain tectonics analysis and modelling. This could involve separating continental data from oceanic to compare the magnetization characteristics of both the crusts, (4) the effect of lithospheric cooling on oceanic magnetic anomalies, and (5) it is shown that the geopotential field anomalies are useful for tectonic analysis. Improved data coverage, especially for gravity and lower elevation magnetics, promises to provide more information for tectonic analysis, particularly for the tectonically rich, relatively little known regions of Antarctica. Combined gravity and magnetic data collected by NASA's proposed GRM satellite can provide such a data set. The Oersted and other satellite mission data can also be used for lithospheric and electrojet variations.

To resolve structural complexities of the Indian plate and to be able to map the source fields at different depths, magnetic anomalies at different levels need to be looked at. Thus as an extension of the ground magnetic surveys, the outings will be formulated to survey different tectonic blocks. This ground data can be coupled with available aeromagnetic and satellite data. The susceptibility of different rock types will provide the necessary constraints for modelling. The aeromagnetic method has given a coherent view by integrating surface and sub-surface features/tectonics of the major portions of the country. Aeromagnetic data have established that Chitradurga divides the eastern and western Dharwar, which has a bearing on prospecting ore and mineral deposits. Thus a plan needs to be formulated for covering the shield areas by systematic aerial surveys. This coverage can be complemented by ground magnetic data over different metamorphosed zones and regions rich in iron deposits, viz. Singbhum-Bastar area, Bababudan in Karnataka and Ratnagiri in Maharashtra.

II. Geoelectromagnetic Studies, MT/GDS/OBM

MT techniques are accepted as a useful tool in exploration studies, especially in the Deccan trap as well as the low velocity sediment covered regions. Further, they are inexpensive compared to their seismic counterparts. The efficacy of these techniques in the area of oil exploration should be consolidated by undertaking surveys in various unexplored sedimentary sequences of the Godavari and Assam region. The ability of MT techniques in identifying repository sites for nuclear waste can be used to demarcate places, where no active faults are connected to the water table.

Earthquake monitoring activity is still in its infancy. MT studies can identify active faults, which should be monitored for possible changes in seismotectonic activity using MT or other similar EM methods. Efforts will be made to develop inexpensive indigenous instrumentation for electrical tomography, which could be of importance in continuous monitoring of electrical resistivity and ground electric current and voltages, which are known to be useful earthquake precursors. MT studies undertaken in geothermal regions to estimate the possible extent of these resources, could be of importance in the future renewable energy resource programmes. Groundwater location could also be detected by suitable magnetic/electrical methods.

A model of the subcontinental conductosphere is planned to undertake with magnetic array and MT measurements, which can be combined with heat flow data and potential field measurements to target natural resources. MT studies in geothermal regions can supplement the conventional energy resources. They can also identify active faults that can be monitored for predictive changes in EM signatures. Extending the EM work to marine environment will throw light on the global dynamics of the lithosphere. In this light, OBM and OBE studies will be very useful. The subduction tectonics at the Andaman arc region have led to seismic and tsunamic activities in the past affecting the coastal areas in many ways. The monitoring and recording of magnetic field changes can forewarn the events. These studies can also map out hydrocarbon deposits. The theoretical and software development for inverting and interpreting 2D/3D EM structure, need augmenting, which would be suitably done in future. Efficient robust algorithms and tensor decomposition schemes are developed to minimize distortions in the response functions.

III. Earthquakes, GPS

Inexpensive indigenous instrumentation for electrical tomography is in different stages of development to monitor electrical resistivity and ground electric currents, which are useful earthquake precursors. At the same time, these precursors should be clubbed with non-seismological deformation field measurements—progressive and continuous stress field mapping, ULF/VLF EM studies, EM response of radio wave propagation, ionospheric perturbations,

infrared emissions in upper atmosphere, geochemical signal monitoring by Rn, He, GEC/TEC measurements in ionosphere (electron contents) and others.

State-of-the-art GPS units monitor minute movement within the subcontinental intracratonic and intercratonic areas and margins. The inferred drift of different lithological units delineates earthquake prone regions. Repeat surveys keep an eye on the changes in the geomagnetic field prior to (and after) an earthquake forewarning a cataclysmic seismic event. New MOs at Kolhapur, Silchar, Andaman and Nicobar islands will monitor co-seismic signals. GPS is also used for detection of ionospheric perturbations (TEC) associated with earthquakes. Two seismological observatories are established at Rewa and Kolhapur, and multi-sensor geophysical observatories at Shillong (Assam) and Port Blair (Andaman and Nicobar islands). The data will be telemetered from these and other observatories either at a fixed timing or in continuous mode to a central location, where the complete history of local and regional changes of geomagnetic and geoelectric field will be continuously analysed and collated with other precursory data to arrive at medium and short-term forecasts of geomagnetic and earthquake activity.

Magnetic and petrological data will be collected over regions, where the GPS data depict maximum plate movements. Resistivity measurements can be taken in regions of maximum stress built up. Gravity and magnetic model will be constructed to evolve comprehensive lithospheric dynamics with ultimate objective of understanding earthquake processes. Areas thus covered will include not only the Himalayan region but also cover seismically interesting areas such as Bhadrachalam and Ongole/Bapatla regions of Andhra Pradesh, parts of Maharashtra, Gujarat, Madhya Pradesh and Karnataka.

Palaeoseismology is fast gaining importance. Continued seismic activity and loss to life and property has put strain on geoscientists and Government to garner short-term earthquake prediction. Apart from all the techniques enumerated above, prediction can be done by signatures left behind by the past earthquakes in lakes and other soft sediments. The dating of these events gives their cyclicity.

IV. Palaeomagnetism

The mechanism that causes 'polarity reversal' of the EMF needs considerable thinking. There is no *a priori* reason why the EMF should have a particular polarity and there is no fundamental reason why its polarity reversal should not change. Reversal has been explained in a number of ways, each of which lacks rigour. One amongst these suggests fluctuations in the distribution of the cyclic convection cells in the core to lead to an abrupt reversal. Such cells are randomly distributed and a reversal occurs when they attain a critical configuration. The retardation/acceleration of the convection due to the interaction at the core-mantle boundary leads to the observed secular changes in the magnetic field. Monitoring the secular change at several strategic locations

on the globe can thus provide inputs to understand the electrodynamics of the Earth's interior, which is otherwise inaccessible. It is of paramount importance to make better use of the palaeomagnetic probe to understand magnetic properties of rocks. Special emphasis is envisaged to map details of the magnetic field during polarity transition, discover more excursions (aborted reversals), mapping systematic departures from the simple dipole structure, magnetic polarity stratigraphy and the acquisition of sedimentary magnetization, secular variation, palaeointensity and short-term geomagnetic field behaviour.

The Indian plate has migrated a phenomenal distance, whose journey can be redrafted from magnetic signatures retained in the magnetizable materials in rocks. The understanding of its tectonic history has considerably increased with the palaeomagnetic studies of south and central Indian dykes, Deccan basaltic rocks, and the Himalayan syntaxial sandstones/dolomites. The studies have placed the upper and lower limits on Deccan volcanic activity and established that the episode lasted for just about half a million years or so. Earlier it was conjectured that this volcanic exhalation continued for quite a long time. Some of the controversial problems on migratory path of the Indian plate will be taken up for definitive answers. Efforts are on to draw apparent polar wander path of India for better correlation with the one available internationally. Palaeomagnetism will also be applied to learn the history of microplates and other crustal fragments caught in evolving plate margins. There is a need to start research to get seafloor information on stratigraphy and tectonics.

The geomagnetic polarity record is central to the construction of geological timescale, and provides the principal tool for calibration of marine and terrestrial biozones. The polarity record continues to evolve with the recognition of brief polarity subchrons, and the limitations to this evolution may lie with sedimentary recording processes. In the Indian context, magnetostratigraphy of important sedimetary basins, e.g. intermontane Kashmir and petroliferous basins will be worked out, and a thorough comparison of biostratigraphic sequences made. Data-base will come from deep-sea piston cores from Bay of Bengal fans and neighbouring oceans. Rock samples from Tethys Himalayas and other regions will be investigated. Their chemical and radiometric analysis will be undertaken along with the preserved records of palaeomagnetic field.

V. Environmental Geomagnetism

Subtle changes in magnetic mineralogy, grain size, oxidation degree, stoichiometry and strain state will be interpreted in terms of changing provenance areas, climatic conditions, diagenetic regimes, and anthropogenic pollution. The interpretive value can be enhanced by utilizing several magnetic proxies together with a few geochemical proxies. Increased use of magnetic proxies is foreseen as a consequence of methodological advances in unravelling mixed magnetic mineralogy and further establishment of more quantitatively based parameters.

The ubiquity and environmental sensitivity of the magnetic mineralogies provide a record of past and present environmental and climate change process. Hence, most environmental magnetic studies aptly focus on environmental interpretations. The measurements are also routinely used because of importance of environmental magnetism to the range of palaeomagnetic application including tectonic, geochronological and geomagnetic investigations. Data-base will come from sediments and sedimentary rocks.

The value of mineral magnetic parameters derives both from the close links apparent between mineral magnetic assemblages and soil forming processes and from the relative ease with which these assemblages can be characterized and distinguished even in very low concentrations well beyond the reach of other techniques. Mineral magnetic studies of particulate flux between terrestrial and fresh-water systems will offer new insights into climatic variation and its bearing on erosion and sedimentation. A pattern underlying the Indian monsoon has been deciphered, the resolution of which needs datasets of longer-term, which can be provided by mineral magnetic studies. Most of the sediment-based studies has revealed LGM, YD and brought about an awareness of the climatic conditions prevailing over the Himalayan, western, eastern and central portions of India during the last 20 ka. Magnetomineralogical S-ratio is found to reflect monsoon quite well. Monsoonal changes can be predicted and planned for future. A new study is planned to know how climate change is magnetically reflected along the marine to continental (nonmarine) gradient in areas of India and its immediate surroundings. In addition, the need of making an inventory of existing magnetic methods and procedures, and selecting the most appropriate ones for SW Indian monsoon study is already underway for further optimization of mineral magnetic approach.

The apparent link between mineral magnetic properties and particulate pollution as a result of fossil-fuel combustion and other industrial processes, points the way to one urgent area of future study. The emphasis has been on the use of magnetic measurements in monitoring heavy metal deposition. Equally, the recent interest in the use of fly ash as a source of magnetite makes magnetic characterization especially important since a quantifiable relationship may be expected between magnetic susceptibility or SIRM and crystalline Fe concentration in any given fly ash. Heavy metal pollution correlates with magnetic enhancement, encouraging the use of magnetic measurements as a surrogate monitoring technique and suggesting that variations in heavy metal contents and mineral magnetic parameters indicative of changes in magnetic assemblages will be of value in identifying aerosol and sediment sources. Metropolitan areas like Mumbai, Navi Mumbai, Thane and Raigad districts, are screened for identification of pollution levels of contaminants in materials of roadside dusts, soils, lake sediments and mangroves using mineral magnetic techniques. This is now a fast emerging field and can be extended to other metropolises. Data-base will come from beach sands, roadside tree leaves, atmospheric dusts, fly ash, and mudflat and mangrove core samples.

10.2 CURRENT TRENDS/GEOMAGNETISM

Looking beyond the aforementioned themes, further applications in the influence of geomagnetic activity on weather and climate, archaeomagnetism, biomagnetism, medical and forensic science, are not difficult to envisage. Idenitification of inhaled particulate type and sources should be possible from lung tissue measurements as well as characterization of work environments in terms of aerosol loadings and types.

I. Geomagnetic Activity, Weather/Climate

One of enigmatic field of research is the influence of geomagnetic activity on weather and climate. Although most of the currents associated with the geomagnetic field flow at altitudes far above the regions which control the weather, intriguing results have emanated from studies of the solar features, geomagnetic activity and meteorological parameters like the atmospheric circulation patterns, drought conditions, rainfall, glaciations, etc. As it is unimaginable that solar activity can provide the requisite amount of energy for the meteorological changes, scientists are on the look out to identify some form of catalyst that can trigger large scale transfer of energy from the Sun and the interplanetary space through the upper atmosphere to the lower altitude regions.

II. Secular Variation/Archaeomagnetism

High-sedimentation-rate marine and lake sediments have revolutionized our understanding of the behaviour of the geomagnetic field. The presence of ubiquitous short-lived (~5 ka duration) polarity subchrons or excursions in the Brunhes and Matuyama chrons, coupled with high-quality relative palaeointensity frequently accompanied by short-lived perturbations of the direction of the geomagnetic field is now well established. The study of sub-Milankovitch-scale palaeoclimate changes requires approximate stratigraphic correlation at millennial-scale resolution. As correlation at this scale is not easily achieved through traditional isotopic methods, geomagnetic palaeointensity records and associated directional perturbations can well serve this purpose. In addition, understanding this short-term geomagnetic behaviour is important for constraining models of the geodynamo. There are two immediate prospects for improving the dating of lake sediments. The establishment of regional records of directions and intensities requires spatial corrections to be applied to individual determinations. Such ‘master curves’ for directional studies are now available for several areas, particularly in Europe, the Middle East, Japan, Australia and America. India does not have a SV master curve and needs to develop it from lake sediments and archaeological materials. The potential of mineral magnetism in archaeological studies has begun to emerge from sites in south India, hence archaeological dating of ancient sites in Maharashtra and Gujarat should be taken up. This development will permit

dating of palaeomagnetic secular variation intensity records by matching with previously established SV time series.

III. Biomagnetism

Geomagnetic study over the years has been responsible for many innovative technologies in instrumentation to detect weaker and weakest magnetic fields. Today, magnetometers based on superconducting materials can detect fluctuations with astounding accuracy (one in a million). This has led to a new branch of application called 'biomagnetism'. Birds and animals use magnetic field for their direction finding, although little is known about their physical and biological skills in using this field. Many experimental studies are being carried out to understand this phenomenon. Developments in biomagnetism have also been significant even though a causal linkage still remains elusive. Association between number of heart attacks or epilepsy and condition of the Earth's magnetic environment; effect of geomagnetic storms on migratory birds do bring out association between man and his geomagnetic environment, though the linkage in quantitative terms is missing. Consequently biomagnetism has not attained the status of an exact science. Hence, biomagnetism will surely be the next big step in environmental geomagnetic studies. Specifically, there is a need to establish the quantitative significance of bacterial magnetite in depositional environments, to specify more fully the conditions under which authigenic and diagenetic processes are magnetically significant. In the course of time, it is hoped to have the health check and diagnosis of human ailments based only on passive magnetic measurements. Magnetotherapy is, nowadays, an accepted alternative for several physiological problems.

As the Earth is, but an ordinary planet of the solar system and as the Sun is, but an insignificant star in the milky way galaxy, it is the fond hope of geomagneticians that their scientific quest will pave way for a better understanding of the entire Universe, not just this planet Earth. The latest initiation of regional centres at places like Tirunelveli and Allahabad, dedicated to upper atmospheric studies and solid Earth geomagnetism respectively, can go a long way in planning and executing research pertaining to fundamental and applied aspects with the express aim of using the know-how for the overall betterment of the society we live in.

SELECT BIBLIOGRAPHY

Achache J., Cohen Y. and Counil J-L., 1988. The magnetic anomalies of the Earth's crust. *Endeavour*, **12**, 154–162.

Adam L.N. and Arora B.R., 1995. The role of telluric and magnetotelluric (MT) methods in the exploration of deep sedimentary basins. *J. Geol. Soc. Ind*., **45**, 393–406.

Agarwal A.K., Singh B.P., Rastogi R.G. and Srinivasan S., 1986. On utility of space-borne vector magnetic measurements in crustal studies. *Phys. Earth Planet. Inter*., **41**, 260–268.

Akasofu Syun-Ichi and Lanzerotti L.J., 1975. The Earth's magnetosphere. *Phys. Today*, 28–36.

Alex S., Pathan, B.M. and Lakhina G.S., 2005. Response of the low latitude geomagnetic field to the major proton event of November 2001. *Advances in Space Research*, **26**, 2434–2439.

Alex S. and Mukherjee S., 2001. Local time dependence of the equatorial counter electrojet effect in a narrow longitudinal belt. *Earth, Planets & Space*, **53**, 1151–1161.

Alex S., Jadhav L. and Rao D.R.K., 1992a. Complexities in the variation of declination component (D) of the geomagnetic field in the Indian region. *Mem. Geol. Soc. Ind*., **24**, 263–274.

Alex S., Kadam B.D. and Rastogi R.G., 1992b. A new aspect of the daily variations of the geomagnetic field at low latitude. *J. Atmos. Terr. Phys*., **54**, 863–869.

Allegre Claude J. and Schneider Stephen H., October 1994. The evolution of the Earth. *Sci. Am*., 44–51.

Anand S.P. and Rajaram M., 2003. Study of aeromagnetic data over part of eastern ghat mobile belt and Bastar craton. *Gondwana Res*., **6**, 859–865.

Anand S.P., Erram V.C. and Rajaram M., 2002. Delineation of crustal structure of Mahanadi basin from ground magnetic survey. *J. Geol. Soc. Ind*., **60**, 283–291.

Arora B.R. and Bharadwaj S.K., 2003. Spatial and frequency characteristics of equatorial enhancement of geomagnetic field variations. *J. Atmos. & Solar Terr. Phys*., **65**, 1283–1292.

Arora B.R., Subba Rao P.B.V. and Nagar Vipul, 2003. Electrical conductivity signatures of plume-lithosphere interactions in the Indian Ocean. *Mem. Geol. Soc. Ind*., **53**, 393–418.

Arora B.R., 2002. Seismotectonics of the frontal Himalaya through the electrical conductivity imaging. Seismotectonics in convergent plate boundary, Eds Fujinawa Y. and Yoshida A. Terra Publications, Tokyo, 261–272.

Arora B.R. and Subba Rao P.B.V., 2002. Integrated modeling of EM response functions from peninsular India and Bay of Bengal. *Earth, Planets & Space*, **54**, 637–654.

Arora B.R., Waghmare S.Y. and Mahashabde M.V., 1995. Geomagnetic depth sounding along the Hirapur-Mandla-Bhandara Profile, central India. *Mem. Geol. Soc. Ind.*, **31**, 519–535.

Arora B.R., Kaikkonen P., Mahashabde M.V. and Waghmare S.Y., 1993. A non-uniform thin sheet model for geomagnetic induction anomalies in Central India. *Phys. Earth Planet. Inter.*, **81**, 201–213.

Arora B.R. and Adam A., 1992. Anomalous directional behaviour of induction arrows above certain conductive structures and its possible causes. *Phys. Earth Planet. Inter.*, **74**, 183–190.

Arora B.R., 1988. Earthquake prediction: present status. Proceedings of a symposium held on July 1986. Eds Guha S.K. and Patwardhan A.M. Pune University, India, 53–62.

Arora B.R. and Mahashabde M.V., 1987. A transverse conductive structure in the northwest Himalaya. *Phys. Earth Planet. Inter.*, **45**, 119–127.

Athavale R.N., Verma R.K., Bhalla M.S. and Pullaiah G., 1970. Drift of the Indian subcontinent since Precambrian times. *In:* Palaeogeophysics, Ed Runcorn S.K. Academic Press, London, 291–305.

Banerjee S.K., King J. and Marvin J., 1981. A rapid method for magnetic granulometry with applications to environmental studies. *Geophys. Res. Letters*, **8**, 333–336.

Banerjee S.K., Lund S.P. and Levi S., 1979. Geomagnetic record in Minnesota lake sediments – absence of the Gothenburg and Erieu excursions. *Geology*, **7**, 588–591.

Banks R.J., 1975. Complex demodulation of geomagnetic data and the estimation of transfer functions. *Geophys. J. R. Astron. Soc.*, **43**, 87–101.

Banola S., Pathan B.M., Rao D.R.K. and Chandra H., 2005. Spectral characteristics of scintillations producing ionospheric irregularities in the Indian region. *Earth, Planets & Space*, **57(1)**, 47–59.

Barton C.E. and McElhinny M.W., 1981. A 10,000 year geomagnetic secular variation record from three Australian maars. *Geophys. J. R. Astr. Soc.*, **67**, 465–485.

Basavaiah N., Appel E., Lakshmi B.V., Deenadayalan K., Satyanarayana K.V.V., Misra S., Juyal N. and Malik M.A., 2010. Revised magnetostratigraphy and nature of the fluvio-lacustrine sedimentation of the Kashmir basin, India, during Pliocene-Pleistocene. *J. Geophys. Res.*, **115**, B08105.

Basavaiah N. and Khadkikar A.S., 2004. Environmental magnetism and its application towards palaeomonsoon reconstruction. *J. Ind. Geophys. Uni.*, **8(1)**, 1–14.

Basavaiah N., Juyal N., Pant R.K., Yadava M.G., Singhvi A.K. and Appel E., 2004. Late Quaternary climate changes reconstructed from mineral magnetic studies from proglacial lake deposits of Higher Central Himalaya. *J. Ind. Geophys. Uni.*, **8(1)**, 27–37.

Basavaiah N., 2003. Workshop reports on Environmental Magnetism, *PAGES News*, **11**, 23.

Basavaiah N. and Singh B.P., 1997. Investigation of crustal structure in the Indian subcontinent using satellite gravity and MAGSAT data. *DST-DCS Newslett.*, **7**, 2–8.

Basavaiah N., 1993. Study of Earth's interior through geomagnetic methods—satellite derived geopotential field anomalies. Unpubl. PhD Thesis, Mumbai University, India.

Basavaiah N., Rajaram M., Qureshy M.N. and Rangzan K., 1992. Geopotential studies over the Iranian plateau. *Mem. Geol. Soc. Ind*., **24**, 81–92.

Basavaiah N., Singh B.P. and Radhakrishnamurthy I.V., 1991. The Himalayan riddle of the free-air satellite gravity and a possible solution. *Phys. Earth Planet. Inter*., **69**, 14–19.

Basavaiah N., Rajaram M. and Singh B.P., 1989. Comments on latitudinal dependance of MAGSAT anomalies in B-field and associated inversion instabilities. *Phys. Earth Planet. Inter*., **55**, 26–30.

Bergeron Lou, March 1996. When north flies. *New Scientist*, 24–29.

Bhardwaj S.K. and Rangarajan G.K., 1997. Geomagnetic secular variation at the Indian observatories. *J. Geomag. Geoelectric*, **49**, 1131–1144.

Biswas S.K., Bhasin A.L. and Ram J., 1993. Classification of Indian sedimentary basins in the framework of plate tectonics. Proc. Sec. Seminar on petroliferous basins of India, v1. Indian Petroleum Publishers, Dehradun, India.

Bloxham Jeremy and Gubbins David, December 1989. The evolution of the Earth's magnetic field. *Sci. Am*., 30–37.

Bonatti Enrico, March 1994. The Earth's mantle below the oceans. *Sci. Am*., 44–51.

Brekke A. and Egeland A., 1986. Christopher Hansteen (1784–1873): A pioneer in the study of terrestrial magnetism. *EOS*, **67(15)**, 185–187.

Cain J.C., 1987. The Earth as a magnet. *In:* The solar wind and the Earth, Eds Akasofu S-I. and Kamide Y. D. Reidel Co., Dordrecht, Holland, 57–69.

Cain J.C. and Sweeney R.E., 1973. The POGO data. *J. Atmos. Terr. Phys*., **35**, 1231–1247.

Campbell W.H., Arora B.R. and Sciffmacher E.R., 1993. External Sq currents in the India-Siberia Region. *J. Geophys. Res*., **98**, 3741–3752.

Cande S.C. and Kent D.V., 1995. A new geomagnetic polarity time scale for the Late Cretaceous and Cenozoic. *J. Geophys. Res*., **100**, 6093–6095.

Carrigan Charles R. and Gubbins David, February 1979. The source of the Earth's magnetic field. *Sci. Am*., 92–101.

Ceccaroni L., Frignani M., Langone L., Ravaioli M., Frank M., Mangini A., Basavaiah N. and Giglio F., 1997. Late Quaternary fluctuations of organic carbon and opal accumulation on the continental slope of the Ross Sea, Antarctica. *The Antarctic Region: Geological Evolution and Processes*, 889–896.

Chakrabarty S.K., 1984. The usefulness of geomagnetic observations for predicting the earthquakes. *Mausam*, **35(2)**, 213–218.

Chandra H., 1977. Earthquake of peninsular India—A seismotectonic study. *Bull. Seism. Soc. Am*., **67**, 1387–1413.

Chandrasekhar E. and Arora B.R., 1992. Upper mantle electrical conductivity distribution beneath the Indian subcontinent using geomagnetic storm time variations. *Mem. Geol. Soc. Ind*., **24**, 149–157.

Chandrasekhar E. and Arora B.R., 1996. Complex demodulation and electromagnetic response function for geomagnetic field variations at 27-day and its harmonics. *J. Assoc. Expl. Geophys*., **XVII (2)**, 91–98.

Chapman S., 1919. The solar and lunar diurnal variation of the Earth's magnetism. *Phil. Trans. Roy. Soc., Lond.*, **A218**, 1–118.

Chauhan O.S., Vogelsang E., Basavaiah N. and Syed Abdul Kader U., 2010. Reconstruction of the variability of the southwest monsoon during the past 3 ka,

from the continental margin of the southeastern Arabian Sea. *J. Quater. Sci*., **25(5)**, 798–807.

Chung Wai-Ying and Gao H., 1995. Source parameters of the Anjar earthquake of July 21, 1956, India and its seismotectonic implications for the Kutch rift basin. *Tectonophys*., **242**, 281–292.

Constable C., 2007. Geomagnetic spectrum, temporal. *In:* Encyclopedia of Geomagnetism and Paleomagnetism, Eds Gubbins D. and Herrero-Bervera E. Springer Publishers, 353–355.

Constable C.G. and Constable S.C., 2004. Satellite magnetic field measurements: application in studying the deep Earth. *In:* The State of the Planet: Frontiers and Challenges in Geophysics. Eds Sparks, R.S.J. and Hawkesworth C.T. *Am. Geophys. Uni*., pp. 147–160.

Daglis L.A., Thorne R.M., Wolfgang B. and Stefano O., 1999. The terrestrial ring current: origin, formation and decay. *Rev. Geophys*., **37(4)**, 407–438.

Dankers P., 1981. Relationship between median destructive field and remanent coercive forces for dispersed natural magnetite, titanomagnetite and hematite. *Geophys. J. R. Astron. Soc*., **64**, 447–461.

Dankers P. and Sugiura N., 1981. The effects of annealing and concentration on the hysteresis properties of magnetite around the PSD-MD transition. *Earth Planet. Sci. Lett*., **56**, 422–428.

Dankers P., 1978. Magnetic properties of dispersed natural iron-oxides of known grain size. Unpubl. PhD Thesis. Utrecht University, The Netherlands.

Das P.K., Misra S., Basavaiah N., Newsom H. and Dube A., 2009. Rock magnetic evidence of asteroid impact origin of Ramgarh structure, India. *Lunar and Planetary Science*, 1466–1467.

Dearing J.A., Bird P.M., Dann R.J.L. and Benjamin S.F., 1997. Secondary ferrimagnetic minerals in Welsh soils: a comparison of mineral magnetic detection methods and implications for mineral formation. *Geophys. J. Int*., **130**, 727–736.

Dearing J.A., Maher B.A. and Oldfield F., 1985. Geomorphological linkage between soils and sediments: the role of magnetic measurements. *In:* Geomorphology and Soils, Eds Richards K., Arnett R.R. and Ellis S. George Allen and Unwin, London. 245–266.

Deenadayalan K., Basavaiah N., Misra S. and Newsom H., 2009. Absence of Archean basement in the genesis of Lonar crater, India. *Meteoritics & Planetary Science*, **44**, A59.

Deepti V.G. Dessai, Nayak G.N. and Basavaiah N., 2009. Grain size, geochemistry, magnetic susceptibility: Proxies in identifying sources and factors controlling distribution of metals in a tropical estuary, India. *Estuarine, Coastal and Shelf Sci*., **85**, 307–318.

Dekkers M.J., 2007. Magnetic proxy parameters. *In:* Encyclopedia of Geomagnetism and Paleomagnetism. Earth Science Series, Eds Gubbins D. and Herrero-Bervera E. Springer Publishers, 524–534.

Dekkers M.J., 1997. Environmental magnetism: an introduction. *Geologie en Mijnbouw*, **76**, 163–182.

Deotare B.C., Kajale M.D., Rajguru S.N. and Basavaiah N., 2004. Late Quaternary geomorphology, palynology and magnetic susceptibility of playas in western margin of the Indian Thar Desert. *J. Ind. Geophys. Uni*., **8(1)**, 15–25.

Deutsch E.R., 1958. The northward drift of India. *J. Alberta Society of Petroleum Geology*, **6**, 158.

Doumouya V., Cohen Y., Arora B.R. and Yumoto K., 2003. Local time and longitude dependence of equatorial electrojet magnetic effects. *J. Atmos. & Solar Terr. Phys*., **65**, 1265–1282.

Dunlop D.J., 1986. Hysteresis properties of magnetite and their dependence on particle size: a test of pseudo-singledomain remanence models. *J. Geophys. Res*., **91**, 9569–9584.

Dunlop D.J., 1981. The rock magnetism of fine particles. *Phys. Earth Planet. Inter*., **26**, 1–26.

Emiliani C., 1955. Pleistocene temperatures. *J. Geol*., **63**, 538–578.

Fang X.M., Ono Y., Fukusawa H., Tian P.B., Li J.J., Dong-Hong G., Oi K., Tsukamoto S., Torri M. and Mishima T., 1999. Asian monsoon instability during the past 60,000 years: magnetic susceptibility and pedogenic evidence from western Chinese loess plateau. *Earth Planet. Sci. Lett*., **168**, 219–232.

Filloux J.H., 1987. Instrumentation and experimental method for oceanic studies. *In:* Geomagnetism, Ed Jacobs J.A. Academic Press, London. 143–248.

Foukal P.V., February 1990. The variable Sun. *Sci. Am*., 26–33.

Gawali P.B., Basavaiah N. and Hanamgond P.T., 2010. Mineral magnetic properties of sediments of beaches, Redi-Vengurla coast, central west coast of India: A seasonal characterization and provenance study. *J. Coastal Res*., **26(3)**, 569–579.

Gazey N.G.J., Lockwood M., Grande M., Perry C.H., Smith P.N., Coles S., Aylward A.D., Bunting R.J., Opgenoorth H. and Wilken B., 1996. EISCAT/CRRES observations: nightside ionospheric ion outflow and oxygen-rich substorm injections. *Ann. Geophys*., **14**, 1032–1043.

Glatzmaier G.A. and Roberts P.H., 1995. A three-dimensional self-consistent computer simulation of a geomagnetic field reversal. *Nature*, **377**, 203–208.

Glaβmeier K.H., 2007. Geomagnetic pulsations. *In:* Encyclopedia of Geomagnetism and Paleomagnetism, Eds Gubbins D. and Herrero-Bervera E. Springer Publishers, 333–334.

Gokarn S.G., 2003. Electrical conductivity patterns along transects over the Indian lithospheric domains of differing temporal evolution: A review. *Mem. Geol. Soc. Ind*., **53**, 129–147.

Gokarn S.G., Gupta G., Rao C.K. and Selvaraj C., 2003. Some interesting observations on the tectonics in the Deccan volcanic province observed from magnetotelluric studies. *J. Virtual Explorer* (Australia), **12**, 55–65.

Gokarn S.G., Rao C.K., Singh B.P. and Nayak P.N., 1992. Magnetotelluric studies across the Kurdwadi gravity feature. *Phys. Earth Planet. Inter*., **72**, 58–67.

Good G.A., 1985. Geomagnetics and scientific institutions in nineteenth century America. *EOS*, **66(27)**, 524–526.

Grant F.S., 1985. Aeromagnetics, geology and ore environments—I. Magnetite in igneous, sedimentary and metamorphic rocks: An overview. *Geoexploration*, **23**, 303–333.

Gupta G., Gokarn S.G. and Singh B.P., 1994. Thickness of the Siwalik sediments in the Mohand-Ramnagar region using magnetotelluric studies. *Phys. Earth Planet. Inter*., **83**, 217–224.

Gurubaran S. and Rajaram R., 2001. Mean winds, tides and gravity waves during the westward phase of the mesopause semiannual oscillation (MSAO). *J. Geophys. Res*., **106**, 31817–31824.

Han L., Li S.Y., Yang Y., Zhao F.M., Huang J. and Chang J., 2008. Research on the structure and performance of bacterial magnetic nanoparticles. *J. Biomater Appl*., **22**, 433–448.

Hirt A.M., 2007. Magnetic remanence, Anisotrophy. *In:* Encyclopedia of Geomagnetism and Paleomagnetism, Eds Gubbins D. and Herrero-Bervera E. Springer Publishers, 535–540.

Horie S.K., Yaskawa K., Yamanoto A., Yokoyama T. and Hyodo M., 1980. Paleolimnology of Lake Kizaki. *Arch. Hydrobiol*., **89**, 407–415.

Huttunen P. and Stober J., 1980. Dating of palaeomagnetic records from Finnish lake sediment cores using pollen analysis. *Boreas*, **9**, 193–202.

Irving Edward, November 1988. The palaeomagnetic confirmation of continental drift. *EOS*, **69(44)**.

Jackson M., 1991. Anisotropy of magnetic remanence: a brief review of mineralogical sources, physical origins and geological application and comparison with susceptibility anisotropy. *Pure and Applied Geophys*., **136**, 1–28.

Jadhav G., Rajaram M. and Rajaram R., 2001. Modification of daytime compressional waves by the ionosphere: First results from Oersted. *Geophys. Res. Lett*., **28(1)**, 103–106.

Jadhav G., Rajaram M. and Rajaram R., 2002a. Detailed study of equatorial electrojet phenomenon using Oersted satellite observations. *J. Geophys. Res*., **107(A8)**, 1175, 10.1029/2001JA000183.

Jadhav G., Rajaram M. and Rajaram R., 2002b. Main field control of the equatorial electrojet: a preliminary study from the Oersted data. *J. Geodyn*., **33**, 157–171.

Jardine M., 2010. Sunscreen for the Young Earth. *Sci*., **327**, 1206–1207.

Juyal N., Pant R.K., Basavaiah N., Bhushan R., Jain M., Saini N.K., Yadava M.G. and Singhvi A.K., 2009. Reconstruction of last glacial to early Holocene monsoon variability from relict lake sediments of the Higher Central Himalaya, Uttrakhand, India. *J. Asian Earth Sci*., **34(3)**, 437–492.

Juyal N., Pant R.K., Basavaiah N. et al., 2004. Climate and seismicity in the Higher Central Himalaya: evidences from Garbayang basin, Uttaranchal, India. *Palaeogeog., Palaeoclimatol., Palaeoecol*., **213**, 315–330.

Juyal N., Kar A., Rajaguru S.N. and Singhvi A.K., 2003. Luminescence chronology of aeolian deposition during the Late Quaternary on the southern margin of Thar Desert, India. *Quarter. Int*., **104**, 87–98.

Kaila K.L. and Narain H., 1976. Evolution of the Himalaya based on seismotectonics and deep seismic soundings. Proc. Himalayan Geology Seminar, Section 11B: Structures, Tectonics, Seismicity and Evolution, pp.1–30.

Kakad A.P, Singh S.V. and Lakhina G.S., 2003. A shear flow instability in plasma sheet region. *Planet. Space Sci*., **51(3)**, 177–181.

Kane R.P., Trivedi N.B., Tanaka Y., Hajime Y. and Pathan B.M., 2003. Day-to-day variability of the equatorial electrojet strength. *Ind. J. Radio & Space Phys*., **32**, 261–265.

Katsura T., 2007. Mantle, Electrical Conductivity, Mineralogy. *In:* Encyclopedia of Geomagnetism and Paleomagnetism, Eds Gubbins D. and Herrero-Bervera E. Springer Publishers, 684–688.

Kayal J.R., 2003. Seismic tomography structures of source areas of the two redevastating earthquakes in peninsular India. *J. Virtual Explorer*, **12**, 66–71.

Khadkikar A.S. and Basavaiah N., 2004. Morphology, mineralogy and magnetic susceptibility of epikarst—Terra Rossa developed in Late Quatemary aeolianite deposits of southeastern Saurashtra, India. *Geomorphology*, **58**, 339–355.

Khadkikar A.S., Basavaiah N., Gundurao T.K. and Rajshekhar C., 2004. Palaeo-environments around the Harappan port of Lothal, Gujarat, Western India. *J. Ind. Geophys. Uni*., **8(1)**, 49–53.

Kim V.P., Hegai V.V. and Lal M., 2002. A modeling study of the nighttime equatorial E-region behaviour during magnetospheric substorms and storms. *J. Geophys. Res*., **107**, A5.

King J., Banerjee S.K., Marvin J. and Özdemir Ö., 1982. A comparison of different magnetic methods for determining the relative grain size of magnetite in natural materials: some results from lake sediments. *Earth Planet. Sci. Lett.*, **59**, 404–419.

Kruiver P.P. and Passier H.F., 2001. Coercivity analysis of magnetic phases in sapropel S1 related to variations in redox conditions, including an investigation of the S-ratio. *Geochem. Geophys. Geosyst*., 14 December 2001, Paper number 2001GC000181.

Kumaran K.P.N., Shindikar M.R. and Mudgal T.R., 2004. Floristic composition, palynology and sedimentary facies of Hadi mangrove swamp (Maharashtra). *J. Ind. Geophys. Uni*., **8(1)**, 55–63.

Lakhina G.S. and Alex S., 2007. Magnetic observatories in India. *In:* Encyclopedia of Geomagnetism and Paleomagnetism, Eds Gubbins D. and Herrero-Bervera E. Springer Publishers, 731–733.

Lakhina G.S., Alex S., Tsurutani B.T. and Gonzalez W.D., 2005. Research on historical records of geomagnetic storms. *In:* Coronal and Stellar Mass Ejections, Eds Dere K.P., Wang J. and Yan Y. Proceedings IAU Symposium No. 226, 3–15.

Lakhina G.S., Tsurutani B.T. and Pickett J.S., 2004. Association of Alfven waves and proton cyclotron waves with electrostatic bipolar pulses: magnetic hole events observed by Polar. *Nonl. Proc. Geophys*., **11**, 205–213.

Lakhina G.S. and Alex S., 2002. Space weather research in India: an overview. *Ind. J. Radio & Space Phys*., **31**, 337–348.

Lakhina G.S., Jadhav G., Alex S. and Dhar A., 2002. Study of Intense Geomagnetic storms and their possible effects on society. *In:* Antarctic Geosciences, Ocean Atmosphere Interaction and Paleoclimatology, Eds Rajan S. and Pandey P.C. National Center for Antarctic and Ocean Research, Goa, 112–126.

Lakhina G.S., 2001. Role of helicon modes in the injection of oxygen ions in the ring current. *J. Atmos. & Solar Terr. Phys*., **63**, 481–487.

Lakhina G.S., 1993. Electrodynamic coupling between different regions of the atmosphere. *Current Sci*., **64(9)**, 660–666.

Lakshmi B.V., 2001. Geological evidences and dating of a paleoseismic event in the meizoseismal area of the 1993 Latur earthquake, Deccan plateau, Maharashtra. unpubl. PhD Thesis, Osmania University, India.

Langel R.A., Schnetzler, C.C., Philips J.D. and Horner R.J., 1982. Initial vector magnetic anomaly map from MAGSAT. *Geophys. Res. Lett*., **9**, 273–276.

Lanzerotti L.J. and Krimigis Stamatios M., 1985. Comparative magnetospheres. *Phys. Today*, 24–34.

Larson Roger L., February 1995. The mid-Cretaceous superplume episode. *Sci. Am*., 66–70.

Lean C.M.B. and McCave I.N., 1998. Glacial to interglacial mineral magnetic and palaeoceanographic changes at Chathlam Rise, SW Pacific Ocean. *Earth Planet. Sci. Lett*., **163**, 247–260.

Lester A.T., 2007. Storms and Substorms, Magnetic. *In:* Encyclopedia of Geomagnetism and Paleomagnetism, Eds Gubbins D. and Herrero-Bervera E. Springer Publishers, 926–928.

Lilley F.E.M. and Day Alan A., 1993. D'Entrecasteaux, 1792: Celebrating a bicentennial in geomagnetism. *EOS*, **74(9)**, 97–112.

Lisiecki L.E. and Raymo M.E., 2005. A Pliocene-Pleistocene stack of 57 globally distributed benthic $\delta^{18}O$ records. *Paleoceanography*, **20**, PA1003.

Lourens L.J., Hilgen F., Shackleton N.J., Laskar J. and Wilson D., 2004. The Neogene period. *In:* A Geologic Time Scale, Eds Gradstein F.M., Ogg J.G. and Smith A.G. Cambridge University Press, Cambridge, 409–440.

Lowenstam H.A., 1981. Minerals formed by organisms. *Sci*., **211**, 1126–1139.

Magee J.W., Bowler J.M., Miller G.H. and Williams D.L.G., 1995. Stratigraphy, sedimentology, chronology, and palaeohydrology of Quaternary lacustrine deposits at Madigan Gulf, Lake Eyre, South Australia. *Palaeogeog., Palaeoclimatol., Palaeoecol*., **113**, 3–42.

Maher B.A., 2007. Environmental magnetism. *In:* Encyclopedia of Geomagnetism and Paleomagnetism, Eds Gubbins D. and Herrero-Bervera E. Springer Publishers, 248–255.

Maher B.A., 1988. Magnetic properties of some synthetic sub-micron magnetites. *Geophys. J. R. Astr. Soc*., **94**, 83–96.

Mathew B., Iyer K.N. and Pathan B.M., 1992a. Patchy occurrence of VHF scintillations at tropical latitudes. *J. Atmos. Terr. Phys*., **54**, 963–968.

Mathew B., Iyer K.N. and Pathan B.M., 1992b, VHF radio scintillations at Rajkot—A station near the crest of the equatorial anomaly in India. *Ind. J. Radio & Space Phys*., **21**, 237–245.

Mazzella A. and Morrison H.F., 1974. Electrical resistivity variations associated with earthquakes on the San Andreas Fault. *Sci*., **185**, 855–857.

McElhinny W.M., 2007. Geocentric axial dipole hypothesis. *In:* Encyclopedia of Geomagnetism and Paleomagnetism, Eds Gubbins D. and Herrero-Bervera E. Springer Publishers, 281–287.

McWilliams M.O., Holocolm R.T. and Champion D.E., 1982. Geomagnetic secular variation from ^{14}C dated lava flows on Hawali and the question of the Pacific non-dipole low. *Phil. Trans. R. Soc. Lond.*, **A306**, 211–221.

Misra S., Arif Md., Basavaiah N., Srivastava P.K. and Dube A., 2010. Structural and anisotropy of magnetic susceptibility (AMS) evidences for oblique impact on terrestrial basalt flows: Lonar crater, India. *Geol. Soc. Am. Bull*., **122(3/4)**, 563–574.

Morley L.W., 1986. Early work leading to the explanation of the banded geomagnetic imprinting of the ocean floor. *EOS*, **67(36)**, 665–666.

Moskowitz B.M., 1980. Theoretical grain-size limits for single-domain, pseudo-single-domain and multidomain behaviour in titanomagnetite ($x = 0.6$) as function of low-temperature oxidation. *Earth planet. Sci. Lett*., **47**, 285–293.

Muffly G., 1946. The airborne magnetometer. *Geophys*., **11**, 321–334.

Mukherjee G.K. and Parihar N., 2004. Measurement of rotational temperature at Kolhapur, India. *Ann. Geophys*., **22**, 1–7.

Mukherjee G.K., 2003a. The signature of short period gravity waves imaged in the 557.7 nm and near infrared OH nightglow emissions over Panhala. *J. Atmos. & Solar Terr. Phys*., **65**, 1329–1335.

Mukherjee G.K., 2003b. Studies of equatorial F-region depletions and dynamics using multiple wavelength nightglow imaging. *J. Atmos. & Solar Terr. Phys*., **65**, 379–390.

Mukherjee G.K., 2002. Mapping of the simultaneous movement of the equatorial ionization anomaly (EIA) and ionospheric plasma bubbles through all-sky imaging of OI 630 nm emission. *Terr. Atmos. Ocean. Sci*., **13**, 53–64.

Mukherjee G.K., Carlo L. and Mahajan S.H., 2000. 630 nm nightglow observations from 17 degree N latitude. *Earth, Planets & Space*, **52(2)**, 105–110.

Mukherjee G.K., Mahajan S.H., Carlo L. and Patil P.T., 1998. First results of all-sky imaging from India. *Earth, Planets & Space*, **50**, 119–127.

Nayak P.N., Saha S.N., Dutta S., Rama Rao M.S.V. and Sarkar N.C., 1983. Geoelectrical and geohydrological precursors of earthquakes in northeastern India. *Geo-exploration*, **21**, 137–157.

Nichols E.A., Morrison H.F. and Channell J.E.T., 1988. Signal and noise in measurements of low-frequency geomagnetic fields. *J. Geophys. Res*., **93**, 13743–13754.

Nityananda N., Agarwal A.K. and Singh B.P., 1977. Induction at short periods in the horizontal field variations in the Indian peninsula. *Phys. Earth Planet. Inter*., **15**, 5–9.

Oldfield F., 1994. Towards the discrimination of fine grained ferrimagnets by magnetic measurements in lake and near-shore marine sediments. *J. Geophys. Res.*, **99**, 9045–9050.

Oldfield F., 1991. Environmental magnetism—a personal perspective. *Quarter. Sci. Rev*., **10**, 73–85.

Olsen N., 2007. Natural sources for electromagnetic induction studies. *In:* Encyclopedia of Geomagnetism and Paleomagnetism, Eds Gubbins D. and Herrero-Bervera E. Springer Publishers, 696–700.

Overpeck J., Anderson D., Trumbore S. and Prell W., 1996. The southwest monsoon over the last 18,000 years. *Climate Dyn*., **12**, 213–225.

Pandey O.P. and Agrawal, P.K., 1999. Lithospheric Mantle Deformation beneath the Indian Cratons. *J. Geol*., **107**, 683–692.

Panneerselvam C., Nair K.U., Jeeva K., Selvaraj C., Gurubaran S. and Rajaram R., 2003. A comparative study of atmospheric Maxwell current and electric field from a low latitude station, Tirunelveli. *Earth, Planets & Space*, **55**, 697–703.

Pant R.K., Agrawal D.P. and Krishnamurthy K.V., 1978. Scanning electron microscopic and other studies on Karewa beds of Kashmir, India. *In:* Scanning Electron Microscopy in the Study of Sediments, Ed Whalley W.B. Geoabstracts, UK, 275–282.

Pant R.K., Basavaiah N., Juyal N., Saini N.K., Yadava M.G., Appel E. and Singhvi A.K., 2005. A 20 ka climate record from Central Himalayan loess deposits. *J. Quater. Sci*., **20(5)**, 485–492.

Pant R.K., Krishnamurthy R.V., Basavaiah N., Appel E. et al., 1999. Periodicity and amplitude of Quaternary glaciation in the Central Himalaya. Project report (DST Project No: ESS/CA/A3-17/95), 1–81.

Paramasivan B., Vijaykumar C.K. and Elango P., 2002. Migration of dip equator – ground magnetic survey. *J. Ind. Geophys. Uni*., **6(1)**, 19–23.

Pathan B.M., Rastogi R.G. and Rao D.R.K., 1992. On the width and complexities of the equatorial night time radio wave scintillation belt in the Indian region. *J. Geomag. Geoelectr*., **44**, 129.

Patil A.R. and Rajaram R., 2001. On the stationariness of the Sq current system. *J. Geophys. Res*., **106(18)**, 589–596.

Patil A.R., Arora B.R. and Rastogi R.G., 1983. Daily variation of the geomagnetic field near the focus of Sq-current system in Indian longitude. *Proc. Indian Acad. Sci. (Earth Planet. Sci.)*, **92(3)**, 239–245.

Patil S.K. and Arora B.R., 2003. Palaeomagnetic studies on the dykes of Mumbai region, west coast of Deccan volcanic province: implications on age and span of the Deccan eruptions. *J. Virtual Explorer*, **12**, 107–116.

Paul D.K., Ray, A., Das B., Patil S.K. and Biswas S.K., 2008. Geochemistry and paleomagnetism of the earliest magmatic rocks of Deccan volcanic province, Kutch, northwest India: interaction between lithospheric rifting and mantle plume. *Lithos*, **102(1–2)**, 237–259.

Phadtare N.R., 2000. Sharp decrease in summer monsoon strength 4000–3500 cal yr B.P. in the central Higher Himalaya of India based on pollen evidence from Alpine peat. *Quarter. Res*., **53**, 122–129.

Pilkington M., Aeromagnetic Surveying. *In:* Encyclopedia of Geomagnetism and Paleomagnetism, Eds Gubbins D. and Herrero-Bervera E. Springer Publishers, 1–3.

Prakash Babu C., Pattan J.N., Dutta K., Basavaiah N., Ravi Prasad G.V., Ray D.K. and Govil P., 2010. Shift in detrital sedimentation in the eastern Bay of Bengal during the late Quaternary. *J. Earth Syst. Sci*., **119(3)**, 285–295.

Prasad J.N., Patil S.K., Venkateshwarlu M., Saraf P.D., Tripathi S.C. and Rao D.R.K., 1997. Palaeomagnetic results from the Cretaceous Bagh Group in the Narmada Basin, Central India: evidence of pervasive Deccan remagnetization and its implications for Deccan volcanism. *Geophys. J. Int*., **133**, 519–528.

Prasad J.N., Satyanarayana K.V.V. and Gawali P.B., 1999. Palaeomagnetic and low-field AMS studies of Proterozoic dykes and their basement rocks around Harohalli, South India. *J. Geol. Soc. Ind*., **54**, 57–67.

Pullaiah, G., Irving, E., Buchanan, K.L. and Dunlop D.J., 1975. Magnetization changes caused by uplift and burial. *Earth Planet, Sci. Lett*., **28**, 133–143.

Rajaram G., Arun T., Dhar A. and Patil A.G., 2002a. Rapid decline in total magnetic field F at Indian Antarctic station—its relationship to core mantle features. *Antarctic Science*, **14 (1)**, 61–68.

Rajaram G., Hanchinal A.N., Kalra R., Unnikrishnan K., Jeeva K., Sridharan M. and Dhar A., 2002b. Velocity of small-scale auroral ionospheric current systems over Indian Antarctic station Maitri. Proc. *Indian Acad. Sci. (Earth Planet. Sci.)*, **111(1)**, 51–62.

Rajaram G., Dhar A. and Kumar S., 2001. Response of geomagnetic variation and 30 MHz Riometer absorption, at Indian Antarctic station Maitri, to conditions of 'Zero' and 'High solar wind'. *Adv. Space Res*., **28(11)**, 1661–1667.

Rajaram G., Samson J.C. and Rostoker G., 1990. Simultaneous ground-based and satellite observations of the auroral Ps6 pulsation—a clue to magnetosphere-ionosphere coupling. *Ind. J. Radio & Space Phys*., **19**, 7–16.

Rajaram, M., 2007. Depth to Curie isotherm. *In*: Encyclopedia of Geomagnetism and Paleomagnetism. Eds Gubbins D. and Herrero-Bervera E. Springer Publishers, 157–159.

Rajaram M., Anand S.P. and Balakrishna V., 2006. Composite magnetic anomaly map of India and its contiguous regions. *J. Geol. Soc. Ind.*, **68**, 569–576.

Rajaram M. and Anand S.P., 2003. Crustal structure of South India from aeromagnetic data. *J. Virtual Explorer*, **12**, 72–82.

Rajaram M., Anand S.P and Erram V.C., 2000. Crustal magnetic studies over Krishna-Godavari Basin in eastern continental margin of India. *Gondwana Res*., **3(3)**, 385–393.

Rajaram M. and Langel R.A., 1992. Lithospheric analysis of magnetic and related geophysical anomalies. *Tectonophys*., **212**, 117–127.

Rajaram R., Ruohoniemi J.M., Greenwald R.A. and Baker K.B., 1992. A new method for detecting the projection of magnetospheric oscillations in the ionosphere. *J. Geophys. Res*., **97**, 16–59.

Rajaram M. and Singh B.P., 1986. Spherical Earth modelling of the scalar magnetic anomaly over the Indian region. *Geophys. Res. Lett*., **13**, 961–964.

Rajshekhar C., Gawali P.B., Mudgal T.R., Reddy P.P. and Basavaiah N., 2004. Micropalaeontology and mineral magnetic evidences of the Holocene mudflats of Navlakhi, Gulf of Kachchh. *J. Ind. Geophys. Uni*., **8(1)**, 71–77.

Raleigh B., Bennet G., Craig H., Hanks T., Molnar P., Nur A., Savge J., Scholz C., Turner R. and Wu F., 1977. Prediction of the Haicheng earthquake. *EOS*, **58**, 236–272.

Ramaswamy K. and Duraiswamy D., 1990. Archaeomagnetic studies on some archaeological sites in Tamilnadu, India. *Phys. Earth Planet. Inter*., **60**, 278–284.

Rangarajan G.K. 1992a. Magnetometry for geomagnetic observations. *Mem. Geol. Soc. Ind*., **24**, 175–193.

Rangarajan G.K., 1992b. Response of low latitude geomagnetic field to solar proton events with energies >10 MeV. *Ind. J. Radio & Space Phys*., **21**, 255–259.

Rangarajan G.K. and Ajay Dhar, 1992. Response of the Sq and equatorial electrojet variations to the north-south asymmetry in geomagnetic activity. *J. Geomag. Geoelectr*., **44**, 899–908.

Rangarajan G.K. and Ajay Dhar, 1988. Scientific report of fifth Indian Antarctic expedition, Depart. Ocean Development, Govt. of India, New Delhi.

Rangarajan G.K., September 1986. Geomagnetism: past, present and prospects. *Sci. Reporter*, 548–552.

Rao C.K., Ogawa Y., Gokarn S.G. and Gupta G., 2004. Electomagmetic imaging of magma across the Narmada-Son lineament, Central India. *Earth, Planets & Space*, **56(2)**, 229–238.

Rao D.R.K. and Pathan B.M., 2003. On some spatial characteristics of ULF pulsations in the Indian region, in very low frequency (VLF) phenomena. Eds Hughes A.R.W., Ferencz C. and Gwal A.K. Narosa Publishing House, New Delhi. 313–326.

Rastogi R.G. and Chandra H., 1974. Interplanetary magnetic field and the equatorial ionosphere. *J. Atmos. Terr. Phys*., **36**, 377–379.

Rastogi R.G. and Patil A.R., 1992. On certain aspects of daily variation of geomagnetic field at low latitudes. *J. Geomag. Geoelectr*., **44**, 495–503.

Rastogi R.G., 1986a. Evolution of geomagnetic studies in India. *Ind. J. of Radio & Space Phys*., **15**, 356–363.

Rastogi R.G., 1986b. On the occurrence of equatorial spread-F in the evening hours. *J. Atmos. Terr. Phys*., **48**, 687–693.

Rastogi R.G., Rangarajan G.K. and Somayajulu V.V., 1992. Complexities of counter equatorial electrojet currents. *Ind. J. Radio & Space Phys*., **21**, 89–96.

Ravat D., 2007. Reduction to pole. *In*: Encyclopedia of Geomagnetism and Paleomagnetism. Eds Gubbins D. and Herrero-Bervera E. Springer Publishers, 856–857.

Rawat R., Alex S. and Lakhina G.S., 2009. Low latitude geomagnetic response to the interplanetary conditions during very intense magnetic storms. *Adv. Space Res*., **43**, 1575–1587.

Raymond J. and Thorne L., May 1993. The core-mantle boundary. *Sci. Am*., 26–33.

Reddy C.D. and Arora B.R., 1992a. A narrow conductive zone south of the main central thrust of the Garhwal Himalaya. *Mem. J. Geol. Soc. Ind*., **24**, 121–131.

Reddy C.D., Gamal El-Fiky, Teruyuki Kato, Seiichi Shimada and Vijay Kumar K., 2000. Crustal strain field in the Deccan trap region, Western India, derived from GPS measurements. *Earth, Planets & Space*, **52**, 965–969.

Reddy R.V., Lakhina G.S., Singh N. and Bharuthram R., 2002. Spiky parallel electrostatic ion cyclotron and ion acoustic waves. *Nonl. Proc. Geophys*., **9**, 25–29.

Regan R.D., Cain J.C. and Davis W.H., 1975. A global magnetic anomaly map. *J. Geophys. Res*., **80**, 794–802.

Richmond A.D., 2007. Ionosphere. *In*: Encyclopedia of Geomagnetism and Paleomagnetism. Eds Gubbins D. and Herrero-Bervera E. Springer Publishers, 452–454.

Richter C. and van der Pluijm B.A., 1994. Separation of paramagnetic and ferrimagnetic susceptibilities using low temperature magnetic susceptibilities and comparison with high field methods. *Phys. Earth Planet. Inter*., **82**, 113–123.

Roberts A.P., Cui Y. and Verosub, K.L., 1995. Wasp-waisted hysteresis loops: Mineral magnetic characteristics and discrimination of components in mixed magnetic systems. *J. Geophys. Res*., **100**, 17909–17924.

Roy M., 1992a. Eigen modes of hot plasma discontinuity in the magnetosphere. *Ind. J. of Radio & Space Phys*., **21**, 362–365.

Roy M., 1992b. Some properties of low latitude Pc-5 pulsations and their relationship with the magnetosphere. *Mem. Geol. Soc. Ind*., **24**, 383–388.

Sagdeev R.Z. and Kennel C.F., April 1991. Collisionless shock waves. *Sci. Am*., 40–47.

Sastri J.H., Rao J.V.S.V., Rao D.R.K. and Pathan B.M., 2001. Daytime equatorial geomagnetic H-field response to the growth phase and expansion phase onset of isolated sub-storm: case studies and their implications. *J. Geophys. Res*., **106**, 29925–29933.

Satyanarayana K.V.V., Arora B.R. and Janardhan A.S., 2003. Rock magnetism and palaeomagnetism of the Oddanchatram anorthosite, Tamil Nadu, South India. *Geophys. J. Int*., **155**, 1081–1092.

Schmidt P.W. and Embleton B.J.J., 1981. A geotectonic paradox: Has the Earth expanded? *J. Geophys*., **49**, 20–25.

Scholz C.H., Sykes L.R. and Aggarwal Y.P., 1973. Earthquake prediction: a physical basis. *Sci*., **181**, 803–809.

Schubert G., 2007. Interiors of planets and satellites. *In*: Encyclopedia of Geomagnetism and Paleomagnetism. Eds Gubbins D. and Herrero-Bervera E. Springer Publishers, 439–448.

Seetharamaiah J., Basavaiah N., Chakraborty S., Nageswara Rao K. and Khadkikar A.S., 2004. Use of magnetic susceptibility for identification of mangrove deposits in vibracores from deltaic environments. *J. Ind. Geophys. Uni*., **8(1)**, 65–70.

Sethana S.F., Sethana B.S., Kothare P., Rao D.R.K, Saraf P.D, Venkateshwarlu M. and Patil S.K., 2001. A note on palaeomagnetic evidence to show tectonic deformation in the Deccan volcanic province of Saurashtra, Western India. *Current Sci*., **80**, 1067–1069.

Shau Y.H., Torii M., Horng C.S. and Peacor D.R., 2000. Subsolidus evolution and alteration of titanomagnetite in ocean ridge basalts from Deep Sea Drilling Project/Ocean Drilling Program Hole 504B, Leg 83: Implications for the timing of magnetization. *J. Geophys. Res*., **105 (B10)**, 23635–23649.

Singh B.P., Basavaiah N. and Qureshy M.N., 1992a. A preliminary study of satellite derived gravity and magnetic anomalies of India and contiguous regions. *Tectonophys*., **212**, 129–139.

Singh B.P., Rajaram M., Basavaiah N., Nagar V.K. and Rajal B.S, 1992b. Assessment of IGRF candidate models over the Indian region. *J. Geomag. Geoelectr*., **44**, 881–886.

Singh B.P., Rajaram M. and Basavaiah N., 1989a. Inversion of magnetic and gravity data in the Indian region. *Geophys. Monogr. AGU*, **51(6)**, 271–277.

Singh B.P., Basavaiah N., Rajaram M. and Geetharamanan G., 1989b. A method of obtaining solutions with only positive dipole moments on inversion of satellite magnetic anomalies. *Phys. Earth Planet. Inter*., **58**, 95–102.

Singh N., Loo S.M., Wells B.E. and Lakhina G.S., 2001. Evolution of electron beam generated waves resulting into transverse ion heating and filamentation of the plasma. *J. Geophys. Res*., **106**, 21165–21182.

Singh B.P., 1987. What Magsat Sees? *Sci. Age*, 20–25.

Singh S.V, Kakad A.P. and Lakhina G.S., 2005. Quasi-Electrostatic instabilities excited by the energetic oxygen ions in the ring current region. *Phys. Plasmas*, **12(1)**, 12903–12906.

Singh S.V. and Lakhina G.S., 2004. Electron acoustic solitary waves with non-thermal distribution of electrons. *Nonl. Proc. Geophys*., **11**, 275–279.

Singh S.V., Reddy R.V. and Lakhina G.S., 2001. Broadband electrostatic noise due to nonlinear electron acoustic waves. *Adv. Space Res*., **28**, 1643–1648.

Sinha A.K., Pathan B.M., Rajaram R. and Rao D.R.K., 2002. Low frequency modulation of transionospheric radio wave amplitude at equatorial latitudes: possible role of field line resonances. *Ann. Geophys*., **20**, 69–80.

Sirocko F., Sarthein M., Erienkeuser H., Lange H., Arnold M. and Duplessy J.C., 1993. Century-scale events in monsoonal climate over the past 24,000 years. *Nature*, **364**, 322–324.

Sivaji Ch., Arora B.R. and Qureshy M.N., 1992. An assessment of the nature of the crust under the Himalayan collision zone through gravity studies. *Mem. Geol. Soc. Ind*., **24**, 103–112.

Smith B.E. and Johnston M.J.S., 1976. A tectonomagnetic effect observed before a magnitude 5.2 earthquake near Hollister, California. *J. Geophys. Res*., **81**, 3556–3560.

Snowball I. and Torii M., 1999. Incidence and significance of magnetic iron sulphides in Quaternary sediments and soil. *In*: Quaternary climates, environments and

magnetism. Eds Maher B.A. and Thompson R. University Press, Cambridge, 199–230.

Soffel H., 1985. Palaeomagnetism and Archaeomagnetism. *In*: Geophysics of the Solid Earth, the Moon and the Planets. Springer Materials—The Landolt-Börnstein Database. Eds Fuchs K. and Soffel H. http://www.springermaterials.com, 184–243.

Sridharan M. and Ramasamy A.M.S., 2002. Multidimensional scaling technique for analysis of magnetic storms at Indian observatories. *Proc. Indian Acad. Sci. (Earth Planet. Sci.)*, **111(4)**, 459–465.

Sridharan S., Gurubaran S. and Rajaram R., 2003. QBO influences on the variability of planetary waves in the equatorial mesopause region. *Earth, Planets & Space*, **55**, 687–696.

Srivastava B.J., Singh B.P. and Lilley F.E.M., 1984. Magnetometer array studies in India and the lithosphere. *Tectonophys*., **105**, 355–371.

Stern D.P., 1989. A brief history of magnetospheric physics before the space flight era. *Rev. Geophys*., **27(1)**, 103–114.

Stern D.P., 2002. A millennium of geomagnetism. *Rev. Geophys*., **40(3)**, 1–30.

Stuiver M. and Quay P.D., 1980. Changes in atmospheric ^{14}C attributed to a variable Sun. *Sci*., **207**, 11–19.

Subba Rao P.B.V., Singh B.P. and Gawali P.B., 2000. A geoelectrical system across the Andaman Sea region, north east Indian Ocean by using OBM. *J. Geol. Soc. Ind.*, **55**, 47–64.

Sukhija B.S., Rao M.N., Reddy D.V., Nagabhushanam P., Hussain S., Chadha R.K. and Gupta H.K., 1999a. Paleoliquefaction evidence and periodicity of large prehistoric earthquakes in Shillong Plateau, India. *Earth Planet. Sci. Lett*., **167**, 269–282.

Sukhija B.S., Rao M.N., Reddy D.V., Nagabhushanam P., Hussain S., Chadha R.K. and Gupta H.K., 1999b. Timing and return period of major paleoseismic events in the Shillong Plateau, India. *Tectonophys*., **308**, 53–65.

Sukhija B.S., Rao M.N., Reddy D.V., Nagabhushanam P., Hussain S., Chadha R.K. and Gupta H.K., 1999c. Paleoseismic studies of the Shillong Plateau, northeast India. *Himalayan Geol*., **20 (1)**, 105–112.

Sunil P.S., Reddy C.D., Ponraj M., Ajay Dhar and Jaypaul D., 2007. GPS determination of velocity and strain-rate fields on Schirmacher glacier, central Dronning Maud Land, Antarctica. *J. Glaciology*, **53**, 558–564.

Tazima M., 1968. Accuracy of recent magnetic survey and a locally anomalous behaviour of the geomagnetic secular variation in Japan. *Bull. Geogr. Survey Inst*., **13**, 1–78.

Thakur N.K., Mahashabde M.V., Arora B.R., Singh B.P., Srivastava B.J. and Prasad S.N., 1986. Geomagnetic variation anomalous in peninsular India. *Geophys. J. R. Astr. Soc*., **86**, 839–854.

Thamban M., Naik S.S, Mohan R., Rajakumar A., Basavaiah N. et al., 2005. Changes in the source and transport mechanism of terrigenous input to the Indian sector of Southern Ocean during late Quaternary and its palaeoceanography implications. *J. Earth Syst. Sci*., **114**, 443–452.

Thompson R, 1986. Modelling magnetization data using SIMPLEX. *Phys. Earth Planet. Inter*., **42**, 113–127.

Thompson R., Tuner G.M., Stiller M. and Kaufman A., 1985. Near East paleomagnetic secular variation recorded in sediments from the sea of Galiee (Lake Kinneret). *Quater. Res*., **23**, 175–188.

Tobias 2007. Magnetic field of sun. *In*: Encyclopedia of Geomagnetism and Paleomagnetism. Eds Gubbins D. and Herrero-Bervera E. Springer Publishers, 505–509.

Tsurutani B.T., Walter D., et al., 2006. Corotating solar wind streams and recurrent geomagnetic activity: A review. *J. Geophys. Res*., **111**, A07S01.

Tsurutani B.T., Gonzalez W.O., Lakhina G.S. and Alex S., 2003. The extreme magnetic storm of September 1–2, 1859. *J. Geophys. Res.*, **108**, 1268.

Tsurutani B.T., Arballo J.K., Galvan C., Zhang L.D., Zhou X.Y., Lakhina G.S. et al., 2001a. Polar cap boundary layer waves: an auroral zone phenomenon. *J. Geophys. Res*., **106**, 19035–19056.

Tsurutani B.T., Zhou X.Y., Arballo J.K., Gonzalez W.O., Lakhina G.S. et al., 2001b. Auroral zone dayside precipitation during magnetic storm initial phases. *J. Atmos. & Solar Terr. Phys*., **63**, 513–522.

Turner G.M. and Thompson R., 1981. Lake sediment record of the geomagnetic secular variation in Britain during Holocene times. *Geophys. J. R. Astr. Soc*., **65**, 703–725.

Venkatachalapathy R., Bakas T., Basavaiah N. and Deenadayalan K., 2008. Mössbauer and mineral magnetic studies on archaeological potteries from Adhichanallur, Tamilnadu, India. *Hyperfine Interact*., **186**, 89–98.

Verma R.K., 1989. Palaeomagnetism of rocks from Indian peninsula and the Himalaya: Implications of continental drift and India-Asia collision, a review. *In*: 'Current trends in Geology–XI, Himalayan mountain building'. Eds Saklani P.S. Today & Tommorow's Printers and Publishers, New Delhi. 163–198.

Vichare G. and Rajaram R., 2009. Comparative study of models of Earth's magnetic field derived from Oersted, CHAMP and SAC-C magnetic satellite data. *J. Ind. Geophys. Uni*., **13(1)**, 33–42.

Vichare G., Alex S. and Lakhina G.S., 2005. Some characteristics of intense geomagnetic storms and their energy budget. *J. Geophy. Res*., **110**, A03204.

Vinit C.E., 2002. Magnetic mapping of basement of India. Unpubl. PhD Thesis. Mumbai University, India.

Von Dobeneck T. and Schmieder F., 1999. Using rock magnetic proxy records for orbital tuning and extended time series analyses into the super- and sub-Milankovitch bands. *In*: Use of proxies in paleoceanography: examples from the south Atlantic. Eds Wafer G. and Fischer G. Springer-Verlag, Berlin, 601–633.

Waghmare S.Y., Carlo L., Gawali P.B. and Patil A.G., 2008. Geomagnetic investigation in the seismoactive area of Narmada-Son Lineament, Central India. *J. Ind. Geophys. Uni*., **12(1)**, 1–10.

Walden J., 1999. Remanence measurements. *In*: Environmental magnetism. Eds Walden J., Oldfield F. and Smith J.P. Quarter. Res. Ass., London, 63–88.

Williams W., 2007. Magnetometers, Laboratory. *In*: Encyclopedia of Geomagnetism and Paleomagnetism. Eds Gubbins D. and Herrero-Bervera E. Springer Publishers, 654–656.

Williams R.J. and Clarke M.F., 1984. Late Quaternary environments in north-central India. *Nature*, **308,** 633–635.

Woolliscroft L.J.C., 1978. International magnetosphetric study. *Phys. Bull*., **29**, 216–218.

Xu Y., Shankland T.J. and Poe B.T., 2000. Laboratory-based electrical conductivity in the Earth's mantle. *J. Geophy. Res*., **105**, 27865–27875.

Books and Special Publications

Asimov Isaac, 1979. Asimov's guide to science. v.1. The physical sciences. Penguin Books.

Barnes Charles W., 1980. Earth, time and life: An introduction to physical and historical geology. Northern Arizona University, John Wiley & Sons.

Barsukov O.M., 1974. Variations in the electrical resistivity of rocks and earthquakes, Earthquake Precursors. Acad. Sci. USSR, Moscow.

Basavaiah N. and Khadkikar A.S. (Guest eds), 2004. Environmental magnetism and palaeomonsoons. *J. Ind. Geophys. Uni*., Special Issue, 8(1).

Butler R.F., 1992. Paleomagnetism: Magnetic Domains to Geologic Terranes. Blackwell Scientific Publications.

Calder Ritchie, 1968. Man and cosmos: The nature of science today, Penguin Books.

Campbell W.H., 1997. Introduction to geomagnetic fields. Cambridge University Press.

Cattermole Peter, 2000. Building Planet Earth. Cambridge University Press.

Colin Reeves, 2005. Aeromagnetic Surveys – principles, practices and interpretation. e-Published by GEOSOFT (http://www.geosoft.com/knowledge).

Cornell R.M. and Schwertmann U., 2003. The Iron Oxides—structure, properties, reactions, occurrences and uses, Second edition. Wiley-VCH Publications.

Dearing J.A., 1994. Environmental magnetic susceptibility: Using the Bartington MS2 system. Chi Publishing, Kenilworth, UK.

Dunlop D.J. and Özdemir Ö., 1997. Rock Magnetism: fundamentals and frontiers. Cambridge University Press, Cambridge.

Evans Michael E. and Heller Friedrich, 2003. Environmental magnetism: Principles and applications of environmagnetics. Academic Press, Elsevier Science (USA).

Hamilton John (ed.), 1991. They made our world: Five centuries of great scientists and inventors. BBC World Service, Broadside Books.

Hancock Paul L. and Skinner Brian J. (eds), 2000. 'The Earth'. Oxford University Press.

Hazard Daniel L., 1938. Directions for magnetic measurements. United States Government Printing Office, Washington.

Holmes Arthur, 1986. Principles of physical geology, Third edition. English Language Book Society (ELBS).

Hoyt D.V. and Schatten K.H., 1998. The role of the sun in climate change, Oxford University Press.

Jacobs J.A. (ed.), 1987. Geomagnetism, v. 1. Academic Press.

Jacobs J.A. (ed.), 1987. Geomagnetism, v. 2. Academic Press.

Jacobs J.A. (ed.), 1989. Geomagnetism, v. 3. Academic Press.

Keller E.A. and Pinter N., 1996. Active tectonics: earthquakes, uplift and landscape. Prentice-Hall, Upper Saddle River, New Jersey 07458.

Lanza R. and Meloni A., 2006. The Earth's magnetism: An introduction for Geologists. Springer.

Mahadevan T.M., Arora B.R. and Gupta K.R. (eds), 2003. Indian continental lithosphere: emerging research trends. Mem. 53, Geol. Soc. Ind., Bangalore, India.

Maher B.A. and Thompson Roy (eds), 1999. Quaternary climates, environments and magnetism, University Press, Cambridge.

Milovsky A.V., 1982. Mineralogy and petrography. Mir Publishers, Moscow.

O'Reilly W., 1984. Rock and Mineral Magnetism. Blackie, Glasgow.

Onwumechili C.A., 1997. The Equatorial Electrojet. Gordon and Breach Science Publishers, Netherlands.

Parkinson W.D., 1983. Introduction to geomagnetism. Scottish Academic Press, Edinburgh and London.

Press Frank and Siever Raymond, 2002. Understanding Earth, Third edition. W.H. Freeman and Company, New York.

Radhakrishnamurty C., 1993. Magnetism and basalts. Mem. 26, Geol. Soc. Ind., Bangalore, India.

Rajaram Girija and Pisharoty P.R., 1998. The Earth's magnetic field. Oxford and IBH Publishing Co., New Delhi.

Rajaram Mita (ed.), 2003. Geophysics: Window to Indian Geology. J. Virtual Explorer (Australia), 12.

Rama Rao B.S. and Murthy I.V.R., 1978. Gravity and magnetic methods of prospecting. Arnold-Heinemann Publishers, New Delhi.

Rangarajan G.K. and Arora B.R. (eds), 1992. Geomagnetic studies at low latitudes. Mem. 24, Geol. Soc. Ind., Bangalore, India.

Rikitake T., 1982. Earthquake forecasting and warning. Center for Academic Publications, Japan, in co-publication with D. Reidel Publishing Company, Dordrecht.

Robinson Edwin Simons, 1982. Basic Physical Geology. John Wiley & Sons.

Rokityansky I.I., 1982. Geoelectromagnetic investigation of the Earth's crust and mantle. Springer-Verlag, Berlin.

Schmucker U., 1985. Sources of the geomagnetic field. Landolt-Bornstein, New Series, 5/2b, Section 4.1, Springer-Verlog, Berlin-Heidelberg.

Sharma A.S., Kamide Y. and Lakhina G.S. (eds), 2003. The storm-substorm relationship, Geophys. Monogr. Ser., AGU, 142, Washington D.C.

Strangway David W., 1970. History of the Earth's magnetic field. McGraw-Hill Book Company.

Tarbuck Edward J. and Lutgens Frederick K., 1994. Earth Science, Seventh edition. Macmillan College Publishing Company Inc.

Tarling D.H., 1983. Palaeomagnetism: Principles and applications in Geology, Geophysics and Archaeology. Chapman and Hall.

Thompson R. and Oldfield F., 1986. Environmental Magnetism. Allen and Unwin, London, UK.

Uberoi Chanchal, 2000. Earth's proximal space. Universities Press.

Walden J., Oldfield F. and Smith J., 1999. Environmental magnetism: a practical guide. Quaternary Research Association, London.

Weaver J.T., 1994. Mathematical methods for geoelectromagnetic induction. Research Studies Press, Taunton.

Wienert K.A., 1970. Notes on geomagnetic observatory and survey practice. UNESCO.

INDEX